SOVIET PHYSICS

JETP

A translation of the Zhurnal Éksperimental'noĭ i Teoreticheskoĭ Fiziki.

Vol. 11, No. 2, pp. 227-479 (Russian original Vol. 38, No. 2, pp. 313-667, February, 1960) August, 1960

INVESTIGATION OF A HIGH-ENERGY INTERACTION EVENT IN PHOTOGRAPHIC EMULSION

Kh. P. BABAYAN, M. G. SARINYAN, and É. R. TUMANYAN

Physics Institute, Academy of Sciences, Armenian S.S.R.

Submitted to JETP editor June 12, 1959

J. Exptl. Theoret. Phys. (U.S.S.R.) **38**, 313-318 (February, 1960)

A star of the 5 + 21 p type produced by a primary particle of $\sim 10^{12}$ ev was investigated. The measured angular distribution of the secondary shower particles exhibits two maxima. The event was interpreted as a peripheral collision of two nucleons. The ratio of the number of neutral π mesons to the total number of charged shower particles was found to be of the order of 0.4. A secondary interaction of the 0 + 6 p type, which is probably due to a single π-N collision in a peripheral collision of nucleons, was detected.

A star of the 5 + 21 p type has been found in a stack of Ilford G-5 nuclear emulsions, irradiated in Italy at an altitude of 25 — 30 km. The particles of the narrow cone are contained within a half-angle of 0.017 radians, while the half-angle of the wide cone is equal to 0.62 radians.

1. DETERMINATION OF THE PRIMARY PARTICLE ENERGY. ANGULAR DISTRIBUTION OF SHOWER PARTICLES.

The angles were measured using a MBI-8M microscope with total magnification of 1800×. Angles smaller than 2° were measured by the coordinate method[1] while a goniometer was used for larger ones. One of the particles, apparently belonging to the shower, was emitted backwards in the laboratory system (very unfortunate geometry). In the following discussion, this particle has not been taken into account.

The energy of the primary particle E_0 was determined, first assuming a nucleon-nucleon, then a tunnel-effect interaction. Under the first assumption, the energy was determined by two methods: 1) the half-angle method[2] and 2) the Castagnoli method.[3] The following results were obtained:

N - N collision

Method 1 $\gamma_c = 20.1$; $E_0 = 7.5 \times 10^{11}$ ev

Method 2 $\gamma_c = 21.0\ ^{+3.8}_{-4.7}$; $E_0 = (8.3\ ^{+3.0}_{-3.7}) \times 10^{11}$ ev

Tunnel-effect collision ($l = 3.3$)

$E_0 = (1.8^{+0.6}_{-0.8}) \times 10^{12}$ ev.

In the above, γ_c is the Lorentz factor of the center-of-mass system of the colliding nucleons with respect to the laboratory system (l.s.), and l is the length of the nuclear tunnel (in terms of the number of nucleons).

The histogram of the differential angular distribution in the l.s. is shown in Fig. 1. The figure also shows the Landau curve[4] (curve 1) for a symmetrical distribution in c.m.s., the Heisenberg curves[5] for an isotropic (curve 2) and anisotropic (curve 3) distribution in c.m.s. for a head-on N-N collision, and the Landau curve for a tunnel-effect collision (curve 4). The probability that the shower is symmetric was determined by the χ^2 method. It has been found that $P(\chi^2) = 92\%$. The probability of a good fit between the histogram of the experimental distribution and the Landau distribution amounts to 1%; with a Heisenberg distribution (assuming an anisotropic distribution) it amounts to 2%. From the theories of Landau and Heisenberg,

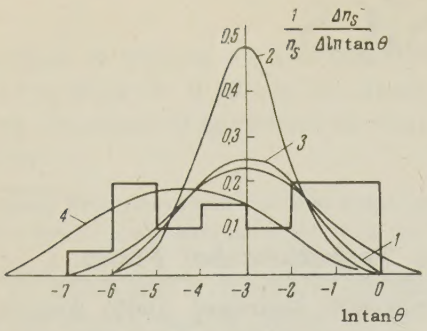

FIG. 1. Histogram of the differential angular distribution in the laboratory system.

one expects the maximum number of particles in the angle range of $1-9°$ in the l.s. for the investigated event. The distribution obtained indicates, however, a marked deficiency of particles in this range, which in c.m.s. corresponds to the vicinity of the angle $\pi/2$.

According to Lindern,[6] in the coordinate system

$$x = \log(\gamma_c \tan\theta), \qquad y = dN / d\log(\gamma_c \tan\theta)$$

(θ represents the angles in l.s.) the differential angular distribution can be approximated by a Gaussian curve with $\sigma = 0.36$ for an isotropic and $\sigma = 0.70$ for an anisotropic Heisenberg distribution. The angular distribution of the event investigated is shown in such coordinates in Fig. 2. The curve represents a Gaussian curve corresponding to the experimental data for $\sigma = 0.9$. As could be expected from the angular distribution in the l.s., the distribution is characterized by the presence of two maxima. A similar angular distribution is expected for a peripheral collision of two nucleons in the case where they are similarly excited[7,8] (a double π-N collision).

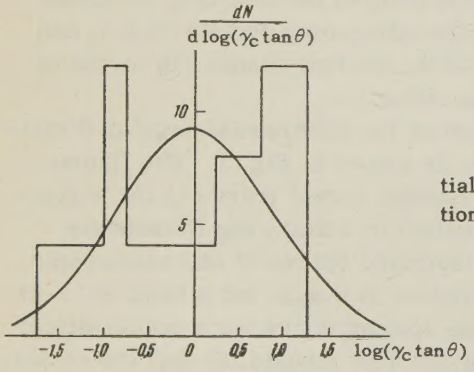

FIG. 2. Differential angular distribution in the c.m.s.

From the energy conservation law, one can determine the Lorentz γ factor of the excited nucleons in the c.m.s.

$$\bar{\gamma} = E_0' / E^*, \qquad (1)$$

where E_0' is the nucleon energy in the c.m.s., $E^* = 2\sqrt{\epsilon E_0'}$ is the energy of the excited nucleon in its proper system, and ϵ is the π-meson energy. For an average value $\bar{\epsilon} = 0.5\mu\gamma_c$, we have $\bar{\gamma} = 1.8$. If the excitation energy E* is known (in our case, it is equal to 11.5 M, where M is the rest mass of the nucleon), one can determine the expected number of shower particles n_s' and the number of particles n_s'' emitted by each of the excited nucleons.[9] It was found that $n_s' = n_s'' = 7$.

To compare the theories with experiment, n_s', n_s'', and $\bar{\gamma}$ have also been determined from an analysis of the experimental data. For a first approximation, the symmetry between the two nucleons in the c.m.s. makes it possible to put $n_s' = n_s''$. However, for a small number of secondary particles, large fluctuations may be expected, and thus the values of n_s' and n_s'' have been estimated by plotting the integral distribution curve in the c.m.s. (see Fig. 3. The quantity F indicated in the figure represents the ratio of the particles with angles smaller than θ to the total number of secondary shower particles.) From this curve, the values $n_s' = 9$ and $n_s'' = 11$ have been obtained.

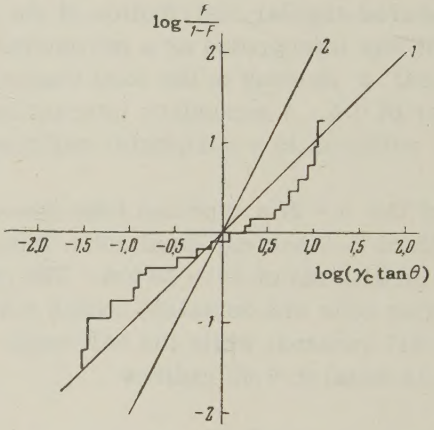

FIG. 3. Integral angular distribution in the c.m.s.

The straight lines 1 and 2 in Fig. 3 correspond to isotropic and anisotropic distributions. It can be seen that the angular distribution in the event investigated cannot be approximated by any straight line, which again indicates a deficiency of particles near the angle $\pi/2$.

For a determination of $\bar{\gamma}$, measurements were made separately for the particles n_s' and n_s''. It was found that

$$\bar{\gamma} = (\gamma_1 + \gamma_2) / 2\sqrt{\gamma_1\gamma_2} = 3.0, \qquad (2)$$

where γ_1 and γ_2 are the Lorentz factors in l.s. of the first and second excited nuclei respectively, determined according to reference 3.

The integral angular distribution of shower particles is shown in Fig. 4 separately for each emitting nucleon. The experimental points lie on a

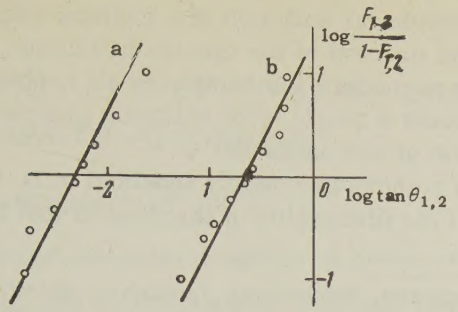

FIG. 4. Integral angular distribution of particles emitted: a – by the first nucleon, b – by the second nucleon.

straight line with slope equal to two, corresponding to an isotropical distribution.

2. THE SOFT COMPONENT

For a study of the soft components accompanying the shower, the cone with an opening angle of 0.06 rad was scanned for about 4 cm from the shower origin. Ten pairs have been detected. The criterion established in reference 10 was used for distinguishing the "associated" and bremsstrahlung pairs. According to this criterion, four "associated" pairs have been detected. The energy of these pairs was determined from the opening angle according to reference 11:

$$\vartheta = \frac{4mc^2}{E}\log\frac{E}{mc^2}, \qquad (3)$$

where θ is the pair opening angle and mc^2 is the rest energy of the electron. For two pairs, it was also possible to determine the energy from the relative scattering (see Table).

Distance from the star X, μ	Pair energy from the opening angle E_ϑ, Bev	Pair energy from the relative scattering E_α, Bev	E_{π^0} from E_ϑ, Bev	E_{π^0} from E_α Bev
319	$2.2^{+2.1}_{-0.8}$	—	$4.3^{+4.2}_{-1.5}$	—
5803	$2.2^{+3.2}_{-1.1}$	5.8 ± 0.7	$5.6^{+6.4}_{-2.8}$	11.6 ± 1.5
5929	$1.1^{+1.4}_{-0.6}$	1.5 ± 0.3	$2.8^{+2.8}_{-1.3}$	2.9 ± 0.6
38203	$8.3^{+6.7}_{-3.5}$	—	$16.6^{+13.4}_{-7.1}$	—

For a known number of electron-positron pairs, one can determine the expected numbers of π^0 mesons.[10] (For π^0 mesons in the energy under consideration, the decay mean free path is $\rho = 33\,\mu$.) The value $N(\pi^0) = 3$ (for the narrow cone) has been obtained, which yields a value of the order of 0.4 for the ratio of the number of neutral π mesons to the total number of charged particles in the narrow cone.

The resulting mean energy of π^0 mesons of the narrow cone is

$\bar{E}_{\pi^0} = \left(7.3\ ^{+6.7}_{-3.0}\right)$ Bev- by the opening-angle method

$\bar{E}_{\pi^0} = (7.3 \pm 1.0)$ Bev-by the relative scattering method.

The energies of six particles in the narrow cone were also determined by the relative-scattering method. The average was ~ 4 Bev. This value is of the same order of magnitude as the π^0-meson energy. However, for the transverse momentum, $p_\perp$, one obtains a considerably lower value as compared with the one generally accepted. The disagreement is possibly due to errors in the measurement of secondary-particle energy in connection with the unfortunate geometry.

3. THE SECONDARY INTERACTION

In the scanning, a secondary interaction of the type 0 + 6p was found at a distance of 3.5 cm from the first star. This interaction was produced by one of the particles of the narrow cone. The event is characterized by a narrow particle jet with a half-angle of two degrees. Strong collimation of the jet particles and their small number indicates the possibility of interpreting this case as a peripheral collision of two nucleons, in which only the incident nucleon was excited (a single π-N collision).[8]

Since, in such a collision, the shower-particle distribution will be symmetrical not in c.m.s. but in the system of the excited nucleons, the angular distribution in the l.s. yields not γ_c but γ', which is the Lorentz factor of the excited nucleons in the l.s. We have found that

$$\gamma' = 19.7\ ^{+9.0}_{-6.1} \text{ by the Castagnoli method}$$

In order to determine the energy of the primary nucleon in the l.s., it is necessary to find E*, the excitation energy of the nucleon in its own system. E* can be determined from curves presented in reference 9 for a known number of shower particles emitted by the excited nucleon. The excitation energy determined in such a way is equal to $E^* = 8\,M$. The energy in the l.s. is

$$E_0 = \gamma' E^* = \left(1.7\ ^{+0.8}_{-0.5}\right)\cdot 10^{11}\ \text{ev}.$$

To strengthen the validity of the above interpretation, the event was tested for a possible N-N collision. For this purpose, assuming the $p_\perp$ of the particle that produced the secondary star to be equal to the generally accepted average value of 0.5 Bev/c, its energy in the l.s. was estimated, and it was found that $E_0 \sim 10^{11}$ ev. This energy value leads to $\gamma_c \sim 7$. This is in sharp disagreement with the value $\gamma_c \sim 20$ determined from the angular distribution of shower particles in the l.s., which should not occur in a head-on N-N collision.

4. DISCUSSION OF EXPERIMENTAL RESULTS

The investigated event has been analyzed assuming a head-on collision of two nucleons and a collision of a nucleon with a tunnel of nuclear matter. However, the angular distribution obtained strongly contradicts the predictions of the theories of Landau and Heisenberg for such collisions. A similar angular distribution with two maxima can be expected in a peripheral collision of two nucleons where both nucleons are excited. In addition, since the probability of a symmetrical distribution for the investigated shower $P(\chi^2) = 92\%$, one should assume that they have an equal degree of excitation. An estimate of the energy of the primary particle by methods presented in references 2 and 3 remains valid, as these methods are correct for all symmetrical stars.

The angular distribution constructed separately for the particles emitted by each excited nucleon is almost isotropic, which, in the energy range under consideration, does not contradict the data presented in the literature[12-14] or the analysis carried out above.

The large number of heavily ionizing tracks N_h can be explained by a mechanism similar to that described in reference 15, namely by an excitation of a nucleus in the interaction of any π meson of the incident nucleon with the nuclear matter in the tunnel (which is possible for $b \sim \hbar/\mu c$). To this assumed interaction, one can also ascribe the $2-3$ particles having the largest angles in the l.s. The symmetry of the shower then becomes more complete.

The experimental values n_s' and n_s'', within the limits of possible fluctuations, do not contradict the theoretical predictions, nor are the latter contradicted by the experimental value of $\bar{\gamma}$.

Thus, the investigated event can be interpreted as a peripheral collision of a nucleon with a peripheric nucleon of the emulsion nucleus.

The secondary interaction in all probability represents a single π-N collision in a peripheral collision of two nucleons.

The authors are deeply indebted to D. S. Chernavskiĭ for discussion of the results and helpful advice.

[1] Zhdanov, Berkovich, Lepekhin, Skirda, and Khokhlova, Приборы и техника эксперимента (Instruments and Measurement Engg.) No. 4, 32 (1957).

[2] Dilworth, Goldsack, Hoang, and Scarsi, Nuovo cimento **10**, 1261 (1953).

[3] Castagnoli, Cortini, Franzinetti, Manfredini, and Moreno, Nuovo cimento **10**, 1539 (1953).

[4] L. D. Landau, Izv. Akad. Nauk SSSR, Ser. Fiz. **17**, 51 (1953).

[5] W. Heisenberg, Kosmische Strahlung (Springer, Berlin, 1953) p. 563.

[6] L. von Lindern, Nuovo cimento **5**, 491 (1957).

[7] E. L. Feĭnberg and D. S. Chernavskiĭ, Dokl. Akad. Nauk SSSR **81**, 795 (1958).

[8] D. S. Cernavsky, Nuovo cimento Suppl. **8**, 775 (1958).

[9] I. A. Ivanovskaya and D. S. Cernavsky, Nucl. Phys. **4**, 29 (1957).

[10] Brisbout, Dahanayake, Engler, Fujimoto, and Perkins, Phil. Mag. **1**, 605 (1956).

[11] Bradt, Kaplon, and Peters, Helv. Phys. Acta, **23**, 24 (1950).

[12] S. Takagi, Progr. Theor. Phys. **7**, 123 (1952).

[13] Ciok, Coghen, Gierula, Holynski, Jurak, Miesowicz, Saniewska, Nuovo cimento **10**, 741 (1958).

[14] G. Cocconi, Phys. Rev. **111**, 1699 (1958).

[15] W. Heitler and C. H. Terreaux, Proc. Phys. Soc. **A66**, 929 (1953).

Translated by H. Kasha
76

TRANSITION EFFECT OF STARS PRODUCED BY COSMIC RAYS IN LEAD AND GRAPHITE ABSORBERS

T. V. VARSIMASHVILI

Physics Institute, Academy of Sciences, Georgian S.S.R.

Submitted to JETP editor June 30, 1959

J. Exptl. Theoret. Phys. (U.S.S.R.) 38, 319-323 (February, 1960)

Results of an investigation of the transition effect of stars produced in lead and graphite absorbers at an altitude of 3100 m above sea level are presented. Photographic emulsions were used in the experiments. The effect amounts to 30% and 10% in lead and in graphite, respectively. A hypothesis is proposed concerning the properties of the particles producing the effects.

CONTRADICTORY results have been obtained by various authors in the study of the transition effect of the stars in dense absorbers. It has been shown[1] that the reason for this might lie in the low efficiency of a single scanning, and in the small depth at which the maximum of the transition curve occurs. It would therefore be of interest to set up an experiment which would enable us to carry out these measurements more accurately. For this purpose, the transition effect of stars in lead and graphite absorbers has been measured on Mount Terskol (3100 m above sea level). The experimental arrangement was placed in a wooden hut with dimensions 1.6 × 2.8 m, and having walls and roof of 1 cm thickness. The hut was set up on an open plateau. (A single-story building was also situated on the same plateau at a distance of 100 m from the hut.)

Emulsion layers of the type NIKFI-BR-400, 5 cm in diameter, were used in the experiments. The emulsion layer was wrapped in black paper and placed in a rubber case (thickness 10^{-2} g/cm^2). A getinax (paper-laminated bakelite) plate 6 cm in diameter and of 1 mm thickness was placed under the emulsion layer to prevent curling.

Stars with a number of prongs ≥ 3 were selected. To increase the efficiency of scanning, each layer was scanned three times, since, as has been mentioned in reference 1, the observed value of the effect is decreased, owing to the low scanning efficiency. All values of the relative number of stars that are presented correspond to the same weight of undeveloped emulsion layer.

The experimental arrangement with the lead absorber (Fig. 1) consisted of nine layers of lead placed one above the other. The dimensions of each layer were 40 × 60 cm. A frame 40 × 60 cm,

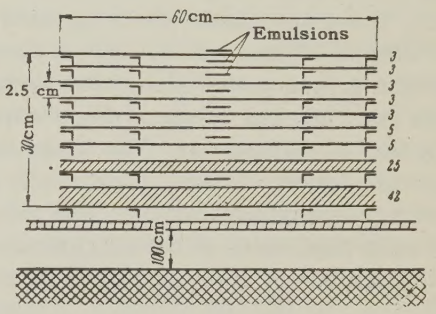

FIG. 1. Diagram of the experimental arrangement for measurements with lead absorber. The numbers on the right denote the thickness of the lead layers in mm.

made of a 25 × 25 mm steel angle 3 mm in thickness, was placed under each lead layer. To prevent the buckling of the lead layers, two duraluminum angles 15 × 15 mm, 1.5 mm thick, were placed on the frame in two places. Each was placed 15 cm from the edge of the longer side of the frame. The position and thickness of the layers are shown in Fig. 1. Instead of additional duraluminum angles, 25 × 25 mm steel angles were placed under the layers of 25 mm and 42 mm thickness, which consisted of separate lead bars. Above these, 1.5 mm thick getinax plates were placed. The remaining lead layers were solid, and were placed on the frames directly. On top of the array and below each lead layer, a single emulsion layer was placed horizontally in the center.

Results of the scanning are shown in Fig. 2. It can be seen that the intensity curve of the stars attains a maximum at the depth of 5 — 6 mm of lead. The value of the transition effect is 30%. At the depth of the order of 2.5 — 3 cm of lead, the transition effect almost completely disappears, and the slope of the curve beyond this point corresponds to the absorption of the N component in lead.

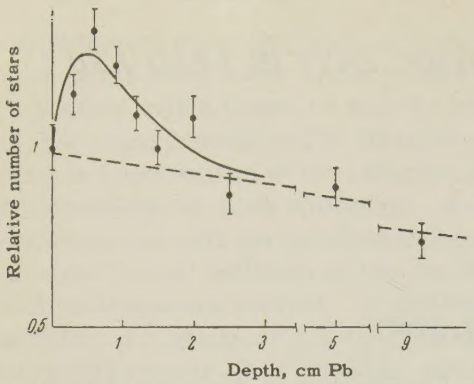

FIG. 2. Variation of the number of stars with the thickness of the lead absorber. Solid curve – the observed number of stars, according to Eq. (1). Dashed curve – the number of stars produced by the N component.

The existence of a transition effect of stars in graphite[2] indicates that the photon component is not the cause of the transition effect of stars. In the experiments of Rössle and Schopper, the value of this effect in graphite was calculated by subtracting from the total number of stars those which were produced by the N component. The latter were obtained by calculation. The purpose of our experiment with the graphite absorber was the measurement at each depth both of the total number of stars and the number of stars produced by the N component.

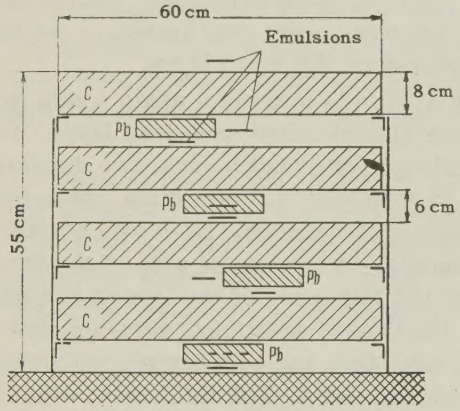

FIG. 3. Schematic diagram of the experimental arrangement with the graphite absorber.

The array consisted of four graphite blocks (Fig. 3), the dimensions of each being 60 × 60 cm. The blocks were placed one above the other, and were supported by steel frames held in a steel shell. A 25 × 25 mm steel angle was used.

Under each graphite block and in its center, two emulsions were placed horizontally. One of these was shielded from above by a 3 cm lead plate of 15 × 15 cm size. In order to decrease the shielding by the lead plates above the higher-placed emulsions, the lower-placed emulsions were turned with respect to the upper emulsions by 90°.

From the experimental data it follows that, at a depth of 3 cm of lead, the transition effect of the stars almost completely disappears, and the shielded emulsion recorded, therefore, only those stars produced by the N components at a given depth. The difference between the number of stars recorded in the unshielded layers, taking the absorption of the N component in 3 cm of lead into account, gives directly the number of stars of the transition effect.

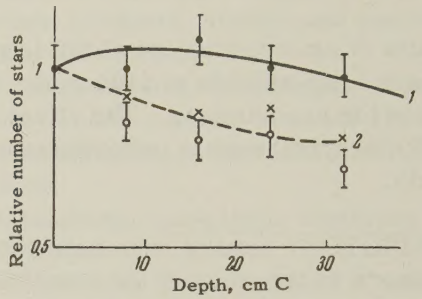

FIG. 4. Variation of the number of stars with the thickness of the graphite absorber. ● – number of stars under graphite absorber (curve 1), ○ – number of stars under the lead plate, × – number of stars under graphite absorber obtained by counting the number of stars detected under the lead plates (curve 2). In calculating this curve, the geometry of the arrangement has been taken into account.

The results of the experiment are shown in Fig. 4. From the figure, it can be seen that the intensity of stars under the graphite absorber (curve 1) is greater than the intensity of stars produced by the N component (curve 2). It is thus evident that there exists a transition effect of stars in graphite. Its value is 10 — 15%. From the existence of the transition effect of stars in graphite it follows that the star-producing particles of this effect are unstable. The presence of a maximum in the intensity curve of stars in lead indicates that these particles are produced in the absorber and, consequently, are secondary ones. According to Rössle and Schopper,[2] they are neutral. It has been shown earlier by the authors[3] that the "primary" particle incident on the absorber and responsible for the production of "secondary" particles cannot be charged.

In order to obtain a good agreement with the experimental data, it is necessary to assume that the mean free path for the production of "secondary" particles by the "primary" ones is approximately equal to the mean free path for star production by "secondary" particles. If, for simplicity, we consider a one-dimensional picture, we obtain the following expression for the intensity of stars at various depths in lead:

$$A\exp\left(-\frac{x}{L}\right)+B\frac{x}{\lambda}\exp\left(-\frac{x}{\lambda}\right) \qquad (1)$$

(solid curve in Fig. 2). The first term gives the intensity of stars produced by the N component (dashed curve in Fig. 2), while the second term gives the intensity of stars of the transition effect (difference between the solid and the dashed curve).

From our experimental data, we obtain: $A \approx 1$, $B \approx 0.8$, $\lambda \approx 0.5$ cm, and $L \approx 33.5$ cm. The value λ is markedly smaller than the mean free path corresponding to the geometrical cross section for nuclear interactions. No known particle possesses such a small mean free path for star production. Knowing A, B, λ, and L we can determine the intensity of the "primary" particles. This was found to be of the order of 4% of the intensity of the star-producing component at the observation altitude.

The expression (1) has been obtained under the assumption that the "primary" particles fall on the absorber from the air. This corresponds to the steep slope of the star-intensity curve after it has passed through its maximum in lead, indicating that the production of "primary" particles in lead is insignificant as compared with air.

From an analysis of experimental data at other altitudes,[4] it follows that these particles are in equilibrium with the N component. In view of the fact that the atomic weights of air and graphite are approximately equal, one can expect that the N component will also produce "primary" particles in graphite. To check this, a graphite array similar to the one described above was surrounded from all sides, except on the bottom, by a 4 cm lead layer. This lead layer shielded the side of the array from the air, both from "primary" and "secondary" particles. The diagram of the position of the experimental arrays in the wooden hut is given in Fig. 5.

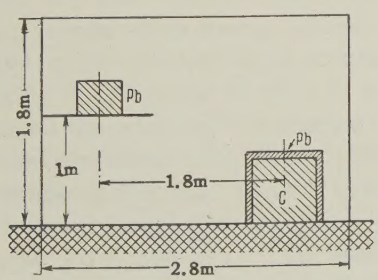

FIG. 5. Schematic diagram of the position of the experimental arrays.

The experiments were carried out in two series. First, the arrays with plane lead absorbers and with a graphite absorber shielded by lead were simultaneously exposed. Then, the graphite array took the place of the lead-shielded graphite array. The time of exposure of each series amounted to about two months. The results of the experiments are shown in Fig. 6.

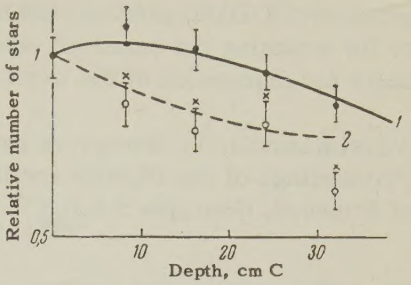

FIG. 6. Variation of the number of stars with the thickness of the graphite absorber in the experiment with the graphite absorber shielded by lead. Notation as in Fig. 4.

The existence of the transition effect in the described array confirms that the particles responsible for this effect are also produced in graphite. Thus, in graphite not shielded by lead, one should observe a total transition effect from "primary" particles produced both in air and in graphite. As a result, the slope of the intensity curve beyond the maximum should correspond to the absorption of the N component in graphite. As can be seen from Fig. 4, the experimental data up to the depth of 32 cm of graphite do not contradict our conclusions.

It should be mentioned that the production of "secondary" particles, as a result of a spontaneous decay of the "primary" ones, is excluded. In fact, in such a case the mean free path of the "primary" particles for the production of the "secondary" ones should be equal to ~ 0.5 cm. Consequently, the transition effect in lead can be produced only by those "primary" particles which were produced in the 0.5 cm of air directly above the lead array. By calculating the number of interactions of the N components with the air nuclei in this layer of air we find that for each such interaction there are 10^3 stars of the transition effect with ≥ 3 prongs. Since one three-prong star has, on the average, an energy of 150-Mev, then the energy lost in a single act of interaction by one particle of the N component to the production of the "primary" particles should be greater than 150 Bev, which contradicts well-known data.

It should be concluded that the "secondary" particles are produced as a result of the interaction of the "primary" particles with nuclei. The energy transferred to the nucleus should, moreover, be insufficient for the production of a visible star. Such a picture does not contradict the energy which is available in the star-producing component of cosmic rays.

In conclusion, the author wishes to express his gratitude to É. L. Andronikashvili for his constant interest in the work, and to N. I. Kostanashvili, G. S. Sherezadashvili, D. B. Bokhua, and I. B. Amirkhanov for scanning the emulsion, and to T. V. Gvaladze for discussion of the work.

[1] T. V. Varsimashvili, Тр. Института физики АН ГрузССР (Proceedings of the Physics Institute, Academy of Sciences, Georgian S.S.R.) 7, (1959), in press.

[2] E. Rössle and E. Schopper, Z. Naturforsch. 9a, 836 (1954).

[3] T. V. Varsimashvili, loc. cit. ref. 1.

[4] J. J. Lord and M. Schein, Phys. Rev. 75, 195 (1949).

Translated by H. Kasha
77

ENERGY DISTRIBUTION OF SPUTTERED AND SCATTERED IONS IN THE BOMBARDMENT OF TANTALUM AND MOLYBDENUM BY POSITIVE CESIUM IONS

V. I. VEKSLER

Central Asia State University

Submitted to JETP editor June 30, 1959

J. Exptl. Theoret. Phys. (U.S.S.R.) **38**, 324-334 (February, 1960)

A method is described for studying the energy spectra of scattered and sputtered ions produced in the bombardment of metals by positive ions. The energy spectra of the Cs^+, Mo^+, and Ta^+ ions obtained by bombarding molybdenum and tantalum targets ($T \sim 1600 - 1800°K$) with Cs^+ ions with energies $U = 900 - 2150$ ev have been investigated. The sputtering and scattering components have been separated from the secondary-emission ion spectra which have been described earlier; the result is a considerable reduction in the limiting energy in the spectrum of Cs^+ scattered on molybdenum. The width of the energy spectrum for the sputtered ions is found to be $30 - 35$ ev for Mo^+ and $35 - 50$ ev for Ta^+; these values are much higher than the value of 5 ev which is quoted in the literature. These results indicate that the probability of ionization of a sputtered atom which escapes from the surface increases as its energy increases.

THE energy distributions of scattered secondary ions which arise in the bombardment of surfaces by accelerated positive ions have been studied by many authors.[1-4] However, the energy distributions of the ions which are emitted in cathode sputtering of surfaces have not been investigated to any great extent, although this process has been studied recently by a number of workers.[5-8] This situation is a result of the difficulty of the required experimental techniques and the fact that a mass-spectroscopic analysis is needed. Honig[7] has studied the energy distributions of Ge^+ and Na^+ ions ejected from the surface of a non-degassed single germanium crystal and reports that at primary-ion energies of $U = 100 - 400$ ev the maximum in the distribution occurs at an energy of the order of 2 ev, although there is a considerable number of ions with energies of the order of $10 - 12$ ev. Bradley[8] has estimated the width of the energy distribution for Mo^+ ions sputtered from a molybdenum surface from the shape of the Mo^+ peak of a mass spectrometer measurement and reports a value of the order of 5 ev ($U \sim 500$ ev). This author concludes that the ionization probability is higher for slower sputtered atoms.

In the work described by Honig[7] and Bradley[8] there is no indication that account has been taken of the variation in transmission of the mass spectrometer with changing initial ion energy; this effect can lead to appreciable distortion of the ion energy distribution (the main distortion is an exaggeration of the number of high-energy ions). An analysis of the operation of the instruments in question indicates that this distortion effect is more important in the work reported by Bradley than in that reported by Honig. Thus, at the present time there are no reliable data on the energy distributions of the ions produced in cathode sputtering. This problem is of interest from the point of view of obtaining information concerning the energy distributions of neutral particles produced in cathode sputtering as well as accumulating information on the nature of electron exchange in the interaction of a slowly moving atom with the surface of a material (effects which are probably different for metals and semi-conductors). There are also certain contradictions in the data on scattering of ions from metallic surfaces.

In the present work we describe an investigation of the energy spectra of different ion-emission components, carried out by means of a method which is free from the shortcomings indicated above; results are reported on the energy distributions of sputtered and scattered ions produced in the bombardment of molybdenum and tantalum surfaces by Cs^+ ions.

1. APPARATUS AND METHOD

The complexity of the isotopic spectra of certain ions and the relatively low resolution of the mass spectrometer at our disposal made it impossible

to carry out an analysis of the energy spectra with the required resolution (several electron volts) by direct examination of the shapes of ion peaks in the mass spectrometer. Hence, in addition to separating the secondary emission products by the mass spectrometer we also used an electrostatic retarding field. Appropriate tests have shown that because of scattering of the secondary ions in the mass spectrometer tube the application of a retarding field at the output of the mass analyzer causes a considerable distortion of the distribution curves. For this reason the retarding field was applied in the region in which the primary-ion target T is located (Fig. 1).

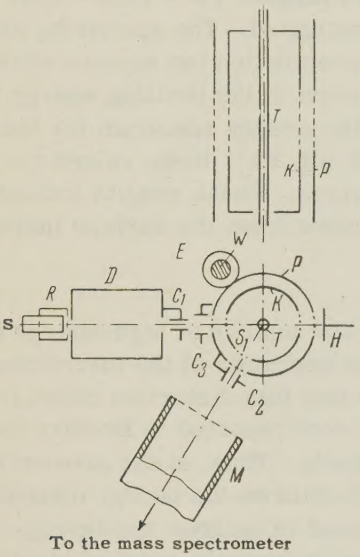

FIG. 1. Diagram of the apparatus: S – primary-ion source, S–R–D – ion gun, C_1, C_2, C_3 – deflection capacitors, T – target, K – cylinder of the energy analyzer, P – accelerating cylinder, M – mass-spectrometer tube, H – collector for "straight-through" ions, E – shield, W – traverse, S_1 – screen.

The Cs^+ ions obtained from the thermo-ionic source S are accelerated by a voltage applied between S and the nickel electrode D which has two longitudinal slits; these define a beam of cross section 0.4 × 5 mm. The width of the beam is estimated from the voltage applied to capacitor C_1, used for transverse deflection of the primary ions and to aim the primary beam on the target (a cylinder 1 mm in diameter made of molybdenum or tantalum foil 0.015 – 0.030 mm thick). The current density of the primary beam at the target was $1 - 6 \times 10^{-6}$ amp/cm^2. This part of the apparatus and its operation have already been described by us in detail in reference 6. The ring R, which is at a positive potential with respect to S, serves to focus the primary Cs^+ ions. The traversing device W, which serves as a current feed for one of the ends of the target, is surrounded by a nickel shield E. The cylinders K and P, which are shown in two projections in the figure, each have three slits which are covered by brass wire mesh with a transmission of 85% and a spacing a = 0.25 mm. The mesh is made by dipping low-transparency mesh in a 30% solution of HNO_3. The presence of these wire-mesh screens and the face shields on cylinder K (diameter 25 mm) prevents the penetration of the external electrostatic field into the space between T and K, in which the secondary ions are slowed down by the retarding voltage V_0. A voltage V_n is applied between cylinders K and P; this voltage provides preliminary acceleration of the secondary ions which move toward the mass spectrometer. The total secondary-ion voltage which is applied between the cylinder K and the mass spectrometer tube M is 1250 v.

Depending on their energies, the secondary ions which leave cylinder K have different probabilities $\varphi(W)$ of passing through the mass spectrometer. The energy distribution of the secondary ions f(W), the mass-spectrometer output current i, and the function φ are related by the expression

$$i(eV_0) = e\int_{eV_0}^{\infty} f(W)\,\varphi(W - eV_0)\,dW \qquad (1)$$

which is an integral equation with kernel $\varphi(W - eV_0)$. In the method used here an approximate form of the function $\varphi(W)$ is found experimentally by plotting the dependence of the current due to the ions, which are produced by surface ionization on an incandescent target and reach the mass spectrometer detector, as a function of the voltage that accelerates these ions (between T and K). These ions can be obtained by letting a stream of neutral particles (formed when the ion source S is operated with no voltage between S and D) strike the incandescent target. It has been found subsequently (cf. below and reference 3) that at a primary-ion energy U = 2150 ev approximately 95% of the secondary Cs^+ ions formed at the incandescent target have energies close to thermal. It is thus possible to obtain the curves under conditions which are similar to the operating conditions (only the sign of V_0 is different). The values of $\varphi(W)$ obtained in both cases are found to be in good agreement. All the $\varphi(W)$ curves used for solving Eq. (1) have been obtained by the second method since it has certain advantages.

The function $\varphi(W)$ is found to be strongly dependent on both the accuracy of the adjustment of the system with respect to the tube M and the voltage V_n; its form was therefore investigated in all cases in which these factors were changed.

To illustrate the change in this function with changes in the voltage V_n, Fig. 2 shows two $\varphi(W)$ curves obtained with one of the molybdenum targets. These curves have been obtained by adjusting the TKP analyzer to achieve maximum current in the detector with minimum voltage applied to capacitor C_2; nevertheless, the shape of the curves indicates that the "transmission" of the mass spectrometer is quite different for ions of different energy. This result verifies the statement made in the introduction with regard to the errors which may have been introduced by Bradley.[8]

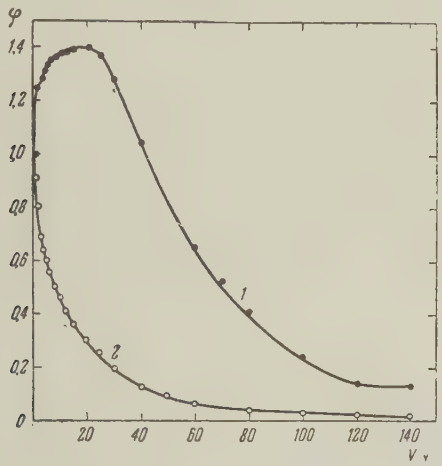

FIG. 2. The transmission of the mass spectrometer as a function of the initial energy of the ions for fixed adjustment and different values of eV_n: curve 1 – 100 ev, curve 2 – 250 ev.

It should be noted that the conditions under which $\varphi(W)$ is obtained by the surface ionization method (acceleration voltage applied to electrode K) differ somewhat from the conditions under which the volt-ampere characteristics are obtained in actual practice (retarding voltage applied to K). Hence, in spite of the measures taken to achieve identical conditions for the ion motion in the region T-K in both cases (cylindrical electrode system, small width of the emitting portion of the target), the effective width of the secondary ion emitter can be somewhat greater than the actual width under operating conditions. The measured results can be distorted by this effect, especially when high retarding potentials are used. Thus, some experimental method for checking the results is required. A check of this kind can be made by measuring a spectrum twice with highly different $\varphi(W)$. In Fig. 3 we show two such spectra for Cs^+ ions scattered on molybdenum (U = 900 ev) obtained by differentiation of the volt-ampere characteristics plotted for different values of V_n (curves 1 and 2, solid points). The hollow circles and triangles denote the results obtained from solutions of the integral equation (1) corresponding to curves

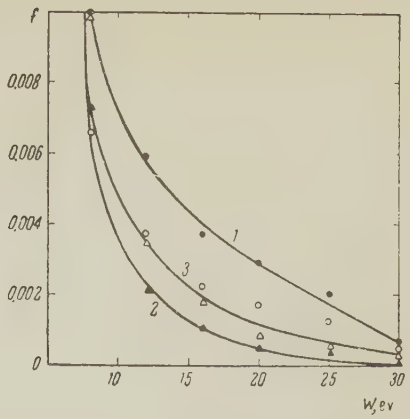

FIG. 3. Energy spectra for Cs^+ ions scattered on molybdenum (U = 900 ev, T = 1800°K) obtained for different functions $\varphi(W)$ and by solution of the integral equation (curve 3). Curves 1 and 2 are obtained by differentiation of the corresponding volt-ampere characteristics.

1 and 2. It follows from the figure that the results obtained by solution of the integral equation (1) with the experimentally determined values of the function $\varphi(W)$ (cf. above) show considerably better agreement between themselves than the curves plotted by simple differentiation. Similar agreement of the curves is found in other cases which have been investigated (Cs^+ on molybdenum at U = 2150 ev with V_n as the variable, Mo^+ at U = 2150 ev with varying alignment of the system, etc.). The distribution functions obtained by using different $\varphi(W)$ can differ by a constant; hence, in comparing these functions it is necessary to normalize the area under the f(W) curve in each case. This has been done in plotting curves shown in Fig. 3. However, in an analysis of the energy distribution of the particles there is no need for such normalization and the results given below have been obtained without normalization.

Knowing that there is a cylindrical field in the operating region T-K-P, we can estimate the variation of the potential in the region of screen S_1 of electrode K using a modified Maxwell formula,[9] which applies for a system of equally spaced parallel wires:

$$V \approx \frac{a}{4\pi}(\alpha V_n - \beta V_0)\ln(1 - 2e^{2\pi x/a}\cos(2\pi y/a) + e^{4\pi x/a}) + [V_0 + (V_0 + V_n)\alpha\gamma](1 + \beta x), \quad (2)$$

where $\alpha^{-1} = r_K \ln(r_P/r_K)$, $\beta^{-1} = r_K \ln(r_K/r_T)$, r_T, r_K, r_P are the radii of cylinders T, K, and P respectively; $\gamma = -(a/2\pi)\ln[2\sin\pi c/a]$, c is the radius of the wire, a is the screen spacing, x is the radial coordinate, which is measured outward from cylinder K, and y is a coordinate which is measured from the center of some wire in the direction perpendicular to the x axis of the wire. An analysis of this formula shows that the minimum

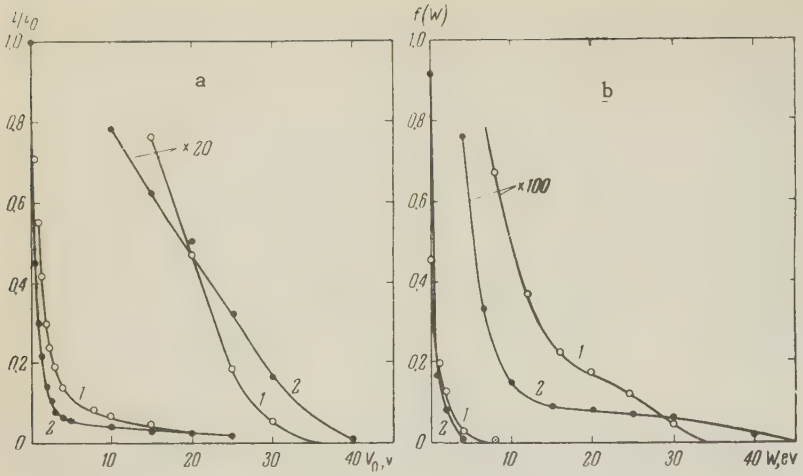

FIG. 4. Retardation curves (a) and energy spectra (b) for Cs^+ ions scattered on a molybdenum (T = 1800°K): curve 1 – U = 900 ev, curve 2 – U = 2150 ev.

departure of the potential from the potential V_K of a wire in the plane y = a/2 is

$$\Delta V'_{min} \approx \alpha\gamma (V_0 + V_n). \quad (3)$$

Under operating conditions V_n is −100 and −250 v, i.e., $\Delta V'_{min}$ with $V_0 = 0$ is respectively −0.8 and −2 v. Actually, these figures should be reduced when account is taken of the fact that wire-mesh screens are used rather than parallel wires. If, to the quantities indicated above we add the potential drop along that part of the heated target which is bombarded by ions, $\Delta V'' = 0.5$ v (the electrical system has a provision for applying the voltage V_0 between cylinder K and the center point of the target), we can determine the radial and angular components of the momentum in terms of energy without taking account of the contact potential, which is 1.3 v when $V_n = 100$ v and 2.5 v when $V_n = 250$ v.

The pressure of the residual gas in the apparatus is measured with an ionization gauge, while the target temperature is measured with an optical pyrometer. Before operation, the glass chamber of the instrument is heated by gas while the target is annealed for a long period of time at T = 2300 – 2500°K by passing current through it. Under these conditions cylinder K is heated to 900°K by radiation while the temperature of the walls in the operating portion of the glass chamber is approximately 370°K. This outgassing procedure is continued until repeated heating of the target is no longer accompanied by a noticeable pressure rise. In operation the system is evacuated by mercury diffusion pumps and liquid-oxygen traps. The pressure by adsorption at the target with the primary ion source on was estimated by the flash method;[10] this pressure is of the order of $5 - 8 \times 10^{-8}$ mm Hg. An adsorption pressure of this order of magnitude has also been obtained by another method which we have used earlier.[11]

The currents due to secondary ions are measured by a vacuum-tube electrometer located at the output of the mass spectrometer; the sensitivity of this instrument is 5×10^{-16} amp/mm.

The integral equation (1) can be easily reduced to the form

$$f(eV_0) = -\frac{1}{\varphi(0)}\left[\frac{di(eV_0)}{d(e^2V_0)} + \int_{eV_0}^{\infty} f(W)\varphi'(W - eV_0)\,dW\right]. \quad (4)$$

This equation is solved by numerical integration using an iteration method in which the first term on the right side of Eq. (4) is used as the zeroth approximation for f(W).

2. EXPERIMENTAL RESULTS AND DISCUSSION

The retardation curves for secondary Cs^+ ions obtained in the bombardment of molybdenum (V_n = 100 v) and tantalum (V_n = 250 v) targets by Cs^+ ions are shown in Figs. 4a and 5a respectively.* The distribution functions f(W) obtained from the retardation curves in Figs. 4a and 5a by means of Eq. (1) are shown in Figs. 4b and 5b.

In all curves obtained at high target temperatures, an especially noteworthy feature is the sharp drop of f(W) at W ~ 1 – 2 ev. This drop is probably due to the presence of Cs^+ ions among the scattered ions; these ions are produced by surface ionization of the cesium atoms which diffuse from inside the material. These atoms, in turn, are formed from Cs^+ ions of the primary beam which penetrate into the volume of the target. This effect has been observed earlier.[2] The energy width of this segment of the curve is found to be in agreement with the estimate of the resolving power given above.

*All these curves, as well as the curves in Figs. 6a and 7a (with the exception of curve 3 in Fig. 5a) are given in units of the current i_0 that corresponds to the curves for $V_0 = 0$. In order to facilitate a comparison with curve 1 in the same figure, curve 3 in Fig. 5a is given in units of the current i_0 for curve 1.

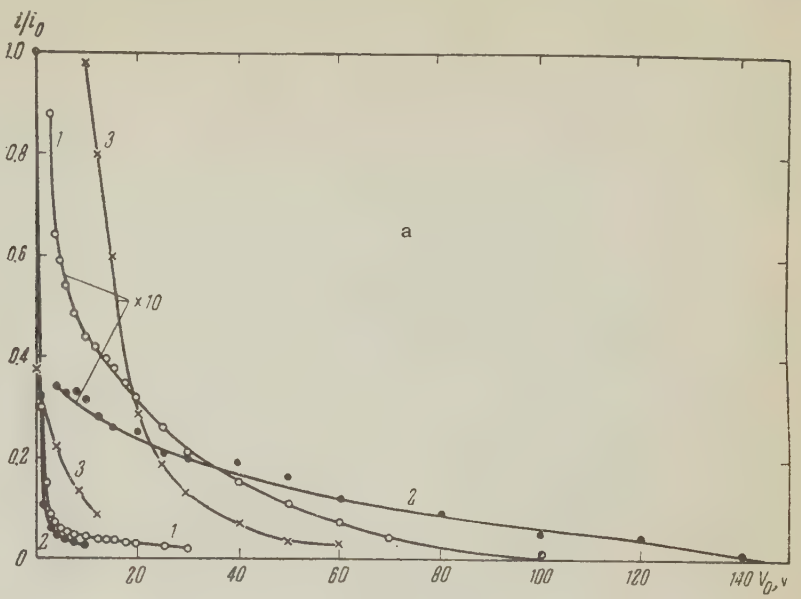

FIG. 5. Retardation curves (a) and energy spectra (b) for Cs^+ ions scattered on a tantalum target: curve 1 – U = 900 ev, T = 1600°K; curve 2 – U = 2150 ev, T = 1600°K; curve 3 – U = 900 ev, T ≈ 300°K.

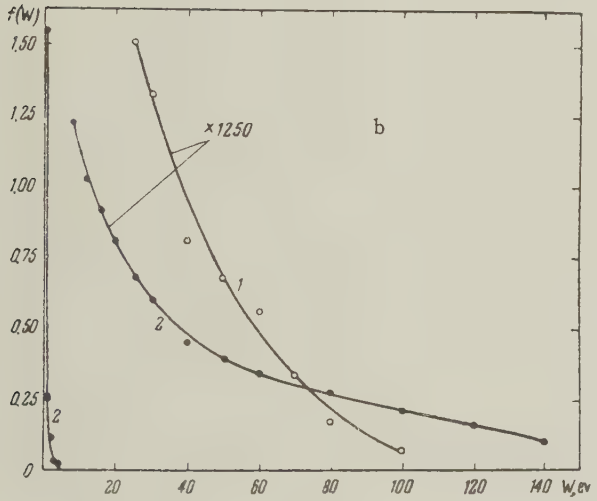

The retardation curves for Mo^+ and Ta^+ ions ejected from molybdenum and tantalum targets are given in Figs. 6a and 7a respectively.

A check on whether or not ions which enter the mass spectrometer come from the target is given by the presence of a clearly defined peak on the mass spectrogram; this peak vanishes when the primary beam is deflected from the target. The peaks corresponding to Mo^+ and Ta^+ ions are also checked by the absence of Ta^+ (Mo^+) peaks when molybdenum (tantalum) is bombarded by Cs^+. It should be noted that at V_n = 250 v and small values of V_0, a peak due to Cs^+ is partially superimposed on the Mo^+ peak; the Cs^+ ions arise as a result of bombardment of the output grid of cylinder P by scattered Cs^+ ions which come from the target. This situation causes a sharp drop in current on the retardation curve in the region of small V_0, which is characteristic of surface ionization of Cs. Hence the Mo^+ peak is always studied with V_n = 100 v.

The identification of the Mo^+ peak is also checked by the temperature dependence of the Mo^+ current (Fig. 8). At high target temperatures, in which case the surface may be assumed clean, this dependence is similar to that obtained by us earlier[5] in the bombardment of molybdenum by Hg^+

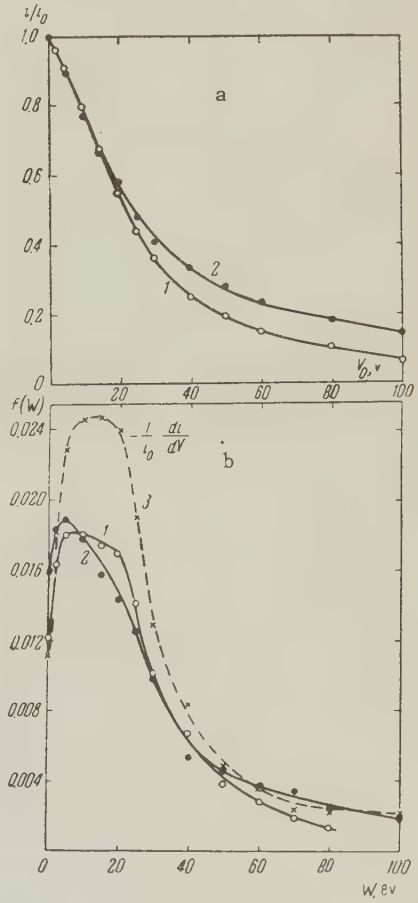

FIG. 6. Retardation curves (a) and energy spectra (b) for sputtered Mo^+ ions (T = 1800°K): curve 1 – U = 900 ev, curve 2 – U = 2150 ev.

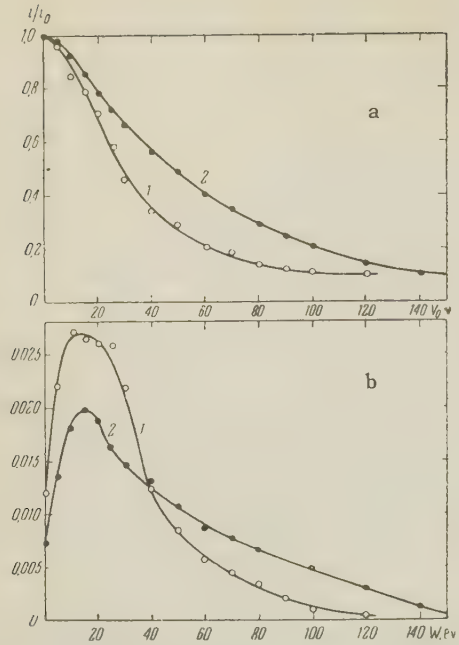

FIG. 7. Retardation curves (a) and energy spectra (b) for sputtered Ta^+ ions (T = 1800°K): curve 1 – U = 1200 ev, curve 2 – U = 2150 ev.

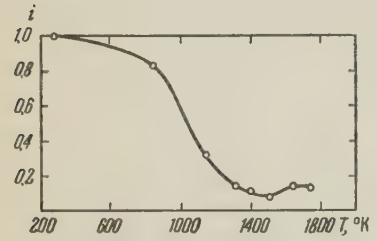

FIG. 8. The current of of sputtered Mo^+ ions as a function of target temperature (U = 2150 ev).

and by Bradley in the bombardment of molybdenum by Ar^+.[8]

The fact that the temperature dependence of the ion component of the cathode sputtering coefficient is not affected by the nature of the bombarding ion is of interest in itself. This result indicates that the structure of the electron shell of the bombarding ion is not a factor in the sputtering of matter in the form of ions.

The energy distribution functions for Mo^+ and Ta^+ obtained from the retardation curves (Figs. 6a and 7a) by means of the integral equation (1) are shown in Figs. 6b and 7b. To demonstrate that the integral equation can be applied in this case in Fig. 6b we also show curve 3, which is obtained from curve 1 of Fig. 6a by direct differentiation. It follows from curves 1 and 3 that in the present case the correction for the change in transmission of the mass spectrometer as a function of W is small, although the position of the maximum on curve 3 is displaced toward higher energies. The reduction of this correction when the retarding-field technique is used, as compared with the analogous correction (Fig. 2) when the energy spectrum is determined from the shape of the peak at the output of the mass spectrometer, apparently results from the fact that at higher values of V_0 ions with a given initial energy W reach screen S_1 with almost zero energy and have approximately the same probability of reaching the detector of the mass analyzer.

Since the probability for surface ionization of Cs on molybdenum and tantalum is approximately 100%, the current i_0 (Figs. 4a and 5a) can, in a rough way, serve as a measure of the primary ion beam at the output of the mass spectrometer;[6] thus we can estimate the scattering coefficient K_0 for Cs and the sputtering coefficient K_S for Mo^+ and Ta^+ (this estimate turns out to be somewhat large since we neglect scattering of cesium in the neutral state, which should have a small probability).

In the case of Cs^+ scattering (U = 900 ev) from a tantalum surface, K_0 is found to be of the order of 6% ($V_0 \geq 4$ ev) a value which is in poor agreement with the value of approximately 18% (U = 400 ev) reported by Arifov and Ayukhanov,[2] but in much better agreement with the data reported by Brunnee[3] on the reflection of Rb^+ ions from a molybdenum surface.

It is likely that the disagreement with the data reported by Arifov and Ayukhanov is due to the difference in the primary-ion energy in their work and the work reported here, or to the existence of noticeable anisotropy effects in the angular distribution of the scattered ions. In references 2 and 3 the scattering was averaged over all angles, whereas in the present work scattering is measured at approximately 120° with respect to the primary beam.

A comparison of curves 1 and 3 (Fig. 5a) indicates that when the surface of the equilibrium layer (T ~ 300°K) contains cesium atoms with an admixture of impurity atoms, the coefficient for secondary ion emission increases although the limiting energy of the distribution is reduced. It is possible that this phenomenon is to be associated with the sputtering of a cesium film at low temperatures, since the mean energy of the sputtered ions exceeds the mean energy of the ions obtained in surface ionization.

In cases of interaction of Cs^+ with a molybdenum surface, in spite of the fact that the mass m of the incident ion is greater than the mass M of the lattice atom,[4] it is found that the Cs^+ scatters on the molybdenum. The numerical value of the scattering coefficient ($K_0 \sim 4\%$ at U = 2150 ev) is of the same order of magnitude as that reported by Brunnee.[3] The energy spectra of the scattered ions obtained by Brunnee and by us are also simi-

lar. However, the values of the limiting energy given in Fig. 4b (approximately 40 ev) are somewhat lower than the values reported by Brunnee. It is possible that this difference is due to an angular dependence for the limiting energy or, what is more probable, the presence of sputtered ions (not taken into account in reference 3). It follows from the data of Fig. 6b that the limiting energy W_{max} in sputtering of the surface is greater than 100 ev (in reference 3 the secondary ion emission components were not analyzed).

Whereas the curves in Fig. 5b indicate a proportionality between W_{max} and U, as has already been observed earlier in references 1 and 3, in the scattering of Cs^+ from a molybdenum surface W_{max} increases very slowly as U increases. This difference can be explained qualitatively as follows.

In recent papers[1-4,12] the interactions of the bombarding atoms with the lattice are treated as elastic pair collisions with atoms of the lattice. Within the framework of this analysis, scattering of the primary ion at angles greater than 90° is possible in single collisions between these ions and lattice ions only if $m < M$, in which case the limiting energy of the scattered ion that escapes from the surface is determined by the energy loss of the ion for a single pair collision. The condition $m < M$ is satisfied when Cs^+ scatters on a tantalum surface, in which case W_{max} must be proportional to U.

In order to explain scattering of primary ions at angles greater than 90° when $m > M$ (Cs^+ on molybdenum) we must assume multiple collisions of these ions with the lattice atoms, owing to the increased path length of the primary ions inside the material as compared with the preceding case, to the increase in the energy loss with increasing U (for motion back to the surface), and, as a consequence, owing to the slower increase in W_{max}.

A further verification of this interpretation can be obtained by a comparison of the distortion of the function f(W) with increasing U in sputtering of Mo^+ and Ta^+ (cf. Figs. 6b and 7b). In one case (Ta^+) this distortion is essentially a change in the scale of the abscissa axis almost proportional to the energy U; because of the normalization of the distribution function this change is proportional to the reduction in the height of the curve f(W). In the case of Mo^+, however, there is no change in scale but the maximum of the f(W) curve is shifted toward lower energies with increasing U. It may be assumed that in the first case the formation site of the sputtered ions remains close to the surface whereas in the second case it is displaced into the material.

The width of the energy distribution of the sputtered ions corresponding to half the maximum energy of f(W) obtained in the present work (Figs. 6b and 7b) is found to be appreciably greater (30 — 35 ev for Mo^+ and 35 — 50 ev for Ta^+) than the corresponding value obtained by Bradley[8] (5 ev for Mo^+). A possible cause for this disagreement is discussed above. It might be thought that the recording of high-energy sputtered ions by the electrometer is subject to error because of ionization of sputtered atoms from deep inside the target which reach the spectrometer. (Ionization can be caused by thermal electrons from the target; under the present experimental conditions this electron current is of the order of one milliampere.) However, as is shown by experiments carried out at lower target temperatures and by a detailed theoretical calculation, the probability for this effect is vanishingly small. The fact that the widths of the energy distributions are about the same for the scattered and sputtered ions seems to indicate that the mechanisms for sputtering and scattering are closely related and that the transition between these phenomena is a smooth one.

The absolute value of the sputtering coefficient ($K_S \sim 2.5 \times 10^{-3}$ in the case of Mo^+ and 6×10^{-3} in the case of Ta^+ for U = 2150 ev and T = 1800° K) agrees with the values reported in the literature.[5,6,8]

A comparison of the mean values of the energies of the neutral particles produced in cathode sputtering (15 — 20 ev, Wehner;[8] 5 — 7 ev, Sporn[13]) with the mean values of the energy of the sputtered ions (Figs. 6b and 7b) (21 — 23 ev for Mo^+ and 26 — 36 ev for Ta^+) indicates that the ionization probability for Mo and Ta atoms which escape from the surface increases as their energy increases. Support for this interpretation is also found in the fact that there is an initial increase in the function f as W increases: although the shape of the energy distribution of the neutral atoms obtained in cathode sputtering has not been investigated as yet, there are a number of indirect data (for example, the behavior of curve 3 in Fig. 5a of the present work) which indicate that the dependence is a monotonically decreasing one.

It should be noted that these facts are in qualitative agreement with the expected small (proportional to $\sqrt{W}$) increase for the ionization probability of an atom which leaves the surface of a metal as its energy increases. This increase is predicted theoretically from an analysis of electron exchange in the interaction of a slowly moving atom with the

surface of a metal.[14] It would be desirable to investigate the energy spectra of sputtered neutral atoms in order to obtain a clearer picture of these phenomena.

[1] M. A. Eremeev, Dokl. Akad. Nauk SSSR **79**, 755 (1951). U. A. Arifov and A. Kh. Ayukhanov, Dokl. Akad. Nauk Uz. S.S.R., No. 4, 12 (1951).

[2] U. A. Arifov and A. Kh. Ayukhanov, Izv. Akad. Nauk, SSSR, Ser. Fiz. **20**, 1164 (1956), Columbia Tech. Transl. p. 1057.

[3] C. Brunnee, Z. Physik **147**, 161 (1957).

[4] Arifov, Ayukhanov, and Starodubtsev, JETP **33**, 845 (1957), Soviet Phys. JETP **6**, 653 (1958).

[5] V. I. Veksler, Dokl. Akad. Nauk Uz. S.S.R. No. 1, 9 (1956).

[6] V. I. Veksler and M. B. Ben'yaminovich, J. Tech. Phys. (U.S.S.R.) **26**, 1671 (1956), Soviet Phys.-Tech. Phys. **1**, 1626 (1957).

[7] R. E. Honig, J. Appl. Phys. **29**, 549 (1958).

[8] R. C. Bradley, J. Appl. Phys. **30**, 1 (1959).

[9] J. C. Maxwell, A Treatise of Electricity and Magnetism, Dover, 1955.

[10] N. D. Morgulis, J. Tech. Phys. (U.S.S.R.) **25**, 1667 (1955).

[11] V. I. Veksler and M. B. Ben'yaminovich, Тр. Среднеазиатского гос. ун-та (Proc. Central Asia State Univ.) **91**, 57 (1957).

[12] O. Roos, Z. Physik **147**, 184 (1957).

[13] H. Sporn, Z. Physik **112**, 278 (1939).

[14] V. I. Veksler, Izv. Akad. Nauk Uz.S.S.R. Ser. Fiz. Mat. No. 4, 34 (1959).

Translated by H. Lashinsky
78

PARAMAGNETIC RELAXATION IN MANGANESE SALT SOLUTIONS

P. G. TISHKOV and G. P. VISHNEVSKAYA

Physico-technical Institute, Kazan' Branch, Academy of Sciences, U.S.S.R.

Submitted to JETP editor July 6, 1959

J. Exptl. Theoret. Phys. (U.S.S.R.) **38**, 335-340 (February, 1960)

Paramagnetic absorption in parallel fields was measured for aqueous manganese salt solutions at concentrations of 0.25 N and higher. It is shown that the thermodynamic theory of paramagnetic relaxation and the Brons-Van Vleck formula are valid for aqueous manganese salt solutions. The spin-lattice relaxation time equals 10^{-8} sec and depends on the nature of the anion and on the concentration of the Mn^{++} ions in the solutions. Its temperature dependence can be described by the Al'tshuler-Valiev theory. The internal field constants have been determined.

THE fast development of paramagnetic resonance and paramagnetic relaxation methods in recent years is connected with the great importance of the obtainable results for certain branches of physics and chemistry. These methods are of particular interest in the study of the structure of solids and liquids. The principal parameters of paramagnetic relaxation are: the spin-lattice relaxation time ρ_L, the spin-spin relaxation time ρ_S, and the constant b/c, which characterizes the internal field in a paramagnet.

In the present investigation, we measured the paramagnetic absorption in parallel and perpendicular fields for aqueous solutions of certain manganese salts at concentrations from 0.25 mole/liter and above.

The measurements were by the Q-meter method, previously described by one of the authors.[1] It was shown in that reference that the spin-lattice relaxation times in liquid solutions of electrolytes and the constant b/c can be determined with the Q-meter from measurements of χ'' at two frequencies assuming the Casimir and du Pré equation, corrected for spin-spin absorption after Shaposhnikov,[2,3] is correct.

The correction was determined by measuring the absorption in zero field as obtained from experiments in perpendicular fields; it was assumed here that the spin-spin absorption becomes negligibly small at fields ≥ 1500 oe.

We shall first treat here in greater detail the applicability of the formula

$$\chi'' = \chi_0 F \rho_L \nu / (1 + \rho_L^2 \nu^2), \qquad F = H^2/(b/c + H^2) \quad (1)$$

to the description of the spin-lattice relaxation in liquid solutions of electrolytes. If the values ρ_L and b/c, obtained from measurements of $\chi''(H)$ at two frequencies, coincide with the values of ρ_L and b/c obtained at two other frequencies, this obviously will serve as evidence of applicability of (1) in the given frequency range to a description of relaxation processes in liquid electrolyte solutions. Frequencies of 12, 21, 32, and 42 Mcs were used in the measurements.

To calculate ρ_L we used all possible combinations of frequencies, with the exception of the combination $\nu = 32$ and $\nu = 42$ Mcs, which were too close to each other. From the values of ρ_L thus obtained the average was taken. The deviation of the individually computed value of ρ_L from the average amounted to approximately $\pm 6\%$. The calculated values of $10^8\ \rho_L$ (sec) for a 1 N solution of $MnSO_4$ at 22° C are given in Table I. The constant b/c, which characterizes the internal magnetic field in the paramagnet, was determined from the experimental curves and from the obtained val-

TABLE I

H, oe / $\nu_1-\nu_2$	1200	1600	2000	2400	2800	3200	3600
12—21	0.9	1.3	1.45	1.6	1.78	1.85	1.94
12—32	1.28	1.47	1.5	1.7	1.77	1.86	1.97
12—42	1.11	1.24	1.45	1.61	1.75	1.8	1.88
21—42	1.25	1.4	1.47	1.63	1.75	1.8	1.86
21—32	1.38	1.52	1.6	1.71	1.8	1.9	2
average $10^8\rho_L$	1.18±0.14	1.39±0.11	1.48±0.04	1.65±0.04	1.77±0.02	1.84±0.03	1.93±0.05

ues of ρ_L.[1] The deviation of individual calculated values of b/c from the average amounted to $\sim \pm 10\%$. Table II lists the values of b/c for a 3.2 N solution of $MnSO_4$ at 22° C.

TABLE II

ν, Mcs	H_1	H_2	$(b/c)\cdot 10^{-8}$
42	2400	3200	2.165
	2800	3600	2.26
32	2400	3200	2.865
	2800	3600	2.56
21	2400	3200	2.43
	2800	3600	2.74
12	2400	3200	2.49
	2800	3600	2.355
		Average:	2.48±0.18

Figure 1 shows, by way of an example, an experimental curve of $\chi''(H)$ for a 3.2 N solution of $MnSO_4$ at 300° K for 12, 21, 32 and 42 Mcs (solid curves); the values of $\chi''(H)$, represented by the circles at 32 and 42 Mcs, were calculated from the values of ρ_L and b/c determined experimentally at 12 and 21 Mcs. It is seen from Fig. 1 that the experimental values of $\chi''(H)$ coincide with the computed ones.

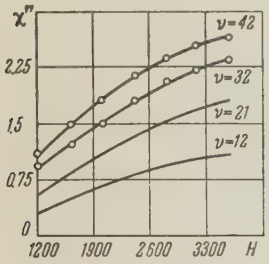

FIG. 1

The results obtained thus testify to the applicability of Eq. (1) for the spin-lattice relaxation in aqueous solutions of electrolytes at the given frequency range. The experimental values of ρ_L for aqueous solutions of $Mn(NO_3)_2$, $MnSO_4$, and $MnCl_2$ at concentrations ranging from 0.25 N upward are on the order of 10^{-8} sec, which is almost one order of magnitude less than the ρ_L of the corresponding solid substances.[2] Experiment has shown that the dependence of ρ_L on the intensity of the constant field H is described by the Brons-Van Vleck equation

$$\rho_L = \rho_0 \frac{b/c + H^2}{b/c + pH^2}; \qquad (2)$$

where ρ_0 is the spin-lattice relaxation time for H = 0 and p is a constant (p < 1).

Figure 2 shows a comparison of the experimental values of $\rho_L(H)$ for 2 N solutions of nitrate, sulfate, and chloride of manganese (circles) and the values calculated by the Brons-Van Vleck formula (solid curves). It is seen from this figure that ρ_L depends substantially on the type of anion.

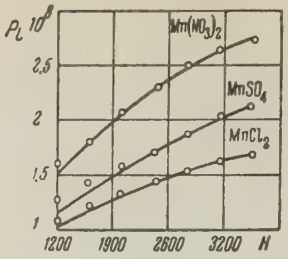

FIG. 2

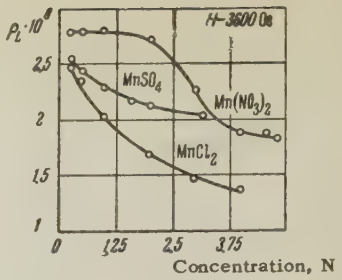

FIG. 3

The dependence of ρ_L on the type of anion and on the concentration (N) of the Mn^{++} ions in aqueous solutions of $Mn(NO_3)_2$, $MnSO_4$, and $MnCl_2$ is shown in Fig. 3. It is found that the spin-lattice relaxation times increase with dilution. The greatest increase in ρ_L with changing concentration is observed in manganese chloride.

The difference in ρ_L between solutions of different salts becomes equalized at small concentrations. At concentrations from 1.5 N to 2 N and lower the value of ρ_L of manganese nitrate remains constant, within the limits of experimental error; ρ_L remains likewise almost constant as the concentration increases from 4 N upward.

An attempt can be made to explain the observed dependence of ρ_L on the concentration, as well as the individual behavior of the curves for all three solutions, by arguing as follows.

In solid crystals the Mn^{++} ion makes up, together with its nearest diamagnetic surrounding, a paramagnetic complex MnX_6, where X is a water molecule or some other diamagnetic particle. Judging from the chemical formulas, one can assume that in solid hydrated sulfate and chloride of manganese the nearest surrounding includes also anions in addition to the water molecules, whereas in the case of manganese nitrate the nearest surrounding consists of six water molecules. One can assume further that in sufficiently concentrated solutions the structure of the corresponding hydrated crystal is retained, i.e., the nearest surrounding of the ion includes anions along with the water molecules and, in addition, entire molecular aggregates may be retained. This conclusion has been obtained by several authors[4-6] on the basis of results of x-ray diffraction investigations, a study of the Raman spectra, etc.

As the dilution increases, the groups break up, the anions become "washed out" with water, and as a result in strongly diluted solutions the paramagnetic ions will be surrounded by water molecules only.

According to the Al'tshuler-Valiev theory,[7] we

shall assume that the relaxation time is determined above all by the interaction within the complex, formed by the paramagnetic ion together with its closest surrounding. The Brownian motion of the molecules in the liquid disturbs the natural oscillations of the complex and this changes the electric field in which the paramagnetic particle is located.

In our case one can assume, for the solution of manganese nitrate, that at high concentrations (starting approximately with 4 or 5 N), entire particle aggregates exist, which begin to break up upon dilution, causing ρ_L to increase, and after these groups have entirely disappeared further dilution should no longer influence the spin-lattice relaxation time.

In the case of manganese sulfate and chloride solutions, the region of strong dilution, when the Mn^{++} ion is surrounded only by six water molecules and where ρ_L should remain constant, lies apparently below 0.25 N and was not investigated here. At a concentration of approximately 0.5 N and above, apparently, the anion begins to penetrate into the first surrounding sphere of the Mn^{++} ion; at concentrations greater than 3.5 N for the sulfate and greater than 5 N for the chloride of manganese, this penetration is essentially complete. At the same time, at these concentrations the influence of the ions becomes most strongly pronounced, and as a result of this the ρ_L of the sulfate and chloride of manganese exhibit the greatest difference from each other in strongly concentrated solutions.

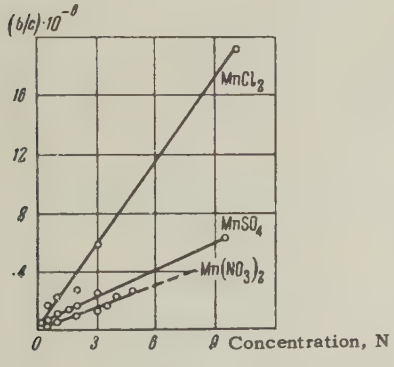

FIG. 4

Figure 4 shows the dependence of the constant of the internal field b/c on the type of the anion and on the concentration N of the solutions of nitrate, sulfate, and chloride of manganese. It is found that b/c varies approximately linearly with concentration, and the values of b/c for the solid salts (6.2×10^6 for $MnSO_4 \cdot 4H_2O$ and 19.3×10^6 for $MnCl_2 \cdot 4H_2O$) fit well on the corresponding straight lines. The linear dependence of b/c on N is typical for each salt, i.e., the dependence on the type of anion becomes manifest. This is an additional confirmation of the correctness of the model used to explain the dependence on the concentration and on the type of anion. In fact, the increase in b/c with increasing concentration can be explained by assuming that the structure of the solution approaches the structure of the solid.

Preliminary measurements of the magnetic absorption in parallel fields for alcohol solutions of $MnCl_2$ at concentrations from 0.25 N to 1.7 N have shown that the ρ_L of alcohol solutions differs very little from those of aqueous solutions within the same concentration range.

To explain the dependence of ρ_L on the temperature, measurements were made with a 2 N solution of $Mn(NO_3)_2$ at -2, $+22$, and $+58°C$. A value of 2 N was chosen for the concentration because further dilution from this value leaves ρ_L almost unchanged and it can be assumed that the Al'tshuler-Valiev mechanism holds in this range of concentration, i.e., ρ_L is determined essentially by the natural oscillations of the paramagnetic complex $Mn(H_2O)_6$, perturbed by the Brownian motion of the molecules of the liquid.

Measurements made at these temperatures have shown that, in agreement with the theory, the curve $\rho_L(T)$ passes through a maximum; the maximum occurs at $t \approx 20°C$ ($\rho_L = 2.7 \times 10^{-8}$ sec at H = 3600 oe); at -2 and $+58°C$, ρ_L decreases to 2.05 and 2.4×10^{-8} sec respectively.

These measurements were performed several times. The difference in the values of ρ_L at different temperatures lies outside the limits of experimental errors.

Such a temperature dependence of the spin-lattice relaxation time is confirmed by measurements of the line widths in solutions of Mn^{++}.[8,9]

However, the minimum line width $\Delta H \approx 1/\rho_L + 1/\rho_S$ is observed not at $\sim 20°C$ but at $\sim 80°C$. This is understandable, for according to Bloembergen, Purcell, and Pound,[10] the contribution of magnetic dipole-dipole interactions to ΔH should decrease monotonically with increasing temperature. A clarification of the temperature dependence of ρ_L in solutions of paramagnetic salts requires further experimental study.

Experimental data make it possible to calculate the spin-spin relaxation time ρ_S. This is calculated from experimental data by the formula

$$\rho_S = [(1 + \rho_L^2 \nu^2)^2 - \sqrt{(1 + \rho_L^2 \nu^2)^2 - 4k^2 F^2 \nu^2 \rho_L^2}\,] / 2kF\rho_L \nu^2, \quad (3)$$

where

$$k = \chi''_{\perp}(0) / \chi''_{\parallel}(H),$$

and ρ_L was taken to be the spin-spin relaxation time for H = 3600 oe. This formula was obtained under the assumption that the Casimir and du Pré equation holds for fields ≥ 2,000 oe and the equation

$$\chi''(H_\perp = 0)/\chi_0 = \rho_S \nu/(1 + \rho_S^2 \nu^2) \qquad (4)$$

is valid. This equation is derived in Shaposhnikov's general theory of paramagnetic relaxation.[3] Rivkind[11] has verified Eq. (4) experimentally and demonstrated its correctness. The sign of the root in (3) is determined from the experimental frequency dependence of $\chi(\nu)$. The values of ρ_S calculated with Eq. (3) are plotted in Fig. 5 as functions of the concentration N of the magnetic ions for solutions of $MnCl_2$.

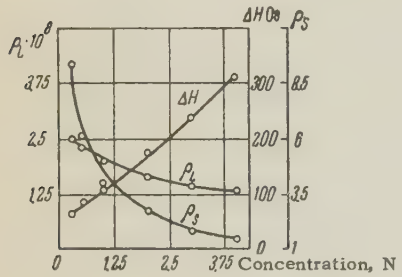

FIG. 5

The paramagnetic-resonance absorption line widths in perpendicular fields and the spin-spin and spin-lattice relaxation times are determined essentially by the same interactions. The line width ΔH and the relaxation times ρ_L and ρ_S are frequently[12] connected by the approximate relation

$$\Delta H \approx 1/\rho_S + 1/\rho_L. \qquad (5)$$

We calculated ΔH by using the value of ρ_L at H = 0, the latter being obtained with the aid of the Brons-Van Vleck equation from the experimental value of $\rho_L(H)$. Figure 5 shows a comparison of the values of ΔH calculated with the foregoing formula (continuous line) and those obtained by measuring χ'' in perpendicular fields[11] [circles on the ΔH(N) curve] for aqueous solutions of $MnCl_2$.

Analogous calculations of ΔH were carried out also for solutions of manganese sulfate and nitrate. For low concentrations (≤ 1 N) the agreement between the calculated and the experimental values of ΔH is just as good as for solutions of manganese chloride. At high concentrations the discrepancy in the calculated values of ΔH reaches in some cases up to ~ 30%. This is not surprising, for actually the connection between ΔH and the relaxation time is much more complicated than that given by (5).

It is seen from the above that a study of the spin-lattice relaxation in liquid solutions of electrolytes also offers great possibilities for the investigation of the structure of these solutions.

In conclusion, we take this occasion to thank B. M. Kozyrev for guidance and continuous aid in this work and B. K. Silant'eva for participating in the experiments.

[1] P. G. Tishkov, JETP **36**, 1337 (1959), Soviet Phys. JETP **9**, 949 (1959).

[2] C. J. Gorter, Paramagnetic Relaxation, Elsevier, N.Y., 1948.

[3] I. G. Shaposhnikov, Doctoral Dissertation, Phys. Inst. Acad. Sci., 1949.

[4] O. Ya. Samoĭlov, Структура водных растворов электролитов и гидратация ионов (Structure of Aqueous Solutions of Electrolytes and Hydration of Ions), Acad. Sci. Press, 1957.

[5] J. Beck, Phys. Z. **40**, 474 (1939).

[6] J. P. Mathieu and M. Lounsbury, Compt. rend. **229**, 1315 (1949).

[7] S. A. Al'tshuler and K. A. Valiev, JETP **35**, 947 (1959), Soviet Phys. JETP **8**, 661 (1959).

[8] B. M. Kozyrev, Doctoral Dissertation, Phys. Inst. Acad. Sci., 1957.

[9] B. M. Kozyrev, Izv. Akad. Nauk SSSR, Ser. Fiz. **21**, 828 (1957), Columbia Tech. Transl. p. 828.

[10] Bloembergen, Purcell, and Pound, Phys. Rev. **73**, 679 (1948).

[11] A. I. Rivkind, Dissertation, Ural University, 1952.

[12] S. A. Al'tshuler and B. M. Kozyrev, Usp. Fiz. Nauk **63**, 533 (1957).

Translated by J. G. Adashko
79

EXPERIMENTAL DETERMINATION OF THE POLARON MASS IN CUPROUS OXIDE

A. I. GUBANOV, N. I. KRIVKO, and N. M. REĬNOV

Leningrad Physico-technical Institute, Academy of Sciences, U.S.S.R.

Submitted to JETP editor July 10, 1959

J. Exptl. Theoret. Phys. (U.S.S.R.) **38**, 341-344 (February, 1960)

The effective mass of the current carriers in cuprous oxide was determined at helium temperatures by the method of diamagnetic resonance. The value obtained is close to the polaron mass calculated for cuprous oxide using Pekar's theory.

1. STATEMENT OF THE PROBLEM

A number of investigations on the theory of polarons have appeared, but so far as we are aware there has been to date no direct experimental confirmation of the existence of mobile polarons. The experimental observation of a carrier mass equal in order of magnitude to the calculated polaron mass would provide such confirmation. We set ourselves the problem of measuring the polaron mass in Cu_2O, using the method of diamagnetic (cyclotron) resonance.

It should be noted that, because the infra-red oscillation frequencies of ions in a crystalline lattice are large in comparison with resonant frequencies in the centimeter band, the polarization of the crystal is able to follow the high frequency field of the absorbed radiation, and, consequently, diamagnetic resonance will reveal the mass of the polaron, if it exists, and not the effective mass of an electron moving relative to the polarization well.

For the polaron mass Pekar[1] has given a formula (10.35) which, using the relationship (10.37) in the same work, can be written in the form

$$M = 9.08 \cdot 10^3 (m^*/m)^3 c_0^4 / \omega_1^2, \qquad (1)$$

where m^* is the carrier effective mass, m is the electronic mass; ω_1 is the limiting frequency of the polarization oscillations of the ions;

$$c_0 = 1/n^2 - 1/\varepsilon_0, \qquad (2)$$

n is the refractive index, and ϵ_0 is the static dielectric constant. Equation (1) was obtained for a crystal of the rock-salt type, but for other crystals it can only differ by a numerical factor of order unity.

If, following Pekar (reference 1, pp. 210 and 214), we take for cuprous oxide

$\varepsilon_0 = 9$, $n^2 = 4$, $c_0 = 0.139$, $m^*/m = 1.81$, $\omega_1 = 4.73 \cdot 10^{13}$,

then formula (1) gives

$$M = 9 \cdot 10^{-27}, \quad M/m = 9.8.$$

These values should, however, be considered in the light of more recent investigations. The ratio $m^*/m = 1.81$ used by Pekar was obtained indirectly and is unreliable. Gross and Pastrnyak,[2] from measurements of the diamagnetic Landau levels, adopt for cuprous oxide $m^*/m = 0.80$; they obtain approximately the same value from the exciton spectrum.[3] In reference 2 are also given more accurate values of ϵ_0 and n^2, viz: $\epsilon_0 = 7.5$ $n = 1.8$, which lead to the value $c_0 = 0.176$. Using these values of m^*/m and c_0, we obtain $M/m = 2.20$.

However, as Haken[4] has remarked, because of the rapid motion of the electron, the polarization of the neighboring electronic orbits does not take place completely. Consequently, instead of the dielectric constant n^2, some effective smaller value, κ, should be taken, because the frequency of oscillation of the electron in the polaron well is much larger than optical frequencies. This viewpoint is confirmed by the calculations of Muto and Okuno[5] who, for the x-ray exciton in KCl, obtained better agreement with experiment by taking $\kappa = 1.5$ instead of $n^2 = 2.12$.

The idea of retarded electronic polarization was used by Toyozawa[6] for a calculation on the electron polaron.

Thus, the creation of the polaron well results not only from ionic polarization, but in part also from the electronic polarization; this leads to an increase in the parameter c_0, to which the polaron mass is very sensitive. It is sufficient, for example, to take $n^2 = 1.6$ and $c_0 = 0.258$ to obtain $M/m = 7.5$.

It should also be remarked that according to Feynman[7] formula (1) for the polaron mass is inaccurate and its error is difficult to estimate. So, even if we take the correct value of c_0, the

calculated ratio M/m is correct only with an accuracy of tens of percent.

2. EXPERIMENTS

The study of the absorption of high-frequency energy was carried out in a microwave-spectrometer of the superheterodyne type similar to that described by Manenko and Prokhorov[8] with an intermediate frequency of 60 Mcs. The wavelength of the radiation used was $\lambda = 3.27$ cm. The range of magnetic fields in which the resonance absorption of the polaron is expected was determined from the resonance condition

$$M = eH / \omega c, \qquad (3)$$

in which, having substituted the theoretical estimates of the polaron mass, values of from 7×10^3 to 3.3×10^4 oe were obtained.

The resonator consisted of a section of rectangular waveguide with a diaphragm of diameter 6.3 mm placed in a liquid-helium Dewar.

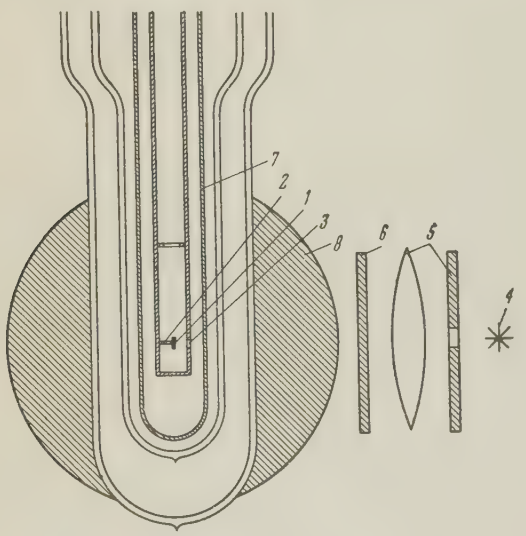

FIG. 1. Experimental apparatus.

The Cu_2O specimen (1 in Fig. 1) in the form of a plate $3 \times 3 \times 1$ mm was affixed to a polystyrene support, 2, situated at an antinode of the electric field of the high frequency wave. The specimen was illuminated through the aperture, 3, of 2 mm diameter in the wide wall of the resonator by a 340-watt PZh lamp (4) through a lens and diaphragm system, 5, and an SZS-14 filter, (6). To avoid contact with the liquid helium, the resonator and the waveguide carrying the energy were placed in a thin-walled glass tube, 7. The electromagnet, 8, with pole diameter 150 mm, produced fields up to 26,000 oe. Modulation of the magnetic field was produced in a number of experiments by additional coils at a frequency of 50 cps. The magnetic field was measured by the ballistic method.

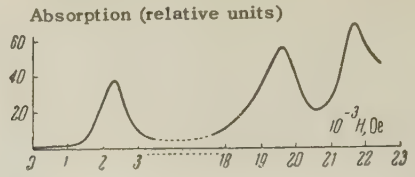

FIG. 2

Polycrystalline specimens of Cu_2O were used; they were optically transparent and aged for a while. A number of curves were obtained for the absorption of electromagnetic energy as a function of the external magnetic field. One of the curves is given in Fig. 2; the others had similar forms. Three absorption maxima were observed at magnetic field values of H = 2350, 19,600 and 21,600 oe, which, according to formula (3), correspond to ratios of carrier masses to the electronic free mass of 0.7, 6, and 6.6.

It should be mentioned that the effect of illumination on the crystal was already very large at H = 0. No maxima were observed on the curve in the absence of illumination at T = 4.2° K. Control experiments also showed that illumination without the filter did not essentially change the results, and the support without the specimen did not give absorption maxima.

3. DISCUSSION OF RESULTS

As was shown by Dresselhaus, Kip, and Kittel,[9] a clearly-displayed maximum of the diamagnetic absorption can only be observed under the conditions

$$\omega\tau > 1, \qquad (4)$$

where ω is the resonance frequency and τ is the free path time of the carriers.

The photomagnetic effect in Cu_2O has been studied in this laboratory at helium temperatures,[10] and it was shown that the effect has a maximum in fields of the order of 6000 oe. This maximum occurs near $\omega\tau = 1$. Consequently, for fields greater than 6000 oe, condition (4) is satisfied. Thus, the two maxima obtained in large magnetic fields are, in fact, due to diamagnetic resonance. The corresponding values of the ratio M/m = 6 and 6.6 lie within the limits obtained by theoretical estimates for polarons. From what has been described, it follows that our experiments confirm the existence of polarons in cuprous oxide crystals.

The maximum at small magnetic fields H = 2350 oe gives a carrier mass close to the effective mass of band electrons or holes obtained by Gross and Pastrnyak.[2,3]

The simultaneous observation of the effective masses of the band electrons and the polarons indicates the existence of some equilibrium between the number of electrons in the band and number of polarons when the crystal is illuminated. It should be remembered that light excites electrons into the conduction band and polarons are formed subsequently. The existence of two polaron masses can, apparently, be explained by the presence of n- and p-type polarons. According to Gross and others,[11] the effective masses of electrons and holes in Cu_2O are approximately the same. But it should be noted that even a small difference in effective masses for the electrons and holes leads to a marked difference in the mass of the polarons, since the polaron masses are proportional to the cubes of the effective masses m^*.[1] This explains the presence of one maximum for electrons and holes and two maxima for polarons. Apparently the maximum of the photomagnetic effect[10] is determined by the polarons, since their concentration is greater than the concentration of electrons in the band; this follows from the larger height of the absorption maxima caused by polarons. So, in fact, $\omega\tau = 1$ at $H = 6000$ oe for polarons, and for electrons in the band this probably occurs at much smaller fields, because the maximum of diamagnetic absorption at $H = 2350$ oe is quite clearly displayed.

[1] S. I. Pekar, Исследование по электронной теории кристаллов (Research on the Electron Theory of Crystals) GITTL (1951).

[2] E. F. Gross and I. Pastrnyak, Физика твердово тела 1, 518 (1959), Soviet Phys.-Solid State 1, 466 (1959).

[3] E. F. Gross and I. Pastrnyak, Физика твердово тела 1, 973 (1959), Soviet Phys.-Solid State 1, 891 (1959).

[4] H. Haken, Fortschr. Phys. 6, 271 (1958).

[5] T. Muto and H. Okuno, J. Phys. Soc. Japan 11, 633 (1956).

[6] J. Toyozawa, Progr. Theor. Phys. 12, 421 (1954).

[7] R. Feynman, Phys. Rev. 97, 660 (1955).

[8] V. V. Manenkov and A. M. Prokhorov, Радиотехника и электроника (Radio Engg. and Electronics) 1, 469 (1956).

[9] Dresselhaus, Kip, and Kittel, Phys. Rev. 98, 368 (1955).

[10] Komar, Reĭnov, and Shalyt, Dokl. Akad. Nauk SSSR 46, 47 (1959).

[11] Gross, Zakharchenya, and Pavinskiĭ, J. Tech. Phys. (U.S.S.R.) 27, 2177 (1957), Soviet Phys.-Tech. Phys. 2, 2018 (1958).

Translated by K. F. Hulme
80

FRAGMENTATION OF Ag AND Br NUCLEI BY 9-Bev PROTONS

N. A. PERFILOV, N. S. IVANOVA, O. V. LOZHKIN, M. M. MAKAROV, V. I. OSTROUMOV, Z. I. SOLOV'EVA, and V. P. SHAMOV

Radium Institute, Academy of Sciences, U.S.S.R.

Submitted to JETP editor August 1, 1959

J. Exptl. Theoret. Phys. (U.S.S.R.) 38, 345-350 (February, 1960)

Formation of multiply-charged particles with $Z \geq 4$, due to interaction of 9-Bev protons with Ag and Br nuclei in photographic emulsions, was investigated. The fragment-production cross section, and the angular, energy, and charge distribution of the fragments were determined. The peculiarities of nuclear disintegrations involving the formation of fragments are examined.

1. INTRODUCTION

THE fragmentation process, formation of multiply-charged particles with $Z \geq 3$ in nuclear disintegrations, a process which plays a rather small role at comparatively low energies of bombarding particles (on the order of several hundreds Mev), assumes great significance at energies greater than 1 Bev. The cross section of the fragmentation process reaches in this energy range, for silver and bromine, values on the order of 10% of the total cross section of inelastic interaction. This circumstance results in a substantial change in the mass curve of nuclear disintegration products in the region near several Bev. Failure to account for fragmentation in the "cascade-evaporation" model of interaction between high-energy particles and nuclei leads thus to a substantial distortion of the actual picture of nuclear disintegration. In addition, fragmentation is in itself an interesting object of study, for it can yield information on the structural features of nuclei and on the interaction between fast particles and nucleon clusters in the nuclei.

We report here the first results of an investigation of fragmentation at proton energies near 10 Bev.

2. EXPERIMENTAL PROCEDURE

Small emulsion chambers containing ten layers of P-R 200-μ emulsions were bombarded by 9-Bev protons in the proton synchrotron of the Joint Institute for Nuclear Research. The individual layers of the chambers were marked by the method described by Sidorov and Trukhin.[1] The thickness of the emulsion chambers made it possible to obtain complete range distributions of multiply-charged particles produced in the nuclear disintegrations, and the sensitivity of the emulsion to relativistic particles made it possible to observe all the charged particles emitted from the nuclei.

In scanning the emulsion we analyzed nuclear disintegrations containing tracks of particles with $Z \geq 4$, which could be reliably distinguished from tracks of singly and doubly charged particles. In the analysis of the nuclear disintegrations, the tracks were classified as "black," "gray," and "thin" ("black" — proton energy less than 30 Mev; "gray" — proton energy ≤ 1 Bev; "thin" — proton energy > 1 Bev). The number of particles, their angles with the direction of the incident proton, and different characteristics of the fragments were determined.

The fragment charge was determined by measuring the integral track width over a fixed length from the end of the range (see reference 2). The widths were measured with an ocular micrometer on seven sections of the track, spaced every 3μ from the end of the range.

3. EXPERIMENTAL RESULTS

In scanning the nuclear emulsions irradiated by 9-Bev protons, a total of 1028 disintegrations with more than four prongs were investigated. This number of ordinary disintegrations included 188 disintegrations containing fragments with $Z \geq 4$. An additional 709 disintegrations with fragments were obtained for the investigation of the fragmentation process. Thus, a total of 997 disintegrations with fragments having $Z \geq 4$ were registered.

a) Characteristics of nuclear disintegrations with fragments. One of the essential features of nuclear disintegrations with fragments produced by 9-Bev protons is, as in the case of lower proton energies, the considerably greater average number of par-

Character of disintegrations	Average number of prongs			
	"black"	"gray"	"thin"	Total
Disintegration without fragments	8.3			
Disintegration with one fragment of $Z \geqslant 4$	10.2	4.8	1.44	16.5
Disintegration with two and more fragments of $Z \geqslant 4$	11.0	5.8	1.5	18.3
Disintegration with fast fragments	11.4±1.5	5.2±0.8	1.8±0.3	18.4

ticles in the disintegration than in ordinary disintegration, this difference being due, essentially, to relatively slow particles.

The table lists data on the average number of particles in disintegrations with fragments and in ordinary stars.[3] In disintegrations with fragments, the fragments themselves are not included in the number of "black" prongs.

The average number of particles in disintegrations with fragments is considerably greater than in ordinary disintegrations. This number is even greater in disintegrations containing several fragments, and in disintegrations with fast fragments at energies greater than the Coulomb barrier (with ranges greater than 100 μ).

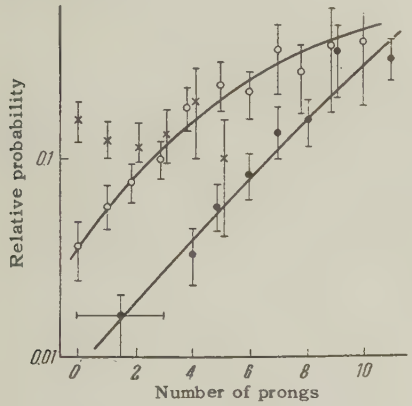

FIG. 1. Dependence of the probability of disintegrations with fragments on the number of prongs: ● – "black," ○ – "gray," and × – "thin."

This increase in the average number of particles in stars with fragments is due to the considerable increase in the probability of fragment emission with increasing number of particles in the disintegration. Figure 1 shows the dependence of the probability of the production of disintegration with fragments on the number of "black," "gray," and "thin" prongs. A strong dependence of the probability of fragment production on the number of "black" and "gray" prongs in the disintegration is observed. The dependence for the production of fast fragments is analogous.

b) Cross section of production of stars with fragments. The cross section of production of fragments was found starting with the proton current, determined from the number of tracks in the emulsion, the number of nuclei per unit volume of the emulsion, and the observed number of disintegrations with fragments. In addition, the fragmentation cross section can be determined from the known cross section of inelastic interaction of 9-Bev protons with photoemulsion nuclei and the distribution of disintegrations by number of prongs,[3] knowing the relative fraction of stars with fragments among all the disintegrations induced by protons.

The results obtained by both methods were in agreement. The cross section for the production of disintegrations with fragments of $Z \geq 4$ was found to be 100 ± 30 mb in Ag and Br nuclei. Thus, the cross section for production of disintegrations with fragments with $Z \geq 4$, for 9-Bev incident protons, was ~ 10% of the total cross section of inelastic interaction. For the sake of comparison with results obtained at lower proton energies, it is useful to determine the cross section of production of Li_3^8 and B_5^8 nuclei. This cross section amounts to approximately 3 mb for 9-Bev protons.

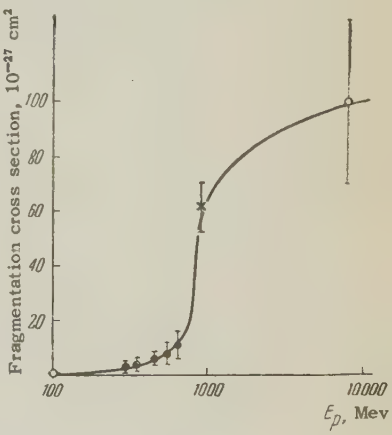

FIG. 2. Dependence of the cross section of production of fragments with $Z \geqslant 4$ in the disintegration of Ag and Br nuclei on the energy of the incident protons, E_p: ● – data of reference 4, × – data of reference 5, ○ – present data.

Figure 2 shows the dependence of the cross section for the production of fragments of $Z \geq 4$ in the disintegration of Ag and Br nuclei on the energy of the incident protons, plotted from data available at the present time. The sharp increase in the cross section at energies near 1 Bev is clearly pronounced.

c) Multiplicity of fragment production. As the the energy of the incident proton increases, the relative fraction of stars containing two or more tracks of multiply-charged particles increases. In the investigation of disintegrations due to 9-Bev protons, it was found that out of 838 disintegra-

tions with one fragment of $Z \geq 4$, there are 144 disintegrations with two, 13 with three, and 2 disintegrations with four such fragments. Thus, the average number of fragments with $Z \geq 4$ in disintegrations with fragments is approximately 1.2. The relative fraction of disintegrations with ≥ 2 fragments amounts to 0.2 at 9-Bev proton energy, whereas for 660-Mev protons this value is approximately 0.05.[6]

d) Nature of the fragments. To measure the charge, we used tracks of fragments with depth angle not greater than 7° in the developed emulsion and with lengths not less than 15 μ. The emulsion was calibrated with the tracks of Li_3^8 and B_5^8. A total of 120 tracks of particles of $Z \geq 4$ were measured. The analysis of the resultant distribution of tracks by integral widths has led to the charge dependence of the fragment yield shown in Fig. 3. The same figure shows the distribution of fragments by charge at proton energies of 6.2 Bev.[7]

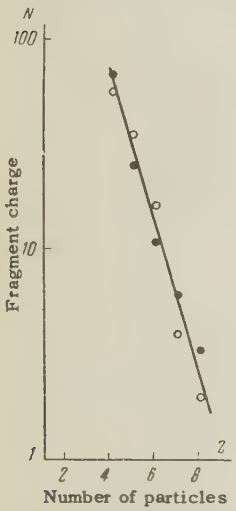

FIG. 3. Distribution of fragments by charge. ● – energy of incident protons 6.2 Bev,[7] ○ – energy of incident protons 9 Bev.

A comparison shows a close agreement between the charge distributions of the fragments at these proton energies. Comparison with the data of references 5 and 6 leads, in addition, to the conclusion that the fragment distribution by charge depends little on the energy of the incident protons.

During the course of the work we investigated the possible β activity of the fragments for the purpose of obtaining certain information on their mass distribution. For this purpose we estimated the effectiveness of registration of decay electrons by stopping a β-active particle in the emulsion; this could be done by observing the decay electrons due to muons and Li_3^8 and B_5^8 ions stopped in the emulsion. This effectiveness was found to be approximately 70%.

From anong the 175 fragments of charge $Z \geq 4$, investigated for this purpose, we could observe tracks of fast electrons at the end of the fragment

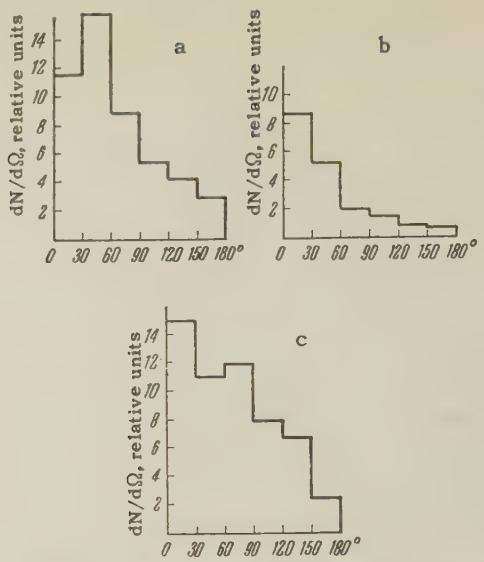

FIG. 4. Angular distribution of fragments with $Z \geq 4$ relative to the direction of incident protons: a – disintegrations with one fragment; b – disintegrations with fast fragments, c – disintegrations with two and more fragments.

range in only nine cases. Of these nine fragments, two are B_5^8 ions. Thus, if fragments with $Z \geq 4$ are considered, allowing for the probability of observing the decay electron, we find that not more than 10% of the fragments can be β-active.

e) Angular and energy distributions of the fragments. The angular distribution of the fragments with $Z \geq 4$ in space, relative to the direction of incident protons, was found by recalculating the angular distribution found in projection on the emulsion plane, by the method described by Ostroumov and Filov.[8]

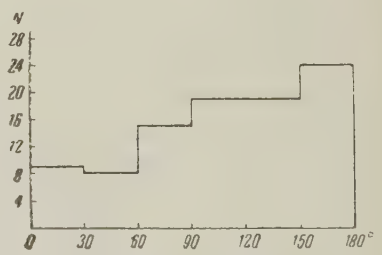

FIG. 5. Distribution of the number of disintegrations with several fragments with respect to the angle between fragment tracks (projected on the emulsion plane).

Figure 4 shows the angular distributions obtained for the fragments, and Fig. 5 shows the distribution of the number of stars with two fragments relative to the angle between these fragments, measured in projection on the emulsion plane. An analogous correlation with the direction of emission of two multiply-charged particles was noted earlier at 660 Mev.[9]

As the fragment energy increases, the angular distribution becomes more anisotropic: for fragments with $R > 100\,\mu$, the forward/backward ratio is 3.6 ± 1.1, while for all other fragments the ratio is 2.1 ± 0.2.

Along with investigating the dependence of the probability of disintegrations with fragments on the number of thin prongs, a study was also made of the angular correlation between the fragments and fast particles (thin prongs). It was found that for the most part small angles ($< 90°$) between fragments and thin prongs are observed. A comparison of this correlation with that calculated on the basis of the experimental angular distributions of fragments and thin prongs shows that the observed angular correlation can be attributed to a random distribution of the angles.

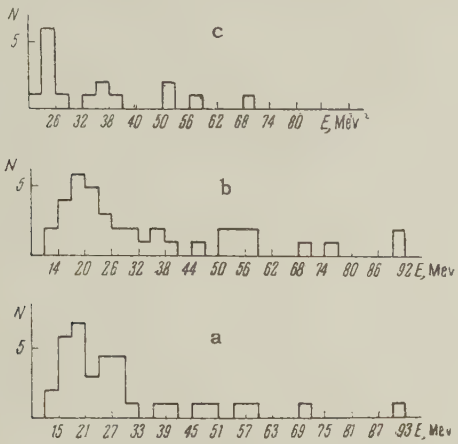

FIG. 6. Energy distribution of fragments with following charges: a – 4, b – 5, c – 6.

The energy distribution (Fig. 6) was plotted for those fragments, the charge of which was determined.

Owing to the identical charge distribution of the fragments at different proton energies, a comparison can be made between the range distribution of the fragments, observed at different energies. Figure 7 shows distributions of fragments with $Z \geq 4$ by ranges at proton energies of 660 Mev (reference 9) and 9 Bev. The difference between the two distributions is due to the different fraction of fragments with ranges greater than 100 μ.

A comparison of these distributions, and also the energy distribution of particles with charges 4, 5, and 6 (Fig. 6) shows that the energy spectrum of the fragments has a weak dependence on the energy of the incident particles. The only important factor is the increase in the relative fraction of fast fragments.

f) Formation of hyperfragments. In a total of 997 investigated fragments with $Z \geq 4$, three cases were found of hyperfragment production, one of which had a charge 6, and the other two had a charge 2 or 3. It must be indicated that the procedure of scanning in our experiment admitted of the possibility of losing sight of a considerable portion of the long-range light hyperfragments (H or He nuclei).

4. CONCLUSION

A comparison of the experimental data, obtained in the present investigation for disintegrations of Ag and Br nuclei, with the data available for lower energies of bombarding protons, leads to the following conclusion:

1. If the energy of bombarding protons is approximately 9 Bev, the fragmentation cross section continues to increase, but apparently more slowly.

2. Disintegrations with fragments, at 9-Bev proton energies, are due to the greater average transfer in energy, than in ordinary disintegrations. The probability of a disintegration with a fragment increases with increasing number of both black and gray prongs and is independent of the number of thin prongs.

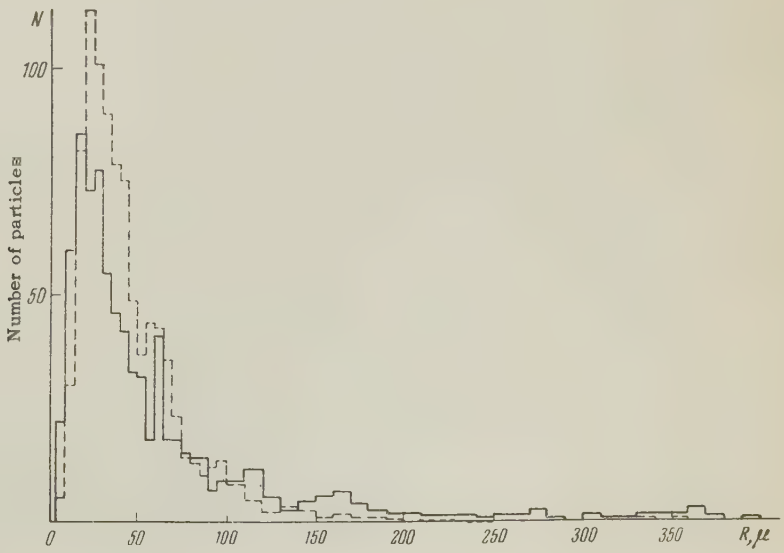

FIG. 7. Distribution of fragments by ranges R at proton energies of 660 Mev (reference 9) (dotted line) and 9 Bev (solid line).

3. The charge distribution differs little from the distributions obtained at lower energies of the bombarding particles.

4. The angular distribution of the fragments at a proton energy of 9 Bev has a lower anisotropy relative to the direction of the incident protons than at energies less than 1 Bev.

5. The fragments produced are for the most part stable isotopes of light nuclei.

6. The energy distribution of the fragments differs little from the distributions obtained at different incoming-particle energies.

In conclusion, the authors take this occasion to thank the High-energy Laboratory staff of the Joint Institute for Nuclear Research for aid in irradiating the emulsion chambers.

[1] V. M. Sidorov and M. I. Trukhin, Материалы совещания по методике толстослойных фотоэмульсий (Materials of the Conference on Procedures with Thick Photoemulsions), vol. 2, p. 36, Dubna.

[2] V. I. Ostroumov and Yu. P. Yakovlev, JETP **35**, 1358 (1958), Soviet Phys. JETP **8**, 949 (1959).

[3] Bogachev, Wang Shu-Fen, Gramenitskiĭ, Kirillova, Lebedev, Lyubimov, Markov, Merekov, Podgoretskiĭ, Sidorov, Tolstov, and Shafranova, Атомная энергия (Atomic Energy) **4**, 281 (1958).

[4] O. V. Lozhkin, JETP **33**, 354 (1957), Soviet Phys. JETP **6**, 273 (1958).

[5] Lozhkin, Perfilov, Rimskiĭ-Korsakov, and Fremlin, JETP **38**, No. 5, 1960, Soviet Phys. JETP **10**, No. 5, 1960 (in press).

[6] O. V. Lozhkin and N. A. Perfilov, JETP **31**, 913 (1956), Soviet Phys. JETP **4**, 790 (1957).

[7] Nakagawa, Tamai, Huzita, and Okudaira, J. Phys. Soc. Jap. **12**, 747 (1957).

[8] V. I. Ostroumov and R. A. Filov, Приборы и техника эксперимента (Instruments and Measurement Engg.) **1**, No. 2, 44 (1957).

[9] O. V. Lozhkin, Dissertation, Radium Inst. Acad. Sci., 1957.

Translated by J. G. Adashko
81

THE HEAT CAPACITY OF BISMUTH TELLURIDE AT LOW TEMPERATURES

E. S. ITSKEVICH

Institute for the Physics of High Pressures, Academy of Sciences, U.S.S.R.; Institute for Physical Problems, Academy of Sciences, U.S.S.R.

Submitted to JETP editor August 3, 1959

J. Exptl. Theoret. Phys. (U.S.S.R.) **38**, 351-358 (February, 1960)

The heat capacity of p-type Bi_2Te_3 was measured between 1.37 and 65°K. At temperatures below 2.5°K the heat capacity can be described by a linear term with $\gamma = 17 \times 10^{-5}$ joule-deg^{-2} (g-atom)$^{-1}$ and a cubic term with $\Theta_0 = 155.5$°K. Between 2.5 and 8°K the heat capacity is proportional to a power of the temperature greater than three. The heat capacity of the laminar Bi_2Te_3 lattice is not consistent with the calculations performed for lattices with a larger difference between the elastic moduli in the layer and between the layers. Data are presented on measurements of the Hall effect and resistivity of Bi_2Te_3 at a number of temperatures between 2° and 300°K. The linear term of the heat capacity is ascribed to holes. The hole mass is estimated as $1.46\,m_0$.

INTRODUCTION

THE intermetallic compounds Bi_2Te_3, Bi_2Se_3 and Sb_2Te_3 are semiconductors with lattices which have strong layer characteristics. This property makes a study of their heat capacity especially interesting

An investigation of the heat capacity of cadmium halides at low temperatures[1] showed that its temperature dependence for these layer lattices is considerably different from that characteristic of less anisotropic structures. The attempt at a quantitative comparison with theory was unsuccessful because the anisotropy of CdI_2, $CdBr_2$, and $CdCl_2$ is not as great as the theory requires.[2,3*] In addition, a temperature range was found for all three salts in which the heat capacity varied with temperature according to a power greater than three. This was ascribed to the effect of soft optical branch modes, corresponding to inter-layer interactions.

In the last 3 or 4 years Bi_2Te_3 has become a much studied substance.[4-9] However, there are only the data of Gul'tyaev and Petrov[10] on the heat capacity in the temperature region attainable with liquid nitrogen. We have undertaken a study of bismuth telluride to widen the investigation of the heat capacity of layer lattices.

1. THE COMPOUND AND METHOD OF MEASUREMENT

Bismuth telluride has a typical layer lattice, which consists of five-chain layers, with the monatomic networks alternating in the order Te-Bi-Te-Bi-Te. The bonding between such layers is produced by van der Waals forces. Within the weakly bound layers the atoms are held considerably more strongly by covalent (with an ionic component) forces.[11-13]

The Semiconductor Institute of the Academy of Sciences kindly prepared the p-type Bi_2Te_3 for us. The alloy was recrystallized twice to increase the purity and was not analyzed for purity. A cylinder consisting of large crystals was cast from this material and pieces were cleaved from the top and bottom for measurements of resistivity, thermal emf and Hall constant. These measurements, made at room temperature in the Semiconductor Institute, gave the following results: for the upper part of the casting the conductivity $\sigma = 470\,\Omega^{-1}\,cm^{-1}$, thermal emf $\alpha = 37.7\,\mu v/deg$ and Hall constant $R = 0.965$ cm^3/coul; for the lower part $\sigma = 173\,\Omega^{-1}\,cm^{-1}$, $\alpha = 30.5\,\mu v/deg$ and $R = 1.06$ cm^3/coul. The upper and lower surfaces of the cylinder were drilled and a cylindrical hole bored along the axis for the thermometer. The weight of the specimen was 567.6 g.

The outside of the cylinder was coated with polymer varnish BF-2, and enamelled constantan wire wound on as a heater of resistance ~180 ohms at 4.2°K. The measurements were made in the calorimetric apparatus described previously.[1] The cylinder was hung on three caproic threads in a vacuum jacket. The high heat capacity of the specimen above 20°K (20.34 joule/deg at 20.8°K and 68.92 joule/deg at 64.8°K), together with the good vacuum obtained with the adsorption pump, made it possible to carry out measurements without any further adiabatic arrangements up to

*It was shown by Itskevich and Kontorovich[3] that graphite shows the required anisotropy.

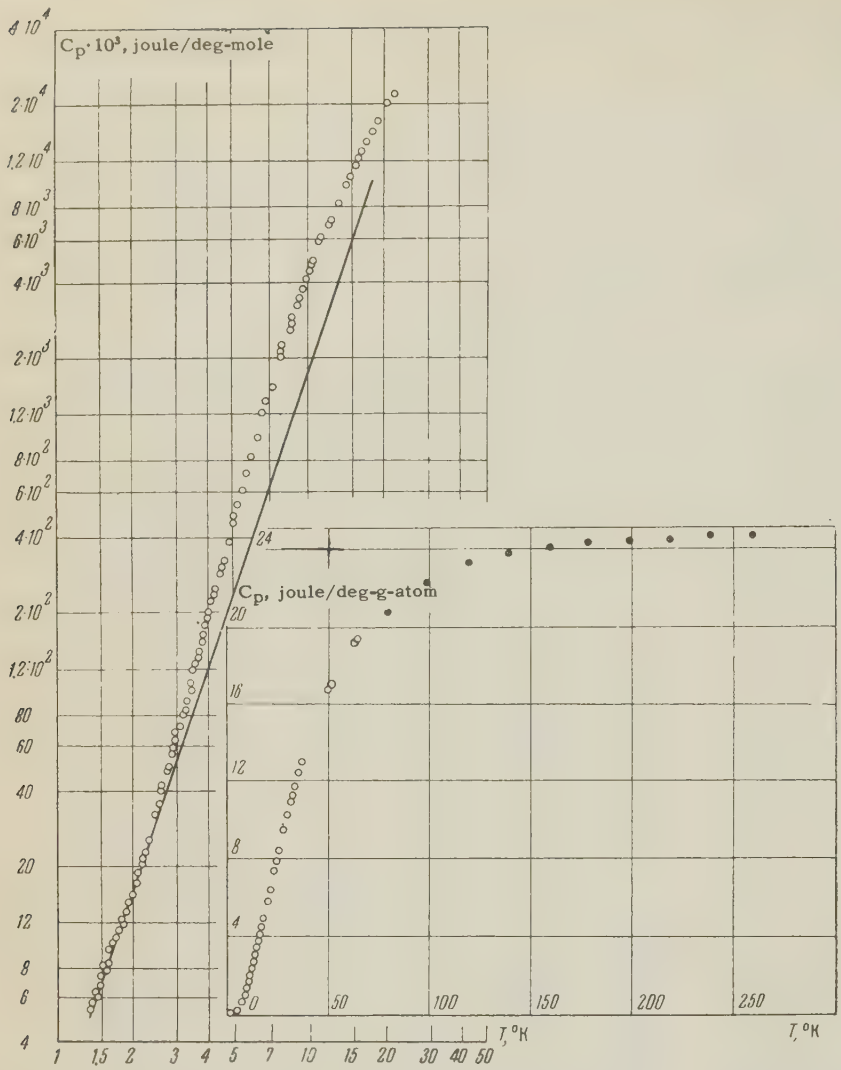

FIG. 1. Heat capacity of p-type bismuth telluride. The straight line corresponds to the law $C_p \sim T^3$. Below right; data of the author (open circles) and the values obtained by Gul'tyaev and Petrov[10] (full circles).

65° K, using liquid and gaseous hydrogen as coolant and heat exchange medium above 20° K. At 30° K the temperature drift was 5×10^{-4} deg/min and at 65° K it was 4×10^{-3} deg/min. A platinum resistance thermometer was used at hydrogen temperatures, a bronze thermometer in the helium range (1958 scale) and a carbon thermometer between 3.5 and 16.3° K. The thermometer construction and calibration and the measuring procedure have been described.[1] Thermal equilibrium was established rapidly in the specimen. Calculation showed that apart from the copper and BF-2 varnish, the heat capacity of all components of the heater and thermometer could be neglected at all temperatures. Corrections were made for the copper and varnish, calculated from the data of Corak et al.[14] and of Kalinkina,[15] extrapolated according to the Debye law above helium temperatures. At all temperatures the total correction was less than 1% of the measured heat capacity and only reached 1.5% below 2° K, so that any error in determining the correction could be neglected.

The measurements made between 3.5 and 4.1° K using both the bronze and carbon thermometers, and those between 12.2 and 16.3° K with the carbon and platinum thermometers almost coincide; there may be an insignificant systematic difference between the data obtained between 12° and 14° K with the two thermometers, which does not influence the final result.

2. RESULTS

A total of 135 measurements was made between 1.37 and 64.8° K. The range between 1.37 and 38.6° K was covered continuously and no phase transition was found. Figure 1 shows the results from 1.37 to 20.0° K. Our data from 1.4 to 65° K are also shown together with the smoothed data of Gul'tyaev and Petrov[10] between 80 and 300° K.

Below 2.3° K the results can be fitted by the expression

$$C = \gamma T + 464.5\,(T/\Theta_0)^3, \qquad (1)$$

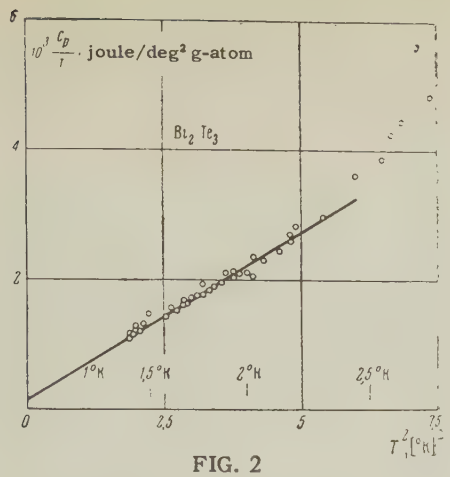

FIG. 2

with $\gamma = (17 \pm 8) \times 10^{-5}$ joule-deg^{-2}/g-atom and $\Theta_0 = (155.5 \pm 3)$°K — the Debye temperature at absolute zero. It can be seen from Fig. 2 that the linear term in (1) shows up clearly and at 1.5°K contributes 12% of the measured heat capacity.

The exponent of the temperature dependence of the heat capacity increases considerably above 2.5 — 3°K (see Fig. 1). In this region the contribution of the linear term is negligible (it comprises 4% at 3°K, and this rapidly falls off with increasing temperature). The experimental points fit a dependence $C = aT^{3.6}$ up to 8°K. Above 8°K the power falls monotonically and again goes through a region of cubic dependence. This can easily be seen in Fig. 3, where there is a minimum in the $\Theta_D(T)$ curve between 8 and 11°K. The greatest deviation from the curve corresponding to Eq. (1) is greater than 200%. There is no extension of the linear and quadratic dependence found previously.[1]

We estimate that the overall mean error in the results is 1% above 20°K and between 2 and 3% below 20°K.

3. DISCUSSION OF THE FORM OF THE HEAT CAPACITY OF THE BISMUTH TELLURIDE LATTICE

It can be seen from Fig. 1 that the heat capacity curve for the Bi_2Te_3 lattice is considerably different from that of the cadmium halides:[1] the cubic law for Bi_2Te_3 (allowing for the linear term below 2.3°K) agrees with Blackman's requirement that it should hold for $R < \Theta_D/50$; the square

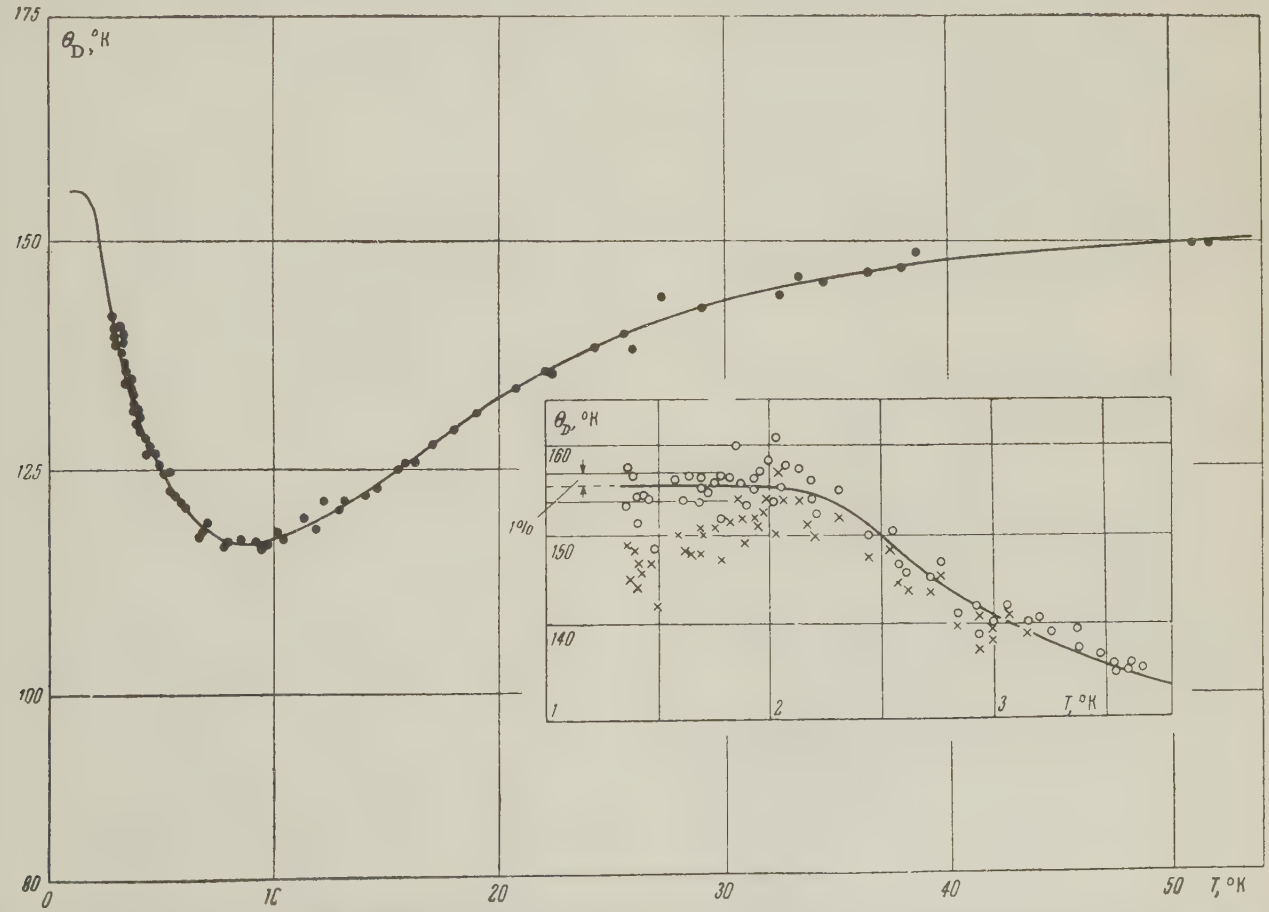

FIG. 3. Characteristic Debye temperature for Bi_2Te_3 between 1.37 and 50°K, derived from the experimental data. The region below 3.5°K is shown separately and corresponds to the portion of the main figure which has no points. The crosses indicate the value of Θ_D calculated on the assumption that the whole measured heat capacity is due to the lattice.

and linear regions are clearly absent; there is a larger interval in which the temperature dependence is greater than cubic and the exponent has a greater maximum value.

Figure 3 shows the $\Theta_D(T)$ curve below 3.5°K and also over a wide temperature range. (The Debye temperature is calculated from the data on C_p. The difference between C_p and C_V is negligible over the whole range; it is 1% at 90°K and rapidly decreases at lower temperatures.) The linear term can be separated out from the trend of the Θ_D points below 2°K. Both this curve and Fig. 2 lead to the conclusion that $\Theta_0 = \Theta_D(0) = (155.5 \pm 3)$°K. Θ_D decreases above 2.3°K, corresponding to a more rapid C-T relation. There is a broad minimum ($\Theta_{D\,min} = 117$°K) at 8 — 11°K, reminiscent of Blackman's pseudo-cubic region,[16] after which there is a more gradual rise: between 30 and 65°K, Θ_D only increases from 144 to 151°K. The dependence of $\Theta_D(T)$ for the cadmium halides is qualitatively similar. Other crystals show a similar variation, and in particular this curve resembles de Sorbo's for bismuth.[17]

From everything described here it is evident that the layer lattice of Bi_2Te_3 is so different from the lattice for which the formula of the Lifshitz theory[2] applies, that we will not attempt to derive quantitative results, as for graphite. It is probable that the increase in the power of the temperature dependence above three is related, as was suggested in the case of the cadmium halides, to the inclusion in the heat capacity of soft optical branches, corresponding to weak inter-layer interactions.

4. HALL EFFECT AND RESISTIVITY OF BISMUTH TELLURIDE AT LOW TEMPERATURES

From the Hall-effect measurements mentioned above, it follows that our specimen had a hole conductivity at room temperature. However, to determine the type of carrier responsible for the linear term in the heat capacity it is necessary to measure the Hall effect at low temperatures. If the conductivity is produced by charge carriers of one sign, their concentration could be deduced from such measurements. From the concentration and the coefficient of the linear term in the heat capacity, if it is assumed that the Fermi surface is an ellipsoid, the limiting Fermi energy can be derived and the effective mass, if it is assumed isotropic.

There are data on the Hall effect in p-type Bi_2Te_3 in several papers in recent years (e.g., references 4 — 9), but the measurements only extend down to nitrogen temperature.* All measurements on Bi_2Te_3 specimens show a slight decrease in the absolute value of the Hall constant on going from room temperature to nitrogen temperature.

Stil'bans and Vlasova[4] found that for a hole specimen with 0.2% bismuth in excess of the stoichiometric proportion, the Hall constant fell sharply with decreasing temperature and was close to zero at 82°K. On this basis, they suggested that there might be a change of sign and an unfilled impurity band with electronic conductivity near 0°K.

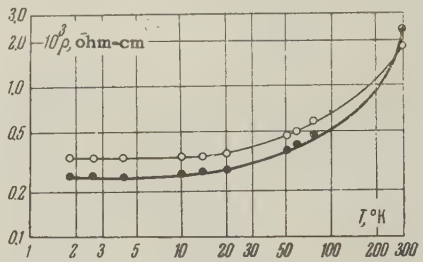

FIG. 4. Resistivity of p-type Bi_2Te_3 between 2 and 300°K: ● — specimen No. 1, ○ — specimen No. 2.

We measured the resistance and Hall effect at low temperatures (helium, hydrogen and nitrogen). The resistance measurements were made on two polycrystalline circular rods, made from the upper and lower parts of the specimen used for the heat capacity measurements. One of these rods was then polished down to a disc for determining the Hall emf. The measurements were made by a null method, and for this, current and potential leads were attached to the ends of the rod. The resistance was compared with a 0.01-ohm standard. The specimens were joined in series and were placed close together in a Dewar vessel containing the appropriate liquid. Temperatures below the boiling point were obtained by pumping. The results are shown in Fig. 4 and in Table I.

TABLE I. Resistance of two specimens of p-type Bi_2Te_3 at low temperatures

T, °K	Specimen No. 1		Specimen No. 2	
	R, Ω	σ, $\Omega^{-1}\cdot cm^{-1}$	R, Ω	σ, $\Omega^{-1}\cdot cm^{-1}$
1.9	0.0057	3880	0.0037	2950
2.6	0.0057	3880	0.0037	2950
4.2	0.0056	3950	0.0037	2950
10.2	0.0059	3780	0.0037	2950
14.0	0.0059	3760	0.0038	2910
20.4	0.0061	3630	0.0040	2760
52	0.0082	2700	0.0051	2140
59	0.0088	2520	0.0054	2020
78	0.0104	2130	0.0064	1700
room temperature	0.052	420	0.020	550

*See the next footnote.

TABLE II. Absolute values of emf and Hall constant, R, for p-type bismuth telluride (specimen No. 1)

T, °K	emf at H=10.2 koe, μv	R, cm³/coul	T, °K	emf at H=10.2 koe, μv	R, cm³/coul
1.9	31.2	+0.182	78.0	37.7	+0.223
4.2	31.8	+0.186	room temperature	50.9	+0.306
20.4	33.7	+0.192			

The results show our specimen to have a metallic type conductivity, starting from the lowest temperatures. The conductivity is independent of temperature below 10°K, which is probably to be explained by the presence of a large impurity concentration. The impurity could be bismuth atoms produced, as Satterthwaite and Ure have shown,[8] by the exact stoichiometric proportions in the liquid not giving rise to the same proportions in the crystals.

The Hall emf was measured on specimen No. 1 at liquid helium temperatures and at the boiling points of hydrogen and nitrogen using a KL-48 potentiometer. Our magnet made measurements possible up to fields of 10,200 oe. The direction of the field was reversed by rotating the specimen. Measurements were made in different fields at each temperature, and no field dependence of the Hall constant, R, was found (in the range 2.0 to 10.2 koe). The results are shown in Table II and in Fig. 5.*

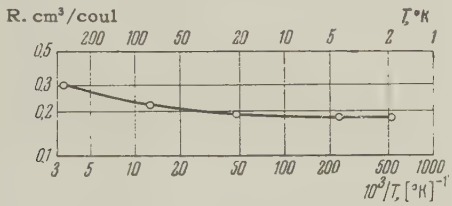

FIG. 5. Hall constant of p-type Bi_2Te_3 between 2 and 300°K.

The Hall constant is always positive, which does not bear out the suggestion of Stil'bans and Vlasova[4] about a change in sign, and the conductivity of our Bi_2Te_3 is by holes at all temperatures. We can deduce the hole concentration at helium temperatures and possibly at hydrogen temperatures, where the Hall constant is practically independent of temperature. Using the formula $R = 3\pi/8ne$ or $n = 7.35 \times 10^{18} R^{-1}$, we obtain $n = 4.0 \times 10^{19}$ cm^{-3} for our sample.

Since the Hall constant increases, although slowly, with increasing temperature, we can presume that one or more further groups of charge carriers come into evidence above hydrogen temperatures. Our data on the temperature dependence of resistance and Hall constant do not fit into the simple scheme with an unfilled impurity band, proposed by Vlasova and Stil'bans.

*We recently learned of Yates' work[18] on the measurement of electrical resistance and Hall effect in Bi_2Te_3 between 1.3 and 660°K. Our results are in satisfactory agreement with Yates' results.

5. DISCUSSION OF THE RESULTS ON THE HEAT CAPACITY OF THE HOLES IN BISMUTH TELLURIDE

On the assumption that in p-type Bi_2Te_3 near 0°K there is one group of holes in a large concentration, giving the main contribution to the linear term in the heat capacity and to the Hall emf, we can deduce their effective mass at 2°K from their concentration and heat capacity.

The atomic heat capacity of a highly degenerate gas of holes is

$$C_v = \gamma T = 3.86 \cdot 10^{-13} V n^{1/3} (m/m_0) T \text{ cal/g-atom-deg}, \quad (2)$$

where V is the atomic volume, n the number of holes per unit volume, and m/m_0 the ratio of the effective hole mass to the mass of the electron. This relation applies for $T \ll T_F$, where T_F is the Fermi temperature:[19]

$$T_F = 4.2 \cdot 10^{-11} n^{2/3} m_0/m.$$

In our case the Fermi temperature comes out to be 336°K, so that Eq. (2) is applicable, and from it we obtain $m/m_0 = 1.46$.

Since the Hall constant changes little between 2 and 300°K it is possible that the activation energy for the impurities in our Bi_2Te_3 is close to zero.

In conclusion, the author considers it a pleasant duty to express his sincere appreciation to Academician P. L. Kapitza for making it possible to carry out this work in the Institute for Physical Problems of the Academy of Sciences and to Professor P. G. Strelkov for his constant interest in the work and for valuable advice.

[1] E. S. Itskevich and P. G. Strelkov, JETP **32**, 467 (1957), Soviet Phys. JETP **5**, 394 (1957).

[2] I. M. Lifshitz, JETP **22**, 471, 475 (1952).

[3] E. S. Itskevich and V. M. Kontorovich, JETP **32**, 175 (1957), Soviet Phys. JETP **5**, 147 (1957).

[4] R. M. Vlasova and L. S. Stil'bans, J. Tech. Phys. (U.S.S.R.) **25**, 569 (1955).

[5] P. P. Konorov, J. Tech. Phys. (U.S.S.R.) **26**, 1400 (1956), Soviet Phys.-Tech. Phys. **1**, 1371 (1957).

[6] Harman, Paris, Miller, and Goering, J. Phys. Chem. Solids **2**, 181 (1957).

[7] Black, Conwell, Seigle, and Spencer, J. Phys. Chem. Solids **2**, 240 (1957).

[8] C. B. Satterthwaite and R. W. Ure, Phys. Rev. **108**, 1164 (1957).

[9] Drabble, Groves, and Wolfe, Proc. Phys. Soc. **71**, 430 (1958), J. R. Drabble, Proc. Phys. Soc. **72**, 380 (1958).

[10] P. V. Gul'tyaev and A. V. Petrov, Физика твердого тела **1**, 368 (1959), Soviet Phys. Solid State **1**, 330 (1959).

[11] P. W. Lange, Naturwiss. **27**, 133 (1939).

[12] S. A. Semiletov, Тр. Ин-та кристаллографии (Proc. Inst. Crystallography) **10**, 76 (1954).

[13] J. R. Drabble and C. H. L. Goodman, J. Phys. Chem. Solids **5**, 142 (1958).

[14] Corak, Garfunkel, Satterthwaite, and Wexler, Phys. Rev. **98**, 1699 (1955).

[15] I. N. Kalinkina, Приборы и техника эксперимента (Instrum. and Meas. Engg.) **1**, 146 (1958).

[16] M. Blackman, Proc. Roy. Soc. **148A**, 365, 384 (1935); **149A**, 117 (1935).

[17] W. de Sorbo, J. Phys. Chem. **62**, 965 (1958).

[18] B. Yates, J. Electron. and Control **6**, 26 (1959).

[19] E. C. Stoner, Phil. Mag. **21**, 145 (1936).

Translated by R. Berman
82

THE POLARIZATION OF NUCLEI OF DIAMAGNETIC ELEMENTS DISSOLVED IN IRON

B. N. SAMOĬLOV, V. V. SKLYAREVSKIĬ, and E. P. STEPANOV

Submitted to JETP editor August 6, 1959

J. Exptl. Theoret. Phys. (U.S.S.R.) **38**, 359-371 (February, 1960)

The possibility of polarizing the nuclei of paramagnetic elements — indium, antimony, and gold — in weak solutions of these elements in iron is established. Samples of ferromagnetic alloys In-Fe, Sb-Fe, and Au-Fe were cooled to a temperature of ~ 0.03°K and magnetized to saturation by a not too large (~ 2000 oe) magnetic field. The gamma-ray anisotropy of In^{114m}, Sb^{122}, and Au^{198} nuclei contained in the samples was measured. Measurements showed that a strong inner magnetic field acts on the nuclei of the elements dissolved in iron; the value of this field has the following limits: for In-H $\geq 2.5 \times 10^5$, for Sb-H $\geq 2.8 \times 10^5$, for Au-H $\geq 1.0 \times 10^6$ oe. The assumption is expressed that this field is created by the conduction electrons, which have a substantial degree of polarization in a ferromagnet. At temperatures of 0.03°K the value of the polarization of the investigated nuclei is not less than 30 — 50%.

1. INTRODUCTION

In recent years a considerable number of experiments with oriented nuclei was performed. In the majority of cases a study was made of the angular distribution of the gamma rays. In these experiments, except for checking the polarization methods themselves, information was also obtained that made the decay schemes of radioactive nuclei more precise. After the widely known experiment by Wu, Ambler et al., a certain number of experiments was performed on the angular distribution of electrons and positrons released during beta decay. Some experiments were also performed to study the interaction of polarized neutrons with polarized nuclei, by observing the anisotropy of the angular distribution of alpha particles during alpha decay and of fragments in neutron-induced fission of nuclei.

In the overwhelming majority of cases two statistical and equilibrium methods, proposed in references 1 and 2, were used for orientation. Both methods are applicable to the limited number of elements that form paramagnetic compounds which retain their paramagnetic properties down to very low temperatures. This requirement is very stringent and explains why all the experiments were performed solely with the isotopes of several elements of the iron group, the rare earths, and actinides. A limitation is also inherent in two other statistical methods — the method of reference 3 and the direct method. The first of these is applicable to a narrow class of compounds whose nuclei have large quadrupole moments; the second requires the use of static magnetic fields with an intensity of 10^5 to 10^6 oe, the production of which entails at present considerable technical difficulties. The use of the method proposed in references 4 and 5 for the polarization of ferromagnetic nuclei is naturally limited to ferromagnetic elements.

The dynamic methods, proposed in references 6, 7, and by others, extend somewhat the circle of elements whose nuclei can be oriented. Thus a sufficiently large degree of orientation of As^{76} nuclei was attained in references 8 and 9; this the authors were able to measure by means of the anisotropy of the gamma radiation. However, obviously even the dynamic methods must not be considered universal. In addition their practical carrying out is more complicated than that of the statistical methods, particularly if a study of beta or alpha radiation emitted by the oriented nuclei is necessary.

We have attemped to find new methods for polarizing nuclei. Earlier we published[10,11] preliminary results of experiments on the polarization of Au^{198}, Sb^{122}, and In^{114m} in weak solutions of these elements in iron. In all three cases a relatively large degree of polarization, which was determined by the extent of the gamma-ray anisotropy, was attained. The method of polarization consists essentially of the cooling of a sample of ferromagnetic alloy, containing active nuclei magnetized to saturation, to a temperature of several hundredths of a degree. The above nuclei were chosen only because both their magnetic moments and their decay schemes[12] are known.

In this paper we publish the final results of the experiments on the polarization of Au^{198}, Sb^{122},

and In^{114m}, nuclei in weak solutions of gold, antimony, and indium in iron. Possible explanations of the polarization mechanism are discussed in Sec. 4 of this paper.

2. EXPERIMENTAL SETUP AND METHOD OF MEASUREMENT

The adiabatic demagnetization method for paramagnetic salt was used to cool the samples down to a temperature of several hundredths of a degree. Potassium chrome alum was used. The thermal contact between the salt and the sample was accomplished by means of a "heat conductor" — a copper rod ~ 150 mm long and with a diameter of 2.5 to 3 mm. The sample was soldered to one end of the "heat conductor." At the other end of the rod, copper plates, serving as the thermal contact between the rod and the salt, were soldered on with silver solder. The previously ground salt was pressed under a pressure of several thousand atm around these plates into the form of a cylinder 50 mm long and with a diameter of 20 mm. The total surface of the copper plates in contact with the salt amounted to $40 - 50$ cm^2.

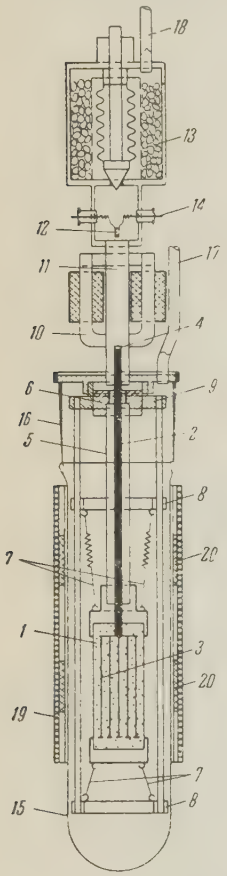

FIG. 1. Arrangement of the instrument.

The salt block with the "heat conductor" was suspended in the vacuum chamber of a cryostat by means of thin stainless-steel wires and was centered with the aid of a thin-walled glass tube in the upper part of the chamber (Fig. 1). On this figure, 1 is the block of paramagnetic salt, 2 — the "heat conductor" between the contact plates 3 and sample 4; 5 — the centering glass tube held by Plexiglas washers surrounding the salt, 6 — a textolite sleeve for centering. The block was suspended on the thin wires 7, whose tension was adjusted by little springs attached to brass hooks 8 sliding in a frame of thin-walled tubes coated with German silver. The tubes of the frame were soldered on to the flange 9, fixed to the lid of the vacuum chamber. A centering sleeve was screwed into the flange. The position of the salt block with the sample was chosen such that the sample was at the lower end of the polepieces of the electromagnet 10. The electromagnet produced fields up to $2 - 2.5$ koe at the position of the target. In these fields the samples used were magnetized practically to saturation. The vacuum chamber was connected by a pipe 11 to a volume where a resistance thermometer 12 was placed, and to an adsorption pump 13 (reference 13). The upper end of the "heat conductor" with the soldered-on sample was also inside this pipe. The thermometer was connected to the measuring circuit through air-tight isolated leads 14 (cf. reference 14) by means of thin constantan wires. The thermometer served as the vacuum indicator in the chamber. A glass test tube 15 served as the outer wall of the vacuum chamber. The test tube was attached to a copper cylinder 16 which was sealed to the chamber lid with low-melting-point solder. Tubes 17 and 18 served for pumping out the small pump and the chamber, and for filling the chamber with helium for heat exchange through a special measuring device placed in the cryostat lid. To measure the magnetic susceptibility of the salt, a coil with two windings, primary winding 19 and secondary winding 20, was placed over the test tube.

The vacuum chamber was fastened inside the helium Dewar flask by means of a thin-walled silver-coated tube joined to the lid of the Dewar. Inside this tube there was a second tube which served as the connection to the valve of the adsorption pump. The electromagnet was fastened to a flange equipped with three stainless-steel wire braces of about 1 mm diameter whose upper ends were attached to the lid of the cryostat, since during magnetization of a paramagnetic salt in the field of a large magnet a considerable force tends to pull the electromagnet in. The whole cryostat was placed on a swinging truss making it possible to transfer the device after demagnetization from the magnet into the measuring setup quickly and without shaking. The helium evacuation line was equipped with an oilseal packing permitting, in ad-

dition to a rotation of the truss, also the adjustment of its height above the field. The end of the evacuation line was fastened to the lid of the cryostat through a bellows which made it possible to change the distance between the axis of the device and the axis of rotation of the truss. This provided the device with a third degree of freedom. The evacuation of the helium was effected by means of a VN-4 pump with a geometric efficiency of about 60 *l*/sec. The pump was in a different room and was secured on a massive foundation. The evacuation line practically did not decrease the efficiency of the pump. With a completely open valve the pump allowed an evacuation up to 0.2 — 0.3 mm Hg above liquid helium; this corresponded to a salt temperature of 1.05 — 1.10° K before demagnetization.

A powerful magnet with an adjustable distance between the poles was used to magnetize the salt. The magnet was equipped with polepieces of "Armco" iron permitting the establishment of fields up to 22 koe in a 90 mm gap with a power dissipation of 40 kw in water-cooled windings. The polepiece diameter was 120 mm.

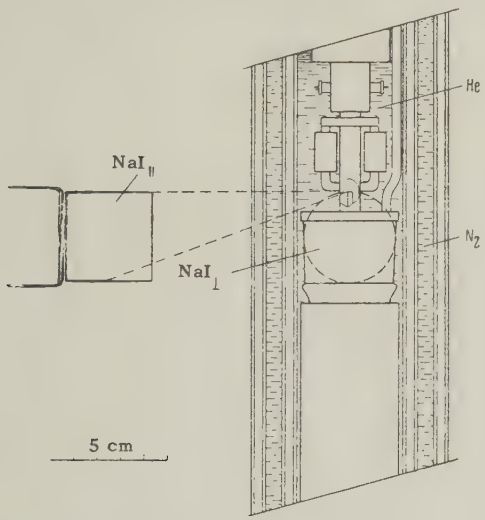

FIG. 2. The geometry of the measurements.

The angular distribution of the gamma quanta emitted by the sample was measured with two scintillation counters fastened to massive iron shields on a support which made it possible to place the counters at angles of 0, 30, 45, 60, and 90° to the direction of the sample magnetization. Inasmuch as the angular distribution of the gamma radiation for the investigated transitions was assumed to be known, the counting was performed in two directions only — parallel and perpendicular to the magnetizing field. Figure 2 shows the relative positions of the sample, the small magnet, and the crystals during the measurement of the angular distribution. As can be seen from the figure, the crystals were placed a little below the sample in order to decrease the shielding influence of the magnet poles.

Every counting channel contained a crystal (as usual, this was a NaI crystal in the form of a 40 × 40 mm cylinder), a FEU-13 photomultiplier with a power pack and a cathode follower, an amplifier, a pulse-height analyzer, and a scaler. The amplitude resolution of the system was 14% for Cs^{137} 662-kev gamma rays. In each channel there were two decade scalers. A special switching device connected each scaler in turn. As one scaler was in operation, the readings of the other one were recorded. The operating precision of the switching device was determined by a crystal-stabilized master generator of standard frequency (60 cps), and was sufficiently high. A PPCh-4 device for watch checking was used as such a generator. The same generator was used also for supplying the primary circuit of the R-56 ac bridge that served to measure the magnetic temperature of the paramagnetic salt. In addition to the secondary winding of the coil, a variable inductance was connected to the secondary circuit of the R-56 bridge; it served to determine the initial potentiometer reading.

The samples were prepared in the form of thin discs (to decrease the demagnetization factor) and had a diameter of 3 mm and a thickness of 0.1 — 0.4 mm. The samples were prepared by alloying "Armco" iron with some of the investigated metal, by heating them inside a high-frequency oven in a helium atmosphere. The alloying took place in quartz ampules. The bead obtained after the alloying was spread and rolled to the required thickness. A disc was punched out from the obtained strip. After this, the alloy samples were irradiated by thermal neutrons in a reactor. The irradiated samples were annealed in vacuum at a temperature of about 1000° C for 2 — 3 hours, after which they were soldered to the end of the "heat conductor" with a soft solder. To improve thermal contact, the end of the "heat conductor" with the sample was covered with an electrolytic layer of copper. Thus the samples containing Au^{198} and Sb^{122} were prepared. Samples with In^{114m} were prepared by alloying previously irradiated metallic indium with iron.

As usual, the experiment began with a calibration of the magnetic thermometer. For this purpose the susceptibility of the salt block was measured at several fixed temperatures, determined from the helium vapor pressure. To control the heat transfer by the gaseous helium, simultaneous measurements of the thermometer resistance

were made. The calibration was made in the temperature interval from 4.2 to 1.2 — 1.1°K. The helium vapor pressure was measured with a mercury manometer, small height differences being determined with the aid of a KM-6 cathetometer. After calibration, the device was placed between the poles of the electromagnet and the field was switched on. Five to ten minutes after the switching on of the field, the valve of the pump was opened. The evacuation of the heat-conducting helium continued for 10 to 15 minutes, after which the valve was shut and the field was slowly switched off (in the course of 3 — 4 minutes). The device was transferred from the magnet to the measuring setup, the field of the small magnetization magnet was switched on, and simultaneous measurements of the gamma-ray intensity along both magnetic temperature directions as a function of time began. The salt temperature was measured at equal intervals of 10 — 15 minutes; for this purpose the variable magnetic field with an amplitude of about 0.1 oe was switched on only for the short measurement time of 15 — 30 seconds. The duration of the experiment was determined by the supply of liquid helium available in the Dewar flask. And since at the end of the experiment, before all the helium had evaporated, it was essential to measure the counting rate for an isotropic gamma-ray distribution of the "warm" sample for a given position of the device relative to the counters, the duration of the experiment usually did not exceed 3 — 4 hours. During that time, in the good experiments, the salt with the sample had time to warm up from a minimum temperature of about 0.005°K to about 0.05°K. In cases where a higher temperature range was of interest, the sample and the salt were heated immediately after the demagnetization by the variable magnetic field employed for measuring the temperature. For this purpose the amplitude of this field was increased by a factor of 10 — 20 (up to 1 — 2 oe). The heat was essentially evolved in the copper contact plates and in the "heat conductor." The sample was heated in a similar manner at the end of the experiment to measure the gamma radiation of a "warm" sample.

3. MEASUREMENT RESULTS

Each experiment yielded the dependence of the counting rate from the two detectors $N(0)$ and $N(\pi/2)$ and of the salt temperature on the time after the demagnetization. These data were processed in the following manner. The background was subtracted from $N(0)$ and $N(\pi/2)$, and the values obtained (for the experiments with Au^{198} and Sb^{122} the values were first adjusted to account for the decay) were normalized by dividing them by the average counting rate for the heated sample. In the case of Au^{198} and Sb^{122} the background (amounting to about 10% of the count) was determined simply by removing the device with the sample from the detectors. In the case of In^{114m}, whose spectrum contains harder gamma rays in addition to the investigated 192-kev lines, the extent of the background was determined by measurements in which a lead filter 2.5 mm thick was placed between the sample and the detector; such a filter absorbed 192-kev gamma rays completely and allowed practically the entire passage of harder radiation. The background which was thus determined amounted to about 15 — 20%.

The sample temperature was determined by the temperature of the salt. The magnetic temperature was measured, and from it the thermodynamic temperature was calculated. For this purpose the magnetic temperature of the cylinder was first converted to the magnetic temperature of a spherical sample.[15] In these calculations the effective demagnetization factor for a salt pressed into the form of a cylindrical block was taken to be 0.95; this was determined in accordance with the data of reference 16, taking account of the change in the susceptibility of the salt with the temperature. This correction, practically constant in the temperature interval 0.01 — 0.1°K, amounted to $+2.0 \times 10^{-2}$ deg. The magnetic temperature so corrected was then converted into the thermodynamic temperature. In this conversion we made use of the data of reference 17 for the temperature region above 0.05°K, and of the data of reference 18 for temperatures below 0.05°K. The sample temperature was assumed to be equal to the temperature of the salt. The correction for their temperature difference, which is due to the energy liberated by the beta-active sample, was estimated in accordance with the data of reference 19. The correction apparently does not exceed 2 to 3×10^{-3}°K for the lowest equilibrium temperature of about 0.03°K, and lies within the limits of the error in the determination of the thermodynamic temperature of the salt, which we estimate to be about 10%. For lower temperatures this correction becomes substantial. Thus for a beta-active sample which emits energy at the rate of about 0.3 erg/sec, the temperature of the sample cannot become lower than 0.015 — 0.020°K, even when the temperature of the salt is arbitrarily low.

In our experiments thermal equilibrium was established within 30 — 60 minutes after the demagnetization of the salt. Up to this time the salt had time to warm up to about 0.03°K. This circumstance was not taken account of in the prelim-

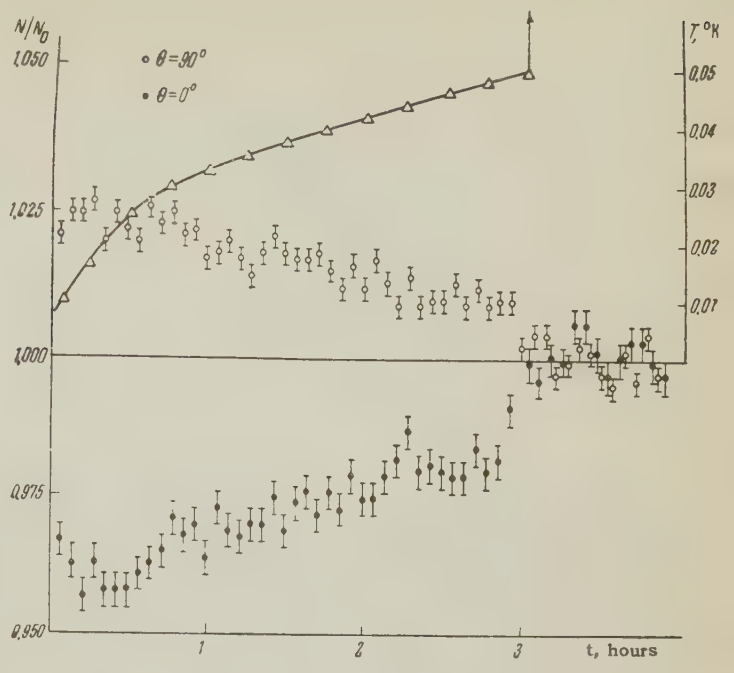

FIG. 3. The dependence of the 566-kev gamma-ray intensity of Sb^{122} on the time after the demagnetization of the salt. The counting rate of the heated sample was taken to be unity. The temperature variation of the salt is shown by the solid curve. The arrow on the temperature curve shows the time when the artificial heating of the salt began.

inary experiments,[10,11] in which the heating of the salt was carried out for 15 — 30 minutes after the demagnetization, i.e., until thermal equilibrium was established. As a result, the sample temperatures used earlier were found to be too low.

Experiments with Sb^{122}

The sample of the Sb-Fe alloy contained 0.6% Sb by weight. There are indications that antimony and iron form a solid solution with an antimony content of up to 6 — 7% (reference 20). The activity of the Sb^{122} nuclei, obtained by irradiating the sample in a reactor, amounted during the experiments to 6 — 8 μC. Only those pulses corresponding to the gamma-ray photopeak with an energy of 566 kev were registered. The fraction of the registered pulses from harder gamma rays did not amount to more than 5%.

The angular distribution of gamma rays with an energy of 566 kev (the $2^+ \xrightarrow{E2} 0^+$ transition), emitted after the beta decay of oriented Sb^{122} nuclei (the $2^- \to 2^+$ transition), is determined by the following expression:[9,21]

$$N(\vartheta) = 2[1 - \tfrac{10}{7} f_2 B_2 P_2(\cos\vartheta) - \tfrac{40}{3} f_4 B_4 P_4(\cos\vartheta)], \quad (1)$$

where ϑ is the angle between the direction of emission of the gamma rays and the axis of orientation; $P_2(\cos\vartheta)$ and $P_4(\cos\vartheta)$ are Legendre polynomials; f_2 and f_4 are orientation parameters of the Sb^{122} nuclei; B_2 and B_4 are coefficients that determine the change in the orientation of the nuclei during beta decay. For the beta transition $2^- \to 2^+$ (reference 9)

$$B_2 = 1 - \alpha_1/2 - 17\alpha_2/14,$$
$$B_4 = 1 - 5\alpha_1/3 - 5\alpha_2/7, \ \alpha_0 + \alpha_1 + \alpha_2 = 1, \quad (2)$$

where α_0, α_1, α_2, are the relative probabilities that during the $2^- \to 2^+$ beta decay the electron and the neutrino are emitted in a state with a total angular momentum L of 0, 1, and 2, respectively

Usually the anisotropy of the gamma radiation of the nuclei is determined in the following manner:

$$\varepsilon = [N(\pi/2) - N(0)]/N(\pi/2), \quad (3)$$

where $N(\pi/2)$ and $N(0)$ are the probabilities of gamma-ray emission at 90° and 0° to the axis of orientation. In our case

$$\varepsilon = (\tfrac{15}{7} B_2 f_2 - \tfrac{25}{3} B_4 f_4)/(1 + \tfrac{5}{7} B_2 f_2 - 5 B_4 f_4). \quad (4)$$

The values of f_2 and f_4 are fully determined by the quantity $\beta = \mu H/kTI$, where μ is the magnetic moment of the Sb^{122} nucleus equal to 1.9 nuclear magnetons,[22] H is the effective magnetic field at the Sb nuclei, T is the absolute temperature, and I is the nuclear spin. For small values of β, $f_4 \approx 0$, and $f_2 \approx a\beta^2$, where $a \approx (2/45) I(I+2)$ and consequently

$$\varepsilon \approx \tfrac{15}{7} B_2 f_2 \approx \tfrac{15}{7} B_2 a\beta^2 = \tfrac{15}{7} B_2 a (\mu H/kTI)^2. \quad (5)$$

From expressions (2) it is possible to find that $-3/14 \le B_2 \le 1$. However, negative values of B_2 are excluded by the fact that the experimental value of ϵ is positive. Therefore $0 < B_2 \le 1$. Substituting in (5) the values of μ and I for Sb^{122} and taking the square root, we obtain

$$\sqrt{\varepsilon} \approx 3.0 \cdot 10^{-8} \sqrt{B_2}\, H/T. \quad (6)$$

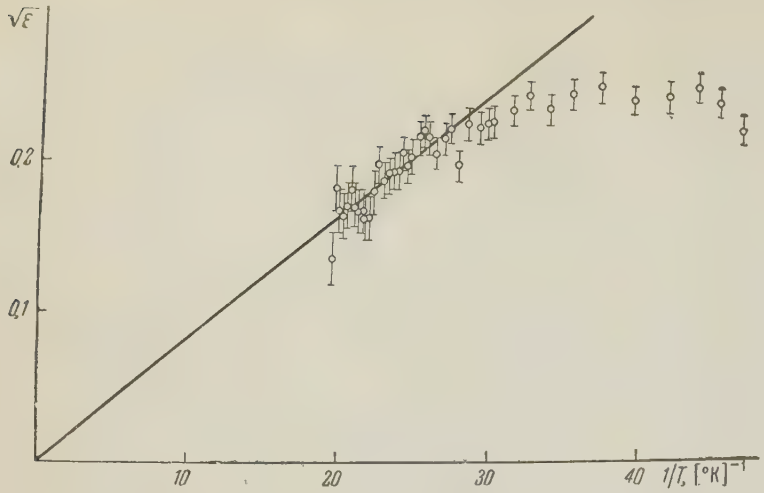

FIG. 4. The dependence of $\sqrt{\epsilon}$ on 1/T for 566-kev gamma radiation of Sb^{122}.

The results of one of the experiments with Sb^{122} are shown on Fig. 3. Figure 4 gives the experimental dependence of $\sqrt{\epsilon}$ on 1/T for Sb^{122}, calculated from Fig. 3. It can be seen that the experimental points fit well on a straight line. The deviations from the straight line for small T are essentially due to the fact that in this temperature region the temperature of the sample differs from that of the salt. From expression (6) and from the slope of the linear portion of the experimental curve of Fig. 4, it can be found that $H \approx 2.8 \times 10^5/\sqrt{B_2}$ oe. Since $0 < B_2 \leq 1$, H must be greater than or equal to 2.8×10^5 oe. Unfortunately, we still do not have data which would enable us to narrow the bounds of B_2, although it is almost obvious that very small (~ 0.1) values of B_2 are highly improbable. Thus from the results obtained it is possible to determine only the lower limit of the field value on the Sb nuclei in the Sb-Fe alloy, namely $H \geq 2.8 \times 10^5$ oe. The degree of polarization of the Sb^{122} nuclei is $f_1 = \bar{I}_z/I \geq 30\%$ for $T = 0.03°K$.

Experiments with Au^{198}

The sample of Au-Fe alloy contained 0.3% Au by weight. It is known that the solubility of gold in iron at 600° C is 0.6% (reference 20). The activity of the Au^{198} nuclei, which were produced in the sample as a result of irradiation in a reactor, amounted during the experiments to $2-3\,\mu C$. The anisotropy of the gamma radiation with an energy of 411 kev (the $2^+ \xrightarrow{E2} 0^+$ transition), emitted after the beta decay (the $2^- \rightarrow 2^+$ transition) of oriented Au^{198} nuclei, was measured. This case is completely identical with the above case of Sb^{122} and therefore expressions (1) — (5) are applicable to Au^{198}. Substituting in (5) I = 2, and the value of μ for Au^{198} which is 0.5 nuclear magnetons,[22] we obtain for small β

$$\sqrt{\varepsilon} \approx 0.79 \cdot 10^{-8} \sqrt{B_2} H/T. \qquad (7)$$

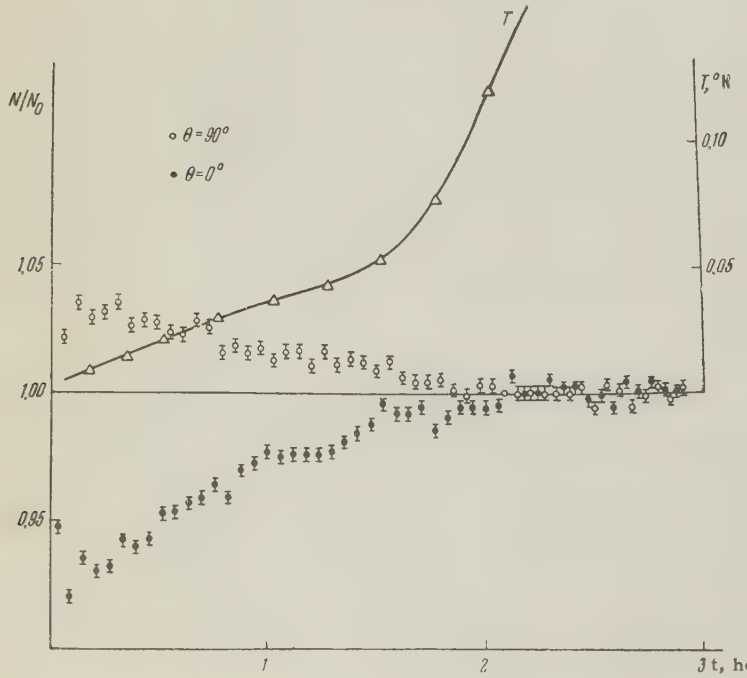

FIG. 5. The dependence of the gamma-ray intensity of Au^{198} on the time after the demagnetization of the salt.

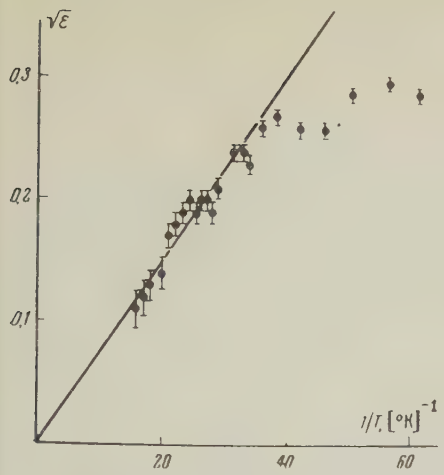

FIG. 6. The dependence of $\sqrt{\epsilon}$ on 1/T for 411-kev gamma radiation of Au^{198}.

Figure 5 shows the results of one of the experiments with Au^{198}, and Fig. 6 shows the experimental dependence of $\sqrt{\epsilon}$ on 1/T obtained from these results. From (7) and the slope of the linear portion of the experimental curve of Fig. 6 it can be found that $H \approx 1.0 \times 10^6/\sqrt{B_2}$ and since $0 < B_2 \leq 1$, $H \geq 1.0 \times 10^6$ oe for Au^{198}. For $T = 0.03°K$ the degree of polarization of Au nuclei is $f_1 = \bar{I}_z/I \geq 30\%$.

Experiments with In^{114m}

The sample of the In-Fe alloy, containing In^{114m} radioactive nuclei, was prepared by alloying metallic indium, previously irradiated in a reactor, with iron. About the solubility of indium in iron, unfortunately, nothing is known. The indium content of the sample was 0.12% by weight, and the activity of the In^{114m} nuclei (the number of decays) was $\sim 10\,\mu C$. In^{114m} nuclei disintegrate basically (96.5%) by gamma transition ($5^+ \xrightarrow{E4} 1^+$) with an energy of 192 kev. The anisotropy of the quanta emitted during this transition was measured. Because of the large conversion coefficient, the number of these quanta per decay is only equal

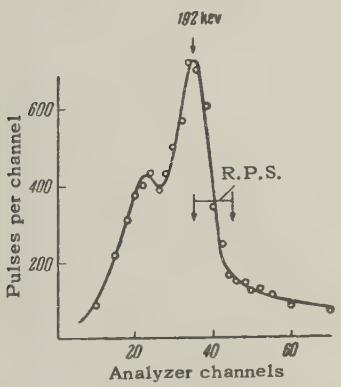

FIG. 7. The gamma-ray spectrum of In^{114m} (R.P.S. – the registered portion of the spectrum).

to 0.18. Figure 7 shows the gamma spectrum of the sample when it is in its operating position inside the Dewar flask. The spectrum was measured by a detector placed at an angle of 0° with respect to the field of the small magnet. As can be seen from Fig. 7, only pulses corresponding to the right half of the gamma-ray photopeak with an energy of 192 kev were registered. This was done in order to exclude the effect of gamma rays scattered by various parts of the device near the source.

The angular distribution of gamma rays with an energy of 192 kev, emitted by oriented In^{114m} nuclei, is of the following form:*

$$N(\vartheta) = 1 - 2.61 f_2 P_2(\cos\vartheta) + 4.97 f_4 P_4(\cos\vartheta) + 1.71 f_6 P_6(\cos\vartheta) - 75 f_8 P_8(\cos\vartheta). \quad (8)$$

For small values of β all terms, except the one depending on f_2, can be neglected, and, using the value of the nuclear magnetic moment for In^{114m}, equal to 4.7 nuclear magnetons,[22] and I = 5, it is possible to obtain the following expression for the anisotropy of the gamma rays:

$$\sqrt{\epsilon} \approx 8.5 \cdot 10^{-8} H/T. \quad (9)$$

The results of two experiments with In^{114m} are shown on Figs. 8a and b. Soon after the start of the second experiment, the sample was heated from ~ 0.01 to $\sim 0.03°K$. It can be seen that this heating was accompanied by a sharp decrease in the anisotropy of the gamma radiation. From a comparison of the temperature curve after the heating with the change in the counting rate, it is possible to conclude that the time for the establishment of thermal equilibrium between the sample and the salt was ~ 20 min.

From the results of the experiment shown in Figs. 8a and b the experimental dependence of $\sqrt{\epsilon}$ on 1/T for In^{114m}, shown in Fig. 9, was obtained. Figure 9 also shows the theoretical curve $\sqrt{\epsilon}(1/T)$ calculated with formula (8), taking into account terms which contain f_2 and f_1. The initial portion of this curve coincides with the experimental points and from its slope, using (9), it is possible to obtain the value of the field on the In^{114m} nuclei $H = 2.47 \times 10^5$ oe. The polarization of the In nuclei is $f_1 = \bar{I}_z/I = 50\%$ at $T = 0.03°K$.

Measurements of the anisotropy were also carried out with Cd^{114} for gamma rays with energies of 540 and 720 kev that are emitted after K capture in In^{114m}. Since the angular distribution of the quanta of these two gamma transitions is the same (a case analogous to the emission of 1170- and 1330-kev gamma quanta in the decay of Co^{60}), they were registered simultaneously. From these measurements a value $H = 2.3 \times 10^5$ oe, coinciding within 10% with that given earlier, was obtained.

*This formula was obtained by L. D. Puzikov.

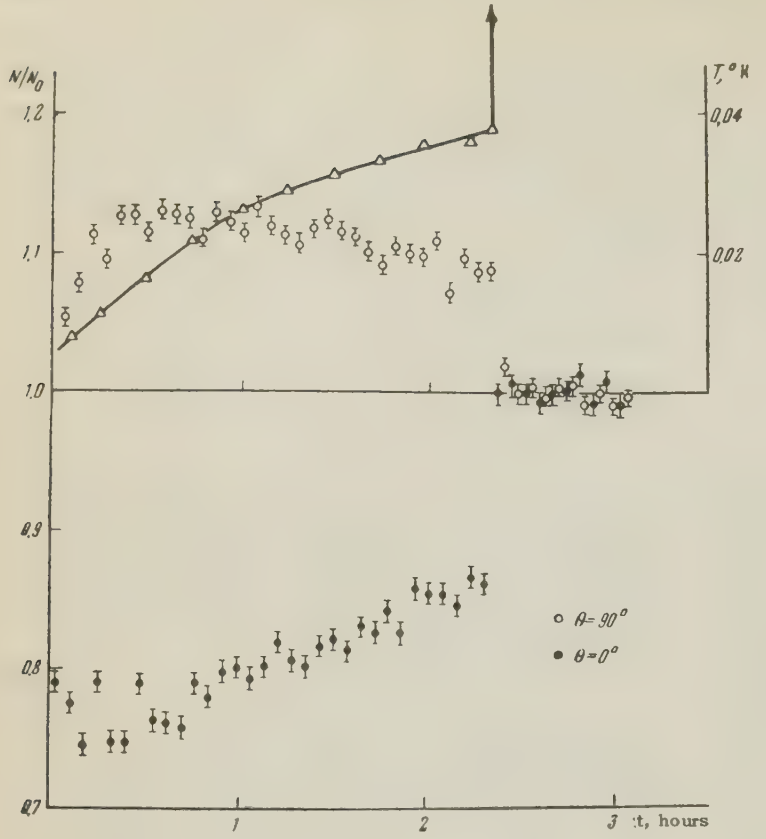

a

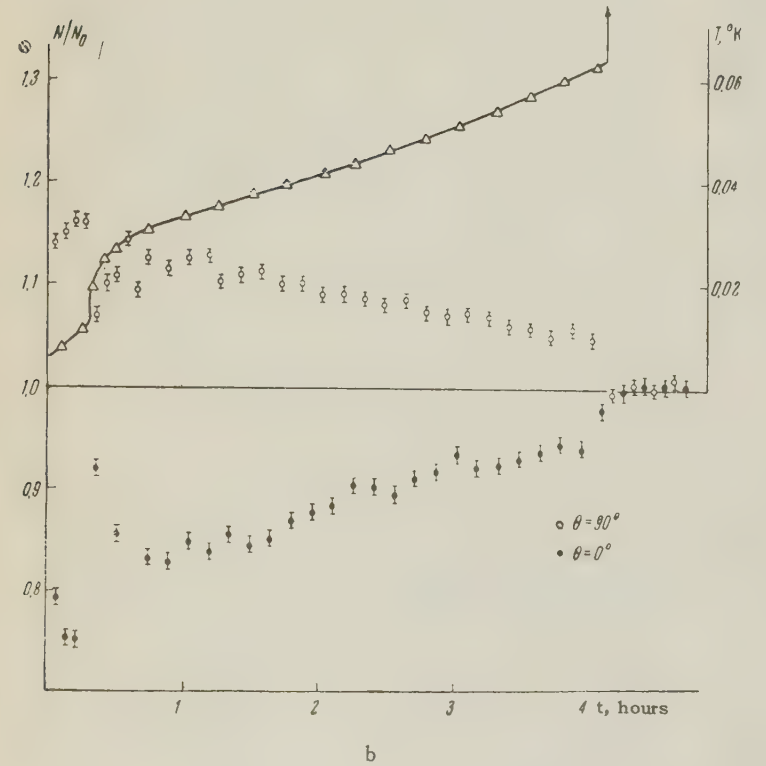

b

FIG. 8. The dependence of the 192-kev gamma-ray intensity of In^{114m} on the time after the demagnetization of the salt in various temperature intervals: a – first experiment, b – second experiment. The notation is the same as in Fig. 3.

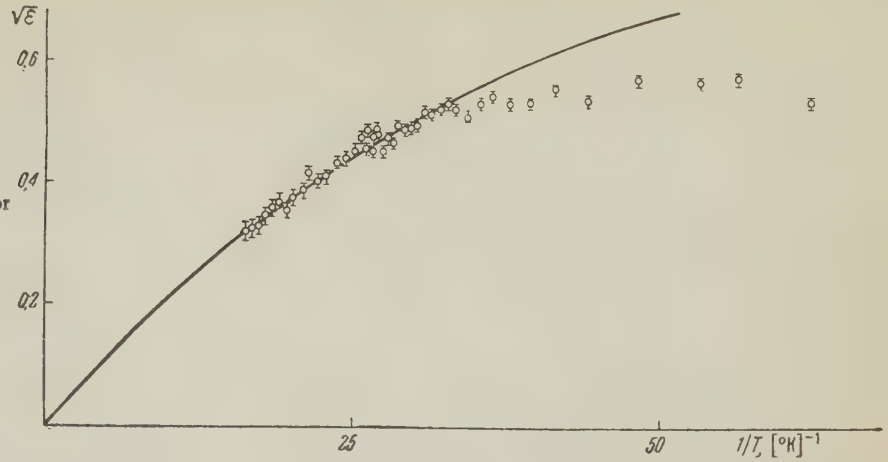

FIG. 9. The dependence of $\sqrt{\epsilon}$ on 1/T for 192-kev gamma radiation of In^{114m}.

Inasmuch as it remains unknown what portion of the indium entered into the alloy with iron, the values obtained can only be considered the lower limit of the magnetic field on the indium nuclei in the In-Fe alloy. We also carried out experiments with a sample of In-Fe alloy which contained 0.6% In by weight. The value of the anisotropy at 0.03°K turned out to be 10%. From this it is possible to conclude that the solubility of indium in iron is less than 0.6% but hardly less than 0.12%, i.e., the true value of the magnetic field on the In nuclei in the In-Fe alloy does not differ greatly from that found in the experiments with the In-Fe alloy containing 0.12% In.

A summary of the results obtained is given in the table.

The element dissolved in the iron	Au	Sb	In
Content of the element by weight	0,3	0,6	0,12
The radioactive nucleus	Au^{198}	Sb^{122}	In^{114m}
ε_γ, % } for $T = 0.03°$ K	6	8	28
f_1 }	$\geqslant 0.3$	$\geqslant 0.3$	$\geqslant 0.5$
H, oe	$\geqslant 1 \cdot 10^6$	$\geqslant 2.8 \cdot 10^5$	$\geqslant 2.5 \cdot 10^5$

4. DISCUSSION OF RESULTS

It follows from the stated results that the introduction of weakly magnetic elements into a ferromagnet is, apparently, a universal method for the polarization of nuclei. This method is based on the fact that a strong magnetic field on the order of 10^6 oe acts upon the nuclei of weakly magnetic elements dissolved in the ferromagnet. As was already stated in an earlier paper,[11] the most probable explanation of the source of this field (first shown to us by E. K. Zavoĭskiĭ) is that it is created by the conduction electrons, which in ferromagnets have a substantial degree of polarization. The determination of the value of this field is of independent interest for the theory of ferromagnetism.

Recently, Marschall[23] investigated the "contact" magnetic field created on the nuclei of a ferromagnet by the conduction electrons. For the value of this field he used the following expression:

$$H_c = -(8\pi/3)\,\mu_0\,|\psi(0)|^2\,nP_{\text{eff}},$$

where μ_0 is the Bohr magneton, $|\psi(0)|^2$ is the mean square value of the s-electron wave function at the nucleus, which can be estimated from the value of the atomic hyperfine-structure constants of a free atom, P_{eff} is the polarization of the conduction electrons. According to Marschall, P_{eff} consists of two terms. The first is due to the direct effect of the d-shell magnetic moments of the atoms on the conduction electrons; the second term is due to the exchange interaction of s and d electrons. A comparison of Marschall's estimates with the results of experiments on the polarization of Co^{60} nuclei in metallic cobalt leads to a value $P_{\text{eff}} \sim 10\%$.

The mechanism investigated by Marschall is, apparently, also applicable to our case, if it is assumed that the conduction electrons are polarized near the iron atoms and go over to the neighboring impurity atoms without reorientation. Unfortunately, it is still impossible to compare the experimental values of the fields on the nucleus with the theoretical values, which are merely estimates. Concerning the experimental values, it was possible in the cases which we investigated to determine only their lower limits. However, we propose later on to find in a number of cases the actual values of the fields (accurate within 10 — 20%) both by measuring the anisotropy of the gamma radiation emitted after allowed beta transitions, and by measuring the anisotropy of the beta radiation.

We intend also to investigate the value of the field on nuclei of elements introduced into various ferromagnets. The measurements of the gamma-ray anisotropy of In^{114m} in an indium-nickel alloy

which have already been carried out yielded a negative answer (accurate within 0.5%). This result is of interest from the point of view of recent widely discussed ideas[24] about two different types of electron structures of transition metals. According to these ideas, the d shells of the atoms of such metals as nickel and cobalt differ little from the d shells of free Ni and Co atoms, and the total number of conduction electrons per atom is only ~ 0.5. Iron and, apparently, the rare earths belong to another type. In iron atoms, for instance, six of the eight d electrons are collectivized and are in the conduction band.

The authors consider it their pleasant duty to express their deep gratitude to E. K. Zavoĭskiĭ and L. V. Groshev for their constant interests in the work, to L. D. Puzikov for help in the theoretical calculations, to V. M. Galitskiĭ and D. P. Grechukhina for a discussion of the work, to G. P. Mel'nikov for the construction of the necessary radio devices, to V. N. Agureev, I. B. Filippova, and N. V. Razzhivina for help in carrying out the experiments, and also to N. E. Yakovich, V. A. Drozdov, and V. D. Sheffer who provided an uninterrupted supply of liquid helium.

Note added in press (January 18, 1960): Until very recently we, unfortunately, did not know the paper by Beun et al.[25] on the connection between the magnetic and thermodynamic temperatures in potassium chrome alum. If in the processing of our results we had used the data of the above paper, the values of the fields on the nuclei of gold, antimony, and indium, would have been lower by 25 — 35%.

[1] B. Bleaney, Proc. Phys. Soc. **A64**, 315 (1951).
[2] C. J. Gorter, Physica **14**, 509 (1948); M. E. Rose, Phys. Rev. **75**, 213 (1949).
[3] R. V. Pound, Phys. Rev. **76**, 1410 (1949).
[4] G. R. Khutsishvili, JETP **29**, 894 (1955), Soviet Phys. JETP **2**, 766 (1956).
[5] Grace, Johnson, Curti, Scurlock, and Taylor, Comm. Conf. de Physique de basses Temperatures, Paris, 1955, p. 263.
[6] A. W. Overhauser, Phys. Rev. **92**, 411 (1953).
[7] C. D. Jeffries, Phys. Rev. **106**, 164 (1957).
[8] F. M. Pipkin and J. W. Culvahouse, Phys. Rev. **109**, 1423 (1958).
[9] F. M. Pipkin, Phys. Rev. **112**, 935 (1958).
[10] Samoĭlov, Sklyarevskiĭ, and Stepanov, JETP **36**, 644 (1959), Soviet Phys. JETP **9**, 448 (1959).
[11] Samoĭlov, Sklyarevskiĭ, and Stepanov, JETP **36**, 1944 (1959), Soviet Phys. JETP **9**, 1383 (1959).
[12] B. S. Dzhelepov and L. K. Peker, Схемы распада радиоактивных ядер, (Decay Schemes of Radioactive Nuclei), Acad. of Sciences Press, 1958.
[13] B. N. Samoĭlov, Dokl. Akad. Nauk SSSR **86**, 281 (1952).
[14] B. N. Samoĭlov, J. Tech. Phys. (U.S.S.R.) **22**, 888 (1952).
[15] N. Kurti and F. Simon, Phil. Mag. **26**, 849 (1938).
[16] K. Warmuth, Arch. Elektrotech. **33**, 747 (1939).
[17] A. H. Cooke, Proc. Phys. Soc. **A62**, 269 (1949).
[18] de Klerk, Steenland, and Gorter, Physica **15**, 649 (1949).
[19] Kurti, Robinson, Simon, and Spohr, Nature **178**, 450 (1956).
[20] M. Hansen, The Structure of Binary Alloys, Russ. Transl., 1941.
[21] H. A. Tolhoek and J. A. M. Cox, Physica **19**, 101, 673 (1953).
[22] Strominger, Hollander, and Seaborg, Revs. Modern Phys. **30**, 585 (1958).
[23] W. Marschall, Phys. Rev. **110**, 1280 (1958).
[24] N. Mott and K. Stevens, Phil. Mag. **2**, 1364 (1957).
[25] Beun, Miedema, and Steenland, Physica **23**, 1 (1957).

Translated by Z. Barnea
83

INVESTIGATIONS OF THE REACTIONS (α, α'), (α, p) AND (α, t) ON LITHIUM NUCLEI

K. V. MAKARYUNAS and S. V. STARODUBTSEV

Leningrad Physico-technical Institute, Academy of Sciences, U.S.S.R.

Submitted to JETP editor August 7, 1959

J. Exptl. Theoret. Phys. (U.S.S.R.) **38**, 372-378 (February, 1960)

The angular distribution of the reaction $Li^7(\alpha, \alpha')Li^{7*}$ ($Q = -4.61$ Mev) for the bombarding α-particle energy $E_\alpha = 13.2$ Mev and also the angular distributions of the reactions $Li^7(\alpha, t)Be^8$ ($Q = -2.56$ Mev), $Li^6(\alpha, p)Be^9$ ($Q = -2.13$ Mev), and $Li^7(\alpha, p)Be^{10}$ ($Q = -2.56$ Mev) for $E_\alpha = 10.15$, 11.5, and 13.2 Mev were investigated.

The results can be derived from direct interaction theories. From an interpretation of the experimental angular distribution of the reaction (α, α') within the framework of Butler's theory it follows that the parity of the 4.61 Mev level in the Li^7 nucleus is negative and the spin is equal to one of the following four values: $1/2$, $3/2$, $5/2$, $7/2$.

1. INTRODUCTION

In many papers published in recent years it has been shown that many nuclear reactions proceed without formation of a compound nucleus. This pertains also to reactions due to α particles with energy ranging from several Mev to several times ten Mev, as a result of which the final nucleus remains in the ground state or in a not too excited state.

Symptoms of direct processes in a nuclear reaction are the asymmetry of the angular distribution of the secondary particles with respect to the plane perpendicular to the direction of the beam of bombarding particles (in the center-of-mass system) and relatively weak dependence of the form of the angular distribution on the energy. A characteristic symptom of reactions that proceed via a compound nucleus, to the contrary, is symmetry of the angular distribution relative to the aforementioned plane. An asymmetrical distribution in the case when a compound nucleus is formed is possible only when the reaction goes through a small number of overlapping levels of the compound nucleus of unequal parity, but in this case the form of the angular distribution should be sensitive even to slight changes in the energy.[1]

A simple approximate formula for the differential cross section of direct nuclear reactions was given by Austern, Butler and McManus.[2] The differential cross section was expressed in terms of the linear combination of the squares of spherical Bessel functions $j_l^2(|\mathbf{q}|R)$, where Q is the wave vector of the recoil nucleus, R a certain radius, and l the quantum number of the orbital angular momentum, acquired (or lost) by the nucleus as a result of the collision. Possible values of l are determined by the selection rules

$$|\mathbf{J}_A + \mathbf{J}_B + \mathbf{s}_a + \mathbf{s}_b|_{min} \leqslant l \leqslant J_A + J_B + s_a + s_b \quad (1)$$

and

$$\pi_A \pi_B = (-1)^l, \quad (2)$$

where $\mathbf{J}_A$, $\mathbf{J}_B$, $\mathbf{s}_a$, and $\mathbf{s}_b$ are respectively the spins of the initial and final nucleus and of the incident and emitted particles, π_A and π_B are the parities of the initial and final nucleus. The theory of direct nuclear reactions was later on developed by Butler,[3] who gave a sufficiently general theory (in the Born and plane-wave approximations) of nuclear reactions that occur when bombarding particles interact with weakly bound particles located in the surface region of the nucleus. In particular, it has been shown that in the expression for the differential cross section of direct nuclear reactions, interference terms may appear. Formulas for the differential cross section given by Butler, Austern, et al. were derived specifically for reactions on nuclei which can be described by the nuclear-shell model, but similar formulas can be obtained also when using other nuclear models.[4-6]

The formulas of Butler, Austern, et al. are suitable for describing angular distributions which are directed forward and which have an oscillating structure. Owen and Madansky[7] have considered the mechanism of "stripping of a heavy particle," which produces a peak in the angular distribution at angles close to 180°.

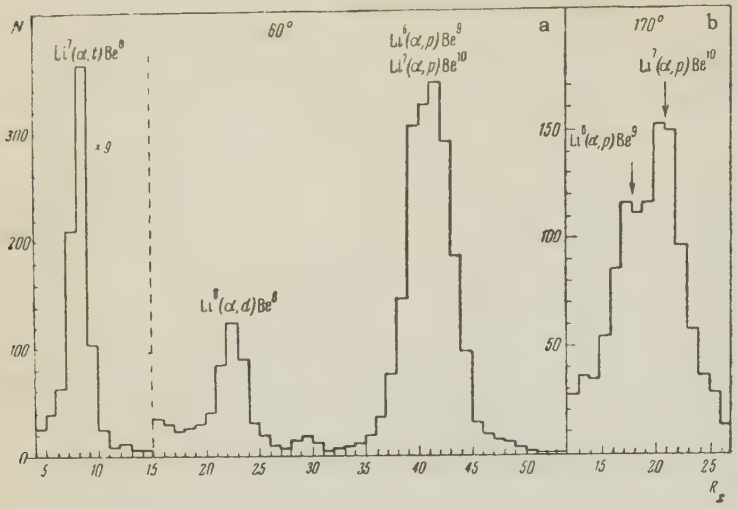

FIG. 1. Track spectra at $E_\alpha = 13.2$ Mev. The abscissas represent the horizontal projection of the track length, a – $\theta_{lab} = 60°$, thickness of aluminum foil in the cassette window $d_{Al} = 62\ \mu$, each division of the horizontal scale corresponds to 5.07 μ; b – $\theta_{lab} = 170°$, $d_{Al} = 8\ \mu$, one division of the horizontal scale = 2.535 μ.

2. MEASUREMENT PROCEDURE

The experiments were performed with the cyclotron of the Leningrad Physico-technical Institute, which produces accelerated particles of different energies (in the experiments reported in this article, α particles of energies 10.15, 11.5, and 13.2 Mev were used). A scattering chamber 50 cm in diameter was attached to the cyclotron. A target was placed in the center of the chamber, surrounded at a radius of 20 cm by special cassettes containing photographic plates (type Ya-2, emulsion thickness 100 μ). The average angle between the plane of the photographic emulsion in the cassette and the direction of particle motion from the target was 10°. The scattering chamber and the cassettes employed made it possible to investigate angular distributions in the range from 10 to 170°, in steps of 5 or 10°, but since the particle energy from the Li + α reaction diminishes very rapidly with scattering angle in the laboratory system, in practice only several high-energy particles could be registered at large angles.

The targets were made by rolling metallic lithium of natural isotopic composition in an atmosphere of dry carbon dioxide. The targets employed were 0.75 – 1.1 mg/cm^2 thick.

The plates, exposed and developed in a standard manner, were scanned with a MBI-3 microscope The lengths of the tracks were measured and the energy spectra of the particles and angular distributions of particle groups were determined. The groups of tracks were associated with the different particles produced in the various reactions by studying the changes in the track lengths with scattering angle.

The absolute values of the differential cross sections obtained in different experiments did not deviate from their average values by more than 30 or 40%.

3. RESULTS AND THEIR DISCUSSION

A. Track groups. In scanning the photographic plate under the microscope, many intense track groups were found. Among the short-range tracks (shorter than the tracks of the elastically scattered α particles), the most intense was a group due to the inelastic scattering reaction $Li^7(\alpha, \alpha')Li^{7*}$ (Q = – 4.61 Mev). Among the long range tracks, the most intense were groups from the reactions $Li^7(\alpha, t)Be^8$ (Q = – 2.56 Mev), $Li^6(\alpha, d)Be^8$ (Q = – 1.59 Mev), $Li^6(\alpha, p)Be^9$ (Q = – 2.13 Mev), and $Li^7(\alpha, p)Be^{10}$ (Q = – 2.56 Mev). The particles from the two last reactions form a single group (see track spectrum at $\theta_{lab} = 60°$ in Fig. 1a) and begin to separate only at large scattering angles (Fig. 1b). What is striking is the large intensity of the triton and deuteron groups.

B. Angular distributions of the reaction $Li^7(\alpha, \alpha')Li^{7*}$ (Q = – 4.61 Mev). The angular distribution of the α particles inelastically scattered by Li^7 (Q = – 4.61 Mev) at energy E_α = 13.2 Mev, is shown in Fig. 2 (experimental points). The errors indicated are the sum of the corresponding statistical errors, the errors in the determination of the solid angle, and the errors which possibly occurred in the separation of track groups (similar errors are indicated also for the other angular distributions). The transverse cross section of the reaction is very large: the section estimated by integrating the angular distribution from 15 to 90° (in the c.m.s.), is 147 ± 60 mb. In a comparison with the Butler theory,[3] under the assumption that the single-particle level of the unpaired proton from the p shell is excited, it is found that it is impossible to obtain a theoret-

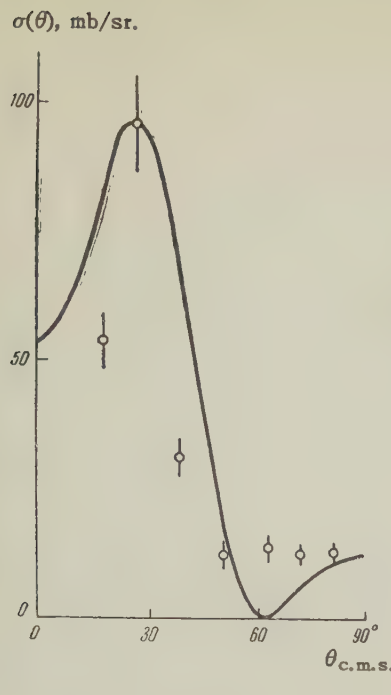

FIG. 2. Experimental and theoretical Butler angular distributions of the reaction $Li^7(\alpha,\alpha')Li^{7*}$ ($Q = -4.61$ Mev) at $E_\alpha = 13.2$ Mev.

ical curve that fits satisfactorily the experimental one, but the forward peak of the experimental angular distribution can be sufficiently well compared with the peak of the Butler curve with $l = 2$ and radius $R = 5.6 \times 10^{-3}$ cm (curve on Fig. 2). This fact, in accordance with the selection rules (1) and (2) and the known spin and parity of the ground state of the Li^7 nucleus $(3/2^-)$,[8] indicates clearly that the 4.61-Mev level of Li^7 has negative parity. The value of the spin can be assumed here to be one of the following four: $1/2$, $3/2$, $5/2$, and $7/2$.

It is seen from Fig. 2 that the experimental peak is narrower than the theoretical one. In explaining this circumstance it must be kept in mind that Butler's theory does not take into account adequately the scattering of the incident and elastically-scattered particles in the field of the nucleus, i.e., the distortions of the plane waves. A refinement of this theory in this sense, as is known, leads indeed to a narrowing of the peaks.[9,10]

C. Angular distributions of the reactions $Li^6(\alpha, p)Be^9$ ($Q = -2.13$ Mev) and $Li^7(\alpha, p)Be^{10}$ ($Q = -2.56$ Mev). The angular distributions of the protons from these reactions in the laboratory system at $E_\alpha = 10.15$, 11.5, and 13.2 Mev are shown in Fig. 3 [the ordinates represent $0.925\,\sigma_{Li^7}(\theta) + 0.075\,\sigma_{Li^6}(\theta)$]. The points with different labels were obtained in different experiments. The same diagram shows curves 1 and 2 corresponding to the isotropic angular distributions of the protons from the reactions $Li^7(\alpha, p)Be^{10}$ and $Li^6(\alpha, p)Be^9$ in the c.m.s.

Since the groups of protons from the two reactions are not separated, and their c.m.s. are somewhat different, an exact recalculation of the angular distribution to the c.m.s. is impossible. Figure 4 shows as an illustration the approximate angular distribution of the protons in the c.m.s. at $E_\alpha = 11.5$ Mev [the additional errors in the recalculation are $\Delta\theta < 1°$, $\Delta\sigma(\theta) < 5\%$].

It is seen from Figs. 3 and 4 that the angular distributions in the c.m.s. are sharply anisotropic and are asymmetrical with respect to $\theta = 90°$. Their shape changes as the α-particle energy varies from 10.15 to 13.2 Mev, but the similarity between the two is retained, which can be considered as an indication of the important role of the process, which takes place in addition to the production of a compound nucleus. The maximum at angles close to 180° (Fig. 4) is apparently connected with the mechanism of the "stripping of the heavy particle." It is still difficult to say more about the details of the mechanism of the reactions, for it is not known whether both reactions proceed without formation of the compound nucleus, or only one of them.

D. Angular distributions of the reaction $Li^7(\alpha, t)Be^8$ ($Q = -2.56$ Mev). The angular distribution of the tritons of the reaction $Li^7(\alpha, t)Be^8$ ($Q = -2.56$ Mev) at $E_\alpha = 10.15$ Mev is shown in Fig. 5 (experimental points). At other energies, up to 14.7 Mev, very similar angular distributions are observed.[11] The form and energy dependence of the angular distributions point to the importance of the role of the direct-interaction mechanism.

When a more detailed picture of the direct-interaction mechanism in the $Li^7(\alpha, t)Be^8$ reaction is established, it appears more likely to consider the triton produced in this reaction as consisting of nucleons belonging prior to the collision to the Li^7 nucleus rather than to He^4. Actually, the reaction is due to the collision of two light nuclei, which do not differ greatly in their masses, but have substantially different structures: the He^4 nucleus is very strongly bound and compact, while Li^7 is weakly bound and "loose." According to the shell model, the Li^7 nucleus should be considered as consisting of four s-nucleons in the filled shell, forming the α particle, and three outer p-nucleons. Following Brueckner's idea[12] we can assume that the outer p-nucleon can form something by nature of a triton and the Li^7 nucleus can be considered at different times as if consisting of an α particle and a triton. It appears little likely that the $Li^7(\alpha, t)Be^8$ reaction is a result of the stripping of a proton from a strong and compact α particle in the field of a loose Li^7 nucleus. A much more probable process is one similar to the knock-out of tritons from Li^7 by α particles, when the tri-

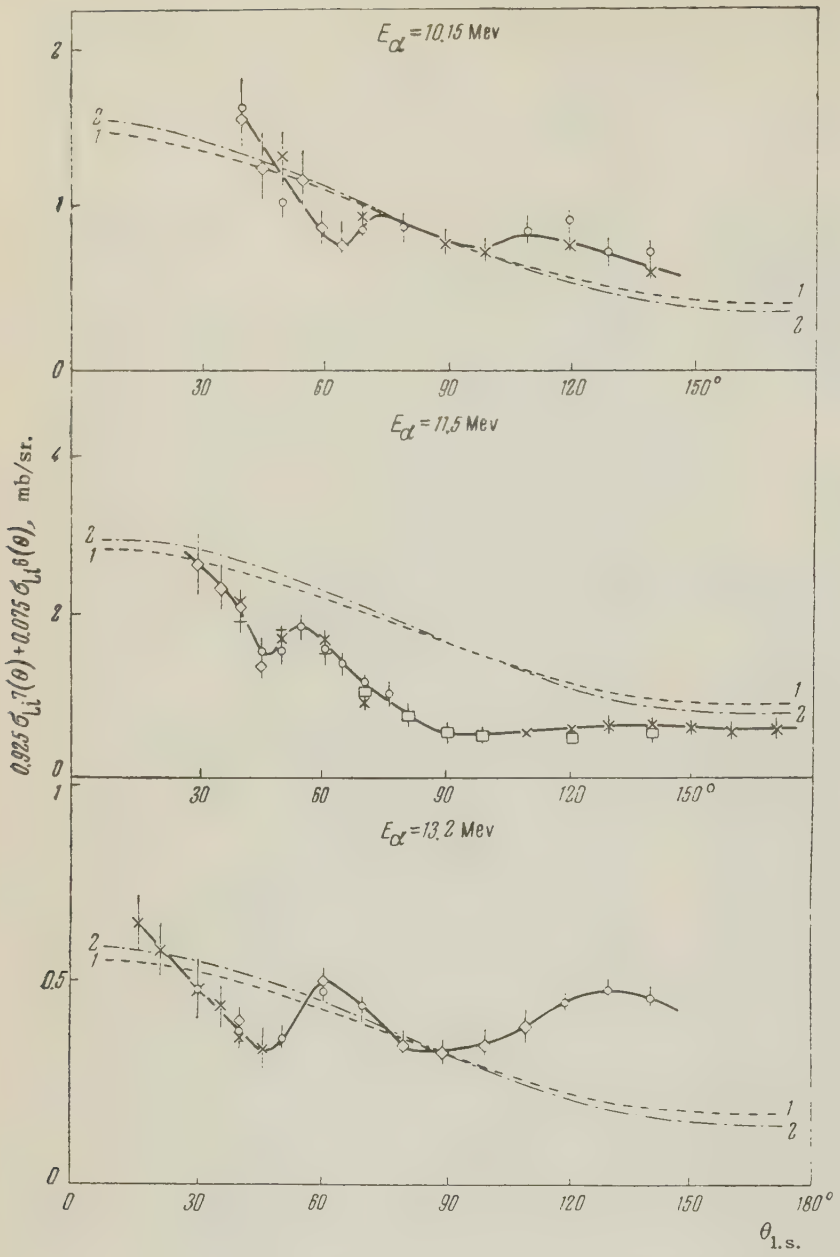

FIG. 3. Angular distribution of the reactions $Li^7(\alpha, p)Be^{10}$ (Q = −2.56 Mev) and $Li^6(\alpha, p)Be^9$ (Q = −2.13 Mev) at E_α = 10.15, 11.5, and 13.2 Mev in the laboratory system.

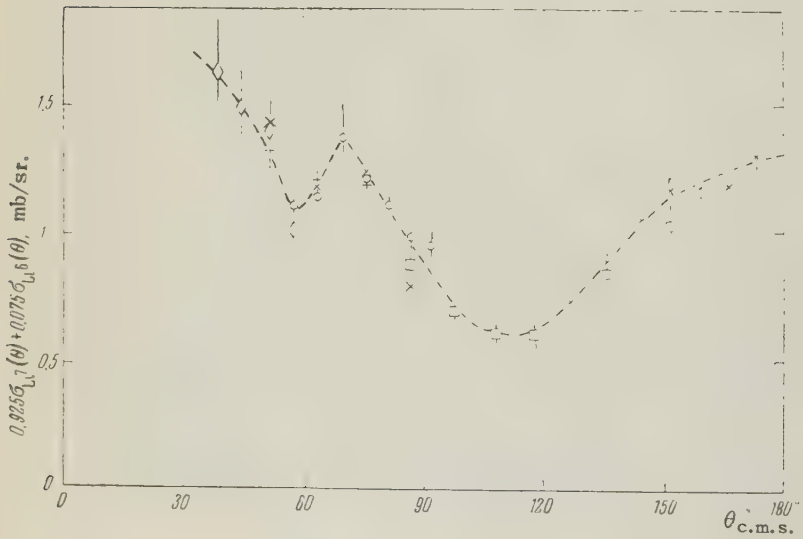

FIG. 4. Angular distribution of the reactions $Li^7(\alpha, p)Be^{10}$ (Q = −2.56 Mev) and $Li^6(\alpha, p)Be^9$ (Q = −2.13 Mev) at E_α = 10.5 Mev in the c.m.s.

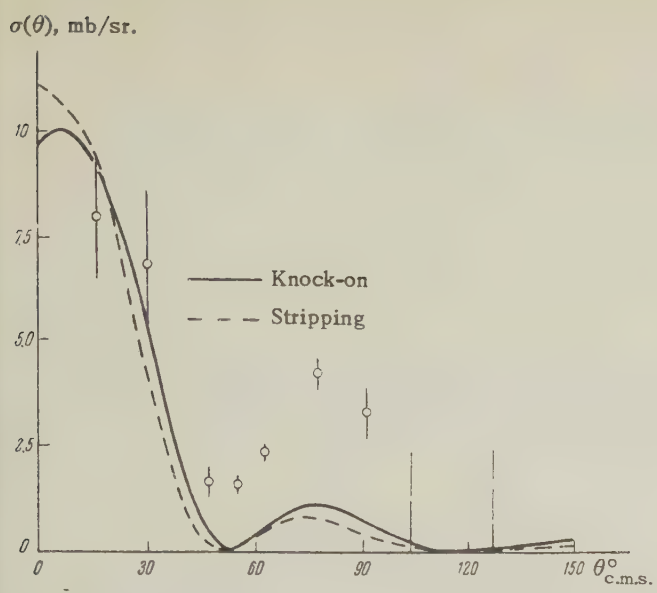

FIG. 5. Experimental and theoretical angular distributions of the reaction $Li^7(\alpha, t)Be^8$ (Q = −2.56 Mev) at E_α = 10.15 Mev.

ton contained in the Li^7 leaves this nucleus as a result of the collision, and the remaining α particle captures the incoming α particle into the Be^8 nucleus. A curve calculated on the basis of such a model with Butler's formula[3] for $l = 1$ (the only possible value compatible with the known values of the spins and parities of the nuclei participating in the reaction[8]), $R = 10 \times 10^{-13}$ cm and $|\mathbf{q}| = \frac{4}{7}|\mathbf{k}_\alpha - \frac{7}{8}\mathbf{k}_t|$ (where $\mathbf{k}_\alpha$ and $\mathbf{k}_t$ are respectively the wave vectors of the α particle and the triton),[13] is shown in Fig. 5. As can be seen, the positions of the maxima of the theoretical and experimental curves are in fair agreement.

The curve calculated from stripping theory (where the α particle is considered as an antisymmetrical deuteron) for $l = 1$, $|\mathbf{q}| = |\mathbf{k}_\alpha - \frac{7}{8}\mathbf{k}_t|$ and $R = 5.6 \times 10^{-13}$ cm is shown dotted in Fig. 5. We see that it is similar to the curve calculated by the knock-on theory.

To obtain a satisfactory agreement between the theoretical curves, calculated by the knock-on theory, the "interaction radius" parameter had to be taken very large: $R = 10 \times 10^{-13}$ cm. When R is reduced the maxima of the theoretical curves broaden and creep towards the larger angles, while the distances between them increase. We note that in explaining the experimental angular distributions of other reactions on light nuclei by means of the knock-on mechanism, it is also necessary to take larger values of the parameter R.[14] This is connected with the fact that in the case when a theory similar to that of Butler is used in the analysis of knock-on reactions, R must be interpreted not as a nuclear radius, but as the distance between the center of gravity of the core of the nucleus (in this case the α particle contained in the Li^7) and the center of gravity of the knocked-on particle (in this case the triton) during the instant of collision. For light nuclei this distance may be much greater than the nuclear radius.

The authors are grateful to the cyclotron crew, headed by A. B. Girshin and also to the staff of the Laboratory of Nuclear Reactions of the Leningrad Physico-technical Institute, who helped with the performance of the experiments.

[1] J. Blatt and V. Weisskopf, Theoretical Nuclear Physics, Wiley, N.Y., 1952.

[2] Austern, Butler, and McManus, Phys. Rev. **92**, 350 (1953).

[3] S. T. Butler, Phys. Rev. **106**, 272 (1957).

[4] J. S. Blair and E. M. Henley, Phys. Rev. **112**, 2029 (1958).

[5] S. Hayakawa and S. Yoshida, Progr. Theoret. Phys. **14**, 1 (1955); Proc. Phys. Soc. **A68**, 656 (1955).

[6] S. Yoshida, Proc. Phys. Soc. **A69**, 668 (1956).

[7] G. E. Owen and L. Madansky, Phys. Rev. **99**, 1608 (1955); **105**, 1766 (1957).

[8] F. Ajzenberg and T. Lauritsen, Rev. Mod. Phys. **27**, 77 (1955).

[9] W. Tobacman, M. H. Kalos, Phys. Rev. **97**, 132 (1955).

[10] S. Butler and O. H. Hittmair, Nuclear Stripping Reactions, New York-Sydney, 1957.

[11] S. V. Starodubtsev and K. V. Makaryunas, JETP **36**, 1594 (1959), Soviet Phys. JETP **9**, 1133 (1959).

[12] Brueckner, Eden, and Francis, Phys. Rev. **98**, 1445 (1955).

[13] G. F. Pieper and N. P. Heydenburg, Phys. Rev. **111**, 264 (1958).

[14] J. Dabrowski and J. Sawicki, Acta Phys. Polon. **14**, 323 (1955).

Translated by J. G. Adashko
84

POSITRON DECAY OF Ir^{192}

S. F. ANTONOVA, S. S. VASILENKO, M. G. KAGANSKIĬ, and D. L. KAMINSKIĬ

Leningrad Physico-technical Institute, Academy of Sciences, U.S.S.R.

Submitted to JETP editor August 8, 1959

J. Exptl. Theoret. Phys. (U.S.S.R.) **38**, 379-383 (February, 1960)

Positron decay of Ir^{192} ($T_{1/2}$ = 74 days) has been detected with the relative intensity 1.5×10^{-7} positron per decay and end-point energy 240 ± 10 kev. The total Ir^{192}-Os^{192} transition energy is 1950 kev. The conversion-electron spectrum above 1 Mev was measured. A new 1088-kev γ transition was detected.

1. INTRODUCTION

Ir^{192} is known to decay to Pt^{192} through β^- emission and to Os^{192} through electron capture. According to Wapstra[1] an Ir^{192}-Os^{192} transition through positron decay is also energetically possible. This decay has heretofore not been detected; in references 2 and 3 its intensity was estimated at less than 10^{-6} positron per decay.

2. EXPERIMENTAL PROCEDURE

Our measurements were obtained with the magnetic beta-ray spectrometer described in references 4 and 5. Iridium sources were prepared by thermal-neutron irradiation of metallic iridium deposited on 5 μ aluminum foil by means of cathode sputtering in an argon atmosphere. Material containing 99.92% Ir, 0.03% Pt and 0.02% Rh was sputtered. 18 × 8 mm sources were used. The spectrometer resolution was 1.5% with the solid angle 0.5% of 4π.

3. POSITRON SPECTRUM OF Ir^{192}

Correct allowance for the background is very important for the study of a very weak positron spectrum in the presence of intense beta and gamma radiation. The background is usually measured by shifting the source with respect to the slit placed before it so that beta rays with normal trajectories cannot enter the spectrometer. The background can also be measured when the diaphragm aperture is closed, but both procedures generally modify the background in such a way as to distort the results. Our beta-ray spectrometer was designed to permit background measurements by a different technique.

In our spectrometer the beta-ray beam which had traversed the first counter after being focused in a sectorial magnetic field was refocused by a magnetic lens, which thus served as a second monochromator. Figure 1B shows the instrumental line for the magnetic lens that was obtained in measuring the electron spectrum. With constant current maintained in the magnet the lens focused beta rays in a small energy range which was determined from the spectrometer resolution. At the same time the background electrons have a very flat energy distribution since the background results mainly from Compton electrons, ejected by gamma rays in the region of the first counter, which enter the first counter and are subsequently focused at the second counter, as well as from beta rays undergoing multiple scattering at the walls and baffles. Consequently, when the lens current is varied within certain limits while the magnet current remains constant the registered radiation will not change much if it results from the background. However, if positrons focused by the sectorial field are being registered the beam intensity will vary as shown by the curve in Fig. 1B. Figure 1A shows how the coincidence intensity observed by us in the study of the Ir^{192} positron spectrum depends on the lens current. Here the background a can be very sim-

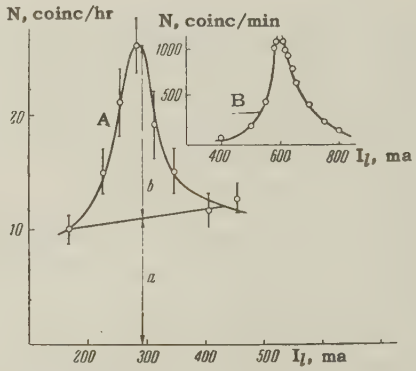

FIG. 1. A) dependence of counting rate on lens current in measurement of Ir^{192} positron spectrum (a – background, b – positrons); B) dependence of counting rate on lens current for β^- spectrum of Ir^{192}.

ply separated from the positron spectrum. The principal advantage of the given technique for background measurements lies in the fact that the position of the source and the conditions for beam passage are not varied.

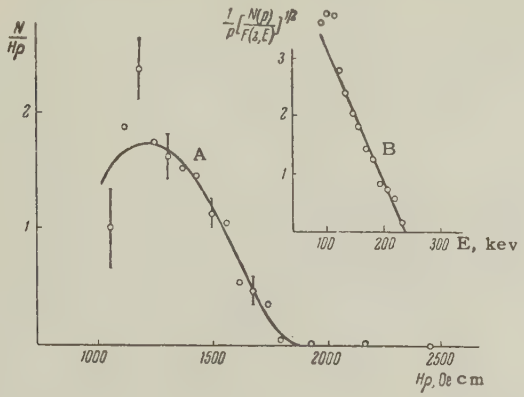

FIG. 2. A) Ir^{192} positron spectrum; B) Fermi plot for positron spectrum.

The positron spectrum of Ir^{192} is shown in Fig. 2 (curve A), where the background was taken into account and a correction was made for the dependence of detector efficiency on positron energy, just as in the case of the earlier work described in reference 5. A Fermi plot (Fig. 2B) shows that the positron spectrum results basically from β^+ decay with end-point $E_0 = 240 \pm 10$ kev. The half-life of the positron spectrum is estimated to be $T_{1/2} = 120 \pm 60$ days. On the basis of the end-point and half-life the observed spectrum is assigned to positron decay of Ir^{192}. Available data[6] indicate that the observed β^+ spectrum cannot be accounted for by impurities.

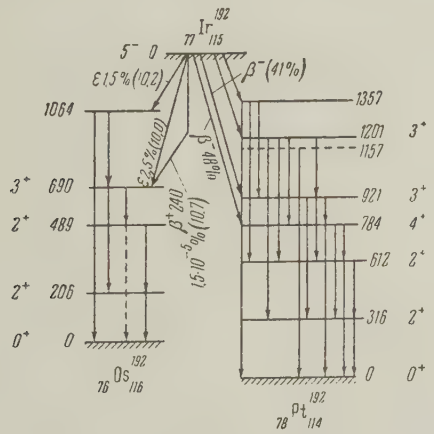

FIG. 3. Ir^{192} decay scheme.

Figure 3 shows the decay scheme[6] of Ir^{192} including the observed β^+ decay. Because of the relatively low statistical accuracy of the experimental data the corresponding unique shape of the β^+-decay spectrum was not determined. The total Ir^{192}-Os^{192} decay energy is 1950 ± 10 kev according to our data, in good agreement with the value 2050 kev obtained by Wapstra using a different procedure.[1]

By comparison with the β^- spectrum the β^+-decay intensity was determined to be $(1.5 \pm 0.4) \times 10^{-7}$ positron per decay. The observed spectrum is the weakest of the partial β spectra known at the present time. According to the decay schemes in reference 6 the K-capture intensity in Ir^{192} with a transition to the 690-kev excited state of Os^{192} is 2.5%. The K-capture to β^+-decay intensity ratio thus becomes $J_K/J_{\beta^+} = 1.6 \times 10^5$, which is about eight times larger than the result obtained by a calculation based on previously published data for allowed transitions[7,8] but which agrees very well with Zyryanova's results[9] for unique transitions.

4. INTERNAL CONVERSION SPECTRUM OF Ir^{192} GAMMA RADIATION ABOVE 1 Mev

The high-energy γ transitions that accompany Ir^{192} decay exhibit low intensities, the data for which are inadequate and to a certain extent inconsistent. No data have been available for the internal conversion spectrum of these hard gamma rays. We have investigated the spectrum of conversion electrons produced by gamma rays with energies above 1 Mev by means of the same apparatus that was used to measure the positron spectrum. The low background and negligible effect of scattered radiation make this spectrometer, as is evident from the data given below, a convenient instrument for investigating the internal conversion of very weak gamma radiation ($10^{-4} - 10^{-5}$ quanta per decay) when the conversion lines lie outside the β^- spectrum.

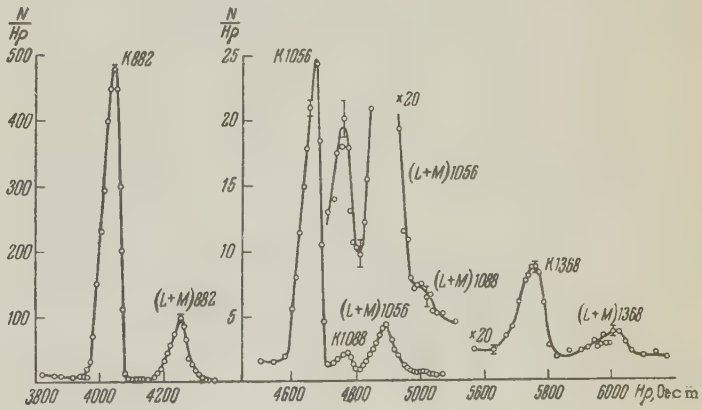

FIG. 4. Spectrum of Ir^{192} conversion electrons.

The results are shown in Fig. 4. We have included measurements of previously investigated

E_γ, kev	882±5	1056±5	1088±10	1368±10
Internal conversion ratio K/(L + M)	4.05	5.40	4.80	3.70
Multipolarity	*E*2 *	*E*1	*E*1 (*M*1)	*E*3 (*M*3)
Relative intensity of K-conversion lines	100	5.6	0.22	0.23
Relative gamma-ray intensity	100	21	0.8 (0.1)	0.3 (0.08)
Gamma-ray intensity	100	27 [10], 16 [11]	—	0.6±0.5 [12]

*E2 according to reference 3.

conversion lines resulting from a 882-kev gamma ray for the purpose of comparing intensities. Three gamma rays, with 1056, 1088 and 1368 kev, were observed in the energy region above 1 Mev. The difference between the K- and L-conversion energies indicates that the 1056-kev quantum is converted in Os^{192} while the other two quanta are converted in Pt^{192}. An analysis of the conversion spectrum yields the energies, multipolarities and relative intensities of these gamma rays, which are given in the table.

Multipole orders were determined from the K/L ratios with M-conversion taken into account through the ratio L/M = 3.5. Whenever a unique multipole order could not be determined a second less likely type is given in parentheses. Correspondingly, two values of the relative intensity are presented. The table shows that the 1056- and 1368-kev intensities agree in general with values given in the literature.[10-12]

The 1088-kev gamma ray was the first to be observed. This transition cannot be included in the Ir^{192} decay scheme shown in Fig. 3 without introducing an additional level. According to our data the 1056-kev transition is of type E1, which, as shown by the Ir^{192} decay scheme, disagrees with the value of log τf for the corresponding K-capture branch and with the relative intensity of the 1060- and 374-kev gamma rays.

It should be noted that, like the authors of reference 12, we failed to detect 1157- and 1201-kev gamma radiation. The corresponding intensities must in any event be considerably lower than those reported in references 11 and 13.

[1] A. H. Wapstra, Physica **21**, 367 (1955).

[2] B. S. Dzhelepov and O. E. Kraft, Izv. Akad. Nauk SSSR, Ser. Fiz. **20**, 318 (1956), Columbia Tech. Transl. p. 293.

[3] Baggerly, Marmier, Boehm, and Du Mond, Phys. Rev. **100**, 1364 (1955).

[4] D. L. Kaminskiĭ and M. G. Kaganskiĭ, Приборы и техника эксперимента (Instruments and Measurement Engg.) **1**, 32 (1959).

[5] Antonova, Vasilenko, Kaganskiĭ, and Kaminskiĭ, JETP **37**, 667 (1959), Soviet Phys. JETP **10**, 477 (1960).

[6] B. S. Dzhelepov and L. K. Peker, Схемы распада (Decay Schemes), Acad. Sci. Press, M.-L., 1958.

[7] B. S. Dzhelepov and L. N. Zyryanova, Влияние электрического поля атома на бета-распад (Influence of the Atomic Electric Field on Beta Decay), Acad. Sci. Press, M.-L., 1956.

[8] Band, Zyryanova, and Ch'eng-Jui, Izv. Akad. Nauk SSSR, Ser. Fiz. **20**, 1387 (1956), Columbia Tech. Transl. p. 1269.

[9] L. N. Zyryanova, Izv. Akad. Nauk SSSR, Ser. Fiz. **23**, 875 (1959), Columbia Tech. Transl., in press.

[10] B. S. Dzelepov and Yu. V. Hol'nov, Nuovo cimento **3**, Suppl. **1**, 49 (1956).

[11] M. W. Johns and S. V. Nablo, Phys. Rev. **96**, 1599 (1954).

[12] Delyagin, Kuznetsova, and Shpinel', Izv. Akad. Nauk SSSR, Ser. Fiz. **20**, 909 (1956), Columbia Tech. Transl. p. 825.

[13] Pringle, Turchinetz, and Taylor, Phys. Rev. **95**, 115 (1954).

Translated by I. Emin
85

FISSION OF Th^{232} *BY 14.9-Mev NEUTRONS*

A. N. PROTOPOPOV, M. I. KUZNETSOV, and É. G. DERMENDZHIEV

Radium Institute, Academy of Sciences, U.S.S.R.

Submitted to JETP editor August 10, 1959

J. Exptl. Theoret. Phys. (U.S.S.R.) **38**, 384-386 (February, 1960)

The energy characteristics of Th^{232} fission induced by 14.9-Mev neutrons were measured with a double ionization chamber with grids. The most probable total kinetic energy and fragment mass ratio were measured and found equal to (157 ± 4) Mev and (1.43 ± 0.05) respectively. The most probable values of the masses of the heavy and light fission fragments are (140 ± 3) and (92 ± 3). Data are obtained which confirm the influence of nuclear shells on fission.

In the investigation of the energy characteristics of the fission of heavy nuclei it was noted[1,2] that the dependence of the kinetic energy of the fragments on their mass ratio exhibits more or less sharply pronounced maxima. It was shown here[2] that in all cases the position of the maxima corresponds to those mass ratios, for which the heavy fragment has a mass number close to 132. A less pronounced maximum is observed at mass ratios for which the light fragments have a mass number in the 82 — 84 region. A hypothesis has been advanced that the increase in the kinetic energy of the fragment at definite mass ratios is connected with the formation during the fission process of heavy fragments with closed shells of 50 protons and 82 neutrons (A = 132) and light fragments with a closed shell of 50 neutrons (A = 82 — 84).

In connection with the fact that the question of the influence of nuclear shells on the fission process is of considerable interest, further experimental data must be accumulated in this field. For this purpose we undertook an investigation of the energy characteristics of the fission of Th^{232} by 14.9-Mev neutrons.

A measurement of the energies of the Th^{232} fission fragments was made by means of a double ionization chamber with grids, with simultaneous recording of the amplitudes of the pulses produced by paired fission fragments.[3] The collimation angle of the fragments was 45°. To reduce the influence of the anisotropy of fission and of the motion of the center of mass of the fragments on the result of the measurements, the neutron beam was aimed at an angle of 3 — 5° to the plane of the target. The bombarding neutrons were obtained from the T(d, n)α reaction.

A thorium target weighing 70 μg/cm² was made by sputtering in an electric field from an alcohol solution of thorium nitrate on a film 25 — 30 μg/cm² thick with subsequent conversion of the hygroscopic thorium nitrate into non-hygroscopic thorium oxide by a method described in the paper by Selitskiĭ.[4] The purity of Th^{232} was determined from the α spectrum plotted with an ionization α spectrometer.

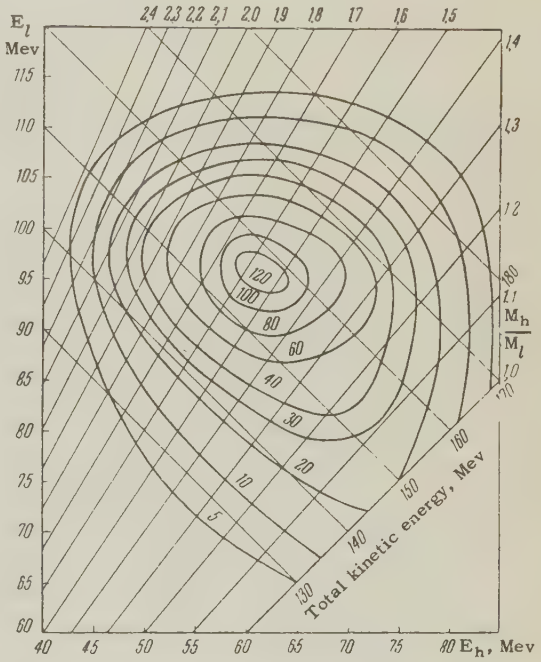

FIG. 1. Contour map of Th^{232} fission by 14.9-Mev neutrons. The subscripts h and *l* refer to heavy and light fragments respectively.

The energy calibration of the apparatus was by comparison with the energies of the α particles from Am^{241} and Th^{232}. A total of 12,500 fission events were observed. The fission-fragment energy was corrected for the ionization defect and for losses in the substrate of the target and in the

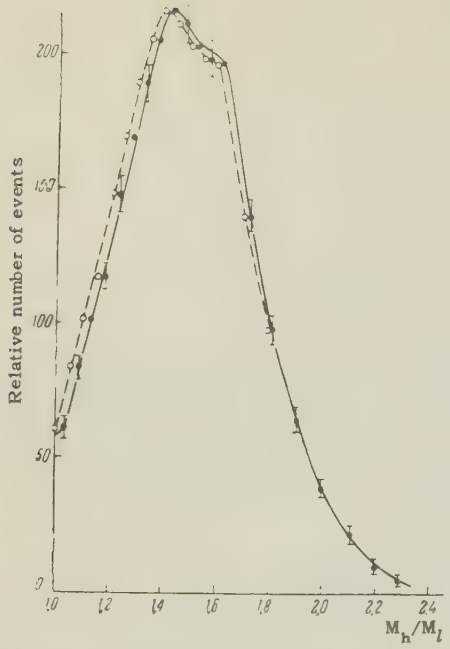

FIG. 2. Fission probability as a function of the mass ratio of the fragments: o – uncorrected data, • – corrected for dropping of neutrons.

collimator. The measurement results are shown on the contour diagram (Fig. 1).

Figure 2 shows the dependence of the probability of fission on the fragment mass ratio. The same diagram shows a curve plotted with allowance for the discarding of neutrons by the fragments.[5] In introducing the corrections it was assumed that the average number of emitted neutrons per fission event was 4.64,[6] and that one neutron evaporates prior to fission. The most probable mass ratio is 1.43 ± 0.05. These data have been used to calculate the most probable masses of the heavy and light fragments, found to be 140 ± 3 and 92 ± 3 respectively.

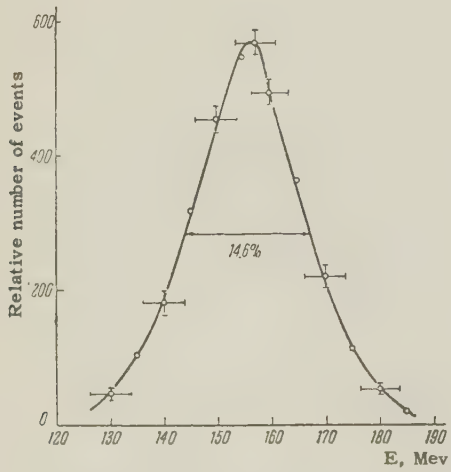

FIG. 3. Distribution of total kinetic energy of Th^{232} fission fragments.

FIG. 4. Dependence of the most probable total kinetic energy of Th^{232} fission fragments on the fragment mass ratio (the statistical errors are indicated).

The distribution of the total kinetic energy of fission fragments is shown in Fig. 3. The half width of the energy distribution is 14.6%. The most probable kinetic energy is 157 ± 4 Mev.

The dependence of the most probable total kinetic energy of fission fragments on their mass ratio is shown in Fig. 4. The curve shows clearly two maxima of kinetic energy at fragment mass ratios 1.32 and 1.8.

Figure 5 shows the dependence of the dispersion of the energy distribution on the ratio of fragment masses. The maximum dispersion is at a mass ratio 1.17. A slight increase in dispersion is noticeable in the region of mass ratio 1.8.

In accordance with the results of reference 2, one might expect that in fission of Th^{232} an increase should be observed in the total kinetic energy of the fragments at mass ratios 1.32 and 1.83. The data obtained in the present work are in good agreement with these values. At the same mass ratios, one might expect also an increase in the dispersion of the total kinetic energy. However, as follows from Fig. 5, the position of the first maximum (1.17) differs considerably from the expected value. This discrepancy is possibly due to an increase in the apparatus dispersion, owing to the great thickness of the thorium layer.

In conclusion, the authors express their indebtedness to Yu. A. Selitskiĭ for preparing the thorium target.

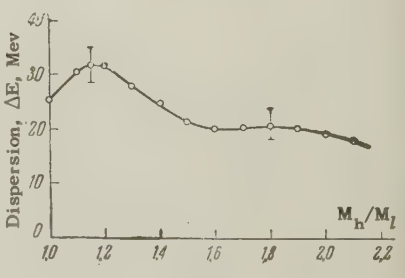

FIG. 5. Dependence of the dispersion of the energy distribution on the fragment mass ratio. The statistical errors are indicated.

[1] D. C. Brunton and G. C. Hanna, Phys. Rev. **75**, 990 (1949).

[2] Protopopov, Baranov, Selitskiĭ, and Éĭsmont, JETP **36**, 1932 (1959), Soviet Phys. JETP **9**, 1374 (1959).

[3] A. N. Protopopov and V. P. Éĭsmont, Атомная энергия (Atomic Energy) **6**, 644 (1959).

[4] Yu. A. Selitskiĭ, ibid, in press.

[5] J. S. Fraser, Phys. Rev. **88**, 536 (1952).

[6] R. B. Leachman, Second United Nations Intern. Conf. on the Peaceful Uses of Atomic Energy, Geneva, 1958, rep. 15 (P) 2467.

[7] Smith, Fields, Friedman, and Sjoblom, Phys. Rev. **111**, 1633 (1958).

[8] H. A. Tewes and R. A. James, Phys. Rev. **88**, 860 (1952).

Translated by J. G. Adashko
86

SINGLE SCATTERING OF 10 — 30 Mev NEGATIVE MUONS ON CARBON

A. I. ALIKHANIAN, V. G. KIRILLOV-UGRYUMOV, L. P. KOTENKO, E. P. KUZNETSOV, and A. V. SAMOĬLOV

P. N. Lebedev Physics Institute, Academy of Sciences, U.S.S.R.

Submitted to JETP editor August 11, 1959

J. Exptl. Theoret. Phys. (U.S.S.R.) **38**, 387-393 (February, 1960)

Single scattering of μ^- mesons in a propane bubble chamber was measured. About 60,000 μ^- meson stoppages were measured. For the scattering analysis 48,100 stopped μ^- mesons possessing energies between 10 and 30 Mev were chosen. Observations were carried out on 1260 carbon nuclear path lengths traversed by the μ^- mesons. The differential angular distribution can be satisfactorily described by a Mott scattering curve if account is taken of the finite size of the nucleus. The present experiment shows that the cross section for "anomalous" scattering (if it exists) through an angle $> 45°$ cannot exceed 1.25×10^{-28} cm^2 per nucleon for the energies under consideration and does not exceed 0.7×10^{-28} cm^2 per nucleon for scattering through an angle $> 90°$. Not one case of μ^- decay of the $\mu^- \rightarrow e^+ + e^- + e^-$ type was detected in the 60,000 stoppage events.

INTRODUCTION

THE measured value of the muon magnetic moment, the cross section for the production of muon pairs by photons, and data on mesic atoms all give grounds for assuming that, at least in the region of small energies, the scattering of muons by nucleons should be the same as that of electrons having the same mass as the muons. On the other hand, on the basis of the analysis of the experimental angular distributions of muons, many authors have concluded the existence of "anomalous" scattering, which is not in agreement with the concluded purely-electromagnetic interaction between muons and nuclei (see, for example, the survey by Fowler and Wolfendale in reference 1, and also reference 2).

The results of most investigations on muon scattering, performed during the past two years at low energies,[3-6] do not contradict the notion of a muon being an ordinary Dirac particle. The scantiness of the statistical material, however, the difficulty in identifying the particles, and the low accuracies of energy and angle measurements, difficulties all characteristic of research on the scattering of cosmic muons, cast a certain doubt on the presence or absence of "anomalous" scattering.

We have measured single scatterings of negative muons on carbon, contained in the working medium of a propane bubble chamber. An important factor is that by selecting the single-scattering cases, it is possible to compare experiment with theory by using simple and exact equations for the elementary processes and to avoid complicated recalculations and averaging, connected with allowance for repeated and multiple scattering. If there actually exists some sort of non-Coulomb interaction between muons and nuclei, it should manifest itself most clearly in the investigation of single scattering by a light nucleus, such as the carbon nucleus.

EXPERIMENTAL CONDITIONS

The scattering of negative muons was measured in a propane bubble chamber (370×104×100 mm).[7] The chamber was bombarded by negative muons produced in the decay of negative pions in the beam of the proton synchrotron of the Joint Institute for Nuclear Research. The 150-Mev negative pions produced on the inner beryllium target of the proton synchrotron were deflected by the stray field of the accelerator and guided to the chamber through a three-meter collimator. The negative pions and negative muons were slowed down in front of the chamber by a copper absorber and stopped within the chamber. The absorber was chosen such as to make the number of stopped negative muons a maximum. To increase the number of stopped muons, a focusing lens was placed at the exit of the collimator, three meters from the chamber; this doubled the number of stopped muons. To register the scattering of high energy muons, three copper plates, each 0.5 cm thick, were placed in the chamber. The operating cycle of the chamber amounted to 4 — 10 seconds. The chamber was photographed with three "Industar-23" lenses (F = 110 mm),

located opposite the plates mounted in the chamber. An average of three or four stopped muons were registered in each photograph. A total of 60,000 such muons was registered.

REDUCTION OF EXPERIMENTAL DATA

We have investigated single scatterings of negative muons scattered and stopped in the working matter of the chamber. Mesons with true range greater than 1.5 cm, corresponding to energies greater than 10 Mev, were selected. The stopped negative muon was identified by the μ-e decay.

To eliminate possible subjective errors in scanning, the statistical material was processed in the following manner.

a) Flux and energy spectrum of negative muons. To determine the flux and energy spectrum of the negative muons stopped in the chamber, two independent scannings of the same statistical material (each 50th frame) were performed. After identifying the stopped muons registered in both scannings, using the method described in reference 8, the probability was established of the observer registering a stopped muon in scanning the film. This probability was found to be 0.94 and independent of the muon range. The form of the spectrum is shown in Table I.

TABLE I. Flux and energy spectrum of negative muons stopped in the chamber

Range, cm	$p\beta$ Mev/c	Integral flux of negative muons, based on each 25th frame	Flux corrected for omissions	Flux for all frames
1.50	18.6	1815	1924	48100
2.04	21.9	1684	1785	44625
2.61	25.2	1531	1623	40575
3.30	28.5	1364	1446	36150
4.05	31.8	1218	1291	32275
4.88	35.1	1045	1108	27700
5.76	38.4	873	925	23125
6.71	41.7	694	736	18400
7.75	45.0	485	514	12850
8.82	48.3	308	326	8150
10.00	51.6	153	162	4050

Data obtained by scanning each 25th frame of the film, together with the previously determined probability of observing a stopped negative muon, yields the total flux of muons with ranges greater than 1.5 cm, stopped in the chamber, a value of 48,100 ($\pm$2.3%) events.

b) Scattering of negative muons. In the first scanning, single scatterings by an angle greater than 10°, projected in the plane of the film, were measured on all the frames. Among these, 292 particles were scattered by more than 15° over the entire range of investigated energies. A thorough second scanning of 25% of the frames showed that in the first scanning not a single scattering event was omitted on these frames. One can therefore conclude that the number of omitted scattering events is apparently less than 1.5%, amounting to four events for all the statistical material. The particle energy at the point of scattering and the energy of the negative muons entering the chamber were determined from the residual range. The error in the energy measurement amounted to 1.5%. The energy interval in which the scattering of the muons was investigated was 10 — 30 Mev, corresponding to negative-muon ranges in propane from 1.5 to 10 cm (the propane density at the instant of passage of the particles was 0.4 g/cm^3).

Before the experimental angular distribution of the negative muons scattered by carbon are compared with the theory, several corrections must be introduced into the data, for the finite dimensions of the chamber, for erroneously assigning a scattering event to the wrong angle interval, for negative-pion impurities, and for scattering by hydrogen.

Correction for the finite chamber dimensions. The finite dimensions of the chamber lead to the following two effects when particle scattering is registered.

a) Some of the scattering events are due to a flux not registered by the chamber. When the trajectory of such a scattered muon is rectified for coincidences with its direction prior to scattering, the muon may be found stopped on the chamber wall or on the plate. Owing to this effect, 22 scattering events were excluded. The result of this correction is seen in column 3 of Table II.

b) Another effect, due to the geometry of the chamber, is the reverse of the first — some of the scattered particles enter the chamber walls and become lost to observation. The probability of registering each scattering event was determined experimentally with allowance for the distribution of the μ^- mesons over the section of the chamber, the angle with which the scattered muon enters the chamber, the length of the visible range after scattering, and the scattering angle. The values of the correction factor, averaged over the angle intervals for the entire registered energy spectrum, are listed in Table III. The influence of this correction is shown in column 4 of Table II.

Assignment of particle to the wrong angle interval. The mean square error in measuring the angle amounted to $\sim$ 1.5°. This error is due essentially to the multiple scattering and also to the finite thickness of the track. Considering the deviations in the angle measurement to be Gaussian, the

TABLE II

Angle interval, degrees	Observed number of scattering events	Number of scattering events after introducing corrections					Expected number of scattering events according to model	
		unregistered flux	finite chamber dimensions	error in angle interval	decay of negative pions in flight	scattering by hydrogen	of the finite nucleus	of a point nucleus
1	2	3	4	5	6	7	8	9
15—25	189	178	203	199	178	166	166.6	172.2
25—35	61	55	67	66	56	52	44.57	47.87
35—45	22	19	24	24	23	21	17.77	19.94
45—55	9	8	11	11	11	10	8.81	10.31
55—65	5	5	7	7	7	6	4.91	6,11
65—75	2	2	3	3	3	3	3.06	3.97
75—85	1	1	2	2	2	2	2.02	2.76
85—180	3	2	3	3	3	3	6.35	10,25

TABLE III. Magnitude of the correction factor, averaged over the angle intervals

15 —25°	1.14	65— 75°	1.47
25— 35°	1.22	75— 85°	1.50
35— 45°	1.29	95—105°	1.50
45— 55°	1.36	105—115°	1.47
55— 65°	1.42		

spilling of particles from one interval to the other was calculated (see column 5, Table II).

Correction for negative-pion impurity. In addition to the negative muons, negative pions were also stopped in the chamber. A special scanning has shown that a total of 8700 stopped pions were registered, terminated with visible and neutral stars; this amounts to 18% of the stopped negative muons. Some of the negative pions, decaying in flight, may simulate the single scattering of a negative muon. When selecting negative muons of energy greater than 10 Mev after scattering, this effect may be significant up to angles of 40°. A kinematic calculation has shown that approximately 120 negative pions should decay, judging from the number and spectrum of the stopped negative pions registered by us in the chamber. Among the negative muons produced in these decays, only 32 have energies in the 10 — 30 Mev range and a projected decay angle greater than 15°. The results of this correction are listed in column 6 of Table II.

Correction for scattering by hydrogen. The number of events of Coulomb scattering of μ^- mesons by hydrogen contained in the working substance of the chamber amounts to 7.41% of the number of scattering events by carbon (the correction is indicated in column 7 of Table II).

The seventh column of Table II lists the final angular distribution of the scattered negative muons with allowance for all the corrections.

RESULTS AND DISCUSSION

A total of 204,350 cm of negative-muon range in propane at energies 10 — 30 Mev, amounting to 1,260 nuclear lengths of carbon, were traced. Here, as can be seen from Table II, 263 of single scatterings by carbon were observed, at angles more than 15° in projection on the photographic film. The differential angular distribution of the scattered negative muons is shown in the diagram. The abscissas represent the projected scattering angles, and the ordinates the number of scattering events within the angular interval. The points designate the experimental data. Continuous curves 1 and 2 represent the expected Coulomb scattering by a finite and point nucleus, recalculated for the case of the projected data. The finite dimensions were taken into account by introducing the form factor, obtained in experiments on scattering of electrons by carbon (see appendix). It can be seen that the experimental data are in good agreement with the expected scattering if a finite nuclear dimension is assumed. The significance level obtained with a χ^2 test is 65%. For the curve corresponding to a point nucleus, the agreement is somewhat poor in the angle range from 85 to 180°. The

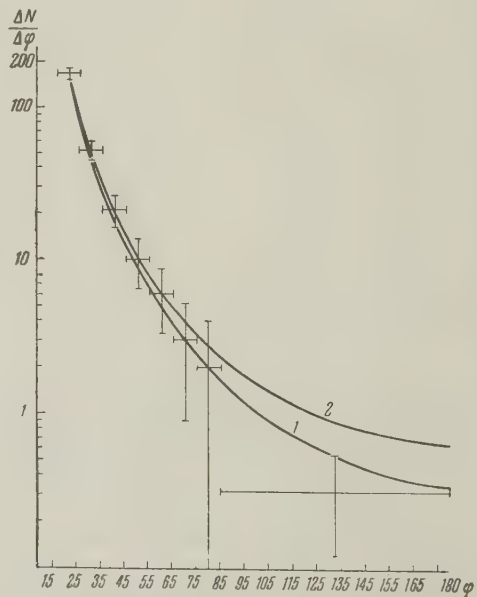

Differential angular distribution of scattered negative muons. φ — projection of the scattering angle on the photographic film. The points represent the experimental data. Curves 1 and 2 — expected Coulomb scattering for a finite and point nucleus respectively.

expected number of events within these angles is 10.25, and the observed is 3 ± 2.1. According to the finite-nucleus model, the expected number of scattering events at these angles is 6.35. Thus, for a single scattering of negative muons at 10 — 30 Mev by a carbon nucleus, no other scattering is observed, with the exception of the ordinary Coulomb scattering. The following estimates can be given for the upper limit of the cross section of "anomalous" scattering, resulting from this experiment (we consider scattering anomalous if it causes an increase in the cross section over that expected from the finite-nucleus model). The cross section of "anomalous" scattering by an angle greater than 45° does not exceed 1.25×10^{-28} cm^2 per nucleon, and that by an angle of 90° does not exceed 0.7×10^{-28} cm^2 per nucleon. The estimate is subject to the condition that the "anomalous" scattering be noted when the excess of the experimental number of scattering events over the theoretical value is greater than one statistical error.

We are now processing the data on single scattering of negative muons at 30 — 50 Mev, namely the muons which have passed after scattering through one of the plates installed in the chamber.

In connection with the increasing recent interest in the possibility of muon decay by the $\mu \to e + e + e$ scheme, we wish to note that in our chamber, from among 60,000 registered muon decays by the $\mu \to e + \nu + \bar{\nu}$ scheme, not a single muon decay into three electrons was observed. This gives a ratio $(\mu \to e + \nu + \bar{\nu})/(\mu \to e + e + e) < 1.7 \times 10^{-5}$.

In conclusion, we express our gratitude to Professor V. P. Dzhelepov for allowing us to perform measurements on the proton synchrotron and for continuous interest in this investigation, and also the staff of the Laboratory of Nuclear Problems, Joint Institute for Nuclear Research, who collaborated in the performance of the experiment, with particular gratitude to N. B. Edovina and V. G. Svyatkina for organizing rapid development of the photographic film as received, and also to A. A. Bednyakov for effective help when working with the accelerator.

APPENDIX

Plotting the theoretical curve.

Single Coulomb scattering of Dirac particles, with allowance for spin, from a point-like nucleus is satisfactorily described, for $Z/137 \ll 1$, by the Mott formula

$$d\sigma_p = \frac{1}{4} Z^2 r_e^2 \left(\frac{m_e c}{p\beta}\right)^2 \sin^{-4}\frac{\theta}{2}\left(1 - \beta^2 \sin^2\frac{\theta}{2}\right) d\Omega, \quad (1)$$

where Z is the nuclear charge, m_e and r_e are the mass and classical radius of the electron, p and β the momentum at the velocity of the incoming particle, and θ the polar scattering angle.

Since we have measured the muon distribution over the projections of the scattering angles on the plane of the photographic film, for comparison with theory one must project Eq. (1) on a plane. When projected, Eq. (1) becomes

$$d\sigma_p = 4Z^2 r_e^2 \left(\frac{m_e c}{p\beta}\right)^2 \left[\frac{\sin\varphi + (\pi - \varphi)\cos\varphi}{\sin^3\varphi} - \frac{\beta^2}{2}\frac{(\pi - \varphi) - 0.5\cdot\pi\cos\varphi}{\sin\varphi\cos\varphi}\right] d\varphi. \quad (2)$$

Here φ is the projection of the scattering angle of the negative muon. We note that at energies of 10 — 30 Mev the spin contribution [second term in the square brackets of formula (2)] does not play any role in the present experiment.

In the transfer of the momenta prevailing in scattering of 10 — 30-Mev muons by carbon nuclei, account must be taken of the influence of the finite nuclear dimensions. This allowance leads to the introduction of a form factor F^2

$$d\sigma_f = F^2 d\sigma_p, \quad (3)$$

where σ_p is the cross section for scattering by a point nucleus, σ_f the scattering cross section by a finite nucleus, and F^2 is a factor that takes into account the charge distribution in the nucleus. The experiments of Fregeau and Hofstadter[9,10] have shown that the distribution of the charge in the carbon nucleus is best described by a form factor obtained on the basis of the oscillator shell model

$$F^2 = [1 - \alpha x^2/2k^2(2 + 3\alpha)]\exp[-x^2/4k^2], \quad (4)$$

where $x = (2a/\lambda\!\!\!^{-})\sin(\theta/2)$, θ is the polar scattering angle, $a = 2.4 \times 10^{-13}$ is the mean square radius of the carbon nucleus, $\alpha = 4/3$, $k^2 = 3(2+5\alpha)/2(2+3\alpha)$. The three dimensional distribution described by formula (3) was projected on a plane to obtain a theoretical distribution of the scattered muons over the projections of the scattering angle, with allowance for the finite nuclear dimensions.

In plotting the theoretical scattering curve, the entire interval of investigated momenta $p\beta$ was broken up into ten sub-intervals with equal $\Delta(p\beta)$. For each such sub-interval, the average scattering cross section was obtained by integration, with allowance for the energy distribution of the muon

flux and under the assumption that the energy losses due to ionization are constant in this interval. The latter approximation leads to an inaccuracy in the cross section for the first sub-interval, where $\Delta(p\beta)/p\beta$, at most, is less than 0.5%. This was followed by calculation of the theoretical value of the number of particles scattered by angles, whose projections are greater than 15°. The ten curves thus obtained were summed over the corresponding angular intervals, and yielded the theoretical differential distribution of particles over the scattering angles.

[1] G. N. Fowler and A. W. Wolfendale, Progress in Elem. Particles and Cosmic Rays, V — IV, Amsterdam 1958, p. 123-153.

[2] N. Bosn and M. Sinha, Proc. Nat. Inst. of Science of India **A24**, 295 (1958).

[3] V. G. Kirillov-Ugryumov and A. M. Moskvichev, JETP **34**, 322 (1958), Soviet Phys. JETP **7**, 224 (1958).

[4] A. I. Alikhanyan and F. R. Arutyunyan, JETP **36**, 32 (1959), Soviet Phys. JETP **9**, 23 (1959).

[5] Kirillov-Ugryumov, Dolgoshein, Moskvichev, and Morozova, JETP **36**, 416 (1959), Soviet Phys. JETP **9**, 290 (1959).

[6] Chidley, Hinmann, Goldstein, Summers, and Adler, Can. J. Phys. **36**, 801 (1959).

[7] Kotenko, Kuznetsov, and Popov, Материалы совещания по камерам Вильсона, диффузионным и пузырьковым камерам (Materials of the Conference on Cloud, Diffusion, and Bubble Chambers), No. III, Dubna, 1958, p. 109.

[8] Bogachev, Mikhul, Petrashku, and Sidorov, JETP **34**, 531 (1958), Soviet Phys. JETP **7**, 367 (1958).

[9] J. H. Fregeau, Phys. Rev. **104**, 225 (1956).

[10] R. Hofstadter, Revs. Modern Phys. **28**, 214 (1956).

Translated by J. G. Adashko
87

TOROIDAL DISCHARGE IN A STRONG MAGNETIC FIELD

G. G. DOLGOV-SAVEL' EV, V. S. MUKHOVATOV, V. S. STRELKOV, M. N. SHEPELEV, and N. A. YAVLINSKIĬ

Submitted to JETP editor August 14, 1959

J. Exptl. Theoret. Phys. (U.S.S.R.) 38, 394-403 (February, 1960)

The results of an investigation of a plasma loop formed in a toroidal chamber with a strong magnetic field are given. When the Shafranov-Kruskal stability condition is satisfied no macroscopic oscillations are observed. The radiation emitted by the plasma in the visible and ultraviolet regions of the spectrum has been studies. It is shown that in a metal chamber with a limiting vacuum of 1 to 2×10^{-6} mm Hg most of the radiated energy is due to impurity ions.

1. INTRODUCTION

A current pinch in a plasma is known to be unstable. A magnetic field is required for stabilization of such a system. One approach is to use a longitudinal field which is uniform over the cross section of the chamber.[1] In this case, H_0, the magnetic field over the entire cross section of the chamber, must be greater than the field due to the discharge current $H_J = 2J/ca$, where a is the radius of the pinch. As has been shown by Shafranov,[2] for stable operation the following condition must be satisfied:

$$H_0 / H_J \geqslant L / 2\pi a, \tag{1}$$

where L is the length of the pinch. In the case of a plasma loop formed in a toroidal chamber of radius R, we have $L = 2\pi R$. If the condition in Eq. (1) is satisfied in the toroid, instabilities characterized by wavelengths $\lambda \sim 2\pi R$ and shorter are suppressed. This method of stabilization, however, does not provide absolute stability. Certain distortions of cylindrical shape of the loop ($m > 1$) remain unstabilized. It can be shown by theoretical analysis, however, that these need not lead to a displacement of the plasma loop with respect to its equilibrium position. In a toroidal system a conducting wall is used in order to contain the current loop, which tends to expand under the influence of the electromagnetic repulsive forces.

The method of stabilization indicated above has a number of advantages; in particular, the pinch stability for $m = 1$ is independent of the distribution of current over the cross section and it is not necessary that the current flow in a thin skin layer. As is shown by theory,[1] for a given value of the current J a plasma loop in a strong longitudinal magnetic field (not interacting with the walls of the chamber) can be heated to a much higher temperature than a toroidal system which is stabilized by a trapped "paramagnetic" field.

We write Eq. (1) in the form:

$$H_0 / (2J / ca) = kR / a, \tag{2}$$

where k is the stability coefficient. Then

$$k = ca^2 H_0 / 2RJ. \tag{3}$$

One of the problems of an experimental investigation of stabilization is that of studying the stability of a plasma loop as a function of k.

2. EXPERIMENTAL ARRANGEMENT. METHOD OF MEASUREMENT

The experiments to be described here have been carried out on a system called "Tokomak," which is a thick-walled copper toroid with a major diameter of 125 cm and a minor diameter of 50 cm, inside which is installed a short-circuit chamber made of stainless steel (wall thickness 0.1 mm). The space between the copper chamber and the inner chamber is evacuated to a pressure of 1×10^{-5} mm Hg. The pressure of the residual gases in the operating chamber is 1 to 2×10^{-6} mm Hg.

The design of the experimental apparatus is due to V. S. Vasil' evskiĭ and his colleagues.

The capacitor bank is discharged through the 19-turn primary winding of an air transformer, inducing a voltage in the toroid circuit and exciting the discharge. A quarter oscillation period for this voltage varies from 1.5 to 3 μsec depending on experimental conditions. The magnetic field in the operating chamber is produced by a coil which is wound on the toroid. This coil is excited by discharging a capacitor bank with a capacity of 0.1 farad at a maximum voltage of 5 kv. The half

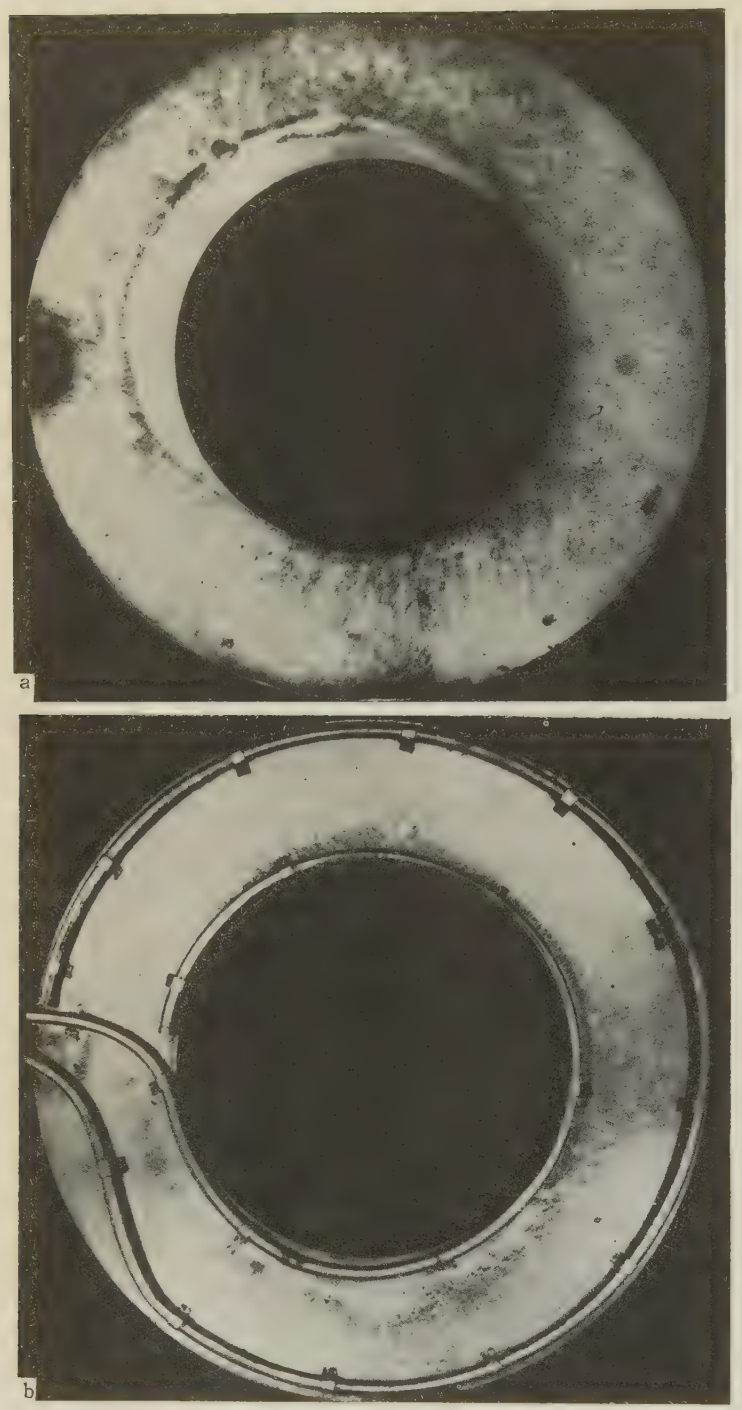

FIG. 1. The diaphragm (which defines the discharge) after several hundred pulses. a) The trace of the ion beam is displaced toward the outer wall of the toroid and upward from the equatorial plane, b) measuring loops on the diaphragm.

period for the magnetic field is 80 μsec. In the present experiments the strength of the longitudinal magnetic field H_0 could be varied from 600 to 12,000 oe. The initial intensity of the electric field along the axis of the chamber could be varied from 0.2 to 0.6 v/cm. The power supply for the system has been described in reference 3.

The work described here has been carried out at pressures ranging from 2×10^{-4} to 5×10^{-3} mm Hg and the operating gases which have been investigated include deuterium, argon and helium.

In order to produce a pinch which remains isolated from the walls of the chamber, thereby reducing the interaction with the walls, the chamber is provided with two diaphragms made of stainless steel 2 mm thick. In the first experiments the apertures in the diaphragms were 26 cm in diameter and the centers of the apertures were on the axis of the toroidal tube.

As is well known, the equilibrium position of a plasma loop in a toroid is displaced with respect to the axis. The photograph in Fig. 1 shows a

diaphragm which was removed from the chamber after several hundred pulses. The plasma loop was displaced toward the outer wall of the chamber and upward. The displacement in the equatorial plane agrees with the calculated displacement. The displacement in the upward direction may be a consequence of some magnetic asymmetry, possibly the effect of fringing fields which penetrate through spaces in the copper shell.

All the principal measurements were carried out with diaphragms in which the apertures were displaced with respect to the axis in accordance with the experimentally determined position of the loop. These diaphragms are furnished with windings. By energizing the diaphragm windings it is possible to change the magnitude and direction of the longitudinal field in regions close to the diaphragms.

On each of the two diaphragms there are two Rogowsky loops. The loops are enclosed in thin-walled tubes of stainless steel. The wall thickness is chosen so that frequencies up to 200 kc are not attenuated. One of these loops is used to measure the current J_g which flows through the apertures in the diaphragm while the other is used to measure the current J_{g+d} which flows through the entire inner cross section of the chamber. In addition, there is a loop which is used to measure the total current J_{tot} which flows in the chamber (including the current in the shell of the inner chamber). By connecting the first and second loops in opposition we measure the current to the diaphragm $J_d = J_{g+d} - J_g$. By measuring the emf in the loop directly we measure the derivative of the current, dJ_g/dt. The loop voltage of the discharge chamber is measured, in the conventional way, by a loop in the equatorial plane of the toroid.

In addition to measuring its electrical characteristics, we investigate other properties of the plasma loop. Streak photographs of the optical radiation of the discharge in the visible region of the spectrum are also taken. A high-speed camera is used for this purpose.

The discharge radiation spectrum is studied with a DFS-6 vacuum spectrometer which is designed (according to its specifications) for the wavelength range between 60 and 2200 A. The time variation of the intensity of the individual spectral lines from deuterium and the impurities is studied by means of a ZMR-3 monochromator which is furnished with an electron photomultiplier at the output slit. The electron concentration in the plasma is estimated by the absorption of microwave radiation (73,000 and 130,000 Mcs). The measurement system is conventional and has been described, for example, in reference 3.

3. RESULTS OF THE MEASUREMENTS

The most interesting results are found in the streak photographs of the pinch. In Fig. 2 are shown streak photographs of a discharge in argon taken with $k_0 = 0.67$, 2.35, and 6.4, where

$$k_0 = ca^2H_0 / 2R\,(J_r)_{max}.$$

It is apparent from Fig. 2a that the pinch is unstable. The luminous region reaches the diaphragm approximately 100 μsec after the discharge is initiated; after 300 μsec the plasma loop moves beyond the limits defined by the aperture in the diaphragm. The photograph shown in Fig. 2b indicates uniform luminosity, and the absence of any marked distortion of the pinch. The photograph in 2c is characterized by uniform luminosity and by the fact the luminosity over the entire cross section of the chamber grows weaker for 600 μsec. In all photographs the radiation is intense in the upper part of the chamber. It is more than likely that this effect

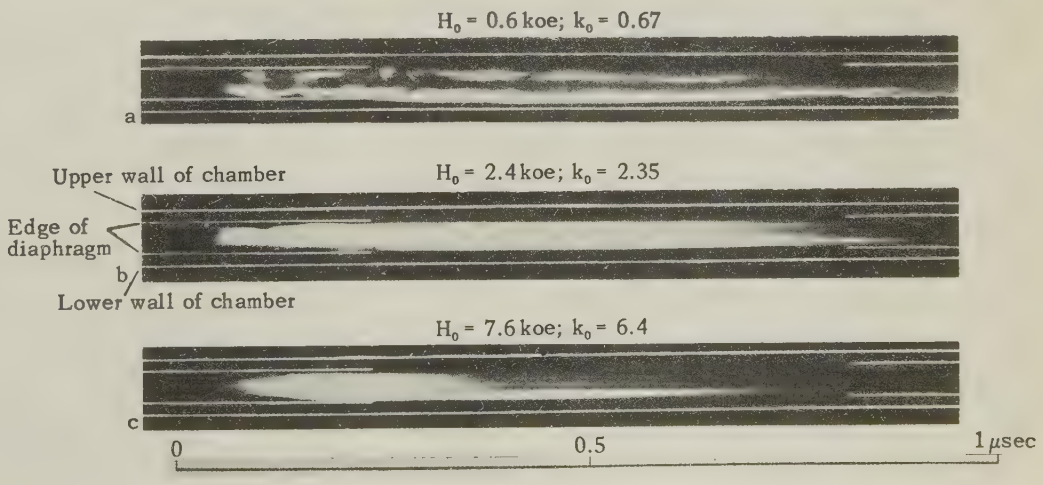

FIG. 2. Streak photographs of a plasma loop limited by diaphragms for different values of H_0 and k_0. The diaphragms are located at distances of 50 and 150 cm along the axis from the window through which the photographs are taken; p = 10^{-3} mm hg (Ar).

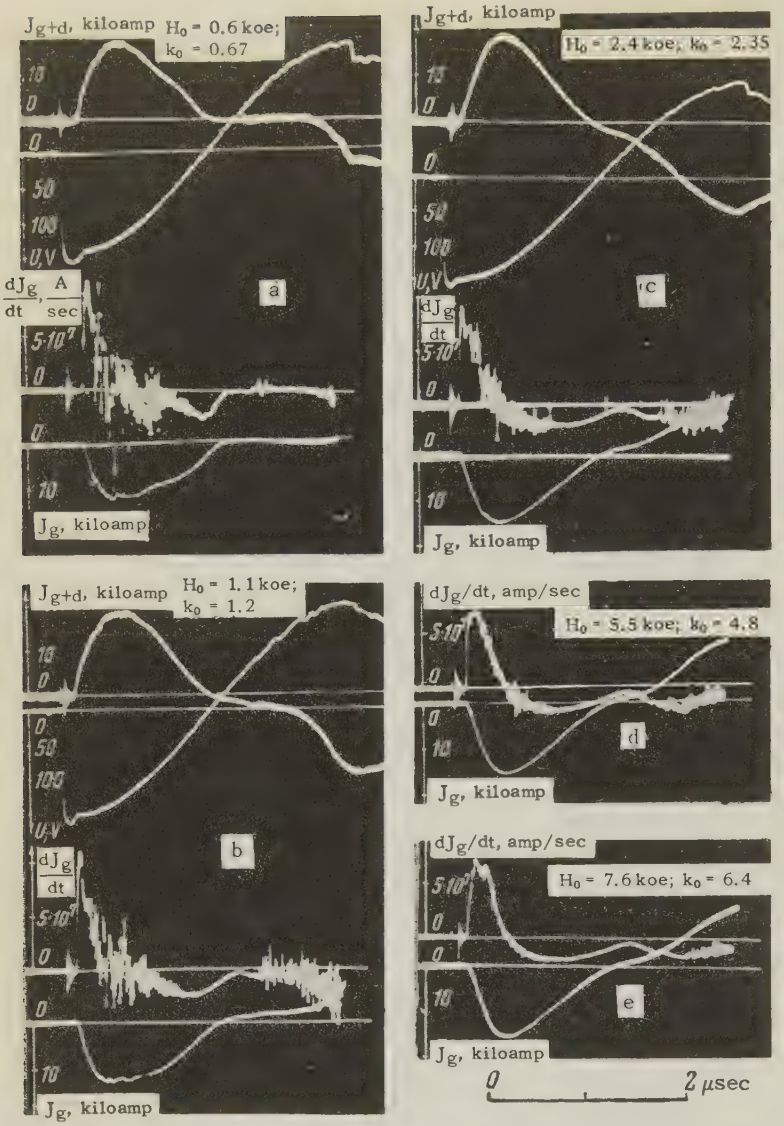

FIG. 3. Oscillograms showing the current J_{g+d}, the loop voltage U, the derivative of the current in the gas dJ_g/dt, and the current in the gas J_g for several values of k_0 (the gas is argon and $p_0 = 10^{-3}$ mm Hg).

is due to the fact that the apertures in the diaphragms and the equilibrium position of the toroidal loop are not exactly in coincidence.

The photographs of the discharge in deuterium are similar to those shown in Fig. 2. However, because of the low intensity of the radiation the films were not exposed completely.

It is interesting to compare these photographs with the other experimental data. In Fig. 3 are shown oscillograms of the current J_{g+d} and the loop voltage U, the derivative of the current in the gas dJ_g/dt, and the current in the gas J_g, all for argon. Oscillograms 3a, 4c, and 4e were obtained under the same conditions of operation as the photographs of the plasma loop.

On the oscillograms showing the current and the current derivative there are characteristic features that occur at the same instant of time. The J_g curve exhibits a discontinuity, indicating a considerable increase in current, while the current derivative dJ_g/dt falls off sharply; simultaneously, oscillations appear on the derivative oscillogram. As k_0 is increased the oscillations in the current derivative are reduced in amplitude. These features on the oscillograms showing the current and the current derivative coincide in time with the appearance of the current at the diaphragm J_d. This coincidence is seen from a comparison of the oscillograms for J_g and J_{g+d} and a careful examination of the current J_d.

A similar pattern is observed in the oscillograms obtained with a deuterium discharge. Typical oscillograms are shown in Fig. 4 for purposes of illustration.

The effect of the coefficient k_0, which characterizes the excess stability of the loop, can be illustrated by oscillograms which show the variation in time of the intensity of the deuterium spectral line $D\beta$ ($\lambda = 4860$ A). Such oscillograms are shown in Fig. 5. In order to relate the intensity of

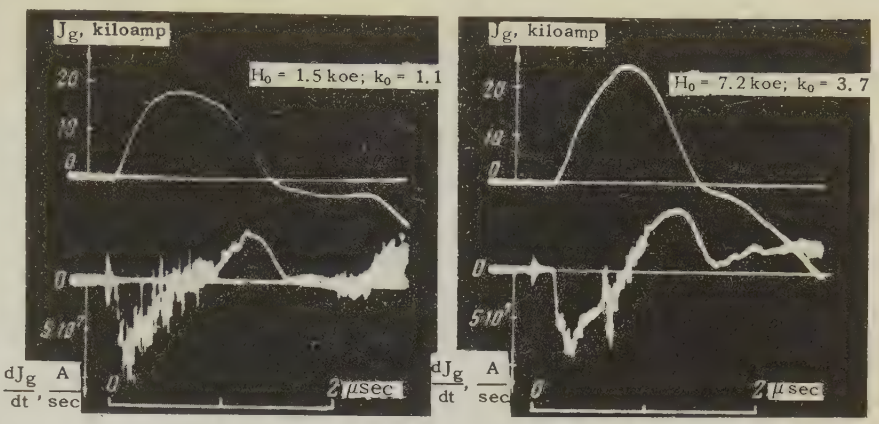

FIG. 4. Oscillograms of the current J_g and its derivative dJ_g/dt for two values of k_0 (the operating gas is deuterium and $p_0 = 10^{-3}$ mm Hg; $E_0 = 0.41$ v/cm).

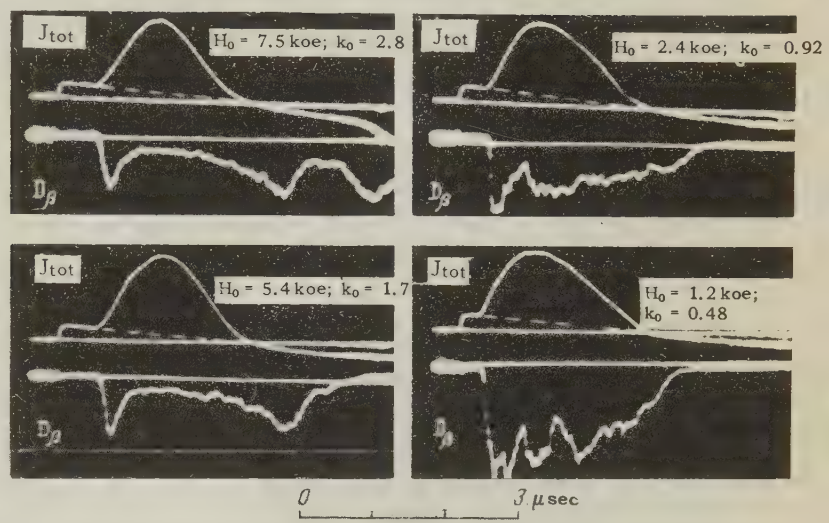

FIG. 5. Oscillograms showing the time variation of the intensity of the deuterium spectral line (D_β, $\lambda = 4860$ A) for various values of k_0 ($p_0 = 50 \times 10^{-4}$ mm Hg and $E_0 = 0.4$ v/cm).

the spectral line with the development of the discharge the upper beam of the oscilloscope is used to display the total chamber current J_{tot}. The small current at the beginning of the process is the current in the inner short-circuit chamber.

With $k_0 = 2.8$ and 1.7, after breakdown of the gas the intensity of the $D\beta$ line first increases sharply, reaching a maximum in approximately 50 μsec. It then falls off for 300 — 400 μsec, after which some increase is observed. With a reduction in excess stability the picture changes markedly. When $k_0 < 1$ there the intensity fluctuates widely as long as current flows in the gas. When a strong magnetic field is used the intensity of the $D\beta$ line remains high one microsecond after the flow of current in the gas is terminated. As H_0 is reduced this time period is also reduced.

In Figs. 6a and b are shown oscillograms for the currents J_{g+d} and J_g, the current derivative dJ_g/dt, the loop voltage U, the intensity of the deuterium $D\beta$ line, and the current to the diaphragm J_d for two values of k_0. Under the oscillograms (same time scale) is shown the mean electrical conductivity (over the cross section of the pinch) σ during the discharge. The electrical conductivity is computed from the formula

$$\sigma = 9 \cdot 10^{11} \frac{2RJ_g}{a^2 (U_{loop} - L_p dJ_g/dt)} \text{ [cgs esu]},$$

where L_p is the inductance of the pinch, which is assumed to be constant and given by $L_p = 4\sigma R \times \ln(b/a)$ (b is the radius of the shielding shell).

Comparing the oscillograms of the current to the diaphragm with the other oscillograms, we see that the time at which the intensity of the $D\beta$ line stops diminishing corresponds to the time at which the current to the diaphragm appears. At the same time the current derivative increases for a period estimated as 30 — 50 μsec. At approximately the same instant of time the conductivity of the plasma starts to drop.

In Fig. 7 are shown oscillograms of the C III line (doubly charged carbon, $\lambda = 4651$ A) which are synchronized with the oscillograms showing the diaphragm current. As the intensity of the longitudi-

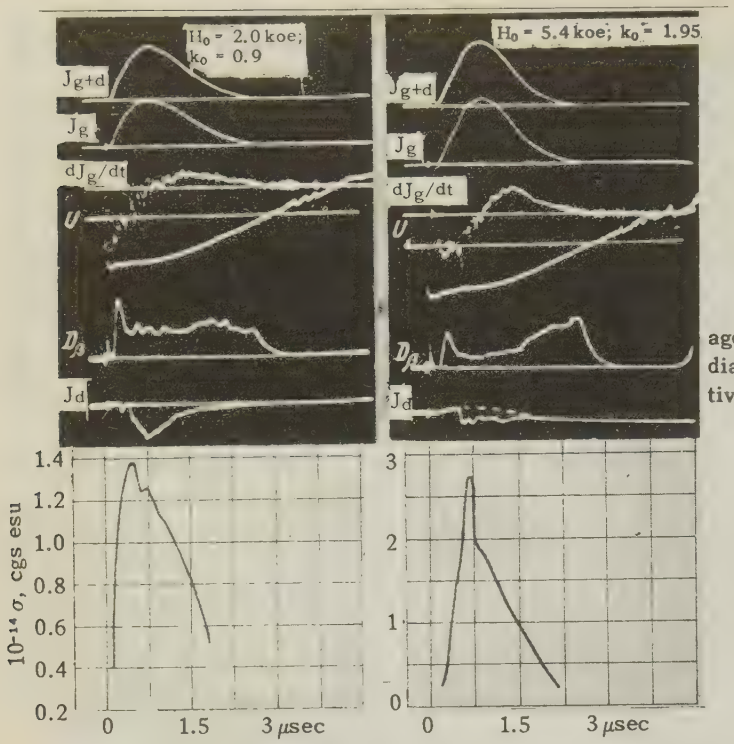

FIG. 6. Oscillograms showing the currents, loop voltage, intensity of the deuterium spectral line, current to the diaphragm and the calculated value of the electrical conductivity of the plasma loop ($p_0 = 10^{-3}$ mm Hg; $E_0 = 0.43$ v/cm).

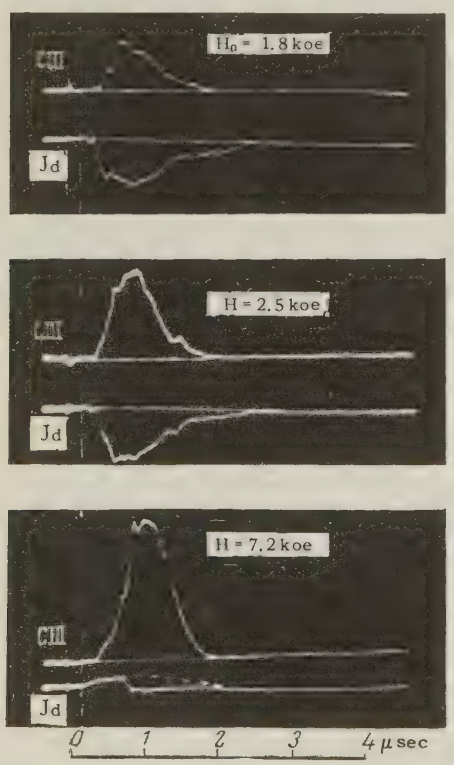

FIG. 7. Oscillograms showing the intensity of the spectral line C III (λ = 4651 A) and the current to the diaphragm for three values of the longitudinal magnetic field. Discharge in deuterium ($p_0 = 10^{-3}$ mm Hg, $E_0 = 0.43$ v/cm).

nal magnetic field H_0 is increased, the intensity of this line also increases.

A number of tests have been made to investigate the role of impurities in the operating gas in processes by which energy is lost from the plasma. In Fig. 8 are shown the relative intensities of the lines on the discharge spectrogram taken with the DFS-6 vacuum spectrometer. This spectrogram represents 150 pulses in stable operation for ($k_0 > 1$).

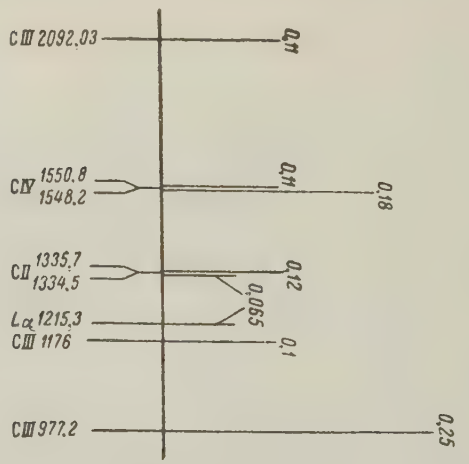

FIG. 8. Relative intensities of the lines on the discharge spectrum taken for 150 pulses with E = 0.42 v/cm and H_0 = 7200 oe; the deuterium pressure is $p = 10^{-3}$ mm Hg.

The photograph film was sensitized by sodium salicylate, which has a uniform quantum yield for wavelengths between 600 and 3,000 A.[4] An exposure of 150 pulses provides normal blackening for the most intense lines L_α (λ = 1215.3 A) and C III (λ = 1176 A). On the spectrogram only the lines for deuterium and carbon were measured. In Fig. 8 the vertical lines indicate the relative energies in the different spectral lines. The total energy of all the lines in the spectrogram is taken

as unity. It is apparent that the radiation from deuterium is only $1/15$ to $1/20$ of the total energy radiated in this region of the spectrum.

A rough estimate of the absolute magnitude of the radiation loss is given by the following experiment. A photographic film, which is first calibrated by means of a thermocouple, is placed in an auxilliary section, which connects to the discharge chamber. The film is sensitized with sodium salicylate. One-third of the film is covered by a glass filter, another third by a quartz filter, and part of the film is left completely exposed. From the blackening of the film we determine the absolute and relative radiation energy emitted in various portions of the spectrum. Preliminary measurements indicate that only 5% of the total energy emitted by the plasma is contained in the visible and near ultraviolet; most of the energy (up to 50%) is emitted as hard radiation.

The electron concentration in the plasma is determined by microwave probing. At a frequency of 130,000 Mcs microwave radiation is transmitted for 400 to 500 μsec after current starts to flow in the gas. After this period the microwave radiation is completely attenuated. Thus, the electron density is at least 2.5×10^{14} cm^{-3}. Furthermore, the measurements indicate that the electron concentration remains large for one microsecond after the discharge is extinguished. This result is in agreement with the data given for the $D\beta$ line for this same time period.

4. DISCUSSION OF THE RESULTS AND CONCLUSIONS

A. Stability. In Fig. 9 the ratio of diaphragm current to gas current (J_d/J_g) is plotted as a function of k_0 from an analysis of the oscillograms; the currents J_d and J_g are taken for times corresponding to the maximum value of the gas current. When $k_0 < 1$ this ratio falls off rapidly with increasing k_0. When $k_0 > 1$ this ratio continues to fall off, but at a much slower rate.*

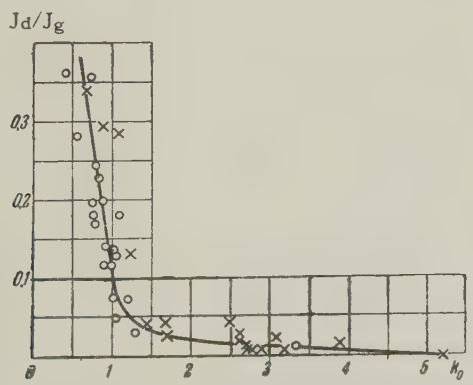

FIG. 9. The ratio of the diaphragm current J_d to the gas current J_g as a function of k_0 for two series of experiments (the gas is deuterium).

The break in the curve which is observed at values of k_0 close to unity indicates the existence of a critical current which characterizes the boundary between stable and unstable states of the plasma loop. The critical current can be estimated as follows:

$$J_{cr} = ca^2 H_0 / 2R.$$

For operating conditions characterized by $J_{max} > J_{cr}$, i.e., $k_0 > 1$, at the beginning of the discharge the gas current is less than the critical value and the pinch is stable. Later the gas current increases, reaching the critical value when $k_0 = 1$. At this point the pinch becomes unstable and there is a large current to the diaphragm. In Fig. 10 the points indicate the values of the gas current J_g at times corresponding to the appearance of the diaphragm current for discharges characterized by $J_{max} > J_{cr}$ for various values of the longitudinal magnetic field H_0. The dashed line shows the calculated value of the critical current. Functional relations of this kind are also found for discharges in helium and argon.

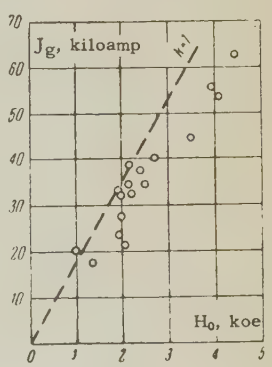

FIG. 10. The gas current J_g as a function of magnetic field at the time corresponding to the appearance of current to the diaphragm. The dashed line is the value calculated for $k = 1$.

When $k_0 > 1$ the current to the diaphragm falls off as k_0 increases; however, higher values of k_0 could not be achieved because the longitudinal magnetic field could not be increased. It is not very fruitful to increase k_0 by reducing the gas current because the energy evolved per pulse becomes small and, under certain conditions, can become smaller than that required for dissociation and ionization of the gas in the chamber. In the pres-

*The dependence is somewhat different when the centers of the apertures in the diaphragms coincide with the axis of the toroidal tube [Report by M. A. Leontovich at the Harwell Research Establishment (Great Britain), April, 1959]. When $k_0 > 1$ considerable current to the diaphragm is observed because the apertures in the diaphragms are not in coincidence with the equilibrium position of the plasma loop in the toroid.

ent experiments, with $k_0 = 5$ the current to the diaphragm was too small to be detected by the measuring apparatus.

The measurements of the intensity of the $D\beta$ line also illustrate the effect of the longitudinal magnetic field on plasma stability. For $k_0 < 1$, when the discharge current is greater than the critical value the intensity of the $D\beta$ line is higher than for $k_0 > 1$ and varies at random. It is possible that this behavior is a consequence of kinks in the plasma loop, which lead to a strong interaction with the diaphragm and perhaps with the walls of the chamber. Under these conditions the plasma tends to de-ionize and neutral atoms are excited a second time. At high magnetic fields ($k_0 > 1$) the oscillograms showing the intensity of the $D\beta$ line are regular and can be reproduced from discharge to discharge.

B. Ionization. The data available to us are inadequate for determining the concentration of charged particles in the plasma loop.

From the results of microwave probing of the plasma it follows that the concentration of electrons in the plasma loop is at least 1.5 times greater than the initial concentration of deuterium atoms. It is possible that the increase in electron concentration is a consequence of ionization of impurity atoms or deuterium atoms which enter the plasma loop from peripheral regions.

As is indicated by the data which have been presented, the electrical conductivity (averaged over the cross section of the plasma loop) increases for some time after the intensity of the $D\beta$ line starts to diminish. This result can be interpreted assuming that ionization of most of the neutral gas is terminated. Hence, it does not contradict the results obtained by microwave probing of the plasma. The increase in electrical conductivity after ionization is terminated is apparently due to heating of the plasma.

The high degree of ionization is indicated by the fact that the discharge spectrum contains intense lines due to doubly charged (C III) and triply charged (C IV) carbon. The corresponding ionization potentials are 22.28 v and 47.55 v. Thus, the plasma contains electrons with energies several times greater than the ionization potential of deuterium.

Finally, we can cite the data obtained by a microphotometric analysis of the films used in the streak photographs of the pinch. An analysis of these data, which takes account of the geometric factors, indicates that the radiation in the center of the pinch is less intense than the radiation from the outer layer. In all probability, the outer layer of the plasma, which is in contact with a layer of neutral particles, radiates a great part of the energy in the visible portion of the spectrum. Rough probe measurements indicate a sharp drop in the concentration of charged particles as a function of distance from the axis of the plasma loop. It follows from these measurements that the concentration of charged particles at the walls of the chamber is no greater than 10^{11} particles/cm^3.

C. Electron temperature. As is well known, the electron temperature in a fully ionized plasma, T_e, can be determined from the electrical conductivity σ. Thus, on the basis of the usual relations, it is found that the mean electron temperature $T_e \sim 7$ ev if the mean conductivity as averaged over the cross section of the plasma loop is $2 - 3 \times 10^{14}$ cgs esu. If we estimate T_e from the relative intensities of the impurity lines (in the present case, C I, C II, etc.) the electron temperature is found to be approximately 15 ev.

It has been noted above that the diaphragms located in the chamber are furnished with windings. Current pulses from a condenser bank can be applied to these windings. When this is done the current to the diaphragms is reduced but the total gas current J_g is increased. Under certain conditions the current increases by a factor of $1.4 - 1.5$. The loop voltage does not change under these conditions. It is more than likely that the increase in current is due to the increase in the cross section of the pinch over the entire chamber because of the deformation of the lines of force in the longitudinal field.

The following conclusions may be drawn from the data reported here.

1. A plasma loop formed in a toroidal chamber in the presence of a longitudinal magnetic field is stable when $k > 1$ and unstable when $k < 1$.

2. The equilibrium position of a plasma loop in a toroidal chamber is determined with a fair degree of accuracy by theory. Certain distortions in the equilibrium orbit found in the present experiments are apparently to be associated with the construction of the chamber.

3. The degree of ionization achieved in these experiments is rather high; the gas is almost completely ionized.

4. The temperature of the electrons in the plasma is not greater than 15 ev in spite of the fact that the amount of energy which goes into the plasma is sufficient to heat the electrons to a higher temperature. A measurement of the radiation losses indicates that impurity atoms are responsible for a considerable portion of the energy loss.

The authors wish to acknowledge the continued attention and useful discussions which have been contributed to the present work by L. A. Artsimovich. They also wish to express their gratitude to their colleagues Yu. A. Gusev and G. A. Egorenkov.

[1] S. I. Braginskiĭ and V. D. Shafranov, Nuclear Physics, Report of Soviet Delegation to 2nd International Conference on the Peaceful Uses of Atomic Energy, Geneva, 1958, Glavatom, 1959 p. 221.

[2] V. D. Shafranov, Атомная энергия (Atomic Energy) **5**, 38 (1956).

[3] Dolgov-Savel'ev, Ivanov, Mukhovatov, Razumova, Strelkov, Shepelev, and Yavlenskiĭ, loc. cit. ref. 1, p. 85.

[4] Watanabe, Edward, and Inn, J. Opt. Soc. Am. **43**, 32 (1953).

Translated by H. Lashinsky
88

ON THE MECHANISM OF URANIUM FISSION INDUCED BY SLOW NEGATIVE MUONS

G. E. BELOVITSKIĬ, N. T. KASHCHUKEEV, A. MIKHUL, M. G. PETRASHKU, T. A. ROMANOVA, and F. A. TIKHOMIROV

Joint Institute for Nuclear Research; P. N. Lebedev Physics Institute, Academy of Sciences, U.S.S.R.

Submitted to JETP editor August 14, 1959

J. Exptl. Theoret. Phys. (U.S.S.R.) **38**, 404-408 (February, 1960)

Photographic emulsions were employed to study the possibility of uranium fission induced by direct transfer to the nucleus of the energy liberated in the $2p-1s$ mesic-atom transition. The upper limit of the probability for fission by this mechanism is ~ 0.01. Uranium fission induced by μ^- mesons is due mainly to nuclear capture of the μ^- meson, the probability of which is of the order of 0.07. Arguments are presented in favor of the notion that the mesic-atom $2p-1s$ transition in uranium is in part non-radiative.

THE fission of uranium by slow negative muons can occur in at least two different ways.

1. By nuclear capture of the μ^- meson according to the reaction $p + \mu^- \rightarrow n + \nu$. According to theoretical[1] and experimental[2] data, the average excitation energy of the heavy nucleus in the capture of a slow μ^- meson is on the order of 15 or 20 Mev, enough to fission a uranium nucleus.

2. The fission of uranium by negative muons is possible also by direct transfer of energy to the nucleus in mesic-atom transition of the negative muon from the state 2p into the state 1s, in which an energy of 6.3 Mev is liberated. This fission mechanism was considered in detail in Zaretskiĭ's theoretical paper.[3] According to him, the probability of non-radiative energy transfer to the uranium nucleus in the $2p-1s$ transition is ten times greater than the probability of radiative transition. Since the lifetime of the negative muon on the K shell of the nucleus is much longer than the lifetime of the excited nucleus, the nuclear capture of the μ^- meson can be preceded by a breakup of the excited nucleus in some manner or another (fission, emission of a neutron or γ^- quantum, etc). Fission will be possible, however, only if the energy of this transition in uranium is greater than the energy of the fission threshold for the state in which the μ^- meson is on the K shell of the nucleus.

In this method of fission, the μ^- meson is not absorbed by the uranium nucleus, and is captured after fission on the orbit of one of the fragments, as a rule the heavier one. The meson is subsequently either absorbed by the fragment, or else is discarded from the excited fragment because of the internal-conversion mechanism (in a small number of events, a $\mu-e$ decay should be observed at the end of the fragment range). If the second possibility is realized, then the negative muon ejected from the fragment can again cause fission of the next uranium nucleus, i.e., conditions are created for a catalytic fission reaction. The probability of emission of a negative muon from the excited fragment by means of the mechanism of internal conversion was estimated by Zaretskiĭ[3] and was found to be 0.25.

When this investigation was begun, very scanty data on the fission of uranium nuclei by negative muons were published in the literature. John and Fry[4] estimated, on the basis of seven fission events, the fission probability and found it to be 0.07. Galbraith and Whitehouse,[5] who used pure uranium samples irradiated by negative muons from cosmic rays, estimated the upper boundary of the fission probability, found to be < 0.25. These papers, therefore, did not yield any information on the possibility of non-radiative fission (fission due to energy liberated in the non-radiative mesic-atom transition $2p-1s$).

In this connection, we set up experiments to ascertain the existence of such a mechanism of uranium fission. A confirmation of such a process would be the observation of conversion μ^- mesons or of heavy charged particles (p, α) and electrons from $\mu-e$ decay, emerging from the stopping point of the fragment.

1. EXPERIMENTAL PART

To observe the fission of uranium nuclei by slow μ^- mesons we used NIKFI type "R" photographic

plates, 200 — 250 μ thick, impregnated with uranyl acetate. The loading and development procedure enabled us to introduce up to 1.5×10^{20} uranium nuclei into a cubic centimeter of emulsion with uniform development of the emulsion over the entire depth. Some of the plates were treated to make the tracks of relativistic particles invisible, while the remainder retained their sensitivity to relativistic particles, a fact that could be monitored by the presence of $\mu - e$ decays. The number of uranium nuclei introduced into the emulsion was determined by counting the α particles from the natural radioactivity of uranium. This quantity, averaged over all the experiments, was found to be 1.7×10^{20} cm^{-3}. The plates were irradiated in the synchrocyclotron of the Joint Institute for Nuclear Research by a beam of slow μ^- mesons, obtained by slowing down the initial negative-pion beam, of energy ~ 160 Mev, in a copper absorber 11.5 cm thick. The admixture of negative pions (~ 1%) was determined from the number of stars with three or more prongs, due to the stopped mesons.

A total of 738 fission events was found, of which 520 were in plates insensitive to relativistic particles, and 218 in relativistic plates. The plates were scanned at an overall magnification of 300×. The fission events detected were analyzed at a magnification of 2000 ×. The accuracy of measurement of the range was $\pm 1\,\mu$. On the basis of 397 fission events, obtained from 271,600 negative muons stopped in the emulsion, we calculated the fission probability P_f of uranium by negative muons, using the formula

$$P_f = \frac{n_f}{0.4 S_\mu N_U Z_U / (N_U Z_U + \Sigma N_i Z_i)},$$

where n_f is the number of fissions, S_μ the number of stopped μ^- mesons, N_U the number of uranium nuclei, N_i the number of carbon, oxygen, or nitrogen nuclei per cubic centimeter of emulsion, contained in the uranium-impregnated gelatin, Z is the nuclear charge, and the factor 0.4 arises because 40% of the negative muons are stopped in the uranium-containing gelatin (see references 6 and 7). The probability of capture of a negative muon by the uranium was calculated from the well known composition of the NIKFI emulsion and the assumption that the Fermi-Teller law[8] holds, whereby the capture of the μ^- meson by the various nuclei contained in the gelatin is proportional to Z.

The probability of uranium fission by μ^- mesons calculated under these assumptions was found to be 0.070 ± 0.008.

Recent experimental investigations[9,10] have shown that in chemical compounds, such as Al_2O_3, SiO_2, AgCl, UF_4, etc, the capture of negative mu-ons is proportional to the number of atoms in the molecule. If this result is applied to our case (gelatin plus uranium), then a quantity greater than unity is obtained for the fission probability, which is absurd. The foregoing is confirmed also by the results of Galbraith and Whitehouse,[5] who used pure uranium specimens, and who obtained a value less than 0.25 for the fission probability. An even more conclusive deduction is made in reference 11, where the photo method was used, in which it is shown that the capture of negative mesons in the (gelatin plus uranium) medium follows more readily the Fermi-Teller law. Thus, the Fermi-Teller law does not distort the results greatly, if at all.

To obtain information on the excitation energy of uranium nuclei fissioned by negative muons, we measured the range of each fragment. This could be done because the track of the negative muon usually makes it possible to determine the point where the fission occurred.

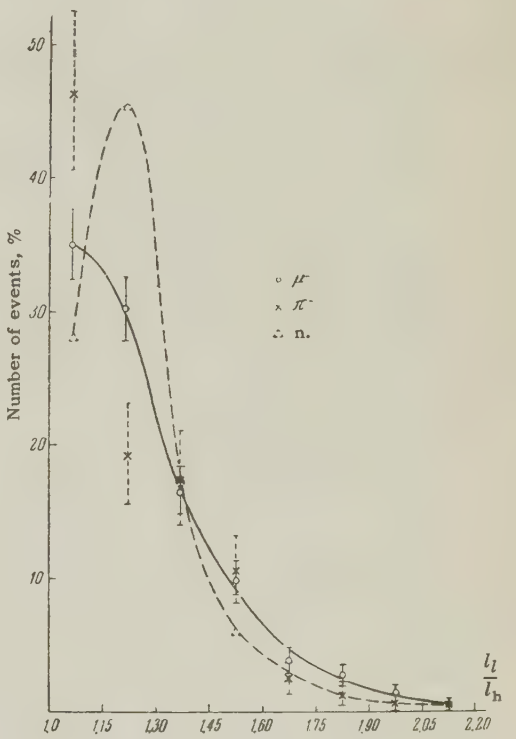

The diagram shows data on the degree of asymmetry of the fission of uranium induced by negative muons (the abscissas represent the ratio of the ranges of the light and heavy fragments, and the ordinates represent the relative number of such events, in percent). For comparison, the same figure shows analogous data for fission of uranium by slow neutrons[12] and slow negative pions.[12,13]

2. DISCUSSION OF THE FISSION MECHANISM

The experimental data we obtained lead to the conclusion that if the process of non-radiative fission of uranium does indeed take place, its probability is ~ 0.01, i.e., more than one order of magnitude smaller than computed.[3] This statement is based on the following facts:

a) Were the fissions observed due to non-radiative transition, then the emission of heavy (p, α) charged particles from the end of the fragment track would be observed in approximately ten cases, and in eight cases electrons from $\mu - e$ decay would be observed. We did not observe a single event of this kind.

b) In the presence of non-radiative fission, emission of conversion μ^- mesons is possible. If the meson energy is less than 1 Mev, the emission of such a meson can be detected from the $\mu - e$ decay. Approximately ten such events were expected, but not a single one was observed among the 228 fission events found in the relativistic plates.

c) A comparison of the distributions of the light to heavy fragment-range ratio in the fission of uranium by μ^- mesons (see the figure) with analogous data for the fission induced by slow neutrons (excitation energy ~ 6 Mev) and slow negative pions (excitation energy ~ 60 Mev) indicates that uranium is fissioned by μ^- mesons essentially at an excitation energy considerably greater than 6 Mev. Were a noticeable role to be played by non-radiative fission, the character of the fragment-range asymmetry in the fission by μ^- mesons (excitation energy ~ 6 Mev) would be similar to that induced by slow neutrons.

Finally, the difference between the probabilities of fission of Th^{232} and U^{238} (0.018 and 0.07) under the influence of μ^- mesons, as reported in reference 14, also apparently indicates that the fission is not via non-radiative excitation. At an excitation energy of 6.3 Mev, the probability of fission of Th^{232} should not be considerably less than that of uranium.

As shown by later calculations (D. F. Grechukhin, private communication), so small a probability of non-radiative uranium fission by negative muons, compared with that previously obtained,[3] is apparently due to the fact that when the μ^- meson lands on the K shell the potential barrier for fission increases by ~ 1 Mev, which should reduce the fission probability by several orders of magnitude. Thus, the fission of U^{238} by negative muons is apparently due essentially to nuclear capture of the μ^- meson. This results in an excited Pa^{238} nucleus with an excitation spectrum from 0 to 20 Mev.[1,2] The probability of fission of Pa^{238} at such excitation energies can be calculated from the empirical formula:[15]

$$\frac{P_f(Pa_{91}^{238})}{P_f(U_{92}^{238})} = 1.3\left[\frac{Z^2}{A} - 34.7\right], \qquad (1)$$

where $P_f(Pa^{238})$ and $P_f(U^{238})$ are the fission probabilities of Pa^{238} and U^{238} at equal excitation energies. This formula is applicable to nuclei with $Z \geq 90$ at least at an excitation energy $8 - 12$ Mev.

To calculate $P_f(U^{238})$ we used the experimental data on the uranium fission probability under the influence of neutron[16] and gamma rays[17] at excitation energies which obtain in the Pa^{238} when a U^{238} nucleus captures a μ^- meson. The fission probability $P_f(U^{238})$, averaged over the entire excitation spectrum obtained by Kaplan et al.[2] was found to be 0.27 ± 0.02. Substituting this quantity in the above formula, we obtain $P_f(Pa^{238}) \approx 0.03$, which is less than the value 0.07 obtained in our experiments.

Thus, if (1) is correct in our case, then to explain the experimental value of $P_f(Pa^{238})$ it is necessary to assume the existence of another channel, by which fission takes place. As established in our investigation, the transition $2p - 1s$ of the negative muon into a mesic atom of uranium, if it is non-radiative, does not lead in a noticeable number of cases to uranium fission. The excited nucleus that is produced thereby apparently emits a neutron (binding energy of the last neutron in uranium is 6 Mev). Consequently, this nuclear capture of the negative muon occurs already in U^{237} with formation of Pa^{237} and its subsequent fission.

Using (1) again, we obtain for the probability of Pa^{237} fission a value of 0.08, close to the experimental value. Considering, however, the possible inaccuracy of the formula at excitation energies greater than 12 Mev, and the inaccuracy of the other quantities used in these estimates, we cannot draw a final conclusion regarding the extent to which the transition $2p - 1s$ is non-radiative.

We have recently become acquainted with the results of reference 18, in which it was established, by measuring the number of γ quanta with energy > 6 Mev per capture of a μ^- meson, that the $2p - 1s$ transition in the mesic atom of uranium is non-radiative with a probability ~ 0.5, confirming our conclusion regarding the mechanism of uranium fission by μ^- mesons. The presence of a non-radiative transition $2p - 1s$ and the small

fission probability ($P_f = 0.07$) allow us to conclude that when the μ^- meson lands on the K shell of the uranium nucleus, the fission barrier increases by more than 0.2 Mev.

The authors express their gratitude to Professor V. P. Dzhelepov and I. M. Frank for constant interest in the work and for useful discussion, and also to I. Ya. Barit and A. E. Ignatenko for help in the work, and to the laboratory staff for participating in scanning the photographic plates.

Three of us (N. T. Kashchukeev, A. Mikhul, and M. G. Petrashku) are also grateful to V. M. Sidorov for help in this work.

[1] V. A. Wheeler, Revs. Modern Phys. **21**, 133 (1949).

[2] Kaplan, Moyer, and Pyle, Phys. Rev. **112**, 968 (1958).

[3] D. F. Zaretskiĭ, Тр. Второй Международной конф. по мирному использованию атомной энергии. Доклады советских ученых (Second Geneva Conference; Papers by Soviet Scientists), Vol. 1, 1959, p. 462.

[4] W. John and W. F. Fry, Phys. Rev. **91**, 1234 (1955).

[5] W. Galbraith and W. J. Whitehouse, Phil. Mag. **44**, 77 (1953).

[6] O. V. Lozhkin and V. P. Shamov, JETP **28**, 739 (1955), Soviet Phys. JETP **1**, 587 (1955).

[7] W. F. Fry, Phys. Rev. **85**, 675 (1952).

[8] E. Fermi and E. Teller, Phys. Rev. **72**, 399 (1947).

[9] Sens, Swanson, Telegdi, and Jovanovith, Nuovo cimento **7**, 536 (1958).

[10] Backenstoss, Bloch, Chidley, Reiter, Romanowski, Siegel, and Sutton, Bull. Am. Phys. Soc. **4**, No. 4, Sec. T, 1959.

[11] G. E. Belovitskiĭ, JETP **38**, 658 (1960), this issue p. 473.

[12] V. P. Shamov and O. V. Lozhkin, JETP **29**, 286 (1955), Soviet Phys. JETP **2**, 111 (1956).

[13] Belovitskiĭ, Romanova, Sukhov, and Frank, JETP **28**, 729 (1955), Soviet Phys. JETP **1**, 581 (1955).

[14] G. M. Petrashku and A. K. Mikhul, Dokl. Akad. Nauk SSSR **126**, 752 (1959), Soviet Phys.-Doklady **4**, 628 (1959).

[15] Huizenga, Gindler, and Duffield, Phys. Rev. **95**, 1009 (1954); J. R. Huizenga, Phys. Rev. **109**, 484 (1958).

[16] Knight, Smith, and Warren, Phys. Rev. **112**, 259 (1958).

[17] Lazareva, Gavrilov, Valuev, Zatsepina, and Stavinskiĭ, Сессия АН СССР по мирному использованию атомной энергии (заседания отд. физ.-мат. наук). (Session of U.S.S.R. Acad. Sci. on Peaceful Uses of Atomic Energy, Div. of Phys.-Math. Sciences), Acad. Sci. Press, 1955, p. 306.

[18] Blats, Kondrat'ev, Landsberg, Lebedev, Obukhov, and Pontecorvo, Preprint R-448 Joint. Inst. for Nucl. Res., Dubna, 1959.

Translated by J. G. Adashko
89

INELASTIC INTERACTION OF PIONS WITH HELIUM NUCLEI AT APPROXIMATELY 300 Mev

M. S. KOZODAEV, M. M. KULYUKIN, R. M. SULYAEV, A. I. FILIPPOV, and Yu. A. SHCHERBAKOV

Joint Institute for Nuclear Research

Submitted to JETP editor August 14, 1959

J. Exptl. Theoret. Phys. (U.S.S.R.) **38**, 409-422 (February, 1960)

Interaction of positive and negative π mesons with helium nuclei at corresponding energies 273 Mev and 330 Mev was studied with the aid of a diffusion cloud chamber. Quasifree scattering on neutrons and protons, multiple scattering and absorption of the mesons were discriminated. The total inelastic interaction cross sections were $(145 \pm 15) \times 10^{-27}$ cm^2 for $E_\pi = 273$ Mev and $(103 \pm 10) \times 10^{-27}$ cm^2 for $E_\pi = 330$ Mev. The relative probabilities for quasifree scattering on neutrons and protons through angles of 45° in the laboratory coordinate system are found to agree with the corresponding probabilities for scattering on free nucleons. The probabilities for multiple scattering processes were found equal to 0.24 ± 0.06 for $E_\pi = 273$ Mev and 0.29 ± 0.05 for $E_\pi = 330$ Mev.

The experimental results confirm current ideas concerning the main role of n-p pairs in absorption of π mesons by nuclei. The angular distribution of inelastically scattered π mesons is compared with the Watson-Zemach calculations.

INTRODUCTION

THE basic phenomena that occur when fast pions are scattered by nuclei are adequately described in first approximation by the Serber-Goldberger model.[1,2] In this model the inelastic scattering is considered as a result of the interaction between the pion and individual nucleons of the nucleus. The nucleons of the nucleus are represented as an aggregate of non-interacting particles, located in a potential well and having a certain momentum distribution.

The absorption of the pions by the nuclei fits the framework of the mechanism of absorption by nucleon pairs, and the principal role is apparently played by n-p pairs.[3-6]

More detailed experimental research is necessary for further development of the notions of the mechanism of interaction between fast pions and nuclei. In particular, it is very important to establish by direct experiment the degree to which the free and bound nucleons exhibit identical properties in the scattering, the role of the interaction processes in which more than one nucleon participates, etc. Such investigations entail great experimental difficulties. The problem becomes somewhat simpler if targets of light nuclei are used and the experiments performed with both positive and negative pions.

The present work covers inelastic interactions between $\pi^\pm$ mesons and helium nuclei at approximately 300 Mev.

EXPERIMENTAL PROCEDURE AND APPARATUS

The interaction between pions and helium nuclei was investigated with a high pressure diffusion chamber using pion beams from the synchrocyclotron of the Joint Institute for Nuclear Research. The arrangement of the experimental apparatus when working with negative and positive pions is shown in Figs. 1 and 2 respectively.

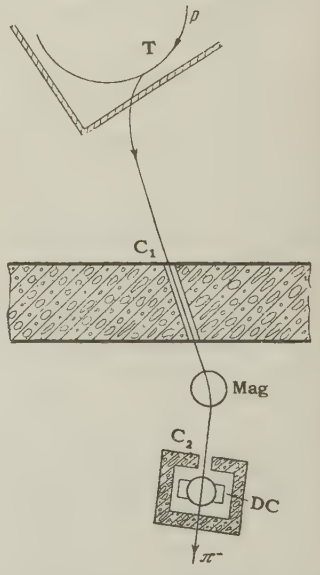

FIG. 1. Setup for the experiment with negative pions.

Negative pions were produced with a carbon target T, placed inside the accelerator chamber along the circular path of a 670-Mev proton beam. The negative pions accelerated in the stray magnetic field of the accelerator, passed through a steel

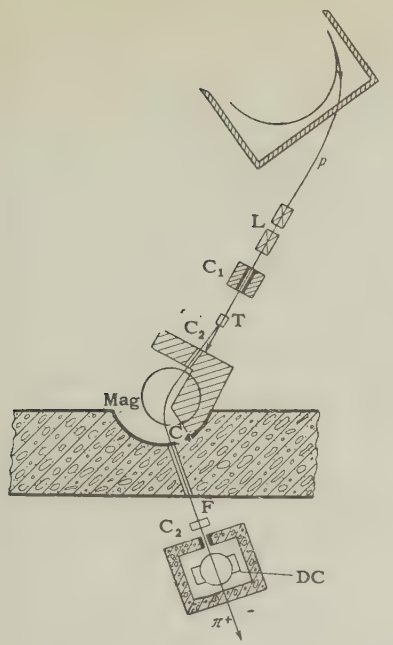

FIG. 2. Setup for the experiment with positive pions.

collimator C_1, 100 mm in diameter, in a four-meter concrete shield, were again deflected by a clearing magnet Mag by 22° and entered the diffusion chamber DC.

Positive pions were produced with the proton beam extracted from the accelerator chamber. A polyethylene target T 200 mm thick was placed at the focus of quadrupole magnetic lenses L past a collimator C_1. A monochromatic beam of positive pions from the reaction $p + p \rightarrow \pi^+ + d$, traveling at an angle of 9° to the direction of the proton beam, was gathered with the aid of collimators C_3 and C_4 and analyzing magnet Mag. The diffusion chamber, as in the first case, was placed in the experiment room behind a four-meter concrete shield.

In both cases, a collimator C_2, with a cross section equal to the size of the inlet window of the diffusion chamber (30×60 mm) was placed in front of the chamber. To clear the positive pion beam of protons having the same momenta as the mesons, a carbon filter F 60 mm thick was placed in front of collimator C_2. To reduce the background of extraneous particles the diffusion chamber was surrounded by additional lead and concrete shields.

The pion energy was determined by simulating their trajectories with a flexible current-carrying conductor. The positive-pion beam was used in addition to plot a range curve in copper. It follows from these measurements that, allowing for ionization losses in the absorber and the chamber walls, the energies of the positive and negative pions were (273 ± 7) and (330 ± 6) Mev respectively.

A diffusion chamber of 270 mm diameter, filled with helium at a pressure of 15 atmos, was used in the experiments.[7] The working liquid was methyl alcohol. The height of the sensitive layer was 5 — 6 cm at a bottom temperature of − 65° C and a vapor source temperature of + 10° C. The sensitive layer was illuminated on both sides by parallel beams of light. The chamber was photographed at an angle of 90° to the direction of the illumination by a stereo camera having lenses with parallel axes and a base of 120 mm. Lenses of focal length F = 35 mm and of relative aperture 1 : 7 were used. 35 mm Pankhrom X with a sensitivity $S_{0.85} = 1000$ GOST units and contrast $\gamma = 1.6$ was used.

During the exposure of the diffusion chamber the accelerator operated in the control mode customary for such experiments. The particle flux through the chamber was regulated by varying the number of acceleration cycles and amounted on the average to approximately 20 particles per photograph. The operating cycle was determined to a considerable extent by the background conditions and ranged from 7 or 10 seconds in the negative-meson beam to 15 or 18 seconds in the positive-meson beam.

2. PROCESSING OF THE PHOTOGRAPHS AND IDENTIFICATION OF INTERACTION EVENTS

The interaction events were selected by scanning the photographs twice through a stereo magnifier. The necessary angles and lengths of the particle ranges were measured on a reprojector.[8] Two angles were measured for all secondary particles: the angle between the direction of the primary and secondary particles, θ, and the azimuth angle φ. Most measurements could be made directly by simply reading the dials of the instrument. For this purpose the axis of rotation of the screen was made to coincide with the direction of the track of the primary particle, after which the position of the scattering plane was found by rotating the screen about this axis. The true position of the track in space was established by making its two projections on the screen coincide. If the secondary-particle track was located in a region in which a stereo projection cannot be obtained in this manner, the axis of rotation was turned by 90° in the horizontal plane, and the angles φ' and θ', connected with φ and θ by the simple relations

$$\sin\theta = \cos\theta'/\cos\varphi, \qquad \tan\varphi = \tan\theta' \sin\varphi',$$

were measured. Here φ' is the projection of the angle θ on the vertical plane, and θ' is the angle

between the track of the secondary particle and the axis of rotation.

Whenever the track fell in the "dead zone" of the reprojector, it became necessary to make the measurements by the coordinate method. The angle at the vertex of the "dead-zone" cone was approximately 40°.

An important role was played in the identification of interaction events by measurements of the ranges and by the specific ionization of the particles. The length of the range was taken to be the distance between the point of interaction (corresponding to the point of intersection of the fast-particle tracks) and the end of the track of the stopped particles, reduced by one half the width of the track. The length obtained in this manner was reduced by another 5%, in view of the change in scale that arises when the image is reprojected, owing to the shrinkage of the film. A careful analysis was made every time to ascertain whether the particle range terminated in the illuminated region of the chamber. The accuracy with which the particle energy was determined in this manner was verified by comparing the measured ranges of the recoil α particles, formed in elastic scattering, with those calculated by the Bethe formula. The average error did not exceed 15%.

The ionization was measured by relative photometry, i.e., by comparing the photograms of tracks made by particles of known and unknown ionization.[9] The ionization was measured only when a visual estimate was found to be insufficient for identification purpose and more exact data were needed.

The chamber contained, along with the helium, methyl alcohol vapor CH_3OH. This admixture, however, was small in the sensitive layer. Estimates show that the ratio of the number of interactions with hydrogen to that with helium should not exceed ~ 0.002 for negative pions and ~ 0.01 for positive pions; the contributions due to events produced by oxygen or carbon should not exceed ~ 0.02. It was therefore assumed in the analysis of the observed events that all, with the exception of the obvious carbon and oxygen stars, are due to interactions with helium nuclei.

Before we proceed to describe the procedure of identifying different interaction processes between $\pi^{\pm}$ mesons and helium nuclei, let us list the principal reactions:

$$\pi^- + He^4 \to \pi^- + He^4, \quad \text{elastic scattering} \quad (1)$$
$$\pi^- + n + He^3 \quad (2)$$
$$\pi^- + He^4 \to \pi^- + p + H^3, \quad \text{inelastic scattering} \quad (3)$$
$$\pi^- + (2n, 2p) \quad (4)$$
$$\pi^- + He^4 \to \pi^0 + n + H^3, \quad \text{exchange scattering} \quad (5)$$
$$\pi^0 + (3n, 1p) \quad (6)$$
$$\pi^- + He^4 \to n + n + d, \quad \text{non-radiative capture} \quad (7)$$
$$3n + p \quad (8)$$
$$\pi^+ + He^4 \to \pi^+ + He^4, \quad \text{elastic scattering} \quad (1')$$
$$\pi^+ + n + He^3 \quad (2')$$
$$\pi^+ + He^4 \to \pi^+ + p + H^3, \quad \text{inelastic scattering} \quad (3')$$
$$\pi^+ + (2n, 2p), \quad (4')$$
$$\pi^+ + He^4 \to \pi^0 + p + He^3, \quad \text{exchange scattering} \quad (5')$$
$$\pi^0 + (1n, 3p) \quad (6')$$
$$\pi^+ + He^4 \to p + p + d, \quad \text{non-radiative capture} \quad (7')$$
$$n + 3p \quad (8')$$

The nucleon combination included in the parentheses may be a deuteron with two free nucleons or else four free nucleons. The elastic scattering events (1) and (1′) were segregated by kinematic particle divergence, as described in detail in references 10 and 11.

As a rule, reactions (2) and (2′) appear on the photographs as two-prong stars with uncorrelated prongs. The pion should have an ionization close to minimum. The He^3 nucleus is slower in this reaction, and its range terminates in most cases in the illuminated region. Quite similar in external appearance to the processes (2′) are certain exchange-scattering events, when a fast proton is emitted in reaction (5′). To segregate such events, we measure the ionization of the fast particle. We had in mind the fact, shown by kinematic calculations, that the ionization produced by the forward-flying fast proton cannot, with any discernible probability, be lower than twofold.

True, another possibility, which is much less probable for reactions (2) and (2′), is a single-prong star, formed whenever the He^3 nucleus has a very small momentum and its range is not discernible in the photograph. Such events are distinguished from reactions (8) and (5′) also by ionization measurements.

Somewhat greater difficulties arise in the identification of processes (3) and (3′). In fact, most events (3) and (3′) are three-prong stars. But processes (4), (4′), (6′), (7′), and (8′) also produce tridents. Therefore, the identification calls

for an all-inclusive analysis, which takes into account all the singularities of these reactions.

The easiest to segregate from the bulk of the tridents are events in which at least one neutral particle is emitted; it is seen from these events immediately that the emitted three particles are not in a position to balance the initial momentum. This manifests itself either in the fact that the charged particles move into the rear hemisphere, or in the fact that the projections of the directions of the charged particles on the azimuth plane lie in one half plane.

The next step in the identification of tridents is also based on the conservation of momentum. If only three particles are emitted in the final state, then the measured angles φ and θ, together with the value of the initial momentum, make it possible to calculate the momenta of these particles. If neutral particles are emitted in this reaction together with the three charged particles, such a calculation does not give the true value of the momentum. In this case the expression for the calculated momentum p'_n can be represented in the form

$$p'_n = p_n - q_n.$$

Here p_n is the true momentum of the n-th particle and q_n is a rather complicated function of many quantities and can assume both positive and negative values. One can therefore consider that a sufficient condition of the emission of at least one neutral particle is the appearance of negative values for p'_n.

The purpose of further identification was to segregate from among the remaining tridents cases in which only three particles are emitted, namely (3), (3′), and (7′). For this purpose, the obtained values of the momenta were used to verify the energy balance, and whenever a particular track could not be assigned to a particular particle, different possible assumptions were made concerning the natures of the particles. In addition to the energy balance, the angular correlation between the pion and the proton in (3) and (3′), or between the two protons in (7′), were examined under the assumption that the initial momentum is represented by the difference $p_0 - p_{H^3}$ or $p_0 - p_d$ respectively. The angular correlation was verified with a special instrument, which readily simulated the vectors of all the momenta in space. Finally, we verified the correspondence between the values of the calculated momenta of the slow particles, and the values determined from the ranges, or their lower bounds.

In segregating events (3), (3′) and (7′), owing to the great variety of the measurement conditions, we did not use any particular selection rules, since an accurate determination of these events was a highly difficult matter. Instead, a thorough individual analysis was made in each specific case of the possible errors in the measurements of φ and θ, and the sensitivity of the calculated values of the particle momenta and energies to these errors was verified. As a result of such an approach, the inaccuracy in the energy balance did not exceed ± 50 Mev for most of the selected three-particle events. The events identified with greatest reliability were those in which the ranges of the H^3 nuclei or of the deuterons terminated in the illuminated region of the chamber.

We also classified as processes (3) and (3′) certain of the two-pronged stars, in which the kinematic conditions of two-particle (π-p) divergence are satisfied. It was assumed that in these cases the H^3 nucleus, owing to its very small momentum, does not leave a visible track in the chamber. After separating the three-particle reactions, the remaining tridents were classified as (4), (4′), (6′), and (8′). Cases of inelastic scattering of positive pions (4′) were selected from among the processes with emission of neutral particles by measuring the ionization produced by the fast particles. We were unable to devise separation methods for the analogous exchange-scattering (6′) and non-radiative capture (8′) processes. A similar situation obtains in the identification of exchange scattering (5) and (6) and non-radiative capture, (7) and (8) of negative pions (all these cases are single-prong stars). We merely attempted here to separate the reaction (8) from events in which a fast proton was emitted (this will be discussed in Sec. 5). Typical photographs of individual reactions are given in Figs. 3, 4, and 5.

3. RESULTS OF IDENTIFICATION AND ABSOLUTE CROSS SECTIONS

We obtained 24,000 photographs in the beam of negative pions and 11,000 photographs in the beam of positive pions. The results of the scannings disclosed a total of 321 and 229 interaction events due to negative and positive pions respectively, of which 222 and 152 were due to inelastic interaction. The results of the identification of these events are listed in Table I.

To determine the absolute cross sections, we selected the photographs of highest quality containing not more than 20 particles per frame. The total number of interactions of events in these selected photographs of positive and negative meson beams was approximately 100 in each selected group. These photographs were subjected to careful scanning, with simultaneous calculation of the number

FIG. 3. Photograph of quasifree scattering of a positive pion by a proton.

FIG. 4. Photograph of quasifree scattering of a negative pion by a neutron.

FIG. 5. Photograph of capture of a positive meson by an n-p pair.

of particles passing through the chamber. This number did not include the particles deviating from the beam direction by angles greater than the divergence angle of the beam. Nor were particles included whose ionization, as estimated visually, exceeded the minimum value. The admixture of muons and fast electrons in the negative-pion beam was estimated by observing the $(\pi-\mu)$ decays in flight in the same beam,[7] and was assumed to equal 6%. The same admixture in the positive-pion beam was determined from the range curve and amounted to 10%. In the calculations of the absolute cross section the gas density was assumed to correspond to the temperature of the midpoint of the sensitive layer, and the effective thickness of the track in the chamber was taken to be 23 cm. The total absolute cross sections of interaction of 330-Mev negative pions and

TABLE I

Positive pions, E_π = 273 Mev			Negative pions, E_π = 330 Mev		
Process	Number of events	Cross section, 10^{-27} cm^2	Process	Number of events	Cross section, 10^{-27} cm^2
1	2	3	4	5	6
(1′)	77	75±9	(1)	99	47±5
(2′) total track of He^3 invisible	14 [5]* —	14±4	(2) total track of He^3 invisible	72 4	34±4
(3′) total track of H^3 invisible	51 [10] 1	50±7	(3) total track of H^3 invisible	27 [7] 4	13±3
(4′)	21 [12]	20±4	(4)	41 [6]	19±3
(5′) total track of He^3 invisible	35 [10] [2]	34±6	(5), (6), (7), (8) total	70	33±4
(7′) total track of d invisible	8 [1] —	8±3	with emission of fast protons	20	9±2
(6′), (8′)	13 [5]	13±4			
Cases of interaction with oxygen or carbon	2		Cases of interaction with oxygen or carbon	4	
Unidentified events	8		Unidentified events	8	
Total	229	220±20	Total	321	150±15

*The numbers in square brackets indicate the events in each group with lower reliability of identification, owing to poor measurement conditions.

of 273-Mev positive pions with helium nuclei were found to be $(150 \pm 15) \times 10^{-27}$ and $(220 \pm 20) \times 10^{-27}$ cm^2, respectively. The partial cross sections of different processes are listed in columns 3 and 6 of Table I. The cross sections are indicated with relative statistical errors.

4. ANALYSIS OF THE INELASTIC AND EXCHANGE SCATTERING PROCESSES

a) Role of multiple scattering processes. The reactions (2), (2′), (3), (3′), and (5′) can be considered as the results of a quasifree scattering by individual bound nucleons, considering that the residual nuclei do not participate directly in the interaction with the incoming pions. Analyzing these reactions, we can verify that the momenta of the He^3 and H^3 nuclei are of the same order of magnitude as the intranuclear momenta of the nucleons; their values range essentially from 0 to 300 Mev/c. The angular distributions of these nuclei (detailed data on which will be published later) also agree with the foregoing scheme. In addition, the momenta and the angles of the mesons and protons in (3) and (3′) are correlated and are close to the correlation that takes place in scattering by free nucleons.

Thus, the singularities of these reactions, together with their high probability (see Table I), illustrate the correctness of the point of view that the pion-nucleon interaction at these energies has essentially a one-nucleon character.

The remaining cases of inelastic scattering (4), (4′), (6), and (6′), in which more than three particles are emitted in the final state, can be interpreted in two ways. Firstly, these cases may be the result of simultaneous interaction between the pions and complexes of nucleons. This assumption can be corroborated partially by the fact that a noticeable probability of non-radiative pion capture exists, in which at least two nucleons participate. The fact that not a single event of a type (π, d, d) reaction was registered cannot serve as a refutation of this point of view, since the probability of emission of a group of nucleons in the bound state may prove to be small.

Secondly, these cases may be the result of the development of a cascade in the nucleus. The few observed events, in which two charged particles (apparently protons) diverge at an angle of 90°, indicates that the cascade processes do take place, at least in those cases. Actually, it is probable that both mechanisms are in operation. To clarify their relative role, the experimental results must be supplemented by cascade calculations.

The processes that proceed via these two channels we shall tentatively call multiple-scattering processes. The relative probability of multiple scattering in inelastic scattering ϵ can be determined directly from the number of cases that correspond to the reactions (2), (2′), (3), (3′), (4) and (4′):

$$\varepsilon_{E_\pi=273} = N_{4'} / (N_{2'} + N_{3'} + N_{4'}) = 0.24 \pm 0.06;$$

$$\varepsilon_{E_\pi=330} = N_4 / (N_2 + N_3 + N_4) = 0.29 \pm 0.05.$$

In exchange scattering this probability cannot be determined, since the corresponding reactions were not identified.

b) Relations between quasifree scattering processes. One can hope that the results obtained for the quasifree scattering by neutrons and protons will throw light on the question whether the properties of the free and bound nucleons that appear in the scattering are identical. In particular, owing to the great difference in the interaction of pions with nucleons in various isotopic states, one can attempt to obtain, by comparison with the corresponding quantities for the free nucleons, information on the purity of the isotopic states in quasifree scattering processes. However, one must bear in mind here several circumstances which make such an analysis difficult. The first of these is that the interaction between pions and nucleons is not confined to quasifree processes. Therefore, for comparison purposes, it would be desirable to separate all the cases that result from pairwise interaction with neutrons and protons, cases due to collective interactions or interference phenomena, and to establish whether the latter influence in a unique manner the probability of interaction with neutrons and protons. In actuality, this cannot be done on the basis of experimental data.

The second difficulty lies in the fact that there is a certain indeterminacy in the choice of the energy for which the cross sections of interaction with free nucleons are to be taken. The comparison could be made within the framework of some theory that describes sufficiently well the entire complex of interactions between pions and nucleons. Unfortunately, no such theory exists. Nevertheless, a comparison of the relative probabilities of scattering by free and bound nucleons can be made under certain simplifying assumptions.

We shall assume that the corrections to the relation between the quasifree processes due to multiple scattering and absorption of pions are small. The influence of elastic scattering can be excluded by using in the comparison cross sections in that range of angles where there is practically no elastic scattering ($> 45°$). For exchange scattering

TABLE II

Pion energy, Mev	Process	Cross sections, 10^{-27} cm²		Cross section ratio	
		total	$\theta>45°$	total	$\theta>45°$
1	2	3	4	5	6
Scattering by free protons					
$E_\pi = 330$	I) $\pi^+p \to \pi^+p$	56	25.1	$\sigma_I / \sigma_{II} = 5.1$	3.9
	II) $\pi^-p \to \pi^-p$	11	6.4	$\sigma_I / \sigma_{III} = 3.7$	
	III) $\pi^-p \to \pi^0n$	15	—		
$E_\pi = 273$	I	96	49.0	$\sigma_I / \sigma_{II} = 7.4$	6.0
	II	13	8.2	$\sigma_I / \sigma_{III} = 4.0$	
	III	24	—		
$E_\pi - V_R = 296$	I	76	34.8	$\sigma_I / \sigma_{II} = 6.3$	5.1
	II	12	6.8	$\sigma_I / \sigma_{III} = 3.6$	
	III	21	—		
$E_\pi - V_R = 244$	I	118	68.2	$\sigma_I / \sigma_{II} = 7.4$	6.6
	II	16	10.4	$\sigma_I / \sigma_{III} = 3.9$	
	III	30	—		
Quasifree scattering					
$E_\pi = 330$	(2)	34±4	25±4	$\sigma_{(2)} / \sigma_{(3)} = 2.6\pm0.7$	4.2±1.3
	(3)	13±3	6±2		
	(5)	—	—		
$E_\pi = 273$	(3′)	50±7	39±6	$\sigma_{(3')} / \sigma_{(2')} = 3.6\pm1.1$	4.9±2.0
	(2′)	14±4	8±3	$\sigma_{(3')} / \sigma_{(5')} = 1.5\pm0.3$	
	(5′)	34±6	—		

this need not be done, since any interaction that leads to a change in charge of an α particle is an inelastic process.

To take into account the change in the relative energy due to intranuclear motion of the nucleons, we shall average the total cross sections for the interaction between pions and free protons over the function of momentum distribution of the nucleons in the nucleus. If the distribution function is taken in the form $A \exp(-p^2/p_0^2)$ with a value p_0 = 150 Mev/c, and we use the experimental energy dependence of the π-p interaction cross section,[12-15] then the calculated effective cross sections hardly differ from the cross sections of the corresponding processes on protons at rest at the same energies in the laboratory system of coordinates. Thus, in this range of energies one can disregard the effect of the intranuclear motion of the nucleons on the value of the relative meson energy.

Finally, we can also take into account the presence of a repelling nuclear potential, which reduces the kinetic energy of the pions in the nucleus. The values of the real part of the average nuclear potential V_R can be assumed to be 29 and 34 Mev for the energies 273 and 330 Mev respectively (more details on this will be reported later). The results of the comparison of the corresponding cross sections are given in Table II. The data pertaining to interaction between $\pi^\pm$ mesons and protons were taken from the literature,[14,15] and the angular distributions were taken for values of energy close to those under consideration, and normalized to the corresponding total cross sections.

The quantities in Table II evidence clearly the influence of the factors considered on the results of the comparison. In accordance with the considerations advanced above, one must compare the values listed in column 6 for E_π-V_R and quasifree scattering. For both pion energies considered, the average values of the relative scattering probabilities by bound neutrons and protons is undervalued. However, owing to the large statistical errors, the reliability of this fact is low. If we consider in addition the roughness of the scheme adopted for the comparison, and also the possible systematic errors in the separation of quasifree scattering cases, it is obvious that the results obtained give no grounds for doubting the purity of the isotopic states in quasifree scattering of pions.

TABLE III

Energy, Mev	γ
$E_\pi = 300$	0.63±0.06
$E_\pi = 273$	0.53±0.06
$E_\pi - V_R = 296$	0.47±0.05
$E_\pi - V_R = 244$	0.44±0.05

Table III lists the values of the coefficient γ, which characterizes the summary influence of the bond on the absolute cross section of interaction with bound nucleons. It is equal to the ratio of the total cross section of inelastic scattering between pions and He^4 nuclei to the sum of cross sections of interaction with free nucleons.

c) Angular distributions. The angular distributions of inelastic scattering in the laboratory system of coordinates are shown in Figs. 6 and 7.

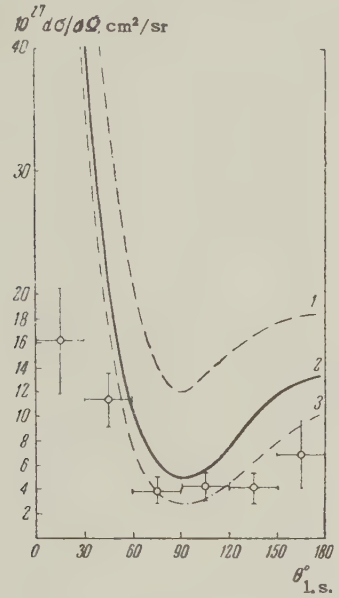

FIG. 6

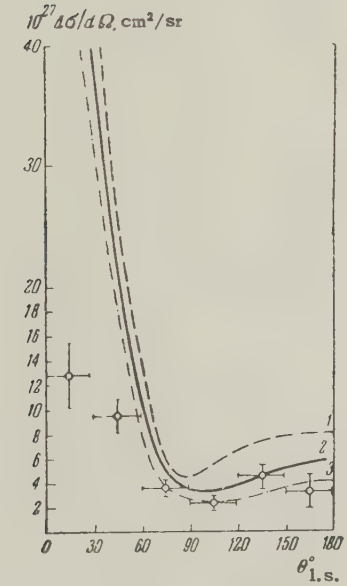

FIG. 7

FIG. 6. Angular distribution of inelastic scattering of π^+ mesons by He^4 at E = 273 Mev; curves – calculated: 1 – values of 2Σ for $E_\pi - V_R$ = 244 Mev, 2 – $(F/F_f) \times 2\Sigma$ at $E_\pi - V_R$ = 244 Mev, 3 – $(F/F_f) \times 2\Sigma$ at E_π = 273 Mev.

FIG. 7. Angular distribution of inelastic scattering of negative pions by He^4 at E = 330 Mev. The curves have been calculated by the same formulas as the corresponding curves of Fig. 6, but at the following energies: 1 – $E_\pi - V_R$ = 296 Mev, 2 – $E_\pi - V_R$ = 296 Mev, 3 – E_π = 330 Mev.

These include both quasifree and multiple-scattering events. The dotted lines in the same figures show the sums (multiplied by two) of the differential cross sections of the scattering of pions by free neutrons and protons[14,15]

$$2\Sigma = 2\,[d\sigma(\pi^- p \to \pi^- p)/d\Omega + d\sigma(\pi^+ p \to \pi^+ p)/d\Omega]$$

for energies $E_\pi - V_R$. The relative variation of the differential cross section of scattering by free nucleons is very similar to the angular dependence of inelastic scattering of pions by He^4. Exceptions are the region of small angles ($\theta < 40°$), where the inelastic scattering is noticeably suppressed. This phenomena can be understood by considering that the inelastic scattering by nuclei is forbidden at a relatively small energy transfer to the bound nucleons, as indeed happens in the case of scattering at small angles.

Watson and Zemach[16] have made an attempt to take into account theoretically the influence of coherent processes on inelastic scattering of pions by nuclei. Actually they have approximately taken account of the variation in the kinematic factors, due to the fact that the mesons are scattered in a medium where the potential differs from zero and varies with the pion energy. The differential scattering cross sections by free $(d\sigma/d\Omega)_f$ and bound $(d\sigma/d\Omega)_b$ nucleons they were able to relate by means of the simple equation

$$(d\sigma/d\Omega)_b = (F/F_f)(d\sigma/d\Omega)_f.$$

The factor F/F_f is a function of the angle θ, and also depends on the initial pion energy and on the value of the optical potential. In accordance with the theory considered, the angular dependence of this factor for meson energies of 273 and 330 Mev is shown in Fig. 8. On the basis of this dependence,

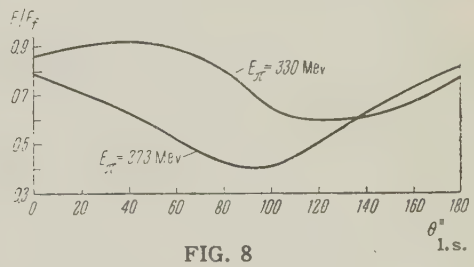

FIG. 8

we calculated the angular distributions of inelastic scattering of pions by He^4 nuclei. The calculations were made for two versions. In the first version $(d\sigma/d\Omega)_f$ were taken for the pion energy in the laboratory system. In the second version, we took into account the change in the pion energy by an amount V_R.

It is seen from Figs. 6 and 7 that the results of the calculations are in good agreement with the ex-

perimental points, particularly for $E_\pi = 330$ Mev. A great discrepancy is observed only in the region of small angles. But this is to be expected, since in the Watson-Zemach calculation no account was taken of the Pauli exclusion rule. Such a success of these calculations appears somewhat strange, since firstly the theory contains a large number of rough approximations, and secondly it does not reflect many factors which undoubtedly influence the size of the inelastic scattering cross section. In particular, the screening action of the nucleons is disregarded.

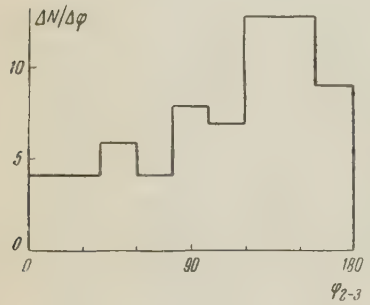

FIG. 9. Dependence of the number of events on the relative azimuth angle φ_{2-3} of the proton and H^3 nucleus in reactions $\pi^\pm + He^4 \to \pi^\pm + p + H^3$.

d) Correlation in the divergence of nucleons and residual nuclei. Figure 9 shows the distribution of the number of cases of quasi-elastic scattering of $\pi^\pm$ mesons by protons as a function of the angle between the projections of the proton and H^3 momenta on the azimuth plane. This distribution indicates that the proton and H^3 have a tendency to diverge in opposite directions (19 cases of travel in the same direction and 49 of travel in opposite directions). A possible interpretation of this phenomenon may be that the scattering of the mesons gives rise to an excited α-particle level, the existence of which is indicated by many experiments.[17] If we adopt this point of view and calculate the value of the excitation energy Q, its average is found to be approximately 20 Mev (Fig. 10) i.e., exactly the expected level. Errors in the determination of Q are quite large, and therefore one must not attach great significance to this result, since the agreement may be quite accidental. In addition, the observed correlation can be understood qualitatively within the framework of the Goldberger model. In fact, at the instant of collision between the pion and the proton, the latter has a momentum equal and opposite to the momentum of the H^3 nucleus. Since the momentum transferred by the meson to the proton by scattering is of the same order as the intranuclear momenta of the nucleons, the initial direction of motion of the proton should be conserved to the some extent.

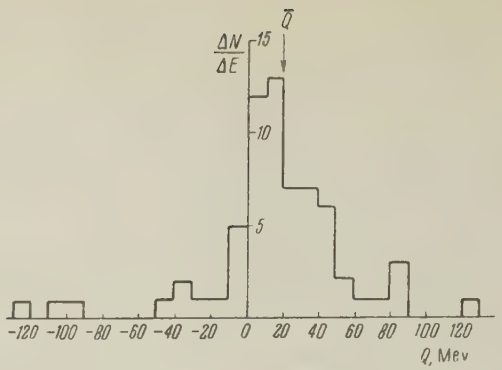

FIG. 10. Distribution of the values of Q for the reactions $\pi^\pm + He^4 \to \pi^\pm + p + H^3$.

5. NON-RADIATIVE CAPTURE

As already noted in Section 4, of all the cases of non-radiative capture of positive pions, the only capture that could be identified directly was the one with emission of two protons and a deuteron in the final state (8′). In all these cases the deuterons are slow, their momenta not exceeding 200 Mev/c. The protons display on the other hand an angular and momentum correlation, corresponding to the absorption of pions by free deuterons (see Fig. 11). Thus, we can interpret reaction (8′) as the capture of a pion by a deuteron pair. For the

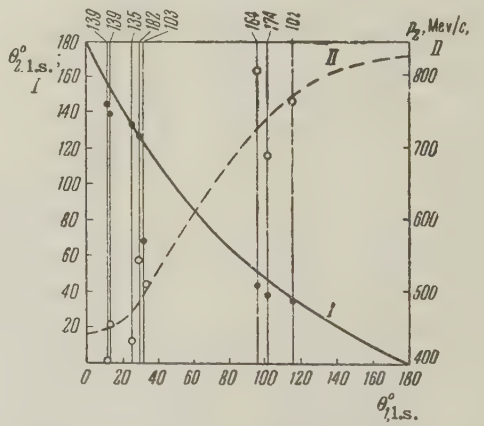

FIG. 11. Angular and momentum correlation in the reaction $\pi^+ + He^4 \to p + p + d$. The curves correspond to correlation in absorption by a free pair of nucleons; the full circles (left-hand scale) show the values of the angles θ_2, while the empty circles (right-hand scale) show the values of the momenta p_2. The numbers on top are the values of the momenta of the residual deuterons.

probability of the other possible cases of positive-pion capture, the only thing that is obtained experimentally is an upper limit. It can be estimated if all the events (6′) and (8′) (see Table I) are considered to be absorption. However, among the latter events there should be also multiple exchange-scattering events. Their fraction can be calculated

by assuming that the probability of the multiple-scattering processes, both with and without charge exchange, are the same. This assumption is partially justified by the roughness of the calculation of the cascade probability in both cases, which indicates that these probabilities are approximately equal. An estimate of the number of events of multiple-exchange scattering, obtained under this assumption, corresponds to 14, where a total of 13 events (6′) and (8′) were observed. This result can be interpreted (naturally, with a reliability determined by the small statistical accuracy) as evidence of the low probability for other processes of pion absorption, including the capture of negative pions by a pair of like nucleons.

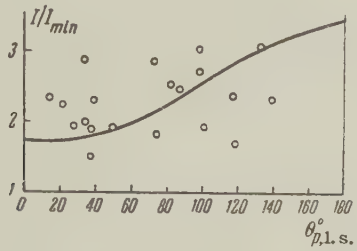

FIG. 12. Correlation between the angle of emission and ionization of fast protons in single-prong stars, produced by negative pions. The curve is obtained from kinematic calculations under the assumption that the absorption is produced by a free pair of nucleons.

We attempted to identify the absorption of negative pion processes by pairs of like nucleons directly from the correlation between the angle θ of emission of the fast proton and the ionization it produced. However, a reliable separation of the cases of absorption by a pair of like nucleons from other processes that lead to the emission of fast protons could not be attained, owing to the large error in the measurement of the ionization, and also owing to the ambiguous connection between the ionization and the angle (due to intranuclear motion). The results of the measurements are given in Fig. 12. For negative pions, as was done for the positive pions, an indirect estimate was made of the number of absorptions by a pair of like nucleons. It was assumed here, too, that the relative probabilities of capture by a deuteron pair at 273 and 330 Mev are equal. With the statistics accumulated for 300 Mev, this corresponds to 12 captures by an n-p pair, whereas an estimate of the number of absorptions by a p-p pair yields a value of 6.

The analysis of the experimental results on the capture of pions in helium indicates that apparently the pion capture is produced essentially by nucleon pairs, and the absorption by a deuteron pair is the principal process. This conclusion agrees with the results of investigation of the absorption of pions by more complex nuclei such as carbon, chlorine, and fluorine.[4-7]

6. RARE EVENTS

Five events of interaction of pions with helium were registered, and these cannot be ascribed to any of the foregoing processes. A characteristic feature of all these cases was that among the secondary products there was more than one fast particle, producing nearly minimum ionization (Fig. 13).

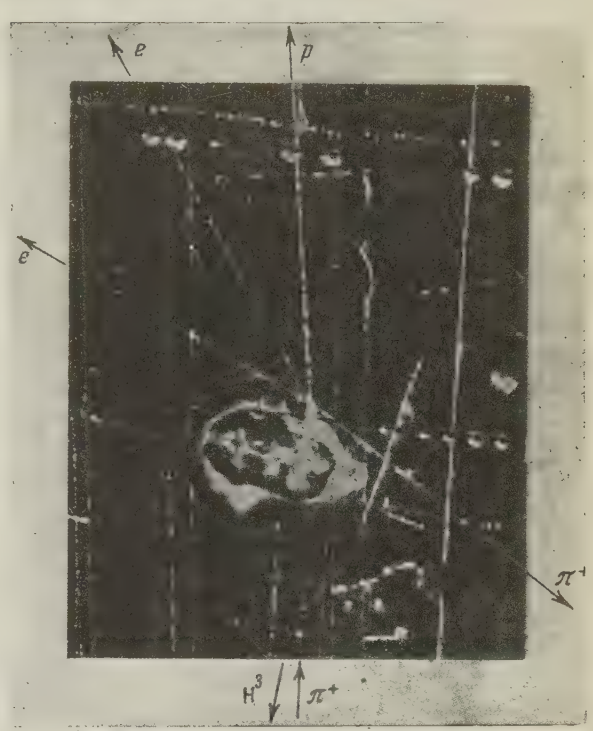

FIG. 13. Photograph of a probable production of a neutral pion with subsequent decay into 2e and a photon.

As noted above, in the scattering of 300-Mev pions there cannot be any protons with less than twofold ionization. These events can therefore be interpreted as the production of particles lighter than nucleons. An additional argument in favor of this statement is also the absence of angular correlation between the fast particles, which would appear in quasifree scattering of pions. Summary data on the observed events are listed in Table IV.

By virtue of the limited information, we cannot identify these events uniquely, and therefore the last column of Table IV lists only a probable interpretation. In addition to the conservation laws, we took into account in the interpretation certain considerations on the probable angles β between the electrons in the processes $\pi^0 \rightarrow 2e + \gamma$.

The authors are grateful to Professor Wang Kang-Ch'ang, L. I. Lapidus, and S. S. Filippov for useful discussions and many valuable comments.

TABLE IV

E_π, Mev	θ_1	θ_2	β	θ_3	θ_4	θ_5	Ionization	Probable interpretation
330	30.0	11.5	31.3	142.1	—	—	$I_1 \approx I_2 \approx I_{min}$	$\pi^- + He^4 \to \pi^0 + n + H^3$, $\pi^0 \to 2e + \gamma$
	162.8	19.8	146.7	116.6	—	—	$I_1 \approx I_2 \approx I_{min}$	$\pi^- + He^4 \to \pi^- + \pi^+ + (p, 3n)$
	63.5	130.5	150.0	17.4	—	—	$I_1 \approx I_2 \approx I_{min}$	
273	139.7	123.6	17.5	20.0	71.3	—	$I_1 \approx I_2 \approx I_{min}$	$\pi^+ + He^4 \to \pi^0 + p + He^3$, $\pi^0 \to 2e + \gamma$
	32.5	66.0	34.1	125.2	5.01	180	$I_1 \approx I_2 \approx I_3 \approx I_{min}$, $I_4 \approx (2-3) I_{min}$	$\pi^+ + He^4 \to \pi^+ + \pi^0 + p + H^3$, $\pi^0 \to 2e + \gamma$

[1] R. Serber, Phys. Rev. **72**, 1114 (1947).

[2] M. L. Goldberger, Phys. Rev. **74**, 1269 (1948).

[3] Brueckner, Serber, and Watson, Phys. Rev. **84**, 258 (1951).

[4] Byfield, Kessler, and Ledermann, Phys. Rev. **86**, 17 (1952).

[5] Blinov, Lomanov, Shalamov, Shabanov, and Shchegolev, JETP **35**, 880 (1958), Soviet Phys. JETP **8**, 609 (1959).

[6] Petrov, Ivanov, and Rusakov, JETP **37**, 957 (1959), Soviet Phys. JETP **10**, 682 (1960).

[7] Kozodaev, Sulyaev, Filippov, and Shcherbakov, Dokl. Akad. Nauk SSSR **107**, 236 (1956), Soviet Phys.-Doklady **1**, 171 (1956).

[8] Vasilenko, Kozodaev, Sulyaev, Filippov, and Shcherbakov, Приборы и техника эксперимента (Instrum. and Meas. Engg.) No. 6, 34 (1957).

[9] Voloshchuk, Kuznetsov, Sulyaev, Filippov, and Shcherbakov, ibid, in press.

[10] Kozodaev, Sulyaev, Filippov, and Shcherbakov, JETP **31**, 701 (1956), Soviet Phys. JETP **4**, 580 (1957).

[11] Kozodaev, Sulyaev, Filippov, and Shcherbakov, JETP **31**, 1047 (1957) [sic!].

[12] Ignatenko, Mukhin, Ozerov, and Pontecorvo, Dokl. Akad. Nauk SSSR **103**, 395 (1955).

[13] S. J. Lindenbaum and C. L. Yuan, Phys. Rev. **100**, 306 (1955).

[14] Mukhin, Ozerov, and Pontecorvo, JETP **31**, 371 (1957), Soviet Phys. JETP **4**, 237 (1957).

[15] V. G. Zinov and S. M. Korenchenko, JETP **33**, 335, 1307, 1308 (1957), **36**, 618 (1958); Soviet Phys. JETP **6**, 260, 1006, 1007 (1958), **9**, 429 (1959).

[16] K. M. Watson and C. Zemach, Nuovo cimento **10**, 453 (1958).

[17] Bogdanov, Vlasov, Kalinin, Rybakov, Samoĭlov, and Sidorov, Ядерные реакции при малых и средних энергих. (Nuclear Reactions at Low and Medium Energies), Acad. Sci. Press, M., 1958.

Translated by J. G. Adashko
90

NON-MESONIC DECAYS OF HYPERFRAGMENTS

I. B. BERKOVICH, A. P. ZHDANOV, F. G. LEPEKHIN, and Z. S. KHOKHLOVA

Radium Institute, Academy of Sciences, U.S.S.R.

Submitted to JETP editor August 28, 1959

J. Exptl. Theoret. Phys. (U.S.S.R.) **38**, 423-425 (February, 1960)

Non-mesonic decays of 18 hyperfragments were studied in the part of an emulsion stack irradiated with 4.5 Bev π mesons. The ratio of the number of decays due to the interaction between the Λ^0 particle and neutron to the number of decays due to interaction with a proton was determined. It turned out to be 1.25.

THERE have been a number of papers published recently on experimental investigations of non-mesonic decays of hyperfragments.[1,2] In these papers the quantity of interest is the ratio of the number of hypernucleus decays due to interaction of a Λ^0 particle with a neutron to the number of decays due to interaction with a proton:

$$R = N/P.$$

According to the theoretical considerations of Ferrari and Fonda,[3] the value of R gives information about the mechanism through which the Λ^0 particle interacts with the nucleons in the nucleus. The Λ^0 particle can interact directly with a nucleon, or through a virtual Σ state.

According to reference 3, in a direct interaction, no matter what the relative parities of the Λ^0 particle and the nucleon are, the value of R is

Kinematics of the particles

Serial Number	Primary Star	Tracks	Presumed Charge	Range μ	Angles $\theta_{F,\pi}$ $\theta_{F,i}$ deg	Presumed Decay Scheme
1	2	3	4	5	6	7
		A. Decays induced by neutrons				
1	14+1π	*F*	3	140.2	97	—
		1		745.6	16	
		2		75.5	68.5	
2	8+0π	*F*	3	145.5	90	—
		1		147.0	43.5	
		2		136.0	36.5	
3	9+2π	*F*	2	105.0	64.0	—
		1		378.0	74.5	
		2		82.0	81	
4	10+0π	*F*	2	46.0	74	—
		1		68.0	84.5	
		2		240.0	50	
5	18+0π	*F*	3	43.7	34	—
		1		17.6	89.5	
		2		66.3	18.5	
		3		16.3	105	
6	10+0π	*F*	2	97.2	123	—
		1		302.6	102.5	
7	9+1π	*F*	2	80.8	60.5	—
		1		20.2	23.6	—
8	12+2π	*F*	2	59.2	139	
		1		40.0	98.6	
9	13+0π	*F*	6	55.0	114	
		1		34.0	57	
		2		821.0	118	$\Lambda^5C^{12} \rightarrow Be^9 + 2H' + n^0$
		3		609.0	90.5	
10	16+0π	*F*	4	47.4	47	
		1		2630	172.5	
		2		72.4	115.3	
		3		32.0	89	
		4		104.5	88	

1	2	3	4	5	6	7
B. Decays induced by protons						
11	15+0π	F	2	153.0	20	
		1		92.0	52	
		2		>12000	36.5	
12	11+3π	F	2	50.0	29	
		1		5900	38	$\Lambda^0He^5 \to 2H^2 + n^0$
		2		3.5	54	
13	15+0π	F	2	77.7	30	
		1		<15000	136.5	$\Lambda^0He^5 \to H' + H^3 + n^0$
		2		16	83.5	
14	17+0π	F	3	181.0	88	
		1		>23000	59	$\Lambda^0Li^6 \to H' + He^4 + n^0$
		2		43	83	
15	18+3π	F	3	87.0	62	
		1		9900	46	
		2		88	32	$\Lambda^0Li^8 \to H' + 2H^3 + n^0$
		3		22	98	
16	7+0π	F	4	28.5	17	
		1		3746	139	$\Lambda^0Be^9 \to H' + H^2 + He^4 + 2n^0$
		2		2983	24	
		3		16.0	90	
17	15+0π	F	5	16.0	115	
		1		10.0	88.8	$\Lambda^0B^{10} \to He^4 + H' + 2H^2 + n^0$
		2		16500	61	
		3		26	91	
		4		47.5	124	
18	13+2π	F	6	94.5	79	
		1		47.0	72	
		2		48.5	132	$\Lambda^0C^{12} \to 2He^4 + H' + H^2 + n^0$
		3		135	154	
		4		<25000	48	

less than or equal to one ($R \leq 1$). Hence, if $R > 1$, the interaction must proceed through a virtual Σ state. At the present time, there is little experimental data on this problem. In the following we present some results obtained in part of a G-5 emulsion stack irradiated by 4.5 Bev π mesons.

After analyzing all the double stars found in a systematic search of 47 cm^3 of emulsion, 18 cases were selected which satisfied the following criteria: 1) the length of the connecting F-track was greater than 20 μ; 2) the connecting F-track was thinner toward the end of its range, as determined from measurements of the track width. The hyperfragments so found were separated into two classes. In the first class were all decays which had a singly charged particle with a range greater than 3 mm, while in the second class were all decays in which the secondary particles were slow ones. The ratio of the number of decays in the second class, N, to the number in the first, P, was 10/8 = 1.25. This ratio is definitely greater than one, since the error can only be positive (the value of N is too small if anything). Taking into account the results of reference 1, we conclude that the interaction of the Λ^0 particle with the nucleons is very likely through a virtual Σ state. We propose to improve the statistics, not only to solve this problem but also to find the parity of the $\Lambda^0 N$ system.

We also examined the angular distribution of the hyperfragments relative to the direction of the incident π-meson beam. Silverstein[2] found the forward/backward ratio to be 2.2 ± 0.5. According to our data, this ratio is 2.6. The forward/backward ratio for lithium fragments ("hammers") was also measured in the same emulsion. For Li fragments with energies comparable to the energies of the hyperfragments, the ratio turned out to be one.

All the experimental results discussed in the text are summarized in the table.

[1] Baldo-Ceolin, Dilworth, Fry, Greening, Huzita, Limentani, and Sichirollo, Nuovo cimento **7**, 328 (1958).

[2] E. M. Silverstein, Nuovo cimento **10**, Suppl. No. 1, 41 (1958).

[3] F. Ferrari and L. Fonda, Nuovo cimento **7**, 320 (1958).

Translated by R. Krotkov
91

INVESTIGATION OF THE ELASTIC SCATTERING OF π^- MESONS WITH MOMENTA 6.8 Bev/c FROM PROTONS IN A PROPANE BUBBLE CHAMBER

WANG KANG-CH'ANG, WANG TS'U-CHIENG, TING TA-TS'AO, V. G. IVANOV, Yu. V. KATYSHEV, E. N. KLADNITSKAYA, L. A. KULYUKINA, NGUYEN DINH TY, A. V. NIKITIN, S. Z. OTVINOVSKIĬ, M. I. SOLOV'EV, R. SOSNOVSKIĬ, and M. D. SHAFRANOV

Joint Institute for Nuclear Research

Submitted to JETP editor August 28, 1959

J. Exptl. Theoret. Phys. (U.S.S.R.) **38**, 426-431 (February, 1960)

The elastic scattering of 6.8 Bev/c negative pions from protons in a propane bubble chamber was studied. The total and differential cross sections for elastic scattering were obtained on the basis of 213 interaction events, and the total cross section for the π^--p interaction was also estimated:

$$\sigma_{el}\ (>6^\circ) = 3.75\ ^{+0.25}_{-0.55}\ \text{mb}, \quad \sigma_{tot} = 30 \pm 5\ \text{mb}.$$

It was found that the elastic scattering agreed, within the limits of experimental error, with the model of a proton as a homogeneous sphere with sharp boundaries: $R = 1.05 \times 10^{-13}$ cm, $K = 0.71 \times 10^{13}\ \text{cm}^{-1}$, $k_1 = 0$.

PION-PROTON scattering at high energies, where the de Broglie wavelength is much smaller than the effective region of the interaction, can give useful information on proton structure. In the present work, the investigation of the elastic scattering from protons of negative pions with momenta 6.8 Bev/c (wavelength $\lambda\!\!\!^{-} = 0.112 \times 10^{-13}$ cm) was done with a 24-liter propane bubble chamber[1] placed in a magnetic field of 13,700 oe.

Figure 1 shows the placement of the chamber and the other equipment in the pion beam.[2] The momentum distribution of the pions was obtained along 112 beam tracks measured in the chamber; it is given in Fig. 2. The average value of the momentum was (6.8 ± 0.6) Bev/c.

RESULTS AND ANALYSIS OF THE MEASUREMENTS

Two different scannings of the photographs obtained were carried out with a stereo lens by two persons. In all, about 3500 exposures were examined. From all the two-pronged stars, 550 cases which suggested elastic and quasi-elastic scattering were picked out. The coordinates of the interaction points and of the tracks were calculated with measuring microscopes on both stereo exposures.

The results of the measurements were analyzed by an electronic computer which gave the spatial coordinates of the tracks, the magnitude of the range of the recoil proton (for stoppings), the pion scattering angle θ_π, the recoil proton angle θ_p, and the azimuthal angles of the pion and of the recoil proton φ_π and φ_p. The error in the angles θ_π and θ_p was determined on the basis of two independent measurements of 80 events. The mean-square errors $\Delta\theta_\pi$ and $\Delta\theta_p$ were found to be 26′ and 1°14′ respectively. A correction was introduced for track curvature, although this did not exceed 20′.

The elastic pion-nucleon scattering cases were identified by the following criteria.

1. Coplanarity. As a measure of coplanarity we selected the angle between the plane formed by the incident and scattered pions and the plane formed by the incident pion and the recoil proton. This angle is equal to the modulus of the difference of the azimuthal angles: $\Delta\varphi = |\varphi_p - \varphi_\pi|$. Those events in which $\Delta\varphi$ did not exceed twice the mean square error were taken to be coplanar. The distribution of all 550 events by coplanarity parameter is given in Fig. 3.

2. Angular correlation. A region determined by the mean-square error was laid out along the correlation curve $\theta_\pi = f(\theta_p)$ for 6.8 Bev/c momentum pions. Elastic scattering cases had to lie in this region. Figure 4 shows the distribution of all the cases as a function of deviation from the correlation curve. The doubled mean-square error $\Delta\theta$ is taken as a measure of the deviation.

3. Range of the Recoil Proton (For Stoppings). This criterion was used in about 30% of the cases.

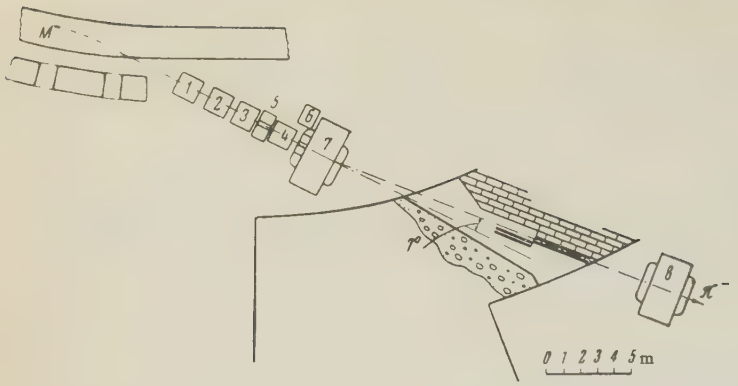

FIG. 1. Setup of equipment in π^- beam. 1–4) fixed focus lenses; 5 and 6) shielding; 7) deflecting magnet; 8) magnet containing chamber; M) beryllium target in accelerator chamber.

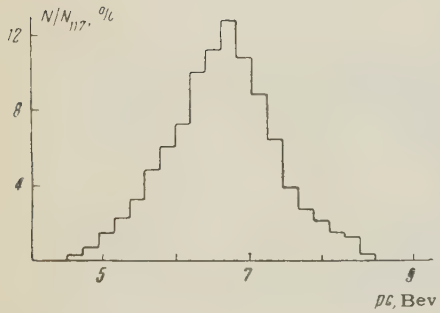

FIG. 2. Relative π- spectrum obtained from measurements of the moments of 112 beam tracks in the chamber.

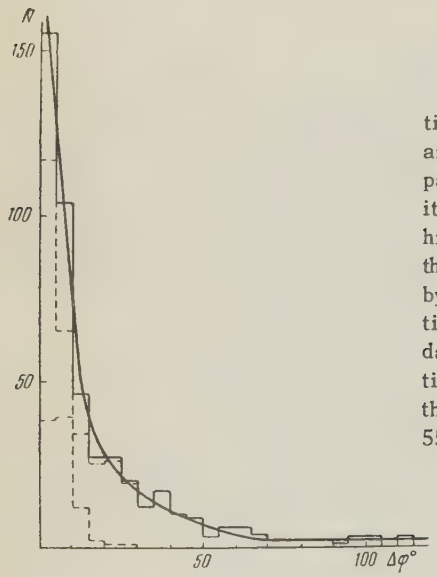

FIG. 3. Distribution of the number of analyzed events by parameter of coplanarity $\Delta\varphi$. The dotted histogram refers to the events identified by all criteria as elastic scattering; the dot-dashed one to inelastic scattering events; the solid one to all 550 events.

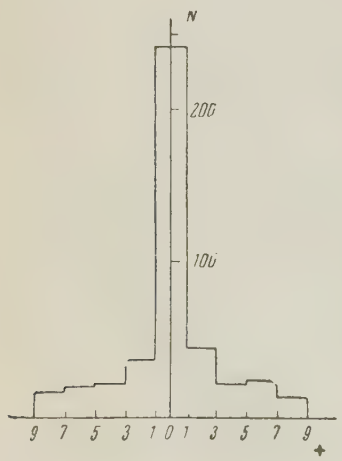

FIG. 4. Distribution of the number of two-pronged stars by deviation from the angular correlation curve. One division of the abscissa corresponds to the doubled mean square error.

Of all of the 550 events measured and analyzed, 218 events were classified as elastic. The distribution of these 218 cases of pion-proton elastic scattering are given in Fig. 5 as a function of longitudinal position in the chamber. A length of 43 cm of the central part of the chamber was taken as the effective region (the overall length of the chamber was 55 cm). Of the 218 events, 213 occurred in the effective region. The distribution of these 213 events by azimuthal angle of the recoil proton is given in Fig. 6.

FIG. 5. Distribution of 218 events of elastic π^--p scattering by length in the chamber. Zero corresponds to the center of the chamber.

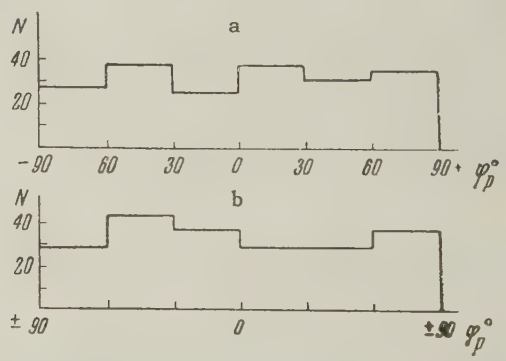

FIG. 6. Distribution of 213 events of elastic π^--p scattering, selected for analysis by azimuthal angle of the recoil proton φ_p: a) distribution above and below, b) left and right.

In 113 events the recoil proton went upwards, in 100 events downwards, in 115 events to the left, and in 98 cases to the right. Since the distribution by recoil proton azimuthal angle was isotropic, corrections for loss in the region near $\varphi_p = \pm 90°$ were not made.

An estimate of the contribution from quasi-

elastic events to the total number of elastic scattering events was made from the distribution of all events as a function of their deviation from the correlation curve. This contribution was about 6%.

To get the value of the elastic interaction cross sections, we counted, twice for each emulsion, the number of beam π^- tracks going through the effective region of the chamber, and the number of stars induced by beam negative pions. Taking into account the admixture of negative muons, estimated to be $(5 \pm 2)\%$, it was found that total length of tracks of negative pions was 1.15×10^6 cm. In 201 events it was found that

$$\sigma_{el}\ (\theta_\pi' > 6^\circ) = 3.75\ {}^{+0.25}_{-0.55}\ \text{mb},$$

where θ'_π is the pion scattering angle in the center-of-mass system.

An estimate of the total π^--p interaction cross section was also made. For this, we counted the number of stars containing an even number of prongs, and from them N_1 which had no more than one black track and N_2 which had an odd number of relativistic prongs and no black track. Under the supposition that at this energy $\sigma_t(\pi^- + p) = \sigma_t(\pi^- + n)$, we find that the number of stars created by negative pions from free protons is equal to $N_1 - N_2$. The value of $N_1 - N_2$ found leads to the cross section $\sigma(\pi^- \pm p) = (30 \pm 5)$ mb.

OPTICAL MODEL CALCULATION

We carried out an analysis of the scattering of negative pions from protons on the basis of the optical model. The homogeneous sphere[3] was used for a model of the proton. Under the hypothesis that elastic scattering has a purely diffraction character ($\sigma_{el} = \sigma_d$), we have the following relations expressing the total cross section of inelastic processes σ_i and the diffraction cross section σ_d by optical model parameters:

$$\sigma_i = \pi R^2 \{1 - [1 - (1 + 2B)e^{-2B}]/2B^2\} \qquad B = KR; \qquad (1)$$

$$\sigma_d = \sigma_d(K, k_1 = 0)\{1 + 4(k_1/K)^2[1 - \tfrac{1}{18}B^2 + \ldots]\}, \qquad (2)$$

$$\sigma_d(K, k_1 = 0) = (\pi R^2/4B^2)\{4B^2 - 14 - 2(1 + 2B)e^{-2B} + 16e^{-B}(1 + B)\}; \qquad \frac{d\sigma}{d\Omega}(\theta) = |f(\theta)|^2,$$

$$f(\theta) = ik_0 \int_0^R [1 - e^{(-K + 2ik_1)s}]\, J_0(k_0 \rho \sin\theta)\, \rho\, d\rho,$$

$$s = \sqrt{R^2 - \rho^2}. \qquad (3)$$

Here $f(\theta)$ is the scattering amplitude, θ is the scattering angle, k_0 is the wave number of the incident pion, k_1 is the change in the real part of the wave number, K is the absorption coefficient of the nucleon, and R is the radius of the sphere.

Calculations of the curves $\frac{d\sigma}{d\Omega}(\theta)$ were carried out for various values of σ_d, σ_i, and R. By comparing the calculated values with the experimental angular distributions, it was ascertained that the experimental data could be best described by a proton model with the following parameters:

$$R = 1.05 \cdot 10^{-13}\ \text{cm}, \quad K = 0.71 \cdot 10^{13}\ \text{cm}^{-1}, k_1 = 0,$$
$$\sigma_d = 5.5\ \text{mb}, \quad \sigma_i = 21.0\ \text{mb}.$$

Figure 7 shows the differential cross section of π^--p scattering for (6.8 ± 0.6) Bev/c, and Fig. 8 gives the dependence of $\lambda\!\!\!^{-2}d\sigma/d\Omega$ on $(\sin\theta'_\pi)/\lambda\!\!\!^{-}$ for negative pions with momentum 1.43 Bev/c, $\lambda\!\!\!^{-} = 0.272 \times 10^{-13}$ cm (reference 4) and 6.8 Bev/c,

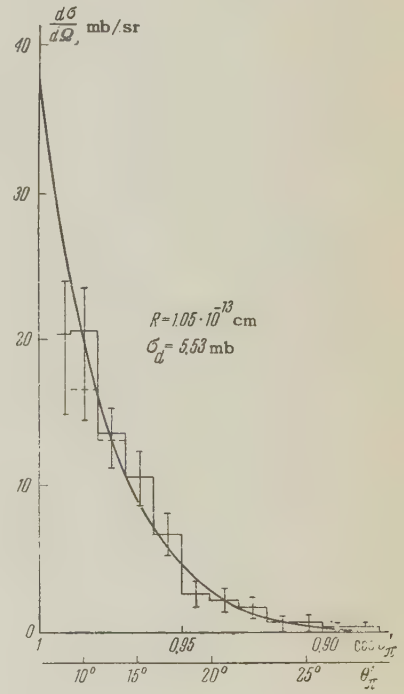

FIG. 7. Differential cross section for elastic π^--p scattering for average pion momentum (6.8 ± 0.6) Bev/c, based on 213 events. In the angular interval $\cos\theta'_\pi > 0.97$ are added 23 events (shown dotted) which could be identified as elastic scattering by the value of their recoil proton range and whose noncoplanarity did not exceed three times the error. The errors are everywhere statistical.

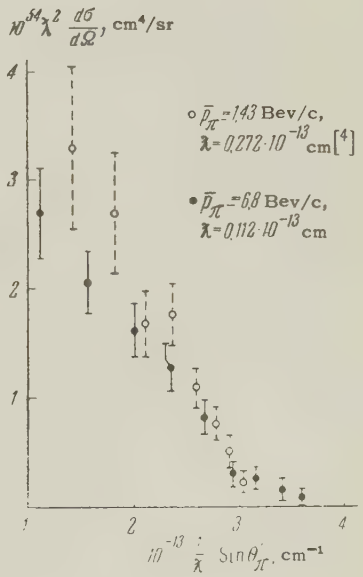

FIG. 8

E, Bev	σ_d, mb	σ_t, mb	10^{13} R, cm	10^{-13} K, cm^{-1}	$10^{-13}k_1$, cm^{-1}	$\sigma_t / \pi R^2$
1.3 [5]	7.4±1.0	26.4±2.2	1.08±0.06	—	—	—
1.4 [6]	7.0±1.0	34±3	1.18±0.10	0.67	~0	0.61±0.10
1.4 [4]	10.1±0.8	30±3	1.08±0.06	—	—	—
4.5 [7]	6.0±1.5	28±2.6	0.90±0.15	—	—	—
5 [8]	4.7±1.0	22.5±2.4	0.90±0.15	1.02	~0	0.6±0.2
6.8	5.5±0.5	30±5 (estimate)	1.05±0.05	0.71	~0	0.61

$\lambda\!\!\!^{-} = 0.112 \times 10^{-13}$ cm (present work). From Fig. 8 it follows that, notwithstanding the large energy difference, the connection between the quantities $\lambda\!\!\!^{-2}d\sigma/d\Omega$ and $(\sin\theta'_\pi)/\lambda\!\!\!^{-}$ is expressed by one curve. Evidently the physical significance of this result consists in the constancy of the average value of the transverse momentum transferred in elastic scattering. Consequently, in the energy region considered, the effective collision parameter determining the value of the cross section for the interaction of pions with nucleons does not depend very much on the energy. Therefore R, K, and k_1 do not depend much on the energy. This fact is also attested to by a comparison with other experimental data (see table). The small difference observed in the region of small values of $(\sin\theta'_\pi)/\lambda\!\!\!^{-}$ can evidently be explained by the fact that the scattering amplitude at momenta 1.4 Bev/c has a small real part, while at our energies the scattering amplitude is purely imaginary.

In conclusion the authors express their deep gratitude to Academician V. I. Veksler and I. V. Chuvilo for advice, to N. A. Smirnov, E. K. Kuryatnikov, Yu. I. Makarov, and M. A. Samarin for help with the experiment, and to L. Ya. Ivanova and K. N. Radina for help in carrying out the measurements.

[1] Wang, Solov'ev, and Shkobin, Приборы и техника эксперимента (Instrum. and Meas. Engg.) No. 1, 41 (1959).

[2] Wang, Ting, Ivanov, Kladnitskaya, Nguyen, Saitov, Solov'ev, and Shafranov, Report, High-Energy Lab. Joint Inst. Nuc. Res., 1959.

[3] Fernbach, Serber, and Taylor, Phys. Rev. **75**, 1352 (1948).

[4] Chretien, Leitner, Samios, Schwartz, and Steinberger, Phys. Rev. **108**, 383 (1957).

[5] J. Leitner, referred to in reference 7.

[6] Eisberg, Fowler, Lea, Shephard, Shutt, Thorndike, and Whittemore, Phys. Rev. **97**, 797 (1955).

[7] W. D. Walker, Phys. Rev. **108**, 872 (1957).

[8] Maenchen, Fowler, Powell, and Wright, Phys. Rev. **108**, 850 (1957).

Translated by W. Ramsay
92

CHARGED PION PRODUCTION IN INTERACTIONS OF 9-Bev PROTONS WITH EMULSION NUCLEI

N. P. BOGACHEV, S. A. BUNYATOV, T. VISHKI, Yu. P. MEREKOV, V. M. SIDOROV, and V. A. YARBA

Joint Institute for Nuclear Research

Submitted to JETP editor August 30, 1959

J. Exptl. Theoret. Phys. (U.S.S.R.) 38, 432-440 (February, 1960)

Nuclear disintegrations produced in photographic emulsions by 9 Bev protons and involving not less than three fast particles were studied. The charged π-meson energy spectrum, measured up to 540 Mev and extrapolated to the high-energy region, is presented. The angular distributions of fast π mesons and protons in the laboratory system were measured. The average number of π mesons and fast protons per disintegration was found. The fraction of primary proton energy carried away by π mesons is estimated. The ratio of the numbers of π and K mesons in the velocity range $\beta = 0.5 - 0.8$ has been derived.

1. EXPERIMENTAL CONDITIONS

SOME general information concerning the interaction of 9-Bev protons with emulsion nuclei[2-5] has been obtained after the proton synchrotron of the High-Energy Laboratory of the Joint Institute for Nuclear Research[1] had begun operation. The present article is an attempt to study the spectrum and the angular distribution of π mesons produced in the interaction of 9-Bev protons with emulsion nuclei.

An emulsion chamber consisting of a hundred layers of the NIKFI-R emulsion 450 μ thick, 10×10 cm in size, was irradiated by the internal proton beam. The emulsion layers were scanned under a microscope along the tracks of primary protons, using 630× magnification. For the study of the spectrum of π mesons produced in interactions of primary protons with complex emulsion nuclei, nuclear disintegrations with a number of fast particles $n_s \geq 3$ were chosen. (Particles with an ionization $J \leq 1.4 J_0$ were considered fast, where J_0 is the ionization along the tracks of primary protons. This ionization corresponds to a pion kinetic energy higher than 80 Mev and a proton kinetic energy higher than 500 Mev.) Such a choice made it possible to select events in which several π mesons are produced. Events recognized as proton-nucleon collisions[6,7] were excluded.

Measurements of multiple Coulomb scattering and ionization were used for identification of the secondary particles. The multiple scattering measurements were carried out for tracks with ionization $J \leq 2 J_0$ and length in one emulsion layer $l \geq 6$ mm. In constructing the spectrum, a geometrical correction was applied, because of the finite thickness of an emulsion layer and the limitation in the dip angle of the tracks (condition $l \geq 6$ mm). This correction was calculated according to the formula

$$\eta = \pi / [\arcsin(h_1 / l \sin\theta) + \arcsin(h_2 / l \sin\theta)].$$

Here l is constant and equal to 6 mm, θ is the spatial angle between the track and the direction of motion of the primary proton, and $h_{1,2}$ are the distances from the center of the star to the emulsion surface and to the glass respectively. Under the assumption of azimuthal symmetry of the angular distribution of secondary particles with respect to the direction of the primary protons, this correction yields the total number of particles at a given angle θ, i.e., takes into account also those tracks for which the scattering was not measured because of large dip angles.

From the distribution of the stars to which the selected tracks belong with respect to the number of fast particles n_s in the star, it was found, taking into account the geometrical correction, that the average multiplicity $\overline{n_s'}$ for the selected class of stars is 4.60 ± 0.14. It should be noted that the value $\overline{n_s'}$ obtained should be somewhat greater than the corresponding value $\overline{n_s}$ determined directly from the distribution of stars with respect to n_s found in scanning along the track,[4] as given by

$$\overline{n_s'} = \overline{n_s} + D/\overline{n_s},$$

where D is the dispersion of star distribution with respect to n_s. The quantity $\overline{n_s'}$ obtained for

stars with $n_s \geq 3$ from data of reference 2 was found to be equal to 4.78 ± 0.10. It can be seen that this value is, within the limits of error, in agreement with the value of the mean multiplicity for our selection criterion. This shows that, in selecting tracks with $l \geq 6$ mm from stars with $n_s \geq 3$, there was no bias against some stars and relativistic tracks.

2. SCATTERING AND IONIZATION MEASUREMENTS. PARTICLE IDENTIFICATION

The particles were identified by measuring the multiple Coulomb scattering and ionization. The scattering was measured using a Koristka MS-2 microscope. The table noise was measured by the multiple-beam interference method, and amounted to 0.03, 0.07, and 0.04 μ for cells of 100, 500, and 1000 μ respectively. The scattering measurements were carried out by the coordinate method.[8] False scattering[9] for different cell lengths was measured in several layers. The average value of false scattering $\bar{D}_f$ over a cell of 400 μ was found to be equal to 0.29 μ, which corresponds to the Coulomb scattering of a singly-charged particle with $p\beta = 1$ Bev/c. Therefore, a quantitative energy computation was carried out only for particles for which the value of $p\beta$, after correcting for false scattering, was not higher than 650 Mev/c; the maximum correction for false scattering was then less than 15%.

Preliminary measurements were made on each track (20 readings with a cell of 250 μ), from which the optimum cell length t was determined. (It was required that $\bar{D}_t/\bar{D}_n \geq 2$, the average value of the measurement noise D_n being equal to about 0.2 μ.) The final measurements were carried out with a cell shorter by a factor of two than the optimum one, in order to exclude the measurement noise (grain noise and reading noise). The value $p\beta$ was calculated according to the formula

$$p\beta = \frac{k}{0.573 \cdot D_{100}} \text{ Mev/c.}$$

$$D_{100} = \sqrt{\frac{(D_t^2 - D_{tf}^2) - (D_{t/2}^2 - D_{t/2\,f}^2)}{t^3 - (t/2)^3}} \ \mu.$$

The scattering constant as a function of the particle velocity and cell size was taken according to Gottstein et al.,[10] and did not vary greatly in the measurements described here, its value being $k = 24 - 25$. To take into account the distortion of tracks, calculation of third, and where necessary, fourth differences, was carried out. The statistical error in the scattering measurements, calculated according to the formula $\sigma = 0.75/\sqrt{N}$, where N is the number of cells, was not greater than 13%. For several tracks, the values of $p\beta$ were calculated taking false scattering into account, according to the maximum likelihood method described by Solntsev.[11] The values of $p\beta$ thus obtained did not differ, within the limits of error, from the results obtained by the method described above.

As a result of scattering measurements on the selected 204 tracks, it was found that 78 tracks have $p\beta \leq 650$ Mev/c and 126 tracks $p\beta > 650$

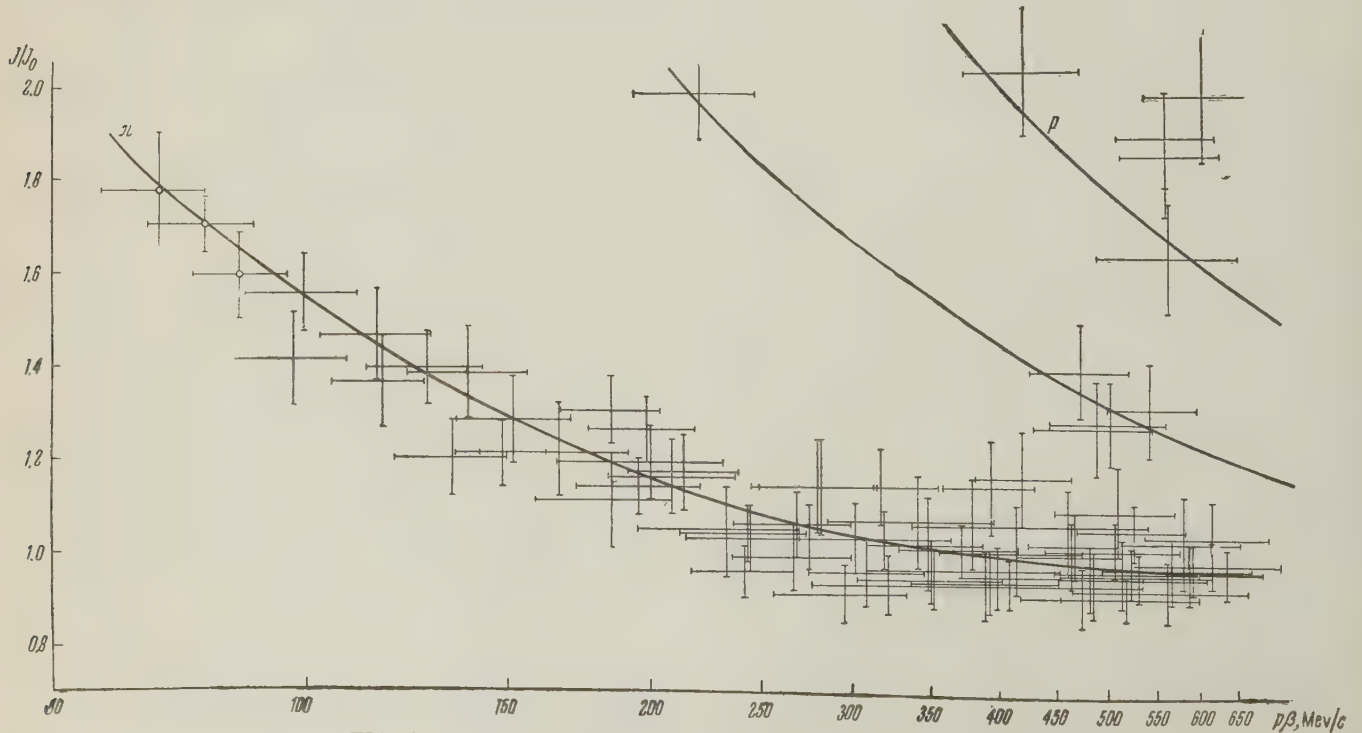

FIG. 1. Variation of ionization with $p\beta$ for the NIKFI-R emulsion.

Data on K mesons produced in collisions between 9 Bev protons and nuclei*

θ, deg	η	J/J_0	pβ, Mev/c	E_K, Mev	Type of parent star	
					n_s	N_h
32	22.5	1.4	475±46	290	4	3
35	24.0	1.3	506±58	315	4	4
26	18.3	1.3	490±57	300	5	6
3	2.0	2.0	222±26	121	6	6
27	19.0	1.3	546±45	345	7	6

*N_h – number of particles with ionization $J > 1.4 J_0$ in the star; E_K – kinetic energy of the K meson.

Mev/c. Ionization was measured by counting of gaps and blobs above a certain size along the given track.[12] Statistical errors of the measurement of the relative ionization were not greater than 7%.

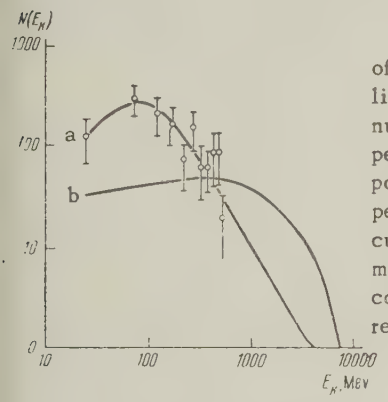

FIG. 2. Energy spectrum of π mesons produced in collisions of 9-Bev protons with nuclei; a – data of the experiments, the curve corresponds to the empirical dependence (1); b – theoretical curve for spectrum of π mesons produced in N–N collisions according to reference 13.

The variation of ionization with pβ obtained in the experiment is shown in Fig. 1. The circles denote π mesons stopping in the emulsion chamber. Their energy, as found from multiple scattering, is in agreement with the energy determined from range measurements. Curves for K mesons and protons are constructed from the π meson curve. It is evident that the experimental points are grouped around these curves. Among the particles with $p\beta \leq 650$ Mev/c and $J \leq 2 J_0$, 69 π mesons, 4 protons, and 5 K mesons were identified. Data concerning K mesons and their parent star are given in the table. In order to detect associated production of charged strange particles, all black and grey tracks ($J > 1.4 J_0$) emerging from stars in which K mesons were identified were scanned. No strange particles were found among the scanned tracks.

Particles with $p\beta > 650$ Mev/c and $J \leq 1.4 J_0$ were not identified; it was assumed that this group of particles consists only of π mesons and protons, and the particles with $p\beta > 650$ Mev/c and ionization in the range $1.4 J_0 \leq J \leq 2 J_0$ were considered to be protons. After introducing geometrical corrections, the following effective numbers of particles were obtained; π mesons — 1326, protons — 266, K mesons — 86, unidentified particles — 879.

In scanning the tracks with ionization $J > 2 J_0$, one event of Σ-hyperon decay was detected among the tracks stopping in the chamber. The hyperon was produced in a parent star of the type 4 + 2p. The emission angle of the hyperon was 29°, ionization $J = 6.5 J_0$, energy determined from ionization and scattering ~ 60 Mev. The hyperon traversed 7.7 mm and decayed in flight according to the scheme $\Sigma^{\pm} \rightarrow n + \pi^{\pm}$; the ionization of the π meson $J = 1.1 J_0$ and the energy was approximately 100 Mev. The angle of emission of the π meson in the c.m.s. was $\theta_{\pi}^{*} = 65°$.

3. ENERGY SPECTRUM OF π MESONS

The energy spectrum of π mesons is shown in Fig. 2. As mentioned above, the measurement of the energy of particles was limited by the value $p\beta \leq 650$ Mev/c (corresponding π meson energy 540 Mev). Moreover, the scattering was measured only for tracks with $J \leq 2 J_0$, which limited the spectrum from the low-energy end. For the determination of the number of slow π mesons emerging from stars with $n_s \geq 3$, all tracks with ionization greater than $2 J_0$ were followed in some of the stars. From the number of π mesons with $J \geq 2 J_0$ found in this fraction of stars, the total number of slow π mesons in all selected stars with $n_c \geq 3$ was determined.

The following empirical formula was found to fit the experimental points of the spectrum in the measured energy range:

$$N(E_k) = E_k / (a - bE_k^{\alpha}). \quad (1)$$

where E_k is the kinetic energy of π mesons in Mev. The coefficients a, b, and α were determined by the least-squares method* and found to

*The computations were carried out using the "Ural" computer. The authors are grateful to N. N. Govorun for carrying these out, and also to V. A. Meshcheryakov for help in reducing the data.

be $a = 0.17 \pm 0.07$, $b = (1.2 \pm 1.4) \times 10^{-6}$, $\alpha = 2.60 \pm 0.35$ (see curve a in Fig. 2). Information on the spectrum in the meson energy range > 540 Mev was obtained by extrapolating the empirical function found up to the energy of 7.6 Bev (maximum energy which can be attained by π mesons in nucleon-nucleon collisions in three-pion production by 9 Bev incident nucleons). The spectrum of π mesons measured in cosmic rays up to the energy of 2 Bev by Baradzeĭ et al.[14] for primary particle energy of about 10 Bev is of the same form. The number of π mesons with $p\beta > 650$ Mev/c, obtained by extrapolating the spectrum, was found to be equal to 400, and hence the number of protons with $p\beta > 650$ Mev/c equals 479.

An estimate of the mean total pion energy, taking into account the inaccuracy due to the extrapolation, leads to a value $\bar{E} = (0.7 \pm 0.2)$ Bev for the whole spectrum and $\bar{E} = (0.8 \pm 0.2)$ Bev for fast mesons. The estimates of the mean energy of π mesons given in references 4 and 5 are in agreement with these results.

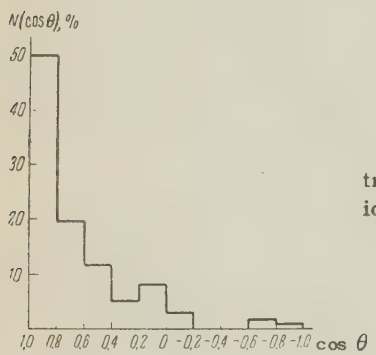

FIG. 3. Angular distribution of π mesons with ionization $J \leq 1.4 J_0$

The ratio of the number of fast π mesons to the number of fast protons was found to be equal to 3.2 ± 1.9, and the fast-particle multiplicity $\bar{n}_s = 4.37 \pm 0.10$. Hence, one can determine the mean number of fast π mesons (n_π) and fast protons (n_p) per interaction. For the stars under consideration, these numbers are $n_\pi = 3.3 \pm 0.5$; $n_p = 1.0 \pm 0.5$. The number of π mesons with $E_k \leq 80$ Mev per interaction as determined from the spectrum equals 0.6 ± 0.2. The number of all charged π mesons N_π (fast and slow) per interaction equals 3.9 ± 0.5. In order to determine the mean energy of π mesons separately for light and heavy nuclei, all π mesons were divided into two groups: π mesons from stars with $N_h > 8$ (60% of the total number of π mesons), and from stars with $N_h \leq 8$ (40% of the total number of π mesons). It was found that, in the measured spectral region, the mean energy of π mesons from heavy nuclei ($N_h > 8$) is smaller by roughly 100 Mev than the energy of π mesons from the group of nuclei with $N_h \leq 8$.

In order to find the variation of the mean π-meson energy with the number of fast particles in a star, all stars were divided into two groups: one with $n_s = 3$ or 4, and the second with $n_s > 4$. The number of stars in the groups was found to be roughly the same. The mean energy of π mesons for these groups over the measured part of the spectrum does not change, within the limits of error.

4. ANGULAR DISTRIBUTION OF FAST π MESONS AND PROTONS

The angular distribution of fast π mesons ($J \leq 1.4 J_0$) in the laboratory system is shown in Fig. 3. π mesons with energy greater than 540 Mev were included in the first interval ($\cos\theta = 1.0 - 0.8$), as found from the angle-energy relation for π mesons shown in Fig. 4. The points in

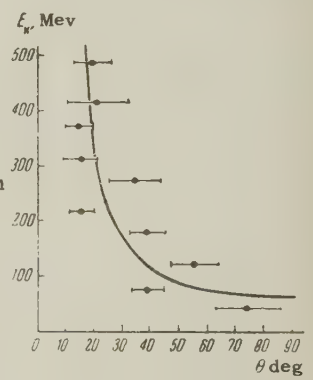

FIG. 4. Variation of π meson energy with emission angle.

Fig. 4 have been obtained by averaging the data over all emission angles of π mesons in the energy interval. The half angle of fast π mesons (the angle which contains half of all particles) $\theta^{\pi}_{1/2} = (36.5 \pm 8.8)°$. The angular distribution of fast protons in the laboratory system is shown in Fig. 5.

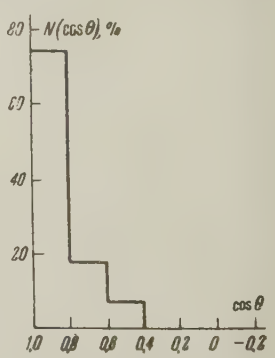

FIG. 5. Angular distribution of protons with ionization $J \leq 1.4 J_0$.

Since none of the fast protons ($p\beta > 650$ Mev/c) have been identified, in order to construct their angular distribution, fast π mesons ($p\beta > 650$ Mev/c) were subtracted from the angular distribution of all fast unidentified particles. (All the π mesons were subtracted from the interval $\cos\theta = 1.0 - 0.8$, as found from the angle-energy relation.)

The half angle for fast protons is $\theta^{p}_{1/2} \sim 29°$. The half angle of all fast particles for stars with $n_s \geq 3$ equals $\theta^{\pi p}_{1/2} = (30.5 \pm 5.0)°$.

5. DISCUSSION OF RESULTS

1. A comparison of the energy spectrum obtained (Fig. 2) with the spectrum of π mesons obtained in cosmic rays[14] shows that, within the limits of error, the spectra are not different. The spectrum obtained in the present experiment has a maximum near 100 Mev. Spectra of secondary π mesons originating in collisions of π mesons with energies of 1.5 and 4.2 Bev with emulsion nuclei, as obtained by other authors,[15,16] also have a maximum in the range 100 — 150 Mev. Thus, independent of the nature of the incident particle, and over a wide energy range, the position of the maximum in the spectrum does not change. This, evidently, indicates that the majority of π mesons, at least in the 100 — 150 Mev energy range, are essentially produced as a result of secondary collisions inside the nucleus. This is also confirmed by a comparison of the spectrum obtained with the spectrum of π mesons calculated[13] for nucleon-nucleon collisions according to the statistical theory of multiple particle production and using the isobar method (see curve b in Fig. 2). It is evident that the observed energy spectrum is shifted towards lower energies. It is natural to assume that the difference between the observed spectrum of π mesons emitted in collisions of protons with nuclei and the theoretical spectrum of π mesons in nucleon-nucleon collisions is due to secondary processes inside the nucleus. (It is also quite possible that the statistical theory does not predict the spectrum of π mesons from N-N collisions accurately enough.)

As has been mentioned above, the mean energy of π mesons originating in stars with $N_h > 8$ in the measured part of the spectrum is, by roughly 100 Mev, lower than for the group of stars with $N_h \leq 8$. In addition, if π mesons with $p\beta < 650$ Mev/c are emitted roughly with the same frequency from stars with $N_h > 8$ and $N_h \leq 8$, then the particles with $p\beta > 650$ Mev/c are emitted from the stars with $N_h \leq 8$ three times more frequently than from stars with $N_h > 8$. These results can be explained by a large number of collisions in heavy nuclei, as compared with the number of collisions in light nuclei. In fact, it is natural to assume that the number of collisions in the nucleus is proportional to the radius of the nucleus, and, consequently, the number of collisions in heavy nuclei of the emulsion should be twice of that in light nuclei. On the other hand, the mean number of fast particles in the groups of stars under investigation does not differ greatly. Thus, for stars with $N_h \leq 8$ and $N_h > 8$, these numbers are 4.24 ± 0.13 and 4.47 ± 0.16 respectively. This can be explained by the fact that, in heavy nuclei, the multiplicity of relativistic particles produced in secondary collisions decreases rapidly with the development of the cascade.

2. The results obtained in the experiment make it possible to find the mean energy spent for the production of π mesons in the collision of 9 Bev protons with nuclei. Using the value of the mean energy of π mesons in the spectrum and the mean number N_π of charged π mesons per interaction for the chosen class of stars, one can find that the following energy is, on the average, spent for meson production

$$E_\pi = \tfrac{3}{2}\bar{E}N_\pi = (4.1 \pm 1.3)\ \text{Bev},$$

which amounts to $(45 \pm 14)\%$ of the energy of the primary proton. (It is assumed here that π^0 mesons carry away half of the energy transferred to charged π mesons.)

In experiments carried out using the proton synchrotron at 9-Bev proton energy,[3-5] the energy fraction carried away by fast π mesons equalled $(44 \pm 9)\%$, $(27 \pm 8) - (33 \pm 8)\%$, and $(33 \pm 9)\%$ respectively.

It should be mentioned that the energy carried away by π mesons obtained in the present experiment should be higher than the average for all disintegrations found in scanning along tracks, since events with $n_s \geq 3$, in which a large number of π mesons is produced, have been selected. Using the value for the energy fraction spent for meson production as obtained in the present article and that of the disintegration energy of nuclei from reference 3, we obtain the value 0.43 ± 0.14 for the energy fraction carried away by the proton after colliding with a nucleus. For nucleon-nucleon collisions, the energy fraction carried away by the proton is, on the average, equal to 0.65.[7]

From these results, it follows that the primary proton undergoes approximately two collisions with an average nucleus of the emulsion.

3. The measurements of the values of $p\beta$ and of the ionization along tracks of particles produced in collisions of primary protons with nuclei made it possible to identify five $K^{\pm}$ mesons in the ionization range $1.2\,J_0 \leq J \leq 2\,J_0$ (corresponding to a velocity interval $\beta = 0.8 - 0.5$). The energy interval for π mesons with such velocities is 22 — 95 Mev. Using the effective number of K mesons (86) and the number of π mesons calculated from

the spectrum (409), we obtain the value 5.0 ± 2.5 for the ratio n_π/n_K in the energy range under consideration. It should be noted that Kostanashvili and Shakhulashvili[17] obtained $n_\pi/n_K = 6$ for the range $\beta \leq 0.67$.

CONCLUSIONS

1. The energy spectrum of charged π mesons produced in interactions between 9-Bev protons and emulsion nuclei, with a number of charged particles $n_s \geq 3$, is described by the empirical formula (1).

2. The mean total π-meson energy $\bar{E} = (0.70 \pm 0.2)$ Bev, and the mean total energy of a fast π meson is equal to (0.8 ± 0.2) Bev.

3. The mean number of fast π mesons and protons per interaction is 3.3 ± 0.5 and 1.0 ± 0.5 respectively. For the mean number of π mesons with energy smaller than 80 Mev, the value of 0.6 ± 0.2 has been obtained.

4. The energy fraction carried away by π mesons (taking π^0 mesons into account) amounts to $(45 \pm 14)\%$.

5. The ratio of the number of charged π mesons and K mesons in the velocity interval $\beta = (0.5 - 0.8)$ equals 5.0 ± 2.5.

6. The experimental data obtained do not contradict the assumption that the interaction of 9-Bev protons with complex nuclei represents, for the stars under consideration, a series of consecutive collisions.

The authors are grateful to Prof. V. P. Dzhelepov and Prof. Kh. Khulubeĭ for the interest and attention they have shown, and also to G. I. Bogorovskaya, L. F. Zakharova, K. D. Sverdlina, and D. A. Flyagina for help in carrying out the measurements. One of the authors (T. Vishki) thanks Prof. I. Auslaender and E. Friedlaender for their discussion.

[1] Veksler, Efremov, Mints, Veĭsbeĭn, Vodop'yanov, Gashev, Zeĭdlits, Ivanov, Kolomenskiĭ, Komar, Malyshev, Monoszon, Nevyazhskiĭ, Petukhov, Rabinovich, Rubchinskiĭ, Sinel'nikov, and Stolov, Атомная энергия (Atomic Energy) **4**, 22 (1956); V. I. Veksler, Proceedings of the Second International Conference on Peaceful Applications of Atomic Energy, Papers of Soviet Scientists, vol. 1, M. 1959, p. 253 (in Russian).

[2] Bogachev, Wang Shu-Fen, Gramenitskiĭ, Kirillova, Lebedev, Lyubimov, Markov, Merekov, Podgoretskiĭ, Sidorov, Tolstov, and Shafranova, Атомная энергия (Atomic Energy) **4**, 281 (1958).

[3] Barashenkov, Belyakov, Wang Shu-Fen, Glagolev, Dalkhazhav, Kirillova, Lebedev, Mal'tsev, Markov, Tolstov, Tsyganov, Shafranova, and Yao Ch'ing-Hsien, Preprint, Joint Institute for Nuclear Research P-331, 1959.

[4] Bayatyan, Gramenitskiĭ, Nomofilov, Podgoretskiĭ, and Skzhipchak, JETP **36**, 690 (1959), Soviet Phys. JETP **9**, 483 (1959).

[5] Zhdanov, Markov, Strel'tsov, Tret'yakova, Cheng P'u-Ying, and Shafranova, JETP **37**, 611 (1959), Soviet Phys. JETP **10**, 433 (1960).

[6] Bogachev, Bunyatov, Merekov, and Sidorov, Dokl. Akad. Nauk SSSR **121**, 617 (1958), Soviet Phys.-Doklady **3**, 785 (1959).

[7] Bogachev, Bunyatov, Gramenitskiĭ, Lyubimov, Merekov, Podgoretskiĭ, Sidorov, and Tuvdendorzh, JETP **37**, 1225 (1959), Soviet Phys. JETP **10**, 872 (1960).

[8] P. H. Fowler, Phil. Mag. **41**, 169 (1950).

[9] Biswas, Peters, and Rama, Proc. Ind. Acad. Sci. **A41**, 154 (1955).

[10] Gottstein, Menon, Mulvey, O'Ceallaigh, and Rochat, Phil. Mag. **42**, 708 (1951).

[11] N. Solntseff, Nucl. Phys. **6**, 222 (1958).

[12] P. H. Fowler and D. H. Perkins, Phil. Mag. **46**, 587 (1955).

[13] Barashenkov, Belyakov, Bubelev, Wang Shou-Feng, Maltsev, Ten Gyn, and Tolstov, Nucl. Phys. **9**, 74 (1958).

[14] Baradzeĭ, Rubtsov, Smorodin, Solov'ev, Tolkachev, and Tulinova, Dokl. Akad. Nauk SSSR **115**, 685 (1957), Soviet Phys.-Doklady **2**, 367 (1958).

[15] J. E. Crew and R. D. Hill, Phys. Rev. **110**, 177 (1958).

[16] Abrahamson, Ben-Arieh, Yekutieli, and Alexander, Nuovo cimento **12**, 27 (1959).

[17] N. I. Kostanashvili and O. A. Shakhulashvili, JETP **36**, 1006 (1959), Soviet Phys. JETP **9**, 713 (1959).

Translated by H. Kasha
93

ELASTIC SCATTERING OF 300-Mev NEGATIVE PIONS BY HYDROGEN

I. M. VASILEVSKIĬ and V. V. VISHNYAKOV

Joint Institute for Nuclear Research

Submitted to JETP editor September 9, 1959

J. Exptl. Theoret. Phys. (U.S.S.R.) **38**, 441-444 (February, 1960)

The elastic scattering of 300-Mev negative pions from hydrogen was studied with the aid of a hodoscopic system with pulse-fed counters. Equation (1) gives the angular distribution for the elastic scattering under the hypothesis that the fundamental contribution to the scattering comes from the S and P waves.

IN the present work, a hodoscopic system with an adjustable pulse feed for the counters[1,2] was used to study the elastic scattering of 300-Mev negative pions. The experimental setup is shown in Fig. 1. Negative pions formed by the bombardment of a beryllium target by 670-Mev protons from the internal beam of the synchrocyclotron of the Joint Institute for Nuclear Research were bent in the magnetic field of the accelerator and were incident on a collimator set into a four-meter concrete shield. On the other side of the collimator stood a magnet which cleared the beam of particles with other momenta.

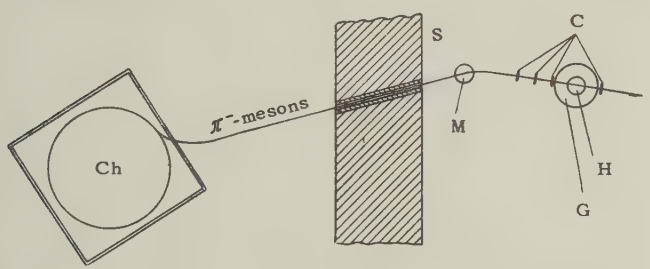

FIG. 1. Diagram of the arrangement of the apparatus: Ch – synchrocylotron chamber, S – shielding wall, M – deflecting magnet, C – scintillation counters, G – hodoscopic system, H – liquid hydrogen target.

The energy of the beam of pions was determined by measuring their range in copper, after taking into account corrections for multiple scattering of the mesons in copper and for slowing-down losses in the walls of the hydrogen target, and was equal to (300 ± 7) Mev, where the energy spread was obtained from the absorption curve. The admixture of negative muons in the pion beam was equal to 4%. The pion beam was picked out by a scintillation counter telescope and was incident on a polystyrene foam target in liquid hydrogen. The intensity of the meson beam, which was detected by the telescope, was about 13,000 particles/minute. The pion scattering process in the hydrogen target was separated by the hodoscope control system which

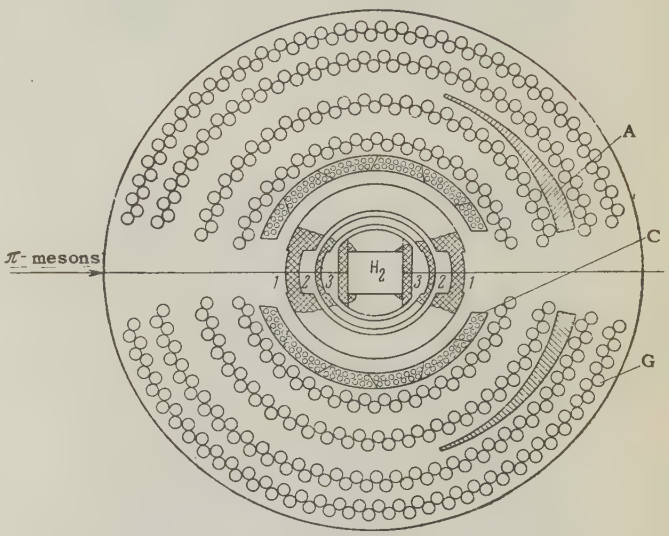

FIG. 2. Setup of the counters in the hodoscopic system: C – counters of the control system, G – hodoscopic system, A – copper absorber, 1, 2, 3 are the walls of the polystyrene foam target with the liquid hydrogen.

contained, besides the scintillation counter telescope, gas-discharge counters with small dead times, set in front of the hodoscope counters.

Figure 2 shows the arrangement of the counters in the hodoscopic system. The counters detected negative pions scattered in the whole angular interval from 20° to 160° in the laboratory system. In the angular interval from 20° to 70° relative to the incident beam, a copper absorber whose thickness varied with angle was set between the second and third rows of counters to separate the recoil proton from the scattered pions. When the scattered pions went into the solid angle determined by the controlling gas-discharge counters, a high voltage pulse was generated which passed through all the counters in the hodoscopic system. A gas discharge, displayed by MTX-90 neon bulbs, was produced by the pulse feed in those counters through which particles passed. A motion picture camera recorded the lighted neon bulbs.

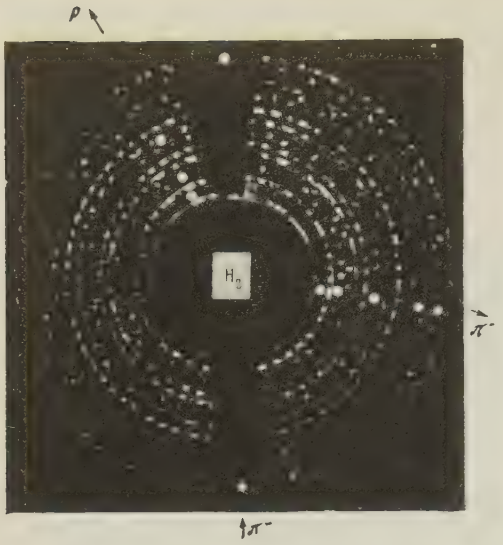

FIG. 3,

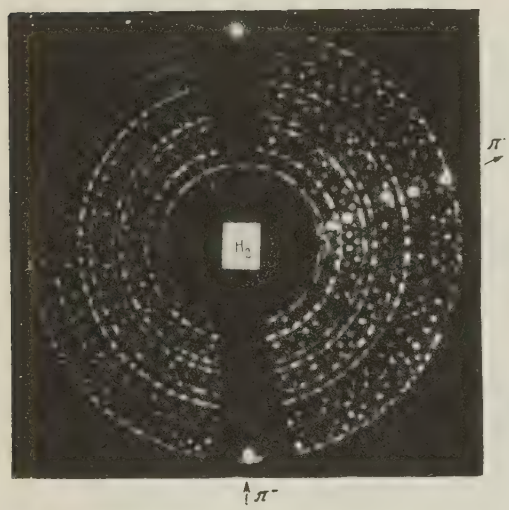

FIG. 4

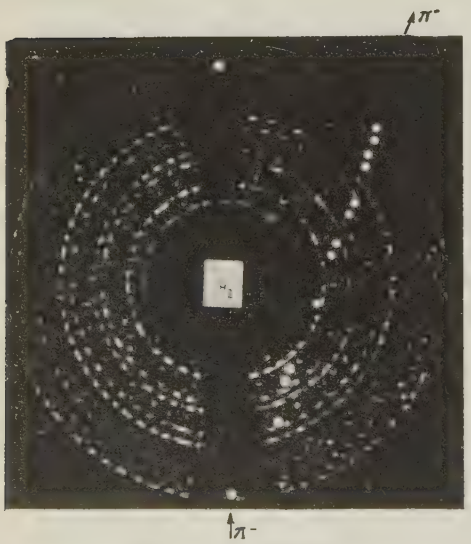

FIG. 5

To investigate negative pion scattering from hydrogen, measurements were carried out with the target first filled with hydrogen and then empty. The analysis of the exposures obtained was carried out in two steps. First the pellicles were examined with a D-1A diascope, and the scattering events were marked. Next each scattering event was analyzed in detail. To do this the activated counters recorded on the photographs were examined on a diagram showing the location of the hodoscopic counters.

In processing the plates only those cases were examined in which simultaneous counts were made in the four rows or in three arbitrary rows when the trajectory of the particle could be described.

All the trajectories obtained were broken down into several groups according to the following criteria:

1. A single photograph shows two trajectories whose angles of scattering relative to the incident beam of negative pions are connected by an angular correlation corresponding to energy and momentum conservation laws. These trajectories represent the tracks of the scattered meson and the recoil proton.

2. Trajectories of particles which can be described by a) scattering in the hydrogen or in the walls of the hydrogen target, b) scattering in the walls of the hydrogen target (1, 2, figure 2), c) scattering in the crystal of the scintillation counter, or d) accidental coincidences.

The photographs (Figs. 3 — 5) show the trajectories of the particles corresponding to groups 1, 2a, and 2c, respectively.

The hodoscope made it possible to discriminate, in a large angular interval, between the scattering events in the hydrogen or in the walls 3 (Fig. 2) and those scattering events in walls 1 and 2, which fact improved the statistical accuracy of the difference methods of measuring.

In analyzing the plates, about 1500 scattering events were found whose trajectories could be attributed to types 1 and 2a. Measurements without hydrogen showed that the scattering events with type 2a trajectories make up about a third of all the cases. Thus the number of events of scattering from hydrogen was about 1000. All the scattering events were broken down into angular intervals of 10°, and the differential cross sections were computed by the formula

$$(d\sigma(\theta)/d\Omega)_{\text{lab}} = (N_{\text{with H}} - N_{\text{without H}})/N_{\text{H}}\Omega(1-\alpha)N_{\pi}\varepsilon,$$

where $(N_{\text{with H}} - N_{\text{without H}})$ is the number of pions scattered from hydrogen, N_{H} is the number

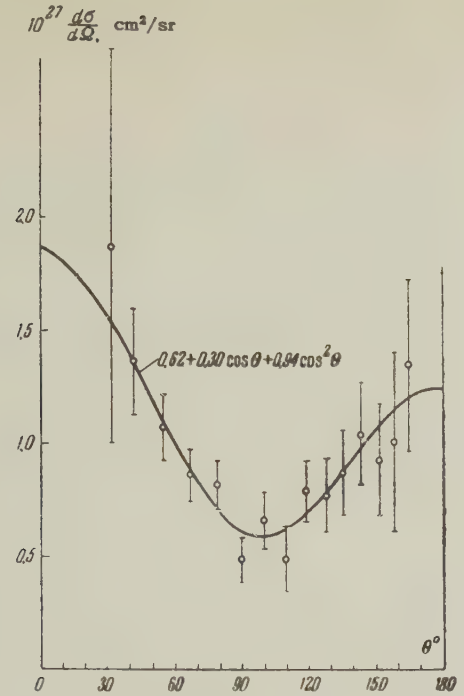

FIG. 6. Angular distribution for elastic scattering of 300-Mev negative pions from hydrogen.

of hydrogen atoms in 1 cm², Ω is the solid angle determined by the gas-discharge control counters, α is the fraction of negative muons and electrons in the beam, N_π is the number of π^- traversals through the hydrogen target (a correction for the dead time of the control system of the hodoscope was made in getting this number), and ϵ is the efficiency of detecting the pions. The efficiency of pion detection was determined, first, by the efficiency of the gas-discharge control system, second, by the efficiency of the hodoscopic counters, and third, by nuclear absorption in the copper absorber. The efficiency of the guide counters was 98%.[3]

For the chosen constant potential,[2] $V_0 = 1$ volt on the hodoscopic counters, the detection efficiency for each row was 85% for a high-potential pulse length of 0.8 μsec. For an individual counter efficiency of 85%, the probability is 52.3% that a particle would be recorded by four rows simultaneously, 36.8% by three, 9.8% by two, 1% by one, and 0.05% by none. The detection efficiency for a markedly higher selection of scattering cases was 89%. To measure the nuclear absorption in the copper absorber, the hodoscopic chamber (Fig. 2) was rotated about the vertical axis so that mesons passed through the copper filter. The energy of the pions was lowered to equal the energy of the pions scattered at the given angle. These measurements were carried out at several angles.

The angular distribution obtained of the differential scattering cross section is shown in Fig. 6, in the center-of-mass system. The errors shown in the differential cross sections are statistical. If it is conceded that the basic contribution to the scattering comes from S and P waves, then the angular distribution of the elastically-scattered pions in hydrogen can be given in the form

$$d\sigma/d\Omega = [(0.62 \pm 0.06) + (0.30 \pm 0.09)\cos\theta + (0.94 \pm 0.19)\cos^2\theta] \cdot 10^{-27} \text{ cm}^2/\text{sr} \quad (1)$$

To find the phase shifts in states with isotopic spin $T = 1/2$, we used the data from the present work on the elastic scattering of negative pions and the results of Mukhin and Pontecorvo for the elastic scattering of positive pions at 307 Mev.[4] The phase analysis was carried out with the aid of the "Strela" electronic computer. The phase shifts obtained by the Ashkin-Vosko graphical methods were used for initial data.

Two sets of phase shifts (see table) were found which gave a minimum value to the quantity

$$M = \sum (\Delta_i/\varepsilon_i)^2,$$

where Δ_i is the deviation of the calculated from the experimental values, and ϵ_i is the experimental error in the cross section. The expectation value of the quantity M was 19.

The introduction into the computer of initial data which differed from those obtained by the graphical method in both the values and signs of α_1, α_{11}, and α_{13} produced two sets of phase shifts, close to the sets given below.

The first set of phases are in satisfactory agreement with those obtained by Zinov and Korenchenko.[5] A better choice between the two sets can probably be made upon completion of the measurement, now in progress, of the polarization of the recoil protons in π^--p scattering.

In conclusion, the authors have the pleasant duty of expressing their thanks to A. A. Tyapkin for his guidance and help in the work and to N. I. Polumordvinova for help in carrying out the phase analysis.

	α_3	α_{31}	α_{33}	α_1	α_{11}	α_{13}	M
Set 1	−23.2°	−8.6°	133.3°	26.6°	10.7°	−3.1°	19.2
Set 2	−22.9°	−8.2°	133.3°	−11.6°	−2.4°	20.1°	18.5

[1] A. A. Tyapkin, Приборы и техника эксперимента (Instruments and Meas. Engg.) **3**, 51 (1956).

[2] V. V. Vishnyakov and A. A. Tyapkin, Атомная энерния (Atomic Energy) No. 10, 298 (1957).

[3] I. M. Vasilevskiĭ and V. V. Vishnyakov, Приборы и техника эксперимента (Instruments and Meas. Engg.), in press.

[4] A. I. Mukhin and B. Pontecorvo, JETP **31**, 550 (1956), Soviet Phys. JETP **4**, 373 (1957).

[5] Transactions of the International Conference on High Energy Physics, report of Prof. B. Pontecorvo, Kiev 1959.

Translated by W. Ramsay
94

ANTIPROTON CHANNEL WITH 2.8 Bev/c MOMENTUM

N. M. VIRYASOV, A. S. VOVENKO, G. G. VOROB' EV, A. D. KIRILLOV, KIM HI IN, B. A. KULAKOV, A. L. LYUBIMOV, Yu. A. MATULENKO, I. A. SAVIN, E. V. SMIRNOV, L. N. STRUNOV, and I. V. CHUVILO

Joint Institute for Nuclear Research

Submitted to JETP editor September 3, 1959

J. Exptl. Theoret. Phys. (U.S.S.R.) **38**, 445-448 (February, 1960)

An arrangement is described for separation of antiprotons, possessing a momentum of 2.8 Bev/c, obtained from the Joint Institute for Nuclear Research proton synchrotron. Data on the relative frequency of generation of antiprotons and π mesons in Be and Cu have been obtained.

THE antiproton channel described in this article is intended for a study of the interaction between antiprotons in a cloud chamber, operating in the controlled mode. The antiprotons are generated in the target by protons accelerated to 9 Bev.

1. ARRANGEMENT OF THE CHANNEL

The arrangement of the channel is shown in Fig. 1. The negative particles produced in the target are analyzed by momentum by the magnetic field of the proton synchrotron and by magnet M_1.

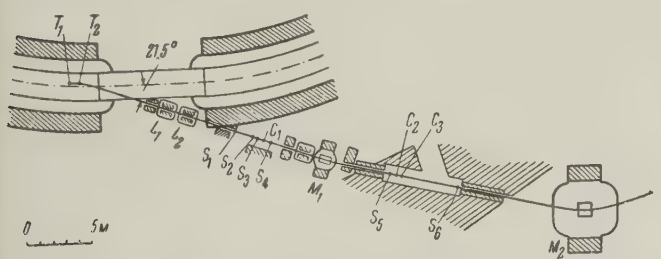

FIG. 1. Diagram of antiproton channel. L_1, L_2 – quadrupole lenses; M_1 – deflecting magnet, M_2 – magnet in which the cloud chamber is located, S_1, S_2, S_3, S_4, S_5 – scintillation counters, 9 cm diameter, 1 cm thick; S_6 – the same, 14.6 cm dia., 1.5 cm thick. C_1, C_2, C_3 – Cerenkov counters, 10 cm diameter, 3 cm thick; T_1, T_2 – targets for aiming the particle beam at 0 and 7° respectively.

The quadrupole lenses L_1 and L_2 focus the particle beam. The gradients in the lenses are chosen to correspond to the maximum number of particles passing through the scintillation telescope $S_1S_4S_5S_6$. The magnetic system segregates the momentum 2.8 ± 0.15 Bev/c.

2. SEGREGATION OF THE ANTIPROTONS

In the momentum-analyzed beam the anti-protons are identified by velocity ($\beta = 0.95$) by means of Cerenkov counters C_1, C_2, and C_3, operating on the total internal reflection principle.* The radiator used is a mixture of glycerine with alcohol (n = 1.430). In each Cerenkov counter two type FEU-33 photomultipliers are used, which can be connected in individual coincidence-circuit channels. The efficiency $\eta_{\bar{p}i}$ of these photomultipliers to antiprotons was determined indirectly, with the aid of the negative pions in the same beams, and the index of refraction of the radiator (n = 1.390) was chosen such as to simulate the identical conditions of the amount and gathering of the light (see Table I). When several photomultipliers are connected in a coincidence circuit, the values of $\eta_{\bar{p}i}$ are multiplied (see Table II). Generally speaking, in the presence of an inhomogeneity in the gathering of the light over the volume of the radiator, the registration of a single particle by several photomultipliers does not represent independent events. This appears in particular in the case of small Cerenkov-counter efficiences $\eta_{\pi i}$ (n = 1.430) to negative pions ($\eta_{\pi i}$ is the efficiency of the i-th photomultiplier to pions).

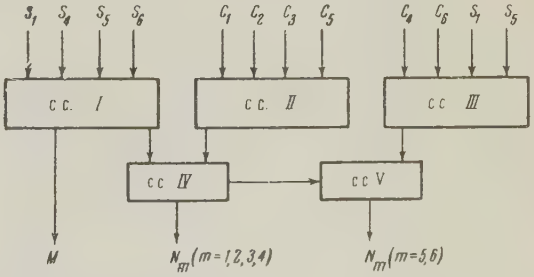

FIG. 2. Block diagram of the electronic circuitry. c.c. I, II, III – four-fold coincidence circuits with $\tau = 1 \times 10^{-8}$ sec; c.c. IV, V – two-fold coincidence circuits with $\tau = 5 \times 10^{-7}$ sec.

*A description of the counter will be published in the journal Приборы и техника эксперимента (Instruments and Measurement Engineering).

TABLE I

No. of photomultiplier	1	2	3	4	5	6
$\eta_{\bar{p}i}$, %	89±0.5	88±0.5	91±0.5	94±0.5	86±0.7	72±1
$\eta_{\pi i} \cdot 10^2$	5.7±0.2	4.2±0.2	8.5±0.4	11±0.4	4.4±0.2	—

TABLE II

Photomultipliers in the coincidence circuit	Experimental efficiency, %	Product of efficiencies, %	Photomultipliers in the coincidence circuit	Experimental efficiency, %	Product of efficiencies, %
1+2	73±2	78±1	1+2+3+4	66±2	61±2
3+4	83±1	85±1	1+2+3+5	—	64±2
1+2+4	69±1	69±1.5	1+2+3+4+5	—	53±2.5
			1+2+3+4+5+6	—	38±3

TABLE III

Photomultipliers in the coincidence circuit	1+2	3+4	1+3	2+4	3+5
Experimental efficiency of the two photomultipliers to pions ($\times 10^3$)	5.5±0.3	12.5±0.5	4.6±0.4	4.5±0.3	3.9±0.5
$\eta_{\pi i}\eta_{\pi j} \cdot 10^3$	2.4±0.2	9.3±0.7	4.8±0.4	4.6±0.4	3.7±0.3

TABLE IV

m	$\epsilon_{\bar{p}m}$, %	$\epsilon_{\pi m} \cdot 10^4$	$\alpha_m \cdot 10^4$	$\beta_m \cdot 10^4$	$n_{\bar{p}} \cdot 10^4$
1	90	600±200	600±200	—	—
2	80	80±40	80±40	—	—
3	70	5.3±0.3	6.7±1	—	—
4	64	0.51±0.03	1.22±0.04	0.71±0.05	1.10±0.08
5	53	0.03±0.01	0.53±0.04	0.50±0.04	0.95±0.1
6	38	0.002	0.35±0.07	0.35±0.07	0.92±0.22

It is seen from Table III that the multiplication takes place only in the case of photomultipliers taken from different counters (1+3; 2+4; 3+5).

A block diagram of the electronic apparatus is shown in Fig. 2. The coincidence circuit I counts all the particles passing through the counters (M). Connected in coincidence circuits II and III are m (from 1 to 6) photomultipliers from the Cerenkov counters. Here $N_m/N = \alpha_m$ is the relative count of the circuits, $\alpha_m - \epsilon_{\pi m} = \beta_m$ is the relative count of the antiprotons, $\epsilon_{\pi m}$ the efficiency of m photomultipliers to pions, $\beta_m/\epsilon_{\bar{p}m} = n_{\bar{p}}$ is the relative number of antiprotons in the beam, $\epsilon_{\bar{p}m}$ the efficiency of m photomultipliers to antiprotons.

It is seen from Table IV that α_m first decreases in proportion to $\epsilon_{\pi m}$ (m = 1, 2, 3) and then, as the relative count acquires a larger number of antiprotons, α_m varies as $\epsilon_{\bar{p}m}$. The ratios β_5/β_4 (70 ± 11)%, β_6/β_5 (66 ± 18)% give the efficiencies of the fifth and sixth photomultipliers to antiprotons. Within the limits of errors, these efficiencies coincide with the efficiencies determined with pions at n = 1.390.

The efficiency of this system to antiprotons is thus 60 — 40%. The corresponding suppression of pions amounts to $2 \times 10^4 - 5 \times 10^6$.

3. CONTROL EXPERIMENTS

1. One of the proofs that the particles separated are antiprotons and not an excess count due to negative pions is that the ratios β_5/β_4 and β_6/β_5 coincide with efficiencies to antiprotons.

2. When the index of refraction of the radiator is increased so that the light radiated by the antiproton experiences total internal reflection from the separation boundary, the efficiency of the counter to $\bar{p}$ and π mesons becomes approximately equal. Actually, when a radiator with a large index (n = 1.54) was placed in one of the Cerenkov counters (C_3), the relative count β_5 was reduced by a factor of approximately 12. This indicates that in this case $\eta_{\bar{p}5}$ became equal to approximately 7%, i.e., approximately the same as $\eta_{\pi i}$ for a radiator with n = 1.430.

3. When the energy of the accelerated protons is reduced to 6.3 Bev, particles with 2.8 Bev/c momentum enter into the channel, leaving the tar-

TABLE V

Angle, degrees	Target	Intensity of proton beam	No. of particles in channel per pulse	Relative number of antiprotons in beam $n_{\bar{p}}$
0	Be	10^9	1000	$(1.03 \pm 0.13) \cdot 10^{-4}$
7	Be	10^9	~700	$(1.37 \pm 0.18) \cdot 10^{-4}$
7	Cu	10^9	~700	$(2.42 \pm 0.53) \cdot 10^{-4}$

get at an angle $\gtrsim 12°$. The number of antiprotons among them should be very small.[1] The relative number of antiprotons, obtained in this experiment, was $n_{\bar{p}} \leq 3 \times 10^{-6}$.

4. RESULTS

The system described yielded the ratio of the number of $\bar{p}$ with momentum (2.8 ± 0.15) Bev/c to the number of remaining particles (essentially negative pions) from a beryllium target (36 g/cm^2) at angles of 0 and 7° and from a copper target (~ 180 g/cm^2) at an angle of 7° to the beam of incident protons, accelerated to 8.1 — 8.9 Bev (Table V). At an internal beam intensity of 10^9 p, the apparatus counted on the average one antiproton every four minutes.

5. DISCUSSION OF THE RESULTS

1. The number of particles in the channel agrees with the data on the interaction of 9-Bev protons, obtained in emulsions.[4]

2. The increase in $n_{\bar{p}}$ upon going from 0 to 7° in the laboratory system is in accordance with predictions based on spectra of particles, calculated by statistical theory.[2,3]

3. Considering the absorption of pions ($\sigma_t \sim 30$ mb) and antiprotons ($\sigma_t \sim 60$ mb) and the attenuation of the beam of primary protons ($\sigma_{in} \sim 30$ mb), we obtain the ratio of differential cross sections of the creation of antiprotons and negative pions with momentum 2.8 Bev/c at an angle of 0° in the laboratory system in beryllium:

$$\frac{d^2\sigma_{\bar{p}}}{d\Omega dp} \Big/ \frac{d^2\sigma_{\pi}}{d\Omega dp} \approx 1.5 \cdot 10^{-4}.$$

In conclusion, the authors consider it their pleasant duty to express their gratitude to the entire staff of the Proton Synchrotron Division for attention and for careful work.

[1] O. Chamberlain et al., Nuovo cimento **3**, 447 (1956).

[2] Barashenkov, Belyakov, Bubelev, Wang, Shu-Fen, Maltsev, Ten Gin, and Tolstov, Joint Institute for Nuclear Research, Preprint P-218, 1958.

[3] Zubarev, Mukhin, and Semenyushkin, Joint Institute for Nuclear Research, Preprint P-302, 1959.

[4] V. Beliakov et al., Proceedings of the Annual International Conference on High-Energy Physics at CERN, p. 309, 1958.

Translated by J. G. Adashko
95

ELECTRON PARAMAGNETIC RESONANCE SPECTRUM OF V^{3+} IN CORUNDUM

G. M. ZVEREV and A. M. PROKHOROV

Institute of Nuclear Physics, Moscow State University

Submitted to JETP editor September 10, 1959

J. Exptl. Theoret. Phys. (U.S.S.R.) **38**, 449-454 (February, 1960)

Electron-spin paramagnetic resonance has been investigated in a corundum single crystal with 0.13% V^{3+}. The experimental results are interpreted with the aid of the spin Hamiltonian, for which the following parameters were determined: $g_{\parallel} = 1.915 \pm 0.002$; $D = 7.0 \pm 0.3$ cm^{-1}; $|A| = (0.959 \pm 0.005) \times 10^{-2}$ cm^{-1}; $|E| < 10^{-2}$ cm^{-1}.

We have previously[1] reported the detection of the electron paramagnetic resonance spectrum of V^{3+} in corundum.* The present paper presents results obtained in a more detailed investigation.

The free V^{3+} ion, which has a $^3F_2$ ground level, contains two unpaired 3d electrons. A vanadium ion replaces an aluminum ion isomorphically in a corundum (Al_2O_3) single crystal, where it is surrounded by six oxygen ions forming a slightly deformed octahedron.[3] At the center of the octahedron, where the paramagnetic ion is located, the crystal electric field possesses basically cubic symmetry with a small admixture of fields having a lower order of symmetry. Figure 1 shows how fields with different symmetries split the F ground level of the free ion.

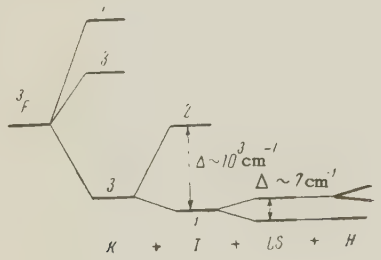

FIG. 1

The field of the corundum lattice is similar in character to the field of hydrated alum resulting from the octahedron of molecules of crystallization water. The splitting of the lowest energy level of V^{3+} in fields with different symmetries has been studied by Siegert[4] and Van Vleck[5] for the purpose of explaining the magnetic behavior of vanadium alum. The ground level of free V^{3+} possesses sevenfold orbital degeneracy ($L = 3$). A cubically symmetric field removes the orbital degeneracy and converts this level into a singlet (lying uppermost) and two triplets (Fig. 1). The components of a crystal field having trigonal symmetry further split the lower triplet into a singlet and a doublet, with a separation Δ on the order of 10^3 cm^{-1}. Thus in the corundum lattice field the lowest vanadium ion level will be a singlet with triple spin degeneracy.

The lower triplet is further split into a singlet and a doublet through spin-orbit interaction. Van den Handel and Siegert[6] in analyzing the magnetic susceptibility of vanadium-ammonium alum found a separation of 5 cm^{-1} between the higher-lying doublet and the singlet. The degeneracy of the triplet is completely removed by the admixture of a field with orthorhombic symmetry; this occurs in corundum.

Since at low temperatures and even at room temperature practically only the lowest energy levels are occupied, in the study of paramagnetic resonance we are interested in only the three lowest spin levels, with which we can associate the effective spin $S' = 1$ (Fig. 2). The singlet level corresponds to $S'_Z = 0$ and is nonmagnetic, while the doublet corresponds to $S'_Z = \pm 1$.

Paramagnetic resonance can be used to observe transitions between these three spin levels. Because of the large initial splitting of levels ϵ_1 and $\epsilon_{2,3}$ observation of absorption lines representing the transitions $\epsilon_1 \leftrightarrow \epsilon_2$ and $\epsilon_1 \leftrightarrow \epsilon_3$ ($|\Delta M| = 1$) would require 7-cm^{-1} quanta. For 1-cm^{-1} quanta a magnetic field of $\sim$ 60 kilo-oersteds is required. With the usual range of frequencies and magnetic fields we can expect to observe the transition between levels ϵ_2 and ϵ_3 ($|\Delta M| = 2$).

The detection of electron-spin resonance may be hindered by short spin-lattice relaxation times resulting in extreme line broadening. In the case of the vanadium ion the spin-lattice relaxation time

*The paramagnetic resonance of V^{3+} in corundum has recently been detected also by Lambe, Ager and Kikuchi.[2]

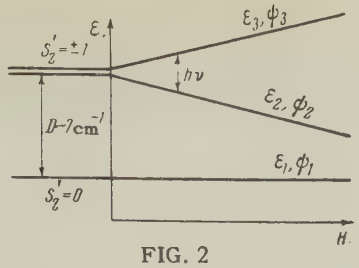

FIG. 2

is very short at room temperature because of close-lying higher orbital levels. Therefore resonance can be observed only at low temperatures.

The resonance spectrum was investigated in corundum single crystals containing 0.13% vanadium together with Cr^{3+} and Fe^{3+} impurities not exceeding 0.001%. Measurements were performed in the frequency range 9000 — 39,000 Mcs at liquid-helium temperature. For the 25,000 — 39,000 Mcs range we used a microwave spectrograph with a reentrant-type cavity resonator. For the 9000- and 15,000-Mcs ranges superheterodyne spectrographs with reflecting resonators were used.

At T = 290° and 77° K we did not succeed in detecting paramagnetic resonance of V^{3+}. At liquid-helium temperature one line with eight hyperfine components was observed, corresponding to the nuclear spin $I = 7/2$ of V^{51} (Fig. 3).

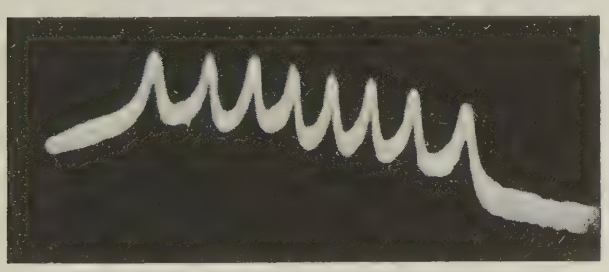

FIG. 3. Electron paramagnetic resonance line of V^{3+} in corundum, ν = 37,450 Mcs, T = 4.2°K, $\theta = 0$.

The positions and widths of the line components were measured as functions of the angle θ between the trigonal crystal axis (the z axis) and the direction of the static magnetic field **H**. We also studied the frequency dependence of line position for different θ and the temperature dependence of intensity at 1.6 — 4.2° K. Intensities were compared for different relative orientations of the static magnetic field **H** and radio-frequency field H_1.

The results were interpreted by means of the spin Hamiltonian for the three lowest levels in a magnetic field:

$$\hat{\mathcal{H}} = D\hat{S}_z'^2 + g_{\parallel}\beta H_z \hat{S}_z' + g_{\perp}\beta\,(H_x\hat{S}_x' + H_y\hat{S}_y') + A\hat{S}_z'\hat{I}_z + B\,(\hat{S}_x'\hat{I}_x + \hat{S}_y'\hat{I}_y) + E\,(\hat{S}_x'^2 - \hat{S}_y'^2), \quad (1)$$

where $\hat{S}_x'$, $\hat{S}_y'$, $\hat{S}_z'$ are the projections of the effective electron spin, $\hat{I}_x$, $\hat{I}_y$, $\hat{I}_z$ are the nuclear-spin projections, H_x, H_y, H_z are the magnetic field components, $g_{\parallel}$ and $g_{\perp}$ are the spectroscopic splitting factors, β is the Bohr magneton, D is the initial splitting factor, E is the orthorhombic field constant, A and B are the hyperfine structure constants. The Hamiltonian (1) resembles that proposed for V^{3+} by Abragam and Pryce,[7] differing by the addition of the term containing E.

By means of perturbation theory with the conditions $D \gg g_{\parallel}\beta H$, $g_{\perp}\beta H$; $g_{\parallel}\beta H \gg E$, A, B we calculate the following energy levels from the Hamiltonian:

$$\varepsilon_1 = (g_{\perp}\beta H \sin\theta)^2 D^{-1};$$

$$\varepsilon_2 = D + g_{\parallel}\beta H\cos\theta + \frac{1}{2}\frac{(g_{\perp}\beta H\sin\theta)^2}{D + g_{\parallel}\beta H\cos\theta} + \frac{E^2}{2g_{\parallel}\beta H\cos\theta} + Am;$$

$$\varepsilon_3 = D - g_{\parallel}\beta H\cos\theta + \frac{1}{2}\frac{(g_{\perp}\beta H\sin\theta)^2}{D - g_{\parallel}\beta H\cos\theta} - \frac{E^2}{2g_{\parallel}\beta H\cos\theta} - Am, \quad (2)$$

where m is the z projection of the nuclear spin.

Transitions with $|\Delta M| = 1$ ($\epsilon_1 \leftrightarrow \epsilon_2$; $\epsilon_1 \leftrightarrow \epsilon_3$) are not observed since $h\nu \ll D$. For the $|\Delta M| = 2$ transition we have

$$h\nu = \left(2 - \frac{(g_{\perp}\beta H\sin\theta)^2}{D^2}\right)[g_{\parallel}\beta H\cos\theta + Am] + \frac{E^2}{g_{\parallel}\beta H\cos\theta}. \quad (3)$$

Figure 4a shows the angular dependence of the vanadium line center for different frequencies. The position of the line center was calculated by averaging all hyperfine components.

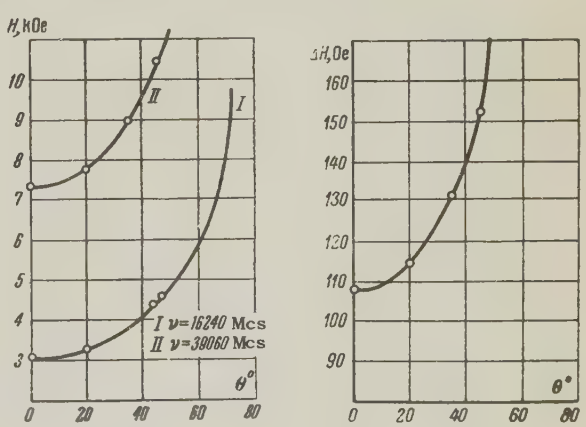

FIG. 4. Center of V^{3+} line (a) and hyperfine splitting (b) as functions of the angle θ. Circles represent experimental values; the solid curves were calculated.

Both for parallel orientation ($\theta = 0$) and for nonzero values of θ the frequency was found to be proportional to the magnetic field within experimental error (0.1%). Second-order corrections are therefore not required in (3). We also obtained $g_{\parallel} = 1.915 \pm 0.002$.

The hyperfine components were equidistant at all angles θ for which measurements were obtained. The angular dependence of the hyperfine splitting is shown in Fig. 4b and is in good agreement with the theoretical relation calculated from (3), neglecting second-order terms, for $|A| = (0.959 \pm 0.005) \times 10^{-2}$ cm^{-1}.*

For the purpose of determining D we used the temperature dependence of line intensities in the range 1.6 — 4.2° K. Relative intensities were measured for the lines of V^{3+} and of Cr^{3+} and Fe^{3+}, which were present in the single crystal as impurities. In order to obviate errors due to saturation the experiments were performed at minimum power levels in the microwave spectrometer resonator; lines were registered by a superheterodyne detector. The temperature dependence of the Cr^{3+} and Fe^{3+} line intensities was calculated using known values of the constants in the spin Hamiltonians of these ions.[8-11] $D = 7.0 \pm 0.3$ cm^{-1} was obtained with accuracy limited by the accuracy with which the relative intensities were measured. At low temperatures, because of the competition between two processes, — the increasing difference between the populations of levels 2 and 3 and the actual decrease of these populations because of the existence of level 1 — the vanadium line maximum should appear at $T \sim 7°$ K.

Experiments performed with parallel orientation showed that the $\epsilon_2 \leftrightarrow \epsilon_3$ transition is induced by the z component of the radio-frequency magnetic field. For this reason the term $E(\hat{S}_x'^2 - \hat{S}_y'^2)$ was introduced into the Hamiltonian to represent the interaction between the spin and the orthorhombic component of the crystal field. The Hamiltonian proposed for V^{3+} by Abragam and Pryce[7] does not account for the fact that the line representing the $|\Delta M| = 2$ transition does not vanish in the parallel orientation. In reference 1 the present authors introduced the term $\Delta\hat{S}_x'$ into the Hamiltonian to represent an interaction that removes the degeneracy of the doublet $S_z' = \pm 1$ in zero magnetic field, while the $|\Delta M| = 2$ transition in parallel orientation is allowed with the probability Δ/D. However, the latter transition should be induced by the x component of the radio-frequency field, which disagrees with experiment. The Hamiltonian is more properly corrected by the addition of the term $E(\hat{S}_x'^2 - \hat{S}_y'^2)$, which appears in second order in (3) and thus has practically no effect on either the line position or the hyperfine splitting. The term is required in order to account correctly for line intensities.

The wave functions for the different levels are

$$\psi_1 = \frac{\sqrt{2}}{2}\frac{g_\perp \beta H \sin\theta}{D}\psi^{-1} + \psi^0 + \frac{\sqrt{2}}{2}\frac{g_\perp \beta H \sin\theta}{D}\psi^{+1};$$

$$\psi_2 = \frac{E}{2g_{\parallel}\beta H \cos\theta}\psi^{-1} + \frac{\sqrt{2}}{2}\frac{g_\perp \beta H \sin\theta}{D}\psi^0 + \psi^{+1};$$

$$\psi_3 = \psi^{-1} + \frac{\sqrt{2}}{2}\frac{g_\perp \beta H \sin\theta}{D}\psi^0 - \frac{E}{2g_{\parallel}\beta H \cos\theta}\psi^{+1}, \qquad (4)$$

where ψ^{-1}, ψ^0, ψ^{+1} are the wave functions of the states with $S_z' = -1$, $S_z' = 0$ and $S_z' = +1$, respectively. The matrix elements for the $\epsilon_2 \leftrightarrow \epsilon_3$ transition are

$$\langle 2|\hat{S}_x'|3\rangle = g_\perp \beta H \sin\theta/D;$$

$$\langle 2|\hat{S}_y'|3\rangle = -ig_\perp \beta H \sin\theta/D;$$

$$\langle 2|\hat{S}_z'|3\rangle = -E/g_{\parallel}\beta H \cos\theta. \qquad (5)$$

Thus the z component of the radio-frequency field will give a nonvanishing line intensity in parallel orientation. The experimentally observed constancy of the integral intensity with varying θ while the radio-frequency field has a fixed orientation with respect to the z axis indicates that for nonzero values of θ the principal contribution to line intensity comes from the matrix element of $\hat{S}_z'$, which does not vary with θ.

In parallel orientation the width of a single component is 24 oersteds. Upon rotation of the crystal the width increases with θ more rapidly than the hyperfine splitting ΔH ($\Delta H \approx \Delta H_0/\cos\theta$), and at angles greater than 70° it is practically impossible to resolve the components.

This effect probably results from smearing of the trigonal crystal axis direction through an angle $\Delta\theta$ because many microdomains with slightly different axial directions are present. In this case the additional line broadening should be $\delta H = H \tan\theta\, \Delta\theta$. This is insignificant in the case of parallel orientation, for which the line width will be determined by other factors such as spin-spin interaction, random inhomogeneities of the crystal field and interactions of ions with the magnetic moments of aluminum nuclei.

The foregoing hypothesis is in agreement with experiment; additional broadening associated with $\Delta\theta$ varies from sample to sample. For example, at $\theta = 36°$ the width of a hyperfine component was 71 oersteds and 38 oersteds, respectively, in two different samples, although in parallel orientation the corresponding widths were 25 and 24 oersteds.

*In reference 1 we gave erroneously 2|A| instead of |A|.

$\Delta\theta$ was calculated to be 0.5° and 0.2° for these samples.

No temperature dependence of line width was detected in the range $1.6 - 4.2°$ K, thus indicating the absence of broadening due to spin-lattice relaxation.

Corundum is still the only single crystal in which a paramagnetic resonance spectrum of V^{3+} has been detected. This may result from the fact that the trigonal component of the crystal field is stronger in corundum than in other commonly used substances such as alum; the splitting Δ of orbital levels of the lower triplet would thus be greater, making the spin-lattice relaxation time T_1 for V^{3+} in corundum longer than in alum. This may possibly account for the failure to detect electron paramagnetic resonance of vanadium in alum.

From our study of the V^{3+} spin resonance spectrum we were able to determine only the parameters $g_{\|}$, A and D in the spin Hamiltonian. E might possibly be determined from measurements of absolute line intensities or relative intensities at different frequencies. Our present estimate, $|E| < 10^{-2}$ cm^{-1}, is based on the fact that the term containing E in (3) may be neglected to within experimental accuracy. $g_{\perp}$ might be determined from the detailed angular dependence of line intensities; it would be difficult to determine B at present. The detection of $|\Delta M| = 1$ lines would be of considerable interest but would require the construction of a microwave spectrometer for the $150 - 250 \times 10^3$ Mcs range.

The authors are indebted to A. A. Popova, R. P. Bashuk, and A. S. Bebchuk, who prepared the corundum-vanadium samples.

[1] G. M. Zverev and A. M. Prokhorov, JETP **34**, 1023 (1958), Soviet Phys. JETP **7**, 707 (1958).

[2] Lambe, Ager, and Kikuchi, Bull. Am. Phys. Soc. Ser. II, **4**, 261 (1959).

[3] E. S. Rudnitskaya, Тр. Ин-та кристаллографии (Trans. Inst. of Crystallography) **8**, 13 (1953).

[4] A. Siegert, Physica **4**, 138 (1937).

[5] J. H. Van Vleck, J. Chem. Phys. **7**, 61 (1939).

[6] J. van den Handel and A. Siegert, Physica **4**, 871 (1937).

[7] A. Abragam and M. H. L. Pryce, Proc. Roy. Soc. (London) **A205**, 135 (1951).

[8] A. A. Manenkov and A. M. Prokhorov, JETP **28**, 762 (1955), Soviet Phys. JETP **1**, 611 (1955).

[9] L. S. Kornienko and A. M. Prokhorov, JETP **33**, 805 (1957), Soviet Phys. JETP **6**, 620 (1958).

[10] G. M. Zverev and A. M. Prokhorov, JETP **34**, 513 (1958), Soviet Phys. **7**, 354 (1958).

[11] G. S. Bogle and H. F. Symmons, Proc. Phys. Soc. (London) **73**, 531 (1959).

Translated by I. Emin
96

PRODUCTION OF PIONS IN p-d COLLISIONS AND MOTION OF NUCLEONS INSIDE THE NUCLEUS

Yu. D. PROKOSHKIN

Joint Institute for Nuclear Research

Submitted to JETP editor September 18, 1959

J. Exptl. Theoret. Phys. (U.S.S.R.) **38**, 455-461 (February, 1960)

It is shown that the energy dependence of the cross section for production of π mesons in nucleon-deuteron collisions and the energy spectra of the π mesons can be calculated rather accurately from the data on free nucleon-nucleon collisions. In the energy range considered from the threshold for meson production to ~ 700 Mev, the effect of nucleon binding results mainly in a change in the magnitude of the cross sections as a result of motion of the nucleons inside the deuteron. The effective momentum distribution of nucleons in the deuteron is found.

1. INTRODUCTION

THE study of reactions following from collisions of protons with deuterons is a convenient method of studying the proton-neutron interaction. In the energy region $\gtrsim$ 1000 Mev, lying substantially above the meson production threshold (280 Mev), this method has been successfully employed both for measuring the total p-n interaction cross section[1] and for obtaining information about π-meson production.[2] The effect of binding of nucleons in the deuteron at such high energies is not large and can easily be taken into account by introducing a small correction into the measured cross sections.[1,2]

The closer the energy is to threshold, the more important is the effect of binding of the nucleons in the deuteron on the π-meson production processes. The main effect of the binding in this energy region is the change in magnitude of the cross section because of the motion of the nucleons inside the nucleus. Among other effects, connected with the presence of the spectator nucleon, one should note: the mutual screening of the nucleons (which is small[1-3] on account of the large radius of the deuteron), reabsorption of the produced π meson by the nucleon pair, exclusion of a number of final states because of the Pauli principle, possible effects from interference of nucleon states, and contributions from reactions proceeding without breakup of the deuteron (the cross sections of these processes are very small[4]).

In order to obtain information in this energy region about π-meson production in p-n collisions from the data on p-d collisions, it is necessary, if only approximately, to take into account the effect of binding of the nucleons in the deuteron and, first of all, to try to evaluate the magnitude of the change in cross section coming from motion inside the nucleus (this variation is especially important near threshold, where the corresponding enhancement factor for the cross section goes to infinity). This problem will be considered below in the impulse approximation, using as example the production of π^0 mesons in p-d collisions:

$$p + d \to \pi^0 + \text{nucleons} \qquad (1)$$

which was studied in detail earlier.[5]

2. MOMENTUM DISTRIBUTION OF NUCLEONS IN THE DEUTERON

If we consider the deuteron to be two nucleons moving relative to each other, and neglect interference, then the total cross section σ_{pd} for reaction (1) can be written as

$$\sigma_{pd} = \int \{\sigma_{pn}[\eta_m(p_1, \mathbf{p}_2), \mathbf{p}_2] + \sigma_{pp}[\eta_m(p_1, \mathbf{p}_2), \mathbf{p}_2]\} F(\mathbf{p}_2)\, d\mathbf{p}_2. \qquad (2)$$

Here $F(\mathbf{p}_2)$ is the momentum distribution of nucleons in the deuteron, $\mathbf{p}_2$ their momentum in the center-of-mass system, η_m the maximum momentum of the produced π^0 meson, p_1 the momentum of the incident proton, σ_{pn} and σ_{pp} the cross sections for π^0 production in collisions of the incident proton with the neutron and proton of the deuteron. For small values of p_1, the dependence of σ_{pn} and σ_{pp} on $\eta_m(p_1, p_2)$ is most important, making it possible to simplify these functions by setting them equal to $k\sigma_{pn}[\eta_m(p_1, p_2)]$ (and analogously for σ_{pp}). The factor k so in-

troduced takes into account all effects of binding other than the motion of the nucleons inside the deuteron. It is assumed that k changes slowly with energy.

Carrying out the integration in Eq. (2) over the unit vector $\mathbf{p}_2/p_2$, we obtain

$$\sigma_{pd} = \int k \{\sigma_{pn}(p_1, p_2) + \sigma_{pp}(p_1, p_2)\} F(p_2) p_2^2 dp_2. \quad (3)$$

Here the cross sections $\sigma_{pn}(p_1, p_2)$ and $\sigma_{pp}(p_1, p_2)$ correspond to the reactions

$$pn \to pn\pi^0, \quad (4)$$

$$pp \to pp\pi^0, \quad (5)$$

occurring with the moving nucleons of the deuteron. Since the cross section for the reaction (5) is comparatively small,[6] the contribution from the second term in the sum (3) is small. The functions $\sigma_{pn}(p_1, p_2)$ and $\sigma_{pp}(p_1, p_2)$ entering into the relation (3) were calculated for a wide range of values of p_1 and p_2 on the "Ural" electronic computer. The experimental data of reference 6 was used to determine the functions $\sigma_{pp}(p_1, p_2)$. According to the phenomenological theory,[7] the cross section $\sigma_{pn}(\eta_m)$ should go as η_m^δ near threshold, where $3 < \delta < 4$. Calculations of $\sigma_{pn}(p_1, p_2)$ were carried out for $\delta = 3$ and $\delta = 4$. The integration in Eq. (3) was carried out for several types of momentum distribution $F(p_2)$ (several of these distributions are shown in Fig. 1). The dependence of σ_{pd} on the energy of the incident proton then found is shown on Fig. 2, where the various curves are compared with the energy dependence for the cross section of reaction (1) found experimentally.[5] Curve 4c on this figure was calculated from a momentum distribution of the Chew-Goldberger type (the so-called improved one):

$$F(p_2) \sim (\alpha^2 + p_2^2)^{-2} (\beta^2 + p_2^2)^{-2},$$

$$\beta = 2.5\alpha, \qquad \alpha = 190 \text{ Mev/c} \quad (6)$$

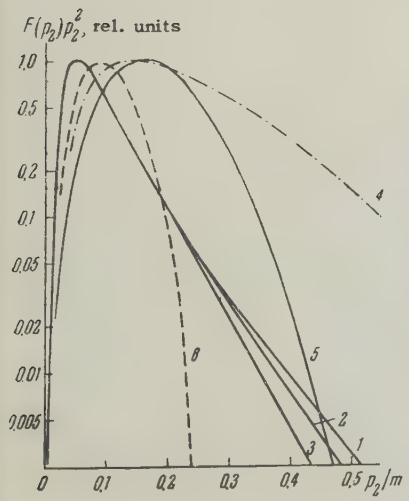

FIG. 1. Momentum distributions. 1, 2, 3 – Salpeter-Goldstein for Yukawa, exponential and Gaussian potentials. 4 – Chew-Goldberger (improved). 5, 6 – Gaussian, with dispersions $(\bar{p^2}/m)^{1/2} = 0.11$ and 0.06 with m the mass of the nucleon.

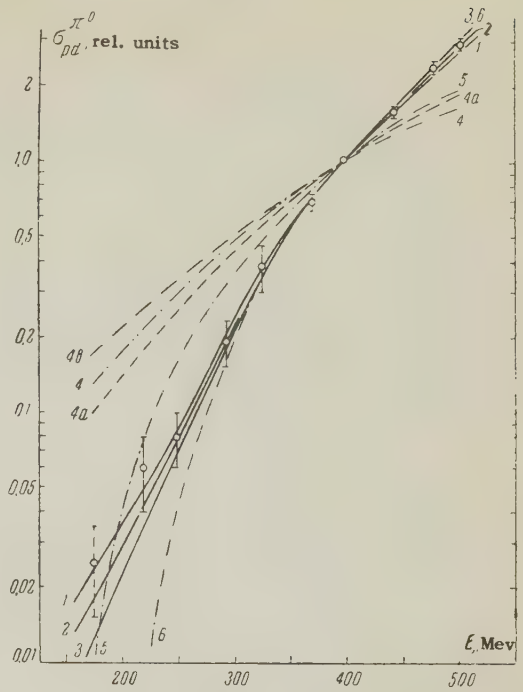

FIG. 2. Energy dependence of the total cross section for reaction (1). o – measured in Ref. 5. 1–6 – energy dependencies, calculated using the momentum distributions given in Fig. 1. 4a and 4c – see text. All data are normalized to unity at incident proton energy E = 400 Mev.

which has a long tail (see Fig. 1).

Together with taking the motion of the nucleons into account, an attempt was also made to estimate in an approximate way the effect of the Pauli principle by excluding from reaction (1) contributions from those collisions in which the secondary nucleons remain inside the Fermi sphere. The change in the size of the cross section because of the Pauli Principle was negligible in this energy range, as can be seen by comparing curve 4c in Fig. 2 with curve 4 which, in contradistinction to 4c, was calculated taking the Paul Principle into account. All of the other curves in Fig. 2 were also calculated with account of the Pauli Principle.

It has already been indicated above that the dependence of the cross section σ_{pd} on energy near threshold is determined mainly by the form of the momentum distribution, and is insensitive to the energy dependence of the cross sections for reactions (4) and (5). One can see this by comparing curves 4 and 4a on Fig. 2, which were calculated for the cases $\sigma_{pn} \sim \eta_m^3$ and η_m^4.

Curves 5 and 6 on Fig. 2 were calculated for a Gaussian distribution

$$F(p_2) \sim \exp(-p_2^2/2p_2^2), \quad (7)$$

which describes the momentum distribution in complex nuclei reasonably. A distribution of this type

differs from the Chew-Goldgerger distribution in that it contains relatively few high momentum components (see Fig. 1). It can be seen from Fig. 2 that both the Gaussian and Chew-Goldberger distributions are in poor agreement with the experimental data[5] for the reaction (1).

It is possible to obtain good agreement with measured cross sections (see curves 1 — 3 on Fig. 2) if one uses the momentum distributions of Salpeter and Goldstein[8] for the deuteron (see Fig. 1). In the low-momentum region these distributions go approximately as

$$F(p_2) \sim (\gamma^2 + p_2^2)^{-2}, \qquad (8)$$

where $\gamma = 46$ Mev/c. The distributions 1 — 3 (calculated in reference 8 for Yukawa, exponential, and Gaussian potentials) differ, as can be seen from Fig. 1, only in the region of very high momenta. All of these are almost equally good in reproducing the experimental dependence of the cross section for reaction (1) on energy.

Thus, analysis of the energy dependence of the cross section for the reaction $p + d \rightarrow \pi^0 +$ nucleons near threshold shows that the momentum distribution of nucleons in the deuteron is described well by the curves from the Salpeter and Goldstein distributions. It should be remarked that the interpretation of results of measurements on the energy dependence, similar to those of reference 5, in the spirit of the impulse approximation, runs into essential difficulties, since large momenta of the nucleons in the nucleus correspond to small distances between them, where threefold interactions become important. Therefore, the momentum distributions given above should be considered as effective distributions, the knowledge of which makes it possible to take into account the effect of motion inside the nucleus on the magnitude of meson production cross sections of the type of reaction (1), but which may differ markedly from the true momentum distribution.

3. RECONSTRUCTION OF THE TOTAL CROSS SECTION FOR p-n INTERACTION

Using the effective momentum distribution obtained above for the deuteron, the integration in Eq. (3) can be carried out, leading to the following relation between the cross sections of reactions (1), (4) and (5)

$$\sigma_{pd} = k(g_{pn}\sigma_{pn} + g_{pp}\sigma_{pp}). \qquad (9)$$

Here $\sigma_{pn} = \sigma_{pn}(p_1, 0)$ and $\sigma_{pp} = \sigma_{pp}(p_1, 0)$ are the usual cross sections, and g_{pn} and g_{pp} are quantities characterizing the change in the cross sections from the motion in the nucleus; they depend only on p_1. In order to carry out such an integration it is necessary to know the energy dependence of the cross sections for reactions (4), (5). In essence, this problem can be solved by the method of successive approximations. However, because the momentum distribution $F(p_2)$ is not broad, the first approximation for the cross section $\sigma_{pn}^{(1)}$ is already sufficient to determine g_{pn}. As first approximation for $\sigma_{pn}^{(1)}$, the dependence η_m^3 was used near threshold and in the high-energy region one can take $\sigma_{pn}^{(1)} = \sigma_{pd} - \sigma_{pp}$. Above 600 Mev the rate of growth of $\sigma_{pn}^{(1)}$ decreases and for energies $\gtrsim$ 1000 Mev, $\sigma_{pn}^{(1)} \approx$ const. The functions $\sigma_{pn}^{(1)}(p_1, p_2)$ so obtained and used to determine g_{pn} are given on Fig. 3. The functions $\sigma_{pp}(p_1, p_2)$ have an analogous form. The coefficients g_{pn} and g_{pp} obtained in the way described above are given on Fig. 4.

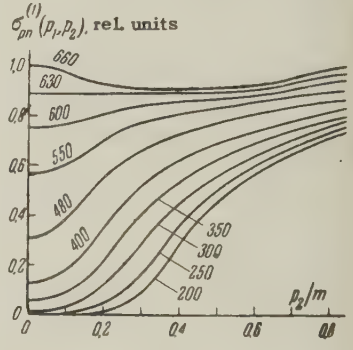

FIG. 3. Functions $\sigma_{pn}^{(1)}(p_1, p_2)$. The numbers near the curves indicate the corresponding values of the kinetic energy $E = \sqrt{p_2^2 + m^2} - m$.

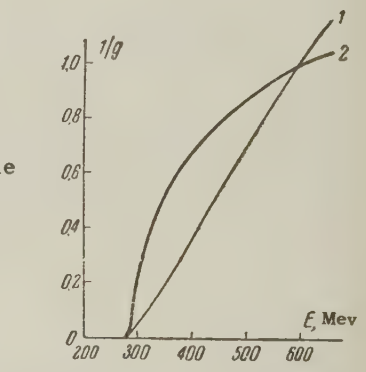

FIG. 4. Dependence of the coefficients g on energy. 1) $1/g_{pp}$; 2) $1/g_{pn}$.

Calculation of the coefficient k, which enters into the expression (9), is practically impossible because of inadequacy of contemporary nuclear theory. One can only say that this coefficient is near to unity at high energies, where $\sigma_{pd} \approx \sigma_{pn} + \sigma_{pp}$. The only factor entering into the coefficient k which one can calculate is the decrease in the cross section because of the mutual screening of the nucleons in the deuteron.[3] The corresponding correction is small (several per cent).

The coefficient k can be found empirically by comparing cross sections measured in proton and

neutron beams of the same mean energy. When the incident particle is a neutron, the cross section for the deuteron is

$$\sigma_{nd} = k(g_{np}\sigma_{np} + g_{nn}\sigma_{nn}), \qquad (9')$$

which is analogous to Eq. (9), since, because of the charge symmetry of nuclear forces, $\sigma_{np} = \sigma_{pn}$, $\sigma_{nn} = \sigma_{pp}$, $g_{np} = g_{pn}$ and $g_{nn} = g_{pp}$. In order to determine k it is convenient not to use the cross sections, which are not measured with high accuracy, but rather the more accurate measurements of the ratios of cross sections $\alpha_p = \sigma_{pd}/\sigma_{pp}$ and $\alpha_n = \sigma_{nd}/\sigma_{np}$. In this notation

$$1/k = g_{pp}/\alpha_p + g_{pn}/\alpha_n. \qquad (10)$$

The values α_p and α_n were measured at 590 Mev:[5,6,9] $\alpha_p = 3.00 \pm 0.15$, $\alpha_n = 1.30 \pm 0.04$. From these, k (590) = 0.89 ± 0.03.

The quantity k can be determined at one other point, at 380 Mev where the cross sections for the reactions (1), (4) and (5) have been measured:[5,6,10]

$$k(380) = 0.72 \pm 0.16.$$

Comparison of the two values obtained gives reason to believe that the coefficient k is constant over the entire energy region from threshold to 600 Mev.

Using the values obtained for g_{pn}, g_{pp} and k it is possible to reconstruct the cross section for production of π^0 mesons in p-n collisions from the experimental data on the σ_{pd} and σ_{pp} cross sections:

$$\sigma_{pn} = \sigma_{pd}/kg_{pn} - \sigma_{pp}g_{pp}/g_{pn}. \qquad (11)$$

4. π-MESON SPECTRA

The energy spectra of π mesons produced in reactions of type 1 depend even more on the binding between the nucleons than does the magnitude of the total cross section σ. Even at high energies, they differ substantially from the spectra of π mesons produced in collisions of free nucleons[11,12] (see Figs. 5 and 6). In particular, the absence of a peak, which is so characteristic of collisions of free protons, is striking. Assuming as previously that the effect of binding leads, in the main, to a change in the magnitude of the differential cross section $d^2\sigma/d\Omega\,dE$ because of motion of the nucleons in the deuteron, it is possible to calculate the change in the form of the spectra by the same method as applied in the preceding paragraphs for obtaining the total cross sections. This calculation was carried out for the spectra of π^+ mesons produced in p-d collisions at 655 Mev, with the

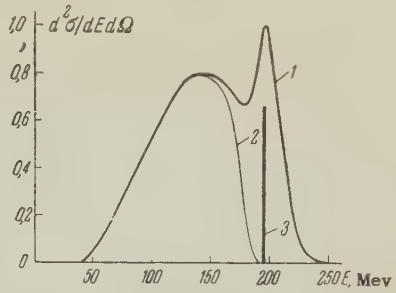

FIG. 5. Energy spectrum of π^+ mesons, produced in p-p collisions (in relative units). 1) measured by Helfer et al.[12] at angle ≈ 90° in the c.m.s. for proton energy 655 Mev. 2) π^+-meson spectrum from the reaction p + p → p + n + π^+. 3) position of the peak corresponding to the reaction p + p → d + π^+.

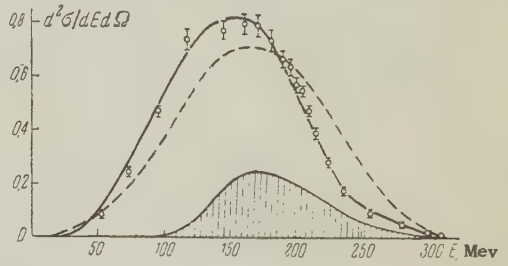

FIG. 6. Spectrum of π^+ mesons, produced in p-d collisions (in relative units). o – measured spectrum of π^+ mesons produced in p-p collisions in the deuteron[12] (obtained as the difference of π^+ and π^- spectra). The thick solid curve is this spectrum, calculated from the Salpeter-Goldstein momentum distribution. The dashed curve shows the spectrum calculated for a Gaussian distribution with dispersion $\sqrt{\overline{p_i^2}}/m = 0.06$. The thin curve is the spectrum of π+ mesons from the reaction p + p → d + π^+, transformed as a result of motion inside the deuteron. The resolution of the spectrometer[12] was taken into account in constructing these spectra; this only slightly changed the form of the spectra because of their large width.

object of comparing the results of the calculation with the experimental data* on the spectrum of π^+ mesons in the reaction p + d → π^+ + nucleons.[12] Calculations were carried out separately for the reactions p + p → d + π^+ and p + p → p + n + π^+ (plots of the spectra corresponding to these reactions are shown in Fig. 5). Functions $d^2\sigma/d\Omega\,dE\,(p_1, p_2)$, analogous to those entering into Eq. (3), were calculated using the experimental results for the energy dependence of the π^+-meson production cross section[13] and the spectra obtained in references 12 and 13. Integration over the momenta of the nucleons in the deuteron was carried out for the Salpeter-Goldstein momentum distribution.

The calculated spectra differ substantially from the spectra of π^+ mesons produced in p-p colli-

*I would like to take this opportunity to thank M. G. Meshchyeryakov and collaborators who kindly furnished me with the results of their measurements before publication.

sions. This is especially true of the peak (shaded region in Fig. 6) relating to the reaction $p + p \rightarrow d + \pi^+$, the width of which is increased as a result of motion of the nucleons up to 50% of the whole, making it practically unobservable in the spectrum of π^+ mesons produced in p-d collisions. At the same time, the relative contribution of the peak is somewhat reduced (by 15%) because the energy dependence of the cross section for the reaction $p + p \rightarrow d + \pi^+$ has a resonance character.

Comparison of the spectra of π^+ mesons produced in p-p collisions in the deuteron[12] with the calculated spectra shows (Fig. 6) that the form of the spectra for p-d collisions can be rather accurately predicted from the data on free p-p collisions. The form of the calculated spectrum depends strongly on the momentum distribution employed in the calculation. A π^+ spectrum, calculated in the same way as previously, but for the case of a Gaussian distribution with $\sqrt{\overline{p_z^2}}/m = 0.06$ is shown on Fig. 6. In spite of the fact that this distribution is rather close to the Salpeter-Goldstein ones (see Fig. 1), the corresponding spectra differ markedly. From this it follows that study of π-meson spectra in p-d collisions also makes it possible to obtain quantitative knowledge about the momentum distribution of nucleons in the deuteron.

The considerations above about the π-meson spectra can be turned around, i.e., from the spectrum of π mesons produced in p-d collisions, if measured with high accuracy, one can reconstruct the spectrum of π mesons produced in collisions of free nucleons. This is of particular interest in cases where direct investigation of the corresponding reaction by collisions between free nucleons would involve substantial experimental difficulties (such as, for example, the reaction $p + n \rightarrow p + p + \pi^-$).

In conclusion, I would like to express my gratitude to A. I. Baz', B. M. Golovin, M. G. Meshcheryakov and Yu. A. Shcherbakov for discussion of results of this work. I am sincerely thankful to L. A. Kulyukina for help in carrying out the long calculations.

[1] Chen, Leavitt, and Shapiro, Phys. Rev. **103**, 211 (1956).

[2] Batson, Cullwick, Klepp, and Riddiford, Proc. Roy. Soc. **A251**, 233 (1959).

[3] R. Glauber, Phys. Rev. **100**, 242 (1955); J. Blair, Nuclear Phys. **6**, 348 (1958).

[4] Crewe, Garwin, Ledley, Lillethun, March, and Marcowitz, Phys. Rev. Letters **2**, 269 (1959).

[5] A. F. Dunaĭtsev and Yu. D. Prokoshkin, JETP **38**, 747 (1960), Soviet Phys. JETP, in press.

[6] A. F. Dunaĭtsev and Yu. D. Prokoshkin, JETP **36**, 1656 (1959), Soviet Phys. JETP **9**, 1179 (1959).

[7] A. Rosenfeld, Phys. Rev. **96**, 139 (1954).

[8] E. Salpeter and J. Goldstein, Phys. Rev. **90**, 983 (1953).

[9] Dzhelepov, Oganesyan, and Flyagin, JETP **29**, 886 (1955), Soviet Phys. JETP **2**, 757 (1956).

[10] Rosenfeld, Solmitz, and Hildebrand, Bull. Am. Phys. Soc. **1**, 72 (1956).

[11] Meshkovskiĭ, Pligin, Shalamov, and Shebanov, JETP **32**, 1328 (1957), Soviet Phys. JETP **5**, 1085 (1957).

[12] Helfer, Kuznetzov, Meshcheryakov, Swiatkowski, and Vovchenko, Acta Phys. Polon., in press.

[13] B. S. Neganov and O. V. Savchenko, JETP **32**, 1265 (1957), Soviet Phys. JETP **5**, 1033 (1957); B. S. Neganov and L. B. Parfenov, JETP **34**, 767 (1958), Soviet Phys. JETP **7**, 528 (1958); Meshcheryakov, Zrevov, Neganov, Yzorov, and Shabudin, Review of CERN Symposium **2**, 347 (1956); Batson, Cullwick, Hill, and Riddiford, Proc. Roy. Soc. **A251**, 218 (1959).

Translated by G. E. Brown
97

ON THE NONLINEAR THEORY OF ELEMENTARY PARTICLES

D. F. KURDGELAIDZE

Moscow State University

Submitted to JETP editor June 10, 1959

J. Exptl. Theoret. Phys. (U.S.S.R.) **38**, 462-474 (February, 1960)

The energies and momenta of spinor fields in theories with pseudovector and scalar nonlinear terms are calculated on the basis of a number of new exact solutions of the wave type. By a semiclassical quantization the mass of the nucleon is determined as $k_0 l = 2^{1/2}\pi^{3/2} \approx 7.84$. The dependence of the energy of the field on the degree of nonlinearity is established. The method of fusion is used to derive from the nonlinear spinor equation a nonlinear undor equation, which on certain assumptions reduces to a nonlinear meson equation of the Klein-Gordon type. The conformal invariance of the nonlinear equations of the meson and spinor fields is discussed.

ACCORDING to the unified nonlinear field theory the theory of the elementary particles is based on the spinor equation

$$\{\gamma_\mu(\partial/\partial x_\mu + l^2\gamma_5(\bar\psi\gamma_\mu\gamma_5\psi)) + A(\bar\psi, \psi)\}\psi = 0, \quad (1)$$

where $x_\mu \equiv (x_n, it)$, $\hbar = c = 1$, and A is an arbitrary function of $\bar\psi$ and ψ. Equations of this type that have been discussed[1-5] are

$$D\psi \equiv \gamma_\mu(\partial/\partial x_\mu + l^2\gamma_5(\bar\psi\gamma_\mu\gamma_5\psi))\psi = 0, \quad (2)$$

$$D\psi \equiv (\gamma_\mu\partial/\partial x_\mu + l^2(\bar\psi\psi))\psi = 0. \quad (2a)$$

We shall call the nonlinear equation with the scalar (pseudovector) nonlinear term simply the "scalar" ("pseudovector") nonlinear equation.

Starting from Eqs. (2) and (2a), Heisenberg[1] determines the spectrum of masses and charges of the elementary particles, using for this purpose the complicated apparatus of quantum field theory and the Tamm-Dancoff approximate method. One can, however, also get close approximations to the masses of the elementary particles from Eqs. (2) and (2a) by a simpler semiclassical method, if one uses a certain approximate condition that is equivalent to quantization.

1. THE ENERGY, MASS, AND CHARGE OF THE NONLINEAR FIELDS

The Nonlinear Pseudovector Equation

1. Let us consider Eq. (2), in which the nonlinear pseudovector term has been chosen by Heisenberg and Pauli[2] from among the possible nonlinear terms suggested by Ivanenko and Brodskiĭ[3] by the use of all the known conservation laws both in ordinary space and in isotopic space. The equation adjoint to Eq. (2) is

$$\bar\psi\overleftarrow{D} \equiv \bar\psi(\overleftarrow{\partial}/\partial x_\mu - l^2\gamma_5(\bar\psi\gamma_5\gamma_\mu\psi))\psi = 0. \quad (2')$$

From Eqs. (2) and (2') we find

$$\partial(\bar\psi\gamma_\mu\psi)/\partial x_\mu = 0, \quad (1.1)$$

$$\partial(\bar\psi\gamma_\mu\gamma_5\psi)/\partial x_\mu = 0. \quad (1.2)$$

Solutions of Eqs. (2), (2') and (1.1), (1.2) in the form

$$\psi = a(s)\varphi(\sigma),$$

$$\bar\psi = \bar a(s)\varphi^*(\sigma), \quad \sigma = k_\mu x_\mu, \quad k_\mu \equiv (k_n, i\omega), \quad (1.3)$$

where s is the spin coordinate and $\varphi(\sigma)$ does not depend on the matrices γ_μ, are found by the method used earlier.[4] As the result we get a complex solution unique for the given type of equation:

$$\varphi = \varphi_0\exp\{ik_\mu x_\mu\}, \quad \varphi^* = \varphi_0^*\exp\{-ik_\mu x_\mu\}. \quad (1.4)$$

The length of the four-vector k_μ and the eigenfunctions $a(s)$, $\bar a(s)$ are determined from the equations

$$\gamma_\mu(k_\mu + \gamma_5 a_{\mu 5})a = 0, \quad (1.5)$$

$$\bar a(k_\mu - \gamma_5 a_{\mu 5})\gamma_\mu = 0, \quad (1.6)$$

where

$$a_{\mu 5} = -il^2(\bar a\gamma_\mu\gamma_5 a), \quad \bar a = a^*\gamma_4. \quad (1.7)$$

Since the energy operator

$$H = \partial/\partial x_4 = -\gamma_4\gamma_n(\partial/\partial x_n + l^2\gamma_5 a_{n5}) - \gamma_5 a_{45} \quad (1.8)$$

commutes with the spin operator

$$\sigma = \begin{pmatrix} 0 & \sigma' \\ \sigma' & 0 \end{pmatrix}, \quad (1.9)$$

(σ' stands for the Pauli matrices), we can add to the list (1.3) the equation for the spin

$$(ks - \sigma k)a = 0, \quad \bar a(s)(ks - \sigma k) = 0. \quad (1.10)$$

To calculate $a_{\mu 5}$ we take the matrices in the form

$$\gamma_5 = \begin{pmatrix} 1 & 0 \\ 0 & -1 \end{pmatrix}, \qquad \gamma_4 = \begin{pmatrix} 0 & 1 \\ 1 & 0 \end{pmatrix}, \qquad \gamma_n = \begin{pmatrix} 0 & i\sigma_n' \\ -i\sigma_n' & 0 \end{pmatrix},$$

$$\sigma_1' = \begin{pmatrix} 0 & 1 \\ 1 & 0 \end{pmatrix}, \qquad \sigma_2' = \begin{pmatrix} 0 & -i \\ i & 0 \end{pmatrix}, \qquad \sigma_3' = \begin{pmatrix} 1 & 0 \\ 0 & -1 \end{pmatrix},$$

$$\alpha(s) = \begin{pmatrix} a_1(s) \\ a_2(s) \end{pmatrix}, \quad a_1(s) = \begin{pmatrix} b_1(s) \\ b_2(s) \end{pmatrix}, \quad a_2(s) = \begin{pmatrix} b_3(s) \\ b_4(s) \end{pmatrix}. \tag{1.11}$$

Then we find

$$a_{45} = -l^2(a_1^* a_1 - a_2^* a_2),$$

$$a_{35} = -sl^2(a_1^* a_1 + a_2^* a_2) = -sl^2(\bar{a}\gamma_4 a),$$

$$a_{25} = il^2(b_1^* b_2 + b_3^* b_4 - b_2^* b_1 - b_4^* b_3),$$

$$a_{15} = -l^2(b_1^* b_2 + b_3^* b_4 + b_2^* b_1 + b_4^* b_3). \tag{1.12}$$

Let us impose on the amplitude constants the conditions

$$a_{15} = a_{25} = 0. \tag{1.13}$$

If now in Eqs. (1.5), (1.6), (1.10) we go over to a primed coordinate system[6] in which k_3' is directed along σ, then on using also the conditions (1.13), we get (dropping the primes)

$$(\omega - s\varepsilon k - i\varepsilon a_{45} - s a_{35})\, a = 0,$$
$$s = \pm 1, \quad \varepsilon = \pm 1. \tag{1.14}$$

From this we get for the eigenvalue of ω

$$\omega = s\varepsilon k + i\varepsilon a_{45} + s a_{35}. \tag{1.15}$$

The function $a(s)$ has been subjected only to the requirement (1.13) and the conditions (1.14). We can satisfy them if we prescribe $a(s)$ in the form

$$a_1(s) = \delta_{\varepsilon,1} \begin{pmatrix} c_1\sqrt{1+s} \\ c_2\sqrt{1-s} \end{pmatrix},$$

$$a_2(s) = \delta_{\varepsilon,-1} \begin{pmatrix} c_1\sqrt{1+s} \\ c_2\sqrt{1-s} \end{pmatrix}. \tag{1.16}$$

Then we get

$$a_{45} = 0, \quad a_{\mu 5}^2 = a_{35}^2,$$

$$a_{35} = -sl^2(\delta_{\varepsilon,1} + \delta_{\varepsilon,-1})[(1+s)c_1 c_1^* + (1-s)c_2^* c_2] \tag{1.17}$$

and for ω we find $\omega = s\epsilon k + s a_{35}$.

2. Let us now determine the momentum, charge, and energy of the field of Eq. (2) that correspond to this solution. The Lagrangian density function of Eq. (2) is

$$\mathfrak{L} = \tfrac{1}{2}\{\bar{\psi}(D\psi) - (\bar{\psi}\overleftarrow{D})\psi - l^2(\bar{\psi}\gamma_\mu\gamma_5\psi)^2\}. \tag{1.18}$$

From this we get for the momentum, charge, and energy of the field

$$G_n = i\int T_{n4}\, d^3x = -k_n(\bar{a}\gamma_4 a)\, L^3,$$

$$Q = \int \rho_e\, d^3x = -e(\bar{a}\gamma_4 a)\, L^3,$$

$$E = \int T_{44}\, d^3x = -\omega(\bar{a}\gamma_4 a)\, L^3 + \tfrac{1}{2} l^{-2} a_{\mu 5}^2 L^3. \tag{1.19}$$

If we consider the solution (1.16), we get

$$\mathbf{G} = \mathbf{Nk}, \qquad -Q = Ne, \qquad E = -\left(\omega + \tfrac{1}{2} Nl^2 L^{-3}\right) N,$$

$$\omega = s\varepsilon k - l^2(\bar{a}\gamma_4 a) = s\varepsilon k - l^2 N L^{-3},$$

$$N = (\bar{a}\gamma_4 a)\, L^3. \tag{1.20}$$

From these formulas we have for $\mathbf{k} = 0$*

$$G = 0, \qquad -Q = Ne,$$

$$E = E_0 = \tfrac{1}{2} N\omega_0, \qquad \omega_0 = NL^{-3}l^2. \tag{1.21}$$

Let us now calculate the energy contained in the basic periodicity volume given by

$$L^3 = (2\pi/\omega)^3. \tag{1.22}$$

For $\mathbf{k} = 0$ we get $L = (2\pi/\omega_0) = l(2\pi/N)^{-1/2}$, and we further find

$$l\omega_0 = (2\pi)^{3/2} N^{-1/2}, \qquad lE_0 = \tfrac{1}{2} N(l\omega_0).$$

In the case $N = 1$ we arrive by this normalization, which is essentially equivalent to a sort of primitive quantization, at the rest mass of an elementary particle†

$$k_0 l = \sqrt{2}\,\pi^{3/2} \approx 7.84, \qquad Q = -e \tag{1.23}$$

($E_0(N=1) = k_0$, $\omega_0(N=1) = k_0' = 2k_0$); this is close to the result of Heisenberg ($k_0 l \approx 6.5$ for the pseudoscalar nonlinear field and $k_0 l \approx 7.4$ for the scalar field[1]).

3. Equation (2) also has a solution of a different form. These solutions can be found by the method of integration of nonlinear equations proposed in reference 4. Equation (2) can be integrated if we introduce new functions φ and $\bar{\varphi}$ by the formulas

$$\psi = -D\varphi, \qquad \bar{\psi} = \bar{\varphi}\overleftarrow{D}, \tag{1.24}$$

which can be rewritten in the form

$$\psi = -\gamma_\mu(\chi_\mu + \eta_{\mu 5}\gamma_5)\, a, \qquad \bar{\psi} = \bar{a}(\chi_\mu^* - \eta_{\mu 5}^*\gamma_5)\gamma_\mu, \tag{1.25}$$

where a is a constant spinor. The functions χ_μ and η_μ can be regarded as two independent unknown functions. Substituting Eq. (1.25) in Eq. (2), we get a system of equations for the determination of χ_μ and η_μ. The solution of this system of equations is difficult, however, because of the presence of the summation over the index of the γ_μ. This difficulty can be evaded if we consider a special form of the function (1.25) without the matrices γ_μ:

$$\psi = (\varphi + \gamma_5\chi)\, a, \qquad \bar{\psi} = \bar{a}(\varphi^* - \gamma_5\chi^*). \tag{1.26}$$

*Regarding the signs of the parameter l^2 and the Lagrangian (and energy) see Sec. 3.

†An elementary particle is taken to correspond to a field which has the momentum k, the charge e, and the volume given by Eq. (1.22).

Equation (2) then gives

$$\gamma_\mu (\partial\varphi / \partial x_\mu + B_{\mu 5}\chi)\, a = 0,$$
$$\gamma_\mu\gamma_5 (\partial\chi / \partial x_\mu + B_{\mu 5}\varphi)\, \alpha = 0. \qquad (2'')$$

$$B_{\mu 5} \equiv l^2 (\bar\psi\gamma_\mu\gamma_5\psi) = l^2 (\bar a\gamma_\mu\gamma_5 a)\,(\varphi^*\varphi + \chi^*\chi)$$
$$+ l^2 (\bar a\gamma_\mu a \quad \chi + \chi^*\varphi). \qquad (1.27)$$

Along with Eq. (2″) we must also take the system of complex conjugate equations.

From Eq. (2″) we can get the equations

$$(\partial\varphi / \partial x_\mu + B_{\mu 5}\chi)^2\, a = 0, \qquad (1.28)$$
$$(\partial\chi / \partial x_\mu + B_{\mu 5}\varphi)^2\, a = 0. \qquad (1.29)$$

If we now seek a solution in the form

$$\varphi = \varphi(\sigma), \quad \chi = \chi(\sigma),$$

$$\varphi^* = \varphi, \quad \chi = i\eta, \quad \eta^* = \eta, \quad \sigma = k_\mu x_\mu, \qquad (1.30)$$

for the system of equations (1.28), we can satisfy Eq. (1.29) with

$$\varphi' = \eta, \quad \eta' = \varphi, \quad \varphi^2 + \eta^2 = \text{const},$$
$$B_{\mu 5} = i a_{\mu 5} = \text{const}, \qquad (1.31)$$

and we get for the solution

$$\psi = e^{i\gamma_5\sigma} a(s), \quad \bar\psi = \overline{a}(s)\, e^{i\gamma_5\sigma} \qquad (1.32)$$

The length k_μ^2 is determined from the equations

$$(k_\mu^2 - a_{\mu 5}^2)\, a = 0, \quad k_\mu a_{\nu 5} - k_\nu a_{\mu 5} = 0 \qquad (1.33a)$$

or

$$(k_\mu^2 + a_{\mu 5}^2 + 2k_\mu a_{\mu 5})\, a = 0. \qquad (1.33b)$$

The eigenfunctions $a(s)$ themselves must be determined from the equation

$$\gamma_\mu (k_\mu + a_{\mu 5})\, a = 0, \qquad (1.34)$$

which in the case (1.33a) gives $a = \gamma_\nu (k_\nu - a_{\nu 5})\, a'$, where a' is an arbitrary constant spinor. In the case (1.33b), on the other hand, Eq. (1.34) is solved in just the same way as Eq. (1.5) with the supplementary condition (1.13). We find as the result

$$(\omega - i a_{45} - s\varepsilon (k + a_{35}))\, a = 0. \qquad (1.35)$$

For the eigenvalues ω we get*

$$\omega = s\varepsilon k + \varepsilon (i\varepsilon a_{45} + s a_{35}). \qquad (1.36)$$

If we now fix $a(s)$ in the form (1.16), we find

$$\omega = s\varepsilon (k + a_{35}). \qquad (1.37)$$

Let us determine the momentum, charge, and energy of the field that correspond to the solution (1.32) and (1.16). We have

$$G = -k (\bar a\gamma_4\gamma_5 a) L^3, \qquad Q = e (\bar a\gamma_4 a) L^3,$$
$$E = -\omega (\bar a\gamma_4\gamma_5 a) L^3 - \tfrac{1}{2} l^{-2} a_{\mu 5}^2 L^3 \qquad (1.38)$$

*An eigenvalue ω is also obtained from Eq. (1.33b), which with the condition (1.13) gives $(i\omega + a_{45})^2 + (k + a_{35})^2 = 0$, i.e., $\omega = k + i a_{45} + a_{35}$ $(s = \varepsilon = 1)$.

and, using Eq. (1.17), we get

$$G = 0, \quad Q = Ne, \quad E = -\tfrac{1}{2} (N l^2 L^{-3}) N, \qquad (1.39)$$
$$\omega = s\varepsilon (k - s\omega_0),$$
$$\omega_0 = -s a_{35} = l^2 N L^{-3}, \quad (\bar a\gamma_4 a)\, L^3 = -s l^2 a_{35} L^3 = N. \qquad (1.40)$$

From these results we find for $\mathbf{k} = 0$:

$$G = 0, \quad Q = Ne, \quad -E_0 = \tfrac{1}{2} N\omega_0, \quad \omega = \varepsilon\omega_0. \qquad (1.41)$$

Let us now again determine the energy contained in the fundamental periodicity volume (1.22). For $\mathbf{k} = 0$ Eq. (1.22) gives $L = 2\pi/\omega_0 = l N^{1/2} (2\pi)^{-1/2}$. We get

$$Q = Ne, \quad \omega_0 l = N^{-1/2} (2\pi)^{3/2}, \quad E_0 l = -\tfrac{1}{2} (l\omega_0) N. \qquad (1.42)$$

In the case $N = 1$ we again arrive at the charge and mass of an elementary particle:

$$k_0 l = \sqrt{2}\, \pi^{3/2} \approx 7.84, \quad Q = e. \qquad (1.43)$$

$$E_0 (N = 1) = -k_0, \quad \omega_0 (N = 1) = k_0' = 2k_0. \qquad (1.44)$$

The Nonlinear Scalar Equation

1. Let us consider the scalar equation (2a), or for the sake of generality the equation

$$(\gamma_\mu \partial / \partial x_\mu + A (\bar\psi\psi))\, \psi = 0. \qquad (2a')$$

The solution of the equation (2a′) in the form (1.3) for real $A(\bar\psi, \psi)$ is given by Eq. (1.4) with

$$(\gamma_\mu k_\mu - i\bar k_0)\, a = 0, \quad k_\mu^2 = -\bar k_0^2 = -A^2 (\rho_0),$$
$$\rho_0 = \dot\varphi_0 \varphi_0. \qquad (1.45)$$

Equation (2a′) also has a solution of a different form, which can be obtained by the method of integration.[4] We must introduce new functions φ and $\bar\varphi$ by the formulas*

$$\psi = \varphi - \gamma_\mu \frac{\partial\varphi}{\partial x_\mu} \frac{1}{A (\bar\psi, \psi)},$$

$$\bar\psi = \bar\varphi + \frac{\partial\bar\varphi}{\partial x_\mu} \gamma_\mu \frac{1}{A (\bar\psi, \psi)}. \qquad (1.46)$$

*Here on the assumption $\varphi = a\Phi$, $\bar\varphi = \bar a\Phi$, $A(\bar\psi, \psi) = A(\rho)$, $\rho = (\bar\psi\psi)$ the integrated equation is of the form[4]

$$\left(\partial^2 / \partial x_\mu^2 - A^2 (\rho) + A^{-1} (\rho) \frac{dA}{d\rho} \frac{\partial\rho}{\partial x_\mu} \frac{\partial}{\partial x_\mu} \right) \Phi = 0,$$

where in the case of Eq. (2a) the quantity ρ is determined from the algebraic equation

$$p^3 - (\bar a a)\, \Phi^2 p^2 + l^{-4}\, (\bar a a)\, (\partial\Phi / \partial x_\mu)^2 = 0,$$

which, as can be shown, has a single real solution for $(i\partial\Phi/\partial x_\mu)^2 > 0$.

If we now look for $\varphi(x_\mu)$ in the form* $\varphi = \varphi(\sigma)\,a$, $\bar{\varphi} = \bar{a}\varphi^*(\sigma)$, then Eq. (1.46) is written

$$\psi = (\varphi - \gamma_\mu k_\mu \bar{k}_0^{-1}\chi)\,a, \quad \bar{\psi} = \bar{a}(\varphi^* + \gamma_\mu k_\mu \bar{k}_0^{-1}\chi^*), \quad (1.47)$$

where φ and χ can be regarded as two independent unknown functions.† As solutions we have $\chi = 0$, $\varphi^*\varphi = \text{const}$, which reduces to Eq. (1.4), and also‡ $\varphi = \varphi_0 \cos(\sigma + c)$, $\chi = \varphi_0 \sin(\sigma + c)$, i.e.,

$$\psi = (\cos(\sigma + c) - \gamma_\mu k_\mu \bar{k}_0^{-1} \sin(\sigma + c))\,a, \quad (1.48)$$

where a is an arbitrary amplitude, and $k_\mu^2 = -\bar{k}_0^2 = A^2(\rho_0)$.

2. Let us determine the momentum, charge, and energy of the field (2a) with the Lagrangian

$$\mathfrak{L} = -\tfrac{1}{2}\{\bar{\psi}(D\psi) - (\overline{\psi D})\psi - l^2(\bar{\psi}\psi)^2\}. \quad (1.49)$$

In the case of the solution (1.4), (1.45) we find

$$\mathbf{G} = \mathbf{k}(\bar{a}\gamma_4 a)\,L^3, \quad Q = e(\bar{a}\gamma_4 a)\,L^3,$$
$$E = \left[\omega - \tfrac{1}{2}l^2(\bar{a}a)^2/(\bar{a}\gamma_4 a)\right](\bar{a}\gamma_4 a)\,L^3, \quad (1.50)$$

and after the normalization $N = (\bar{a}\gamma_4 a)\,L^3$ we get $(\bar{a}a) = NL^{-3}(\omega_0/\omega) = \bar{k}_0 l^{-2}$,

$$\mathbf{G} = N\mathbf{k}, \quad Q = Ne, \quad E = \tfrac{1}{2}N\omega\left(1 - \tfrac{1}{2}(k^2/\omega^2)\right),$$
$$\omega = NL^{-3}l^2. \quad (1.51)$$

Finally we get for the charge and mass of the elementary particle

$$G = 0, \quad Q = e, \quad k_0 l = \sqrt{2}\,\pi^{3/2} \approx 7.84. \quad (1.52)$$

In the case of the solution (1.48) we have

$$\mathbf{G} = \mathbf{k}(\bar{a}a)\frac{\omega}{\omega_0}L^3, \quad Q = e(\bar{a}\gamma_4 a)\,L^3,$$
$$E = \left(\omega - \frac{l^2}{2}\left(\frac{\omega_0}{\omega}\right)(\bar{a}a)\right)(\bar{a}a)\left(\frac{\omega}{\omega_0}\right)L^{-3} \qquad (\omega_0 = \bar{k}_0) \quad (1.53)$$

and after the normalization $(\bar{a}a)(\omega/\omega_0)\,L^{-3} = N$ we find* $(\bar{a}\gamma_4 a) = NL^{-3}$,

$$\mathbf{G} = N\mathbf{k}, \quad Q = Ne, \quad E = \tfrac{1}{2}N\omega\left(1 + (k_0/\omega)^2\right),$$
$$\omega = NL^{-3}l^2. \quad (1.54)$$

Determining the energy in the volume defined by Eq. (1.21), we again arrive at the results (1.52).

Dependence of the Rest Mass of the Elementary Particle on the Degree of Nonlinearity

To find the dependence of the rest mass of the elementary particle on the degree of nonlinearity, we call attention to the fact that when $A(\bar{\psi}, \psi)$ is an arbitrary function of $\rho = (\bar{\psi}\psi)$ the functions (1.4), (1.45), and (1.48) are also solutions of the general equation (2a′). The Lagrangian density corresponding to Eq. (2a′) can be written in the form

$$\mathfrak{L} = -\tfrac{1}{2}\{\bar{\psi}(D\psi) - (\overline{\psi D})\psi + [B(\hat{\rho}) - \hat{\rho}\,dB(\hat{\rho})/d\hat{\rho}]\}, \quad (1.55)$$

where $\hat{\rho} = l(\bar{\psi}\psi)$ and $B(\hat{\rho})$ is an arbitrary function.

From the Lagrangian (1.55) we at once find the field equation (2a′), in which

$$A(\hat{\rho}) = \tfrac{1}{2}l\,dB(\hat{\rho})/d\hat{\rho},$$

and the expressions for the momentum, charge, and mass take the forms

$$\mathbf{G} = N\mathbf{k}, \quad Q = Ne, \quad E = (\omega - [A(\hat{\rho}_0) - l\hat{\rho}_0^{-1}B(\hat{\rho}_0)])\,N,$$
$$N = (\bar{a}\gamma_4 a)\,L^3, \quad \omega^2 = k^2 + \omega_0^2,$$
$$\omega_0 = A(\hat{\rho}_0), \quad \hat{\rho}_0 = lNL^{-3}(\omega_0/\omega). \quad (1.56)$$

For $\mathbf{k} = 0$, $N = 1$ we obtain as the charge and mass of the elementary particle

$$Q = e, \quad k_0 = (l/2\hat{\rho}_0)\,B(\hat{\rho}_0) \quad (\omega_0(N=1) = k_0'). \quad (1.57)$$

From the conditions

$$\rho_0 = L^{-3}, \quad k_0' = A(\hat{\rho}_0) = (l/2\hat{\rho}_0)\,B(\hat{\rho}_0)$$

with the additional requirement $L = 2\pi/k_0'$ we get

$$dB(\rho_0)/d\rho_0 = 4\pi\rho_0^{1/3}. \quad (1.58)$$

For a prescribed form of the function $B(\hat{\rho})$ we

---

*If we look for solutions in the form $\varphi = \varphi(\xi)\,a$, $\varphi^* = \bar{a}\varphi(\varepsilon)$, $\xi = -x_\mu^2$, then Eq. (1.46) gives $\psi = (\varphi + \gamma_\mu x_\mu \chi)\,a$, $\bar{\psi} = \bar{a}(\varphi - \gamma_\mu x_\mu \chi)$, $\rho = (\bar{\psi}\psi) = (\bar{a}a)(\varphi^2 + \xi^2\chi^2)$, and from Eq. (2a′) we find

$$4\chi + 2\xi\chi' + A(\rho)\varphi = 0, \quad (a)$$
$$2\varphi' - A(\rho)\chi = 0. \quad (b)$$

In the case $A(\rho) = l^2(\bar{\psi}\psi)$ the equations (a) and (b) coincide with the equations obtained by Heisenberg.[5] If we now eliminate $A(\rho)$ from Eqs. (a) and (b), we get

$$\chi^2 = -\rho'/3(\bar{a}a) \quad (c)$$

and then substituting Eq. (c) in Eq. (a) we find

$$\xi\rho'' + 4\rho' - A(\rho)\sqrt{-\rho'(3\rho + \xi\rho')} = 0, \quad \rho' \equiv d\rho/d\xi.$$

With a special choice of $A(\rho)$ it may be possible in this way to find also the corresponding exact solution of Eq. (2a′).

†Then Eq. (2a′) gives

$$\gamma_\mu k_\mu(\varphi' + \bar{k}_0^{-1}A(\rho)\chi)\,a = 0, \quad \gamma_\mu k_\mu(\chi' + A(\rho)\varphi\bar{k}_0 k_\mu^{-2})\,a = 0,$$
$$\rho = \rho_0 + \rho_1, \quad \rho_1 = (\bar{a}a)(\varphi^*\varphi - k_\mu^2\bar{k}_0^{-1}\chi^*\chi), \quad (A)$$
$$\rho_2 = (\bar{a}\gamma_\mu k_\mu a)(\varphi^*\chi - \chi^*\varphi).$$

We must take along with Eq. (A) the system of complex conjugate equations. It is easy to show further that

$$\varphi^*\varphi + \chi^*\chi = \text{const}, \quad \varphi^*\chi - \chi^*\varphi = \text{const},$$
$$\rho = \rho_0 = \text{const}, \quad k_\mu^2 = -\bar{k}_0^2 = -A^2(\rho_0).$$

‡It is easy to verify that

$$\frac{\partial}{\partial x_\mu}(\bar{\psi}\gamma_\mu\psi) = \frac{d}{d\sigma}(\bar{\psi}\gamma_\mu k_\mu\psi) = \frac{d}{d\sigma}(\bar{a}(\varphi^2 - \chi^2 k_\mu^2/\bar{k}_0^2)\,a) = 0.$$

*Since the a(s) are arbitrary functions, they can be taken to be the solution of Eq. (1.45).

can use Eq. (1.58) to express $\rho_0 = (\bar{a}a)$ in terms of absolute constants. For example, taking $B(\hat{\rho})$ in the form

$$B(\hat{\rho}) = l^n (\bar{\psi}\psi)^n. \tag{1.59}$$

we get

$$\hat{\rho}_0 = (4\pi/n)^{3/(3n-4)} l^{-4/(3n-4)},$$
$$k_0' = A(\hat{\rho}_0) = \tfrac{1}{2} n l \rho_0^{n-1}$$
$$= \tfrac{1}{2}(4\pi)^{(3n-3)/(3n-4)} l^{-n/(3n-4)} n^{-1/(3n-4)}, \tag{1.60}$$

and the mass of the elementary particle is

$$k_0 = \hat{\rho}_0^n / 2\rho_0 = \tfrac{1}{2} l \hat{\rho}_0^{n-1} = k_0'/n,$$

that is,

$$k_0 l^{n/(3n-4)} = \tfrac{1}{2}(4\pi/n)^{(3n-3)/(3n-4)}. \tag{1.61}$$

Let us note some features of the function (1.61). For $n = 1$ (linear theory) Eq. (1.61) gives $k_0 l^{-1} = \frac{1}{2}$, in complete agreement with reality. For $n = 2$ [the case of the nonlinear equation (2a)] we get $k_0 l = 2^{1/2}\pi^{3/2} \approx 7.84$, as was to be expected. For $n \to \infty$ we find

$$l^{1/3} k_0 (n \to \infty) \to \tfrac{1}{2}(4\pi/n)_{n\to\infty} \to 0.$$

For $n \to 0$ we have

$$k_0 (n \to 0) \to \tfrac{1}{2}(4\pi/n)_{n\to 0} \to \infty.$$

Thus in this interpretation we can get any value of the mass by varying the degree of nonlinearity n. For example, we can use for the neutrino the case of an infinite degree of nonlinearity, and for the electron the case of a finite but very large value of n.

The function (1.61) is meaningless for one case, $n = 4/3$ (the Gürsey case[7]), i.e., for

$$B(\hat{\rho}) = \hat{\rho}^{4/3} = l^{4/3} (\bar{\psi}\psi)^{4/3}. \tag{1.62}$$

The peculiarity of this case is that there is now no need for the requirement (1.22). The expression analogous to Eq. (1.22) is obtained automatically. Besides this, the parameter l of the nonlinear term is a dimensionless quantity in this case, and the length L plays the role of the dimensional parameter in the theory. In fact, in the case (1.62) Eq. (1.56) gives the relations

$$G = Nk, \quad Q = Ne, \quad E = \left(\omega + \tfrac{1}{2} l \hat{\rho}_0^{1/3}\right) N, \quad N = (\bar{a}\gamma_4 a) L^3,$$

$$\hat{\rho}_0 = l(\bar{a}a) = lNL^{-3}(\omega_0/\omega), \quad \omega_0 = \tfrac{2}{3} l^{4/3} (N(\omega_0/\omega))^{1/3}.$$

From these we find for $k = 0$, $N = 1$

$$G = 0, \quad Q = e, \quad k_0 L = \tfrac{1}{2} l^{4/3}, \quad k_0' = \tfrac{4}{3} k_0$$

and the condition analogous to Eq. (1.22) is

$$L k_0' = \tfrac{2}{3} l^{4/3}. \tag{1.22'}$$

Equation (1.22') becomes identical with Eq. (1.22) for a suitable choice of the constant* $l^{4/3}$:

$$l^{4/3} = 3\pi, \qquad k_0 L = \tfrac{3}{2}\pi \approx 4.71. \tag{1.63}$$

2. ON THE THEORY OF THE FUSION OF NONLINEAR FIELDS

The introduction of a single fundamental spinor field as the basis of the theory of elementary particles requires the definition of some procedure for getting other fields from the fundamental field.

As has been pointed out in reference 8, the de Broglie fusion method, together with the use of group theory, indicates a possibility for such a procedure. Group theory is too general, however, and in particular does not fix any connection between the nondifferential parts of the equations of the various fields. For example, if we start the fusion with Eq. (2a), group theory will give no information about the concrete form of the nonlinear terms in the equations obtained after the fusion. For this reason in the present paper, in dealing with the problem of the fusion of nonlinear fields, we apply the second, fundamental, fusion method of de Broglie, which can be called the "method of fusion of equations."[6]

If we take two spinor fields $\bar{\psi}_i^{(1)}$ and $\psi_k^{(2)}$ that obey the linear Dirac equation, we can form a function $\psi_{ik} = \bar{\psi}_i^{(1)} \psi_k^{(2)}$, which is a component of an undor of the second rank $(\psi\Gamma)$, so that $(\psi\Gamma)$ obeys the Dirac equation or the corresponding Klein-Gordon equation. The undor $(\psi\Gamma)$ can be expanded in the following way:

$$(\psi\Gamma) = \gamma_0\varphi_0 + \gamma_5\varphi_5 + \gamma_\mu\varphi_\mu + \gamma_\mu\gamma_5\varphi_{\mu 5} + \sigma_{\mu\nu}\varphi_{\mu\nu} = \sum_{\alpha=1}^{16} \theta_\alpha \varphi_\alpha,$$

$$\gamma_0 \equiv \gamma_4, \tag{2.1}$$

where θ_α is one of the sixteen independent Dirac matrices.

Let us now consider fusion, starting with the nonlinear Dirac equation

$$(\gamma_\mu \partial/\partial x_\mu + k_0(\bar{\psi}, \psi))\psi = 0. \tag{2.2}$$

As in the case of the linear theory, we consider two fields $\bar{\psi}_i^{(1)}$ and $\psi_k^{(2)}$ that satisfy Eq. (2.2) and the adjoint equation. We form the function $\psi_{ik} = \bar{\psi}_i^{(1)} \psi_k^{(2)}$ and go over to the undor equation

$$(\gamma_\mu \partial/\partial x_\mu + \bar{k}_0(\bar{\psi}, \psi))(\psi\Gamma) = 0,$$

$$\bar{k}_0(\bar{\psi}, \psi) = \tfrac{1}{2}[k_0(\bar{\psi}^{(1)}, \psi^{(1)}) + k_0(\bar{\psi}^{(2)}, \psi^{(2)})]. \tag{2.3}$$

If we now impose on $\bar{k}_0(\bar{\psi}, \psi)$ the requirement

*It is easily verified that Eq. (1.62) with the value (1.63) inserted, i.e., the function $B(\hat{\rho}) = 3\pi\hat{\rho}^{4/3}$, is a solution of Eq. (1.58).

$$\bar{k}_0(\bar{\psi}, \psi) = k_0(\bar{\psi}^{(1)}, \psi^{(2)}) = k_0(\bar{\psi}^{(2)}, \psi^{(1)}) = \bar{k}_0(\bar{\psi}^{(1)}, \psi^{(2)}) \quad (2.4)$$

and use the fact that when we confine ourselves to the lowest powers of the invariants $\bar{k}_0(\bar{\psi}^{(1)}, \psi^{(2)})$ has the form[3]

$$\bar{k}_0(\bar{\psi}^{(1)}, \psi^{(2)}) = \sum_{\alpha=1}^{16} \lambda_\alpha \theta_\alpha (\bar{\psi}^{(1)} \theta_\alpha \psi^{(2)}), \quad (2.5)$$

where λ_α are arbitrary constants, we arrive at the conclusion that $\bar{k}_0(\bar{\psi}^{(1)}, \psi^{(2)})$ is also an undor. Let us now choose the constants λ_α so that

$$\lambda_\alpha (\bar{\psi}^{(1)} \theta_\alpha \psi^{(2)}) = \lambda_0 \varphi_\alpha. \quad (2.6)$$

Then Eq. (2.5) can be written in the form

$$\bar{k}_0(\bar{\psi}^{(1)} \psi^{(2)}) = \lambda_0 (\psi\Gamma). \quad (2.7)$$

Substituting Eq. (2.7) in Eq. (2.3), we get the nonlinear undor equation

$$(\gamma_\mu \partial/\partial x_\mu + \lambda_0 (\psi\Gamma))(\psi\Gamma) = 0. \quad (2.8)$$

Applying the operator $\gamma_\nu \partial/\partial x_\nu$ to Eq. (2.8), we find

$$(\partial^2/\partial x_\mu^2 - 2\lambda_0^2 (\psi\Gamma)^2)(\psi\Gamma) = 0. \quad (2.9)$$

Let us now consider the expression

$$(\psi\Gamma)^2 = \varphi_0^2 + \varphi_5^2 + \varphi_\mu^2 - \varphi_{\mu 5}^2 + (\sigma_{\mu\nu}\varphi_{\mu\nu})^2 + f(\ldots), \quad (2.10)$$

where $f(\ldots)$ denotes terms containing mixed derivatives of the various fields. In a similar way we get for $(\psi\Gamma)^3$

$$(\psi\Gamma)^3 = \gamma_0 \varphi_0^3 + \gamma_5 \varphi_5^2 + \gamma_\mu \varphi_\mu \varphi_\nu^2 - \gamma_\mu \gamma_5 \varphi_{\mu\nu} \varphi_{\nu 5}^2 + \sigma_{\mu\nu}\varphi_{\mu\nu} (\sigma_{\alpha\beta}\varphi_{\alpha\beta})^2 + U(\ldots). \quad (2.11)$$

The mixed derivatives of various fields lead to a nonlinear interaction of these fields. In the case in which we consider only the self-interactions of the fields, the quantities $f(\ldots)$ and $U(\ldots)$ are to be neglected. We then get

$$(\partial^2/\partial x_\mu^2 - 2\lambda_0^2 \varphi_\alpha^2)\varphi_\alpha = 0, \quad (2.12)$$

where φ_α is one of the components of the undor.*

We have previously considered[4] an expression of the type of Eq. (2.12) and have shown that it leads to a spectrum of meson masses.

*If we take into account the fact that according to field theory there are three relations[1] between the invariants φ_0^2, φ_5^2, $\varphi_{\mu 5}^2$, φ_μ^2, $\varphi_{\mu\nu}^2$, we can put the expression (2.10) in the form

$$(\psi\Gamma)^2 = \alpha_1 \varphi_0^2 + \alpha_2 \varphi_5^2 + f(\ldots).$$

Then Eq. (2.11) will have the corresponding form

$$(\psi\Gamma)^3 = \alpha_1 \gamma_0 \varphi_0^3 + \alpha_2 \gamma_5 \varphi_5^3 + U(\ldots),$$

and instead of Eq. (2.12) we get

$$\left(\frac{\partial^2}{\partial x_\mu^2} - 2\lambda_0^2 \begin{pmatrix} \alpha_1 \varphi_0^2 \\ \alpha_2 \varphi_5^2 \end{pmatrix}\right) \begin{pmatrix} \varphi_0 \\ \varphi_5 \end{pmatrix} = 0, \qquad \frac{\partial^2}{\partial x_{\mu^2}} \begin{pmatrix} \varphi_\mu \\ \varphi_{\mu 5} \\ \varphi_\mu \end{pmatrix} = 0, \quad \frac{\partial \varphi_\mu}{\partial x_\mu} = 0.$$

3: THE CONFORMAL INVARIANCE OF THE NONLINEAR EQUATIONS

As a rule nonlinear equations possess the property of so-called conformal invariance, which makes it possible to go from one particular solution to another by a simple change of scale of the coordinates. We have already called attention to the property of conformal invariance of the nonlinear meson-field equation

$$(\Box - \lambda\varphi^2)\varphi = 0 \quad (3.1)$$

in an earlier paper,[9] where in particular we showed that if $\psi(x_\mu, \lambda)$ is a solution of Eq. (3.1) then the function

$$\psi'(x_\mu, \lambda) = AB^{1/2}\psi(Ax_\mu, B\lambda) \quad (3.2)$$

is also a solution of that equation.*

Let us introduce coordinate transformations (regarding the nonlinear parameter as a fifth coordinate):

$$x'_\mu = Ax_\mu, \quad \lambda' = B\lambda. \quad (3.3)$$

The invariance of Eq. (3.1) under (3.3) gives

$$\psi'(x', \lambda') = S(AB)\psi(x_\mu, \lambda), \quad (3.4)$$

where S(AB) satisfies the conditions

$$SS^{-1} = 1, \quad S^2 A^2 B = 1, \quad S^{-1} = AB^{1/2}, \quad (3.5)$$

which also leads to the expression (3.2).

Let us use the property of conformal invariance of the field equation to derive conservation laws. According to Noether's theorem, for this we need invariance of the Lagrangian function under the transformations in question.

Under the transformation (3.3), (3.4) and the condition (3.5) the Lagrangian of Eq. (3.1),

$$\mathfrak{L} = \frac{1}{2}\int \left\{ \left(\frac{\partial\varphi}{\partial x_\mu}\right)^2 + \frac{1}{2}\lambda\varphi^4 \right\} (d^4x) \quad (3.6)$$

transforms according to the formula

$$\mathfrak{L}'[\psi'(Ax_\mu, B\lambda)] = g(AB)\,\mathfrak{L}[\psi(x_\mu, \lambda)].$$

*From this it follows in particular that the functions $A\psi(Ax_\mu, \lambda)$ and $B^{1/2}\psi(x_\mu, B\lambda)$ are solutions of Eq. (3.1). For example, the second of these forms expresses the fact that the solution of Eq. (3.1) can contain the nonlinear parameter only in the combination $\lambda\varphi_0^2$, where φ_0 is the amplitude of the solution.

From this we get*

$$\mathfrak{L}(\lambda) = B\mathfrak{L}(B\lambda), \quad g(AB) = g(B) = B^{-1}. \tag{3.7}$$

Confining ourselves to the case $B = +1$, $S^{-1}(AB) = S^{-1}(A) = A$, we find

$$\psi'(x'_\mu, \lambda) = S(A)\psi(x_\mu, \lambda),$$
$$\psi'(x_\mu, \lambda) = S(A)\psi(A^{-1}x_\mu, \lambda). \tag{3.8}$$

Let us now introduce the representative operator $T(A)$ and write

$$\psi'(x'_\mu, \lambda) = T(A)\psi(x_\mu, \lambda) = S(A)\psi(A^{-1}x_\mu, \lambda). \tag{3.9}$$

Confining ourselves to a consideration of the continuous group, let us introduce a small parameter α by the relation $A = 1 + \alpha$, and also the infinitesimal operators† $\hat{J}$ and $\hat{S}$; we then find from Eq. (3.9)

$$\{\hat{J} - (\hat{S} - x_\mu\partial/\partial x_\mu)\}\psi(x_\mu, \lambda) = 0. \tag{3.10}$$

Let us now consider the case of the nonlinear spinor equation

$$\{\gamma_\mu(\partial/\partial x_\mu + l_1^2\gamma_5(\bar{\psi}\gamma_\mu\gamma_5\psi)) + l_2^2(\bar{\psi}\psi)\}\psi = 0. \tag{3.11}$$

The conformal invariance of Eq. (3.11) was pointed out recently by Heisenberg and his coworkers.[1] They also made an attempt to connect the conformal invariance of Eq. (3.11) with a definite conservation law. Here we shall consider the conformal invariance of Eq. (3.11) in a different aspect, in particular in connection with the meson field equation (3.1).

The Lagrangian function corresponding to Eq. (3.11) is

$$\mathfrak{L} = \frac{1}{2}\int\left\{\bar{\psi}\gamma_\mu\frac{\partial\psi}{\partial x_\mu} - \frac{\partial\bar{\psi}}{\partial x_\mu}\gamma_\mu\psi + l_1^2(\bar{\psi}\gamma_\mu\gamma_5\psi)^2 + l_2^2(\bar{\psi}\psi)^2\right\}(d^4x). \tag{3.12}$$

Under the transformation (3.3) the quantities $\psi(x_\mu, \lambda_i)$ and $\mathfrak{L}[\psi(x_\mu, \lambda_i)]$ transform according to the formulas‡

$$\psi'(Ax_\mu, B\lambda_i) = S(AB)\psi(x_\mu, \lambda_i),$$
$$S^{-1}(AB) = \sqrt{AB}, \quad \lambda_i \equiv l_i^2;$$
$$\mathfrak{L}'[\psi'(Ax_\mu, B\lambda_i)] = g(AB)\mathfrak{L}[\psi(x_\mu, \lambda_i)], \quad g(AB) = A^2/B. \tag{3.13}$$

Taking $g(AB) = 1$; $A^2 = B$, i.e., $S(AB) = B^{-3/4} = A^{-3/2}$, and introducing the representative operator $T(A)$, we get

$$\psi'(x'_\mu, \lambda'_i) = T(A)\psi(x_\mu, \lambda_i) = S(A)\psi(A^{-1}x_\mu, A^{-2}\lambda_i). \tag{3.14}$$

Introducing the small parameter $\alpha = A - 1$ and the infinitesimal operators J and S, we find*

$$\{\hat{J} - (\hat{S} - x_\mu\partial/\partial x_\mu - l_i\partial/\partial l_i)\}\psi(x_\mu, \lambda_i) = 0, \quad \lambda_i \equiv l_i^2. \tag{3.15}$$

As the eigenvalues of the operator $\hat{S}$ we get $+1$ for bosons and $-3/2$ for spinors.

We now turn out attention to the sign of the nonlinear parameter l_1^2. It follows from Eqs. (3.7) and (3.13) that if $B = -1$ the Lagrangian merely changes sign, and therefore as long as the sign of the Lagrangian does not impose any conditions on physical processes both signs are permissible in nonlinear equations.

In conclusion I express my gratitude to D. Ivanenko for a discussion on the nonlinear theory.

Note added in proof (December 12, 1959). Introducing the operator $\hat{p}\psi \equiv (\hat{J} - \hat{S})\psi = p\psi$ and the new coordinates $\xi_j(x_\mu, l_i)$ [in the case of Eq. (3.10)], or $\xi_j(x_\mu)$ [in the case of Eq. (3.15)], we can write Eqs. (3.10) and (3.15) in the form $(\xi_j\partial/\partial\xi_j + p)\psi = 0$, with the solution

$$\psi = c_1\sigma_1^{-p} + c_2\sigma_2^{-p/2} + c_3\sigma_1^{\lambda}\sigma_2^{-(p+\lambda)/2}, \tag{a}$$

where c_1, c_2, c_3, λ are arbitrary constants, $\sigma_1 = k_j\xi_j$, and $\sigma_2 = -\xi_j\xi_j$. Now comparing Eq. (a) with the particular solution $\psi = \lambda^{-1/2}\sigma_2^{-1/2}$ of Eq.

*It may be helpful to indicate the analogy with the linear theory, in which the field equation is invariant with respect to the transformation

$$\psi'(x_\mu, k_0) = N^{1/2}\psi(x_\mu, k_0),$$

where N is a number. Under this the Lagrangian function transforms in the following way:

$$\mathfrak{L}'[N^{1/2}\psi'(x_\mu, k_0)] = N\mathfrak{L}[\psi(x_\mu, k_0)],$$

which gives the possibility of introducing the number of particles. In reference 9 we have used the analogy of these transformations with Eqs. (3.4) and (3.7) to introduce the number of particles $N = B$ in the nonlinear field theory.

†$\hat{J} = \partial T(\alpha)/\partial\alpha|_{\alpha=0}$, $\hat{S} = \partial S(\alpha)/\partial\alpha|_{\alpha=0}$, and, as follows from Eq. (3.9), the eigenvalue of $\hat{S}$ is $+1$.

‡As we see, the transformation (13) also gives the possibility of introducing the number of particles $N = BA^{-2}$

*The compatibility of the quantum number and the conformal invariance require that the conformal transformation operator commute with the translation operator. Generally speaking these operators do not commute, but Heisenberg[1] prescribes the transformation of translation in the form

$$x'_\mu = x_\mu + \alpha l_i,$$

and since in the case of Eq. (3.11), according to Eq. (3.15), l_i transforms in just the same way as x_μ, the operators do commute. In the case of Eq. (3.1), according to Eq. (3.9), prescription of the translations in the form (a) does not lead to commuting operators: instead of (a) we must write $x'_\mu = x_\mu + \alpha\varphi_0$, where φ_0 is the amplitude of the solution, which, according to Eq. (3.9), transforms just like x_μ. In the case of Eq. (3.11) the translation can be prescribed in the form $x'_\mu = x_\mu + \alpha\varphi_0^{2/3}$, where φ_0 is the amplitude of the solution, which, according to Eq. (3.15), transforms just like $x^{2/3}$ and secures commutativity of the operators of translation and conformal transformation.

(3.1) and the particular solution $\psi = c\sigma_2^{-1/4} \times \{1 + \gamma_\mu x_\mu \sigma_2^{-1/2}\}$ of Eq. (3.11) (with $\sigma_2 = -x_\mu^2 + l_1^2 \approx -x_\mu^2$), we find $p = 1$ for bosons and $p = 1/2$ for spinors. From this we get for the eigenvalues

$$J = 2\begin{pmatrix} -1/2 \\ 1 \end{pmatrix}, \qquad p = \begin{pmatrix} 1/2 \\ 1 \end{pmatrix}, \qquad s = \begin{pmatrix} -3/2 \\ 1 \end{pmatrix} \begin{matrix} \text{spinors} \\ \text{bosons} \end{matrix}.$$

If in the derivation of (4.16) (sic) we start not from (4.15) (sic) but from

$$\psi'(x'_\mu, \lambda'_i) = T(B)\psi(x_\mu, \lambda_i) = S(B)\psi(B^{-1/2}x_\mu, B^{-1}\lambda_i),$$

we again arrive at Eq. (3.15), but now with $\hat{J}$ replaced by $2\hat{J}$.

The results obtained also remain valid if instead of from Eq. (3.12) we start from the nonlinear Lagrangian (1.59), where, however, it is expedient to introduce instead of l the parameter

$$l_1 = (l^n / 3\pi)^{1/(3n-4)},$$

which has the dimensions of k_0^{-1} ($k_0 l_1 = \text{const}$, $B(\hat{\rho}) = 3\pi l_1^{3n-4}(\bar{\psi}\psi)^n$).

[1] W. Heisenberg, Revs. Modern Phys. **29**, 269 (1957). Dürr, Heisenberg, Mitter, Schlieder, and Yamazaki, Z. Naturforsch. **14a**, 441 (1959).

[2] W. Heisenberg and W. Pauli, On the Isospin Group in the Theory of the Elementary Particles, preprint.

[3] D. Ivanenko and A. Brodskiĭ, Dokl. Akad. Nauk SSSR **84**, 683 (1952); JETP **24**, 383 (1953).

[4] D. F. Kurdgelaidze, JETP **34**, 1587 (1958), Soviet Phys. JETP **7**, 1093 (1958); JETP **36**, 842 (1959), Soviet Phys. JETP **9**, 594 (1959).

[5] W. Heisenberg, Z. Naturforsch. **9a**, 292 (1954).

[6] A. Sokolov and D. Ivanenko, Квантовая теория поля (Quantum Field Theory), Gostekhizdat, 1952.

[7] F. Gürsey, Nuovo cimento **3**, 988 (1956).

[8] D. F. Kurdgelaidze, JETP **35**, 1572 (1958), Soviet Phys. JETP **8**, 1099 (1959). G. A. Sokolik, Dokl. Akad. Nauk SSSR **106**, 429 (1956), Soviet Phys.-Doklady **1**, 57 (1956).

[9] D. D. Ivanenko and D. F. Kurdgelaidze, Dokl. Akad. Nauk SSSR **96**, 39 (1954). D. F. Kurdgelaidze, Вестник МГУ (Bull. Moscow State Univ.) **8**, 81 (1954).

Translated by W. H. Furry
98

NUCLEON-NUCLEON SCATTERING IN THE TWO-MESON APPROXIMATION FOR LARGE ORBITAL ANGULAR MOMENTA

A. D. GALANIN, A. F. GRASHIN, B. L. IOFFE, and I. Ya. POMERANCHUK

Submitted to JETP editor June 12, 1959

J. Exptl. Theoret. Phys. (U.S.S.R.) **38**, 475-488 (February, 1960)

The method previously developed by the authors is used to calculate the nucleon-nucleon scattering amplitude in the two-meson approximation for large orbital angular momenta. Specific calculations are carried out for the singlet amplitude in the non-relativistic approximation for orbital angular momenta which are not very large, $1 \ll l \ll 4m^2/\mu^2$ (m is the nucleon mass, μ the meson mass). The results obtained indicate that the F and G phase shifts for nucleon energies $E_{lab} \lesssim 200$ Mev are given to good accuracy by the one-meson approximation. This conclusion may prove important in the phase shift analysis of nucleon-nucleon scattering.

1. CALCULATION OF THE TWO-MESON AMPLITUDE

In a previous paper[1]* it was shown that, in order to calculate the nucleon-nucleon scattering amplitude in the two-meson approximation for large orbital angular momenta, it is necessary to know the meson-nucleon scattering amplitude $f_{\alpha\beta}$. The latter amplitude, according to formulas (2.25, I), (3.1, I), (3.6, I), (3.20, I), is expressed as follows:

$$f_{\alpha\beta}(p_1,\ p_1+q;\ k+q/2,\qquad k-q/2) = f_{p\alpha\beta} + \tilde{f}'_{\alpha\beta} + \tilde{f}''_{\alpha\beta},$$

$$f_{p\alpha\beta} = -g^2\tau_\alpha\tau_\beta \frac{\hat{k}}{(k+q/2)^2 + 2p_1(k+q/2)} + g^2\tau_\beta\tau_\alpha \frac{\hat{k}}{(k-q/2)^2 - 2p_1(k-q/2)},$$

$$\tilde{f}'_{\alpha\beta} = \frac{g^2}{m}\alpha\delta_{\alpha\beta},$$

$$\tilde{f}''_{\alpha\beta} = i\frac{g^2}{\mu^2}\varepsilon_{\alpha\beta\gamma}\tau_\gamma\left(\beta_1\hat{k} + \beta_2\frac{p_1 k}{m}\right), \qquad (1.1)$$

where $\alpha = 1.2$, $\beta_1 = 0.025$, and $\beta_2 = -0.029$.

We insert (1.1) into (2.29, I). Omitting the term quadratic in $\tilde{f}''_{\alpha\beta}$ [it would give a contribution to the scattering phase shift containing an extra factor $1/L$, where L is defined by (2.16, I)], we obtain

$$M^2(q^2) = \frac{g^4}{\pi m}\left[\frac{3\alpha^2}{4}B_0 - \frac{3\alpha}{2}B_1 + \tau_\alpha^{(1)}\tau_\alpha^{(2)}B_2 + (3 + 2\tau_\alpha^{(1)}\tau_\alpha^{(2)})B_3 + (3 - 2\tau_\alpha^{(1)}\tau_\alpha^{(2)})B_4\right], \qquad (1.2)$$

where

$$B_0 = \frac{2}{i}\int \Delta(k,\ q)\, d^4k\, (\bar{u}_{p_1+q}u_{p_1})(\bar{u}_{p_2-q}u_{p_2}),$$

$$B_1 = \frac{2m}{i}\int\left[\frac{(\bar{u}_{p_1+q}|\hat{k}|u_{p_1})(\bar{u}_{p_2-q}u_{p_2})}{(k+q/2)^2 + 2p_1(k+q/2)} + \frac{(\bar{u}_{p_2-q}|\hat{k}|u_{p_2})(\bar{u}_{p_1+q}u_{p_1})}{(k-q/2)^2 + 2p_2(k-q/2)}\right]\Delta(k,q)\, d^4k,$$

$$B_2 = -\frac{2m^2}{i\mu^2}\int\left[\frac{(\bar{u}_{p_1+q}|\beta_1\hat{k} + \beta_2 p_1 k/m|u_{p_1})(\bar{u}_{p_2-q}|\hat{k}|u_{p_2})}{(k-q/2)^2 + 2p_2(k-q/2)} + \frac{(\bar{u}_{p_1+q}|\hat{k}|u_{p_1})(\bar{u}_{p_2-q}|\beta_1\hat{k} + \beta_2 p_2 k/m|u_{p_2})}{(k+q/2)^2 + 2p_1(k+q/2)}\right]\Delta(k,q)\, d^4k,$$

$$B_3 = \frac{m^2}{i}\int\frac{(\bar{u}_{p_1+q}|\hat{k}|u_{p_1})(\bar{u}_{p_2-q}|\hat{k}|u_{p_2})\Delta(k,q)}{[(k+q/2)^2 + 2p_1(k+q/2)][(k-q/2)^2 + 2p_2(k-q/2)]}\, d^4k,$$

$$B_4 = -\frac{m^2}{i} \times \int\frac{(\bar{u}_{p_1+q}|\hat{k}|u_{p_1})(\bar{u}_{p_2-q}|\hat{k}|u_{p_2})\Delta(k,q)}{[(k+q/2)^2 + 2p_1(k+q/2)][(k+q/2)^2 - 2p_2(k+q/2)]}\, d^4k,$$

$$\Delta(k,\ q) = [(k-q/2)^2 - \mu^2]^{-1}\ [(k+q/2)^2 - \mu^2]^{-1}.$$

Introducing, as usual, the Feynman parameter x, we express B_0 in the form

$$B_0 = \frac{2w}{i}\int_0^1 dx\int d^4k\,[k^2 - \mu^2 + q^2/4 - qk(1-2x)]^{-2}, \qquad (1.3)$$

$$w = (\bar{u}_{p_1+q}u_{p_1})(\bar{u}_{p_2-q}u_{p_2}). \qquad (1.4)$$

The integral over d^4k in (1.3) extends to infinity, but the high momentum contribution appears as an additive constant, independent of q^2, and it need not be taken into account. We separate the finite term, differentiating (1.3) with respect to μ^2, then integrating over d^4k and then integrating back again with respect to μ^2. Integrating, finally, over dx we obtain the singular part of the integral in the form

$$B_0 = -w\frac{s}{\sqrt{1-s^2}}\tan^{-1}\frac{\sqrt{1-s^2}}{s}, \qquad (1.5)$$

*This paper will be referred to as I.

$$s = \sqrt{1 - q^2/4\mu^2}. \quad (1.6)$$

For the square root (1.6) we choose the branch which is positive in the physical region. In this case, on the upper side of the cut, $s = -i|s|$.

We restrict the discussion below to the singlet amplitude in the nonrelativistic approximation and for this case only we shall calculate the matrix elements of the type (1.4). Expanding w in powers of p^2/m^2 and setting $\cos\theta = 1 + 2\xi^2$, we obtain, to an accuracy including up to second-order terms*

$$w = 1 + (p^2/2m^2)(1 - \cos\theta) = 1 - \varepsilon^2; \ \varepsilon = \mu/m. \quad (1.7)$$

Now expanding (1.5) in powers of s, and retaining the leading term, we obtain finally,

$$B_0 = -\pi(1 - \varepsilon^2)\, s/2. \quad (1.8)$$

For the integration in B_1, we introduce two Feynman parameters x_1 and x_2 (taking into account that $2p_1q = -q^2$, $2p_2q = q^2$):

$$B_1 = \frac{4m}{i}\int_0^1 dx_2 \int_0^{1-x_2} dx_1 \int d^4k \left\{ \frac{(\bar{u}_{p_1+q}\,|\,\hat{k}\,|\,u_{p_1})(\bar{u}_{p_2-q}\,u_{p_2})}{(k^2 - 2\bar{p}k - \Delta)^3} + \ldots \right\},$$

$$\bar{p} = -q/2 + qx_1 - p_1x_2, \ \Delta = -q^2/4 - p_1qx_2 + \mu^2(1 - x_2), \quad (1.9)$$

the dots indicating a similar term with p_1 replaced by p_2.

Integrating over d^4k, we obtain

$$B_1 = w\int_0^1 dx_2 \int_0^{1-x_2} dx_1 \frac{x_2}{b^2}, \ b^2 = x_2^2 + \varepsilon^2(1 - x_2)$$
$$- 4\varepsilon^2(1 - s^2)\, x_1(1 - x_1 - x_2). \quad (1.10)$$

Making the substitution $x_1 = (1 - \epsilon y - z)/2$, $x_2 = \epsilon y$ and integrating over dz, we obtain

$$B_1 = \frac{w}{\sqrt{1 - s^2}}\int_0^{1/\varepsilon} \frac{y}{a}\tan^{-1}\frac{(1 - \varepsilon y)\sqrt{1 - s^2}}{a}\, dy, \quad (1.11)$$

where

$$a^2 = s^2 + \varepsilon(1 - 2s^2)\, y + [1 - \varepsilon^2(1 - s^2)]\, y^2. \quad (1.12)$$

For small s^2, small values of y are important in (1.11), so that $\tan^{-1}[(1 - \epsilon y)\sqrt{1 - s^2}/a]$ can be replaced by $\pi/2$ [it is shown in the Appendix that by doing this we obtain an accurate value for the singular part of the integral (1.11)]. After this is done the integral is easy to evaluate, since the upper limit gives a term, nonsingular in the neighborhood of $s^2 = 0$, which can be discarded. Consequently, expanding the result in powers of s^2 and ϵ^2 and substituting into (1.7), we obtain

$$B_1 = -\frac{\pi}{2}\left(1 + \frac{1}{2}\varepsilon^2\right)\left[s - \frac{\varepsilon}{2}\ln(\varepsilon + 2s)\right]. \quad (1.13)$$

The integral B_1 corresponds to the interference term already discussed in Sec. 2 of reference 1, and its discontinuity across the cut coincides with (2.28, I).

As already mentioned,[1] in calculating the phase shift we are interested in those cases in which $|2s| \gg \epsilon$ for the effective region of integration in (2.15, I) (corresponding to $L \ll 4m^2/\mu^2$), so that we do not expand terms of the type $\ln(\epsilon + 2s)$ in powers of s. Since $s > 0$ in the physical region, the argument of the logarithm in (1.13) does not vanish. However, on the other sheet of the Riemann surface, where $s < 0$, this argument does vanish, and on this sheet there occurs a singular point at $4s^2 = \mu^2/m^2$, or $q^2 = 4\mu^2 - \mu^4/m^2$.

We express the integral B_2 in the form

$$B_2 = -\frac{4}{\varepsilon^2}\int_0^1 dx_2 \int_0^{1-x_2} dx_1 F,$$

$$F = \frac{1}{i}\int d^4k \left\{ \frac{(\bar{u}_{p_1+q}\,|\,\hat{k}\,|\,u_{p_1})(\bar{u}_{p_2-q}\,|\,\beta_1\hat{k} + \beta_2 p_2 k/m\,|\,u_{p_2})}{(k^2 - 2\bar{p}k - \Delta)^3} + \ldots \right\}, \quad (1.14)$$

where the quantities $\bar{p}$ and Δ are defined in (1.9), and the dots represent a similar term with p_2 replaced by p_1. Differentiating F with respect to μ^2, and then integrating over d^4k, we obtain

$$\frac{dF}{d\mu^2} = \frac{1 - x_2}{4}\left\{ \frac{m^2x_2^2\beta_1w_1 + x_2[x_2(m^2 + 2p^2) + q^2(1 - 2x_1)/4]\,\beta_2w}{(\bar{p}^2 + \Delta)^2} \right.$$
$$\left. - \frac{1}{2}\frac{\beta_1w_2 + \beta_2w_1}{\bar{p}^2 + \Delta} \right\}, \quad (1.15)$$

where

$$w_1 = [(\bar{u}_{p_2-q}\,u_{p_2})(\bar{u}_{p_1+q}\,|\,\hat{p}_2\,|\,u_{p_1})$$
$$+ (\bar{u}_{p_2-q}\,|\,\hat{p}_1\,|\,u_{p_2})(\bar{u}_{p_1-q}\,u_{p_1})]/2m,$$
$$w_2 = (\bar{u}_{p_1+q}\,|\,\gamma_\alpha\,|\,u_{p_1})(\bar{u}_{p_2-q}\,|\,\gamma_\alpha\,|\,u_{p_2}).$$

With accuracy up to terms quadratic in p^2/m^2 and ϵ^2 we have

$$w_1 = 1 + \frac{p^2}{m^2}\left(2 - \frac{1 - \cos\theta}{2}\right) = 1 + \frac{2p^2}{m^2} + \varepsilon^2,$$
$$w_2 = 1 + \frac{2p^2}{m^2}. \quad (1.16)$$

The subsequent calculations are not difficult. Neglecting terms nonsingular in the neighborhood of $s^2 = 0$, using (1.7) and (1.16), and setting

$$\beta = -(\beta_1 + \beta_2)\left(1 + 2p^2/m^2 + \tfrac{5}{2}\varepsilon^2\right) - 2\varepsilon^2\beta_1, \quad (1.17)$$

we obtain

*We note the fact that the next correction term to the expresion in (1.7), in the present case p^4/m^4, is absent. Similar cancellations take place in the matrix elements (1.16) and (1.23).

$$B_2 = -\frac{\pi}{4}\beta\left[s - \frac{\varepsilon}{2}\ln(\varepsilon + 2s)\right]. \qquad (1.18)$$

We now turn to the calculation of the integrals B_3 and B_4, which correspond to fourth order perturbation theory. Introducing four Feynman parameters and integrating over d^4k, we obtain

$$B_3 = \frac{m^2}{4}\int dx_1 dx_2 dx_3 dx_4\, \delta\left(\sum x_i - 1\right) \times\left[\frac{(\bar{u}_{p_2-q}\,|\,\hat{h}\,|\,u_{p_2})(\bar{u}_{p_1+q}\,|\,\hat{h}\,|\,u_{p_1})}{(h^2+\Delta)^2} - \frac{1}{2}\frac{w_2}{h^2+\Delta}\right], \qquad (1.19)$$

$$B_4 = -\frac{m^2}{4}\int dx_1\, dx_2 dx_3 dx_4\, \delta\left(\sum x_i - 1\right) \times\left[\frac{(\bar{u}_{p_2-q}\,|\,\hat{h}'\,|\,u_{p_2})(\bar{u}_{p_1+q}\,|\,\hat{h}'\,|\,u_{p_1})}{(h'^2+\Delta)^2} - \frac{1}{2}\frac{w_2}{h'^2+\Delta}\right], \qquad (1.20)$$

where

$$h = p_2x_1 + p_1x_2 - q(x_1 - x_2 + x_3 - x_4)/2,$$
$$h' = p_2x_1 - p_1x_2 - q(x_1 + x_2 + x_3 - x_4)/2,$$
$$\Delta = \mu^2(x_3 + x_4) - q^2(1 - 2x_1 - 2x_2)/4.$$

Taking into account the fact that, to accuracy p^2/m^2, ϵ^2, the numerator in (1.19) can be written in the form [cf. (1.22)]

$$(u_{p_2-q}\,|\,\hat{h}\,|\,u_{p_2})(\bar{u}_{p_1+q}\,|\,\hat{h}\,|\,u_{p_1}) = m^2(x_1 + x_2)^2 w_1,$$

we transform B_3 to the following form:

$$B_3 = -\frac{1}{4}\left[\frac{w_2}{2} + w_1\frac{\partial}{\partial\gamma}\right]_{\gamma=1}\int dx_1 dx_2 dx_3 dx_4\, \delta\left(\sum x_i - 1\right) \times[\gamma(x_1 + x_2)^2 + \varepsilon^2(x_3 + x_4 - 4(1 - s^2)x_3x_4) + 4(p^2/m^2 + \varepsilon^2(1 - s^2))x_1x_2]^{-1}.$$

Making the change of variables

$$x_1 = (\varepsilon y + \varepsilon x)/2,\quad x_2 = -x_1 + \varepsilon y,\quad x_3 = (1 - x_1 - x_2 - z)/2$$

and integrating over dz, we obtain

$$B_3 = -\frac{1}{4\sqrt{1-s^2}}\left[\frac{w_2}{2} + w_1\frac{\partial}{\partial E^2}\right]\int_0^{1/\varepsilon} dy\int_0^{y}\frac{dx}{b_1}\tan^{-1}\frac{(1-\varepsilon y)\sqrt{1-s^2}}{b_1},$$

$$b_1^2 = s^2 + \varepsilon(1 - 2s^2)y + E^2y^2 - [p^2/m^2 + \varepsilon^2(1 - s^2)]x^2 \quad (E^2 = 1 + p^2/m^2).$$

Just as in the calculation of B_1 and B_2, we replace the arctangent in the integrand by $\pi/2$ and integrate over dx:

$$B_3 = -\frac{\pi}{8\sqrt{1-s^2}}\left(\frac{w_2}{2} + w_1\frac{\partial}{\partial(E^2)}\right) \times\int_0^{1/\varepsilon}\frac{dy}{\sqrt{p^2/m^2 + \varepsilon^2(1-s^2)}} \times\sin^{-1}\left[\frac{y}{a_1}\sqrt{p^2/m^2 + \varepsilon^2(1-s^2)}\right],$$

$$a_1^2 = s^2 + \varepsilon(1 - 2s^2)y + E^2y^2.$$

For p^2/m^2, $\epsilon^2 \ll 1$ the arcsine can be expanded as a series (taking two terms into account), after which integration over dy and subsequent differentiation with respect to E^2 gives, for $|s|^2 \ll 1$:

$$B_3 = -\frac{\pi}{16}\left\{\left(1 + 4\varepsilon^2\right)s - \varepsilon\left(1 + \frac{5}{2}\varepsilon^2\right)\ln(\varepsilon + 2s) + \left(1 + \varepsilon^2\right)\frac{\varepsilon s}{\varepsilon + 2s}\right\}. \qquad (1.21)$$

To calculate B_4 the exact value of the numerator in (1.20) is needed.

$$(\bar{u}_{p_2-q}\,|\,\hat{h}'\,|\,u_{p_2})(\bar{u}_{p_1+q}\,|\,\hat{h}'\,|\,u_{p_1}) = m^2(x_1 - x_2)^2 w_1 + m^2x_1x_2w_3, \qquad (1.22)$$

$$w_3 = -\frac{4p^4}{m^4}\left(1 - \frac{1 - \cos\theta}{2}\right) = -\frac{4p^2}{m^2}\left(\frac{p^2}{m^2} + \varepsilon^2\right). \qquad (1.23)$$

Making the change of variables

$$x_2 = (1 - x_3 - x_4 - \varepsilon z)/2,$$
$$x_3 = (1 - \varepsilon y - x)/2,\quad x_4 = 1 - \varepsilon y - x_3$$

and integrating over dz, we obtain

$$B_4 = \frac{1}{4}\mathfrak{L}\frac{1}{E}\int_0^{1/\varepsilon} dy\int_0^{1-\varepsilon y} dx\,\frac{1}{b_2}\tan^{-1}\frac{yE}{b_2},$$

$$\mathfrak{L} = \frac{w_2}{2} + \left(w_1 - \frac{w_3}{4}\right)\frac{\partial}{\partial E^2} - \frac{w_3}{4}\frac{\partial}{\partial(p^2/m^2)},$$

$$b_2^2 = s^2 + \varepsilon(1 - 2s^2)y - [p^2/m^2 + \varepsilon^2(1 - s^2)]y^2 + (1 - s^2)x^2. \qquad (1.24)$$

The calculation of B_4 (see Appendix) gives the following result in the nonrelativistic approximation:

$$B_4 = -\frac{\pi}{16}\left\{(1 + 3\varepsilon^2)s - \varepsilon\left(1 + \frac{3}{2}\varepsilon^2\right)\ln(\varepsilon + 2s) + \frac{\varepsilon}{2Ev}\ln\frac{2sE + \varepsilon v}{\xi E(1+v)} - i\pi\frac{\varepsilon}{4v\sqrt{1-s^2}}\right\}, \qquad (1.25)$$

$$v = \sqrt{1 + 4s^2/\xi^2},\quad \xi = \mu/p. \qquad (1.26)$$

The branch of the square root is defined as in (1.6) with the cut from $s^2 = -\xi^2/4$ to $-\infty$.

Characteristic of this part of the amplitude is the presence of a second singular point at $v = 0$, which corresponds to $q^2 = 4\mu^2(1 + \xi^2/4)$, with a singularity of the form

$$[4\mu^2(1 + \xi^2/4) - q^2]^{-1/2}.$$

For $\xi^2/4 \ll 1$, the second point is found in the neighborhood of the first point ($s^2 = 0$) but for $\xi^2 \to \infty$ it moves far away from the first; therefore terms in (1.25) which are singular only at the second point contribute to the phase shift only for $\xi^2/4 \lesssim 1/L$. In view of this, in calculating such terms an expansion is made in powers of ξ^2 which

ensures that the phase shift is calculated with error $< 1/L$ (see Appendix). The last term in (1.25) is the only term in the whole two-meson amplitude giving a contribution to $\operatorname{Im} I_l^{(2)}$, so that it is calculated exactly for any $s^2 \leq 0$, since the effective region of the integration over $|s|$ for $\operatorname{Im} I_l^{(2)}$ is in the close neighborhood of the second point, $|s| = \xi/2$.

Substituting (1.8), (1.13), (1.18), (1.21), and (1.25) into (1.2), we obtain, for the singular part of the singlet amplitude, the following expression ($|s|^2 \ll 1$, $|v|^2 \ll 1$):

$$M^{(2)}(s^2) = -\frac{3g^4}{8m}\left\{c_0 s + \varepsilon c_1 \ln(\varepsilon + 2s) + \varepsilon c_2 \frac{s}{\varepsilon + 2s} + \varepsilon \frac{3 - 2\lambda_\tau}{12}\left[\frac{1}{Ev}\ln\frac{2Es + \varepsilon v}{\xi E(1+v)} - \frac{i\pi}{2v\sqrt{1-s^2}}\right]\right\},$$

$$c_0 = (\alpha - 1)^2 + (7/2 - \alpha - \alpha^2)\varepsilon^2 + \lambda_\tau(\varepsilon^2 + 2\beta)/3,$$

$$c_1 = \alpha - 1 + (\alpha/2 - 2)\varepsilon^2 - \lambda_\tau(\varepsilon^2 + \beta)/3,$$

$$c_2 = (3 + 2\lambda_\tau)(1 + \varepsilon^2)/6, \qquad (1.27)$$

where λ_T is the eigenvalue of the operator $\tau_\alpha^{(1)}\tau_\alpha^{(2)}$. The amplitude has been calculated taking into account first order corrections in powers of ϵ^2 and $p^2/m^2 = \epsilon^2/\xi^2$.

2. CALCULATION OF THE TWO-MESON PHASE SHIFT

To calculate the two-meson singlet phase shift, it remains to integrate the scattering amplitude with respect to $|s|$ along the cut, making use of the relation (2.15, I) for each of the functions occurring in (1.27).

Taking into account that the discontinuity of the function s across the cut is $\Delta s = -2i|s|$, we obtain, for the contribution of this function to I_l,

$$[s]_l = -4\pi^{-1/2}\xi^2 Q_l(1 + 2\xi^2) L^{-3/2}. \qquad (2.1)$$

Inserting into (2.15, I) the discontinuity in the function $\ln(\epsilon + 2s)$, equal to $-2i\tan^{-1}(2|s|/\epsilon)$, we obtain for the corresponding contribution to I_l:

$$[\ln(\varepsilon + 2s)]_l = -(16\xi^2/\pi) Q_l(1 + 2\xi^2)\int_0^\infty e^{-L|s|^2} \times \tan^{-1}(2|s|/\varepsilon)\,|s|\,d|s|. \qquad (2.2)$$

We calculate the integral (2.2), first differentiating it with respect to ϵ,

$$\frac{\partial}{\partial\varepsilon}\int_0^\infty e^{-L|s|^2}\tan^{-1}\left(\frac{2|s|}{\varepsilon}\right)|s|\,d|s| = -\frac{1}{4}\sqrt{\frac{\pi}{L}} + \frac{\varepsilon\pi}{8}e^{\varepsilon^2 L/4}\left[1 - \Phi\left(\frac{\varepsilon\sqrt{L}}{2}\right)\right], \qquad (2.3)$$

where $\Phi(\epsilon\sqrt{L}/2)$ is the probability integral. If we restrict the discussion to not too high orbital angular momenta, then the parameter $\zeta = \epsilon\sqrt{L}/2 \ll 1$. At any energy, this makes it necessary to restrict l by the inequality

$$l \ll 4/\varepsilon^2 = 180. \qquad (2.4)$$

Now expanding (2.3) in powers of ζ, we obtain, after integrating back with respect to ϵ,

$$[\ln(\varepsilon + 2s)]_l = -4\xi^2 Q_l(1 + 2\xi^2) L^{-1}[1 - 2\pi^{-1/2}\zeta + \ldots]. \qquad (2.5)$$

Note that both terms written out in (2.5) can easily be obtained directly from (2.2), expanding the arctangent in powers of $\epsilon/2|s|$; however, it is already impossible to obtain the next term in the expansion in terms of ζ in this way, since the integral of each separate term diverges.

For the term $s/(\epsilon + 2s)$, expanding in powers of $\epsilon/2|s|$, we obtain the first term in the expansion in ζ:

$$\Delta\frac{s}{\varepsilon + 2s} = -\frac{2i\varepsilon|s|}{\varepsilon^2 + 4|s|^2} = -i\frac{\varepsilon}{2|s|} + \ldots,$$

$$\left[\frac{s}{\varepsilon + 2s}\right]_l = -\frac{2\xi^2}{\sqrt{\pi}}\varepsilon L^{-1/2} Q_l(1 + 2\xi^2). \qquad (2.6)$$

In integrating the remaining terms, we consider separately two regions of integration: $0 \leq |s| \leq \xi/2$ (from the first singular point to the second) and $|s| \geq \xi/2$ (beyond the second point). For the function

$$[\ln(2Es + \varepsilon v) - \ln E\xi(1 + v)]/Ev$$

in the first region we obtain

$$\Delta\frac{1}{Ev}\ln\frac{2Es + \varepsilon v}{E\xi(1+v)} = -\frac{2i}{Ev}\tan^{-1}\frac{2E|s|}{\varepsilon v} = -\frac{2i}{Ev}\left(\frac{\pi}{2} - \frac{\varepsilon v}{2E|s|} + \ldots\right). \qquad (2.7)$$

The first term of the expansion in terms of $\epsilon/2|s|$ gives a contribution to I_l:

$$-\frac{8\xi^2}{E} Q_l(1 + 2\xi^2)\int_0^{\xi/2} e^{-L|s|^2}\frac{|s|\,d|s|}{\sqrt{1 - 4|s|^2/\xi^2}} = -\frac{4\xi^3}{E\sqrt{L}} Q_l(1 + 2\xi^2) e^{-\xi^2 L/4}\int_0^{\xi\sqrt{L}/2} e^{z^2}\,dz. \qquad (2.8)$$

In the second region of integration

$$\Delta\frac{1}{Ev}\ln\frac{2E|s| + \varepsilon v}{E\xi(1+v)} = \frac{2i}{E|v|}\left[\ln(\varepsilon|v| + 2E|s|) - \ln 2E|s|\right] = \frac{i\varepsilon}{E^2|s|} + \ldots. \qquad (2.9)$$

Combining the contributions of the first term of the expansion (2.9) and of the second term in (2.7), we obtain

$$4\pi^{-1/2}\xi^2\varepsilon L^{-1/2}(1 - p^2/m^2) Q_l(1 + 2\xi^2). \qquad (2.10)$$

In (2.10) we set $E^2 = 1 + p^2/m^2$ and include terms of first order in p^2/m^2.

Ratio of two-meson to one-meson phase shifts

E_{lab}, Mev	2,5	10	40	90	160	360	650
^1P	—0.08	—0.15	—0.2				
^1D	0.02	0.04	0.1	0.25			
^1F	$-3\cdot10^{-3}$	$-6\cdot10^{-3}$	—0.02	—0.04	—0.05	—0.1	
^1G	10^{-3}	$3\cdot10^{-3}$	0.01	0.04	—0.1	0.25	
^1H	-10^{-4}	$-4\cdot10^{-4}$	$-3\cdot10^{-3}$	$-7\cdot10^{-3}$	—0.015	—0.035	—0.08

The final term in the amplitude (1.27) is the only one contributing to Im $I_l^{(2)}$. Its cut only begins at the second point,* so that we cannot use formula (2.15, I), obtained for the end-point $t = 1+2\xi^2$. For the end point $t_\xi = 1+2\xi^2(1+\xi^2/4)$ which corresponds to $v = 0$ $[q^2 = 4\mu^2(1+\xi^2/4)]$, similar considerations give the formula

$$I_l = \frac{\xi^4}{\pi i} Q_l(t_\xi) \int_0^\infty e^{-L_\xi |v|^2} \Delta M(v^2)\, d|\vartheta|^2,$$

$$L_\xi = (l+1)\xi^3 / \sqrt{(1+\xi^2/4)[1+\xi^2(1+\xi^2/4)]}. \quad (2.11)$$

Substituting $i/v\sqrt{1-s^2} \approx i/v\sqrt{1+\xi^2/4}$ in (2.11) we obtain for the corresponding contribution to I_l:

$$[i/v\sqrt{1-s^2}]_l = 2i\xi^3 (\pi L)^{-1/2} Q_l(t_\xi). \quad (2.12)$$

Taking account of (2.1), (2.5), (2.6), (2.10), and (2.12), we obtain, for the two-meson singlet integral I_l:

$$I_l^{(2)} = \frac{3g^4}{2m} \frac{\xi^2}{\sqrt{\pi} L^{3/2}} \left\{ Q_l(1+2\xi^2)[c_0 + \zeta d_1 + \zeta^2 d_2] + i\pi \frac{3-2\lambda_\tau}{12s} \zeta^2 \xi Q_l(t_\xi) \right\}, \quad (2.13)$$

where

$$d_1 = 2\sqrt{\pi}[c_1 + \tfrac{1}{6}(3-2\lambda_\tau)(1-p^2/2m^2)\psi(z)],$$

$$d_2 = 2c_2 - 4c_1 - (1-\tfrac{2}{3}\lambda_\tau)(1-p^2/m^2),$$

$$\psi(z) = ze^{-z^2} \int_0^z e^{x^2} dx, \quad z^2 = L\xi^2/4$$

Inserting numerical values for α, β, and $\epsilon^2 = 0.0223$, we obtain

$$c_0 = 0.06 + 0.01\lambda_\tau,$$
$$d_1 = 0.6 - 0.03\lambda_\tau + 0.6\lambda_\tau^2(1-p^2/2m)\psi(z),$$
$$d_2 = -0.7 + p^2/m^2 + \lambda_\tau(1.4 - 2p^2/3m^2). \quad (2.14)$$

The singlet phase shift is related to the integral I_l in the following way:

$$p\,\mathrm{Re}\, I_l = 2\sin 2\delta_l \approx 4\delta_l, \qquad p\,\mathrm{Im}\, I_l = 2(1-\cos 2\delta_l) \approx 4\delta_l^2.$$

Hence it follows that for large orbital angular momenta (when $|\delta_l| \ll 1$), the two-meson phase shift $\delta_l^{(2)} = (\epsilon m/4\xi)\,\mathrm{Re}\, I_l^{(2)}$. Im $I_l^{(2)}$ is proportional to the square of the one-meson phase shift $\delta_l^{(1)}$, since Im $I_l^{(1)} = 0$, and the square of the "total" phase-shift is $(\delta_l)^2 \approx [\delta_l^{(1)}]^2$.

The results (2.13) and (2.14), which we have obtained, show that there exists a strong compensation between the contributions from perturbation theory (fourth-order diagrams) and the terms obtained with the help of dispersion relations (containing α and β). Furthermore, there is mutual compensation of terms containing β_1 and β_2 (the final result involves their linear combination $\beta \ll \beta_1, \beta_2$), as a result of which the part $\tilde{f}''_{\alpha\beta}$ of the meson-nucleon scattering amplitude [cf. (1.1)] gives a negligible contribution to (2.13).

Formula (2.13) is the main part of an asymptotic expansion in the parameter 1/L (cf. Sec. 2 of reference 1) and therefore its accuracy should be, generally speaking, of order 1/L. In the result given above, the cancellations in the main term may increase the importance of higher terms in the asymptotic expansion. For a rough order of magnitude estimate we can apply the formula obtained also to cases when the expansion parameter is not extremely small, $1/L \lesssim 1$.

The table shows values of $\delta_l^{(2)}/\delta_l^{(1)}$ calculated for several l and ξ, using formulas (2.13) and (2.9, I). We see that, to good accuracy, one can use the one-meson ^1D phase shift for energies $E_{lab} \lesssim 40$ Mev, and the one-meson ^1F and ^1G phase shifts for $E_{lab} \lesssim 150$ Mev. The estimates of the order of magnitude should also be valid for the triplet phase shifts. Hence it follows, that for the phase shift analysis of nucleon-nucleon scattering for $E_{lab} \lesssim 150$ Mev, all phase shifts corresponding to $l \geq 3$ can be taken to be the one-meson ones, and only the S, P, and D phase shifts determined from experiment.

3. CONCLUSIONS

The results we have obtained indicate that already for moderate orbital angular momenta the nucleon-nucleon elastic scattering phase shifts are determined by the one-meson interaction. This

*It is interesting to note that this result does not depend on the approximation we have applied (expansion in 1/L) and it is valid for the exact scattering amplitude, i.e. values of $t \geq t_\xi$ give a contribution to ImI_l.

circumstance may be of importance in carrying out phase shift analyses of nucleon scatterings since (as has already been noted[2,3]) this makes it unnecessary to treat every significant phase shift as an arbitrary variable parameter. If for given l and E the two-meson amplitude (2.13) appears appreciably smaller than the one-meson one (2.9, I), then with good justification one can take account of the corresponding phase shift with the one-meson approximation. The absence of a given angular momentum state from the whole analysis of nucleon-nucleon scattering apparently makes impossible a unique shift analysis of the experimental data. The best available data on p-p scattering at an energy of 310 Mev give eight sets of phase shifts[4] of which only two have phase shifts for large l agreeing with the one-meson ones. Undoubtedly the use of the one-meson "tail," within the limits indicated in the present paper, should facilitate phase shift analyses.

The results of this paper depend strongly on the dispersion relations for momentum transfer near $4\mu^2$. Although there is no reason to doubt the applicability of the dispersion relations under these conditions, nevertheless experimental verification of the results obtained might shed light on the region of applicability of the dispersion relations. Since we have considered only the singlet scattering, naturally we have not obtained the complete matrix (in spin space) of the scattering operator responsible for the two-meson exchange. However, the calculations for the triplet state do not introduce any difficulties of principle and have been carried out by Grashin and Kobzarev.[6]

In all the above discussion, we have been making an expansion in powers of 1/L, retaining only the first nonvanishing term, so that the accuracy of our results should be of order 1/L. It is not difficult to see, however, that the basic formulas (2.12, I) and (2.20, I) must hold for appreciably weaker restrictions on the value of the orbital angular momentum. For these to be applicable the inequality

$$1 \gg \frac{Q_l\left(1+\frac{9}{2}\xi^2\right)}{Q_l(1+2\xi^2)} \approx \begin{cases} \exp\{-(l+1/2)\,\xi\} & \text{for } \xi^2 \ll 1 \\ (4/9)^{l+1} & \text{for } \xi^2 \gg 1 \end{cases},$$

must hold, in order to make it possible to neglect three-meson states in the sum over intermediate states in $A_1(E, q^2)$. Under these conditions formula (2.21, I) remains. In this case, of course, one cannot restrict the calculation of $\tilde{f}_{\alpha\beta}$ to the point $\omega = 0$ and $q^2 = 4\mu^2$, but it is necessary to know the meson-nucleon scattering amplitude in some limiting region round the point $\omega = 0$, $q^2 = 4\mu^2$. Therefore the problem of analytic continuation of the meson-nucleon scattering amplitude becomes much more complicated. If, however, such an analytic continuation is feasible, then it may be possible to obtain with sufficient accuracy an expression for the two-meson nucleon-nucleon scattering phase shift for quite small l. It should be emphasized that such an extension to small l depends fundamentally on Mandelstam's results,[5] while the results obtained in this paper depend essentially only on the following: (1) the nearest singular point (apart from the one-meson pole) lies at $q^2 = 4\mu^2$; (2) near $q^2 = 4\mu^2$ there are no other singular points [except for $q^2 = 4\mu^2(1+\xi^2/4)$].

As a result of the strong compensation of the leading terms, which we discussed above, errors in the determination of $L^{(1)}(0, 4\mu^2) = \alpha$ (Sec. 3 of reference 1) may appreciably change (for example by two degrees) the final two-meson phase shifts given in the table. However, if the ratio $\delta_l^{(2)}/\delta_l^{(1)}$ is, for example, less than 10%, these errors do not alter the conclusion that in the given case the scattering phase shift is basically determined by the one-meson interaction.

It has proved possible to express the nucleon-nucleon scattering, caused by two-meson exchange, in terms of the pion-nucleon scattering and, in this way, a connection has been established between these two distinct processes. This is not accidental. If it were possible to do the calculation for small l, then the nucleon-nucleon scattering would be expressed in terms of the meson-nucleon scattering amplitude, the amplitude for the process $\pi + n \to 2\pi + n$, etc.

The authors express their gratitude to L. D. Landau for numerous discussions, and also to V. B. Berestetskiĭ, L. B. Okun', A. P. Rudik, Ya. A. Smorodinskiĭ, K. A. Ter-Martirosyan, and I. M. Shmushkevitch for a number of useful remarks.

APPENDIX

1. Calculation of B_1. For calculating the integral B_1, we introduce the auxiliary function

$$B_1(u) = \frac{1}{\sqrt{1-s^2}} \int_0^{1/\varepsilon} \frac{y}{a} \tan^{-1} \frac{(1-\varepsilon y)\sqrt{1-s^2}+u}{a}\, dy,$$

$$a^2 = s^2 + \varepsilon(1-2s^2)\,y + [1-\varepsilon^2(1-s^2)]\,y^2. \quad \text{(A.1)}$$

The desired integral is equal to the value of this function for $u = 0$, which can be written in the form

$$B_1(0) = B_1(\infty) - \int_0^{\infty} \frac{\partial B_1(u)}{\partial u}\, du, \quad \text{(A.2)}$$

$$B_1(\infty) = \frac{\pi}{2\sqrt{1-s^2}} \int_0^{1/\varepsilon} \frac{y\,dy}{a}, \qquad (A.3)$$

$$\frac{\partial B_1(u)}{\partial u} = \frac{1}{\sqrt{1-s^2}} \times \int_0^{1/\varepsilon} \frac{y\,dy}{1-\varepsilon y + y^2 + u^2 + 2(1-\varepsilon y)\sqrt{1-s^2}}; \quad u \geqslant 0. \qquad (A.4)$$

We consider the analytic properties of the functions (A.2), (A.3), (A.4) of the variable s^2. The original integral was analytic in the whole plane with a cut from $s^2 = 0$ to $-\infty$ (corresponding to $q^2 \geq 4\mu^2$, $t \geq 1 + 2\xi^2$). In the integral (A.3) there appears an additional singularity at the point $s^2 = 1$ ($q^2 = 0$), so that for (A.3) it is necessary to make a second cut from $s^2 = 1$ to $+\infty$ ($q^2 \leq 0$, $t \leq 1$). The integral (A.4) is analytic as a function of the variable $\sqrt{1-s^2}$ in the right half-plane, and as a function of s^2 in the whole plane with a cut from $s^2 = 1$ to $+\infty$, since we took $\sqrt{1-s^2} > 0$ for $s^2 < 1$. Since for the calculation of the phase shift we need to integrate along the cut $s^2 \leq 0$ ($q^2 \geq 4\mu^2$), the contribution of the second term in (A.2) vanishes identically and it need not be taken into account. The calculation of the remaining integral is elementary. Thus the method we have indicated has enabled us to calculate exactly the singular part of the original integral (1.11), giving a contribution to (2.15, I), while "spoiling" the behavior of the function in other regions which do not contribute to the subsequent integration (2.15, I).

2. Calculation of B_4. In contrast to the previous integral, the integral B_4, which corresponds to the fourth-order Feynman diagram shown in the figure,

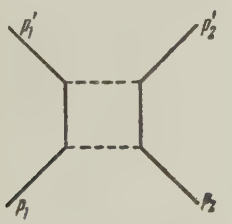

Diagram for the integral B_4

possesses singularities such that the integrand in (1.20) as a function of its parameters is singular for any real q^2. It follows from this that the real axis for the integral $B_4(q^2)$, considered formally for any complex values of q^2, is a singular line. However, direct calculation shows that the function B_4 may be analytically continued from the physical region to all densities with a cut from $q^2 = 4\mu^2$ to $+\infty$, which corresponds to the analytic continuation used in Sec. 2 of reference (1). This will agree with the original Feynman integral only in the upper half-plane. To calculate the phase shift we need just this function and we will not discuss its singularities.

To calculate the remaining integral over two parameters in (1.24), we introduce the function

$$f(u) = \int_0^{1/\varepsilon} dy \int_0^{1-\varepsilon y} dx \frac{1}{b_2} \tan^{-1} \frac{yE+u}{b_2},$$

$$b_2^2 = s^2 + \varepsilon(1-2s^2)\,y - [p^2/m^2 + \varepsilon^2(1-s^2)]\,y^2 + (1-s^2)\,x^2 - i0. \qquad (A.5)$$

The desired integral is equal to the value of $f(u)$ for $u = 0$:

$$f(0) = f(\infty) - \int_0^\infty \frac{\partial f(u)}{\partial u}\,du, \qquad (A.6)$$

$$f(\infty) = \frac{\pi}{2} \int_0^{1/\varepsilon} dy \int_0^{1-\varepsilon y} \frac{dx}{b_2} = \frac{\pi}{2\sqrt{1-s^2}} \times \int_0^{1/\varepsilon} [\ln(R_1 + \sqrt{1-s^2}(1-\varepsilon y)) - \ln R]\,dy,$$

$$R^2 = s^2 + \varepsilon(1-2s^2)\,y - [p^2/m^2 + \varepsilon^2(1-s^2)]\,y^2 - i0,$$

$$R_1^2 = 1 - \varepsilon y - p^2 y^2/m^2 - i0, \qquad (A.7)$$

$$\frac{\partial f(u)}{\partial u} = \int_0^{1/\varepsilon} dy \int_0^{1-\varepsilon y} dx \left[s^2 + \varepsilon(1-2s^2)y + \left(E^2 - \frac{p^2}{m^2} - \varepsilon^2(1-s^2)\right)y^2 + (1-s^2)\,x^2 + 2Eyu + u^2\right]^{-1}. \qquad (A.8)$$

The integrand in (A.7) is singular, as before, on the whole real axis, so that for the following integration over dy it is necessary to take s^2 real and analytically continue the integrated result to the unphysical region. The integrand in (A.8) is already singular only for $s^2 \leq 0$ ($q^2 \geq 4\mu^2$), i.e., the second term in (A.6) is an analytic function in the whole plane with a cut from $s^2 = 0$ to $-\infty$. After integrating with respect to x (A.8) takes the form

$$\frac{\partial f(u)}{\partial u} = \frac{1}{\sqrt{1-s^2}} \int_0^{1/\varepsilon} \frac{dy}{a_2} \tan^{-1} \frac{\sqrt{1-s^2}(1-\varepsilon y)}{a_2},$$

$$a_2^2 = s^2 + \varepsilon y(1-2s^2) + [E^2 - p^2/m^2 - \varepsilon^2(1-s^2)]\,y^2 + 2Eyu + u^2. \qquad (A.9)$$

From this integral we select the part which is singular on the cut, introducing another auxiliary parameter in the same way as in (A.1), (A.2):

$$\frac{\partial f(u)}{\partial u} = \frac{\partial f(u,\infty)}{\partial u} - \int_0^\infty \frac{\partial^2 f(u,v)}{\partial u\,\partial v}\,dv, \qquad (A.10)$$

$$\frac{\partial f(u,\infty)}{\partial u} = \frac{\pi}{2\sqrt{1-s^2}} \int_0^{1/\varepsilon} \frac{dy}{a_2}, \qquad (A.11)$$

$$\frac{\partial^2 f(u,v)}{\partial u\,\partial v} = \int_0^{1/\varepsilon} \left[1 - \varepsilon y + \left(E^2 - \frac{p^2}{m^2}\right) y^2 + 2Eyu + u^2 + v^2 + 2(1-\varepsilon y)\, v\sqrt{1-s^2}\right]^{-1} dy, \qquad u,\ v \geqslant 0. \tag{A.12}$$

The second term in (A.10) need not be taken into account since it is an analytic function for Re $s^2 < 1$ (Re $q^2 > 0$). In the remaining singular part (A.11) there appears an additional singularity at $s^2 = 1$ and a second cut from $s^2 = 1$ to $+\infty$ ($q^2 \leq 0$). We now insert (A.10) and (A.11) into (A.6) and integrate over du. At the upper limit the integral diverges, but the dependence on s^2 disappears, so that we need only take account of the lower limit. Thus the singular part, contributing to (2.15, I), takes the form

$$f = f(\infty) + \frac{\pi}{2\sqrt{1-s^2}} \int_0^{1/\varepsilon} \ln[R_2 + Ey]\, dy,$$

$$R_2^2 = s^2 + \varepsilon y(1-2s^2) + [E^2 - p^2/m^2 - \varepsilon^2(1-s^2)]\, y^2 - i0. \tag{A.13}$$

The integral over dy remaining in (A.13) is calculated exactly, since integrating by parts and removing the irrationality in the denominator of the integral leads to the elementary result:

$$f(\infty) = i\pi \frac{2p^2/m^2 + \varepsilon^2}{4pP^2/m} \ln\frac{\varepsilon - 2ip/m}{\varepsilon} - \frac{\pi K_1}{4\sqrt{1-s^2}} \ln(-K_1) + \frac{\pi K_2}{4\sqrt{1-s^2}} \ln K_2 + i\pi^2 \frac{\varepsilon(1-2s^2)}{8P^2\sqrt{1-s^2}} - \pi \frac{\varepsilon(1-2s^2)}{8P^2\sqrt{1-s^2}} \times \ln\left(\frac{4p^2}{m^2} + \varepsilon^2\right) - \frac{\pi K}{8P^2\sqrt{1-s^2}} \ln\frac{2\sqrt{1-s^2}\,p/m - iK}{2\sqrt{1-s^2}\,p/m + iK} + \frac{\pi\varepsilon(1-2s^2)}{8P^2\sqrt{1-s^2}} \ln\left[\frac{1}{4P^2}(F_1 - KF_2)(F_1 + KF_2)\right] + \frac{\pi K}{8P^2\sqrt{1-s^2}} \ln\frac{F_1 - KF_2}{F_1 + KF_2}. \tag{A.14}$$

Here we introduce

$$F_1 = 2(2p^2/m^2 + \varepsilon^2)(\sqrt{1-s^2} + 1 - s^2) + K^2,$$

$$F_2 = \varepsilon(1 + 2\sqrt{1-s^2}),$$

$$P^2 = p^2/m^2 + \varepsilon^2(1-2s^2), \qquad K = \sqrt{4s^2p^2/m^2 + \varepsilon^2},$$

$$K_1 = [K + \varepsilon(1-2s^2)]/2P^2, \qquad K_2 = [K - \varepsilon(1-2s^2)]/2P^2.$$

The root K is defined so that it is positive in the physical region with a cut running from $s^2 = -\xi^2/4$ to $-\infty$ [$q^2 \geq 4\mu^2(1 + \xi^2/4)$]. The function (A.14) is analytic in the whole plane with the indicated cut. Leaving only terms singular for $s^2 < 1$ ($q^2 > 0$), we obtain

$$f(\infty) = \frac{\pi}{4\sqrt{1-s^2}}[-K_1 \ln(-K_1) + K_2 \ln K_2]. \tag{A.15}$$

The other term in (A.13) is calculated similarly:

$$\int_0^{1/\varepsilon} dy\, \ln[R_2 + Ey] = \frac{1}{\varepsilon}[\ln(\sqrt{E^2 - p^2/m^2} + E) - 1] + \frac{K_1}{2}\ln(-K_1) - \frac{K_2}{2}\ln K_2 + K_2 \ln(1/\varepsilon + K_2) - \frac{i\pi K_1}{2} + \frac{K}{2P^2}\ln(2Es + K) - \frac{E\varepsilon(1-2s^2)}{2WP^2}\ln[2Ws + \varepsilon(1-2s^2)] + \frac{K_1 + K_2}{2}\ln(2P^2\varepsilon) - \frac{K_1}{2}\ln\{2(E + \sqrt{E^2 - p^2/m^2})[K\sqrt{E^2 - p^2/m^2} + \varepsilon E(1-2s^2)] + \varepsilon K(K - \varepsilon)\} - \frac{K_2}{2}\ln\{2(E - \sqrt{E^2 - p^2/m^2})[K\sqrt{E^2 - p^2/m^2} + \varepsilon E(1-2s^2)] + \varepsilon K(K + \varepsilon)\} + \frac{\varepsilon E(1-2s^2)}{2WP^2}\ln\left(\frac{2W}{\varepsilon}\sqrt{E^2 - p^2/m^2} + 2\frac{E^2 - p^2/m^2}{\varepsilon} - \varepsilon\right),$$

where we have introduced $W^2 = E^2 - P^2$. Leaving out terms nonsingular for $s^2 < 1$, and also the last term, singular for $W = 0$ (which corresponds to $q^2 = 4m^2$), and combining with (A.15), we obtain finally the singular part of the original integral (for $4\mu^2 \leq q^2 < 4m^2$):

$$f = \frac{\pi}{2\sqrt{1-s^2}}\left\{-\frac{E\varepsilon(1-2s^2)}{2WP^2}\ln[2Ws + \varepsilon(1-2s^2)] + \frac{K}{2P^2}\ln(2Es + K) - \frac{i\pi K}{4P^2} + K_2 \ln\left(2\frac{p^2}{m^2} + \varepsilon^2 + \varepsilon K\right) - \frac{K_1}{2}\ln\{2(E + \sqrt{E^2 - p^2/m^2})[K\sqrt{E^2 - p^2/m^2} + \varepsilon E(1-2s^2)] + \varepsilon K(K - \varepsilon)\} - \frac{K_2}{2}\ln\{2(E - \sqrt{E^2 - p^2/m^2})[K\sqrt{E^2 - p^2/m^2} + \varepsilon E(1-2s^2)] + \varepsilon K(K + \varepsilon)\}. \tag{A.16}$$

The singularities of the functions $f(s^2)$ and $B_4(s^2)$, obtained from $f(s^2)$ by the application of some differential operator [cf. (1.24)], consist of two singular points: the point $s^2 = -\xi^2/4$, which corresponds to the value $K = 0$ [$q^2 = 4\mu^2(1 + \xi^2/4)$]. For $\xi^2/4 \ll 1$ the second point is found in the neighborhood of the first, but for $\xi^2 \to \infty$ it moves away to an extremely large distance from the first. It is evident that terms singular only at the second point contribute to the integration (2.15, I) only for $\xi^2/4 \lesssim 1/L$ since for them the cut begins for $|s|^2 = \xi^2/4$ and compared with terms singular at the first point they will have, after integration, an additional factor $\exp(-\xi^2 L/4)$. In view of this, such terms in (A.16) can be expanded in powers of ξ^2 and the leading term in the expansion retained. To this accuracy the phase shift will depend on the parameter $\xi^2 \exp(-\xi^2 L/4)$, vanishing as $\xi^2 \to 0$ (high energy) and as $\xi^2 \to \infty$ (low energy). The

largest error will be in the intermediate region $\xi^2/4 \approx 1/L$, where this parameter takes its maximum value $4/2.7\,L \approx 1/L$. But even in this region the expansion in ξ^2 provides just the same accuracy as comes from our asymptotic expansion in $1/L$. Besides this, it is necessary to consider only the first term of the expansion in powers of K^2, just as we considered only the first term in the expansion in powers of s^2. Taking this into account we simplify the last three terms in (A.16), after which we obtain, in the nonrelativistic approximation, for $|s^2| \ll 1$, $|K|^2 \ll \epsilon^2$:

$$f = \frac{\pi}{4P^2}\left\{-\frac{E\varepsilon}{W}\ln[2Ws + \varepsilon(1-2s^2)] + K\ln\left[\frac{p}{m}\frac{2Es+K}{E(\varepsilon+K)}\right] - \frac{i\pi K}{2\sqrt{1-s^2}}\right\}. \quad \text{(A.17)}$$

The next correction terms in (A.17) vanish in this case, and the largest of the discarded terms takes the form $K\xi^4/P^2$, $K(p/m)^4/P^2$. Operating on (A.17) with the differential operator $\mathfrak{L}(1/4E)$ [cf. (1.24)], we obtain formula (1.26).

[1] Galanin, Grashin, Ioffe, and Pomeranchuk, JETP **37**, 1663 (1959), Soviet Phys. JETP **10**, 1179 (1960).

[2] A. F. Grashin, JETP **36**, 1717 (1959), Soviet Phys. JETP **9**, 1223 (1959).

[3] Moravcsik, Cziffra, MacGregor, and Stapp, Bull. Am. Phys. Soc. **4**, 49 (1959).

[4] Stapp, Ypsilantis, and Metropolis, Phys. Rev. **105**, 302 (1957).

[5] S. Mandelstam, Phys. Rev. **112**, 1344 (1958).

[6] A. F. Grashin and I. Yu. Kobzarev, JETP **38**, 863 (1960), Soviet Phys. JETP, in press.

Translated by R. F. Peierls
99

THE SHAPE AND TEMPERATURE DEPENDENCE OF THE ELECTRON-SPIN RESONANCE LINES OF LOCALIZED ELECTRON CENTERS IN CRYSTALS

M. F. DEĬGEN and A. B. ROĬTSIN

Institute of Physics, Academy of Sciences, Ukrainian S.S.R.

Submitted to JETP editor July 18, 1959

J. Exptl. Theoret. Phys. (U.S.S.R.) **38**, 489-498 (February, 1960)

The hyperfine structure of localized electron centers in crystals is evaluated and their electron spin resonance is considered, taking the vibrations of the ions (atoms) into account. We have obtained the shape of the electron paramagnetic resonance (EPR) lines and its temperature dependence. It turns out that they have the Lorentz shape. The EPR of F-centers in NaCl type crystals is considered as an example. The theoretical results agree with experiments. The determination of the EPR half width makes it possible to evaluate the spin-lattice relaxation time. Numerical estimates performed for F-centers lead to agreement between the theoretical results and experiments.

INTRODUCTION

In those papers which are known up to the present and which are devoted to the theory of the electron paramagnetic resonance (EPR) of localized electron centers, it is assumed that the ions were immovably fixed at lattice sites.[1-5] In a number of cases it was possible in this approximation to explain the shape of the overall EPR spectrum of localized centers.[1,2] The shapes of the separate lines, however, were not explained satisfactorily in a quantitative way. Attempts to estimate the line broadening taking dipole-dipole interactions between spatially separated localized centers into account led therefore to a discrepancy of one or two orders of magnitude between the theoretical results and the experiments. In this approximation, of course, one cannot consider the temperature dependence of either the shapes of the separate lines or the shape of the overall EPR spectrum.

There are, nevertheless, recent experimental evidences of an appreciable temperature dependence of the EPR spectrum shape.[6,7] Moreover, direct experimental measurements performed with F-centers[7] show that the spin-lattice interaction is the decisive factor for the shape.

We shall develop in the present paper a theory of EPR of localized centers which will include the hyperfine interaction of a localized electron with the magnetic moments of the nuclei of the vibrating crystal. The latter turns out to be not a small perturbation, in contradistinction to the situation in investigations in the theory of spin-lattice relaxation, and will be taken into account in the zeroth approximation of the theory. The calculations will be performed in the approximation of extremely long wavelengths of the lattice vibrations which turns out to be justified in the case under consideration.

The theory leads to a Lorentz shape of the separate lines and to its correct temperature dependence. The Lorentz shape agrees also with the results of phenomenological investigations. Portis[8] has given a satisfactory explanation of the saturation effect of the EPR of F-centers assuming that the shape of the separate lines is close to the Lorentz shape. A similar assumption enabled Wolga and Strandberg[9] to obtain the correct shape of the smoothed out EPR line of F-centers.

1. THE HAMILTONIAN AND THE ENERGY SPECTRUM OF THE SYSTEM

The Hamiltonian of the system (a localized electron interacting with the lattice vibrations, with the nuclear magnetic moments, and with the external static magnetic field) can be written in the form

$$\hat{H} = \hat{T} + \hat{V}(\mathbf{r}, \mathbf{u}) + \hat{H}_{\text{vib}} + \hat{H}_{\text{s}} + \sum_n \hat{Q}_n, \qquad (1)$$

where $\hat{T}$ is the electronic kinetic energy operator, $\hat{V}(\mathbf{r}, \mathbf{u})$ the operator of the interaction energy between the electron and the lattice, which does not take into account the hyperfine interaction (this term contains, in particular, also the operator of the energy of the electron in the periodic crystalline field); $\hat{H}_{\text{vib}}$ the lattice vibration energy oper-

ator, $\hat{H}_3$ the operator of the energy of the interaction between the electronic magnetic moment μ and the external static magnetic field $\mathcal{H}$, $\sum_n \hat{Q}_n$ the operator of hyperfine interaction of the localized electron with the magnetic moments of the nuclei in the neighborhood, $\mathbf{u}$ the displacement vector of an arbitrary lattice point, and $\mathbf{n}$ the vector determining the position of a lattice site. The Hamiltonian (1) does not contain spin-orbit interaction terms as we shall in the following consider systems for which $\bar{\mathbf{L}} = 0$.

For small displacements $\mathbf{u}$ we can expand the operators $\hat{V}$ and $\hat{Q}_n$ in a power series in $\mathbf{u}$ and restrict ourselves to the linear terms in the expansion. Equation (1) can then be rewritten as follows

$$\hat{H} = \hat{T} + \hat{V}_0(\mathbf{r}) + \mathbf{u}\,(\operatorname{grad}\hat{V})_0 + \hat{H}_{\text{vib}} + \hat{H}_3 + \sum_n \hat{Q}_n^0 + \sum_n \mathbf{u}\,(\operatorname{grad}\hat{Q}_n)_0 \tag{2}$$

Writing $\mathbf{u}$ as an expansion in a complete set of functions

$$\mathbf{u} = \sum_{\varkappa,\alpha} \mathbf{u}_{\varkappa\alpha}\chi_\varkappa(\mathbf{r}), \tag{3a}$$

$$\chi_\varkappa(\mathbf{r}) = \sqrt{2/L^3}\sin(\varkappa\mathbf{r} + \pi/4) \tag{3b}$$

and using in (2) dimensionless normal coordinates, we get

$$\hat{H} = \hat{T} + \hat{V}_0(\mathbf{r}) + \sum_{\varkappa,\alpha}\mathbf{B}_{\varkappa\alpha}\mathbf{q}_{\varkappa\alpha} + \tfrac{1}{2}\sum_{\varkappa\alpha}\hbar\omega_{\varkappa\alpha}(q_{\varkappa\alpha}^2 - \partial^2/\partial q_{\varkappa\alpha}^2) + \hat{H}_3 + \sum_n \hat{Q}_n^0 + \sum_{n,\varkappa,\alpha}\mathbf{A}_{\varkappa\alpha}^n\,\mathbf{q}_{\varkappa\alpha}. \tag{4}$$

where α is the number of the branch of the lattice vibrations and $\omega_{\kappa\alpha}$ the frequency of the κ-th vibration of the α-th branch.

The energy spectrum of the system can be obtained without writing down explicitly the operator coefficients $\mathbf{B}_{\kappa\alpha}$ and $\mathbf{A}_{\kappa\alpha}^n$. The energy of the spectrum is determined by minimizing the functional

$$J = \int \Psi^* \hat{H}\Psi\, d\tau \ldots dq_{\varkappa\alpha}\ldots dS_z \ldots di_{nz}\ldots \tag{5}$$

The symbolic integration over the spin coordinates of the electron S_Z and of all the nuclei of the surroundings of the defect $\ldots, i_{nz}, \ldots$ means summation over the spin variables.

We shall choose the wave function of the system in the form

$$\Psi = \psi(\mathbf{r})\,\Phi(\ldots q_{\varkappa\alpha}\ldots)\,\chi(S_z, \ldots, i_{nz}, \ldots). \tag{6}$$

Substituting (6) into (5), restricting ourselves to the contact terms in the hyperfine interaction operator and in the approximation of strong magnetic fields, we get

$$J = \bar{\hat{T}} + \bar{\hat{V}}_0 + \sum_{\varkappa\alpha}\bar{\mathbf{B}}_{\varkappa\alpha}\int \Phi^*\mathbf{q}_{\varkappa\alpha}\Phi\ldots dq_{\varkappa\alpha}\ldots + \frac{1}{2}\int\Phi^*\sum_{\varkappa\alpha}\hbar\omega_{\varkappa\alpha}\left(q_{\varkappa\alpha}^2 - \frac{\partial^2}{\partial q_{\varkappa\alpha}^2}\right)\Phi\ldots dq_{\varkappa\alpha}\ldots + (\mu/S)\,S_z\mathcal{H}_z + \sum_n (8\pi\mu\mu_n/3SI_n)\,|\psi(\mathbf{r}=\mathbf{R}_n)|^2 S_z I_{nz} + \sum_{n\varkappa\alpha}\bar{\mathbf{A}}_{\varkappa\alpha}^n\int\Phi^*\mathbf{q}_{\varkappa\alpha}\Phi\ldots dq_{\varkappa\alpha}\ldots, \tag{7}$$

where I_{nz} is the quantum number of the operator of the z-component of the spin of the n-th nucleus. The bars on top indicate averaging over $\psi(\mathbf{r})$. Without loss of generality it was assumed in (7) that the axis of the system coincided with the direction of the external static field.

Varying (7) with respect to Φ^* leads to the following equation for Φ

$$\left\{\tfrac{1}{2}\sum_{\varkappa\alpha}\hbar\omega_{\varkappa\alpha}(q_{\varkappa\alpha}^2 - \partial^2/\partial q_{\varkappa\alpha}^2) + \sum_{\varkappa\alpha}\left(\bar{\mathbf{B}}_{\varkappa\alpha} + \sum_n \bar{\mathbf{A}}_{\varkappa\alpha}^n\right)\mathbf{q}_{\varkappa\alpha}\right\} \times \Phi(\ldots q_{\varkappa\alpha}\ldots) = \lambda\Phi(\ldots q_{\varkappa\alpha}\ldots) \tag{8}$$

One can write Eq. (8) in the form

$$\left\{\tfrac{1}{2}\sum_{\varkappa\alpha}\hbar\omega_{\varkappa\alpha}[(q_{\varkappa\alpha} - q'_{\varkappa\alpha})^2 - \partial^2/\partial q_{\varkappa\alpha}^2] - \sum_{\varkappa\alpha}\tfrac{1}{2}\hbar\omega_{\varkappa\alpha}q_{\varkappa\alpha}'^2\right\}\Phi = \lambda\Phi, \tag{9}$$

$$q''_{\varkappa\alpha} = q'_{\varkappa\alpha} + q^0_{\varkappa\alpha}, \tag{10}$$

$$q'_{\varkappa\alpha} = -(\bar{\mathbf{B}}_{\varkappa\alpha}\mathbf{k}_{\varkappa\alpha})/\hbar\omega_{\varkappa\alpha}, \tag{11}$$

$$q^0_{\varkappa\alpha} = -\left[\sum_n(\bar{\mathbf{D}}_{\varkappa\alpha}^n\mathbf{k}_{\varkappa\alpha})\,I_{nz}S_z\right]\Big/\hbar\omega_{\varkappa\alpha}, \qquad \bar{\mathbf{D}}_{\varkappa\alpha}^n I_{nz}S_z = \bar{\mathbf{A}}_{\varkappa\alpha}^n, \tag{12}$$

where $\mathbf{k}_{K\alpha}$ is a unit vector with components

$$k_{\varkappa\alpha x} = \sin\theta_{\varkappa\alpha}\cos\varphi_{\varkappa\alpha},\ k_{\varkappa\alpha y} = \sin\theta_{\varkappa\alpha}\sin\varphi_{\varkappa\alpha},\ k_{\varkappa\alpha z} = \cos\theta_{\varkappa\alpha},$$

with $\theta_{K\alpha}$ and $\varphi_{K\alpha}$ being polar angles determining the direction of the vector $\mathbf{q}_{K\alpha}$.

It follows from (9) that

$$\lambda = \sum_{\varkappa\alpha}\hbar\omega_{\varkappa\alpha}\left(n_{\varkappa\alpha} + \tfrac{1}{2}\right) - \sum_{\varkappa\alpha}\tfrac{1}{2}\hbar\omega_{\varkappa\alpha}q''^2_{\varkappa\alpha}, \tag{13}$$

$$\Phi = \prod_{\varkappa\alpha}\Phi_{n_{\varkappa\alpha}}(q_{\varkappa\alpha} - q''_{\varkappa\alpha}), \tag{14}$$

where $\Phi_{n_{K\alpha}}$ are the eigenfunctions of an oscillator with its equilibrium position at the point $q''_{K\alpha}$.

Using (13) and (14) we get for J

$$J = \bar{\hat{T}} + \bar{\hat{V}}_0 + \sum_{\varkappa\alpha}\hbar\omega_{\varkappa\alpha}\left(n_{\varkappa\alpha} + \tfrac{1}{2}\right) + (\mu/S)\,S_z\mathcal{H}_z + \sum_n(8\pi\mu\mu_n/3SI_n)\,\psi^2(\mathbf{r}=\mathbf{R}_n)\,S_zI_{nz} - \tfrac{1}{2}\sum_{\varkappa\alpha}q''^2_{\varkappa\alpha}\hbar\omega_{\varkappa\alpha}. \tag{15}$$

The electron-coordinate part of the wave function (6) is determined by minimizing (15) with respect to $\psi(\mathbf{r})$. The evaluation of the $\psi(\mathbf{r})$ corresponding to the minimum of J and the substitution of that function into (15) determines the energy terms of the system. We note in passing that the presence in (15) of spin dependent terms can in

no way appreciably influence the wave function parameters, as these terms are several orders of magnitude smaller than all the others. We can thus to a high degree of accuracy use for our calculations the ψ-function evaluated without taking the "magnetic" terms into account. $\psi(\mathbf{r})$ has been evaluated in this approximation for a number of localized electron centers (see, for instance, references 10 and 11).

The frequency of the quantum transition involving a change in the electron spin and the emission (absorption) of phonons is determined by the expression

$$\hbar\Omega = q\boldsymbol{\mu}\mathcal{H}_z + \sum_n (8\pi\mu\mu_n / 3SI_n)\,\psi^2(\mathbf{r}=\mathbf{R}_n)\,I_{nz} + \sum_{\varkappa\alpha}\hbar\omega_{\varkappa\alpha}(\eta_{\varkappa\alpha} - n'_{\varkappa\alpha}) - \sum_{\varkappa\alpha}\hbar\omega_{\varkappa\alpha}\,q'_{\varkappa\alpha}\,q^0_{\varkappa\alpha}/S_z. \quad (16)$$

By comparison with the paramagnetic resonance frequency in a crystal with "clamped" ions, (16) contains a term (the third one) corresponding to the emission (absorption) of phonons accompanying the electron-spin transition. The fourth term determines the constant shift of the EPR frequency in a vibrating lattice. This last term must lead to an additional change in the g-factor of an electron in a crystal.

2. SHAPE AND TEMPERATURE DEPENDENCE OF EPR LINES

To evaluate the absorption coefficient for lines corresponding to the frequencies (16) we can use the general expression for the intensity of the absorption of electromagnetic radiation by localized centers given by Krivoglaz and Pekar[12]

$$\tau_e = K(2\pi i)^{-1}\oint dz\cdot z^{-(\omega_e+1)}\exp\sum_{\varkappa\alpha}(q_{\varkappa\alpha 1} - q_{\varkappa\alpha 2})^2 \times\left[\tfrac{1}{2}(n_{\varkappa\alpha}+1)\,z^{\omega_{\varkappa\alpha}} + \tfrac{1}{2}n_{\varkappa\alpha}\,z^{-\omega_{\varkappa\alpha}} - n_{\varkappa\alpha} - \tfrac{1}{2}\right]. \quad (17)$$

In the case under consideration $q_{K\alpha_1}$ and $q_{K\alpha_2}$ are the equilibrium positions of the normal coordinates in the ground state (as far as the electron spin is concerned) and the excited states. The coefficient K depends in the given case on the amplitude of the incident radio-frequency field and on the temperature determining the difference in population of the magnetic levels. If $2\mu\mathcal{H}/kT \ll 1$, K is inversely proportional to the temperature. The integration is over a closed contour encircling the point $z = 0$,

$$\hbar\omega_e = \sum_{\varkappa\alpha}\hbar\omega_{\varkappa\alpha}(n_{\varkappa\alpha} - n'_{\varkappa\alpha}), \quad (18)$$

$$n_{\varkappa\alpha} = [\exp(\hbar\omega_{\varkappa\alpha}/kT) - 1]^{-1}. \quad (19)$$

It follows from (10) that

$$q_{\varkappa\alpha 1} - q_{\varkappa\alpha 2} = q^0_{\varkappa\alpha,\,1/2} - q^0_{\varkappa\alpha,\,-1/2}, \quad (20)$$

where $q^0_{K\alpha,\,1/2}$ and $q^0_{K\alpha,\,-1/2}$ are the values of $q^0_{K\alpha}$ for $S_z = \frac{1}{2}$ and $S_z = -\frac{1}{2}$.

It is convenient to go over to new variables $z = \rho e^{i\varphi}$ in (17) and to put $\rho = 1$. Separating moreover the real and imaginary parts of τ_e one sees easily that the imaginary part of τ_e is identically equal to zero. Using also the fact that the integrand in the expression for the real part of τ_e is even we can rewrite (17) in the form

$$\tau_e = (K/\pi)\int_0^\pi d\varphi\cos\Big[\sum_{\varkappa\alpha}\tfrac{1}{2}a_{\varkappa\alpha}\sin\omega_{\varkappa\alpha}\varphi - \omega_e\varphi\Big] \times\exp\Big\{\sum_{\varkappa\alpha}a_{\varkappa\alpha}\Big(n_{\varkappa\alpha}+\tfrac{1}{2}\Big)[\cos\omega_{\varkappa\alpha}\varphi - 1]\Big\}, \quad (21)$$

$$a_{\varkappa\alpha} = (q^0_{\varkappa\alpha,\,1/2} - q^0_{\varkappa\alpha,\,-1/2})^2. \quad (22)$$

It is appropriate to emphasize once again that the summation over α in (21) includes all branches of the dispersion. One can, however, show that in the case under consideration the optical frequencies do not play an important role in (21). To show that, we estimate the indices of the exponentials corresponding to the optical vibrations. We shall restrict ourselves for the sake of simplicity to lattices containing two ions in the elementary cell. One can in that case determine the displacements of the positive and negative ions $\mathbf{u}_+$ and $\mathbf{u}_-$ in the lattice from the following equations

$$M_+\mathbf{u}_+ + M_-\mathbf{u}_- = 0, \quad (23a)$$

$$(e/n^2\Omega_0)(\mathbf{u}_+ - \mathbf{u}_-) = \mathbf{P}, \quad (23b)$$

where M_+ and M_- are the masses of the positive and negative ions, Ω_0 the volume of the elementary cell, n the refractive index in the crystal, and $\mathbf{P}$ the vector of the specific inertial polarization of the crystal in the case of extremely long wavelengths. It follows from (23) that

$$\mathbf{u}_+ = \mathbf{P}\Omega_0 n^2/e(1 + M_+/M_-); \qquad \mathbf{u}_- = -M_+\mathbf{u}_+/M_-. \quad (24)$$

An expansion of $\mathbf{P}$ in a series in terms of a complete set of functions $\chi_K(\mathbf{r})$ and the transition to dimensionless coordinates using the relations

$$\mathbf{q}_\varkappa = \sqrt{4\pi/\hbar\omega_0 c}\,\mathbf{P}_\varkappa \quad (25)$$

leads to the following expression for $\mathbf{u}_+$

$$\mathbf{u}_+ = \frac{\Omega_0 n^2 M_-}{e(M_- + M_+)}\sum_\varkappa\sqrt{\frac{\hbar\omega_0 c}{4\pi}}\,\mathbf{q}_\varkappa\chi_\varkappa(\mathbf{r}), \quad (26)$$

where ω_0 is the frequency of the limiting optical vibrations, $c = 1/n^2 - 1/\epsilon$, and ϵ is the dielectric constant of the crystal

We shall assume that the radius of the state of the localized electron is not much larger than the lattice constant (this occurs in a wide range of crystals). In that case only the hyperfine interaction with the nearest ions in the lattice will play an important role. Let these be, for instance, the positive ions of the first coordination sphere surrounding the defect (the estimate is not essentially altered if we take several coordination spheres into account). For our estimate we can put

$$(\operatorname{grad}\hat{Q}_n)_0=(8\pi\mu\mu_n/3SI_n)\,(\nabla\psi^2)_{\mathbf{r}=\mathbf{R}_n^+}S_zI_{nz}.$$

Using (26) we get for q^0_{κ} opt

$$q^0_{\varkappa,\,\mathrm{opt}}=-\frac{8\pi\mu\mu_n\Omega_0 n^2M_-}{3\hbar\omega_0 SI_n\,(M_-+M_+)\,e}\sqrt{\frac{\hbar\omega_0 c}{4\pi}}\sum_n\chi_{\varkappa}(R_n^+)(\nabla\psi^2)_{\mathbf{r}=\mathbf{R}_n^+}\mathbf{k}. \tag{27}$$

The summation is over the positive ions of the first coordination sphere.

A direct numerical estimate of the index of the exponent in (21) using (22) and (27) and strongly overestimating shows that this index is practically equal to zero ($10^{-15}-10^{-16}$). A similar estimate of the sum in the argument of the cosine in (21) leads to the result that here also the role of the optical vibrations is insignificant. As we shall show directly in the following, the index of the exponent in (21) is for the case of the acoustic vibrations, generally speaking, not small (of the order of unity). The interaction with the long wavelength acoustical vibrations turns out to be very substantial, which follows both from the expression for the coupling constant for the spin-lattice interaction

$$C_{\varkappa\alpha}=\sqrt{\hbar/\omega_{\varkappa\alpha}\rho}\sum(\operatorname{grad}\hat{Q}_n)_0\,\mathbf{k}_{\varkappa\alpha}, \tag{28}$$

and from the general physical picture of the phenomenon.*

We note that for the optical vibrations the coupling constant is equal to

$$C_{\mathrm{opt}}=\frac{\Omega_0 n^2M_-}{e\,(M_-+M_+)}\sqrt{\frac{\hbar\omega_0 c}{4\pi}}\sum_n(\operatorname{grad}\hat{Q}_n)\,\mathbf{k}. \tag{29}$$

For small κ, $C_{\kappa\alpha}$ will thus be appreciably larger than C_{opt}. Taking the above remarks into account we can with great accuracy in (21) in both sums over κ and α retain only the three branches of the acoustical vibrations.

For the actual case of the extremely long wavelengths we can introduce the normal coordinates of the acoustical vibrations using the relations

$$\mathbf{u}_{\varkappa\alpha}=\mathbf{q}_{\varkappa\alpha}\sqrt{\hbar/\rho\omega_{\varkappa\alpha}}. \tag{30}$$

Taking (30) and (12) into consideration we can write $q^0_{\kappa\alpha}$ in the form

$$q^0_{\varkappa\alpha}=\omega_{\varkappa\alpha}^{-1/2}\sum_n(\mathbf{E}^n\mathbf{k}_{\varkappa\alpha})\,\chi_{\varkappa}(\mathbf{R}_n)\,S_zI_{nz}. \tag{31}$$

$$\mathbf{E}^n=-\frac{\overline{(\operatorname{grad}Q_n)_0}}{I_{nz}S_z\sqrt{\hbar\rho}}. \tag{32}$$

We note that (32) is independent of $I_{nz}S_z$.

It follows from (22) and (31) that

$$a_{\varkappa\alpha}=\omega_{\varkappa\alpha}^{-3}\sum_{nn'}(\mathbf{E}^n\mathbf{k}_{\varkappa\alpha})\,(\mathbf{E}^{n'}\mathbf{k}_{\varkappa\alpha})\,\chi_{\varkappa}(\mathbf{R}_n)\,\chi_{\varkappa}(\mathbf{R}_{n'})\,I_{nz}I_{n'z}. \tag{33}$$

By generously overestimating, we find from a numerical estimate similar to (27) but for the acoustical vibrations that the sums

$$\frac{1}{2}\sum_{\varkappa\alpha}a_{\varkappa\alpha}\,[\cos\omega_{\varkappa\alpha}\varphi-1],\qquad\frac{1}{2}\sum_{\varkappa\alpha}a_{\varkappa\alpha}\sin\omega_{\varkappa\alpha}\varphi$$

are appreciably less than unity (of the order of 10^{-6}). Therefore

$$\tau_e\approx\frac{K}{\pi}\int_0^{\pi}\cos\omega_e\varphi\cdot\exp\left\{\sum_{\varkappa,\alpha}a_{\varkappa\alpha}n_{\varkappa\alpha}\,[\cos\omega_{\varkappa\alpha}\varphi-1]\right\}d\varphi. \tag{34}$$

Replacing the summation over κ by an integration over κ-space we are by a direct integration over θ_α and φ_α and a summation over α led to the following result

$$\tau_e\approx(K/\pi)\int_0^{\pi}d\varphi\cos(\omega_e\varphi)\exp\left\{M\int_0^{\varkappa_c}[\cos\omega_{\varkappa}\varphi-1]\,n_{\varkappa}\varkappa^{-1}d\varkappa\right\}, \tag{35}$$

$$M=(6\pi^2)^{-1}(2/c_{\perp}^3+1/c_{\parallel}^3)\sum_{nn'}(\mathbf{E}^n\mathbf{E}^{n'})\,I_{nz}I_{n'z}, \tag{36}$$

where $c_{\parallel}$ and $c_{\perp}$ are the velocities of the longitudinal and transverse waves. We note that $M>0$. To obtain (35) we took into account that in the sums over κ in which the extremely long wavelengths play the dominant part, $\kappa\mathbf{R}_n\ll\pi/4$ and thus $\sin(\kappa\mathbf{R}_n+\pi/4)\approx1/\sqrt{2}$.

For the integration it is convenient to write (35) in the form

$$\tau_e\approx(K/\pi)\int_0^{2/\omega_1}d\varphi\cos(\omega_e\varphi)\exp\left\{M\int_0^{\varkappa_0}[\cos\omega_{\varkappa}\varphi-1]\,n_{\varkappa}\varkappa^{-1}d\varkappa\right\}$$

$$+(K/\pi)\int_{2/\omega_1}^{\pi}d\varphi\cos(\omega_e\varphi)\exp\left\{M\int_0^{\varkappa_0}[\cos\omega_{\varkappa}\varphi-1]\,n_{\varkappa}\varkappa^{-1}d\varkappa\right\}, \tag{37}$$

where ω_1 is the frequency within the interval $(0,\ \omega_0)$ which satisfies the condition

$$\omega_1\ll kT/\hbar. \tag{38}$$

We shall show that the first integral in (37) is appreciably less than the second one. To do this we note that

*One sees easily that for the spin resonance phenomenon the long wavelength phonons with frequencies $\omega\sim2\mu H/\hbar$ play the most important part. This follows, though, directly from the expression given in the following for u_2, where the second integral with the limits $\omega_1\sim2\mu H$ and ω_0 does not play a part.

$$\int_0^{\omega_0} \frac{\cos\omega\varphi - 1}{\exp(\hbar\omega/kT) - 1}\frac{d\omega}{\omega}$$

cannot be positive. Its largest value is equal to zero.

$$u_1 = \frac{K}{\pi}\int_0^{2/\omega_1} d\varphi \cos(\omega_e\varphi)$$

$$\times \exp\left\{M\int_0^{x_0}(\cos\omega_x\varphi - 1)\, n_x x^{-1}dx\right\} \leqslant \int_0^{2/\omega_1} d\varphi = 2/\omega_1.$$

We write the second integral in the form

$$u_2 = \frac{K}{\pi}\int_{2/\omega_1}^{\pi} d\varphi \cos(\omega_e\varphi)$$

$$\times\exp\left\{M\left[\int_0^{\omega_1}\frac{\cos\omega\varphi - 1}{\exp(\hbar\omega/kT)-1}\frac{d\omega}{\omega} + \int_{\omega_1}^{\omega_0}\frac{\cos\omega\varphi - 1}{\exp(\hbar\omega/kT)-1}\frac{d\omega}{\omega}\right]\right\}$$

One can show that in the index of the exponent the first integral (J_1) plays the dominant role. To show this we expand $n(\omega)$ in powers of $\hbar\omega/kT$. We can restrict ourselves by virtue of (38) in J_1 to the first term of the expansion. The second integral J_2 is only increased when we replace $n(\omega)$ by $kT/\hbar\omega$. Thus

$$J_1 = \left[\frac{1-\cos\omega_1\varphi}{\omega_1} - \varphi\int_0^{\omega_1\varphi}\frac{\sin x}{x}dx\right]\frac{kT}{\hbar}, \qquad (39a)$$

$$J_2 \leqslant \frac{kT}{\hbar}\left[\frac{1-\cos\omega_0\varphi}{\omega_0} - \frac{1-\cos\omega_1\varphi}{\omega_1}\right.$$

$$\left. - \varphi\int_0^{\omega_0\varphi}\frac{\sin x}{x}dx + \varphi\int_0^{\omega_1\varphi}\frac{\sin x}{x}dx\right]. \qquad (39b)$$

$\omega_1\varphi > 1$ in the range of values of $\varphi\,(2/\omega_1, \pi)$. Using the asymptotic expression for the sine integral we can write (39) in the form

$$J_1 = (kT/\hbar)(1/\omega_1 - \pi\varphi/2) \approx -kT\pi\varphi/2\hbar, \qquad (40a)$$

$$J_2 \leqslant (kT/\hbar)(1/\omega_0 - 1/\omega_1). \qquad (40b)$$

It follows from (40) that J_1 is larger than the right hand side of (40b). Therefore

$$u_2 = \frac{K}{\pi}\int_{2/\omega_1}^{\pi} d\varphi\cos(\omega_e\varphi)\exp\left(-\frac{\pi}{2}\frac{kT}{\hbar}M\varphi\right). \qquad (41)$$

Integrating, we get

$$u_2 \approx \frac{K}{\pi}\frac{\exp(-2m/\omega_1)}{m^2+\omega_e^2}\left(m\cos\frac{2\omega_e}{\omega_1} - \omega_e\sin\frac{2\omega_e}{\omega_1}\right), \qquad (42)$$

$$m = MkT\pi/2\hbar. \qquad (43)$$

Since for the range of frequencies of interest (for which τ_e is still appreciable) $2\omega_e/\omega_1 \ll 1$, we find

$$u_2 \approx \frac{K}{\pi}\frac{m}{m^2+\omega_e^2}. \qquad (44)$$

Comparing (44) and $u_1 \leq 2/\omega_1$ it follows that in this interval $u_2 \gg u_1$.

Therefore

$$\tau_e \approx \frac{K}{\pi}\frac{m}{m^2+\omega_e^2}, \qquad (45)$$

if ω_1 is chosen within the range

$$m \ll \omega_1 \ll kT/\hbar. \qquad (46)$$

Numerical estimates show that $m \approx 10^6 - 10^7$ sec^{-1}. Therefore (46) is not a strong inequality restricting the range of temperatures. For $\omega_1 \approx 10^9$, for instance, $T \geq 0.01°\text{K}$.

Equation (45) is a general expression for the absorption coefficient at frequency ω_e. It can be seen from this expression that the curve has the Lorentz shape. The half width of the line δ is determined by the expression

$$\delta = 2m. \qquad (47)$$

The total intensity of the absorption in the line turns out to be equal to

$$\int_{-\infty}^{+\infty}\tau_e d\omega_e = K. \qquad (48)$$

It follows from (47) and (43) that the EPR line half width increases linearly with temperature. The absorption coefficient at the maximum

$$\tau_{e\,max} = K/\pi m, \qquad (49)$$

is thus

$$\tau_{e\,max}\delta = 2K/\pi. \qquad (50)$$

3. THE SHAPE OF THE EPR LINES OF F-CENTERS

For the sake of simplicity we restrict ourselves to such colored crystals for which the hyperfine interaction of the electron with the nuclei of the first coordination sphere, for instance with alkali halide nuclei of the NaCl type is substantial (the generalization to the case of interactions with several coordination spheres does not present any difficulties in principle). It is well known that there are in that case 19 lines corresponding to the different values of the z-component of the total spin I_z. The intensity of each of the 19 lines is determined by the interaction of the electron spin with the lattice vibrations without taking the statistical weight of the state with a well defined value of I_z into account.

The consideration given above shows that the line corresponding to one of the possible distributions of the values of I_{nz} (for given I_z) is broad-

ened. The intensity of each of the 19 lines τ_e is thus made up of the intensities of broadened lines with a well defined distribution of I_{nz}

$$\tau_e = \frac{K}{\pi}\sum_i \frac{m_i}{m_i^2+\omega_e^2}, \qquad (51)$$

where the summation extends over all states with different I_{nz} but fixed I_z.

One shows easily, using (51), that the total line intensity turns out to be equal to $K\sigma$, where σ is the statistical weight of the state. One sees easily that (51) has also the Lorentz shape for ω_e which are small or large compared to the m_i. The range of intermediate values is small so that (51) to a good approximation has the Lorentz shape for the whole interval over which the frequency varies. What has been said above substantiates the assumption of the phenomenological theory of the saturation effect of the EPR of F-centers which agrees well with experiments, if one assumes that the shape of each of the 19 lines is the Lorentz shape[8] in their "tails."

To obtain the overall shape of the EPR line of F-centers in accordance with experiments it was also just assumed[9] that each of the 19 lines had a Lorentz shape. It was then again emphasized that to obtain the correct shape of the EPR band it is sufficient that the Lorentz shape occur in the "tails" of the curve.

The frequency dependence of the absorption coefficient of the whole EPR band can be written in the form

$$\tau = \frac{K}{\pi}\sum_{iI_z} \frac{m_i}{m_i^2+(\omega_e-\omega_{I_z})^2}, \qquad (52)$$

if we use (51), where ω_{I_z} is the frequency of the maximum of each of the 19 lines.

Equations (51) and (52) enable us to obtain the temperature dependence of the band width in the frequency range near the maximum. If $\omega_e \ll m_i$, it follows from (51) that

$$\tau_e \approx \left\{\frac{K}{\pi}\sum_i m_i^{-1} - \omega_e^2\sum_i m_i^{-3}\right\}. \qquad (53)$$

We shall as an example determine the line width in the neighborhood of the maximum for $\tau_{e\alpha} = (1-\alpha)\tau_{max}$ where $\alpha < 1$. It follows from (53) that the line width is equal to

$$\delta_\alpha = 2\left[\alpha\sum_i m_i^{-1}\Big/\sum_i m_i^{-3}\right]^{1/2}. \qquad (54)$$

Taking (43) into account we find that

$$\delta_\alpha \sim T. \qquad (55)$$

A similar consideration enables us to obtain the temperature dependence of the width of the whole EPR band in the neighborhood of the maximum. The dependence turns out to be more complicated. The band width increases slowly with the temperature in accordance with the experimental results.[6,7]

One sees easily that the m_i depend on the values of the gradient of the wave function of the localized electron at different lattice sites. A comparison of the results of the theory developed in the foregoing with experiment may thus serve as a method to determine the gradient of the wave function. This can be especially simply done for those crystals in which the localized electron interacts only with one magnetic moment of the nuclei of the surrounding atoms (such a situation occurs, for instance, for F-centers in MgO crystals).

In conclusion we note that knowing the width of the absorption lines enables us to estimate the spin-lattice relaxation time t. In the weak coupling limit (which is valid in the case under consideration) t is inversely proportional to the line width. Preliminary estimates performed for F-centers, show that $t \approx 10^{-5}-10^{-6}$ sec. This magnitude agrees well with the corresponding experimental results (see, for instance, reference 8).

[1] Kip, Kittel, Levy, and Portis, Phys. Rev. **91**, 1066 (1953).

[2] M. F. Deĭgen, JETP **33**, 773 (1957), Soviet Phys. JETP **6**, 594 (1958).

[3] W. Kohn and J. M. Luttinger, Phys. Rev. **97**, 883 (1955).

[4] B. S. Gouray and F. J. Adrian, Phys. Rev. **105**, 1180 (1957).

[5] M. F. Deĭgen and A. B. Roĭtsin, JETP **36**, 176 (1959), Soviet Phys. JETP **9**, 120 (1959).

[6] M. Tinkham and A. F. Kip, Phys. Rev. **83**, 657 (1951).

[7] E. E. Schneider and T. S. England, Physica **17**, 221 (1951).

[8] A. M. Portis, Phys. Rev. **91**, 1071 (1953).

[9] G. J. Wolga and M. W. P. Strandberg, J. Phys. Chem. Solids **9**, 309 (1959).

[10] S. I. Pekar, Исследование по электронной теории кристаллов, (Investigations on the Electron Theory of Crystals) Gostekhizdat, 1951, [Untersuchungen uber die Elektronentheorie der Kristalle, Akademieverlag, Berlin, 1954].

[11] M. F. Deĭgen, Investigations on the Theory of Localized States of Electrons in Dielectrics and Semiconductors, Doctoral Thesis, Physico-technical Institute of the Academy of Sciences, U.S.S.R., 1959.

[12] M. A. Krivoglaz and S. I. Pekar, Тр. Института физики АН УССР (Proc. Inst. Phys., Acad. Sci., Ukr. S.S.R.), **4**, 37 (1953).

Translated by D. ter Haar
100

EXCITATION OF NUCLEAR COLLECTIVE STATES IN CHARGED PARTICLE SCATTERING

S. I. DROZDOV

Submitted to JETP editor July 29, 1959

J. Exptl. Theoret. Phys. (U.S.S.R.) 38, 499-502 (February, 1960)

The differential excitation cross section of the 4^+ even-even nucleus collective level in fast nucleon small-angle scattering is derived. The cross section is strongly dependent on the absolute value and sign of the nuclear shape parameter α_4.

IN the scattering of nucleons on nonspherical nuclei, excitation of the collective states of the nucleus takes place as a consequence of the process of direct interaction of the incident particle with the nuclear surface. We shall show that the angular distribution of particles scattered elastically in these processes is always strongly dependent on the nuclear shape parameter α_l entering into the equation of the surface of the nucleus $r(\mu) = R \times [1+\Sigma\alpha_l P_l(\mu)]$. For this purpose we shall compute the excitation cross section of the rotational 4^+ level of an even-even nucleus in the scattering of fast charged particles by making use of the method of diffraction theory.[1,2]

The excitation of the first rotational level 2^+ has been considered previously.[3] As before, we assume that the energy of the particles exceeds the Coulomb barrier ($kR \gg \eta = ZZ'e^2/\hbar v$), that the adiabatic condition is satisfied ($kR\Delta E/E \ll 1$), and that the nucleus is black. The differential scattering cross section with excitation of the rotational level of an even-even nucleus with moment λ is given by the equation

$$\sigma_\lambda(\theta) = \sum_\mu |\langle Y^*_{\lambda\mu}(\omega) f(\Omega, \omega) Y_{00}\rangle|^2, \quad (1)$$

which is easily generalized to the case of an odd nucleus.[3]

According to the diffraction-theory method, the amplitude is determined by the expression ($z_0 \to \infty$)

$$f(\Omega, \omega) = -\frac{ik}{2\pi}\int_0^{2\pi} d\varphi \int_{\rho(\varphi)}^{\infty} \rho d\rho e^{-ik\rho}\Psi_k(\rho, z_0)e^{-ikz_0}, \quad (2)$$

where the angles $\Omega = (\theta, \varphi')$ determine the scattering direction while the angles ω determine the direction of the symmetry axis of the nucleus; the function $\rho(\varphi)$ describes the shape of the nuclear shadow in the transverse plane; $\mathbf{k}'$ = the wave vector of the scattered particle. The wave function Ψ_k describes the scattering of charged particles on a black nucleus, and has the form[1]

$$\Psi_k(\rho, z) = \exp\left\{i\left[kz - (\hbar v)^{-1}\int_{-z_0}^{z} U(\rho, z)\,dz\right]\right\}. \quad (3)$$

in cylindrical coordinates with the polar z axis along the wave vector of the incident particles $\mathbf{k}$. The quantity $U(\rho, z)$ represents the energy of the electrical interaction of the particle with the nucleus.

If we assume the nucleus to be uniformly charged, we then obtain in second approximation in the small parameter of nonsphericity α_l:

$$\frac{U(\rho, z)}{ZZ'e^2} = \frac{1}{r}\left[1 + 3\sum_{l'}\alpha_{l'}(C^{00}_{l'0l'0})^2\right] + \sum_{lm}\left[\alpha_l + \sum_{l'l''}\alpha_{l'}\alpha_{l''}(C^{l0}_{l'0l''0})^2\frac{2+l}{2}\right] \times \frac{12\pi R^l}{(2l+1)^2}Y^*_{lm}(\omega)Y_{lm}(\mathbf{r})\,r^{-l-1} \quad (4)$$

and similarly for the nuclear shadow function:

$$\frac{\rho(\varphi)}{R} = 1 + \sum_{lm}\frac{4\pi\alpha_l}{2l+1}Y^*_{lm}(\omega)Y_{lm}(0, \varphi) + \frac{1}{2}\sum_{Ll'mm'}\frac{(4\pi)^{3/2}\alpha_l\alpha_{l'}C^{L0}_{l0l'0}C^{Lm+m'}_{lml'm'}}{\sqrt{(2L+1)(2l+1)(2l'+1)}}Y^*_{Lm+m'}(\omega) \times\left[\frac{\partial}{\partial\mu}Y_{lm}(\mu, \varphi)\right]_{\mu=0}\left[\frac{\partial}{\partial\mu}Y_{l'm'}(\mu, \varphi)\right]_{\mu=0}, \quad (5)$$

where $C^{Lm+m'}_{lml'm'}$ are the Clebsch-Gordan coefficients.

By substituting (3) — (5) in (2), we can compute the amplitude $\langle Y^*_{\lambda\mu}(\omega) f(\Omega, \omega) Y_{00}\rangle$ corresponding to excitation of the rotational state of the nucleus $Y_{\lambda\mu}(\omega)$ in the form of an expansion in powers of α_l ($\alpha_l kR^\theta \ll 1$). For simplicity, we shall assume that the nuclear shape parameter $\alpha_4 \ll \alpha_2$. Then the amplitude of the excitation of the state 4^+ of the even-even nucleus in the scattering of charged particles has the form ($\xi = \alpha_4/\alpha_2^2$, $a = kR^\theta$, $\lambda = 4$):

$$i^{-\mu}e^{-i\mu\varphi'}(2\lambda+1)^{1/2}\alpha_2^{-2}k(kR)^{-2(1+i\eta)}\langle Y^*_{\lambda-\mu}(\omega)f(\Omega,\omega)Y_{00}\rangle$$
$$= 2\eta(A_\mu^{(3)}-A_\mu^{(2)})J_\mu(a)+\eta(\xi B_\mu^{(2)}+A_\mu^{(5)})\,\mathrm{Re}(F_{4\mu}-\Phi_{4\mu})$$
$$+\eta^2A_\mu^{(4)}\,\mathrm{Im}(F_{4\mu}-\Phi_{4\mu})+i[(\xi B_\mu^{(1)}+A_\mu^{(1)}+A_\mu^{(2)})J_\mu(a)$$
$$+A_\mu^{(2)}aJ'_\mu(a)+\eta(\xi B_\mu^{(2)}+A_\mu^{(5)})\,\mathrm{Im}(F_{4\mu}-\Phi_{4\mu})$$
$$-\eta^2A_\mu^{(4)}\,\mathrm{Re}(F_{4\mu}-\Phi_{4\mu})]. \qquad (6)$$

Here $A_\mu^{(i)}$, $B_\mu^{(i)}$ are numbers representing combinations of the Clebsch-Gordan coefficients and the spherical harmonics, for example,

$$A_\mu^{(2)}=\frac{4}{10}\pi C^{40}_{2020}\sum_{mm'}C^{4\mu}_{2m2m'}Y_{2m}(0,0)\,Y_{2m'}(0,0).$$

These equations are given in the table; they differ from 0 only for even μ and do not depend on the sign of μ.

μ	$B_\mu^{(1)}$	$B_\mu^{(2)}$	$A_\mu^{(1)}$	$A_\mu^{(2)}$	$A_\mu^{(3)}$	$A_\mu^{(4)}$	$A_\mu^{(5)}$
0	0.375	0	—0.514	0.0964	0.0257	0.0206	0
2	—0.395	0	0.407	—0.102	—0.0407	0	0
4	0.523	0.159	0	0.134	0.108	0.0861	0.246

The complex functions $F\lambda\mu(a,\eta)$, $\Phi\lambda\mu(a,\eta)$ entering into (6) depend on a and η. These functions can be computed from the following formulas:

$$\Phi_{\lambda\mu}(a,\eta)=a^{\lambda-2(1+i\eta)}2^{1-\lambda+2i\eta}\frac{\Gamma(i\eta+(\mu-\lambda)/2+1)}{\Gamma(-i\eta+(\mu+\lambda)/2)},$$

$$F_{\lambda\mu}(a,\eta)=\sum_{m=0}^{\infty}\frac{a^mJ_{\mu+m}(a)}{2^{m+1}}\frac{\Gamma(i\eta+(\mu-\lambda)/2+1)}{\Gamma(i\eta+(\mu-\lambda)/2+m+2)}. \qquad (7)$$

For $\eta=0$, we get the amplitude of inelastic scattering of neutrons ($\lambda=4$) from Eq. (6):

$$i^{-\mu-1}e^{-i\mu\varphi'}(2\lambda+1)^{1/2}\alpha_2^{-2}k(kR)^{-2}\langle Y^*_{\lambda-\mu}(\omega)f(\Omega,\omega)Y_{00}\rangle$$
$$=[A_\mu^{(1)}+A_\mu^{(2)}+\xi B_\mu^{(1)}]J_\mu(a)+A_\mu^{(2)}aJ'_\mu(a). \qquad (8)$$

In a fashion similar to what was done earlier[3] for the amplitude of excitation of the 2^+ state, one can divide the amplitude of inelastic scattering (6), corresponding to excitation of the 4^+ state, into two components: the amplitude of electrical excitation E4 and the part of the amplitude connected with nuclear interaction. It is not difficult to show that the terms in (6) containing the function $\Phi_{\lambda\mu}$ give the amplitude of the Coulomb excitation E4. The remaining terms correspond to the nuclear part of the scattering amplitude n4. Thus the excitation cross section of the level 4^+ can be represented in the form of a sum of the Coulomb excitation cross section and σ_{E4}, the nuclear part of the cross section σ_{n4} and the interference term $\sigma_{int\,4}$:

$$\sigma_4(\theta)=\sigma_{E4}(\theta)+\sigma_{n4}(\theta)+\sigma_{int4}(\theta). \qquad (9)$$

The angular distributions of protons and neutrons with energies of 20 and 30 Mev scattered with excitation of the state 4^+ of the nucleus Gd_{64}^{160} are shown in Figs. 1 — 3. As is seen in Fig. 1, the role

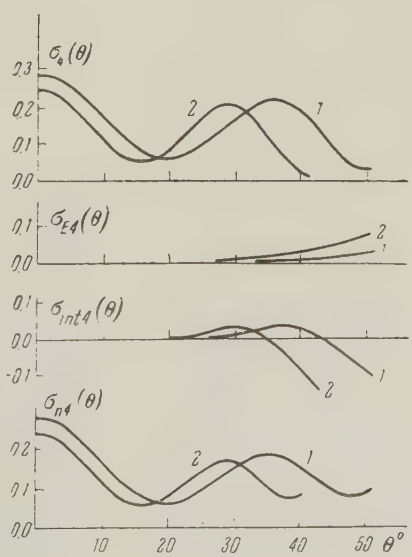

FIG. 1

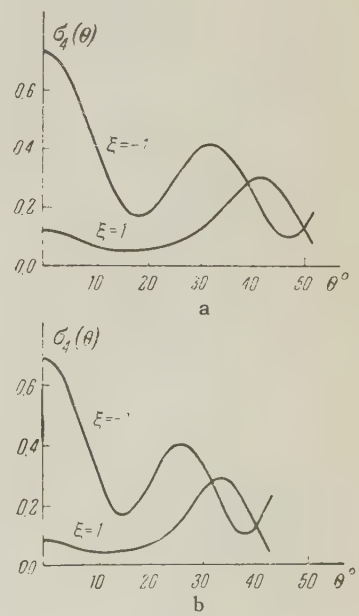

FIG. 2

FIG. 1. The functions $\sigma_4(\theta)$, $\sigma_{E4}(\theta)$, $\sigma_{int\,4}(\theta)$, $\sigma_{n4}(\theta)$, in units of $\alpha_2^4(kR)^4/9k^2$, describing the angular distribution of protons with energy 20 Mev (curve 1) and 30 Mev (curve 2), scattered on the Gd_{64}^{160} nucleus with excitation of its rotational level 4^+. The calculation was made at $\alpha_4=0$ and $R=1.3\times10^{-13}A^{1/3}$ cm.

FIG. 2. The function $\sigma_4(\theta)$ in units of $\alpha_2^4(kR)^4/9k^2$, describing the angular distribution of protons with energies of 20 Mev (a) and 30 Mev (b), inelastically scattered by the Gd_{64}^{160} nucleus. The calculation was made for $\xi=\alpha_4/\alpha_2^2=\pm1$.

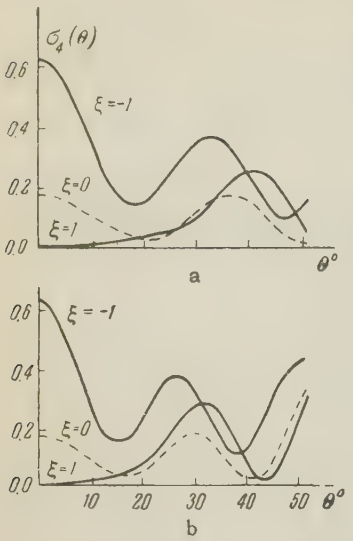

FIG. 3. Graph of the same quantity as in Fig. 2, for the case of inelastic scatterings of neutrons (a – 20 Mev, b – 30 Mev). The calculation was made for $\xi = 0, \pm 1$.

of Coulomb excitation E4 is small in small angle scattering $\theta \ll 1$, inasmuch as in this region of angles, $\sigma_{E4}(\theta)$ is proportional to θ^4. It should be noted that in the excitation of the level 2^+, the role of Coulomb excitation is quite significant.[3]

The form of the angular distribution $\sigma_4(\theta)$ for neutrons and protons is strongly dependent on the absolute value and the sign of the nuclear shape parameter (Figs. 2 – 3); for $\xi = \alpha_4/\alpha_2^2 \approx -1$, there is a large maximum in the angular distribution, corresponding to forward scattering; for $\xi \approx 1$, this maximum has essentially vanished.

The author sincerely thanks A. V. Babykin, T. V. Novikov, and V. Z. Mel'gunov for the numerical calculations.

[1] L. Landau and E. Lifshitz, Квантовая механика (Quantum Mechanics) (Gostekhizdat, 1948, p. 184). English translation, Addison Wesley, 1958.

[2] A. I. Akhiezer and A. G. Sitenko, JETP **32**, 794 (1957), Soviet Phys. JETP **5**, 652 (1957).

[3] S. I. Drozdov, JETP **36**, 1875 (1959), Soviet Phys. JETP **9**, 1335 (1959).

Translated by R. T. Beyer
101

INTERNAL STRUCTURE OF SUPER-DENSE STARS

D. A. KIRZHNITS

P. N. Lebedev Physics Institute, Academy of Sciences, U.S.S.R.

Submitted to JETP editor August 8, 1959

J. Exptl. Theoret. Phys. (U.S.S.R.) **38**, 503-508 (February, 1960)

The peculiarities of a "condensed state -- plasma" transition in ultra-compressed matter are considered, and it is concluded that the cores of dense white dwarfs may be in a condensed state. As a result, the nuclear processes have much lower rates than in a plasma, and the possible hydrogen concentration in the matter of white dwarfs may be much higher.

1. INTRODUCTION

WHITE dwarfs (w.d.), stars of exceedingly high density and small radius and luminosity, do not lack interest for many branches of physics. The exceedingly high density of matter, approaching 10^9 g/cm^3, the presence of relativistic degenerate electron gas, the specific features of the nuclear processes — this is a far from complete list of the distinguishing properties of w.d. (see reference 1).

In the present article we consider the aggregate state of matter in w.d. One usually assumes that it is in a plasma state; accordingly, for example, the speeds of nuclear reactions in w.d. are calculated with the aid of relations applicable only to ionized gases.

Such a representation, which is true for a majority of stars, necessitates when applied to w.d., generally speaking, a review. The point is that owing to the high density of the w.d. the Coulomb coupling between nuclei may be so rigid, that even stellar temperatures ($\sim 10^7$ deg) are found to be insufficiently high for the "evaporation" of the condensate.*

A consistent examination of this problem requires the calculation of thermodynamic potentials of the condensed and plasma phases and the determination of which is the smaller. It is important to emphasize that, for uncompressed matter, even a qualitative examination of this problem would be very difficult owing to the important role of electron shells. The situation is considerably simplified, however, at high compressions, corresponding to a small value of the parameter $RZ^{1/3}/a_0$ (see below for notation). We deal essentially with a practically ideal and homogeneous electron gas, which plays the role of a background that compensates for the positive charge of the nuclei.

In spite of this simplification, the problem remains exceedingly complex. We shall therefore employ here a simpler and clearer, although rougher approach.* There are grounds for assuming that not far from the phase curve the results obtained will be sufficiently reliable.

The presence of a condensed core in the w.d. influences greatly the rate of the nuclear processes (p-p reaction) and the chemical composition of the w.d. What is radically changed (compared with the plasma) is the kinetic mechanism of the process: the factors that come to the forefront are the height of the barrier, (which causes the binding of the particle in the condensate), the frequency of particle vibration, etc.

Wildhack[2] and Zel'dovich[3] have considered the reaction in cold crystalline hydrogen, due to the tunnel effect. The reaction yield was found to be large and incompatible with the small luminosity and the long lifetime of the w.d. This conclusion becomes even more aggravated at a temperature different from 0. Thus, even in a condensed w.d. a hydrogen content on the order of several times ten percent becomes impossible.†

Hydrogen concentrations on the order of several percent ($< 10^{-3}$% according to the plasma model) are possible, however, if a configuration is produced, in which the protons are uniformly

*We make no special distinction between the solid and liquid state (see, incidentally, Section 2), since for nuclear reactions only "near order" is significant.

*This approach is used in the theory of the metallic bond to derive the equation of state of matter, etc.

†We note that even a few years ago[5] the question of the discrepancy between the values of the hydrogen concentration, obtained on the basis of the mass and radius (50–70%) and on the basis of luminosity ($<10^{-5}$, obtained for Sirius B), was quite acute. At the present time, owing to the more precise determination of the radius, this question apparently has become less acute.[1]

"frozen" in the bulk of heavy nuclei. The reaction is then suppressed because the protons must overcome not only the mutual repulsion, but also the potential barrier produced by the neighboring inactive nuclei. We note that the presence of even such a relatively small hydrogen concentration may be of prime significance for the theory of stellar evolution and the theory of novas and supernovas (in this connection see reference 4).

Nuclear reactions are apparently the only factor influenced by the presence of condensate. Such quantities as the pressure, conductivity, etc are determined as before essentially by the electronic component.*

To conclude this section, we give numerical values of the parameters of w.d., which will be used henceforth. The density ρ is chosen to be 10^6 g/cm^3. Only indirect data are available on the temperature; we assume a probable value of 10^7 deg (see references 1 and 5). Finally, the average atomic number Z is taken to be on the order of 10 (reference 6).

2. PHASE TRANSITION IN SUPERDENSE MATTER

We shall start with a consideration of the condensed phase and find the range of temperatures and densities in which it is stable.

We consider first matter containing nuclei of one kind. We separate an isolated neutral spherical cell with a nucleus at the center. The remaining matter is ignored in this approach; its influence manifests itself only in boundary effects, which prevent the expansion of the separated cell.

The cell radius R, which has the significance of the average distance between nuclei, is equal to

$$R = (3\eta ZM/4\pi\rho)^{1/3}, \tag{1}$$

where M is the proton mass and η is the ratio of the atomic weight to Z.

Introducing the Bohr radii of the electron, $a_0 = \hbar^2/me^2$, and of the nucleus $A_0 = \hbar^2/\eta MZ^3e^2$, we have

$$R/a_0 = 3.8\cdot 10^{-2} \ll 1, \quad R/A_0 = 1.4\cdot 10^5 \gg 1, \tag{2}$$

i.e., the system is dense from the point of view of electrons and rarefied from the point of view of nuclei.

An elementary calculation gives the following expressions for the potential energy of the nucleus in the cell

$$U(r) = -3Z^2e^2/2R + Z^2e^2r^2/2R^3, \tag{3}$$

where r is the distance from the center of the cell ($r < R$). The nucleus is thus in an oscillator potential well. The corresponding oscillation frequency is

$$\omega = (Z^2e^2/\hbar R)(A_0/R)^{1/2}. \tag{4}$$

At 0 temperature the level occupied by the nucleus corresponds to an energy (reckoned from the bottom of the well)

$$E_0 = \tfrac{3}{2}\hbar\omega = (3Z^2e^2/2R)(A_0/R)^{1/2}. \tag{5}$$

By virtue of (2) this quantity is considerably less than the depth of the potential well, which also is evidence of the strong bond between the nuclei in the cold condensate, and thereby of the stability of the latter.*

As R decreases the value of E_0 increases more rapidly than U, and at extremely high compression when R becomes of the order of A_0, the nucleus cannot be held by the potential well. In spite of the 0 temperature, the condensate is destroyed by a process that can be called "cold evaporation." It must be noted, incidentally, that electron capture begins long before that and leads to a transition of the matter into a neutron state; in view of this, the upper part of the figure given here is only tentative.

We now consider the influence of the temperature, an effect that reduces to an increase in the average energy of the nucleus. The corresponding factor for an oscillator is $\coth(\hbar\omega/2kT)$. Thus, the ratio of the nuclear energy to the depth of the well is of the form

$$\xi = (A_0/R)^{1/2}\coth[(Z^2e^2/2RkT)(A_0/R)^{1/2}]. \tag{6}$$

It plays the role of a criterion of phase transition: when $\xi \ll 1$ and $\xi \gg 1$ we deal with condensed and plasma states respectively. If $\xi \sim 1$, no definite conclusions can be made, owing to the inapplicability of the approach itself. The figure shows the approximate course of the curve $\xi = 1$. When $T > T_{cr} \sim 10^8Z^5$ deg, the condensed state is altogether impossible, and when $T < T_{cr}$ the condensate region is bounded both from below (the usual thermal evaporation) and from above ("cold evaporation").

Under the conditions of w.d., $Z^2e^2/RkT = 84 \gg 1$, $\hbar\omega/2kT = 0.11 \ll 1$. Hence

$$\xi \approx 2RkT/Z^2e^2 = 0.024 \ll 1.$$

*We note that the usual arguments that lead to the equation of equilibrium of a w.d. become, strictly speaking, unsuitable for w.d. heavier than Sirius B, owing to the Klein paradox. This question will be considered separately.

*With this, the amplitude of the zero oscillations of the nucleus is approximately one order of magnitude less than R (cf. the basic premise of the Lindeman melting theory).

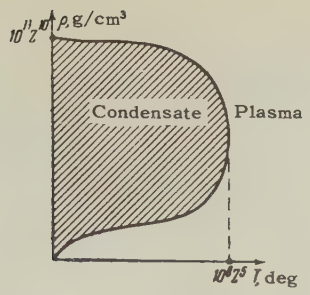

The latter estimate makes it possible to speak with a great degree of confidence on the condensed state of the matter in w.d.

Let us determine the displacement of the nucleus during a time t in the diffusion process; according to Seit[7]

$$l \sim R\,(\omega t)^{1/2} \exp\,(-\,W/2kT).$$

The activation energy W cannot be obtained from an examination of an isolated cell; therefore the estimates given below are quite tentative.

Putting $W \sim Z^2e^2/R$, we find that during the entire time of existence of w.d. ($\sim 10^{17}$ sec) the nucleus shifts merely by a distance on the order R. One can therefore speak of a solid (possibly amorphous) state of the matter in w.d.

Let us make two remarks. We have seen earlier that for the condensate to exist the system of nuclei must be rarefied [see Eq. (2)]. Under this condition, an important role is played by the internuclear correlation, which, in the final analysis, causes the plasma condensation. A "crystallization" of similar kind of a rarefied degenerate electron gas was considered by Wigner.[8]

We note furthermore that during the process of formation of the w.d. the latent heat of condensation should be liberated. This source of energy can apparently play a noticeable role and should be taken into account in the theory of stellar evolution.

We proceed to consider a model in which, in addition to the heavy component with average $Z \neq 10$, there exist also protons. The heavy nuclei, as noted above, form a more or less stable skeleton of the system; with this, at least "in the small," one can speak of a crystalline lattice. The latter will be considered, for the sake of being definite, as face-centered cubic (close packing). We shall also assume that one proton belongs to each crystalline cell of this lattice. This makes the concentration of hydrogen by weight on the order of $[\eta\,(4Z+1)]^{-1} \approx 1\%$ (for heavy w.d. the volume of condensate is close to the total volume of the w.d.).

Let us separate an individual crystal cell and replace it by an equivalent sphere, where the charge of the heavy nuclei is uniformly distributed over the surface of the sphere. Designating the corresponding quantity with a subscript 1, we shall have $R_1 = 4^{1/3}R$. The potential energy of the proton in the cell is

$$U_1(r) = -\,(4Z+3)/2R_1 + (4Z+1)\,r^2/2R_1^3, \qquad (7)$$

whence $\omega_1 = \sqrt{2}\,\omega$.

We have furthermore $\xi_1 = [2 \times 4^{1/3}Z^2/(4Z+3)]\,\xi = 0.17$. Thus, the protons are more weakly bound in the condensate than the heavy nuclei; however, the character of their motion differs greatly from thermal. The protons are displaced relatively slowly over the condensate and vibrate with high frequency about the equilibrium positions.

Let us find the diffusion path l (see above) for protons. Assuming that W is not less than the depth of the potential well, and taking accordingly $W \sim 2Z/R_1$, we obtain $l \sim 10^5$ cm, which is approximately four orders less than the radius of the w.d. Thus, (if this estimate is confirmed by more accurate calculation), there is no need to fear that the greater part of the protons will diffuse into the plasma periphery of the w.d., and will be taken out of play there by the nuclear reaction.

3. RATE OF NUCLEAR REACTION IN WHITE DWARFS

In the introduction we already indicated that, other conditions being equal, the rate of the principal reaction for w.d., $p + p = d + e^+ + \tilde{\nu}$ in the solid phase should be less than in the plasma phase.

We shall estimate now the rate of this reduction for the model considered in the end of the last section (we shall henceforth drop the subscript 1).

The rate of reaction in the plasma phase is

$$q' \sim \overline{\sigma' v}\, n^2, \qquad (8)$$

where σ' is the reaction cross section (allowing for the penetration coefficient) and n is the proton concentration.

In the condensed phase, as can be readily seen, the rate of reaction is independent of the rate of diffusion of nuclei (the change in the number of nuclei which the given nucleus encounters per unit time is exactly compensated for by the opposite change in the fraction of the time spent near them). If ω is the frequency of the oscillation (the number of approaches of the nucleus to the barrier per unit time) then the rate of reaction in the condensate is

$$q \sim b(\sigma/R^2)\,\omega n \sim b\sigma\omega R n^2, \qquad (9)$$

where $b = 6$ is the number of neighboring protons. In practice $b\omega R/v = 1$ and

$$q/q' \sim \sigma/\sigma'$$

(the velocity v is taken at the saddle point, see below). Thus, in spite of the different kinetic mechanism, the rates of reaction in the plasma and condensed phases differ only in the characteristics of the elementary act (more accurately speaking, in the penetration factors).

Let us proceed to calculate the latter. If the interaction potential between protons has the form $V(r) = e^2\varphi(x)/r$, $x = r/R$, then the usual procedure (see, for example, reference 1) leads to the following expression for the coefficient of penetration:

$$K(\varphi) \sim \exp\{-\tau(\varphi - {}^2/_3 x_0\varphi')/(\varphi - x_0\varphi')^{3/2}\}.$$

The saddle point x_0 is determined by the equation

$$x_0^{3/2} = \alpha(\varphi - x_0\varphi').$$

Here $\tau = 3(\pi^2 e^2/4A_0 kT)^{1/2}$, $\alpha = (2/\pi)(A_0/R)^{1/2} \times (e^2/RkT)$, the functions φ and φ' refer to the argument x_0. For pure Coulomb interaction $K(1) = e^{-\tau}$. In finding φ we shall assume that the protons react while in different (neighboring) cells.* For plasma one usually assumes the following expression for V:[1]

$$V(r) = (e^2/r)(1 - \tfrac{3}{2} r/R_0 + \tfrac{1}{2} r^3/R_0^3) \quad \text{for } r < R_0,$$
$$V(r) = 0 \quad \text{for } r > R_0.$$

Here $R_0 = R[\eta(4Z+1)]^{-1/3}$ is the radius of a neutral sphere containing the proton. Thus, allowance for the screening of the protons by the electron gas yields

$$\varphi(x) = \begin{cases} 1 - 3Z^{1/3}x + 4Zx^3, & x < 1/2Z^{1/3}, \\ 0, & x > 1/2Z^{1/3}. \end{cases}$$

In the case of a condensate it is necessary to add a term that takes into account the proton bond in the lattice. Considering that the protons are on the average arranged symmetrically with respect to the boundary that separates their cells, we obtain with the aid of (7)

$$\delta\varphi = Zx(2-x)^2.$$

This term corresponds to the potential well referred to in Section 2, and leads to an effective increase in the repulsion between protons.

The sought reduction in reaction rate is given by the ratio $A = K(\varphi + d\varphi)/K(\varphi)$. Numerical calculations yield $\alpha = 0.0315$, $x_0 = 0.094$, and

$$A \sim 10^{-9}. \qquad (10)$$

Since this quantity has the significance of a probability of emergence from the potential well and depends relatively little on ρ, one can assume this estimate to be valid for a greater portion of the core of a dense w.d. The smallness of A is evidence that the factor that limits the hydrogen content is not the reaction rate, but the model selected by us (see end of Sec. 2). Models with greater hydrogen contents require a special investigation; in any case, a concentration on the order of several percent is quite possible.

I express my deep gratitude to Academician I. E. Tamm, V. L. Ginzburg, and I. S. Shklovskiĭ for interest in this work and for useful advice. I sincerely thank S. A. Kaplan and N. N. Pariĭskiĭ for numerous discussions and valuable comments.

*The statistical weight of the configuration, in which a noticeable number of cells contain two or more protons, is negligible.

[1] E. Schatzman, White Dwarfs, North-Holland, Amsterdam, 1958. J. Greenstein, Scient. American, No. 1, 46 (1959).

[2] W. Wildhack, Phys. Rev. **57**, 81 (1940).

[3] Ya. B. Zel'dovich, JETP **33**, 991 (1957), Soviet Phys. JETP **6**, 760 (1958).

[4] G. and E. Burbridge, Handb. der Physik, **51**, 190 (1959).

[5] R. Marshak, Astrophys. J. **92**, 321 (1940). T. Lee, ibid. **111**, 625 (1950), S. A. Kaplan, Астрономический журнал (Astronomy Journal) **27**, 31 (1950).

[6] E. Öpick, Anthology, Nuclear Processes in Stars (Russ. Transl.), IIL, M., 1957.

[7] W. Seit, Diffusion in Metals, Russ. Transl., IIL, M., 1958.

[8] E. Wigner, Phys. Rev. **34**, 678 (1938).

Translated by J. G. Adashko
102

STATISTICAL THEORY OF MULTIPLE PARTICLE PRODUCTION

A. I. NIKISHOV

P. N. Lebedev Physics Institute, Academy of Sciences, U.S.S.R.

Submitted to JETP editor August 8, 1959

J. Exptl. Theoret. Phys. (U.S.S.R.) **38**, 509-512 (February, 1960)

If equilibrium does not set in during a collision, one can employ the statistical theory for estimating the mean values of the squares of the matrix elements. In this case, one can hope to obtain satisfactory agreement with experiments for the multiplicity, charge state, and momentum distributions irrespective of the charge of the particle.

1. In the work of Witten and Block the energy spectra of π^+- and π^--mesons were given for the reaction $\pi^- + p \to n + \pi^- + \pi^+$ at an energy of 1.8 Bev. Corresponding calculations carried out by Maksimenko[2] according to statistical theory, with account of isobaric states, did not give agreement for these spectra which were considered separately for each sign of the charge of the pions. However, the total spectrum of the charged mesons agrees satisfactorily with the calculation.[2] Better agreement of the results of the statistical theory with experimental data on multiplicity, total spectrum and distribution over charge states (see references 2 — 4) leads to the thought that the circumstance just mentioned is not accidental.

Let us consider in detail the reaction $\pi^- + p \to n + \pi^- + \pi^+$.[2] By first using only isotopic invariance, we find the general expression for the matrix element and investigate its perturbation symmetry. We shall use the method of Belinfante.[5] We denote by $f(1, 2, 3) \equiv f(p_1, p_2, p_3)$ the part of the wave function of the system $n\pi^+\pi^-$ which is independent of the isotopic variables. We shall assume that variables 1 and 2 refer to mesons, while the variable 3 refers to the nucleon. As usual we denote the isotopic function of the proton by $[\frac{1}{2}, \frac{1}{2}]_3$, and that of the neutron by $[\frac{1}{2}, -\frac{1}{2}]_3$. The analogous functions for the π^+-meson will be $[1, 1]_1$ or $[1, 1]_2$, depending on whether it refers to the first or second meson (i.e., it refers to a particle whose momentum is denoted by p_1 or p_2). The total wave function of the system $n\pi^+\pi^-$ is obtained by symmetrization of the function $f(1, 2, 3)[\frac{1}{2}, -\frac{1}{2}]_3[1, 1]_1[1, -1]_2$ over the momentum and isotopic variables of the mesons:

$$\Psi_f = \Psi_{n+-} = \sqrt{\tfrac{1}{2}}\{f(1, 2, 3)[1,1]_1[1,-1]_2 + f(2, 1, 3)[1,1]_2[1,-1]_1\}\left[\tfrac{1}{2},-\tfrac{1}{2}\right]_3 \quad (1)$$

Expanding the isotopic functions in definite total isotopic spins, we transform Eq. (1) to the form

$$\Psi_{n+-} = f_s\{\sqrt{\tfrac{1}{10}}\left[\tfrac{5}{2},-\tfrac{1}{2}\right]_{312} - \sqrt{\tfrac{1}{15}}\left[\tfrac{3}{2},-\tfrac{1}{2}\right]_{312}\} - f_a\{\sqrt{\tfrac{1}{3}}\left[\tfrac{3}{2},-\tfrac{1}{2}\right]_{312} - \sqrt{\tfrac{1}{6}}\left[\tfrac{1}{2},-\tfrac{1}{2}\right]_{312}\} + f_s\sqrt{\tfrac{1}{3}}\left[\tfrac{1}{2},-\tfrac{1}{2}\right]_{312};$$

$$f_s = \sqrt{\tfrac{1}{2}}\{f(1, 2, 3) + f(2, 1, 3)\},$$

$$f_a = \sqrt{\tfrac{1}{2}}\{f(1, 2, 3) - f(2, 1, 3)\}$$

(see the similar calculations of Belinfante[5]). If now for simplicity we limit ourselves to a definite total spin, for example $T = \frac{1}{2}$, then

$$M_{n+-} = \sqrt{\tfrac{1}{6}}\, M_a + \sqrt{\tfrac{1}{3}} M_s,$$

$$|M_{n+-}|^2 = \tfrac{1}{6}|M_a|^2 + \tfrac{1}{3}|M_s|^2 + \sqrt{\tfrac{2}{9}}\,\mathrm{Re}\, M_a M_s^*. \quad (2)$$

If summation is carried out over the isotopic variables of the mesons, then the term $\mathrm{Re}\, M_a M_s^*$ drops out, since it is antisymmetric relative to a permutation of the isotopic variables of the mesons. Summation shows that we are interested in the momentum distribution irrespective of the sign of the charge of the mesons. We now make use of the assumption

$$\overline{\sum |M_a|^2} = \overline{\sum |M_s|^2} = \Omega^3.$$

It then follows from Eq. (2) that

$$\overline{\sum |M_{n+-}|^2} = \tfrac{1}{2}\Omega^3.$$

Thus even if $\mathrm{Re}\, M_a M_s^* \neq 0$, the statistical theory can give the correct results relative to the total energy spectrum.

2. We now consider the annihilation processes

$$\tilde{n} + p \to \pi^+ + \pi^+ + \pi^-, \qquad \tilde{n} + p \to \pi^+ + \pi^0 + \pi^0.$$

We symmetrize the function $\varphi(1, 2, 3)[1, 1]_1 \times [1, 1]_2 [1, -1]_3$ in similar fashion:

$$\Psi_{++-} = \sqrt{\tfrac{1}{3}} \{\varphi(1, 2, 3)[1, 1]_1[1,1]_2[1,-1]_3 + \varphi(1, 3, 2)[1,1]_1[1,1]_3[1,-1]_2 + \varphi(2, 3, 1)[1,1]_2[1,1]_3[1,-1]_1\}. \quad (3)$$

Since the mesons 1 and 2 are identical, we can assume

$$\varphi(1, 2, 3) = \varphi(2, 1, 3).$$

Expansion of the isotopic functions entering into Eq. (3) in terms of functions with a definite total isotopic spin T is given in the table. For example, according to the table we have

$$[1,1]_1[1,1]_3[1,-1]_2 \equiv [1_+3_+2_-] = \sqrt{\tfrac{4}{15}} e_0 - 2\sqrt{\tfrac{1}{12}}(e_1 - e_2) + \sqrt{\tfrac{1}{15}} e_3.$$

The Young diagrams[6] corresponding to irreducible representations are shown in the drawing. The diagram a corresponds to the functions e_0 and

e_3, the diagram b to the functions e_1, e_1', e_2, and e_2'. The quantity $e_0 = [1, 1]$ is the isotopic function of three mesons forming a system with a total isotopic spin T = 1. The Young diagram in the figures shows that in a permutation of the isotopic variables of the mesons 1, 2, 3, the function e_0 is transformed into itself.[7] Similarly, $e_2 = [2, 1]$ is the isotopic function with T = 2, $T_3 = 1$. In the permutation of the isotopic variables, e_2 and e_2' are transformed into linear combinations of themselves without involving the other e. All of the e functions are orthogonal.

By making use of the table, we transform Eq. (3) to the form

$$\Psi_{++-} = \sqrt{\tfrac{4}{15}} \varphi_s e_0 + \sqrt{\tfrac{1}{6}}(\varphi_1 e_1 + \varphi_1' e_1') + \sqrt{\tfrac{1}{15}} \varphi_s e_3;$$

$$\varphi_s = \sqrt{\tfrac{1}{3}} \{\varphi(1, 2, 3) + \varphi(1, 3, 2) + \varphi(2, 3, 1)\},$$

$$\varphi_1 = \sqrt{\tfrac{1}{6}} \{\varphi(1, 2, 3) - 2\varphi(1, 3, 2) + \varphi(2, 3, 1)\},$$

$$\varphi_1' = \sqrt{\tfrac{1}{2}} \{\varphi(1, 2, 3) - \varphi(2, 3, 1)\}. \quad (4)$$

We immediately note the structure of Eq. (4). Each term of it represents the product of a momentum part by an isotopic part. The factors in the product have the same permutation symmetry, as follows from the table and the form of the functions φ_S, φ_1, and φ_1' in (4). This property is preserved even for systems with an arbitrary

	e_0	e_1	e_1'	e_2	e_2'	e_3
$1_+2_+3_-$	2	1	1	−1	−1	1
$1_+3_+2_-$	2	−2	0	2	0	1
$2_+3_+1_-$	2	1	−1	−1	1	1
$1_0 2_0 3_+$	−1	1	1	1	1	2
$1_0 3_0 2_+$	−1	−2	0	−2	0	2
$2_0 3_0 1_+$	−1	1	−1	1	−1	2
Square of the normalizing factor	$\frac{1}{15}$	$\frac{1}{12}$	$\frac{3}{12}$	$\frac{1}{12}$	$\frac{3}{12}$	$\frac{1}{15}$
T	1	1	1	2	2	3

number of mesons, as will be shown somewhat later. In this case it is essential that the isotopic functions are orthonormalized (see reference 7), while the functions e are not orthonormalized. In the language of group theory, this means that the product φe contains only a single representation of the product of two groups of permutations when the permutation symmetry of φ and e is identical.

Returning now to Eq. (4), we have the matrix element corresponding to it:

$$M_{++-} = \sqrt{\tfrac{4}{15}} M_0 + \sqrt{\tfrac{1}{6}}(M_1 + M_1').$$

Once again it is easy to see that the sum over the isotopic variables is equal to

$$\sum |M_{++-}|^2 = \tfrac{4}{15} |M_0|^2 + \tfrac{1}{6}(|M_1|^2 + |M_1'|^2)$$

By making further use of the assumption of Fermi, we obtain

$$\overline{\sum |M_{++-}|^2} = \tfrac{3}{10} \Omega^3.$$

In this formula the identity of the two π^+ mesons is also taken into account.

Similarly one can find

$$\overline{\sum |M_{+00}|^2} = \tfrac{1}{5} \Omega^3$$

Unfortunately, such a complete cancellation of the term $M_i M_k^*$ $(i \neq k)$ does not always take place. For example, it is not difficult to prove that

$$\Psi_{n+--} = \sqrt{\tfrac{1}{3}} \{\sqrt{\tfrac{4}{5}} \varphi_s e_0 + \sqrt{\tfrac{1}{2}}(\varphi_1 e_1 + \varphi_1' e_1') - \sqrt{\tfrac{1}{2}}(\varphi_1 e_2 + \varphi_1' e_2') + \sqrt{\tfrac{1}{5}} \varphi_s e_3\} [\tfrac{1}{2}, -\tfrac{1}{2}].$$

It can also be demonstrated that

$$M_{n+--} = \sqrt{\tfrac{4}{15}} M_0 + \sqrt{\tfrac{1}{6}}(M_1 + M_1') - \sqrt{\tfrac{1}{30}}(M_2 + M_2').$$

After summation over the isotopic variables, the terms $\mathrm{Re}\, M_1 M_2^*$ and $\mathrm{Re}\, M_1' M_2'^*$ do not generally vanish. The fact that the results of the calculation by means of statistical theory with account of isobaric states agree with experiment points to the fact that the remaining cross terms are small.

3. In the case of a system consisting only of mesons and having a definite total spin T, all of the cross terms cancel each other identically upon summation over the isotopic variables. This can be established in the following way. The total wave function of the final state in which we are interested is obtained by symmetrization of the functions $f(1, 2, \ldots n)[1, 2, \ldots n]$, i.e.,

$$\Psi = cf(\ldots j \ldots)[\ldots j \ldots], \tag{5}$$

c is the normalizing coefficient and $[\ldots j \ldots]$ is the isotopic function of the system obtained from the initial $[1, 2, \ldots n]$ as the result of the j-th permutation (compare the obtaining of Eq. (3) for the system $\pi^+\pi^+\pi^-$, where $[1, 2, 3] = [1, 1]_1[1, 1]_2[1, -1]_3$).

We further represent $[\ldots j \ldots]$ in the form

$$[\ldots j \ldots] = a_{ij}e_i, \tag{6}$$

where the e_i are orthonormalized functions forming the bases of an irreducible representation of the permutation group (so that summation over i is a summation over types of irreducible representations and over the numbers of basic functions of the representation of the given type); for the particular n = 3, and total charge 1, see the table. Hence,

$$\Psi = cf(\ldots j \ldots)a_{ij}e_i = c\varphi_i e_i. \tag{7}$$

It is important that $\varphi_i = a_{ij}f(\ldots j \ldots)$ have exactly the same permutation structure as e_i, if all the e_i are orthonormal. Actually,

$$e_i = bc_{ij}[\ldots j \ldots] + b'c_{ij}[\ldots j \ldots]' + \ldots. \tag{8}$$

The terms $[\ldots j \ldots]'$ etc refer to other charge states with the same total charge as $[\ldots j \ldots]$; c_{ij} are determined by the type of permutation symmetry; b, b′ etc (actually these are the Clebsch-Gordan coefficients) depend on what total spin T corresponds to e_i. Since $e_i e_k = \delta_{ik}$, then it follows from (6) and (8) that $c_{ij} = a_{ij}$. In this connection the cross terms $\mathrm{Re}\, M_i M_k^*$ $(i \neq k)$ vanish in the square of the matrix element upon summation over the isotopic variable because, for $i \neq k$, there is no unique representation[8] in the product $M_i M_k^*$.

In conclusion, I express my gratitude to I. L. Rozental' and V. M. Maksimenko for interested discussions, and also thank F. Cerulus and R. Hagedorn for supplying preprints of their work.

[1] R. C. Witten and M. M. Block, Phys. Rev. **111**, 1676 (1958).

[2] Maksimenko, Nikishov, and Rozental', Материалы конференции по физике высоких энергий в Киеве (Materials of the Conference on High-energy Physics, Kiev, 1959) (paper of V. I. Veksler).

[3] Belen'kiĭ, Maksimenko, Nikishov, and Rozental', Usp. Fiz. Nauk **62**, 1 (1957).

[4] F. Cerulus and R. Hagedorn, Particle Production in 6.2-Bev p-p Collisions by a Statistical Model (preprint). R. Hagedorn, Calculation of High-energy Particle Production on an Electronic Computer (preprint).

[5] F. J. Belinfante, Phys. Rev. **92**, 145 (1953).

[6] L. Landau and E. Lifshitz, Квантовая механика (Quantum Mechanics) Gostekhizdat, 1948; English translation, Addison Wesley, 1958.

[7] V. B. Berestetskiĭ, Dokl. Akad. Nauk SSSR **92**, 519 (1953).

[8] L. Landau and E. Lifshitz, op. cit., Par. 94.

Translated by R. T. Beyer
103

RADIATIVE CORRECTIONS TO PHOTOPRODUCTION AND SINGLE-PHOTON ANNIHILATION OF PAIRS

S. Ya. GUZENKO and P. I. FOMIN

Physico-technical Institute, Academy of Sciences, Ukrainian S.S.R.

Submitted to JETP editor August 10, 1959

J. Exptl. Theoret. Phys. (U.S.S.R.) **38**, 513-517 (February, 1960)

General formulas have been obtained for radiative corrections to photoproduction and single photon annihilation of electron-positron pairs. Some limiting cases are considered.

1. An expression for radiative corrections to the differential cross section of pair production by a photon in a Coulomb field (photoproduction) can be obtained from the general formula for corrections to bremsstrahlung,[1,2] by making use of the well-known "substitution rule" (see, for example, reference 3, p. 162) which reduces in the given case to the substitution

$$p_1 \to -p_+, \qquad p_2 \to p_-, \qquad k \to -k, \tag{1}$$

where $p_1 = (\mathbf{p}_1, i\epsilon_1)$, $p_2 = (\mathbf{p}_2, i\epsilon_2)$ and $k = (\mathbf{k}, i\omega)$ are the initial and final momenta of the electron and the momentum of the photon in the bremsstrahlung; $p_+ = (\mathbf{p}_+, i\epsilon_+)$, $p_- = (\mathbf{p}_-, i\epsilon_-)$ and $k = (\mathbf{k}, i\omega)$ are the momenta of the positron, electron, and photon in photoproduction.

In addition to the substitution (1), it is necessary to take the following into account. The expression for the radiative corrections to the bremsstrahlung contains the parameter y, which is determined by the equation

$$4\sinh^2 y = \rho - \varkappa - \tau \tag{2}$$

and, in particular, the transcendental function

$$h(y) = y^{-1}\int_0^y u \coth u du. \tag{3}$$

A similar parameter will enter into the correction for photoproduction. In the case of bremsstrahlung, y is real, since

$$\rho - \varkappa - \tau = 2(\varepsilon_1\varepsilon_2 - \mathbf{p}_1\mathbf{p}_2) - 2 \geqslant 0. \tag{4}$$

For photoproduction we have, with account of (1),

$$\rho - \varkappa - \tau = -2(\varepsilon_+\varepsilon_- - \mathbf{p}_+\mathbf{p}_-) - 2 \leqslant -4. \tag{5}$$

This means that y becomes complex, and the integration in (3) is carried out in the complex plane.

In the case of photoproduction, we define a new parameter z by the relation

$$y = z - i\pi/2. \tag{6}$$

On the basis of (2), we obtain

$$4\cosh^2 z = \varkappa + \tau - \rho \geqslant 4, \tag{7}$$

i.e., z is real.

Carrying out the integration in (3) over the appropriate path (in this connection, see the paper by Harris and Brown[4]) and taking it into account that only the real parts of the corresponding functions enter into the cross section, we obtain as a result the following substitution rule:

$$yh(y) \to zg(z) \equiv \int_0^z u\tanh u du,$$

$$2yh(2y) \to 2zh(2z) - \pi^2/2 \equiv \int_0^{2z} u\coth u du - \pi^2/2,$$

$$(y \pm x)h(y \pm x) \to (z \pm x)g(z \pm x) \equiv \int_0^{z\pm x} u\tanh u du. \tag{8}$$

As a result of the changes, which are connected with (1), (6) and (8), the following result is obtained for the cross section of photoproduction:*

$$d\sigma = d\sigma_0[1 - (e/2\pi)^2\delta_R], \tag{9}$$

where $d\sigma_0$ is given by the Bethe-Heitler formula[5,6] and

$$\delta_R = 2W(x) + [U(\varkappa, \tau, \rho; -\varepsilon_+, \varepsilon_-) + U(\tau, \varkappa, \rho; \varepsilon_-, -\varepsilon_+)]/U_0, \tag{10}$$

$$W(x) = (1 - x\coth x)\left(1 - \frac{1}{3}\coth^2 x\right) - \frac{1}{9},$$

$$4\sinh^2 x = \rho, \tag{11}$$

*We shall use units in which $c = \hbar = m = 1$, $e^2/4\pi = 1/137$.

$$2U(\varkappa, \tau, \rho; -\varepsilon_+, \varepsilon_-) = -T^2 2z/\sinh 2z$$
$$+ U_0\{2(1-2z\coth 2z)\ln\lambda$$
$$+ 4z\coth 2z\,[h(2z) - g(z) - \pi^2/4z] + 2 - z\tanh z$$
$$+ (4+\rho)\,z/\sinh 2z + 2\tau M\} + (-\tau U_0 - S_1\partial/\partial\varkappa$$
$$+ S_5\partial/\partial\varkappa + S_6\partial/\partial\alpha + S_7\partial/\partial_t)\,J(u^2) + (S_2\partial/\partial\varkappa$$
$$+ S_3\partial/\partial\alpha + S_4\partial/\partial\rho)\,J(u) + (\tau U_0 + S_1\partial/\partial\varkappa + S_8\partial/\partial\alpha$$
$$+ S_9\partial/\partial_t)\,J(u^2V) + (S_{10} - S_{11}\varkappa\partial/\partial\varkappa$$
$$+ {}^1/_2 S_{12}\varkappa^2\partial^2/\partial\varkappa^2)\,J(isu) + (S_{13} - S_{14}\varkappa\partial/\partial\varkappa$$
$$+ {}^1/_2 S_{15}\varkappa^2\partial^2/\partial\varkappa^2)\,J(isuv_1). \qquad (12)$$

The expressions $J(\ldots)$ appearing here are expressed by Eqs. (A 5) and (37)—(40) of reference 1, with the substitution $y\coth y \to z\tanh z$, and

$$L = 2\left(z^2 - x^2 - \frac{\pi^2}{4}\right) + F(\varkappa - 1) - F(-1),$$
$$M = 2\sinh^{-1}2z\,\{z\ln\varkappa + zg(z) - (z+x)\,g(z+x)$$
$$- (z-x)\,g(z-x)\},$$
$$N = \int_0^1 \frac{dv}{1+(1-v)\,v\rho - \varkappa v}\ln\left|\frac{1+(1-v)\,v\rho}{\varkappa v}\right|,$$
$$F(x) = \int_0^1 \frac{\ln|1+v|}{v}\,dv \qquad (13)$$

with the new values of the parameters:

$$\varkappa = 2\omega(\varepsilon_- - p_-\cos\theta_-),\quad \theta_- = \widehat{\mathbf{kp}}_-,$$
$$\tau = 2\omega(\varepsilon_+ - p_+\cos\theta_+),\quad \theta_+ = \widehat{\mathbf{kp}}_+,$$
$$\alpha = \varkappa + \tau,\quad \omega = \varepsilon_+ + \varepsilon_-,$$
$$\rho = -2 + \varkappa + \tau - 2(\varepsilon_+\varepsilon_- - p_+p_-\cos\theta),$$
$$\theta = \widehat{\mathbf{p}_+\mathbf{p}_-},\quad p = |\mathbf{p}|, \qquad (14)$$

U_0, T^2 and S_i are obtained from the corresponding expressions in the case of bremsstrahlung [Eqs. (14) and (41) of reference 1] by direct substitution of (1).

It is necessary to add the cross section of pair photoproduction, which is accompanied by radiation of a soft photon, to the cross section (9); the energy of this photon does not exceed a certain $\Delta E \ll m$, which is determined by the accuracy of the measurements. This cross section, integrated over the momentum of the soft photon, is equal to[3]

$$d\sigma_D = d\sigma_0\,(e/2\pi)^2\delta_D, \qquad (15)$$
$$\delta_D = \frac{1}{4\pi}\int_0^{\Delta E}\frac{dk_1}{\sqrt{k_1^2+\lambda^2}}\left(\frac{p_-}{p_-k_1} - \frac{p_+}{p_+k_1}\right)^2 = 2(1-2z\coth 2z)\ln\frac{\lambda}{2\Delta E}$$
$$+ \frac{1}{2}\left[\frac{1}{v_+}\ln\frac{1+v_+}{1-v_+} + \frac{1}{v_-}\ln\frac{1+v_-}{1-v_-} - Y(z, \varepsilon_+, \varepsilon_-)\cosh 2z\right],$$
$$v_+ = p_+/\varepsilon_+,\qquad v_- = p_-/\varepsilon_-,$$
$$Y(z, \varepsilon_+, \varepsilon_-) = \int_{-1}^{1}\frac{dv}{\cosh^2 z - v^2\sinh^2 z}\,\frac{\varepsilon_v}{p_v}\ln\left|\frac{\varepsilon_v v + p_v}{\varepsilon_v - p_v}\right|,$$
$$2\varepsilon_v = \varepsilon_+ + \varepsilon_- + (\varepsilon_+ - \varepsilon_-)\,v,\quad p_v^2 = \varepsilon_v^2 + v^2\sinh^2 z - \cosh^2 z.$$

In the total cross section, which has the form

$$d\sigma = d\sigma_0\{1 - (e/2\pi)^2(\delta_R - \delta_D)\}, \qquad (17)$$

the term containing the "mass" of the photon λ disappears.

2. From the principle of detailed balance, it is easy to obtain the result that the radiative corrections to the single photon pair annihilation in a Coulomb field are described by the same expressions as the corrections to the photoproduction, if we mean by p_+, p_-, k the momenta of the annihilating pair and the radiated photon.

3. Let us consider some limiting cases of radiative correction to photoproduction:

1) Photoproduction at threshold ($p_+, p_- \ll 1$)

$$\delta_R = -\frac{\pi^2}{|v_+ - v_-|} + a + b\,\frac{\cos\theta - \cos\theta_+\cos\theta_-}{\frac{p_+}{p_-}\sin^2\theta_+ + \frac{p_-}{p_+}\sin^2\theta_-} + O(p_+, p_-), \qquad (18)$$
$$\delta_D = O(p_+, p_-),$$
$$a = \frac{65}{18} - \frac{13}{48}\pi^2 + \frac{5}{8}F(3) + \frac{7}{4}\Delta + \frac{29}{9}\ln 2$$
$$- \frac{53}{12}\sqrt{2}\ln(1+\sqrt{2}) - \frac{3}{2}\ln^2(1+\sqrt{2}) = 2,4;$$
$$b = 3 - \frac{5}{24}\pi^2 + \frac{1}{4}F(3) - \Delta - 2\ln 2 + 2\sqrt{2}\ln(1+\sqrt{2})$$
$$- \ln^2(1+\sqrt{2}) = -1,\ 0;$$
$$\Delta = F\left(\frac{-3}{2+\sqrt{2}}\right) + F\left(\frac{-3}{2-\sqrt{2}}\right) - F\left(\frac{-1}{2+\sqrt{2}}\right)$$
$$- F\left(\frac{-1}{2-\sqrt{2}}\right) - F(-3) + F(1) = 2.8. \qquad (19)$$

The first term in (18), which diverges as the relative velocity approaches zero, arises as a result of the fact that account of the interaction of the produced electron and positron is carried out automatically in radiative corrections in the first Born approximation. For a more detailed discussion, see reference 4.

2) Relativistic case of equal energies ($\epsilon_+ = \epsilon_- \gg 1$) at small angles ($\theta^2, \theta_+^2, \theta_-^2 \ll 1/\epsilon^2$). In this case, the momentum transferred to the external field is small ($\rho \ll 1$).

$$\delta_R = -\pi^2/2z + \frac{13}{2} - \pi^2/4 + O(\varepsilon^2\theta^2), \qquad (20)$$
$$\delta_D = O(\varepsilon^2\theta^2\ln\varepsilon). \qquad (21)$$

The small invariant quantity $2z$ in the center-of-mass system of the pair has the meaning of relative velocity of the electron and positron. The term $-\pi^2/2z$ is completely analogous to the first term of Eq. (18) in the threshold case.

3) Ultrarelativistic case. Assuming the angles to be sufficiently large, we write

$$\ln(\alpha - \rho),\quad \ln\varkappa,\quad \ln\tau,\quad \ln\rho \gg 1,$$

However,

$$\ln\frac{\alpha-\rho}{\varkappa},\quad \ln\frac{\alpha-\rho}{\tau},\quad \ln\frac{\rho}{\varkappa},\quad \ln\frac{\rho}{\tau} \sim 1.$$

It is not difficult to prove that in this case δ_R and δ_D can be obtained directly from the asym-

ptotic expressions (5) and (6) of reference 2* by the substitution

$$y = \frac{1}{2}\ln(\rho - \alpha) \to z = \frac{1}{2}\ln(\alpha - \rho),\ \varepsilon_1 \to \varepsilon_+,\ \varepsilon_2 \to \varepsilon_-.$$

The equations thus obtained can be written in the form:

$$\delta_R = 2(1 - \ln 2p_+p_-)\ln\lambda + \ln 2p_+p_-\left(\frac{1}{2}\ln 2p_+p_- - \frac{13}{6}\right) + O(1), \quad (22)$$

$$\delta_D = (1 - \ln 2p_+p_-)(2\ln\lambda + \ln[\varepsilon_+\varepsilon_-/(\Delta E)^2]) + \frac{1}{2}\ln^2 2p_+p_- + O(1), \qquad p_+p_- = \varepsilon_+\varepsilon_- - \mathbf{p}_+\mathbf{p}_-. \quad (23)$$

In the limiting case under consideration, the radiative corrections to photoproduction were calculated earlier by Drell et al.[7] Our result (22) coincides with their formula (27), while (23) differs somewhat from their Eq. (28) which is brought about by a different determination of ΔE in the reference mentioned.[7]†

*We note that an error in sign occurred in (5) of reference 2 and in (56) of reference 1 in front of the term 4x/3.

†We note that the expression obtained in reference 8 for the ultrarelativistic case of radiative corrections to the bremsstrahlung does not coincide with the corresponding formula (5) of reference 2 [or (56) of reference 1] and, consequently, does not agree (for corresponding substitution of parameters) with the result (27) of reference 7.

4. Analogous limiting cases for single photon pair annihilation are described by the same equations (18) – (23) with corresponding change in the meaning of the parameters.

The authors are grateful to Professor A. I. Akhiezer for advice and discussion.

[1] P. I. Fomin, JETP **35**, 707 (1958), Soviet Phys. JETP **8**, 491 (1959).

[2] P. I. Fomin, JETP **34**, 227 (1958), Soviet Phys. JETP **7**, 156 (1958).

[3] J. M. Jauch and F. Rohrlich, Theory of Photons and Electrons, Cambridge, Mass., 1955.

[4] I. Harris and L. M. Brown, Phys. Rev. **105**, 1656 (1957).

[5] H. Bethe and W. Heitler, Proc. Roy. Soc. (London) **146**, 83 (1934).

[6] A. I. Akhiezer and V. B. Berestetskiĭ, Квантовая электродинамика (Quantum Electrodynamics), Gostekhizdat, 1953, AEC Tr.

[7] Bjorken, Drell, and Frautschi, Phys. Rev. **112**, 1409 (1958).

[8] Mitra, Narayanaswamy, and Pande, Nucl. Phys. **10**, 629 (1959).

Translated by R. T. Beyer
104

S-MATRIX IN THE GENERALIZED QUANTIZATION METHOD

D. V. VOLKOV

Physico-technical Institute, Academy of Sciences, Ukrainian S.S.R.

Submitted to JETP editor August 10, 1959

J. Exptl. Theoret. Phys. (U.S.S.R.) **38**, 518-523 (February, 1960)

The formalism of the S-matrix for interacting electromagnetic field and half-spin particle field is considered. Particle field quantization is carried out according to a scheme suggested in the works of Green[1] and the author.[2] It is shown that the basic concepts of the conventional theory of S-matrices (N-product, Wick's theorem, Feynman graphs) allow a simple generalization within the framework of the quantization scheme considered.

1. The customary methods of quantization of wave fields use as commutation relations commutators or anticommutators based on a choice of completely symmetric or completely antisymmetric wave functions in the configuration space of many identical particles. The confinement to symmetric or antisymmetric wave functions corresponds to the experimental data known at present as regards the statistics of elementary particles, but is evidently not rigorously established from the theoretical point of view. The problem as to why other possibilities are not realized in nature, "equally valid in the sense of the correspondence principle," in which "lies the essence of this limited choice of nature" (Pauli[3]), has been discussed in lively fashion in the literature in the period of the development of quantum mechanics (see, for example, reference 3).

With the development of methods of quantum theory, great progress has been achieved in the understanding of the connection of symmetric and antisymmetric wave functions with the value of the spin of particles[4] and with the TCP invariance.[5,6] However, consideration of the problems mentioned has always been carried out within the framework of the following alternative: either symmetric or antisymmetric wave functions; all other possibilities have been entirely neglected.

In this connection it is of interest to attempt to formulate this old problem, which arises in nonrelativistic quantum mechanics, in terms of the theory of wave fields.

The generalization of the existing methods of quantum field theory, which takes into consideration the presence not only of symmetric and antisymmetric wave functions, but which is also compatible with the fundamental premises of relativistic quantum theory, was carried out in the work of Green[1] and later in a research of the author.[2]*

In references 1 and 2, however, questions connected with interaction were not considered. At the same time the possibility was not excluded that precisely the interaction between fields could be decisive for explanation of the separation of the existing methods of quantization.†

In the present article we consider the formalism of the scattering matrix (S-matrix) for interacting electromagnetic field and the field of half-spin charged particles. Quantization of the field of the particles is carried out on the basis of transformed commutation relations [see below, Eq. (3)]. It is shown that, in spite of the change of the quantization rules, there exists a unique procedure of expansion of the S-matrix in a series of normal derivatives (analogous to the usual technique of Wick[8]), which makes it possible to isolate the vacuum effects in the S-matrix. The results obtained without any essential change are applicable also to other local variants of interacting fields.

2. The scattering matrix for the case under consideration has the form

$$S = T\left(\exp\left(-i\int H(x)\,d^4x\right)\right), \qquad (1)$$

where H(x) is the Hamiltonian density in the interaction representation

$$H(x) = ie\,[\bar{\psi}(x),\ \gamma_\alpha\psi(x)]\,A_\alpha(x), \qquad (2)$$

*The work of Green was not known to the author during preparation of reference 2 for publication.

†The possible connection of the symmetry of a wave function with a definite type of interaction in nonrelativistic quantum mechanics has been investigated by Yaffe.[7]

$\psi(x)$ and $\bar{\psi}(x) = \psi^+(x)\gamma_4$ are the field operators of particles satisfying the Dirac equation without interaction in the commutation representation*

$$\psi_\alpha(x)\psi_\beta(x')\psi_\gamma(x'') + \psi_\gamma(x'')\psi_\beta(x')\psi_\alpha(x) = 0$$

$$\psi_\alpha(x)\bar{\psi}_\beta(x')\psi_\gamma(x'') + \psi_\gamma(x'')\bar{\psi}_\beta(x')\psi_\alpha(x) = -iS_{\alpha\beta}(x-x')\psi_\gamma(x'') - iS_{\gamma\beta}(x''-x')\psi_\alpha(x),$$

$$\bar{\psi}_\alpha(x)\bar{\psi}_\beta(x')\psi_\gamma(x'') + \psi_\gamma(x'')\bar{\psi}_\beta(x')\bar{\psi}_\alpha(x) = -iS_{\gamma\beta}(x''-x')\psi_\alpha(x). \quad (3)$$

$A_\mu(x)$ are the operators of the electromagnetic field, which satisfy the usual rules of commutation.

Thanks to the commutability of the operators $H(x)$ and $H(x')$, the T-product in Eq. (1) outside the light cone is determined in a unique, relativistically-invariant fashion.

The operators of the electromagnetic field and the field of particles commute with one another; therefore the T-product in Eq. (1) can be represented in the form of the products of two independent T-products, one of which contains only the field operators of the particles, while the other contains only the operators of the electromagnetic field. The latter of these T-products will not be considered, since it has the same form as in ordinary theory.

The absence in the quantization method under consideration of simple commutation rules between the two operators makes difficult the separation of the vacuum effects in the T-product, which depend on the field operators of the particles, and requires a generalization of the concept of normal product.

In order to make clear the idea of such a generalization, let us look first at the simplest case, in which there are two operators: a_k is the destruction of a particle in the state k and a_l^+ that of the creation of a particle in the state l [or, similarly the operators b_k (b_k^+) of destruction (creation) of antiparticles].

The fundamental properties of these vectors are defined by the relations (9), (13), and (14) of I.

Let us determine the normal product $N(a_l^+ a_k)$ of the operators a_l^+ and a_k by the direct action of the N-product on the arbitrary basis vector:†

$$N(a_l^+ a_k)\, a_1^+ a_2^+ \ldots a_n^+\Phi_0 = \delta_{k1} a_l^+ a_2^+ \ldots a_n^+\Phi_0 + \delta_{k2} a_1^+ a_l^+ \ldots a_n^+\Phi_0 + \ldots + \delta_{kn} a_1^+ a_2^+ \ldots a_l^+\Phi_0 = \sum_{j=1}^{n} \delta_{kj}\, a_1^+ \ldots a_{j-1}^+ a_l^+ a_{j+1}^+ \ldots a_n^+\Phi_0, \quad (4)$$

where Φ_0 is the vector of the vacuum state for noninteracting fields and the indices 1, 2, ... n determine the state of the particle.

As is seen directly from the definition (4), the N-product in the first place preserves the symmetry of the wave function, which is important in the establishment of the connection with nonrelativistic theory, and, in the second place, does not contain the vacuum effects, which are connected with the possibility of the destruction by the operator a_k of a particle previously created by the operator a_l^+.

We note that in the quantization with anticommutators, the determination just considered of the normal derivative coincides with the usual one.

Making use of the commutation relations for the operators a and a^+ (9,I), it is easy to find an explicit expression for the normal product $N(a_l^+ a_k)$ in terms of the operators a_l^+ and a_k:

$$N(a_l^+ a_k) = a_l^+ a_k - a_k a_l^+ - \delta_{lk}. \quad (5)$$

The normal product of the operators b_k^+ and b_l is determined in similar fashion:

$$N(b_l b_k^+)\, b_1^+ b_2^+ \ldots b_n^+\Phi_0 = -\sum_{j=1}^{n} \delta_{jl}\, b_1^+ \ldots b_{j-1}^+ b_k^+ b_{j+1}^+ \ldots b_n^+\Phi_0, \quad (6)$$

where

$$N(b_l b_k^+) = b_l b_k^+ - b_k^+ b_l + \delta_{kl}. \quad (7)$$

For the case of two particle and antiparticle creation operators, and correspondingly for two destruction operators, we determine the normal product with the aid of the following relations:

$$N(a_l^+ b_k^+) = a_l^+ b_k^+ - b_k^+ a_l^+, \quad (8)$$

$$N(b_l a_k) = b_l a_k - a_k b_l. \quad (9)$$

The relations (5), (7) — (9) make it possible to write down the current operator in the form of a normal product. Actually, if the wave functions of the particle and antiparticle in the state k are connected by the relation $v_k = C\bar{u}_k$, where C is the charge-conjugation matrix, u_k and v_k are the coefficients in the expansion (7, I), then $\bar{u}_k\gamma_\mu u_k = \bar{v}_k\gamma_\mu v_k$, as a consequence of which,

$$ie[\bar{\psi}(x),\ \gamma_\mu\psi(x)] = ieN[\bar{\psi}(x)\gamma_\mu\psi(x)]. \quad (10)$$

In the general case, the N-product depends on an arbitrary number of pairs of operators* and is determined by the following relations:

*We use the notation of reference 2, which is cited below as I.

†In Eq. (4) [and in the subsequent formula (6)] the operators b^+ (or a^+) which can enter into the determination of the basis vector are omitted. Such operators, if there are any, do not affect the action of the N-products considered in (4) and (6), and without change in their position go over into the right-hand parts of the corresponding equations.

*We limit ourselves here to a consideration of the N-products only of an even number of field operators of the particles. Such a limitation is not essential in what follows, since an even number of particle field operators always enters into the S-matrix and into all observable physical quantities.

$$N(a_1^+a_2; \ldots;\ a_{1'}^+b_{2'}^+; \ldots;\ b_{1''}a_{2''}; \ldots;\ b_{1'''}b_{2'''}^+; \ldots)$$
$$= N(a_1^+b_{2'}^+) \ldots N(a_1^+a_2; \ldots) N(b_{1'''}b_{2'''}^+; \ldots) N(b_{1''}a_{2''}) \ldots \quad (11)$$

The order of arrangement of pairs of operators under the sign of the N-product in this formula is arbitrary.

The normal products $N(a_1^+a_2; \ldots)$ and $N(b_1b_2^+; \ldots)$ in Eq. (11) depend only on pairs of operators of the form a^+a and bb^+, respectively. The N-products of such a type are determined, similarly to (4) and (6), by the action of these products on the basis vectors:

$$N(a_k^+a_l;\ a_m^+a_r; \ldots)\, a_1^+a_2^+ \ldots a_n^+\Phi_0 =$$
$$= \sum_{i,\ j, \ldots = 1}^{n} \delta_{li}\,\delta_{rj} \ldots a_1^+ \ldots a_{i-1}^+a_k^+a_{i+1}^+ \ldots a_{j-1}^+a_m^+a_{j+1}^+ \ldots a_n^+\Phi_0, \quad (12)$$

$$N(b_kb_l^+;\ b_mb_r^+; \ldots)\, b_1^+b_2^+ \ldots b_n^+\Phi_0 = (-1)^P \sum_{i,\ \ldots = 1}^{n} \delta_{ki}\,\delta_{mj}$$
$$\ldots b_1^+ \ldots b_{i-1}^+b_l^+b_{i+1}^+ \ldots b_{j-1}^+b_r^+b_{j+1}^+ \ldots b_n^+\Phi_0, \quad (13)$$

summation in (12) and (13) is carried out over all non-coinciding indices; P is the number of pairs of operators of the form bb^+ (see the last footnote but one).

Equations (8), (9), and (11) — (13) determine the N-product for an arbitrary even number of operators and make it possible to represent any product of N-products (including the T-product) in the form of a sum of normal products.

As an example, let us consider the product $N[\bar\psi(1)\psi(2)]\,N[\bar\psi(3)\psi(4)]$ (the numbers 1, 2, 3, 4 indicate the dependence of the operators on the coordinates and spinor indices). Making use of the commutation relations for the operators a, a^+, b and b^+ [Eqs. (3) and (9,I)] and the determination of the normal products, we obtain

$$N(\bar\psi(1)\psi(2))\,N(\bar\psi(3)\psi(4)) = N(\bar\psi(1)\psi(2);\ \bar\psi(3)\psi(4))$$
$$- iS^+(2,\ 3)\,N(\bar\psi(1)\psi(4)) + iS^-(4,\ 1)\,N(\bar\psi(3)\psi(2))$$
$$- 2S^+(2,\ 3)\,S^-(4,\ 1), \quad (14)$$

where S^+ and S^- are the usual (+)- and (−)-fold commutation functions:

$$S^+(x) = -\frac{i}{(2\pi)^3}\left(\gamma\frac{\partial}{\partial x} - m\right)\int_{p_0>0} \delta(p^2 + m^2)\, e^{ipx}d^4p,$$

$$S^-(x) = \frac{i}{(2\pi)^3}\left(\gamma\frac{\partial}{\partial x} - m\right)\int_{p_0<0} \delta(p^2 + m^2)\, e^{ipx}d^4p. \quad (15)$$

A similar formula holds for the T-product

$$T[N(\bar\psi(1)\psi(1'))\,N(\bar\psi(2)\psi(2'))] = N(\bar\psi(1)\psi(1');\bar\psi(2)\psi(2'))$$
$$+ S^F(1',\ 2)\,N(\bar\psi(1)\psi(2')) + S^F(2',\ 1)\,N(\bar\psi(2)\psi(1'))$$
$$- 2S^F(1',\ 2)\,S^F(2',\ 1), \quad (16)$$

where

$$S^F(x) = \frac{i}{(2\pi)^4}\left(\gamma\frac{\partial}{\partial x} - m\right)\int \frac{1}{p^2 + m^2 - i\varepsilon}\, e^{ipx}d^4p;\ \varepsilon \to 0 \quad (17)$$

The prime indicates the possible difference of spinor indices in the corresponding operators.

In the general case of a T-product from an arbitrary number of N-products, the following rule holds, similar to the rule of Wick in the ordinary quantization theory.

In order to expand a T-product of the form

$$T[N(\bar\psi(1)\psi(1'))\,N(\bar\psi(2)\psi(2'))\ldots N(\bar\psi(n)\psi(n'))$$

in a sum of normal products, it is necessary to consider all possible couplings of operators $\psi(a')$ and $\bar\psi(b)$, which do not enter into the composition of one and the same normal product, and to substitute these couplings in the functions $S^F(a', b)$. As a result of the superposition of the couplings, all the N-products located under the sign of the T-product are united in groups which are uncoupled among themselves, and which either contain no operators (closed loops) or contain two operators $\bar\psi(a)$ and $\psi(b')$ (open lines). In the latter case, it is necessary to join the two disconnected operators in a pair and to put under the sign N-products of the form $N(\bar\psi(a)\psi(b')\ldots)$. In the presence of closed loops, each of them must be multiplied by an additional factor of 2.*

We note that the rule formulated above has the usual graphical interpretation in terms of a Feynman diagram.

3. The relations considered in the preceding section make it possible to investigate in a simple fashion the matrix element of the scattering matrix corresponding to some particular process. As an illustration, we consider the process of scattering of two particles.

In order to determine completely the state of the two particles (in the given system of quantization), it is necessary, in addition to the quantities that characterize the individual states (spin, momentum), also to give the symmetry of the wave function (in the case of pure states) or the rela-

*The fundamental difference between the ordinary technique of Wick[8] and its generalization considered here consists in the appearance of an additional factor of 2 in the closed loops. The appearance of this factor takes place not only for virtual processes, but also for processes which occur with the creation of pairs of real particles and antiparticles (as a consequence of the normalization of the operator wave function). In the case of more complicated schemes of quantization,[1] which lead in the general case to statistics of particles with maximal occupation number m for each of the individual states, the expansion of the T-product in a sum of N-products takes place in precisely the same fashion, but in this case each closed loop acquires an additional factor of m.

tive weights* of the symmetric and antisymmetric functions (for mixed states).

The basic orthonormalized vectors of states for different types of symmetry have the form

$$\frac{1}{\sqrt{2}}(a_k^+ a_l^+ \pm a_l^+ a_k^+)\Phi_0; \quad k \neq l,$$

k and l are indices characterizing the spin and angular momentum of the individual states.

To determine the probability amplitudes of the scattering process under consideration, we compute the matrix elements of the N-product between the different basis vectors.

Separating in the N-products the terms giving non-vanishing contributions to the matrix element $N(\bar{\psi}(1)\gamma_\mu\psi(1);\bar{\psi}(2)\gamma_\mu\psi(2))$

$$= 2N(a_{k'}^+ a_k; a_{l'}^+ a_l)\,\bar{u}_{k'}(1)\gamma_\mu u_k(1)\bar{u}_{l'}(2)\gamma_\nu u_l(2)$$
$$+ 2N(a_{l'}^+ a_k; a_{k'}^+ a_l)\,\bar{u}_{l'}(1)\gamma_\mu u_k(1)\,\bar{u}_{k'}(2)\gamma_\nu u_l(2), \qquad (18)$$

where the primed indices characterize the state of the particles in the final states, while $u_k(1)$ etc are wave functions of single particle states, and noting that as a consequence of (12),

$$N(a_k^+ a_k;\ a_l^+ a_l)\frac{1}{\sqrt{2}}(a_k^+ a_l^+ \pm a_l^+ a_k^+)\Phi_0$$
$$= \frac{1}{\sqrt{2}}(a_k^+ a_{l'}^+ \pm a_{l'}^+ a_{k'}^+)\Phi_0,$$

$$N(a_{l'}^+ a_k;\ a_{k'}^+ a_l)\frac{1}{\sqrt{2}}(a_k^+ a_l^+ \pm a_l^+ a_k^+)\Phi$$
$$= \frac{1}{\sqrt{2}}(a_{l'}^+ a_{k'}^+ \pm a_{k'}^+ a_{l'}^+)\Phi_0, \qquad (19)$$

we get the following expression for the non-vanishing matrix elements:

*A more detailed realization of the state (furnishing of coefficients in the expansion of the wave function over symmetric and antisymmetric states) has no meaning because of the identity of the particles.

$$\Phi_0^* \frac{1}{\sqrt{2}}(a_{l'}a_{k'} \pm a_{k'}a_{l'})\,N(\bar{\psi}(1)\gamma_\mu\psi(1);\bar{\psi}(2)\gamma_\nu\psi(2))\frac{1}{\sqrt{2}}$$
$$\times(a_k^+ a_l^+ \pm a_l^+ a_k^+)\Phi_0 = 2(\bar{u}_{k'}(1)\gamma_\mu u_k(1)\,\bar{u}_{l'}(2)\gamma_\nu u_l(2)$$
$$\pm \bar{u}_{l'}(1)\gamma_\mu u_k(1)\,\bar{u}_{k'}(2)\gamma_\nu u_l(2)). \qquad (20)$$

Taking into account the sign (−) in Eq. (20), we obtain the well-known formula of Møller. The sign (+) in Eq. (20) leads to the following expression for the scattering cross section (in the center-of-mass system):

$$d\sigma_{(+)} = \frac{r_0^2}{\varepsilon^2(\varepsilon^2-1)^2}\left\{\frac{(2\varepsilon^2-1)^2}{\sin^4\theta} - \frac{4\varepsilon^4 - 5\varepsilon^2 + 5/4}{\sin^2\theta} + \frac{(\varepsilon^2-1)^2}{4}\right\}.$$

For the case of a mixed state, the scattering cross sections $d\sigma^+$ and $d\sigma^-$ are averaged with the corresponding weighting factors.

In conclusion the author expresses his gratitude to A. I. Akhiezer, S. V. Peletminskiĭ and P. I. Fomin for valuable discussions.

[1] H. Green, Phys. Rev. **90**, 270 (1953).
[2] D. V. Volkov, JETP **36**, 1560 (1959), Soviet Phys. JETP **9**, 1107 (1959).
[3] W. Pauli, General Principles of Wave Mechanics (Russian translation, IIL, 1947).
[4] W. Pauli, Relativistic Theory of Elementary Particles (Russian translation, IIL, 1957).
[5] J. Schwinger, Phys. Rev. **82**, 914 (1951).
[6] W. Pauli, article in the volume, Niels Bohr and the Development of Physics (Russian translation IIL, 1958).
[7] G. Yaffe, Z. Physik **66**, 748 (1930).
[8] G. C. Wick, Phys. Rev. **80**, 268 (1950).

Translated by R. T. Beyer
105

ELECTRON RELAXATION TIME IN A HIGH FREQUENCY ELECTROMAGNETIC FIELD AND THE SURFACE IMPEDANCE OF A METAL

R. N. GURZHI and M. Ya. AZBEL'

Physico-technical Institute, Academy of Sciences, Ukrainian S.S.R.

Submitted to JETP editor August 12, 1959

J. Exptl. Theoret. Phys. (U.S.S.R.) **38**, 524-528 (February, 1960)

The effect of quantization of the electromagnetic field and electron orbits in a constant magnetic field on the relaxation time of electrons in a metal due to electron-phonon interactions is studied; the effect on the surface impedance of the metal is also considered. The complete frequency region (normal skin effect, anomalous skin effect, infrared region) up to the internal photoeffect limit has been investigated. It is shown that the quantization of the orbits is significant only in the anomalous skin effect region for $\omega \sim \Omega \gtrsim kT/\hbar$ (Ω is the cyclotron frequency, T = temperature). Quantization of the electromagnetic field is always important in the infrared region and for the anomalous skin effect in a constant magnetic field (throughout the whole magnetic field region for $\omega \sim \Omega$ and only for cyclotron resonance when $\omega \gg \Omega$).

THE surface impedance of a metal in a variable electromagnetic field either in the absence or in the presence of a constant magnetic field has been investigated in a number of researches (see, for example, references 1 — 3). In almost all researches devoted to this problem, the classical collision integral for electrons and phonons has been employed.

At the same time, quantum effects can have a strong effect on the relaxation time of the electron gas in a metal, thus changing the dependence of the surface impedance of the metal on frequency, temperature and magnetic field (see, for example, the researches of one of the authors[4]). These effects become important when the characteristic energy entering into the problem is of the order of or greater than kT (k is Boltzmann's constant, and T the temperature). Such an energy can arise for several reasons.

In the first place, as a consequence of the quantization of the levels of the electron in a constant magnetic field **H**, the distance between the levels $\Delta\epsilon = \hbar\Omega$ (Ω is the frequency of revolution of the electron, see reference 5) becomes of the order of kT at helium temperatures in a field $H \sim 10^4$ oe.

In the second place, owing to the quantization of the energy of the electromagnetic field, the value of the quantum $\hbar\omega$ is already of the order of kT (ω is the frequency) at helium temperatures for centimeter waves.

In the third place, when the energy is associated with the spatial inhomogeneity of the distribution of electrons in the metal (spatial dispersion) $v_z\Delta p \sim v_z\hbar/\Delta$ (the z axis is directed along the normal to the surface of the metal, v is the velocity of the electron, **p** its momentum, and Δ a depth, characterizing the spatial inhomogeneity). In different cases, Δ has different forms; however, if we take $\Delta \sim 10^{-5}$ cm and $v_z \sim v$, then $\hbar v_z/\Delta \sim kT$ at $T = 100°$.

We shall now consider under what conditions each of the characteristic energies appears.

1. EFFECT OF QUANTUM PHENOMENA ON THE FREQUENCY OF ELECTRON-PHONON COLLISIONS

The results given below were obtained by means of a rigorous analysis of the corresponding equations, which we shall not write down because of their comparatively complicated form; we shall instead limit ourselves to qualitative considerations.

As is well known, in the consideration of the skin effect in metals, the following three important regions are usually distinguished: the region of the normal skin effect ($l \ll \delta$, where l is the mean free path, and δ the skin depth), the region of the anomalous skin effect ($l \gg \delta$), and the infrared region ($v/\omega \ll \delta$).

We first investigate the role of quantum phenomena in the region of the normal skin effect and in the infrared region since the analysis is relatively simple in these cases.

a) It is easy to prove that quantum phenomena

are not important in the case of the normal skin effect. This is connected with the fact that long before any of the characteristic energies exceeds kT, one has reached the region of the anomalous skin effect.*

b) In the infrared region of the spectrum, as had been noted previously, the inequality $v/\omega \ll \delta$ is satisfied (in the case of a quadratic law of dispersion of the electrons, $\delta^{-2} = 4\pi ne^2/mc^2$, where n n is the density of the electrons and m is the electronic mass). Since in the given case $\Delta \approx \delta$, it follows from this inequality that $v\hbar/\Delta \ll \hbar\omega$. It can be shown that the effect is nonetheless important, since the energy connected with the spatial inhomogeneity frequently exceeds the energy of the phonon which can be absorbed or emitted by the electron; actually, the usual condition is $v\hbar/\delta \gtrsim k\Theta$ (Θ is the Debye temperature of the material, which characterizes the upper boundary of the phonon spectrum). However, as a quantitative analysis shows, the only determining quantity in the given case is the ratio $v/\omega\delta$; therefore, account of spatial dispersion has no effect on the time of free flight.

It is easy to establish the fact that quantization of the electron levels in a magnetic field in the infrared region is not important. Actually, at practically obtainable fields, the inequalities $\hbar\Omega \ll \hbar\omega$ and $\hbar\Omega \ll k\Theta$ are satisfied; therefore, the energy of the phonons with which the electrons interact is large in comparison with $\hbar\Omega$ (independent of the relations between the quantities kT, $k\Theta$, and $\hbar\omega$).

Account of the quantization of the electromagnetic field in the infrared region was taken earlier (see reference 4).

c) In the case of the anomalous skin effect, the fundamental contribution to the surface impedance in the classical consideration is made, as is well known, by the small fraction of the electrons which move almost parallel to the surface of the metal (see, for example, reference 6), for which $v_z/v \lesssim (\delta/l)^{1/3}$. For these electrons, the quantity $v_z\hbar/\Delta$, even if it exceeds kT, is still small, which leads to a mean free path which is large in comparison with the length l, determined, say, by the collisions with atomic impurities. For the remaining electrons, spatial dispersion leads to a significant decrease in the mean free path (it is shown that $l \sim v_z^{-3}$) and, consequently, their contribution to the impedance increases. However, as calculations show, the "slipping" electrons still play the principal role. The considerations given here evidently remain valid even in the presence of a magnetic field.*

The situation is different in the consideration of quantum effects brought about by the quantization of the electromagnetic field and electronic orbits. In the anomalous skin effect, in the absence of a constant magnetic field, the time of free flight, as is well known, generally drops out of the expression for the surface impedance (see reference 7).† However, in the presence of a constant magnetic field parallel to the boundary of the metal, the surface impedance depends essentially on τ, and the quantum effect connected with $\hbar\omega$ and $\hbar\Omega$ must generally be taken into account.

In the present work, we limit ourselves to the case $\Omega \ll \omega$; consideration of the region $\Omega \gtrsim \omega$, where it is necessary to take into account both types of quantization, will be the subject of another article.

2. RELAXATION TIME FOR CYCLOTRON RESONANCE IN METALS

The anomalous skin effect in the presence of a constant magnetic field parallel to the boundary of the metal was considered by one of the authors and Kaner.[6,8] In these researches, an expression was obtained for the surface impedance in an arbitrary magnetic field. However, if one is not speaking of the rather uninteresting case of square law dispersion of electrons, then the simple formulas for frequency and temperature dependence hold in three cases: weak magnetic fields (when the radius of revolution of the electron in the magnetic field $r \gg l^2/\delta$), strong fields ($r \ll l$) and, finally, resonance frequency ($\omega \approx \Omega n$; $n = 1, 2, \ldots$).

In the case of weak magnetic fields, the surface impedance depends upon the relaxation time τ only in the combination $l^* = l/(1+i\omega\tau)$ (see ref-

*In the region of the normal skin effect, $\hbar\Omega \sim kT$ at practically unattainable fields, $H \sim 10^6$ oe. Here we are dealing with the fundamental electron bands; the case of anomalously small bands requires special consideration (which can lead to the appearance of quantum oscillations of the impedance with the magnetic field).

*The effect of spatial inhomogeneity on the frequency of electron-phonon collisions is possibly important in the consideration of the fluctuations of the electron density in a metal. Actually, in this case, the spatial inhomogeneity of the distribution of electrons is important, and at the same time electrons with all velocity directions play a role.

†We note that in the quantum consideration ($\hbar\omega \gg kT$) this result is valid not with accuracy up to terms of higher order in δ/l (as was the case in the classical approximation), but with accuracy up to terms of higher order in $1/\omega\tau(\omega) \sim \omega^2$ [see Eq. (3) of the present article]. However, these terms become important in a frequency region of little interest – for $\lambda = 2\pi c/\omega \lesssim 10^{-2}$ cm.

erence 8). On the other hand, for $\hbar\omega \gg kT$, $\omega\tau(\omega) \gg 1$ always [this follows from Eq. (3) of the present article] and consequently τ drops out in the first approximation.

In the case of strong fields, i.e., for $r \ll l$ or, what is the same thing, for $\Omega\tau \gg 1$ (and simultaneously, $\omega\tau \gg 1$), as is easily seen, τ also does not enter into the final formula for the surface impedance.

Finally, we come to the consideration of the resonance region. Here the surface impedance depends essentially on the relaxation time. Quantization in the magnetic field has not been considered in the present research, the results obtained being applicable only to harmonics of the cyclotron resonance ($\omega \approx 2\Omega, 3\Omega, \ldots$), where $\Omega < \omega$.

In the region of frequencies of the electromagnetic field that is of most interest, $\hbar\omega \ll k\Theta$ (this inequality is equivalent to $\lambda \gg 1/\Theta$, where λ is in centimeters, and Θ is in degrees), so that in what follows we shall assume

$$k\Theta \gg \hbar\omega \gg kT. \tag{1}$$

An expression was obtained in reference 9 for the quantum collision integral of electrons with phonons. If we write the collision integral in the form

$$\left(\frac{\partial}{\partial t} f_1(\mathbf{p})\right)_{\text{col}} = f_1(\mathbf{p}) \int d\mathbf{p}' K(\mathbf{p}, \mathbf{p}') + \int d\mathbf{p}' f_1(\mathbf{p}') Q(\mathbf{p}, \mathbf{p}')$$

(here $f_1(\mathbf{p})$ is a nonequilibrium addition to the electron distribution function, $\mathbf{p}$ is the momentum of the electron) then under the conditions of the anomalous skin effect the second term on the right hand side is small; consequently the time of free flight of the electron $\tau(\mathbf{p})$ can be introduced (see reference 6);

$$\left(\frac{\partial}{\partial t} f_1(\mathbf{p})\right)_{\text{col}} \approx \frac{1}{\tau(\mathbf{p})} f_1(\mathbf{p}), \qquad \frac{1}{\tau(\mathbf{p})} = \int d\mathbf{p}' K(\mathbf{p}, \mathbf{p}').$$

In finding the surface impedance, one must calculate integrals of the form

$$\int_0^\infty d\varepsilon \frac{\partial f_0}{\partial \varepsilon} \psi\left(\frac{1}{\tau(\mathbf{p})}\right),$$

where $f_0(\epsilon)$ is the Fermi electron distribution function, $\epsilon(\mathbf{p})$ is the energy of the electron, ψ is some function of $1/\tau$ (see reference 6).

Since the function $\psi(1/\tau)$ generally has a complicated form, the calculation of similar integrals in the general case meets with difficulties (in particular, such is the case in the classical consideration). However, if the inequalities (1) are satisfied, then, as is not difficult to show, $1/\tau(\mathbf{p})$ is a relatively slowly changing function which varies appreciably when the energy changes by an amount of the order of $\hbar\omega$. It is evident that the integral under consideration in this case is simply equal to $-\psi[1/\tau(\mathbf{p}_0)]$, where $\mathbf{p}_0$ is the momentum of the electron on the Fermi surface $\epsilon(\mathbf{p}_0) = \epsilon_0$ (ϵ_0 is the limiting energy).

Starting out from the results of reference 9, it is not difficult to prove that

$$\frac{1}{\tau(\mathbf{p}_0)} = C \int d\mathbf{q} \frac{q^2}{h\nu(\mathbf{q})} \delta(\varepsilon(\mathbf{p}+\mathbf{q}) - \varepsilon_0) \left\{ \coth \frac{h\nu(\mathbf{q})}{2kT} - \frac{1}{2}\left[\tanh \frac{h\nu(\mathbf{q}) + \hbar\omega}{2kT} + \tanh \frac{h\nu(\mathbf{q}) - \hbar\omega}{2kT}\right]\right\}, \tag{2}$$

where the integration is carried out over all possible momenta of the phonons $\mathbf{q}$; $h\nu(\mathbf{q})$ is the energy of the phonon, C is some constant.

As a consequence of (1), the principal contribution to the integral (2) comes from the region of low phonon energy; $h\nu(\mathbf{q}) \lesssim \hbar\omega \ll k\Theta$. In this region, the dispersion law of the phonons can be assumed to be linear (but, in general, anisotropic); $h\nu(\mathbf{q}) = qu(\mathbf{n})$, where $\mathbf{n}$ is the unit vector in the direction of $\mathbf{q}$.

Simple calculations lead to the following results:

$$1/\tau(\mathbf{p}_0) = \tfrac{1}{3}(\hbar\omega/k\Theta)^3 / \tau_0(\mathbf{p}_0),$$
$$\frac{1}{\tau_0(\mathbf{p}_0)} = C(k\Theta)^3 \int d\Omega_{\mathbf{n}} \delta[(\mathbf{v}(\mathbf{p}_0), \mathbf{n})] / [u(\mathbf{n})]^4, \tag{3}$$

where $d\Omega_{\mathbf{n}}$ is the element of solid angle in $\mathbf{q}$-space.

Choosing a spherical system of coordinates with the z axis along the vector $\mathbf{v}(\mathbf{p}_0)$, we find

$$\frac{1}{\tau(\mathbf{p}_0)} = C \frac{(k\Theta)^3}{|\mathbf{v}(\mathbf{p}_0)|} \int_0^{2\pi} \frac{d\varphi}{[u(\varphi)]^4},$$

where $u(\varphi) \equiv u(\theta = \pi/2, \varphi)$.

We note that τ_0 coincides in order of magnitude with the classical high temperature time of free flight, taken at the Debye temperature τ_0^{cl} ($\tau^{cl}(T) = (\Theta/T)\tau_0^{cl}$ for $T \gg \Theta$), in particular for a square law dispersion, $\tau_0 = 3\tau_0^{cl}$.

Now the expression (3) that has been obtained should be substituted in the corresponding equation of reference 6 for resonant values of the real R and imaginary X parts of the surface impedance.*

The frequency and temperature dependence of the quantities R_{res}, X_{res}, $(X/R)_{res}$ have been given, as well as the corresponding frequencies of revolution Ω_{res} in the quantum and classical cases. These quantities also depend on the number of harmonics n; however this dependence is not connected with the form of τ, and therefore remains as before.

*In these equations, the quantity $1/\tau(\mathbf{p}_0)$ appears, averaged over the trajectory of the electron in the magnetic field.

1) Square-law dispersion:

$R_{res}^{qu} \sim \omega^2$, $\Delta^{qu} \sim \omega^2$; $R_{res}^{cl} \sim T^2$, $\Delta^{cl} \sim \omega^{1/2}T^{3/2}$; $X_{res}^{qu} \sim \omega^{4/3}$, $\Delta^{qu} \sim \omega^3$; $X_{res}^{cl} \sim \omega^{1/3}T$, $\Delta^{cl} \sim T^3$; $(X/R)_{res}^{qu} \sim \omega^{-1}$, $\Delta^{qu} \sim \omega^2$; $(X/R)_{res}^{cl} \sim \omega^{1/2}T^{-3/2}$, $\Delta^{cl} \sim \omega^{1/2}T^{3/2}$; $\Delta = |\omega - n\Omega_{res}|$.

2) Ω has a maximum:

$R_{res}^{qu} = X_{res}^{qu} \sim \omega$, $\Delta^{qu} \sim \omega^3$; $R_{res}^{cl} = X_{res}^{cl} \sim \omega^{1/2}T^{1/2}$, $\Delta^{cl} \sim T^3$.

3) Ω has a minimum:

$R_{res}^{qu} \sim \omega^{14/3}$, $\Delta^{qu} \sim \omega^{7/3}$; $R_{res}^{cl} \sim \omega^{2/3}T^{4/3}$, $\Delta^{cl} \sim \omega^{1/3}T^2$; $X_{res}^{qu} \sim \omega$, $\Delta^{qu} \sim \omega^3$; $X_{res}^{cl} \sim \omega^{1/2}T^{1/2}$, $\Delta^{cl} \sim T^3$; $(X/R)_{res}^{qu} \sim \omega^{-2/3}$, $\Delta^{qu} \sim \omega^{7/3}$; $(X/R)_{res}^{cl} \sim \omega^{1/3}T^{-1}$, $\Delta^{cl} \sim \omega^{1/3}T^2$.

[1] E. H. Sondheimer, Adv. in Phys. **1**, 1 (1952).

[2] R. G. Chambers, Canad. J. Phys. **34**, 1395 (1956).

[3] V. L. Ginzburg, Usp. Fiz. Nauk **55**, 469 (1955).

[4] R. N. Gurzhi, JETP **33**, 660 (1957); **35**, 965 (1958), Soviet Phys. JETP **6**, 506 (1958); **8**, 673 (1959).

[5] I. M. Lifshitz and A. M. Kosevich, JETP **29**, 730 (1955), Soviet Phys. JETP **2**, 636 (1956).

[6] M. Ya. Azbel' and E. A. Kaner, JETP **32**, 896 (1957), Soviet Phys. JETP **5**, 730 (1957).

[7] M. Ya. Azbel' and E. A. Kaner, JETP **29**, 876 (1955), Soviet Phys. JETP **2**, 749 (1956).

[8] E. A. Kaner and M. Ya. Azbel', JETP **33**, 1461 (1957), Soviet Phys. JETP **6**, 1126 (1958).

[9] R. N. Gurzhi, JETP **33**, 541 (1957), Soviet Phys. JETP **6**, 422 (1958).

Translated by R. T. Beyer
106

THE MOTION OF A CONDUCTING PISTON IN A MAGNETOHYDRODYNAMIC MEDIUM

I. A. AKHIEZER and R. V. POLOVIN

Physico-technical Institute, Academy of Sciences, Ukrainian S.S.R.

Submitted to JETP editor August 12, 1959

J. Exptl. Theoret. Phys. (U.S.S.R.) **38**, 529-533 (February, 1960)

The types of waves excited in a magnetohydrodynamic medium by a uniformly moving conducting plane (piston) are investigated. The question of the resolution of an initial discontinuity is discussed.

THE purpose of the present paper is the study of the character of waves excited in a magnetohydrodynamic medium of infinite conductivity in which a conducting body moves. This problem is a generalization of the piston problem in ordinary hydrodynamics.

We consider the motion of an infinite plane (piston) with constant velocity $\mathbf{u}$; the conductivity of the piston is assumed to be infinite. The magnetohydrodynamic waves excited in this case can be either stationary shock waves of compression or self-similar rarefaction waves. A fast shock or a self-similar wave moves forward; behind it comes an Alfven discontinuity and, finally, a slow wave, shock or self-similar.[1] Taking it into account that some of the waves enumerated can be absent, we obtain 17 qualitatively different pictures of motion of the liquid, which are realized for different values of the velocity of the piston. The particular case $H_y = H_z = 0$, $u_x = 0$ (the x axis is directed along the normal to the piston) was studied by Bazer,[2] while the special case $u_y = u_z = 0$ was considered by Lyubarskiĭ and Polovin.[3]

1. The problem of the character of the waves excited by the motion of the piston can be studied in the limiting case $V \ll c$, $u \ll c$, where $\mathbf{V} \equiv \mathbf{H}\sqrt{4\pi\rho}$, $\mathbf{H}$ is the intensity of the magnetic field, ρ the density, and c the speed of sound.

Upon satisfaction of these conditions, the density discontinuities in the fast and slow shock and self-similar waves will be small, the relations between the discontinuities of magnetohydrodynamical quantities in the shock and the corresponding quantities in the self-similar waves will be the same; the difference between the shock and the self-similar waves in this approximation is only that the density increases in the shock waves ($\Delta_\rho > 0$), while it decreases in the self-similar wave ($\Delta_\rho < 0$).

The relations between the discontinuities of the magnetohydrodynamic quantities in the fast waves (shock or self-similar) have the form

$$\Delta_+ v_x = (c/\rho)\,\Delta_+\rho\,[1 + (\gamma - 3)\,\Delta_+\rho/4\rho],$$
$$\Delta_+ p = c^2\Delta_+\rho\,[1 + (\gamma - 1)\,\Delta_+\rho/2\rho],$$
$$\Delta_+ \mathbf{v}_t = -V_x\mathbf{V}_t\Delta_+\rho/c\rho, \quad \Delta_+\mathbf{H}_t = \mathbf{H}_t\Delta_+\rho/\rho, \tag{1}$$

where $\gamma \equiv C_p/C_V$, $\mathbf{v}$ the velocity of the liquid, and p the pressure; the index t denotes the tangential component of the vector.

At the Alfven discontinuity, the relations

$$\Delta_A\mathbf{v}_t = -\Delta_A\mathbf{V}_t, \quad \Delta_A(V_t^2) = \Delta_A\rho = \Delta_A p = \Delta_A v_x = 0. \tag{2}$$

are satisfied.

Finally, for the slow waves (shock and self-similar), we have the conditions

$$\Delta_- v_x = (V_{1x}/\rho_1)\,\Delta_-\rho, \quad \Delta_- p = c_1^2\Delta_-\rho,$$
$$\Delta_-\mathbf{v}_t = \mathbf{V}_{1t}\,[1 - (1 - 2c_1^2\Delta_-\rho/V_{1t}^2\rho_1)^{1/2}],$$
$$\Delta_-\mathbf{H}_t/\sqrt{4\pi\rho_1} = \mathbf{V}_{1t}\,[(1 - 2c_1^2\Delta_-\rho/V_{1t}^2\rho_1)^{1/2} - 1] \tag{3}$$

(the index 1 refers to the region lying between the Alfven discontinuity and the slow wave).

Taking into consideration the fact that the medium at infinity is at rest, while on the surface of the piston the boundary condition[2,3] $\mathbf{v} = \mathbf{u}$ ($H_x \neq 0$) is satisfied, we obtain

$$\Delta_+\mathbf{v} + \Delta_A\mathbf{v} + \Delta_-\mathbf{v} = \mathbf{u}. \tag{4}$$

Making use of Eqs. (1) — (4), we can find the values of $\Delta_+\rho$, $\Delta_-\rho$, $\Delta_A\mathbf{V}_t$:

$$\Delta_+\rho/\rho = (u_x/c)\,[1 - (\gamma - 3)\,u_x/4c],$$
$$\frac{\Delta_-\rho}{\rho} = -\frac{u_t^2 - 2\mathbf{u}_t\mathbf{V}_t}{2c^2} + \frac{u_t^2 u_x}{2c^3}(\gamma - 2) - \frac{\mathbf{u}_t\mathbf{V}_t u_x(2\gamma - 5)}{2c^3},$$
$$\Delta_A\mathbf{V}_t = V_{1t}(\mathbf{V}_{1t} - \mathbf{u})/|\mathbf{V}_{1t} - \mathbf{u}| - \mathbf{V}_{1t}. \tag{5}$$

If $\Delta_+\rho > 0$, then the fast wave is a shock; if $\Delta_+\rho < 0$, then it is self-similar; if $\Delta_+\rho = 0$, then the fast wave is absent. Similar relations hold for the slow waves.

2. Let us consider in more detail the case in which the magnetic field, the velocity of the piston,

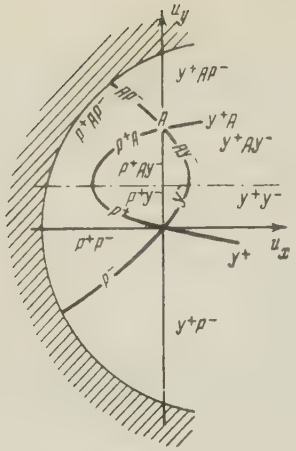

FIG. 1

and the surface normal to it lie in a single plane (the xy plane).

The picture of the motion of the liquid in this case is indicated in Fig. 1 (for definiteness we have set $H_z = 0$, $H_x > 0$, $H_y > 0$). The normal lies along the abscissa, while the tangential component of the velocity of the piston lies along the ordinate. The letters $Y^{\pm}$, $P^{\pm}$, A denote the presence of the shock wave, the rarefaction (self-similar) wave, and the Alfven wave, while the symbol "+" refers to the fast wave and the symbol "–" to the slow wave.

The equations of the curves separating the different regions in Fig. 1 can be obtained from Eqs. (5). Simple transformations lead to the following results.

Equation of the P^+-curve:

$$u_y + \frac{u_x}{c}\frac{V_x V_y}{c + {}^1/_2(\gamma-1)u_x} = 0, \quad -\frac{2c}{\gamma-1} < u_x < 0. \qquad (6)$$

Equation of the P^+A-curve:

$$u_y + \frac{u_x}{c}\frac{V_x V_y}{c + {}^1/_2(\gamma-1)u_x} - 2V_y\left(1 + \frac{\gamma-1}{2}\frac{u_x}{c}\right)^{1/(\gamma-1)} = 0.$$
$$-2c/(\gamma-1) < u_x < 0. \qquad (7)$$

Equation of the Y^+-curve:

$$u_y + u_x V_x V_y / U(U-u_x) = 0; \quad u_x > 0, \quad u_y < 0, \qquad (8)$$

where U is the velocity of the fast shock wave, equal to

$$U = \tfrac{1}{4}(\gamma+1)u_x + \left(\tfrac{1}{16}(\gamma+1)^2 u_x^2 + c^2\right)^{1/2}.$$

The equation of the Y^+A-curve:

$$u_y + u_x V_x V_y / U(U-u_x) - 2V_y\sqrt{U/(U-u_x)};$$
$$u_x > 0, \; u_y > 0. \qquad (9)$$

The curves AP^-, AY^-, Y^-, P^- are described by the equation

$$u_x + V_x u_y (u_y - 2V_y)/2c^2 = 0, \qquad (10)$$

where we have for AP^-, $u_x < 0$, $u_y > 2V_y$; for AY^-, $u_x > 0$, $V_y < u_y < 2V_y$; for Y^-, we have $u_x > 0$, $0 < u_y < V_y$, and for P^-, $u_x < 0$, $u_y < 0$.

Equations (8), and (9) have a region of applicability that is somewhat larger than $V \ll c$, $u \ll c$; to be precise, they are valid under the condition

$$V \ll c, \quad u/c \ll (c/V_y)^{2/(2-\gamma)}.$$

3. The topological structure of Fig. 1 can be obtained even without calculation, on the basis of qualitative considerations. In this case we dispense with the requirement of the smallness of the magnetic field and velocity of the piston.

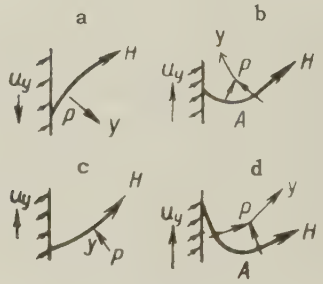

FIG. 2

We first determine through what region the axis of the ordinate passes ($u_x = 0$). Since the magnetic lines of force are "glued" to the particles of the liquid and to the piston, then for $u_y < 0$, the magnetic line of force is deformed as shown in Fig. 2a. The bending of the magnetic line of force leads to the appearance of quasi-elastic tension forces, directed to the side of the concavity (see the arrow in Fig. 2a). Since $v_x = 0$ close to the piston and at infinity, then a compressional wave (shock) arises in front of the arrow, while the rarefaction (self-similar) wave lies behind it. The Alfven wave in the given case does not appear, since H_y close to the piston and at infinity has the same sign. (We recall that the sign of H_y does not change in the shock and self-similar waves,[4] while the contrary is true in the Alfven case.) Thus, for $u_x = 0$, $u_y < 0$, the shock wave travels ahead and the self-similar wave travels behind (the combination Y^+P^-).

Similar considerations show that in the case shown in Fig. 2b, the combination P^+Y^- is realized. Upon increase in the velocity u_y, the sign of H_y close to the piston changes, which leads to the appearance of an Alfven wave (P^+AY^-) (see Fig. 2c). Upon further increase in u_y, the value of $|H_y|$ close to the piston becomes larger than H_y at infinity; in this case the resultant tensile stress is directed out from the piston (see Fig. 2d), which corresponds to the combination Y^+AP^-.

For a sufficiently large value of $|u_y|$, the amplitude of the rarefaction wave becomes so large that the density of the liquid behind the wave vanishes — cavitation sets in.

A picture of the motion of the liquid for $u_x \neq 0$, $u_y \neq 0$, $u_z = 0$ can be obtained by starting out from a consideration of the case $u_x = 0$ given above. Upon increase of u_x, the amplitude of the rarefaction wave decreases, while the amplitude of the compressional wave increases. For a certain value of u_x, the rarefaction wave is transformed into a compressional wave. In a similar way, a decrease of u_x leads to a transformation of the compressional wave into a rarefaction wave. From the qualitative consideration just given, it is also evident that the negative values of u_x make cavitation possible, while positive values hinder it. The region in which cavitation sets in in back of the rarefaction wave is shown in Fig. 1 by the shaded area. The characteristic value of the velocity at which cavitation begins is the velocity of sound.

For $u_t = 0$, $H = 0$, the cavitation condition has the form[5]

$$u_x \leqslant -2c/(\gamma - 1).$$

For $u_x = 0$, $H^2/4\pi \ll p$, numerical calculations[2] lead to the cavitation condition $u_t \geq 3.67\,c$ ($\gamma = 5/3$).

The wave Y^-, AY^-, P^+, AP^+ are possible only for not too large values of the piston velocity; this is connected with the fact that in these waves the value of $|H_y|$ falls off; therefore their amplitude is limited. The waves P^+, AP^+ cannot lead to cavitation, since the relation

$$|\Delta\rho/\rho| < |\Delta H_y/H_y| \leqslant 1$$

is satisfied in the P^+-wave.

The dividing line between the region P^+P^- and P^+AP^- is the curve on which H_y returns to zero after passage of the P^+-wave; the line dividing the regions P^+Y^- from P^+AY^- and Y^+Y^- from Y^+AY^- corresponds to the case in which the tangential magnetic field H_y vanishes in back of the Y^--wave (the special Y^--wave[6]).

4. The problem of the decay of a discontinuity in the initial conditions also reduces to the piston problem. This problem, in the case $\Delta v \ll c$, $\Delta v \ll V$ was considered in reference 7 ($\Delta\mathbf{v}$ is the velocity jump at the initial discontinuity). In the present research, the problem of the decay of an arbitrary discontinuity is investigated under the assumption $\Delta v \ll c$, $V \ll c$ for an arbitrary relation between the characteristic velocities Δv and V. This makes it possible to consider the Alfven discontinuities, in which the angle of deflection of the magnetic field is not small; in particular, it is equal to π if $\Delta\mathbf{v}$, $\mathbf{H}$ on both sides of the discontinuity and the normal to the surface of discontinuity lie in a single plane.

At the initial instant of time $t = 0$, let arbitrary discontinuities of the magnetohydrodynamic quantities Δp, $\Delta\rho$, Δv_x, Δv_t, ΔV_t be given on the surface $x = 0$ (such a situation arises, for example, in the collision of two ionized gaseous masses in a magnetic field). If, the necessary boundary conditions[8] are not satisfied on the surface of the discontinuity, then such a discontinuity decays into seven waves.[7] Velocities of the waves generated are such that not more than three waves can be propagated on each side: in front is the fast magneto-acoustic wave (shock or self-similar); in back is a rotational discontinuity and, finally, the slow magneto-acoustic wave (shock or self-similar). The waves traveling to the left are separated from the waves traveling to the right by a contact discontinuity.

Since the liquid is at rest relative to the contact discontinuity, then the picture of the motion of the liquid on the two sides of the discontinuity will be the same as in the case when the contact discontinuity is replaced by an ideally conducting plane (piston), moving with the same velocity. In contrast with the problem of the piston considered above, the liquid at $x = \pm\infty$ is not at rest, but moves with the given velocities. The velocities of the piston $\mathbf{u}$ relative to the liquid at $+\infty$ and of $\mathbf{u}'$ relative to the liquid at $-\infty$ are related by the self-evident expression:

$$\mathbf{u}' - \mathbf{u} = \Delta\mathbf{v}. \tag{11}$$

In order to determine the velocities of the piston $\mathbf{u}$ and $\mathbf{u}'$, it is necessary to add three more equations, containing $\mathbf{u}$ and $\mathbf{u}'$, to the three equations (11). These equations follow from the condition of continuity of the magnetic field and the pressure on the contact discontinuity:

$$\begin{aligned} \Delta'_+\mathbf{H}_t \div \Delta'_A\mathbf{H}_t \div \Delta'_-\mathbf{H}_t &= (\Delta_+\mathbf{H}_t \div \Delta_A\mathbf{H}_t + \Delta_-\mathbf{H}_t) \div \Delta\mathbf{H}_t, \\ \Delta'_+ p \div \Delta'_- p &= (\Delta_+ p \div \Delta_- p) + \Delta p \end{aligned} \tag{12}$$

(Δ'_+, Δ'_A, Δ'_- denote the jumps of magnetohydrodynamic quantities in the three waves moving to the left. We note that for the waves moving to the left, it is possible to make use of Eqs. (1) to (3) and (5), if $\Delta_\pm\mathbf{v}$, $\Delta_A\mathbf{v}$, $\Delta_\pm p$, $\Delta_\pm\rho$, $\Delta_\pm\mathbf{H}$, $\Delta_A\mathbf{H}$, $\mathbf{u}$ are substituted by $-\Delta'_\pm\mathbf{v}$, $-\Delta'_A\mathbf{v}$, $\Delta'_\pm p$, $\Delta'_\pm\rho$, $\Delta'_\pm\mathbf{H}$, $\Delta'_A\mathbf{H}$, $-\mathbf{u}'$).

If we express the discontinuities of all the quantities in terms of $\mathbf{u}$ and $\mathbf{u}'$ by means of Eqs. (1) to (3) and (5), and make use of Eq. (12), we get

$$u_x + u'_x = -\Delta p / c\rho, \quad \mathbf{u}_t + \mathbf{u}'_t = \Delta \mathbf{V}_t. \qquad (13)$$

Solving Eqs. (11) and (13), we find that the waves traveling to the right of the initial discontinuity will be the same as in the case of motion of a piston in an undisturbed liquid, where the velocity of the piston is equal to

$$u_x = -\tfrac{1}{2}(\Delta p / c\rho + \Delta v_x); \quad \mathbf{u}_t = \tfrac{1}{2}(\Delta \mathbf{V}_t - \Delta \mathbf{v}_t). \qquad (14)$$

Waves traveling to the left from the initial discontinuity will be the same as for a piston moving in the positive direction along the x axis with the velocity $\mathbf{u}''$:

$$u''_x \equiv -u'_x = \tfrac{1}{2}(\Delta p / c\rho - \Delta v_x);$$

$$\mathbf{u}''_t \equiv -\mathbf{u}'_t = -\tfrac{1}{2}(\Delta \mathbf{V}_t + \Delta \mathbf{v}_t) \qquad (15)$$

[in Eqs. (14) and (15), the x axis is directed into the liquid].

The discontinuity in the velocity at the contact discontinuity is shown to be equal to

$$\Delta_c \rho = \Delta\rho - \Delta p / c^2. \qquad (16)$$

The authors express their gratitude to L. I. Serov for suggesting the theme, and to A. I. Akhiezer and G. Ya. Lyubarskiĭ for valuable discussions.

[1] Akhiezer, Lyubarskiĭ, and Polovin, JETP **35**, 731 (1958), Soviet Phys. JETP **8**, 507 (1959).

[2] J. Bazer, Astrophys. J. **128**, 685 (1958).

[3] G. Ya. Lyubarskiĭ and R. V. Polovin, Dokl. Akad. Nauk SSSR **128**, 977 (1959), Soviet Phys.-Doklady **4**, 684 (1960).

[4] R. V. Polovin and G. Ya. Lyubarskiĭ, Ukr. Phys. J. **3**, 571 (1958).

[5] L. D. Landau and E. M. Lifshitz, Механика сплошных сред (Mechanics of Continuous Media) Moscow, Gostekhizdat, 1954, p. 440.

[6] S. I. Syrovatskiĭ, JETP **35**, 1466 (1958), Soviet Phys. JETP **8**, 1024 (1959).

[7] G. Ya. Lyubarskiĭ and R. V. Polovin, JETP **35**, 1291 (1958), Soviet Phys. JETP **8**, 901 (1959).

[8] L. D. Landau and E. M. Lifshitz, Электродинамика сплошных сред (Electrodynamics of Continuous Media) Moscow, Gostekhizdat, 1957, p. 284.

Translated by R. T. Beyer
107

INTERFERENCE OF FORM FACTORS IN LEPTONIC DECAY OF HYPERONS

V. M. SHEKHTER

Leningrad Physico-technical Institute, Academy of Sciences, U.S.S.R.

Submitted to JETP editor August 14, 1959

J. Exptl. Theoret. Phys. (U.S.S.R.) **38**, 534-540 (February, 1960)

It is possible to deduce the energy dependence of the coefficients in front of the products of various form factors in the expression for the probability of leptonic decay of hyperons, and also to predict when part of these coefficients vanish by making use of the invariance of the four-fermion interaction matrix element under some formal transformations, no straightforward calculations being required for this purpose.

1. FORM FACTORS

THE matrix element of the four-fermion interaction H corresponding to the leptonic decay of hyperons

$$Y \to N + l + \bar{\nu}, \tag{1}$$

have, in the most general case, the form (we shall omit the bar over $\bar{\nu}$ in the indices)

$$\langle Nl\bar{\nu}|H|Y\rangle = \sum [(\bar{u}_N \Gamma_j^{(+)} u_Y)(\bar{u}_l O_j u_\nu) + (\bar{u}_N \Gamma_j^{(-)} u_Y)(\bar{u}_l O_j \gamma_5 u_\nu)], \tag{2}$$

where u_k is a spinor of the k-th particle, and

$$O_j = 1,\ \gamma_5,\ \gamma_\mu,\ i\gamma_\mu\gamma_5,\ \tfrac{1}{2}\sigma_{\mu\nu} \quad (j = S,\ P,\ V,\ A,\ T). \tag{3}$$

Because of the presence of virtual strong interactions, the vertices $\Gamma_j^{(\pm)}$ can have a complicated structure. The most general expression for $[q_\mu \equiv (p_Y - p_N)_\mu]$ follows[1] from relativistic invariance:

$$\Gamma_S^{(\mp)} = C_S^{(\pm)}, \quad \Gamma_P^{(\mp)} = C_P^{(\pm)}\gamma_5;$$

$$\Gamma_V^{(\mp)} = C_V^{(\mp)}\gamma_\mu + B_V^{(\mp)}\sigma_{\mu\nu}q_\nu + iD_V^{(\pm)}q_\mu;$$

$$\Gamma_A^{(\pm)} = iC_A^{(\mp)}\gamma_\mu\gamma_5 + iB_A^{(\pm)}\sigma_{\mu\nu}q_\nu\gamma_5 - D_A^{(\mp)}q_\mu\gamma_5;$$

$$\Gamma_T^{(\pm)} = C_T^{(\mp)}\sigma_{\mu\nu} + B_T^{(\pm)}(\gamma_\mu\hat{q}\gamma_\nu - \gamma_\nu\hat{q}\gamma_\mu) + D_T^{(\pm)}\tfrac{1}{2}(\gamma_\mu\hat{q}\gamma_\nu - \gamma_\nu\hat{q}\gamma_\mu) + iF_T^{(\pm)}(p_{Y\mu}p_{N\nu} - p_{Y\nu}p_{N\mu} - \varepsilon_{\mu\nu\alpha\beta}p_{Y\alpha}p_{N\beta}). \tag{4}$$

The form factors $C_j^{(\pm)}$, $B_j^{(\pm)}$, $D_j^{(\pm)}$, $F_T^{(\pm)}$ are functions of the invariant

$$Q^2 = -(p_Y - p_N)^2. \tag{5}$$

In the work of Weinberg,[1] the coefficient of $F_T^{(\pm)}$ has a somewhat different form; however, the transformation properties of the expression described in (4) are much simpler.

Calculation of the energy correlation and the asymmetry of the decay (1) are given in reference 2, and also of the spectrum and polarization of the nucleons, either with $\Gamma_V^{(\pm)}$ and $\Gamma_A^{(\pm)}$ left in (2) (since $C_S^{(\pm)}$ is equivalent to $-D_V^{(\pm)}/m_l$, while $C_P^{(\pm)}$ corresponds to $D_A^{(\pm)}/m_l$, then essentially only the tensor vertex $\Gamma_T^{(\pm)}$ is not considered in this calculation), or with all five variants considered, but without form factors. Calculations with all (including the tensor) vertices would be too cumbersome; however, certain information on the interference of the form factors can be obtained without calculation by studying the behavior of the matrix element (2) — (4) in certain formal transformations which are considered in Sec. 2. In this case, as is shown in Sec. 3, a prediction of the energy dependence of the coefficients in front of the different products of form factors is possible, as is also the vanishing of part of these coefficients. The absence of the interference of certain variants or of form factors, for example, in the ordinary β decay, is a well known fact; its explanation from the general formal point of view has a certain interest. Moreover, the relations that have been obtained can serve as a control of the results of calculations.

2. TRANSFORMATIONS

In calculations with the matrix element (2), it is necessary to calculate an expression having the structure

$$\sum_{r,s} R_F R_G (\bar{u}_{2\lambda}^s F_{\lambda\sigma} u_{1\sigma}^r)(\bar{u}_{1\alpha}^r G_{\alpha\beta} u_{2\beta}^s), \tag{6}$$

where $F_{\lambda\sigma}$ and $G_{\alpha\beta}$ are any of the spinor operators (matrices) written down in (4); R_F and R_G are the form factors standing in front of them in (4); u_1 and u_2 are spinors, either Y and N,

or $\bar{\nu}$ and l. As a rule, $G^+ = \pm G$. It seems that the expression (6) should be multiplied by $(\bar{u}_4 F' u_3) \times (\bar{u}_3 G'^+ u_4)$; however, inasmuch as the spinors u_3 and u_4 do not take part in the transformations (12) (see below), this factor is not essential for our consideration.

Strictly speaking, one should compute not the expression (6), but

$$R_F R_G \operatorname{Sp}\{F\rho_1 G\rho_2\}, \tag{7}$$

because only in the case of a pure state is the density matrix $\rho_{\sigma\alpha}$ expressed in terms of u_α:

$$\rho_{\sigma\alpha} = \sum_r u_\sigma^r \bar{u}_\alpha^r, \tag{8}$$

and (7) reduces to (6). In the general case, the density matrix of the i-th particle ρ_i, as is well known,[3] has the form

$$\rho_i = (1 + i\gamma_5 \hat{\zeta}_i')(m_i - i\hat{p}_i)/4E_i, \tag{9}$$

while if we introduce a unit vector $\mathbf{n_i} \equiv \mathbf{p_i}/|\mathbf{p_i}|$ in the direction of the momentum $\mathbf{p_i}$, and the vector $\boldsymbol{\zeta}_i$ of the spin of the i-th particle in its rest system, then

$$\zeta_{i\mu}' = (\zeta_i \mathbf{n}_i)\,\mathbf{n}_i E_i/m_i + [\zeta_i - (\zeta_i \mathbf{n}_i)\,\mathbf{n}_i]; \quad \zeta_{i\mu}' p_{i\mu} = 0, \tag{10}$$

i.e., (the notation is obvious),

$$\zeta_{i\parallel}' = E_i \zeta_{i\parallel}/m_i\ \zeta_{i\perp}' = \zeta_{i\perp},\ \zeta_{i0}' = (\boldsymbol{\zeta}_i, \mathbf{p}_i)/m_i. \tag{11}$$

Let us consider further three types of formal transformations:

I. $u_1 \to \gamma_5 u_1, \quad u_2 \to u_2;$

II. $u_2 \to \gamma_5 u_2, \quad u_1 \to u_1;$

III. $u_1 \to u_2^c = C\bar{u}_2, \quad u_2 \to u_1^c = C\bar{u}_1.$ (12)

In transformations I and II, we have

$$\rho_i \to -\gamma_5 \rho_i \gamma_5 = (1 - i\gamma_5 \hat{\zeta}_i')(-m_i - ip_i)\hat{}/4E_i, \quad (i = 1, 2), \tag{13}$$

i.e., $\mathbf{m_i} \to -\mathbf{m_i}$ (or $\mathbf{p_i} \to -\mathbf{p_i}$), $\boldsymbol{\zeta}_i' \to -\boldsymbol{\zeta}_i'$.

If we consider (11), then this means

$$m_i \to -m_i \text{ (or } \quad p_i \to -p_i), \qquad \zeta_{i\perp} \to -\zeta_{i\perp}. \tag{14}$$

In the case of transformation III,

$$\rho_1 \to -(C^{-1}\rho_2 C)^T = (1 + i\gamma_5 \hat{\zeta}_2')(-m_2 - i\hat{p}_2)/4E_2, \quad \rho_2 \to -(C^{-1}\rho_1 C)^T, \tag{15}$$

whence

$$p_1 \overset{\to}{\leftarrow} -p_2,\ m_1 \overset{\to}{\leftarrow} m_2 \text{ (or } \quad p_1 \overset{\to}{\leftarrow} p_2,\ m_1 \overset{\to}{\leftarrow} -m_2);$$
$$\zeta_{1\parallel} \overset{\to}{\leftarrow} -\zeta_{2\parallel},\ \zeta_{1\perp} \overset{\to}{\leftarrow} \zeta_{2\perp}. \tag{16}$$

If we now return to (7), it is not difficult to see that it is invariant under transformations I or II, i.e., upon replacement of (14) with simultaneous transformation of the spinor operators:

I. $F \to F\gamma_5, \quad G \to G\gamma_5,$

II. $F \to -\gamma_5 F, \quad G \to -\gamma_5 G;$ (17)

and similarly in case III, i.e., in the transformation (16), together with

$$\text{III. } F \to -(C^{-1}FC)^T, \quad G \to -(C^{-1}GC)^T \tag{18}$$

(if the particles 1 and 2 are Y and N, while F or G is equal to $p_{Y\mu}p_{N\nu} - p_{Y\nu}p_{N\mu} - \epsilon_{\mu\nu\alpha\beta}p_{Y\alpha}p_{N\beta}$, then an additional change in sign should take place).

The transformation of the operators (17) and (18) is equivalent to a transformation of form factors for unchangeable operators. If the particles 1 and 2 are $\bar{\nu}$ and l, then the transformations I, II and III in (17), (18) correspond to [$R_j^{(\pm)}$ are arbitrary form factors in (4)]

$$\text{I. } R_j^{(\pm)} \to R_j^{(\mp)}; \tag{19}$$

$$\text{II. } \begin{matrix} R_j^{(\pm)} \to -R_j^{(\mp)} & (j = S,\ P,\ T), \\ R_j^{(\pm)} \to R_j^{(\mp)} & (j = A,\ V); \end{matrix} \tag{20}$$

$$\text{III. } \begin{matrix} \text{change sign} & R_S^{(\pm)},\ R_P^{(\pm)},\ R_A^{(+)},\ R_V^{(-)}, \\ \text{do not change sign} & R_T^{(\pm)},\ R_A^{(-)},\ R_V^{(+)}. \end{matrix} \tag{21}$$

If particles 1 and 2 are Y and N, then the form factors transform in the following fashion:

$$\text{I. } C_S^{(\pm)} \overset{\to}{\leftarrow} C_P^{(\mp)}, \quad C_V^{(\pm)} \overset{\to}{\leftarrow} -C_A^{(\mp)}, \quad B_V^{(\pm)} \overset{\to}{\leftarrow} -B_A^{(\mp)},$$
$$D_V^{(\pm)} \overset{\to}{\leftarrow} -D_A^{(\mp)}, \quad C_T^{(\pm)} \overset{\to}{\leftarrow} C_T^{(\mp)}, \quad B_T^{(\pm)} \overset{\to}{\leftarrow} D_T^{(\mp)}, \quad F_T^{(\pm)} \overset{\to}{\leftarrow} F_T^{(\mp)}; \tag{22}$$

$$\text{II. } C_S^{(\pm)} \overset{\to}{\leftarrow} -C_P^{(\mp)}, \quad C_V^{(\pm)} \overset{\to}{\leftarrow} -C_A^{(\mp)}, \quad B_V^{(\pm)} \overset{\to}{\leftarrow} B_A^{(\mp)},$$
$$D_V^{(\pm)} \overset{\to}{\leftarrow} D_A^{(\mp)}, \quad C_T^{(\pm)} \overset{\to}{\leftarrow} -C_T^{(\mp)}, \quad B_T^{(\pm)} \overset{\to}{\leftarrow} D_T^{(\mp)}, \quad F_T^{(\pm)} \overset{\to}{\leftarrow} -F_T^{(\mp)}; \tag{23}$$

$$\text{III. } \begin{matrix} \text{change sign} & C_S^{(\pm)},\ C_P^{(\pm)},\ D_V^{(\pm)},\ C_A^{(\pm)},\ D_A^{(\pm)},\ D_T^{(\pm)}; \\ \text{do not change sign} & C_V^{(\pm)},\ B_V^{(\pm)},\ B_A^{(\pm)},\ C_T^{(\pm)},\ B_T^{(\pm)},\ F_T^{(\pm)}. \end{matrix} \tag{24}$$

The invariance of (7) means that the even (odd) combinations of the quantities m_k, p_k, ξ_k (k = Y, N, l, $\bar{\nu}$) relative to any of the transformations considered should be multiplied in formulas for the probability of decay by a combination of form factors that is even (odd) relative to the same transformations in (19) — (24).

3. INTERFERENCE OF FORM FACTORS

We shall now make clear how the conclusions can be obtained.

1) Inasmuch as $m_\nu = 0$, while summation is carried out over $\boldsymbol{\zeta}_\nu$, the variables $\bar{\nu}$ do not remain in (14), so that the probability of decay can contain only even [relative to (19)] bilinear combinations of form factors, namely,

$$R_j^{(+)}R_h^{(+)} + R_j^{(-)}R_h^{(-)},\ R_j^{(+)}R_h^{(-)} + R_j^{(-)}R_h^{(+)}. \tag{25}$$

2) If we are not interested in $\boldsymbol{\zeta}_{l\perp}$, then it fol-

lows from (14) and (20) that the products of form factors inside each of the groups (20) which must enter into the combinations (25) should not be multiplied by m_l, whereas the coefficient in the interference between the groups certainly contains m_l. In formulas with $\zeta_{l\perp}$ the contrary would be true.

3) If we are not interested in ζ_l and ζ_ν, then the interference of form factors inside each of the lines of (21) should be multiplied by even [relative to (16)] products of the quantities E_l, $\mathbf{p}_l$, m_l and E_ν, $\mathbf{p}_\nu$ ($m_\nu = 0$), while the interference between the lines must be multiplied by odd products.

In what follows, we limit ourselves to an investigation of the spectrum, the asymmetry of emission and the polarization N. It is then necessary to integrate over the variables l and $\bar{\nu}$. This is most convenient to do in the system of coordinates where

$$\mathbf{p}_Y = \mathbf{p}_N, \quad \mathbf{p}_l = -\mathbf{p}_\nu. \tag{26}$$

Integration over the variables l and $\bar{\nu}$ means here simply integration over the angles $\mathbf{p}_l$, after which all the components which are linear in $\mathbf{p}_l$ $= -\mathbf{p}_\nu$ disappear. Therefore, the expressions that are even relative to (16) are

$$\mathscr{E}_l\mathscr{E}_\nu, \quad -\mathbf{p}_l\mathbf{p}_\nu = \mathbf{p}_l^2 = \mathbf{p}_\nu^2 = \mathscr{E}_\nu^2, \quad m_l\mathscr{E}_\nu - m_\nu\mathscr{E}_l = m_l\mathscr{E}_\nu, \tag{27}$$

while the odd is

$$m_l\mathscr{E}_\nu + m_\nu\mathscr{E}_l = m_l\mathscr{E}_\nu. \tag{27'}$$

In order to distinguish the system $\mathbf{p}_Y = \mathbf{p}_N$ from the system $\mathbf{p}_Y = 0$, all the energies in the first are denoted by the letter $\mathscr{E}$, and in the second by E. It is not difficult to see that here

$$|\mathbf{p}_Y| = |\mathbf{p}_N| = m_Y\sqrt{E_N^2 - m_N^2}/Q, \quad \mathscr{E}_l = (Q^2 + m_l^2)/2Q,$$
$$\mathscr{E}_Y = m_Y(m_Y - E_N)/Q, \quad |\mathbf{p}_l| = |\mathbf{p}_\nu| = \mathscr{E}_\nu = (Q^2 - m_l^2)/2Q,$$
$$\mathscr{E}_N = (m_Y E_N - m_N^2)/Q, \quad Q^2 = m_Y^2 + m_N^2 - 2m_Y E_N. \tag{28}$$

If now the form factors in (20) are found in one line, i.e., they should not be multiplied by m_l, but in (21), in different lines:

$$R_S^{(\pm)}R_T^{(\pm)}, \quad R_P^{(\pm)}R_T^{(\pm)}, \quad R_S^{(\pm)}R_T^{(\mp)}, \quad R_P^{(\pm)}R_T^{(\mp)},$$
$$R_V^{(\pm)}R_V^{(\mp)}, \quad R_A^{(\pm)}R_A^{(\mp)}, \quad R_V^{(\pm)}R_A^{(\pm)}, \tag{29}$$

then (the signs must be chosen either both upper or both lower), by virtue of (27) such interference is forbidden. Since $C_S^{(\pm)}$ and $C_P^{(\pm)}$ can be reduced to $-D_V^{(\pm)}/m_l$ and $D_A^{(\pm)}/m_l$ and conversely, then the forbiddenness of the interferences

$$C_S^{(\pm)}C_P^{(\pm)}, \quad C_S^{(\pm)}C_S^{(\mp)}, \quad C_P^{(\pm)}C_P^{(\mp)}, \quad D_V^{(\pm)}R_T^{(\pm)}, \quad D_V^{(\pm)}R_T^{(\mp)},$$
$$D_A^{(\pm)}R_T^{(\pm)}, \quad D_A^{(\pm)}R_T^{(\mp)} \tag{30}$$

also follows from (29).

From a comparison of (27) and (21) with (20), it is further clear that the product of form factors from one line both in (20) and in (21), i.e., (the expressions $R_V^{(\pm)}R_V^{(\pm)}$, etc, denote products both of identical and also different form factors, in this case of the vector type

$$R_S^{(\pm)}R_S^{(\mp)}, \quad R_P^{(\pm)}R_P^{(\pm)}, \quad R_V^{(\mp)}R_V^{(\pm)}, \quad R_A^{(\pm)}R_A^{(\pm)},$$
$$R_T^{(\pm)}R_T^{(\pm)}, \quad R_S^{(\pm)}R_P^{(\mp)}, \quad R_T^{(\pm)}R_T^{(\mp)}, \quad R_V^{(\pm)}R_A^{(\mp)}, \tag{31}$$

should be multiplied by $\mathscr{E}_l\mathscr{E}_\nu$ or $\mathbf{p}_l^2 = \mathscr{E}_\nu^2$. If the form factors in (20) are found in different lines, then they interfere with the factor $m_l\mathscr{E}_\nu$:

$$R_S R_A, \quad R_S R_V, \quad R_P R_A, \quad R_P R_V, \quad R_T R_A, \quad R_T R_V. \tag{32}$$

In the case of electron decays, one can neglect m_l. This means an absence of interference both in (29) — (30) and in (32). This result was obtained in somewhat stronger fashion by Weinberg,[1] who used only the invariance relative to the transformation III, and obtained forbiddenness for the interference of two groups in (21). The γ_5 invariance leading to Eq. (20) gives the additional information here.

Thus, in the case of electron decays, the $R_T^{(\pm)}$ interfere only with one another; in the group V, A, only the expressions

$$R_V^{(+)}R_V^{(+)} + R_V^{(-)}R_V^{(-)}, \quad R_A^{(+)}R_A^{(+)} + R_A^{(-)}R_A^{(-)},$$
$$R_V^{(+)}R_A^{(-)} + R_V^{(-)}R_A^{(+)},$$

can be encountered, while in the group S, P, only

$$R_S^{(+)}R_S^{(+)} + R_S^{(-)}R_S^{(-)}, \quad R_P^{(+)}R_P^{(+)} + R_P^{(-)}R_P^{(-)},$$
$$R_S^{(+)}R_P^{(-)} + R_S^{(-)}R_P^{(+)}.$$

When only the form factors C_j remain, this conclusion is confirmed by direct calculation.[2,4] Inasmuch as the form of the matrix element $(\bar{u}_N\Gamma_j u_Y)$ has no effect on the considerations given here, all the above results are applicable to the case of ordinary β decay, where they are generally well known.

Application of the transformations (22) — (24) to the baryon part of the matrix element (2) gives new relations. If in this case one calculates the probability of decay with given energy E_n, angle between $\mathbf{n}_N$ and ζ_Y, and polarization ζ_N ($|\zeta_N| = 1$) then

$$dW \sim dE_N d\Omega_N S_N(E_N)\{1 + \alpha_N(E_N)(\zeta_Y\mathbf{n}_N)\}$$
$$\times\{1 + P_1(E_N)(\zeta_N\mathbf{n}_N) + P_2(E_N)(\zeta_N\mathbf{n}_N)(\zeta_Y\mathbf{n}_N)$$
$$+ P_3(E_N)[(\zeta_Y\zeta_N) - (\zeta_N\mathbf{n}_N)(\zeta_Y\mathbf{n}_N)]\}, \tag{33}$$

where S_N characterizes the spectrum, α_N — the asymmetry of the flight, and P_1, P_2, P_3 — the polarization of N. The quantities α_N and P_1 can be different from zero only in parity nonconservation.

A discussion completely analogous to that given

above shows that in S_N and $S'_N P_2$ ($S'_N \equiv S_N[1 + \alpha_N(\zeta_Y \cdot n_N)]$ the following expressions are multiplied by $\mathscr{E}_Y \mathscr{E}_N$ and p_N^2 ($R_j R_h \equiv R_j^{(+)} R_h^{(+)} + R_j^{(-)} R_h^{(-)}$; the form factors B_j and D_j have the additional factors $\mathscr{E}_Y - \mathscr{E}_N = Q$ while F_T has the factor $\mathscr{E}_Y \mathscr{E}_N$ or p_N^2; C_S and C_P behave as $-D_V$ and D_A):

$$C_V^2 + C_A^2,\ B_V^2 + B_A^2,\ D_V^2 + D_A^2,\ C_T^2,\ B_T^2 + D_T^2,$$
$$F_T^2,\ B_T D_T,\ C_T F_T \quad C_V B_T - C_A D_T,$$
$$(B_V - B_A) C_T,\ (B_V - B_A) F_T. \tag{34}$$

The factor $m_Y m_N$ multiplies

$$C_V^2 - C_A^2,\ B_V^2 - B_A^2,\ D_V^2 - D_A^2,\ B_T^2 - D_T^2,\ C_V B_T + C_A D_T,$$
$$(B_V + B_A) C_T,\ (B_V + B_A) F_T. \tag{35}$$

Moreover, interference expressions of the form

$$(R_i R_j + R_h R_k)\, m_l \mathscr{E}_N + (R_i R_j - R_h R_k)\, m_N \mathscr{E}_l \tag{36}$$

are possible in S_n and $S'_N P_2$, where

$$R_i R_j + R_h R_k = C_A B_A - C_V B_V,\ C_V D_V - C_A D_A,$$
$$C_A C_T + C_V C_T,\ C_A F_T + C^V F_T,\ B_A D_T + B_V B_T,$$
$$B_V D_T + B_A B_T,\ C_T D_T - C_T B_T,\ D_T F_T - B_T F_T. \tag{37}$$

The components (34) in the coefficient $S'_N P_3$ which determine, in accord with (33), the transverse polarization, are multiplied by $m_Y m_N$, while (35) is multiplied by $\mathscr{E}_Y \mathscr{E}_N$ and p_N^2. The expressions (37) interfere according to the rule

$$(R_i R_j + R_h R_k)\, m_N \mathscr{E}_l + (R_i R_j - R_h R_k)\, m_l \mathscr{E}_N. \tag{38}$$

Besides (29) and (30), the interference

$$B_V D_V,\ B_A D_A,\ C_V D_T,\ C_A B_T. \tag{39}$$

in S_N, $S'_N P_2$, $S'_N P_3$ is shown to be forbidden.

As far as the components with parity nonconservation are concerned, i.e., $S'_N \alpha_N$ and $S'_N P_1$ in (33), a similar discussion leads to the result that the interference (35) does not enter into it (here $R_j R_h \equiv R_j^{(+)} R_h^{(-)} + R_j^{(-)} R_h^{(+)}$) while the coefficients for the remaining products of form factors in $S_N \alpha_N$ and $S'_N P_1$ are simply related to each other. For example, in the products (34) (with the substitution of $C_V^2 + C_A^2$, $B_V^2 + B_A^2$, $D_V^2 + D_A^2$ by $C_V C_A$, $B_V B_A$, $D_V D_A$) the factors $\mathscr{E}_Y$ and $\mathscr{E}_N$ appear, while the transition from α_N to P_1 is connected with $\mathscr{E}_Y \rightleftarrows -\mathscr{E}_N$. In the interference (37) (with the substitution of $C_A B_A - C_V B_V$, $C_V D_V - C_A D_A$ by $C_A B_V - C_V B_A$, $C_V D_A - C_A D_A$) we get

$$(R_i R_j + R_h R_k)\, m_Y \rightleftarrows -(R_i R_j - R_h R_k)\, m_N. \tag{40}$$

According to the general rule, one can also ascertain that the form factors $B_V D_A - B_A D_V$ and $C_A B_T + C_V D_T$ should not make a contribution to α_N and P_1, while $B_V D_A + B_A D_V$ and $C_A B_T - C_V D_T$ should be multiplied by $\mathscr{E}_Y$ and $\mathscr{E}_N$, while in the transition from α_N to P_1, $\mathscr{E}_Y \rightleftarrows \mathscr{E}_N$. Direct calculation[2] shows that the coefficients for $B_V D_A$ and $B_A D_V$ are equal to zero. Thus, if α_N is computed, then the expression for P_1 can be obtained without additional calculation.

The results of the present section can be put in a form suitable for comparison with the formulas of reference 2, where the notation

$$J \equiv Q^2/(m_Y - m_N)^2,\quad \xi \equiv (m_Y - m_N)/(m_Y + m_N),$$
$$\eta_l \equiv m_l^2/(m_Y - m_N)^2 \tag{41}$$

is used.

According to (41) and (28),

$$\mathscr{E}_l = m_Y (1 + \xi J)/\sqrt{J}\,(1 + \xi),$$
$$\mathscr{E}_N = m_N (1 - \xi J)/\sqrt{J}\,(1 - \xi),$$
$$p_N^2 = m_l m_N (1 - J)(1 - \xi^2 J)/(1 - \xi^2) J,$$
$$\mathscr{E}_l = \tfrac{1}{2}(m_Y - m_N)\sqrt{J}\,(1 + \eta_l/J),$$
$$\mathscr{E}_\nu = |p_\nu| = |p_l| = \tfrac{1}{2}(m_l - m_N)\sqrt{J}\,(1 - \eta_l/J). \tag{42}$$

Therefore, in addition to the added factors (Q or $\mathscr{E}_Y \mathscr{E}_N$, p_N^2), for B_j, D_j or F_T, the expressions (34) in S'_N and $S'_N P_2$ [and (35) in $S'_N P_3$] are multiplied by $(1 - J)(1 - \xi^2 J)$ or $(1 - \xi^2 J^2)$, while (35) [(34) in $S'_N P_3$] should be multiplied by $(1 - \xi^2) J$. The interference of (36) or (37) can now be written as

$$\sqrt{J}\,[R_i R_j (1 - \xi^2 J) \pm R_h R_k \xi (1 - J)]. \tag{43}$$

In the transition from α_N to P_1, the rule $\mathscr{E}_Y \rightleftarrows \mp \mathscr{E}_N$ is equivalent to $1 \to \mp 1$, $\xi J \to \mp \xi J$; the rule (40) now means that for $R_i R_j$ we have $1 \to -1$, $\xi \to \xi$, while for $R_h R_k$ we have $1 \to 1$, $\xi \to -\xi$. The factors $\mathscr{E}_l$, $\mathscr{E}_\nu$, $p_l^2 = \mathscr{E}_\nu^2$ and $m_l \mathscr{E}_\nu$ in (31) and (32) are proportional to $1 + \eta/J$, $1 - \eta/J$ and $\sqrt{\eta/J}$.

Direct calculation[2] agrees with the results given here, in particular with the absence of interference of the form factors in (29), (30), and (39). It should be noted that in the expression for the energy correlation, such interference will certainly appear with the factor

$$X \sim E_l - E_\nu [1 + m_l^2/Q^2]/[1 - m_l^2/Q^2], \tag{44}$$

the contribution from which vanishes upon integration over the variables l and $\bar{\nu}$.

In conclusion, I express my deep gratitude to S. V. Maleev for stimulating discussions.

[1] S. Weinberg, Phys. Rev. 112, 1375 (1958).

[2] Belov, Mingalev, and Shekhter, JETP **38**, 541 (1960), this issue p. 411.
[3] H. A. Tolhoek, Revs. Modern Phys. **28**, 214 (1956).
[4] L. B. Okun' and V. M. Shekhter, JETP **34**, 1250 (1958), Soviet Phys. JETP **7**, 864 (1958); Nuovo cimento **10**, 359 (1958).

Translated by R. T. Beyer
108

POSSIBILITY OF DETERMINING THE FORM FACTORS IN LEPTONIC DECAY OF HYPERONS

V. P. BELOV, B. S. MINGALEV, and V. M. SHEKHTER

Leningrad Physico-technical Institute, Academy of Sciences, U.S.S.R.

Submitted to JETP editor August 14, 1959

J. Exptl. Theoret. Phys. (U.S.S.R.) **38**, 541-552 (February, 1960)

The energy correlation and asymmetry of emission of particles produced in leptonic decay of hyperons, and also the polarization of the emitted nucleons or secondary hyperons, have been calculated with account of all six form factors of the decay V-A interaction. A method of comparison of the theoretical formulas with the experimental data is suggested, which permits in principle to determine the form factor. A similar calculation is presented in the appendix, when all five types of decay interaction are retained and the form factors are neglected.

1. INTRODUCTION

THE recent observation[1,2] of the decay $\Lambda \to p + e^- + \bar{\nu}$ gives grounds for hoping that leptonic decays of hyperons will soon be experimentally investigated. Such an investigation is particularly interesting for the following reasons. On the one hand, the theoretical analysis is made much easier here by the fact that all the particles in the final states are free (accurate to inessential Coulomb forces). This permits an exact calculation of the process with account of the weak decay interaction, naturally, only in first-order perturbation theory. On the other hand, the influence of strong interactions should lead to the appearance of energy-dependent form factors of the decay interaction, which affect the experimental results. An investigation of the β decay of hyperons can therefore yield certain information on the role of strong interactions, as takes place in the scattering of fast electrons by nucleons.

The present work is devoted to a theoretical analysis of leptonic decays of hyperons. It is assumed from the outset that this decay is due to the universal four-fermion V-A interaction.[3,4] This assumption is natural, since the universal V-A theory has thus far been most brilliantly confirmed by all experiments on weak interactions (incidentally, always without participation of strange particles). The question of the possibility of determining the variants of the interaction responsible for the leptonic decay of hyperons directly from experimental data is considered in Appendix B.

The form factors of the V-A interaction are introduced in Sec. 2. Section 3 is devoted to the possibility of determining all the form factors in an investigation of the energy correlation and asymmetry of the particles emitted in the hyperon decay. Formulas for the energy distribution, asymmetry of emission, and polarization of the emitted nucleons (or secondary hyperons), and also the total probability of the decay, are written out in Sec. 4. The indicated quantities where calculated previously by one of the authors[5] only for the C_V and C_A form factors. Reference 5 contains, however, many inaccuracies which are corrected in the present paper. In section 5, some features of the decays $\Sigma \to \Lambda + e + \nu$ are considered.

2. FORM FACTORS

Leptonic decays of hyperons can be written in a unique manner

$$Y \to N + l + \bar{\nu}, \tag{1}$$

where Y is the decaying hyperon, N the nucleon or hyperon in the final state (processes of the type $\Xi^- \to \Lambda + l^- + \bar{\nu}$ are meant), l is the electron or muon, and $\bar{\nu}$ is the antineutrino. We shall henceforth omit bar over ν in the indices.

In calculating the decay probability in first-order perturbation theory, the matrix element of the S matrix is given (in the case of the VA theory) by the expression[6]

$$i(2\pi)^4\delta(p_Y - p_N - p_l - p_\nu)\left\langle N\left|\frac{G}{\sqrt{2}}J_\mu(0)\right|Y\right\rangle \times (u_l\gamma_\mu(1+\gamma_5)u_\nu), \tag{2}$$

where for each particle B, $|B\rangle$ is its real state, u_B is the free spinor, p_B the four-momentum, and $G = 1.4 \times 10^{-49}$ erg-cm^3 is the Feynman-Gell-

Mann constant.[3] The current $J_\mu(x) \equiv J_\mu^V(x) + J_\mu^A(x)$ is a superposition of the currents $(\bar{\psi}_N(x)\gamma_\mu\psi_Y(x)) + (\bar{\psi}_N(x)\gamma_\mu\gamma_5\psi_Y(x))$, where Y and N are different baryons ($\psi_B(x)$ is the operator of the particle B in the Heisenberg representation), and also of the currents that can be made up of the boson (i.e., K and π meson) operators.

The existence of strong interactions makes a direct calculation of $2^{-1/2}\langle N|GJ_\mu(0)|Y\rangle$ impossible. The most common form of this matrix element follows from the relativistic invariance

$$\left\langle N\left|\frac{G}{\sqrt{2}}J_\mu(0)\right|Y\right\rangle = (\bar{u}_N\{\gamma_\mu(C_V - C_A\gamma_5) + \sigma_{\mu\nu}(p_Y - p_N)_\nu(B_V - B_A\gamma_5) + i(p_Y - p_N)_\mu(D_V - D_A\gamma_5)\}u_Y). \quad (3)$$

In Eq. (3), C_V, C_A, B_V, B_A, D_V, and D_A are real (because of the CP invariance) functions of the invariant

$$Q^2 = -(p_Y - p_N)^2 = m_Y^2 + m_N^2 - 2m_Y E_N$$

(the last equation is true in the rest system of Y). From the conservation laws we have

$$m_l^2 \leqslant Q^2 \leqslant (m_Y - m_N)^2, \quad m_N \leqslant E_N \leqslant (m_Y^2 + m_N^2 - m_l^2)/2m_Y. \quad (4)$$

Unlike ordinary β decay,[6] in the decay of hyperons there are no grounds for assuming B_A and D_V equal to zero, so that the expression for the decay probability should include, generally speaking, the interferences of all six form factors. In the case when l is an electron, only four form factors remain, C_V, C_A, B_V, and B_A, since D_V and D_A make a contribution proportional to the square of the electron mass, which is negligibly small compared with the other quantities of the theory.

The dependence of the form factors on Q^2 is not known beforehand. If we write the power-series expansion

$$C_V(Q^2) = C_V(0)\left[1 - \frac{1}{6}Q^2a^2(C_V) + \cdots\right] \quad (5)$$

with analogous expressions for C_A, B_V, B_A, D_V, and D_A, this dependence will be determined by the quantity a, the β-decay "radius" of the hyperon, analogous to the corresponding electromagnetic radius, which characterizes the distribution of the charge or magnetic moment in the nucleon. It follows from the experimental data[7] that in electromagnetic interactions $a \sim 0.8 \times 10^{-13}$ cm $\sim 1/2m_\pi$. We have no grounds for assuming the β-decay radius to be much greater than this. But if this is so, then in (5), for example, $Q^2a^2/6 \leq 0.09$ for the decay $\Lambda \to p + l^- + \bar{\nu}$ and $Q^2a^2/6 \leq 0.18$ for $\Sigma^- \to n + l^- + \bar{\nu}$. Since these quantities are relatively small, the series (5) will apparently converge rapidly, and the high powers of Q^2 can be neglected in it. It is natural also to expect that in order of magnitude

$$B(0) \sim D(0) \sim aC(0) \quad (6)$$

with $a \sim 0.8 \times 10^{-13}$ cm; Eqs. (5) and (6) will be used later on for various estimates.

3. ENERGY CORRELATIONS AND EXPERIMENTAL DETERMINATION OF THE FORM FACTORS

The largest amount of information for the experimental determination of the form factors entering in (3) can be obtained by investigating the energy correlation of the particles produced in hyperon decays. It is convenient here to introduce the dimensionless variables (all the energies are taken in the Y rest system)

$$X = \frac{2m_Y}{m_Y^2 - m_N^2}\left[E_l - E_\nu\frac{1+\eta/J}{1-\eta/J}\right], \quad J = Q^2/(m_Y - m_N)^2, \ \eta = m_l^2/(m_Y - m_N)^2, \quad (7)$$

analogous to the corresponding variables for the $K_{\pi 3}$ and K_{e3} decays, considered by Dalitz[8] and Kobzarev.[9] The conservation laws limit the range of permissible variation of X and J to the line $J = \eta$ ($\eta = 0$ in the case of electronic decays) and the hyperbola

$$X^2 = X_m^2(J) \equiv (1 - J)(1 - \xi^2 J), \quad (8)$$

where the small parameter ξ is determined by the equation

$$\xi = (m_Y - m_N)/(m_Y + m_N). \quad (9)$$

The values of ξ and η (for $l = \mu$) for different decays are listed in the table. The range of variation of X and J is shown in the figure. The focus of the hyperbola is located at the point $X = 0$, $J = (\xi^{-2} + 1)/2$. When $\xi \ll 1$, the hyperbola is almost identical with the parabola

$$X^2 + J = 1. \quad (10)$$

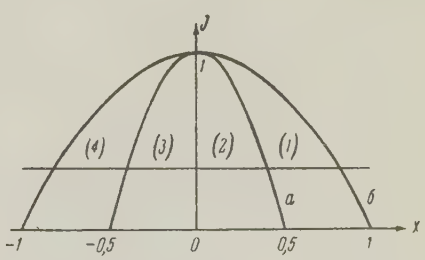

Energy correlation on the XJ plane. Curve a: $X^2 = \frac{1}{4}(1-J) \times (1-\xi^2 J)$, curve b: $X^2 = (1-J)(1-\xi^2 J)$, line parallel to the abscissa axis: $J = \eta = m_\mu^2/(m_Y - m_N)^2$.

According to (7), E_N, $|p_N|$, E_l and E_ν are expressed in terms of X and J by the equations

$$E_N = m_N + \frac{m_Y - m_N}{1+\xi}\xi(1-J),$$

$$|p_N| = \frac{m_Y - m_N}{1+\xi} X_m(J) = \frac{m_Y - m_N}{1+\xi}\sqrt{(1-J)(1-\xi^2 J)},$$

$$E_l = \frac{m_Y - m_N}{2(1+\xi)}\left[(1+\xi J)\left(1+\frac{\eta}{J}\right) + X\left(1-\frac{\eta}{J}\right)\right],$$

$$E_\nu = \frac{m_Y - m_N}{2(1+\xi)}[1+\xi J - X]\left(1-\frac{\eta}{J}\right). \qquad (11)$$

It is seen from (11) that for electronic decays ($\eta = 0$) and for $\xi \ll 1$, E_e is expressed only in terms of X. To obtain the dependence of the decay probability on E_e it is sufficient in this case to integrate with respect to J from 0 to $1-X^2$. The integration is always elementary, for the dependence on J is that of a power law.

The leptonic decay probability calculated according to (2) and (3) with given X and J, and also with given angle between the vector of polarization of the decaying hyperon, ζ_Y, and the unit vector n_N in the direction of motion of N, has the form

$$dW(X, J; \zeta_Y, n_N) = \frac{dX dJ}{16\pi^3}\frac{d\Omega_N}{4\pi}\frac{(m_Y - m_N)^5}{(1+\xi)^3}\left(1-\frac{\eta}{J}\right)^2 \times [S(X, J) + R_N(X, J)(\zeta_Y n_N)]. \qquad (12)$$

Formulas for $S(X, J)$ and $R_N(X, J)$ are given in Appendix A.

If each decay event is now represented by the points X and J on the figure, then an analysis of the distribution of these points leads to certain conclusions regarding the magnitudes of the form factors, all of which are functions of J, but not of X. In such an analysis, in particular, one can determine independently the six coefficients of X^0, X^1, and X^2 in $S(X, J)$ and $R_N(X, J)$. Actually, if the hyperbola $X^2 = \frac{1}{4}X_m^2(J) = \frac{1}{4}(1-J)(1-\xi^2 J)$ is drawn, the region of variation of X and J is broken up in four parts, as shown in the figure, and an integration performed with respect to X in each of the sections, one can obtain the energy distribution $S^{(i)}(J)$ and the asymmetry of emission of the nucleons $R_N^{(i)}(J)$ in the i-th section:

$$dW_i(J; \zeta_Y, n_N) = \frac{dJ}{16\pi^3} X_m(J)\frac{d\Omega_N}{4\pi}\frac{(m_Y - m_N)^5}{(1+\xi)^3}(1-\eta/J)^2 \times [S^{(i)}(J) + R_N^{(i)}(J)(\zeta_Y n_N)]. \qquad (13)$$

For electronic decays ($\eta = 0$), the only ones considered in this section, it follows from (A.1) and (A.2) that

$$S^{(1)} + S^{(2)} + S^{(3)} + S^{(4)} = \tfrac{4}{3}\{C_A^2(1+2J)(1-\xi^2 J) + C_V^2(1-J)(1+2\xi^2 J) + (m_Y - m_N)^2 J[B_A^2(2+J)(1-\xi^2 J) + B_V^2(1-J)(2+\xi^2 J)] - 6(m_Y - m_N)J[C_A B_A(1-\xi^2 J) - C_V B_V \xi(1-J)]\},$$

$$[S^{(1)} + S^{(4)}] - [S^{(2)} + S^{(3)}] = \tfrac{1}{2}X_m^2(J)[-(C_V^2 + C_A^2) + (m_Y - m_N)^2 J(B_V^2 + B_A^2)],$$

$$[S^{(1)} + S^{(2)}] - [S^{(3)} + S^{(4)}] = 4\xi J X_m(J)[-C_V C_A + B_V B_A(m_Y^2 - m_N^2) + (m_Y - m_N)C_V B_A - (m_Y + m_N)C_A B_V],$$

$$R_N^{(1)} + R_N^{(2)} + R_N^{(3)} + R_N^{(4)} = \tfrac{8}{3}X_m(J)\{C_V C_A(1-2\xi J) + (m_Y - m_N)^2 J B_V B_A(2-\xi J) - (m_Y - m_N)J[C^V B_A(1-2\xi) + C_A B_V(2-\xi)]\}$$

$$[R_N^{(1)} + R_N^{(4)}] - [R_N^{(2)} + R_N^{(3)}] = X_m(J)\{[-C_V C_A + (m_Y - m_N)^2 J B_V B_A](1+\xi J) + (m_Y - m_N)J(1+\xi)(C_V B_A - C_A B_V)\},$$

$$[R_N^{(1)} + R_N^{(2)}] - [R_N^{(3)} + R_N^{(4)}] = 2J\{[C_A - (m_Y - m_N)B_A]^2(1-\xi^2 J) + [\xi C_V + (m_Y - m_N)B_V]^2(1-J)\}. \qquad (14)$$

Further analysis, generally speaking, requires that the expressions obtained upon substitution of (5) in (14) be compared with the experimental dependence of $S^{(i)}$ and $R_N^{(i)}$ on J. Such a comparison, however, requires the accumulation of much statistical material. If, however, we neglect in first approximation quantities of order $(m_Y - m_N)^2 a^2/3$, i.e., leave only the statistical values of the form factors, then (14) can be integrated with respect to J, after which comparison with experiment means simply the counting of the number of points entering into each of the four regions on the diagram. The total probability of decay with entry into the i-th region and the integral asymmetry in the same region are given by

$$dW_i(\zeta_Y; n_N) = \frac{(m_Y - m_N)^5}{30\pi^3(1+\xi)^3}\frac{d\Omega_N}{4\pi}[s^{(i)} + r_N^{(i)}(\zeta_Y n_N)]; \qquad (15)$$

if we neglect quantities of order $(m_Y - m_N)^2 a^2/3$ and ξ, then, taking (6) into account:

$$s^{(1)} + s^{(2)} + s^{(3)} + s^{(4)} = 3C_A^2 + C_V^2 - 4(m_Y - m_N)C_A B_A,$$

$$[s^{(1)} + s^{(4)}] - [s^{(2)} + s^{(3)}] = -\tfrac{3}{8}(C_V^2 + C_A^2),$$

$$[s^{(1)} + s^{(2)}] - [s^{(3)} + s^{(4)}] = -\tfrac{5}{4}\xi[C_V C_A + (m_Y + m_N)C_A B_V + (m_Y^2 - m_N^2)B_V B_A],$$

$$r_N^{(1)} + r_N^{(2)} + r_N^{(3)} + r_N^{(4)} = \tfrac{5}{2}\left[C_V C_A - \tfrac{1}{3}(m_Y - m_N)(C_V B_A + 2C_A B_V)\right],$$

$$[r_N^{(1)} + r_N^{(4)}] - [r_N^{(2)} + r_N^{(3)}] =$$
$$- \tfrac{5}{16}[3C_VC_A + (m_Y - m_N)(C_AB_V - C_VB_A)],$$
$$[r_N^{(1)} + r_N^{(2)}] - [r_N^{(3)} + r_N^{(4)}] = C_A^2 - 2(m_Y - m_N)C_AB_A. \quad (16)$$

It is interesting to note that if estimate (6) is correct then, both in (16) and in (14), the decisive role is played in the third expression by the product C_AB_V; the effect itself is in this case of order $(m_Y - m_N)a$, i.e., it is not too small.

Expressions (16) make it possible in principle to determine C_V, C_A, B_V, and B_A in such an approximation, that their dependence on J can be disregarded. If expansion (5) is substituted in (14) for the form factors, then additional terms appear in (16). An experimental determination of $s^{(i)}$ and $r_N^{(i)}$ would then yield six relations between the eight unknowns

$$C_V(0), C_A(0), B_V(0), B_A(0), a(C_V), a(C_A), a(B_V), a(B_A). \quad (17)$$

The additional relations between these quantities, and consequently also the possibility of their determination, can be obtained by investigating the emission asymmetry not of the nucleon alone, but of the electron and neutrino, too. If $R_e(X, J)$ is defined in analogy with (12), its expression is

$$R_e(X,J) = \frac{J(1+\xi)^2}{1+X+\xi J}\{-(C_V - C_A)^2 (1 + X - \xi J)$$
$$- (m_Y - m_N)^2 \times (B_V - B_A)^2 J(1 - X - \xi J)$$
$$+ 2(m_Y - m_N) J(1-\xi)(C_V - C_A)(B_V - B_A)\}$$
$$+ (C_V^2 + C_A^2) 2\xi XJ + (C_V^2 - C_A^2)(1 - \xi^2) J$$
$$- 2C_VC_A(1 - X^2 - \xi^2J^2) + (m_Y - m_N)^2 J\{-(B_V^2 + B_A^2)$$
$$\times 2X + (B_V^2 - B_A^2)(1 - \xi^2) J - 2B_VB_A(1 + X^2 - \xi^2J^2)\}$$
$$+2(m_Y - m_N) J\{(C_VB_V + C_AB_A)(1 - \xi) X$$
$$+ (C_AB_A - C_VB_V)(1+\xi)(1-\xi J) + (C_AB_V - C_VB_A)$$
$$\times(1 + \xi) X + (C_VB_A + C_AB_V)(1 - \xi)(1 + \xi J)\} \quad (18)$$

with $R_\nu(X, J)$ obtainable from (18) by substituting $-X$ for X, $-C_A$ for C_A, and $-B_A$ for B_A, and reversing the sign of the entire expression. Integrating R_e and R_ν with respect to X and [after substituting (5)] with respect to J within the limits of each of the four regions in the diagram, and comparing the resultant expressions with the experimental data on the asymmetry of emission of the electron and the neutrino, new relations are obtained between the parameters (17).

To determine the remaining form factors, i.e., $D_V(0)$, $D_A(0)$, and $a(D_V)$, it is necessary to investigate analogously the μ-mesic decays of hyperons, starting with the equations of Appendix A.

4. ENERGY DISTRIBUTION, EMISSION ASYMMETRY, AND POLARIZATION OF THE EMITTED NUCLEONS OR HYPERONS

The energy distribution and the emission asymmetry of N in the case of electronic decays are given by the first and fourth equations of (14). Analogous expressions for μ-mesic decays are obtained by integrating Eqs. (A.1) and (A.2) with respect to X. The result is

$$dW(J; \zeta_Y, \mathbf{n}_N) = \frac{dJ}{24\pi^3}\frac{(m_Y - m_N)^5}{(1+\xi)^3} X_m(J)\left(1 - \frac{\eta}{J}\right)^2 \frac{d\Omega_N}{4\pi}$$
$$\times S_N(J)[1 + \alpha_N(J)(\zeta_Y \mathbf{n}_N)], \quad (19)$$

$$S_N(J) = (C_V^2 + C_A^2)\{2 + J + \xi^2 J(1 - \tfrac{4}{3}J)$$
$$+ \eta[4 - J - \xi^2 J(1 + 2J)]/J\}$$
$$+ 3(C_A^2 - C_V^2)(1 - \xi^2) J + 2(m_Y - m_N)^2 J(1 + \eta/2J)$$
$$\times [B_V^2(1 - J)(2 + \xi^2 J) + B_A^2(2 + J)(1 - \xi^2 J)]$$
$$+ 3\eta(m_Y - m_N)^2 J[D_V^2(1 - \xi^2 J) + D_A^2 \xi^2 (1 - J)]$$
$$- 12(m_Y - m_N) J(1 + \eta/2J)[C_AB_A(1 - \xi^2 J)$$
$$- C_VB_V \xi(1 - J)] - 6\eta(m_Y - m_N)[C_VD_V(1 - \xi^2 J)$$
$$- C_AD_A \xi(1 - J)]; \quad (20)$$

$$\alpha_N(J) = 4S_N^{-1}(J) X_m(J)\{C_VC_A[1 - 2\xi J + \eta(2 - \xi J)/J]$$
$$+ (m_Y - m_N)^2 J(1 + \eta/2J)(2 - \xi J) B_VB_A$$
$$- \tfrac{3}{2}\eta(m_Y - m_N)^2 J\xi D_VD_A - \tfrac{3}{2}\eta(m_Y - m_N)$$
$$\times (C_AD_V - C_VD_A\xi)$$
$$- (m_Y - m_N) J(1 + \eta/2J)[C_VB_A(1 - 2\xi)$$
$$+ C_AB_V(2 - \xi)]\}. \quad (21)$$

The polarization vector of the emitted nucleon (or hyperon) is determined by

$$\mathbf{P}_N = P_1(J)\mathbf{n}_N + P_2(J)\mathbf{n}_N(\zeta_Y \mathbf{n}_N) + P_3(J)[\mathbf{n}_N[\zeta_Y \mathbf{n}_N]], \quad (22)$$

with (the method of calculating P_i was described earlier[5])

$$P_1(J) S_N(J)[1 + \alpha_N(J)(\zeta_Y \mathbf{n}_N)] = 4X_m(J)\{C_VC_A[1 + 2\xi J$$
$$+ (\eta/J)(2 + \xi J)] - (m_Y - m_N)^2 J(1 + \eta/2J)$$
$$\times (2 + \xi J) B_VB_A - \tfrac{3}{2}\eta(m_Y - m_N)^2 J\xi D_VD_A$$
$$- \tfrac{3}{2}\eta(m_Y - m_N)(C_AD_V - C_VD_A\xi) + (m_Y - m_N)$$
$$\times J(1 + \eta/2J)[C_AB_V(2 + \xi) - C_VB_A(1 + 2\xi)]\};$$
$$P_2(J) S_N(J)[1 + \alpha_N(J)(\zeta_Y \mathbf{n}_N)] = (C_V^2 + C_A^2)\{2 - 3J - \xi^2 J$$
$$\times (3 - 4J) + \eta[4 - 3J - \xi^2 J(3 - 2J)]/J\} + (C_V^2 - C_A^2)$$
$$\times (1 - \xi^2) J(1 + 2\eta/J) - 2(m_Y - m_N)^2 J(1 + \eta/2J)$$
$$\times [B_V^2(1 - J)(2 - \xi^2 J) + B_A^2(2 - J)(1 - \xi^2 J)]$$
$$+ 3\eta(m_Y - m_N)^2 J[D_V^2(1 - \xi^2 J) + D_A^2 \xi^2 (1 - J)]$$
$$+ 4(m_Y - m_N) J(1 + \eta/2J)[C_AB_A(1 - \xi^2 J)$$
$$- C_VB_V \xi(1 - J)] - 6\eta(m_Y - m_N)[C_VD_V(1 - \xi^2 J)$$
$$- C_AD_A \xi(1 - J];$$

$$P_3(J)\,S_N(J)\,[1+\alpha_N(J)\,(\zeta_Y\,n_N)] =$$
$$-(C_V^2+C_A^2)(1-\xi^2)J\,(1-\eta/J)$$
$$+(C_V^2-C_A^2)\,(1+2\eta/J)\,(2-J-\xi^2J)$$
$$-2\,(m_Y-m_N)^2\,J^2\,(1+\eta/2J)\,[B_A^2\,(1-\xi^2J)-B_V^2\xi^2\,(1-J)]$$
$$+3\eta\,(m_Y-m_N)^2\,J[D_V^2\,(1-\xi^2J)-D_A^2\,\xi^2\,(1-J)]$$
$$+4\,(m_Y-m_N)\,J\,(1+\eta/2J)\,[C_AB_A\,(1-\xi^2J)$$
$$+C_VB_V\xi\,(1-J)]-6\eta\,(m_Y-m_N)\,[C_VD_V\,(1-\xi^2J)$$
$$+C_AD_A\xi\,(1-J)]. \qquad (23)$$

We see that (20) — (23) do not contain interferences between the form factors B and D. In addition, S_N, P_2, and P_3 have no "cross products" C_VC_A, C_VB_A, C_VD_A, C_AB_V, C_AD_V, B_VB_A, or D_VD_A, which enter only in α_N and P_1. This is the consequence of certain formal properties of the invariance of the matrix element (2) — (3), discussed in reference 10.

To obtain the energy distribution and the emission asymmetry for l (or $\bar{\nu}$), it is necessary to integrate over variable N and $\bar{\nu}$ (or l). It is possible to obtain in this manner also the polarization of the emitted muons (the electrons should be almost totally polarized). The foregoing integration can be performed, however, only by specifying a concrete dependence of the form factors on Q^2, such as the expansion (5). The results are too cumbersome and will not be written out here.

Similarly, to obtain the total decay probability and emission asymmetry of N, it is necessary to integrate over J in (19) — (21) and substitute (5) therein. If quantities of order ξ^2, $\xi\,(m_Y-m_N)^2a^2$, and $(m_Y-m_N)^4a^4$ are neglected and the estimate (6) is used, the integration is easy. In this approximation, the total decay probability is

$$W=\frac{1}{30\pi^3}\frac{(m_Y-m_N)^5}{(1+\xi)^3}\{[C_V^2(0)+3C_A^2(0)]\,\sigma_1$$
$$+\tfrac{1}{3}\,(m_Y-m_N)^2\,[B_V^2(0)\,(-4\sigma_2-(4-2\eta)\,\sigma_1+2\eta\sigma_0)$$
$$+B_A^2(0)\,(2\sigma_2+(4+\eta)\,\sigma_1+2\eta\sigma_0)]$$
$$+\eta\,(m_Y-m_N)^2\,D_V^2(0)\,\sigma_1$$
$$-2\eta\,(m_Y-m_N)\,[C_V(0)\,D_V(0)\,\sigma_0$$
$$+C_A(0)\,D_A(0)\,\xi\,(\sigma_1-\sigma_0)]-2\,(m_Y-m_N)\,[C_A(0)\,B_A(0)$$
$$\times(2\sigma_1+\eta\sigma_0)+C_V(0)\,B_V(0)\,\xi\,(2\sigma_2-(2-\eta)\,\sigma_1-\eta\sigma_0)]$$
$$-\tfrac{1}{9}\,(m_Y-m_N)^2\,[C_V^2(0)\;a^2(C_V)+C_A^2(0)\,a^2(C_A)]$$
$$\times[\sigma_2+(2-\eta)\,\sigma_1+4\eta\sigma_0]-\tfrac{1}{3}\,(m_Y-m_N)^2\,[C_A^2(0)\,a^2(C_A)$$
$$-C_V^2(0)\,a^2(C_V)]\,\sigma_2+a^2(B_A)]\,(2\sigma_2+\eta\sigma_1)$$
$$+\tfrac{1}{3}\,(m_Y-m_N)^3\,C_A(0)\,B_A(0)\,[a^2(C_A)$$
$$+\tfrac{1}{3}\,\eta\,(m_Y-m_N)^3\,C_V(0)\,D_V(0)$$
$$\times[a^2(C_V)+a^2(D_V)]\,\sigma_1\}. \qquad (24)$$

The quantities

$$\sigma_k\equiv\frac{15}{4}\int_\eta^1 dJ\,\sqrt{1-J}\,(1-\eta/J)^2\,J^k$$

have values

$$\sigma_0=\frac{5}{4}(2+13\,\eta)\,\sqrt{1-\eta}-\frac{15}{8}\,\eta\,(4+\eta)\ln\left|\frac{1+\sqrt{1-\eta}}{1-\sqrt{1-\eta}}\right|,$$
$$\sigma_1=\left(1-\frac{9}{2}\,\eta-4\eta^2\right)\sqrt{1-\eta}+\frac{15}{4}\,\eta^2\ln\left|\frac{1+\sqrt{1-\eta}}{1-\sqrt{1-\eta}}\right|,$$
$$\sigma_2=\frac{4}{7}\,(1-\eta)^3\sqrt{1-\eta}. \qquad (25)$$

To estimate the probabilities of leptonic hyperon decays, one can put in (24) $B_V=B_A=D_V=D_A=0$, $a(C_V)=a(C_A)=0$, and $C_V=-C_A=G/\sqrt{2}$. We give below a table of the probabilities thus calculated. Also given are the values of ξ, η (for $l=\mu$), τ (the experimental lifetime of the hyperon), and $W_{l\tau}$ (ratio of the number of events of corresponding lepton decay to the total number of hyperon decay). The last two columns list the experimental values[2] of $W_{l\tau}$. In the case of Ξ^- decays, $W_{l\tau}$ is assumed to be less than 0.7, since up to now 14 $\Xi^-\to\Lambda+\pi^-$ events have been observed,[17,11] but not a single leptonic decay. For the sake of completeness, the table includes the decays $\Sigma^+\to n+l^++\nu$ for a reduction of 1 in the baryon charge and $\Xi^-\to n+l^-+\bar{\nu}$ for a change of 2 in strangeness.

5. THE DECAYS $\Sigma\to\Lambda+e+\nu$

The table includes also the decays $\Sigma^+\to n+e^\pm+\nu(\bar{\nu})$, in which both baryons have the same strangeness, as in ordinary β decay. According to reference 3, the divergence of the current responsible for these processes is equal to zero. This means[12,13] that in (3) we have for the same spatial parity of Σ and Λ

$$C_V=D_VQ^2/(m_\Sigma-m_\Lambda), \qquad (26)$$

and for different parity

$$C_A=-D_AQ^2/(m_\Sigma+m_\Lambda). \qquad (27)$$

It is seen from (26) and (27) that as $Q^2\to 0$, $C_V(C_A)$ also vanishes. This is the consequence of the absence of a direct interaction, responsible for the decay $\Sigma\to\Lambda+e+\nu$, if the divergence of the vector portion of the baryon current is zero.[14] It is therefore natural to turn again to the analogy with electrodynamics and, assuming as in Sec. 2 that $C_V(C_A)\sim GQ^2a^2/6\sqrt{2}$, put $a\sim 0.8\times10^{-13}$ cm. In this case $C_V(C_A)\lesssim 0.014\,G/\sqrt{2}$, i.e., it is sufficiently small. Inasmuch as the form factor $C_A(C_V)$ should not vanish as $Q^2\to 0$, there are

Type of decay	ξ	η	$10^{10}\tau$, sec	W_e, sec^{-1}	W_μ, sec^{-1}	$W_e\tau$, %	$W_\mu\tau$, %	Experimental values	
								$W_e\tau$, %	$W_\mu\tau$, %
$\Lambda \to p + l^- + \bar{\nu}$	0.086	0.355	2.8	$5.8\cdot10^7$	$9.4\cdot10^6$	1.7	0.26	~0.13	<0.12
$\Sigma^- \to n + l^- + \bar{\nu}$	0.12	0.17	1.7	$3.4\cdot10^8$	$1.5\cdot10^8$	5.7	2.5	≲0.5	≲0.5
$\Xi^- \to \Lambda + l^- + \bar{\nu}$	0.084	0.265	~2	$1.2\cdot10^8$	$3.2\cdot10^7$	2.4	0.64	<7	<7
$\Xi^- \to \Sigma^0 + l^- + \bar{\nu}$	0.052	0.66	~2	$1.4\cdot10^7$	$2.1\cdot10^5$	0.3	0.004	<7	<7
$\Sigma^+ \to n + l^+ + \nu$	0.12	0.18	0.8	$3.0\cdot10^8$	$1.3\cdot10^8$	2.4	1.0	<1.1	<1.3
$\Xi^- \to n + l^- + \bar{\nu}$	0.17	0.077	~2	$2.1\cdot10^9$	$1.5\cdot10^9$	40	30	<7	<7
$\Sigma^- \to \Lambda + e^- + \bar{\nu}$	0.035		1.7	$1.4\cdot10^6$		0.024			
$\Sigma^+ \to \Lambda + e^+ + \nu$	0.032		0.8	$8.6\cdot10^5$		0.007			

no grounds for assuming it to be as small. Therefore one can expect in the decays $\Sigma \to \Lambda + e + \nu$ that $C_A \gg C_V$ ($C_V \gg C_A$). There are less grounds for assuming that $C_A \gg B_V$ ($m_\Sigma - m_\Lambda$) [$C_V \gg B_A$ ($m_\Sigma - m_\Lambda$)], but if it assumed in analogy with (6) that $B \sim Ga/\sqrt{2}$, then when $a \sim 0.8 \times 10^{-13}$ cm we have $(m_\Sigma - m_\Lambda)\, a \sim 1/3$, i.e., an additional small factor arises. If the foregoing inequalities are correct, then according to (19) — (23) the asymmetry of emission of $\Lambda(\alpha)$ and the polarization of $\Lambda(P_1)$ will be small in the decay of unpolarized Σ. It would be interesting to verify this fact experimentally.

Unfortunately, the $\Sigma \to \Lambda + e + \nu$ decays can hardly be observed in the near future; the lack of a direct decay current [$\bar{\psi}_\Lambda \gamma_\mu (1 + \gamma_5) \psi_\Sigma$] can reduce the decay probability by an additional several times.

APPENDIX

A. Energy Correlation and Asymmetry of Hyperon Decay

The formulas for $S(X, J)$ and $R_N(X, J)$, determined in accordance with (12), are

$$
\begin{aligned}
S(X,J) &= (C_V^2 + C_A^2)\{1 - X^2 - \xi^2 J^2) + \eta[(1-X)^2 - \xi^2 J^2]/J\} \\
&+ (C_A^2 - C_V^2)(1-\xi^2) J - 4 C_V C_A \xi X J \\
&+ (m_Y - m_N)^2 J\{(B_V^2 + B_A^2)[(1 + X^2 - \xi^2 J^2) \\
&+ \eta[1 - X^2 - J(1+\xi^2)/2]/J] + (B_A^2 - B_V^2)(1 + \eta/2J) \\
&\times (1-\xi^2) J + 4 B_V B_A X\} + \eta (m_Y - m_N)^2 J\{D_V^2 (1 - \xi^2 J) \\
&+ D_A{}^2 \xi^2 (1-J)\} + 4 (m_Y - m_N) J\{-C_A B_A[(1-\xi^2 J) \\
&+ \eta(1 - X - \xi^2 J)/2J] + C_V B_V \xi[1 - J \\
&+ \eta(1 - J - X)/2J] - C_A B_V X \\
&+ C_V B_A \xi X\} \\
&- 2\eta (m_Y - m_N)\{C_V D_V (1 - \xi^2 J - X) \\
&- C_A D_A \xi (1 - J - X)\} \\
&+ 2\eta (m_Y - m_N)^2 (B_V D_V + B_A D_A) \xi X J. \qquad \text{(A.1)}
\end{aligned}
$$

$$
\begin{aligned}
R_N(X,J) &= 2 X_m(J)\{[C_A^2 (1 - \xi^2 J) + C_V^2 \xi^2 (1-J)] X J / X_m^2 \\
&+ C_V C_A [(1 - \xi J) - X^2 (1 + \xi J)/X_m{}^2 + \eta\{(1 - \xi J) \\
&+ X^2 (1 + \xi J)/X_m^2 - X[2 - J(1+\xi^2)]/X_m^2\}/J] \\
&+ (m_Y - m_N)^2 X J [B_V^2 (1-J) + B_A^2 (1 - \xi^2 J)]/X_m^2 \\
&+ (m_Y - m_N)^2 J B_V B_A [(1 - \xi J) + X^2 (1 + \xi J)/X_m^2 \\
&+ \eta\{1 - X^2 X_m^{-2} (1 + \xi J)\}/J] - \eta (m_Y - m_N)^2 J \xi D_V D_A \\
&- 2 (m_Y - m_N) J X X_m^{-2} [C_A B_A (1 - \xi^2 J) \\
&- C_V B_V \xi (1 - J)] - (m_Y - m_N) J C_A B_V [(1 - \xi) \\
&+ X^2 (1 + \xi)/X_m^2 + (\eta/J)\{1 - X^2 (1+\xi)/X_m^2 + \xi X \\
&\times (1 - J)/X_m^2\}] \\
&- (m_Y - m_N) J C_V B_A [(1 - \xi) - X^2 (1 + \xi)/X_m^2 \\
&- \eta J^{-1} \times \{\xi - X^2 (1 + \xi)/X_m^2 + X (1 - \xi^2 J)/X_m^2\}] \\
&- \eta (m_Y - m_N)[C_A D_V \{1 - X (1 - \xi^2 J)/X_m^2\} \\
&- C_V D_A \xi \{1 - X (1 - J)/X_m^2\}] \\
&- \eta (m_Y - m_N)^2 X J X_m^{-2} \\
&\times [B_A D_V (1 - \xi^2 J) + B_V D_A \xi^2 (1 - J)]\}. \qquad \text{(A.2)}
\end{aligned}
$$

B. Variants of Decay Interaction

The universal V-A interaction scheme[3,4] is at present in splendid agreement with all experimental data on β decay, K capture, induced antineutrino absorption, and pion and muon decay. An extension of this scheme to include the decays of strange particles is at the same time a hypothesis the likelihood of which is based essentially on the agreement between the orders of magnitude of the decay constants of strange and ordinary particle. Contemporary experimental data[2] indicate, in particular, that the $\Lambda \to p + e^- + \bar{\nu}$ decay is approximately one-tenth as frequent as in the universal V-A scheme without renormalization. This agree both with the relatively low probability of $K_{\mu 2}$, $K_{\mu 3}$, and K_{e3} decays,[13,15] and with the fact that i the V-A scheme one must have a renormalizatio of the decay constants[16,14] which can fully lead to their reduction by a factor of several times. At

the same time, the rule $\Delta T = \pm 1/2$, which holds with good accuracy for leptonless decays of strange particles,[17,18] is accidental in the Feynman-Gell-Mann theory, if one excludes from it the neutral baryon and meson currents. In the latter case, the universality of the scheme would necessitate also the introduction of neutral lepton currents, which would lead to the presence of the decays $K^0 \to \mu^+ + \mu^-$, $K^+ \to \pi^+ + e^+ + e^-$, $K^+ \to \pi^+ + \nu + \bar{\nu}$, and $K^+ \to \pi^+ + \mu^+ + \mu^-$, which have not been observed experimentally. Therefore, the extent to which the V-A scheme describes the decay of strange particles remains, strictly speaking, moot.

The fullest answer to this question could be obtained by an experimental study of leptonic hyperon decays. The determination of the variations of decay interaction, to be sure, is made difficult here by the presence of many (12) energy-dependent form factors, the determination of which calls for an accuracy and completeness of experimental data hardly attainable now. The problem becomes much simpler if the contribution from the form factors is assumed small. Under this assumption one can start the calculations with the form of the Lee-Yang matrix element of the S matrix

$$i(2\pi)^4\delta(p_Y - p_N - p_l - p_\nu)\sum_{j=1}^{5}(\bar{u}_N O_j u_Y)(\bar{u}_l O_j (C_j + C_j'\gamma_5) u_\nu), \tag{A.3}$$

where

$$O_j = 1,\ \gamma_5,\ 2^{-1/2}\sigma_{\alpha\beta},\ \gamma_\mu,\ i\gamma_\mu\gamma_5,$$

and C_j and C_j' are assumed constant.

If the energy correlation and the decay asymmetry are investigated on the basis of the matrix element (A.3), the following expressions will hold for $S(X, J)$, and $R_N(X, J)$, determined according to (12),

$$\begin{aligned}S(X,J) &= (a_{VV}+a_{AA})\{(1-\xi^2J^2-X^2)+\eta_l J^{-1}[(1-X)^2-\xi^2J^2]\}+(a_{AA}-a_{VV})(1-\xi^2)J-4a_{AV}\xi XJ\\ &+J[a_{SS}(1-\xi^2J)+a_{PP}\xi^2(1-J)-2(a_{ST}+a_{PT})\xi X]+a_{TT}\{[2-2X^2-J-\xi^2J]+2\eta_l J^{-1}[(1-X)^2-\xi^2J^2]\}\\ &+2\eta_l^{1/2}[(a_{SV}+3a_{AT})(1-X-\xi^2J)+\xi(a_{PA}+3a_{VT})(1-X-J)];\end{aligned} \tag{A.4}$$

$$\begin{aligned}R_N(X,J) &= 2X_m(J)\{[b_{AA}(1-\xi^2J)+b_{VV}\xi^2(1-J)]XJ/X_m^2+b_{VA}[(1-\xi J)-X^2(1+\xi J)/X_m^2+\eta_l J^{-1}\{(1-\xi J)\\ &+X^2(1+\xi J)/X_m^2-X[2-J(1+\xi^2)]/X_m^2\}]+J[b_{SP}\xi-XX_m^{-2}\{b_{ST}(1-\xi^2J)+b_{PT}\xi^2(1-J)\}]\\ &-b_{TT}[1-X^2(1+\xi J)/X_m^2+\eta_l J^{-1}\{(1-\xi J)+X^2(1+\xi J)/X_m^2-X[2-J(1+\xi^2)]/X_m^2\}]+\eta_l^{1/2}b_{AS}[1-X(1-\xi^2J)/X_m^2]\\ &+\eta_l^{1/2}\xi b_{VP}[1-X(1-J)/X_m^2]-\eta_l^{1/2}b_{AT}[2-\xi-XX_m^{-2}\{2-\xi(1-J)-2\xi^2J\}]\\ &+\eta_l^{1/2}b_{VT}[1-2\xi-XX_m^{-2}\{1-2\xi(1-J)-\xi^2J\}]\},\end{aligned} \tag{A.5}$$

where

$$a_{jk} \equiv (C_jC_k + C_j'C_k')/2, \qquad b_{jk} \equiv (C_jC_k' + C_j'C_k)/2. \tag{A.6}$$

An analysis fully analogous to the one of Sec. 3, allows separation of the coefficients of the different powers of X in (A.4) and (A.5). In the case of electronic decays ($\eta = 0$) and neglecting terms of order ξ, one can obtain, as in (16),

$$\begin{aligned}&s^{(1)}+s^{(2)}+s^{(3)}+s^{(4)} = a_{SS}+a_{VV}+3(a_{AA}+a_{TT}),\\ &[s^{(1)}+s^{(4)}]-[s^{(2)}+s^{(3)}] = -\tfrac{3}{8}(a_{VV}+a_{AA}+2a_{TT}),\\ &[s^{(1)}+s^{(2)}]-[s^{(3)}+s^{(4)}] = -\tfrac{5}{8}\xi(a_{ST}+a_{PT}+2a_{VA}),\\ &r_N^{(1)}+r_N^{(2)}+r_N^{(3)}+r_N^{(4)} = \tfrac{5}{2}(b_{VA}-b_{TT}),\\ &[r_N^{(1)}+r_N^{(4)}]-[r_N^{(2)}+r_N^{(3)}] = -\tfrac{15}{16}(b_{VA}-b_{TT}),\\ &[r_N^{(1)}+r_N^{(2)}]-[r_N^{(3)}+r_N^{(4)}] = b_{AA}-b_{ST}.\end{aligned} \tag{A.7}$$

For the asymmetry of emission of l, in the case of electronic decays, the following expression holds

$$\begin{aligned}R_e(X,J) &= -J(1+\xi)^2(1+X-\xi J)(1+X+\xi J)^{-1}\\ &\times[(b_{VV}+b_{AA}-b_{TS}-b_{TP})-2(b_{VA}-b_{TT})]\\ &+(b_{VV}+b_{AA}-b_{TS}-b_{TP})\\ &\times 2\xi XJ-(b_{AA}-b_{VV}+b_{TP}-b_{TS})(1-\xi^2)J\\ &-2(b_{VA}-b_{TT})(1-X^2-\xi^2J^2)\\ &-2(b_{SP}-b_{TT})\xi J[1+\xi J-J(1+\xi)^2/(1+X+\xi J)].\end{aligned} \tag{A.8}$$

As in (A.7), we neglect terms of order ξ and obtain

$$\begin{aligned}&r_e^{(1)}+r_e^{(2)}+r_e^{(3)}+r_e^{(4)} = -2[(b_{AA}-b_{TS})+(b_{VA}-b_{TT})],\\ &[r_e^{(1)}+r_e^{(4)}]-[r_e^{(2)}+r_e^{(3)}] = \tfrac{3}{4}(b_{VA}-b_{TT}),\\ &[r_e^{(1)}+r_e^{(2)}]-[r_e^{(3)}+r_e^{(4)}] = \tfrac{5}{24}\xi\{(b_{VV}+b_{AA}-b_{TS}\\ &\quad -b_{TP})+2(2b_{VA}-b_{TT}-b_{SP})\}.\end{aligned} \tag{A.9}$$

$R(X, J)$ is obtained from (A.8) by reversing the

sign of X and of the constants C_T, C'_T, C_V, and C'_A, followed by reversal of the sign of the entire expression. It is easily seen that knowledge of (A.7) and (A.9) alone is not enough for the determination of the variants of the decay interactions, since these formulas yield only the combinations of constants

$$a_{VV} + a_{AA} + 2a_{TT},\ b_{VA} - b_{TT},$$
$$a_{AA} - a_{VV} - a_{TT} + a_{SS},\ b_{AA} - b_{ST} \qquad \text{(A.10)}$$

(the combinations of constants which are further multiplied by ξ cannot be determined with any degree of accuracy, since the unaccounted form factors should make a large contribution to the corresponding terms).

Such a result was obvious from the very outset, since the transition from the V-A to the S+P-T variant for $C' = C$ leads in the case of hyperon decay, as shown in the Appendix of reference 5, only to a reversal of the polarization of N and l, and this cannot affect in any manner the energy distribution and asymmetry of emission of N, l, and $\bar{\nu}$. To determine the decay interaction it is therefore necessary to study the polarization of N or l. In particular, in the case of electronic decays the polarization of N can be determined from the formulas of reference 19, where the muon decay is calculated, by making the substitutions $\mu \to Y$, $e \to N$. In our notation, these formulas are [S_N, α_N, and P_i are determined from (19) and (22)]:

$$S_N(J) = 2a_{AA}(1 + 2J)(1 - \xi^2 J) + 2a_{VV}(1 - J)(1 + 2\xi^2 J) + 3a_{SS}J(1 - \xi^2 J) - 3a_{PP}\xi^2 J(1 - J) + a_{TT}[4 - J - \xi^2 J(1 + 2J)],$$

$$\alpha_N(J) = 2S_N^{-1}(J)\, X_m(J)\{2b_{VA}(1 - 2\xi J) + 3b_{SP}\xi J - b_{TT}(2 - \xi J)\},$$

$$P_1(J) = 2S_N^{-1}(J)[1 + \alpha_N(J)(\zeta_Y \mathbf{n}_N)]^{-1} X_m(J)\{2b_{VA}(1 + 2\xi J) + 3b_{SP}\xi J + b_{TT}(2 + \xi J)\},$$

$$P_2(J) = S_N^{-1}(J)[1 + \alpha_N(J)(\zeta_Y \mathbf{n}_N)]^{-1}\{2a_{VV}(1 - J)(1 - 2\xi^2 J) + 2a_{AA}(1 - 2J)(1 - \xi^2 J) + 3a_{SS}J(1 - \xi^2 J) + 3a_{PP}\xi^2 J(1 - J) - a_{TT}[4 - 3J - \xi^2 J(3 - 2J)]\},$$

$$P_3(J) = S_N^{-1}(J)[1 + \alpha_N(J)(\zeta_Y \mathbf{n}_N)]^{-1}\{2a_{VV}(1 - J) - 2a_{AA}(1 - \xi^2 J) + 3a_{SS}J(1 - \xi^2 J) - 3a_{PP}\xi^2 J(1 - J) - a_{TT}(1 - \xi^2)J\}. \qquad \text{(A.11)}$$

When $\xi \ll 1$, we obtain in (A.11) $\alpha_N S_N = 4(b_{VA} - b_{TT})$, $P_1 \sim (b_{VA} + b_{TT})$, i.e., a study of the asymmetry of emission as well as the polarization of N make it possible to determine the variant of the decay interaction. The situation here is fully analogous with the case of muon decay.[19]

The formulas for the polarization of l when $\xi \ll 1$ coincide with the known expression for electron polarization in the decay of the free neutron.

To find the polarization of Λ in the decay $\Xi^- \to \Lambda + l^- + \bar{\nu}$ one can use the known asymmetry of the decay $\Lambda \to p + \pi^-$. Analogously, in the decays $Y \to N + \mu + \nu$ the polarization of μ leads to asymmetry of the decay $\mu \to e + \nu + \bar{\nu}$.

[1] Crawford, Cresti, Good, Kalbfleisch, Stevenson, and Ticho. Phys. Rev. Lett. **1**, 377 (1958).

[2] Nordin, Orear, Read, Rosenfeld, Solmitz, Taft, and Tripp. Phys. Rev. Lett. **1**, 380 (1958).

[3] R. P. Feynman and M. Gell-Mann, Phys. Rev. **109**, 198 (1958).

[4] E. C. G. Sudarshan and R. E. Marshak, Phys. Rev. **109**, 1860 (1958).

[5] V. M. Shekhter, JETP **35**, 458 (1958), Soviet Phys. JETP **8**, 316 (1959).

[6] M. L. Goldberger and S. B. Treiman, Phys. Rev. **111**, 354 (1958).

[7] R. Hofstadter, Revs. Modern Phys. **28**, 214 (1956).

[8] R. H. Dalitz, Phil. Mag. **44**, 1068 (1953).

[9] I. Yu. Kobzarev, JETP **34**, 1347 (1958), Soviet Phys. JETP **7**, 930 (1958).

[10] V. M. Shekhter, JETP **38**, 534 (1960), this issue p. 406.

[11] Fowler, Powell, and Shonle, Nuovo cimento **11**, 458 (1959).

[12] G. Feldman and T. Fulton, Nucl. Phys. **8**, 106 (1958).

[13] L. B. Okun', Ann. Rev. Nucl. Sci. **9** (1959).

[14] V. M. Shekhter, JETP **36**, 581 (1959), Soviet Phys. JETP **9**, 403 (1959).

[15] V. M. Shekhter, JETP **36**, 1299 (1959), Soviet Phys. JETP **9**, 920 (1959).

[16] M. L. Goldberger and S. B. Treiman, Phys. Rev. **110**, 1478 (1958).

[17] M. Gell-Mann and A. Rosenfeld, Ann. Rev. Nucl. Sci. **7**, 407 (1957).

[18] Cool, Cork, Cronin, and Wenzel, BAPS **4**, 83 (1959).

[19] L. B. Okun' and V. M. Shekhter, JETP **34**, 1250 (1958), Soviet Phys. JETP **7**, 864 (1958); Nuovo cimento **10**, 359 (1958).

Translated by J. G. Adashko
109

THE POSSIBILITY OF THE DETERMINATION OF THE SCATTERING AMPLITUDES OF UNSTABLE PARTICLES AT ZERO ENERGY

V. N. GRIBOV

Leningrad Physico-technical Institute, Academy of Sciences, U.S.S.R.

Submitted to JETP editor August 14, 1959

J. Exptl. Theoret. Phys. (U.S.S.R.) 38, 553-569 (February, 1960)

The possibility of determining the scattering amplitudes of unstable particles by analyzing the energy and angular distributions of reactions in which they are produced is considered. Reactions are discussed involving the formation of two particles ($\pi + N \to \Lambda + K$, $\Sigma + K$) and three particles ($N + N \to N + \Lambda + K$), two of which interact by resonance at low energy.

1. INTRODUCTION

OF the elementary particles known at the present time, the majority are unstable. This circumstance greatly complicates the study of their interaction, inasmuch as it is impossible to carry out direct experiments on the scattering of unstable particles by each other. Therefore, it is important to find indirect means for the measurement of quantities characterizing the interaction of unstable particles.

In the recent papers of Chew,[1] Chew and Low,[2] and Pomeranchuk and Okun'[3] the possibility was considered of measuring the scattering amplitudes of unstable particles by each other by means of an analytic continuation of the cross sections of processes taking place with stable particles or by measurement of the phases of the scattering corresponding to large orbital momentum. This mode of measurement is extremely attractive inasmuch as it can give information on the interaction of unstable particles over a wide range of energies and transferred momenta. However, practical application of this method is at present complicated because of the non-uniqueness of the analytic continuation of cross sections and the difficulties of measurement of phases with large momenta.

Another method of measurement of quantities characterizing the interaction of unstable particles is based on a study of reactions with production of these particles close to threshold or at the limit of the spectrum.[4-6] This method is more limited by reason of the fact that it affords a possibility of determining the scattering amplitudes of unstable particles only for zero energy of their relative motion. However, it is entirely unambiguous and much simpler than the method of Chew et al. Up to recent times, this method has been used only in the case of reactions with production of three particles, two of which interact by resonance at low energy (Migdal and Watson[4]).

In references 5 and 6, reactions were considered with the production of three particles of low energy which interact in nonresonant fashion. For the determination of the scattering amplitudes of the generated particles in certain reactions, for example, $\pi^- + p \to n + \pi^+ + \pi^-$, $n + \pi^0 + \pi^0$, $p + \pi^- + \pi^0$, it was shown to be sufficient to measure their energy distribution, and in the others ($K^+ \to 2\pi^0 + \pi^-$, $2\pi^0 + \pi^+$) it was necessary to measure the correlation between directions of their emission.

The possibility of determining amplitudes in these cases is brought about for different physical reasons, as will be made clear in what follows.

In the first case, the possibility of determining the amplitudes is based on the fact that if we consider the matrix element of a reaction (taking place in a certain volume of radius r_0) as a function of the momenta of the produced particle p_i, then the terms linear in $p_i r_0$ are completely determined by the amplitudes of pair scattering. In turn this is explained by the fact that the wave function of the three particles at $p_i \neq 0$, in the region of distances of the order of r_0 between particles, differs from the function for zero energy ($p_i = 0$), with accuracy up to terms linear in $p_i r_0$, only by a factor that is determined by the behavior of the wave function at large distances between the particles.

However, in a number of cases (for example in the reactions $K^+ \to 2\pi^+ + \pi^-$, $2\pi^0 + \pi^+$) in squaring the matrix element terms linear in $p_i r_0$ drop out from the expression for the cross section. In these cases, measurement of the energy distribution does not allow us to determine the amplitudes of pair scattering. None the less, as was shown in detail in reference 5, thanks to the effect of the

centrifugal barrier, correlations between the directions of flight of the particles are fundamentally determined by pair interactions.

In the present work, the possibilities are discussed (Sec. 2) of the determination of scattering amplitudes of unstable particles (Λ, K; Σ, K) from a study of reactions with the formation of two particles ($\pi + N \to \Lambda + K$, $\pi + N \to \Sigma + K$). The basic idea used in the study of reactions with the formation of three particles also becomes clear from this section.

In Secs. 3 and 4 we study in detail reactions with formation of three particles (of the type $N + N \to N + \Lambda + K$) under the assumption that the interaction of two of the particles (N, Λ) has a resonance character for low energies.

In contrast to Migdal,[4] we consider not only the resonance interaction but also the interaction of a third particle (for example, K) with two resonant interacting particles (N, Λ). Account of these interactions leads to corrections to the energy distribution of the produced particles [see, for example, Eq. (52)]. These corrections are of the order $p_i r_0$ and are expressed only by amplitudes of pair interactions and the effective radius of the resonant interaction.

Study of the energy distribution of the particles produced allows us in this case to measure the scattering amplitudes of all three formed particles on each other and also the effective radius of resonance interaction.

2. REACTIONS WITH FORMATION OF TWO LOW-ENERGY PARTICLES

Let us consider a reaction of the type

$$A + B \to A' + B', \tag{1}$$

where $m_A + m_B < m_{A'} + m_{B'}$ (m = mass of the corresponding particle). The matrix element of such a reaction

$$M = \langle \Psi_E^{(-)}(A', B') \mid \Psi_E^{(+)}(A, B) \rangle, \tag{2}$$

depends on the energy E in the center of mass system (c.m.s.) as an explicit function of the initial and also the final state.

However, as was noted in reference 6, one can show that the matrix element

$$\langle \Psi_{E_0}^{(-)}(A', B') \mid \Psi_E^{(+)}(A, B) \rangle,$$

where E_0, the threshold energy of the reaction (1), is an analytic function of E near $E = E_0$, with the exception of special cases. It can therefore, with accuracy up to terms of order kr_0, be replaced by the matrix element $M_0 = \langle \Psi_{E_0}^{(-)}(A', B') \mid \Psi_{E_0}^{(+)}(A, B) \rangle$, where r_0 is the effective interaction radius, $k^2 = 2\mu(E - E_0)$ and μ is the reduced mass of the particles A′ and B′. Therefore, accurate to terms linear in kr_0, the dependence of the matrix element M on the energy is determined as a function of the final state. This dependence is usually easily found because of the fact that the Schrödinger equation for the function $\Psi_E^{(-)}(A', B')$ contains only k^2 and, consequently, the dependence on k appears only as a result of the boundary condition at infinity. Since only the S-state gives a contribution to (2) at low energy, then (for distances between particles $r \gg r_0$),

$$\Psi_E^{(-)}(A', B') = e^{-i\delta} \frac{\sin(kr + \delta)}{kr},$$

δ is the phase of S-scattering of the particles A′ and B′. For $r_0 \ll r \ll 1/k$,

$$\Psi_E^{(-)}(A', B') = e^{-i\delta} \frac{\sin\delta}{kr} [1 + k\cot\delta + O(k^2 r^2)]$$
$$= e^{-i\delta} \frac{\sin\delta}{kr} \left[1 + \frac{r}{a} + O(k^2 r^2)\right], \tag{3}$$

where $a = \delta/k|_{k=0}$ is the scattering amplitude, whence it follows that, with accuracy up to terms of order kr_0, the function $\Psi_E^{(-)}$ differs from the function $\Psi_{E_0}^{(-)}$ by the factor

$$F = e^{-i\delta} \frac{\sin\delta}{ka} \text{ и } M = \langle \Psi_E^{(-)}(A', B') \mid \Psi_{E_0}^{(+)}(A, B) \rangle$$
$$= F^* \langle \Psi_{E_0}^{(-)} \mid \Psi_{E_0}^{(+)} \rangle. \tag{4}$$

However, if $a \sim r_0$ (nonresonant case), then we may expand $e^{-i\delta} \sin\delta$ in a series with the accuracy considered thus far. Then $F = 1 - ika$ and, consequently, the cross section of reaction (1) is

$$\sigma(A + B \to A' + B') = k(1 + 2k \operatorname{Im} a) |M_0|^2. \tag{5}$$

Thus, by measuring the cross section of the reaction (1), one can determine $\operatorname{Im} a = (k/4\pi)\sigma'$; σ' is the total interaction cross section of particles A′ and B′, which, because of the possibility of the reaction $A' + B' \to A + B$, is proportional to $1/k$. If other channels than $A' + B' \to A + B$ are possible in the interaction of A′ and B′, then σ' is not expressed directly in terms of σ.

Evidently the most interesting reactions of this type are

$$\pi^- + p \to \Lambda^0 + K^0, \tag{6}$$

$$\pi^+ + p \to \Sigma^+ + K^+. \tag{6'}$$

Since the reactions

$$\Lambda^0 + K^0 \to N + \pi, \quad N + 2\pi, \quad N + 3\pi, \quad N + 4\pi, \tag{7}$$

are possible at zero energies of Λ^0 and K^0, then σ' is not expressed directly in terms of σ. Furthermore, from the unitarity property of the S-matrix, considering that the contribution of the

last two reactions of (7) is small because of the smallness of the phase volume, we find that

$$\mathrm{Im}\, a = (k/4\pi)\{\sigma(\Lambda^0, K^0 \to N, \pi) + \sigma(\Lambda^0, K^0 \to N, \pi, \pi)\}. \quad (8)$$

Thus, by measuring the dependence of the cross section of reaction (5) on energy, we measure the cross section of the reaction $\Lambda^0 + K^0 \to N + \pi + \pi$ at low energy of Λ^0 and K^0.

The reaction (6′) can be considered in an analogous manner. One deficiency of this method is that only the imaginary part of the scattering amplitude is determined. As will be seen below, the real part of a can be determined from a study of the reactions

$$p + p \to \Lambda^0 + K^+ + p, \quad p + p \to \Sigma^+ + K^+ + n,$$
$$p + p \to \Sigma^+ + K^0 + p, \quad p + p \to \Sigma^0 + K^+ + p. \quad (9)$$

Other interesting possibilities of measurement of scattering amplitudes of unstable particles are uncovered if several channels with neighboring thresholds are possible in a reaction of type (1). As an example, let us consider a reaction with the formation of Σ and K particles:

$$\pi^- + p \to \Sigma^- + K^+, \quad (10a)$$
$$\pi^- + p \to \Sigma^0 + K^0. \quad (10b)$$

In this case it is immediately advantageous to make use of isotopic invariance. The state (π^-, p) is the superposition of states with isotopic spin $T = 1/2$ and $T = 3/2$. For matrix elements with the definite isotopic spins $M_{1/2}$ and $M_{3/2}$, one can write down relations that are analogous to (4):

$$M_{1/2} = (1 + ika_{1/2}^*) M_{1/2}^0, \quad M_{3/2} = (1 + ika_{3/2}^*) M_{3/2}^0, \quad (11)$$

$a_{1/2}$ and $a_{3/2}$ are the scattering amplitudes of Σ and K in the states with isotopic spin $1/2$ and $3/2$.

From this it is easy to obtain the following expression for the cross section of the reactions (10a) and (10b):

$$\sigma_{-+} = \frac{1}{3} k |M_{3/2}^0|^2 (1 + 2\sqrt{2}\, x \cos\varphi + 2x^2) \times \left[1 - 2k\, \mathrm{Im}\, \frac{(a_{3/2}^* + \sqrt{2} a_{1/2}^* e^{i\varphi})(1 + \sqrt{2} x e^{-i\varphi})}{1 + 2\sqrt{2} x \cos\varphi + 2x^2}\right], \quad (12)$$

$$\sigma_{00} = \frac{2}{3} k |M_{3/2}^0|^2 \left(1 - \sqrt{2}\, x \cos\varphi + \frac{x^2}{2}\right) \times \left[1 - 2k\, \frac{(a_{3/2}^* + x a_{1/2}^* e^{i\varphi}/\sqrt{2})(1 - x e^{-i\varphi}/\sqrt{2})}{1 - \sqrt{2}\, x \cos\varphi + x^2/2}\right], \quad (13)$$

where x, φ are the modulus and phase relation of the matrix elements $M_{1/2}^0/M_{3/2}^0$. The values of x and φ can be determined, for example, from the ratio of the cross section of reactions (10a) and (10b) to the cross section of the reaction (6′) (in which the same $M_{3/2}$ and $a_{3/2}$ enter). Then, by measuring the energy dependence of the cross section one can, by means of (12) and (13), find two relations between $a_{1/2}$ and $a_{3/2}$. Inasmuch as $\mathrm{Im}\, a_{3/2}$ is determined independently from the cross section of the reaction (6′), then three unknown quantities enter into these two relations. For a unique determination of all the quantities, it is necessary to study simultaneously reactions with the production of three particles.

3. REACTIONS WITH THE FORMATION OF THREE LOW-ENERGY PARTICLES, TWO OF WHICH UNDERGO RESONANCE INTERACTION

a) Nonresonant interaction

To establish the energy distribution in a reaction of the type

$$A + B \to A' + B' + C' \quad (14)$$

at energies close to threshold, one can proceed in a fashion similar to what was done for binary reactions. The wave function $\Psi_E^{(-)}$ of the S-state of the three particles, A′, B′, C′ in the center-of-mass system (in what follows we shall enumerate these with the indices 1, 2, 3) has the form

$$\Psi_E^{(-)}(\mathbf{r}_1, \mathbf{r}_2, \mathbf{r}_3) = \Phi(\mathbf{r}_1, \mathbf{r}_2, \mathbf{r}_3) + \frac{a_{12}}{\rho_{12}} \exp(-ik_{12}\rho_{12}) \frac{\sin p_3\rho_3}{p_3\rho_3} + \frac{a_{13}}{\rho_{13}} \exp(-ik_{13}\rho_{13}) \frac{\sin p_2\rho_2}{p_2\rho_2} + \frac{a_{23}}{\rho_{23}} \exp(-ik_{23}\rho_{23}) \frac{\sin p_1\rho_1}{p_1\rho_1} \quad (15)$$

at large distances between all particles. The spin variables are omitted everywhere in what follows for simplicity; ρ_{ik} is the distance between particles "i" and "k", ρ_l is the distance from the particle l to the center of mass of the two other particles,

$$\mathbf{k}_{il} = (m_l \mathbf{p}_i - m_i \mathbf{p}_l)/(m_i + m_l), \quad (15a)$$

$\mathbf{p}_i$ are the momenta of the particles in the c.m.s., a_{il} are the amplitudes of scattering of pairs of particles at zero energy, m_l are the masses of the particles, and $\Phi(\mathbf{r}_1, \mathbf{r}_2, \mathbf{r}_3)$ is the wave function of three free particles with a total orbital momentum equal to zero and with a fixed energy for each particle. The function $\Phi(\mathbf{r}_1, \mathbf{r}_2, \mathbf{r}_3)$ is the mean value of the function

$$\exp(i\mathbf{p}_1\mathbf{r}_1 + i\mathbf{p}_2\mathbf{r}_2 + i\mathbf{p}_3\mathbf{r}_3) = \exp(i\mathbf{k}_{12}\boldsymbol{\rho}_{12} + i\mathbf{p}_3\boldsymbol{\rho}_3) = \ldots \quad (15b)$$

over all orientations of the plane in which the vectors $\mathbf{p}_1$, $\mathbf{p}_2$ and $\mathbf{p}_3$ lie. If the state of the three particles is to be characterized not by the momenta $\mathbf{p}_1$, $\mathbf{p}_2$ and $\mathbf{p}_3$, but by their magnitudes p_1, p_2, p_3, and the Euler angles θ_i of the coordinate system that has two axes in the plane of these vectors, then

$$\Phi(\mathbf{r}_1, \mathbf{r}_2, \mathbf{r}_3) = \Phi_{p_1, p_2, p_3}(\rho_{12}, \rho_{13}, \rho_{23})$$
$$= \frac{1}{8\pi^2}\int \exp(i\mathbf{p}_1\mathbf{r}_1 + i\mathbf{p}_2\mathbf{r}_2 + i\mathbf{p}_3\mathbf{r}_3)\, d\theta_i. \quad (16)$$

Equation (16) is almost self-evident, and can easily be obtained from equations which will be presented below. We note only that it is valid under the conditions

$$\rho_{il} \gg r_0, \quad \rho_{il} \gg a_{il}. \quad (17)$$

We assume as in the case of two particles that the distances ρ_{il} are such that

$$1/k_{il} \gg \rho_{il} \gg a_{il},\ r_0. \quad (18)$$

Then, expanding in a series and limiting ourselves to terms that are linear in a/ρ, ka, we obtain

$$\Psi_E^{(-)} = 1 + a_{12}/\rho_{12} + a_{13}/\rho_{13} + a_{23}/\rho_{23} - ik_{12}a_{12}$$
$$- ik_{13}a_{13} - ik_{23}a_{23} = (1 - ik_{12}a_{12} - ik_{13}a_{13} - ik_{23}a_{23})$$
$$\times (1 + a_{12}/\rho_{12} + a_{13}/\rho_{13} + a_{23}/\rho_{23}) \quad (19)$$

in place of (15). Inasmuch as terms linear in kr_0 cannot appear from the interaction at small distances, as has already been noted, then even at small distances between the particles, the function $\Psi_E^{(-)}$ differs from the function $\Psi_{E_0}^{(-)}$ only in the factor $1 - ik_{12}a_{12} - ik_{13}a_{13} - ik_{23}a_{23}$. This result was used in references 5 and 6.

However, as is well known, in the interaction of nucleons, the scattering amplitude at zero energy $a \gg r_0$ and the condition $ka \ll 1$ are observed only in a very narrow range of energies. Therefore it is necessary to obtain a result which is free from the restriction $ka \ll 1$ (the restriction $kr_0 \ll 1$, naturally, remains).

In the case in which all the amplitudes $a_{il} \gg r_0$, the problem becomes very complicated[7] and therefore we shall limit ourselves to the case in which only a single amplitude $a_{12} \gg r_0$, while the amplitudes a_{13}, $a_{23} \sim r_0$. This case takes place for reactions of the type $N + N \to N + N + \pi$, and in the reactions

$$N + N \to N + \Lambda + K, \quad N + N \to N + \Sigma + K, \quad (20)$$

if we assume that all the baryons interact in resonant fashion at low energies. Since the simple formula (15) is no longer useful in this case, more detailed analysis of the wave function of the three-particle system is necessary to obtain results.

b) The System of Equations for the Wave Function of Three Particles

For the investigation of the wave function of three particles, it is convenient to introduce the Jacobi coordinates ρ_{12}, ρ_3, or ρ_{13}, ρ_2, or ρ_{23}, ρ_1. In the variables ρ_{12} and ρ_3, the Schrödinger equation has the form

$$\Big[-\frac{1}{2\mu_{12}}\nabla^2_{\rho_{12}} - \frac{1}{2\mu_3}\nabla^2_{\rho_3} + V_{12}(\rho_{12}) + V_{13}(\rho_{13})$$
$$+ V_{23}(\rho_{23}) + V_{123}\Big] + \Psi_E = E\Psi_E, \quad (21)$$
$$1/\mu_{12} = 1/m_1 + 1/m_2,\ 1/\mu_3 = 1/m_3 + 1/(m_1 + m_2).$$

We note that the assumption as to the existence of interaction potentials is introduced only for simplicity and final results are not dependent on it.

In order to take the asymptotic conditions into account explicitly (since we are interested in functions of the final state, Ψ_E at infinity must have the form of an incident plus an outgoing wave), it is convenient to write down the equation in integral form:

$$\Psi_E(\rho_{12}, \rho_3) = \Phi(\rho_{12}, \rho_3)$$
$$- \int G(\rho_{12} - \rho'_{12}, \rho_3 - \rho'_3)\, V_{12}(\rho'_{12})\, \Psi_E(\rho'_{12}, \rho'_3)\, d^3\rho'_{12} d^3\rho'_3$$
$$- \int G(\rho_{13} - \rho'_{13}, \rho_2 - \rho'_2)\, V_{13}(\rho'_{13})\, \Psi_E(\rho'_{13}, \rho'_2)\, d^3\rho'_{13} d^3\rho'_2$$
$$- (1 \to 2) - \int G(\rho_{12} - \rho'_{12}, \rho_3 - \rho'_3)\, V_{123}(\rho'_{12}, \rho'_3)$$
$$\times \Psi_E(\rho'_{12}, \rho'_3)\, d^3\rho'_{12} d^3\rho'_3. \quad (22)$$

$\Phi(\rho_{12}, \rho_3)$ is a function defined by (16),

$$G(\rho_{12}, \rho_3) = G(\rho_{13}, \rho_2) = G(\rho_{23}, \rho_1)$$
$$= \int \frac{d^3p\, d^3k}{(2\pi)^6} \frac{\exp\{i(\mathbf{p}\rho_3 + \mathbf{k}\rho_{12})\}}{p^2/2\mu_3 + k^2/2\mu_{12} - E + i\varepsilon}. \quad (23)$$

The following expressions will also be convenient:

$$G(\rho_{12}, \rho_3) = \frac{\mu_{12}}{2\pi}\int \frac{d^3p}{(2\pi)^3} e^{i\mathbf{p}\rho_3} \frac{e^{-ik_p\rho_{12}}}{\rho_{12}}$$
$$= -\frac{i}{8\pi^2}(\mu_{12}\mu_3)^{1/2} \frac{\varkappa^2 H_2^{(2)}\left(\varkappa\sqrt{\gamma_{12}\rho_{12}^2 + \gamma_3\rho_3^2}\right)}{\gamma_{12}\rho_{12}^2 + \gamma_3\rho_3^2},$$
$$k_p = \sqrt{2\mu_{12}(E - p^2/2\mu_3)},$$
$$\varkappa = \sqrt{2(\mu_{12}\mu_3)^{1/2}E},\ \gamma_{12} = 1/\gamma_3 = (\mu_{12}/\mu_3)^{1/2}, \quad (24)$$

$H_2^{(2)}$ are the Hankel functions. All the quadratic roots of the type k_p entering into what follows are determined for $p^2/2\mu_3 > E$ as $-i\sqrt{p^2/2\mu_3 - E}$.

In the matrix element of production of three particles in which we are interested, the wave function Ψ_E enters in the region $\rho_{12} \sim \rho_3 \sim r_0$. We want to prove that in this region, with accuracy up to terms linear in $\varkappa r_0$, Ψ_E differs from Ψ_0 only by an energy dependent factor; we want to find an expression for this factor in terms of the amplitude of the pair interaction ($E_0 = 0$).

In order to accomplish this, it suffices to show that Ψ_E differs from Ψ_0 by a factor in region

$$1/\varkappa^2 \gg \rho_{12}^2 + \rho_3^2 \gg r_0^2. \quad (25)$$

In this region one can always neglect the contribution of the three particle interaction [the last term

in (22)]. Actually, by making use of the explicit expression of the Green's function (24), we obtain the result that the last term is equal to

$$\frac{-i(\mu_{12}\mu_3)^{1/2}}{(\gamma_{12}\rho_{12}^2+\gamma_3\rho_3^2)^2}\int V_{123}(\rho'_{12},\rho'_3)\,\Psi(\rho'_{12},\rho'_3)\,d^3\rho'_{12}\,d^3\rho'_3$$

$$\sim \frac{r_0^4}{(\gamma_{12}\rho_{12}^2+\gamma_3\rho_3^2)^2}\,\overline{\Psi}(r_0,r_0),$$

if $V_{123}r_0^2(\mu_{12}\mu_3)^{1/2}\sim 1$. If the interactions of particles 1, 3; 2, 3 and 1, 2, 3 are nonresonant, then $\overline{\Psi}(r_0, r_0)\sim a_{12}/r_0$. Consequently, it is of the order $a_{12}r_0^3/(\gamma_{12}\rho_{12}^2+\gamma_3\rho_3^2)^2$, which, as will be seen, is much smaller than the contribution from the two particle interactions. Omitting this term, we consider in more detail the remaining terms in Eq. (22). In this case, it is easy to make note of the following important circumstance: if the variables on the left hand side are changed in the region (25) or even simply in the region $\rho_{12}^2+\rho_3^2\gg r_0^2$, then the function appears in one of the three regions $\rho_{12}\sim r_0$, $\rho_3\gg r_0$; $\rho_{13}\sim r_0$, $\rho_2\gg r_0$; $\rho_{23}\sim r_0$, $\rho_1\gg r_0$, on the right hand side under the integral. Therefore, if we were to know Ψ in all these regions, then we would find Ψ in the region $\rho_{12}^2+\rho_3^2\gg r_0^2$ and, consequently, in the region (25).

We shall show that in each of these regions, respectively, the function Ψ_E has the form $\varphi_{12}(\rho_{12})\Psi_3(\rho_3)$, $\varphi_{13}(\rho_{13})\Psi_2(\rho_2)$, $\varphi_{23}(\rho_{23})\Psi_1(\rho_1)$ with accuracy up to terms linear in κr_0, where φ_{il} is the wave function of the particles "i" and "l" at zero energy, while the functions $\Psi_i(\rho_i)$ satisfy some set of equations in which as unknown parameters there appear only the amplitudes of pair interactions. For solution of these equations it is shown that if $\rho_i\ll 1/\kappa$, then all the functions $\Psi_i(\rho_i)$ differ from their values for $E=0$ by one and the same factor. The latter also leads to the result that the entire function $\Psi(\rho_{12},\rho_3)$ differs from its value at $E=0$ by the same factor. Simultaneously, the functions $\Psi_i(\rho_i)$ are found; these can be used in a number of other problems.

In order to prove these assertions, we consider as an example the region $\rho_{12}\sim r_0$, $\rho_3\gg r_0$.

In this region we want to expand the right hand side of (22) in powers of κr_0 and r_0/ρ_3. For this purpose, it is convenient to represent the function $G(\rho_{12}-\rho'_{12},\ \rho_3-\rho'_3)$ in the form

$$G(\rho_{12}-\rho'_{12},\ \rho_3-\rho'_3)=\delta(\rho_3-\rho'_3)\,\frac{\mu_{12}}{2\pi|\rho_{12}-\rho'_{12}|}$$
$$+\frac{\mu_{12}}{2\pi}\int\frac{d^3p}{(2\pi)^2}e^{ip(\rho_3-\rho'_3)}\,\frac{\exp\{ik_p|\rho_{12}-\rho'_{12}|\}-1}{|\rho_{12}-\rho'_{12}|}. \qquad (26)$$

We can now carry out the indicated expansion in all terms except that containing $\delta(\rho_3-\rho'_3)$. In first approximation, we obtain ($\rho_{12}\sim r_0$, $\rho_3\gg r_0$):

$$\Psi(\rho_{12},\rho_3)=\Psi_3(\rho_3)-\frac{\mu_{12}}{2\pi}\int\frac{V_{12}(\rho'_{12})}{|\rho_{12}-\rho'_{12}|}\Psi(\rho'_{12},\rho_3)\,d^3\rho'_{12}, \qquad (27)$$

$$\Psi_3(\rho_3)=\frac{\sin p_3\rho_3}{p_3\rho_3}-\frac{\mu_{12}}{2\pi}\int G_{12}(\rho_3-\rho'_3)\,\Psi(\rho'_{12},\rho'_3)\,V_{12}(\rho'_{12})\cdot$$
$$\times d^3\rho'_{12}\,d^3\rho'_3-\int G\Big(\rho_3,-\frac{\mu_{13}}{m_1}\rho_3-\rho'_2\Big)V_{13}(\rho'_{13})\Psi(\rho'_{13},\rho'_2)d^3\rho'_{13}\,d^3\rho'_2$$
$$-\int G\Big(\rho_3,-\frac{\mu_{23}}{m_2}\rho_3-\rho'_1\Big)V_{23}(\rho'_{23})\,\Psi(\rho'_{23},\rho'_1)\,d^3\rho'_{23}\,d^3\rho'_1, \qquad (28)$$

where

$$G_{12}(\rho_3-\rho'_3)=-i\int\frac{d^3p}{(2\pi)^3}e^{ip(\rho_3-\rho'_3)}\,\sqrt{2\mu_{12}(E-p^2/2\mu_3)}$$

and the relations among ρ_{13}, ρ_2, ρ_{23}, ρ_1 and ρ_{12}, ρ_3, and the smallness of ρ_{12} are taken into account in the latter terms of (28). But it follows immediately from (27) that $\Psi(\rho_{12},\rho_3)=\varphi_{12}(\rho_{12})\Psi_3(\rho_3)$ for $\rho_{12}\sim r_0$, $\rho_3\gg r_0$, where $\varphi_{12}(\rho_{12})$ satisfies the equation

$$\varphi_{12}(\rho_{12})=1-\frac{\mu_{12}}{2\pi}\int\frac{V_{12}(\rho'_{12})}{|\rho_{12}-\rho'_{12}|}\varphi_{12}(\rho'_{12})\,d^3\rho'_{12}, \qquad (29)$$

i.e., it is the wave function of particles 1 and 2 for zero energy.

Repeating these discussions for two other regions, we obtain

$$\Psi(\rho_{13},\rho_2)=\varphi_{13}(\rho_{13})\Psi_2(\rho_2)\ \text{ for }\ \rho_{13}\sim r_0,\ \rho_2\gg r_0,$$
$$\Psi(\rho_{23},\rho_1)=\varphi_{23}(\rho_{23})\Psi_1(\rho_1)\ \text{ for }\ \rho_{23}\sim r_0,\ \rho_1\gg r_0 \qquad (30)$$

with the expressions for $\Psi_1(\rho_1)$ and $\Psi_2(\rho_2)$ obtained from (28) by substitution of indices.

However, if we now take it into account that the wave function enters the right hand side of (28) in precisely the regions under consideration, then we can substitute (29) and (30) in (28). In this case we obtain the following relation among the functions Ψ_1, Ψ_2, and Ψ_3:

$$\Psi_3(\rho_3)=\frac{\sin p_3\rho_3}{p_3\rho_3}+a_{12}\int G_{12}(\rho_3-\rho'_3)\,\Psi_3(\rho'_3)\,d^3\rho'_3$$
$$+\frac{2\pi}{\mu_{13}}a_{13}\int G\Big(\rho_3,-\frac{\mu_{13}}{m_1}\rho_3-\rho'_2\Big)\Psi_2(\rho'_2)\,d^3\rho'_2$$
$$+\frac{2\pi}{\mu_{23}}\int G\Big(\rho_3,-\frac{\mu_{23}}{m_2}\rho_3-\rho'_1\Big)\Psi_1(\rho'_1)\,d^3\rho'_1,$$

$$a_{il}=-\frac{\mu_{il}}{2\pi}\int V_{il}(\rho'_{il})\,\varphi_{il}(\rho'_{il})\,d^3\rho'_{il}, \qquad (31a)$$

where a_{il} is the scattering amplitude of the particles "i" and "l" at zero energy.

Substituting (29) — (30) in the expressions for $\Psi_2(\rho_2)$ and $\Psi_1(\rho_1)$ (which we have not written out), we obtain

$$\Psi_2(\rho_2)=\frac{\sin p_2\rho_2}{p_2\rho_2}+a_{13}\int G_{13}(\rho_2-\rho'_2)\,\Psi_2(\rho'_2)\,d^3\rho'_2$$
$$+\frac{2\pi}{\mu_{12}}\int G\Big(\rho_2,-\frac{\mu_{12}}{m_1}\rho_2-\rho'_3\Big)\Psi_3(\rho'_3)\,d^3\rho'_3$$
$$+\frac{2\pi}{\mu_{23}}\int G\Big(\rho_2,-\frac{\mu_{23}}{m_3}\rho_2-\rho'_1\Big)\Psi_1(\rho'_1)\,d^3\rho'_1, \qquad (31b)$$

$$\Psi_1(\rho_1) = \frac{\sin p_1\rho_1}{p_1\rho_1} + a_{23}\int G_{23}(\rho_1-\rho_1')\,\Psi_1(\rho_1')\,d^3\rho_1'$$
$$+ \frac{2\pi}{\mu_{12}}\int G\left(\rho_1, -\frac{\mu_{12}}{m_2}\rho_1 - \rho_3'\right)\Psi_3(\rho_3')\,d^3\rho_3'$$
$$+ \frac{2\pi}{\mu_{13}}\int G\left(\rho_1, -\frac{\mu_{13}}{m_3}\rho_1 - \rho_2'\right)\Psi_2(\rho_2')\,d^3\rho_2'. \qquad (31c)$$

Equations (31a), (31b), and (31c) represent a system of three integral equations with functions $\Psi_1(\rho)$, $\Psi_2(\rho)$, and $\Psi_3(\rho)$. This system of equations is identical with the system of equations obtained by Skornyakov and Ter-Martirosyan[7] with the help of boundary conditions for the wave functions in the case in which all three interactions have a resonance character. As is seen from the foregoing, these equations follow naturally from the initial Schrödinger equation without any assumptions on the resonance of all interactions. In order to estimate the order of magnitude of the individual terms in each of these equations, and also the order of magnitude of the terms neglected in their derivation, we consider their solution by the method of successive approximations. For this purpose, we substitute, on the right hand side of (31a) for example,

$$\Psi_1^{(0)} = \frac{\sin p_1\rho_1}{p_1\rho_1}, \quad \Psi_2^{(0)} = \frac{\sin p_2\rho_2}{p_2\rho_2}, \quad \Psi_3^{(0)} = \frac{\sin p_3\rho_3}{p_3\rho_3}. \qquad (32)$$

By making use of (24), we obtain

$$\Psi_3(\rho_3) = \frac{\sin p_3\rho_3}{p_3\rho_3}(1 - ik_{12}a_{12}) + \frac{a_{13}}{\rho_3}e^{ik_{13}\rho_3}\frac{\sin(p_2\rho_3\mu_{13}/m_1)}{p_2\rho_3\mu_{13}/m_1}$$
$$+ \frac{a_{23}}{\rho_3}e^{ik_{23}\rho_3}\frac{\sin(p_1\rho_3\mu_{23}/m_2)}{p_1\rho_3\mu_{23}/m_2}, \qquad (33)$$

from which it follows that if all the interactions are nonresonant ($a_{il} \sim r_0$), then the correction terms $\sim \kappa r_0$, $r_0/\rho_3 \ll 1$ and the application of successive approximations is valid. The neglected terms in this case are of the order $(\kappa r_0)^2$, $r_0\kappa r_0/\rho_3$, r_0^2/ρ_3^2.

If $r_0 \ll \rho_3 \ll 1/\kappa$, then

$$\Psi_3(\rho_3) = (1 - ik_{12}a_{12} - ik_{13}a_{13} - ik_{23}a_{23})(1 + a_{13}/\rho_3 + a_{23}/\rho_3) \qquad (34)$$

in agreement with (20).

When all three interactions are resonant ($a_{il} \gg r_0$, $\kappa a_{il} \sim 1$), none of the correction terms is small, and it is necessary to find a method of exact solution of Eqs. (31). The neglected terms in this case are of the order of κr_0 and r_0/ρ_3.

In our present work, we are interested in the case in which only one of the interactions has a resonance character ($a_{12} \gg r_0$, $a_{13} \sim a_{23} \sim r_0$). In this case, we can neglect the last two terms in Eq. (31a) in the zeroth approximation. This equation is then easily solved. If we set $\Psi_3^{(0)} = A(\sin p_3\rho_3)/p_3\rho_3$, then it follows from Eq. (31a) that

$$A = (1 + ik_{12}a_{12})^{-1}. \qquad (35a)$$

To find $\Psi_2(\rho_2)$, $\Psi_1(\rho_1)$ in this same approximation, it suffices to substitute $\Psi_3^{(0)}(\rho_3)$ in the third term on the right in (31b) and (31c), and to neglect the second and fourth terms. We then have

$$\Psi_1^{(0)}(\rho_1) = \frac{\sin p_1\rho_1}{p_1\rho_1} + \frac{a_{12}}{1+ik_{12}a_{12}}\frac{e^{-ik_{12}\rho_1}}{\rho_1}\frac{\sin(\mu_{12}p_3\rho_1/m_2)}{\mu_{12}p_3\rho_1/m_2} \qquad (35b)$$

and, similarly,

$$\Psi_2^{(0)}(\rho_2) = \frac{\sin p_2\rho_2}{p_2\rho_2} + \frac{a_{12}}{1+ik_{12}a_{12}}\frac{e^{-ik_{12}\rho_2}}{\rho_2}\frac{\sin(\mu_{12}p_3\rho_2/m_1)}{\mu_{12}p_3\rho_2/m_1}. \qquad (35c)$$

If we assume in (35b) and (35c) that $r_0 \ll \rho_1 \ll 1/\kappa$ and $r_0 \ll \rho_2 \ll 1/\kappa$, respectively, then we obtain

$$\Psi_1^{(0)}(\rho_1) = \frac{1}{1+ik_{12}a_{12}}\left(1 + \frac{a_{12}}{\rho_1}\right)$$
$$\Psi_2^{(0)}(\rho_2) = \frac{1}{1+ik_{12}a_{12}}\left(1 + \frac{a_{12}}{\rho_2}\right), \qquad (36)$$

i.e., in these regions the functions differ from their values for zero energy by the same factor.

In order to find the form of $\Psi^{(0)}(\rho_{12}, \rho_3)$ in this region, where the distance between an arbitrary pair of paricles is much larger than r_0, but much smaller than the wavelength, Eqs. (35a) — (35c) can be substituted in the initial equation (22). Direct calculation gives

$$\Psi^{(0)}(\rho_{12}, \rho_3) = \frac{1}{1 + ik_{12}a_{12}}\left(1 + \frac{a_{12}}{\rho_{12}}\right), \qquad (37)$$

i.e., it differs from $\Psi^{(0)}$ at $E = 0$ by the same factor.

Thus, in all the regions (25), the functions $\Psi_E^{(0)}(\rho_{12}, \rho_3)$ and $\Psi_0^{(0)}(\rho_{12}, \rho_3)$ differ only by the factor $(1+ik_{12}a_{12})^{-1}$. Consequently, such a situation also prevails in the region $\rho_{12}^2 + \rho_3^2 \sim r_0^2$. Therefore the matrix element of the reaction (15) for the presence of resonance has the form

$$\langle\Psi_E^{(-)}(A', B', C')\,|\,\Psi_E^{(+)}(A, B)\rangle =$$
$$= \frac{1}{1 - ik_{12}a_{12}^*}\langle\Psi_0^{(-)}(A', B', C')\,|\,\Psi_0^{(+)}(A, B)\rangle, \qquad (38)$$

in zeroth approximation in κr_0; this is the well-known result of reference 4.

The purpose of the present work is to obtain corrections to (38) of the order of κr_0 which contain the amplitude a_{13} and a_{23}.

a) Corrections to the Matrix Element of Order κr_0

To find corrections of order κr_0, it is first necessary in the solution of Eqs. (31a) — (31c) to take into consideration terms containing a_{13} and a_{23}, and in the second place to consider corrections of order κr_0 from the interaction of particles 1 and 2, which were not treated in the devel-

opment of these equations (in the derivation of (31a) — (31c), terms of order κr_0 relative to those considered were discarded). However, since the interaction of particles 1 and 2 is a resonant one ($\kappa a_{12} \sim 1$), corrections to it are of the order of the contribution from the other interactions.

Corrections of the second type are easily taken into account since in their computation the interaction with a third particle is unimportant (consideration of this interaction would give a correction to a correction), the interaction of the particles 1 and 2 changes only the factor in the wave function, with accuracy up to terms linear in κr_0 [see Eq. (3)]. Therefore, account of corrections of this type reduces to replacing the factor $(1+ik_{12}a_{12})^{-1}$ in (35a) by the quantity

$$e^{-i\delta_{12}}\frac{\sin\delta_{12}}{k_{12}a_{12}} = (1+ik_{12}a_{12})^{-1}\left\{1-\frac{k_{12}^2 r_0 a_{12}}{2(1+ik_{12}a_{12})}\right\}, \quad (39)$$

r_0 is the effective radius of interaction of particles 1 and 2.

To find corrections of the first type we shall solve (31a) — (31c) by successive approximations relative to a_{13} and a_{23}. In Eq. (31a) we set

$$\Psi_3(\rho_3) = (1+ik_{12}a_{12})^{-1}\frac{\sin p_3\rho_3}{p_3\rho_3} + \Psi_3'(\rho_3). \quad (40)$$

Then the following equation holds for $\Psi_3'(\rho_3)$:

$$\Psi_3'(\rho_3) = a_{12}\int G(\rho_3-\rho_3')\,\Psi_3'(\rho_3')\,d^3\rho_3' + \Phi_{13}(\rho_3) + \Phi_{23}(\rho_3), \quad (41)$$

where $\Phi_{13}(\rho_3)$ and $\Phi_{23}(\rho_3)$ are the results of substitution in the last two terms of (31a) of the functions $\Psi_1^{(0)}(\rho_1)$ and $\Psi_2^{(0)}(\rho_2)$ from (35b) and (35c);

$$\Phi_{13}(\rho_3) = \Phi_{13}'(\rho_3) + \Phi_{13}''(\rho_3), \quad (41')$$

where $\Phi_{13}'(\rho_3)$ and $\Phi_{13}''(\rho_3)$ are the result of substitution of the first and second terms, respectively, from (35b) in Eq. (31a):

$$\Phi_{13}'(\rho_3) = \frac{a_{13}}{\rho_3}e^{-ik_{12}\rho_3}\frac{\sin p_2'\rho_3}{p_2'\rho_3} \equiv \frac{a_{13}}{2p_2'}\int_{k_{13}-p_2'}^{k_{13}+p_2'} dz\,\frac{e^{-iz\rho_3}}{\rho_3}, \quad (42)$$

$$\Phi_{13}''(\rho_3) = \frac{a_{12}a_{13}}{1+ik_{12}a_{12}}\frac{1}{2p_3'}\int_{k_{12}-p_3'}^{k_{12}+p_3'} dz\int\frac{d^3q}{(2\pi)^3}\frac{\exp\left[-iq\rho_3\frac{\mu_{13}}{m_1}-ik_q\rho_3\right]}{\rho_3(q^2-z_\varepsilon^2)},$$

$$p_2' = \mu_{13}p_2/m_1, \qquad p_3' = \mu_{12}p_3/m_1,$$

$$k_q = \sqrt{2\mu_{13}(E-q^2/2\mu_2)}. \quad z_\varepsilon = z - i\varepsilon, \quad \varepsilon\to 0. \quad (43)$$

The function $\Phi_{23}(\rho_3)$ differs from $\Phi_{13}(\rho_3)$ by a permutation of indices.

Equation (41) is easily solved if we proceed to the momentum representation. If

$$\Psi_3'(\rho_3) = 4\pi\int\frac{\sin p\rho_3}{p\rho_3}\Psi_3'(p)\,p^2dp, \quad (44)$$

then

$$\Psi_3'(p) = [\Phi_{13}(p)+\Phi_{23}(p)]/(1+ik_pa_{12}),$$

$$k_p = \sqrt{2\mu_{12}(E-p^2/2\mu_3)} \quad (45)$$

$$\Phi_{13}(p) = \Phi_{13}'(p)+\Phi_{13}''(p), \quad \Phi_{13}'(p) = \frac{a_{13}}{4\pi^2p_2'}\int_{k_{13}-p_2'}^{k_{13}+p_2'}dz\,\frac{1}{p^2-z_\varepsilon^2},$$

$$\Phi_{13}''(p) = \frac{a_{12}a_{13}}{1-ik_{12}a_{12}} \times\frac{1}{2p_3'}\int_{k_{12}-p_3'}^{k_{12}+p_3'}dz\int\frac{d^3q}{4\pi^4}\frac{1}{(q^2-z_\varepsilon^2)\left[(p-\mu_{13}q/m_1)^2-k_q^2+i\varepsilon\right]} \quad (46)$$

and similarly for $\Phi_{23}(p)$.

As in the previous cases, we are interested in $\Psi_3'(\rho_3)$ for $r_0 \ll \rho_3 \ll 1/\kappa$. In this region, the expression for $\Psi_3'(\rho_3)$ is greatly simplified. We shall first consider the contribution from $\Phi_{13}'(p)$. It can be written in a form that is suitable for further work by separating out the component that does not vanish at E = 0:

$$\frac{a_{13}}{\pi p_2'}\int_{k_{13}-p_2'}^{k_{13}+p_2'}dz\int_0^\infty p^2dp\,\frac{\sin p\rho_3}{p\rho_3} \times\left[\frac{1}{(p^2-z_\varepsilon^2)(1+ik_pa_{12})}-\frac{1}{p^2(1+\gamma_{12}a_{12}p)}\right] + \frac{a_{13}}{\rho_3}\frac{2}{\pi}\int_0^\infty\frac{\sin p\rho_3 dp}{p(1+\gamma_{12}a_{12}p)}. \quad (47)$$

The first integral vanishes at E = 0 while the second does not depend on E. Moreover the first converges at $\rho_3 = 0$. Therefore, in the region $r_0 \ll \rho_3 \ll 1/\kappa$ one can set $\rho_3 = 0$, neglecting terms of order κr_0, r_0/a_{12}. In this case the contribution from $\Phi_{13}'(p)$ takes the form

$$a_{13}F_{13}\left(\varkappa a_{12}, \frac{p_2}{\varkappa}\right) + \frac{a_{13}}{\rho_3}\frac{2}{\pi}\int_0^\infty\frac{\sin x dx}{x(1+x\gamma_{12}a_{12}/\rho_3)}, \quad (48)$$

where

$$F_{13}\left(\varkappa a_{12}, \frac{p_2}{\varkappa}\right) = \frac{1}{\pi p_2'}\int_{k_{13}-p_2'}^{k_{13}+p_2'}dz\int_0^\infty dp\,\frac{a_{12}p^2(\gamma_{12}p-ik_p)+z^2(1+ik_pa_{12})}{(p^2-z_\varepsilon^2)(1+ik_pa_{12})(1+p\gamma_{12}a_{12})}.$$

The contribution from $\Phi_{13}''(p)$ can be similarly transformed, but by a somewhat more awkward method. As shown in the appendix, it has the form

$$\frac{a_{12}a_{13}}{1+ik_{12}a_{12}}G_{13}\left(\varkappa a_{12}, \frac{p_3}{\varkappa}\right) - \frac{ik_{12}a_{12}}{1+ik_{12}a_{12}}\frac{a_{13}}{\rho_3}\frac{2}{\pi}\int_0^\infty\frac{\sin x dx}{x(1+x\gamma_{12}a_{12}/\rho_3)} + \frac{a_{12}a_{13}C}{(1+ik_{12}a_{12})\rho_3^2}\frac{2}{\pi}\int_0^\infty\frac{\sin xax}{1+x\gamma_{12}a_{12}/\rho_3},$$

$$C = \frac{m_1}{\mu_{13}}\tan^{-1}\sqrt{\frac{\mu_{12}\mu_3}{m_1^2}}, \quad (49)$$

where

$$G_{13}\left(\varkappa a_{12}, \frac{p_3}{\varkappa}\right) = -\frac{i}{2\pi p_3'}\int\limits_{k_{12}-p_3'}^{k_{12}+p_3'} dz \int\limits_{-1}^{1} dx \int\limits_{0}^{\infty} p^2 dp \left\{\frac{z}{1+ik_p a_{12}}\right.$$

$$\times\left(z^2 + 2pzx\frac{\mu_{12}}{m_1} + \frac{\mu_{12}}{\mu_{13}}p^2 - 2\mu_{12}E\right)^{-1}\frac{\mu_{12}}{\mu_{13}} - \frac{z}{p^2(1+p\gamma_{12}a_{12})}$$

$$+\frac{\mu_{12}}{\mu_{13}}\left[2\mu_{12}\left(E-\frac{p^2}{2\mu_{13}}\right)+\frac{\mu_{12}^2}{m_1^2}p^2x^2\right]^{-1/2}$$

$$\times\left[1+\frac{z^2}{\left(\sqrt{2\mu_{12}(E-p^2/2\mu_{13})+\mu_{12}^2p^2x^2/m_1^2}+\mu_{12}px/m_1\right)^2-z_\varepsilon^2}\right]$$

$$\left.\times\frac{1}{1+ik_p a_{12}} - \frac{i}{p(1+p\gamma_{12}a_{12})}\sqrt{\frac{\mu_{12}}{\mu_{13}}}\frac{1}{\sqrt{1-\frac{\mu_{12}\mu_{13}}{m_1^2}x^2}}\right\}.$$

Taking (48) and (49) into account, we obtain the result that for $r_0 \ll \rho_3 \ll 1/\kappa$,

$$\Psi_3'(\rho_3) = \frac{1}{1+ik_{12}a_{12}}\left[a_{13}a_{12}G_{13} + a_{23}a_{12}G_{23} + \frac{a_{13}+a_{23}}{\rho_3}\frac{2}{\pi}\right.$$

$$\left.\times\int\limits_0^\infty \frac{\sin x dx}{x(1+x\gamma_{12}a_{12}/\rho_3)} + \frac{a_{13}+a_{23}}{\rho_3}C\frac{a_{12}}{\rho_3}\frac{2}{\pi}\int\limits_0^\infty \frac{\sin dx}{1+x\gamma_{12}a_{12}/\rho_3}\right]$$

$$+ a_{13}F_{13} + a_{23}F_{23}. \qquad (50)$$

Also, considering the correction (39), we conclude that, with the initial accuracy, $\Psi(\rho_{12}, \rho_3)$ can be written for $\rho_{12} \sim r_0$, $\rho_3 \gg r_0$, and $\rho_3 \ll 1/\kappa$ in the form

$$\Psi(\rho_{12}, \rho_3) = L\varphi_{12}(\rho_{12})\left[1 + \frac{a_{13}+a_{23}}{\rho_3}\frac{2}{\pi}\int\limits_0^\infty \frac{\sin x dx}{x(1+x\gamma_{12}a_{12}/\rho_3)}\right.$$

$$\left. + \frac{C(a_{13}+a_{23})a_{12}}{\rho_3^2}\frac{2}{\pi}\int\limits_0^\infty \frac{\sin x dx}{1+x\gamma_{12}a_{12}/\rho_3}\right], \qquad (51)$$

where

$$L = \frac{1}{1+ik_{12}a_{12}}\left[1 - \frac{1}{2}\frac{k_{12}^2 r_0 a_{12}}{1+ik_{12}a_{12}} + a_{12}a_{13}G_{13} + a_{12}a_{23}G_{23}\right]$$

$$+ a_{13}F_{13} + a_{23}F_{23}. \qquad (52)$$

Thus we have found the correction of order κr_0 to the factor $(1+ik_{12}a_{12})^{-1}$ in the wave function and the correction to the wave function in the region $\rho_{12} \sim r_0$, $\rho_3 \gg r_0$ of order r_0/ρ_3, which can be of interest in a number of problems.

To find the corrections to the function $\Psi_2(\rho_2)$, we set

$$\Psi_2(\rho_2) = \Psi_2^{(0)}(\rho_2) + \Psi_2'(\rho_2).$$

To determine $\Psi_2'(\rho_2)$, it is necessary to substitute $\Psi_3'(\rho_3)$ from (44) in the third term on the right-hand side of (31b), with account of the correction (39), and in the second and fourth terms, $\Psi_2^{(0)}(\rho_2)$ and $\Psi_1^{(0)}(\rho_1)$ from (35b) and (35c), respectively.

The expression for $\Psi_2(\rho_2)$ resulting from such substitutions has the form

$$\Psi_2(\rho_2) = L\frac{a_{12}}{\rho_2}\left\{1 + \frac{\rho_2}{a_{12}} + \frac{a_{13}}{\rho_2}f_1\left(\frac{a_{12}}{\rho_2}\right) + \frac{a_{23}}{\rho_2}f_2\left(\frac{a_{12}}{\rho_2}\right)\right\},$$

$$f_i\left(\frac{a_{12}}{\rho_2}\right) = \frac{m_i}{\mu_{12}}\frac{2}{\pi}\int\limits_0^\infty \frac{\sin x e^{-\alpha_i x}}{1+\alpha_i x\frac{a_{12}}{\rho_2}}\left(\frac{1}{x} + \frac{Ca_{12}}{\rho_2}\right)dx, \qquad \alpha_i = \frac{m_i}{\sqrt{\mu_{12}\mu_3}}, \qquad (53)$$

for $r_0 \ll \rho_2 \ll 1/\kappa$, i.e., it contains the same constant factor.

Similar results are obtained for $\rho_{23} \sim r_0$, $r_0 \ll \rho_1 \ll 1/\kappa$ and $r_0 \ll \rho_{12}$, ρ_{13}, $\rho_{23} \ll 1/\kappa$.

Therefore, as in the previous cases, it can be proved that the matrix element of the reaction (14) has the form

$$\langle\Psi_E^{(-)}(A', B', C')\,|\,\Psi_E^{(+)}(A, B)\rangle$$

$$= L^*\langle\Psi_0^{(-)}(A', B', C')\,|\,\Psi_0^{(+)}(A, B)\rangle. \qquad (54)$$

with accuracy up to terms linear relative to κr_0.

The quantities G_{13}, G_{23}, F_{13}, F_{23} entering into the expression for L depend both on the energy distribution among the particles and on the resonance amplitude of scattering a_{12}. If we introduce the variables

$$u = p_1^2/2\mu_1 E, \quad v = p_2^2/2\mu_2 E, \quad w = p_3^2/2\mu_3 E, \qquad (55)$$

which determine the fraction of the entire kinetic energy which is associated with the relative motion of one of the particles (1, 2, and 3 respectively) and the center of mass of the other two, then it is easy to show that

$$G_{13} = \varkappa_{12}\varkappa_3 G(\beta_1, w, a), \quad G_{23} = \varkappa_{12}\varkappa_3 G(\beta_2, w, a),$$

$$F_{13} = \varkappa_3 F(\beta_1, v, a), \quad F_{23} = \varkappa_3 F(\beta_2, u, a), \qquad (56)$$

where

$$\varkappa_{12} = \sqrt{2\mu_{12}E}, \quad \varkappa_3 = \sqrt{2\mu_3 E}, \quad \beta_1 = \mu_{13}/\mu_3 = \mu_{12}/\mu_2,$$
$$\beta_2 = \mu_{23}/\mu_3 = \mu_{12}/\mu_1, \quad a = \varkappa_{12}a_{12}.$$

The functions F and G, after computation of the part of the intervals entering into (48) and (49), can be written in the form

$$F(\beta, u, a) = \frac{1}{2\pi\sqrt{u(1-\beta)}}\int\limits_{z_1}^{z_2}\frac{z dz}{1+a^2(1-z^2)}\left[2a\sqrt{1-z^2}\arccos z\right.$$

$$\left. - i\pi - \frac{4az}{\sqrt{1+a^2}}\left(\sinh^{-1}a + \frac{i\pi}{2}\right)\right] - \frac{2}{\pi a\sqrt{1+a^2}}$$

$$\times\left[\ln\frac{1}{2}(1+\sqrt{1+a^2}) - \frac{i\pi}{2}(\sqrt{a^2+1}-1)\right], \qquad (57)$$

here $z_{1,2} = \sqrt{(1-u)\beta} \mp \sqrt{u(1-\beta)}$;

$$G(\beta, w, a) = \frac{1}{2\pi\sqrt{\beta(1-\beta)}(z_2-z_1)}\int\limits_{z_1}^{z_2} dz\left\{\int\limits_0^1 dy\frac{-iy}{1+ia\sqrt{1-y^2}}\right.$$

$$\times\ln\left|\frac{(y\sqrt{1-\beta}+\sqrt{\beta(1-y^2)})^2 - z^2\beta}{(y\sqrt{1-\beta}-\sqrt{\beta(1-y^2)})^2 - z^2\beta}\right| + \int\limits_1^\infty y dy\left[\frac{1}{1+a\sqrt{y^2-1}}\right.$$

$$\times\tan^{-1}\frac{2\sqrt{\beta(1-\beta)}y^2(1-y^2)}{\beta z^2 - y^2(1-2\beta) - \beta} - \frac{1}{1+ay}\tan^{-1}\frac{2\sqrt{\beta(1-\beta)}}{2\beta-1}\Big]$$

$$- i\int\limits_0^\infty y dy\frac{1}{1+ia\sqrt{1-y^2}}\left[\ln\frac{\beta z^2 + 2zy\sqrt{1-\beta}+y^2-\beta}{\beta z^2 - 2zy\sqrt{1-\beta}+y^2-\beta}\right.$$

$$\left.\left. - \frac{4z\sqrt{1-\beta}}{y(1+ay)}\right] + \pi\theta(1-\beta-z^2\beta)z\int\limits_{y_0}^1\frac{y dy}{1+ia\sqrt{1-y^2}}\right\}, \qquad (58)$$

where

$$z_{1,2} = \sqrt{\beta(1-w)} \mp \sqrt{w(1-\beta)},$$

$$v_0 = \sqrt{\beta(1-z^2\beta)} + z\sqrt{\beta(1-\beta)},$$

$$\theta(x) = \begin{cases} 1 & x > 0 \\ 0 & x < 0 \end{cases}, \qquad 0 < \tan^{-1} x < \pi.$$

In spite of the crudeness of the expressions for F and G, these functions can be tabulated without great difficulty.

The differential cross section of the reaction (14), as a function of the energy of the third particle (which interacts in nonresonant fashion) for example, and of its angle of emission, which is determined by the angle between the direction of the momentum of the incident particles and the plane in which the momenta of the particles produced lie, has the form

$$\frac{d^2\sigma(E, w, \cos\vartheta)}{dw\, d\cos\vartheta} = |M_0|^2 |L|^2 \sqrt{w(1-w)}\,(E-E_0)^2, \qquad (59)$$

$$L = (1 + ik_{12}a_{12})^{-1}\{1 - k_{12}^2 r_0 a_{12}/2(1+ik_{12}a_{12}) + \varkappa_{12}a_{12}[\varkappa_3 a_{13} G(\beta_1, w, a) + \varkappa_3 a_{23} G(\beta_2, w, a)]\} + \varkappa_3 a_{13} F(\beta_1, v, a) + \varkappa_3 a_{23} F(\beta_2, u, a),$$

where ϑ is the angle between $\mathbf{p}_3$ and $\mathbf{k}_{12}$.

For given w and ϑ,

$$v = w(1-\beta_1) + \beta_1(1-w) + 2\sqrt{w(1-w)\beta_1(1-\beta_1)}\cos\vartheta,$$
$$u = w(1-\beta_2) + \beta_2(1-w) - 2\sqrt{w(1-w)\beta_2(1-\beta_2)}\cos\vartheta. \qquad (60)$$

Thus the terms in the variables w and ϑ in the square brackets of (59) are responsible only for the energy distribution, while the terms containing $F(\beta_1, v, a)$ and $F(\beta_2, u, a)$ also involve the correlation between the momenta $\mathbf{p}_3$ and $\mathbf{k}_{12}$.

4. ENERGY DISTRIBUTION $p + p \to p + \Lambda^0 + K^+$, $p + p \to N + \Sigma + K$

Let us consider the energy distribution in the following reactions:

$$p + p \to p + \Lambda^0 + K^+, \qquad (I)$$

$$p + p \to p + \Sigma^0 + K^+, \qquad (IIa)$$

$$p + p \to p + \Sigma^+ + K^0, \qquad (IIb)$$

$$p + p \to n + \Sigma^+ + K^+, \qquad (IIc)$$

and assume that the interactions (Λ, N) and (Σ, N) are resonant.

In order that this be done, it is necessary to take into account the spin and isotopic variables of the particles generated. In the case of reaction (I), in view of the impossibility of charge exchange, the presence of the isotopic spin is not important. Account of the usual spin leads only to the result that p and Λ^0 can be produced both in the singlet and in the triplet states. In this case a system of three particles of small energy (p, Λ^0, K^+) can depend on the internal parity of the system (Λ^0, K^+) relative to the proton, either in the state $(0^+, 1^+)$, or in the states $(0^-, 1^-)$.

However, inasmuch as two protons, as fermions, cannot be found in the state 1^+, then, depending on the parity of (Λ, K^+) in the final state, either only the singlet state (p, Λ^0) or the singlet plus the triplet states are possible. In the first case, the expression (59) is completely applicable for the reaction (I) if by a_{12} one means the amplitude of scattering of p on Λ^0 in the singlet state — a_0. In the second case, since the states 0^- and 1^- do not interfere, after averaging over the directions of the momenta of the incident particles, the reaction cross section has the form

$$\frac{d^2\sigma(E, w, \cos\vartheta)}{dw\, d\cos\vartheta} = \sqrt{w(1-w)}\,(E-E_0)^2 \times\left\{\frac{1}{4}|M_0|^2|L_0|^2 + \frac{3}{4}|M_1|^2|L_1|^2\right\}, \qquad (61)$$

where $|M_0|^2$ and $|M_1|^2$ are the squares of the moduli of the matrix elements of creation in the singlet and triplet states for zero energy. The quantities $|L_0|^2$ and $|L_1|^2$ are expressions entering into (59), in which, in place of a_{12}, there are substituted respectively a_0 and a_1 — the scattering amplitudes of (p, Λ^0) in the singlet and triplet states.

In the case of the reactions (IIa, b, c) the situation is entirely similar in the behavior of the spin variables; however consideration of the isotopic spin materially changes the final result. In this case, the equations (31a, b, c) are more complicated, inasmuch as for $\rho_{il} \sim r_0$ the wave function $\varphi_{il}(\rho_{il})$ of the particles i and l is a superposition of functions with different isotopic spin T_{il} ($\frac{1}{2}$, $\frac{3}{2}$ for N, Σ; 0, 1 for N and K; $\frac{1}{2}$, $\frac{3}{2}$ for Σ and K). We shall not repeat the calculations but merely write down the final result which is almost self-evident.

In place of the matrix element of the reactions (IIa, b, c), which we denote by M_{+0+}, M_{++0}, M_{0++}, we introduce the matrix elements $M_{1/2}$, $M_{3/2}$ of transitions into states with a total isotopic spin T = 1 and isotopic spin of N and Σ, $T_{12} = \frac{1}{2}$ and $\frac{3}{2}$:

$$M_{+0+} = (1/\sqrt{3})M_{1/2} - (1/\sqrt{6})M_{3/2}, \quad M_{++0} = (\sqrt{3}/2)M_{3/2},$$
$$M_{0++} = -\sqrt{2/3}M_{1/2} - (1/2\sqrt{3})M_{3/2}. \qquad (62)$$

We can now write

$$M_{T_{12}} = \sum_{T'_{12}} \langle T_{12}|L|T'_{12}\rangle^* M^0_{T'_{12}}. \qquad (63)$$

in place of Eq. (54).

To obtain $\langle T_{12}|L|T'_{12}\rangle$ from (52), it suffices to note the following. The term

$$(1+ik_{12}a_{12})^{-1}[1-k_{12}^2r_0a_{12}/2(1+ik_{12}a_{12})]$$

depends only on the interaction of N, Σ, for which T_{12} coes not change. Therefore, it gives a contribution to $\langle T_{12}|L|T'_{12}\rangle$ of the form

$$(1+ik_{12}a_{T_{12}})^{-1}[1-k_{12}^2r_0^{T_{12}}a_{T_{12}}/2(1+ik_{12}a_{T_{12}})]\times\delta_{T_{12}T'_{12}}\equiv\alpha_{T_{12}}\delta_{T_{12}T'_{12}}, \quad (64)$$

$a_{T_{12}}$, $r_0^{T_{12}}$ are the scattering amplitude and the effective radius in the state with isotopic spin T_{12}. The term $\kappa_3a_{13}F(\beta_1, v, a) + \kappa_3a_{23}F(\beta_2, u, a)$, as is easily seen from the derivation, is a contribution from processes in which the interaction of particles 1 and 2 enter, and then the interaction of particles 1 and 3 or 2 and 3. The interaction of particles 1 and 3 or 2 and 3 changes the isotopic spin of the particles 1 and 2 (T_{12}). Therefore a_{13} and a_{23} are replaced by

$$\langle T_{12}|b|T'_{12}\rangle=\sum_{T_{13}}S(T_{12},T_{13})\,b_{T_{13}}S(T_{13},T'_{12}),$$

$$\langle T_{12}|c|T'_{12}\rangle=\sum_{T_{23}}\widetilde{S}(T_{12},T_{23})\,c_{T_{23}}\widetilde{S}(T_{23},T'_{12}), \quad (65)$$

where $b_{T_{13}}$ and $c_{T_{23}}$ are the scattering amplitudes of (K, N) and (K, Σ), respectively, in states with a definite isotopic spin.

The coefficients $S(T_{12}, T_{13})$ and $\widetilde{S}(T_{12}, T_{23})$ are determined by the rules of addition of moments and are simply connected with the Racah coefficients, for example

$$S(T_{12},T_{13})=\sqrt{(2T_{12}+1)(2T_{13}+1)}\,W(1,1/2,1,1/2;T_{12},T_{13}).$$

Simultaneously,

$$F(\beta_1,v,a)\to F(\beta_1,v,\varkappa_{12}a_{T'_{12}}).$$

The remaining terms correspond to the successive interactions of particles 1 and 2, 1 and 3, or 2 and 3, and then again 1 and 2. Therefore, they are replaced by

$$\frac{\varkappa_{12}a_{T_{12}}}{1+ik_{12}a_{T_{12}}}[\varkappa_3\langle T_{12}|b|T'_{12}\rangle G(\beta_1,w,\varkappa_{12}a_{T'_{12}})+\varkappa_3\langle T_{12}|c|T'_{12}\rangle G(\beta_2,w,\varkappa_{12}a_{T'_{12}})].$$

By making use of all of the above, it is easy to obtain the following relations between $M_{1/2}$ or $M_{3/2}$ and their values at zero energy, $M^0_{1/2}$ or $M^0_{3/2}$,

$$\begin{aligned}M_{1/2}=&\Big\{\alpha_{1/2}+\varkappa_3\frac{1}{3}(2b_1+b_0)f_1\Big(\frac12,\frac12\Big)\\&+\varkappa_3\frac19(8c_{3/2}+c_{1/2})f_2\Big(\frac12,\frac12\Big)\Big\}M^0_{1/2}\\&+\varkappa_3\Big\{\frac{\sqrt2}{3}(b_1-b_0)f_1\Big(\frac12,\frac32\Big)\\&+\frac{2\sqrt2}{9}(c_{3/2}-c_{1/2})f_2\Big(\frac12,\frac32\Big)\Big\}^*M^0_{3/2},\end{aligned} \quad (66)$$

$$\begin{aligned}M_{3/2}=&\Big\{\alpha_{3/2}+\varkappa_3\frac13(b_1+2b_0)f_1\Big(\frac32,\frac32\Big)\\&+\varkappa_3\frac19(c_{3/2}+8c_{1/2})f_2\Big(\frac32,\frac32\Big)\Big\}^*M^0_{3/2}\\&+\varkappa_3\Big\{\frac{\sqrt2}{3}(b_1-b_0)f_1\Big(\frac32,\frac12\Big)\\&+\frac{2\sqrt2}{9}(c_{3/2}-c_{1/2})f_2\Big(\frac32,\frac12\Big)\Big\}^*M^0_{1/2},\end{aligned}$$

where

$$f_1(T_{12},T'_{12})=F\Big(\beta_1,v,\varkappa_{12}a_{T'_{12}}\Big)+\frac{\varkappa_{12}a_{T_{12}}}{1+ik_{12}a_{T_{12}}}G\Big(\beta_i,w,\varkappa_{12}a_{T'_{12}}\Big),$$

$$f_2(T_{12},T'_{12})=F\Big(\beta_2,u,\varkappa_{12}a_{T'_{12}}\Big)+\frac{\varkappa_{12}a_{T_{12}}}{1+ik_{12}a_{T_{12}}}G\Big(\beta_2,w,\varkappa_{12},a_{T'_{12}}\Big). \quad (67)$$

Equations (62) and (66) allow us to find the cross section of the three reactions (II) depending on the ratio $M^0_{1/2}/M^0_{3/2}$ and the amplitudes of pair interactions.

In conclusion I wish to express my gratitude to Academician L. D. Landau, K. A. Ter-Martirosyan, I. T. Dyatlov, and A. A. Ansel'm for valuable discussions.

APPENDIX

Calculation of the contribution from Φ''_{13} [Eq. (49)]. To obtain (49) it is convenient first to integrate over the modulus q in (46). In this case we obtain

$$\Phi''_{13}(p)=\frac{a_{12}a_{13}}{1+ik_{12}a_{12}}\frac{-i}{2p'_3}\int_{k_{12}-p'_3}^{k_{12}+p'_3}dz\int_{-1}^{1}\frac{dx}{4\pi^2}$$

$$\times\Big\{\frac{z}{z^2\mu_{13}/\mu_{12}+2pzx\mu_{13}/m_1+p^2-2\mu_{13}E+i\varepsilon}$$

$$+\frac{\mu_{12}}{\mu_{13}}\frac{1}{\sqrt{2\mu_{12}(E-p^2/2\mu_{13})+\mu_{12}^2p^2x^2/m_1^2}}$$

$$\cdot\Big[1-\frac{z^2}{(\sqrt{2\mu_{12}(E-p^2/2\mu_{13})+\mu_{12}^2p^2x^2/m_1^2}+\mu_{12}px/m_1)^2-z_\varepsilon^2}\Big]\Big\}, \quad (a)$$

where the relation $\mu_{12}\mu_3/m_1^2 + 1 = \mu_3/\mu_{13} = \mu_2/\mu_{12}$ is employed.

The contribution from $\Phi_{13}''(p)$ in $\Psi_3(\rho_3)$ has the form

$$4\pi\int\frac{\sin p\rho_3}{p\rho_3}\frac{\Phi_3''(p)}{1+ik_p a_{12}}p^2dp. \qquad \text{(b)}$$

For $p/\kappa \to \infty$,

$$\frac{\Phi_{13}''(p)}{1+ik_p a_{12}} = \frac{a_{12}a_{13}}{1+ik_{12}a_{12}}\left\{\frac{1}{p(1+p\gamma_{12}a_{12})}\cdot\right.$$

$$\times\sqrt{\frac{\mu_{12}}{\mu_{13}}}\int_{-1}^{1}\frac{dx}{4\pi^2}\frac{1}{\sqrt{1-\mu_{12}\mu_{13}x^2/m_1^2}}$$

$$\left.-\frac{ik_{12}a_{12}}{2\pi^2p^2(1+p\gamma_{12}a_{12})}+O\left(\frac{1}{p^4}\right)\right\}. \qquad \text{(c)}$$

Therefore, if we write down

$$\frac{\Phi_{13}''(p)}{1+ik_p a_{12}} = \frac{a_{12}a_{13}}{1+ik_{12}a_{12}}\left\{G_{13}(p)+\frac{C}{2\pi^2p(1+p\gamma_{12}a_{12})}\right.$$

$$\left.-\frac{ik_{12}a_{12}}{2\pi^2p^2(1+p\gamma_{12}a_{12})}\right\}, \quad C=\frac{m_1}{\mu_{13}}\tan^{-1}\sqrt{\frac{\mu_{12}\mu_3}{m_1^2}}, \qquad \text{(d)}$$

then $G_{13}(p) \sim 1/p^4$ for $p/\kappa \to \infty$ and, consequently, one can set $\rho_3 = 0$ in the term containing G_{13}, in the integral (b) for $\rho_3 \ll 1/\kappa$. Substituting (a) in (b) and taking into account this observation, we obtain the result given in the text [Eq. (49)].

[1] G. F. Chew, Phys. Rev. **112**, 1380 (1958).

[2] G. F. Chew and F. E. Low, Phys. Rev. **113**, 1640 (1959).

[3] I. Ya. Pomeranchuk and L. B. Okun', JETP **36**, 300 (1959), Soviet Phys. JETP **9**, 207 (1959).

[4] A. B. Migdal, JETP **28**, 10 (1955), Soviet Phys. JETP **1**, 7 (1955); K. Watson, Phys. Rev. **88**, 1163 (1952).

[5] V. N. Gribov, Nuclear Phys. **5**, 653 (1958).

[6] A. A. Ansel'm and V. N. Gribov, JETP **36**, 1890 (1959), **37**, 501 (1959); Soviet Phys. JETP **9**, 1345 (1959), **10**, 354 (1960).

[7] G. V. Skornyakov and K. A. Ter-Martirosyan, JETP **31**, 775 (1956), Soviet Phys. JETP **4**, 648 (1957).

Translated by R. T. Beyer
110

QUANTUM TRANSITIONS IN THE ADIABATIC APPROXIMATION

A. M. DYKHNE

Institute of Radiophysics and Electronics, Siberian Branch of the Academy of Sciences, U.S.S.R.

Submitted to JETP editor August 24, 1959

J. Exptl. Theoret. Phys. (U.S.S.R.) **38**, 570-578 (February, 1960)

The probabilities of quantum transitions in the discrete spectrum have been found in the adiabatic approximation assuming a very simple time dependence of the Hamiltonian. The time behavior of the adiabatic invariants has been examined on the example of the classical linear oscillator.

1. ACCURACY OF THE ADIABATIC INVARIANTS

In certain physical problems we encounter quantities which change very little for slow variations of the external conditions. Such quantities are called adiabatic invariants. Examples of adiabatic invariants are the ratio of the energy over the frequency of the harmonic oscillator or the magnetic moment of a particle in a space or time dependent magnetic field. The adiabatic invariants of quantum mechanics are the quantum numbers, as was first noted by Einstein.[1] It is clear that the adiabatic invariants are not exact integrals of motion. The problem of the accuracy with which the adiabatic invariants are conserved has been discussed in a number of papers.[2-5]

Let α be a small parameter which characterizes the "slowness" of the change in the external conditions as compared to the characteristic period of the motion of the system. For example, in the case of a particle moving in a magnetic field which varies slowly in space or time, we have the parameters $r_L H^{-1}\nabla H$ and $\omega_L^{-1}H^{-1}dH/dt$, respectively, where H is the magnetic field, and r_L and ω_L are the Larmour radius and frequency. In the case of the oscillator this parameter is the ratio $\omega^{-2}d\omega/dt$.

Alfvén[2] has shown that the magnetic moment of a particle in a magnetic field is conserved with an accuracy up to first order in the small parameter. It was then found by Helwig[3] that the invariants are conserved with an accuracy up to the next order of smallness. Later it was shown by Kruskal for the motion of a particle in a magnetic field, and by Kulsrud[4] for the classical harmonic oscillator, that the adiabatic invariants are conserved with an accuracy including all powers of the small parameter. Finally, Lenard[5] proved the same for the nonlinear one-dimensional oscillator

The following derivation refers to the case in which the variation of the external conditions can be described by an analytic function of the time. It will be shown that in this case the variation of the adiabatic invariant of the classical oscillator is exponentially small. The calculation of this variation will be carried out.* Let us assume that the oscillator frequency $\omega(t)$ takes the constant values $\omega_\pm$ as $t \to \pm\infty$. The asymptotic values of the action $J = E/\omega$ for $t \to \pm\infty$ are equal to $J_\pm$. We seek the variation $\Delta J = J_+ - J_-$.

The real solution of the oscillator equation

$$\ddot{x} + \omega^2(t)\,x = 0 \tag{1.1}$$

has the asymptotic form

$$x_\pm = \tfrac{1}{2}(c_\pm e^{i\omega_\pm t} + c_\pm^* e^{-i\omega_\pm t}). \tag{1.2}$$

It is known, on the other hand, that there exists a complex solution of the equation of the type (1.1) which has the asymptotic form

$$y_- = e^{i\omega_- t} + Re^{-i\omega_- t}, \quad y_+ = De^{i\omega_+ t}, \tag{1.3}$$

where R and D are the amplitudes of the reflected and transmitted waves. Taking the real part of (1.3) and comparing with (1.2), we find

$$c_- = 1 + R^*, \; c_+ = D. \tag{1.4}$$

From the conservation law for the number of particles we obtain the following relation between R and D:

$$\omega_-(1 - |R|^2) = \omega_+ |D|^2. \tag{1.5}$$

For the action of the oscillator we find from (1.2)

$$J_\pm = \tfrac{1}{2}\omega_\pm c_\pm c_\pm^*. \tag{1.6}$$

Using (1.4) and (1.5) we can write the equation (1.6) in the form

*The idea of this derivation is due to L. P. Pitaevskiĭ.

$$J_- = \tfrac{1}{2}\omega_- |1+R|^2,\ J_+ = \tfrac{1}{2}\omega_- (1-|R|^2). \quad (1.7)$$

We have thus

$$J_- - J_+ = \omega_- (|R|^2 + \mathrm{Re}\, R). \quad (1.8)$$

We emphasize that this expression is exact.

In order to go over to the adiabatic approximation, we must substitute in (1.8) the reflection amplitude R as calculated in the quasi-classical approximation. This calculation was done by Pokrovskiĭ et al.[6] If $\omega^2(t)$ is an analytic function without zeroes on the real axis and a simple root at the point t_0 of the complex plane, we have thus

$$R = -i\exp\left\{2i\int^{t_0}\omega(t)\,dt\right\}. \quad (1.9)$$

Substituting (1.9) in (1.8), we obtain

$$J_- - J_+ = \omega_- (e^{-4\sigma} + \sin 2\rho e^{-2\sigma}),$$
$$\rho + i\sigma = \int^{t_0}\omega(t)\,dt, \quad (1.10)$$

where ρ and σ are real numbers.

We see that the variation of the adiabatic invariant is an exponentially small quantity. Besides this, the variation depends on the "initial" phase, owing to the presence of the term Re R in (1.8). It is easily shown that, if the k-th derivative of the function $\omega(t)$ has a finite discontinuity on the real axis, the variation of the adiabatic invariant is proportional to the k-th power of the small parameter.

2. QUANTUM TRANSITIONS IN THE DISCRETE SPECTRUM

As is known,[7] the adiabatic invariants of quantum mechanics are the quantum numbers and the distribution over the stationary states of the system. The problem of the variation of the adiabatic invariants with time is, therefore, essentially the problem of calculating the transition probabilities between the stationary states. This problem of quantum mechanics can be solved only by a few methods, in particular, that of perturbation theory. Below we shall develop a method which permits the computation of transition probabilities in a special case in which perturbation theory is not applicable.

Let us assume that the Hamiltonian of the system with a discrete spectrum depends on some parameter $\lambda(t)$ which is a slowly varying function of time. The parameter $\lambda(t)$ goes asymptotically to $\lambda_\pm$ for $t \to \pm\infty$. For $t \to \pm\infty$ the system then has stationary states. We emphasize that the difference between the asymptotic values of the energy at $t \to \pm\infty$ is not assumed to be small, but can have any arbitrary value. The small parameter used in the solution is the ratio

$$\omega_{mn}^{-1}\, d\ln\lambda/dt = \alpha, \quad (2.1)$$

where ω_{mn} is the transition frequency of the Hamiltonian $H(\lambda)$.

Our procedure is the following: let us assume that for $t \to -\infty$ the system was in the n-th stationary state of the Hamiltonian H (the value of the Hamiltonian H for $\lambda(t) = \lambda_-$). The wave function of the system was then ψ_{n-}. For $t \to +\infty$ the wave function can be expanded in terms of the eigenfunctions of the Hamiltonian H_+ ($\lambda = \lambda_+$):

$$\psi = \sum_k a_{nk}\psi_{k+}. \quad (2.2)$$

The problem consists in finding the transition amplitudes a_{nk}. We note that it is meaningless to ask for the transition amplitudes at intermediate times, since the Hamiltonian depends on the time and stationary states can be defined only with an accuracy given by $\omega_{mn}^{-1}\partial H/\partial t$.

The solution of the proposed problem will be discussed first on the example of the harmonic oscillator.

3. THE QUANTUM OSCILLATOR IN THE ADIABATIC APPROXIMATION

The problem consists in solving the Schrödinger equation

$$i\partial\psi/\partial t = H\psi \quad (3.1)$$

with the Hamiltonian

$$H = -\tfrac{1}{2}\partial^2/\partial x^2 + \tfrac{1}{2}\omega^2(t)\,x^2. \quad (3.2)$$

Here and in the following we set $\mu = \hbar = 1$. Let us assume that for $t = t_0 \to -\infty$ there exists a solution of the stationary equation

$$H(t_0)\,\psi(t_0) = E(t_0)\,\psi(t_0). \quad (3.3)$$

As is well known (see, for example, reference 8), the solution of (3.1), $\psi(t)$, can then be expressed through $\psi(t_0)$,

$$\psi(t) = S(t_0, t)\,\psi(t_0), \quad (3.4)$$

with the help of the S matrix, which satisfies the equation

$$i\partial S/\partial t = HS. \quad (3.5)$$

Using (3.4), we can rewrite (3.3) in the form of an equation for $\psi(t)$:

$$H(t_0, t)\,\psi(t) = E(t_0)\,\psi(t), \quad (3.6)$$

where

$$H(t_0, t) = S^{-1}(t_0, t)\,H(t_0)\,S(t_0, t)$$

is the usual oscillator Hamiltonian made up of the operators $\hat{p}(t_0, t)$ and $\hat{x}(t_0, t)$. These latter can be determined from the equation of motion

$$\ddot{\hat{x}} + \omega^2(t)\,\hat{x} = 0. \tag{3.7}$$

By virtue of its linearity we can solve this equation assuming that $\hat{x}$ is a c number. The solution for $t \to \pm\infty$ is asymptotically

$$\hat{x}_\pm = \hat{c}_\pm e^{i\omega_\pm(t-t_0)} + \hat{c}_\pm^+ e^{-i\omega_\pm(t-t_0)},$$
$$\hat{p}_\pm = i\omega_\pm[\hat{c}_\pm e^{i\omega_\pm(t-t_0)} + \hat{c}_\pm^+ e^{-i\omega_\pm(t-t_0)}]. \tag{3.8}$$

From the definition of the operators in the Heisenberg representation we have for $t_0 = t$

$$\hat{x}\ (t,\ t) = \hat{x},\ \hat{p}\,(t,t) = \hat{p}. \tag{3.9}$$

From this we find easily

$$\hat{c}_+ = \tfrac{1}{2}\,(\hat{x} - i\omega_+^{-1}\hat{p}). \tag{3.10}$$

The connection between $\hat{c}_+$ and $\hat{c}_-$ is readily obtained by a method analogous to that described in Sec. 1 for the classical oscillator. The result is

$$\hat{c}_- = (1 - |R|^2)^{-1} D^*\,(\hat{c}_+ - R\hat{c}_+^+). \tag{3.11}$$

Here R and D are the reflection and transmission amplitudes in the corresponding scattering problem.

Using (3.8), we find

$$\hat{c}_- = \frac{D^*}{2(1-|R|^2)}\left[(1-R)\,\hat{x} + \frac{\hat{p}}{i\omega_+}(1+R)\right]. \tag{3.12}$$

Substituting (3.8) in the Hamiltonian

$$H_- = \omega_-^2\,(\hat{c}_-\,\hat{c}_-^+ + \hat{c}_-^+\,\hat{c}_-)$$

and using the law of conservation of the number of particles, we obtain

$$H(t_0, t) = \frac{\omega_+\omega_-}{2(1-|R|^2)}\Big\{|1-R|^2\hat{x}^2 + \frac{\hat{p}^2}{\omega_+^2}|1+R|^2$$
$$+ \frac{1}{\omega_+}\,\mathrm{Im}\,[(1+R)\,(1-R^*)]\,(\hat{p}\hat{x} + \hat{x}\hat{p})\Big\}. \tag{3.13}$$

As can be readily verified, the normalized solution of equation (3.6) with the Hamiltonian (3.13) has now the form

$$\psi_n(t) = \left(\frac{\omega_+}{\pi}\,\mathrm{Re}\,\frac{1-R}{1+R}\right)^{1/4}(2^n n!)^{-1/2}\exp\left\{-\frac{\omega_+ x^2}{2}\,\frac{1-R}{1+R}\right\}$$
$$\cdot H_n\left[\left(\omega_+\,\mathrm{Re}\,\frac{1-R}{1+R}\right)^{1/2} x\right], \tag{3.14}$$

where the H_n are Hermite polynomials. For the computation of the transition amplitudes we must expand this function in terms of the eigenfunctions ψ_{k^+} of the Hamiltonian H_+,

$$\psi_{k+} = (\omega_+/\pi)^{1/4}(2^k k!)^{-1/2}\exp\{-\omega_+ x^2/2\}\,H_k(\omega_+^{1/2}x). \tag{3.15}$$

The amplitudes are equal to

$$a_{nk} = \int_{-\infty}^{\infty}\psi_n(t)\,\psi_{k+}^*\,dx. \tag{3.16}$$

If we assume that $R \ll 1$, the main part of the transition amplitude can be calculated from the leading term in the integral defining a_{nk}:

$$I_{nk} = \int_{-\infty}^{\infty}\exp(-\xi^2)\exp(R\xi^2)\,H_n[(1-\mathrm{Re}\,R)\,\xi]\,H_k(\xi)\,d\xi$$
$$\xi = \sqrt{\omega_+}\,x. \tag{3.17}$$

The integral (3.17) is calculated in the Appendix. The result is

$$a_{nk} = \left(\frac{k!}{n!}\right)^{1/2}2^{(n-k)/2}\left[\left(\frac{k-n}{2}\right)!\right]^{-1}R^{(k-n)/2}$$
$$+ O(R^{(k-n)/2+1}) \text{ for } k > n,$$
$$a_{nk} = \left(\frac{n!}{k!}\right)^{1/2}2^{(k-n)/2}\left[\left(\frac{n-k}{2}\right)!\right]^{-1}(-R^*)^{(n-k)/2}$$
$$+ O(R^{(n-k)/2+1}) \text{ for } k < n, \tag{3.18}$$

in particular

$$a_{nn} = 1 + O(R). \tag{3.19}$$

We see in this way that the main part of the transition amplitude is a universal matrix multiplied by some power of the reflection amplitude.

Since $\omega(t)$ is assumed to be a slowly varying function of time, we must find the reflection amplitude R in the quasi-classical approximation. We quote here the corresponding results from the paper of Pokrovskiĭ, Savvinykh, and Ulinich,[6] where this computation was carried out.

If $\omega^2(t)$ is an analytic function without zeroes on the real axis and a simple root at the point t_0 of the complex plane, the reflection amplitude is equal to

$$R = F(\mu/\alpha)\exp\left\{2i\int^{t_0}\omega(t)\,dt\right\},$$
$$F(x) = \frac{2\pi i\exp\{ix\ln(x/2e) - \pi x/2\}}{\Gamma(ix/2)\,\Gamma(1+ix/2)}. \tag{3.20}$$

Here μ is a parameter of the order of the quantity $(\omega_+ - \omega_-)/(\omega_+ + \omega_-)$ (not necessarily small), and α is a small parameter of the order of the quantity ω'/ω^2 (for the exact definition of these parameters see reference 6).

If $x = \mu/\alpha \to 0$, $|F(x)| \approx \pi x$, which corresponds to the case where perturbation theory is valid. For $x \to \infty$, $F(x) \approx -i$. Then

$$a_{nk} = \begin{cases}\left(\frac{k!}{n!}\right)^{1/2}2^{(n-k)/2}\left[\left(\frac{k-n}{2}\right)!\right]^{-1}\exp\left\{i(k-n)\int^{t_0}\omega(t)dt\right\} & (k>n)\\ \left(\frac{n!}{k!}\right)^{1/2}2^{(k-n)/2}\left[\left(\frac{n-k}{2}\right)!\right]^{-1}\exp\left\{i(n-k)\int^{t_0^*}\omega(t)dt\right\} & (k<n).\end{cases} \tag{3.21}$$

We see that the transition amplitude is exponentially small and the transition probability does not depend on the "initial" phase.

By taking the classical limit of (3.18) we readily obtain the variation of the adiabatic invariant for the classical oscillator. We shall present here the corresponding calculation with an accuracy up to

the first order in the reflection coefficient R. To obtain the quasi-classical wave function, we must take a wide selection of states in the region of large quantum numbers.

Let this wave function be

$$\Phi_{\pm} = \sum \gamma_n^{\pm} \psi_n^{\pm} \text{ for } t \to \pm\infty. \tag{3.22}$$

We note here that the $\gamma_n^{\pm}$ must satisfy the following condition in order that the function $\Phi_{\pm}$ describe a classical particle on a trajectory:

$$(1/\gamma_n^{\pm})\, d\gamma_n^{\pm}/dn \ll 1. \tag{3.23}$$

The average value of the action $J_{\pm}$ is determined by

$$J_{\pm} = \sum_n |\gamma_n^{\pm}|^2 \left(n + \tfrac{1}{2}\right). \tag{3.24}$$

We have the following relation between γ_n^+ and γ_n^- with an accuracy up to order R:

$$\gamma_n^+ = \gamma_n^- a_{nn} + \gamma_{n-2}^- a_{n-2,\,n} + \gamma_{n+2}^- a_{n+2,\,n}. \tag{3.25}$$

The transition amplitudes a_{mn} for large m and n can be written asymptotically

$$a_{nn} = 1 + i \operatorname{Im} R\left(n + \tfrac{1}{2}\right), \qquad a_{n+2,\,n} = \tfrac{1}{2}\left(n - \tfrac{1}{2}\right) R,$$

$$a_{n-2,\,n} = -\tfrac{1}{2}\left(n + \tfrac{3}{2}\right) R^*. \tag{3.26}$$

Substituting (3.26) in (3.25) and using (3.23), we readily obtain

$$|\gamma_n^+|^2 = |\gamma_n^-|^2 (1 - 2 \operatorname{Re} R). \tag{3.27}$$

As can be seen from (3.24), we have then

$$(J_+ - J_-)/J_+ = -2 \operatorname{Re} R.$$

This result agrees with an accuracy up to order R with the variation of the action of the classical oscillator as found in Sec. 1 [cf. Eq. (1.8)].

4. TRANSITION PROBABILITIES FOR POTENTIALS OF THE FORM $\lambda(t)\,V(x)$

Let us now consider the problem of calculating the transition amplitudes for a potential of the type $\lambda(t)\,V(x)$ with a discrete spectrum. We determine the eigenfunctions and the eigenvalues of the time dependent Hamiltonian from the equation

$$H(x|t)\,\psi_n(x|t) = E_n(t)\,\psi_n(x|t) \tag{4.1}$$

and expand the wave function in terms of these functions. For the expansion coefficients we obtain a system of equations which is usually taken as the basis of adiabatic perturbation theory (see, for example, reference 8):

$$a_n = \sum_{k \neq n} \omega_{nk}^{-1} a_k (\partial H/\partial t)_{nk} \exp\left\{i \int^t \omega_{nk}(t)\, dt\right\}. \tag{4.2}$$

If $a_k \to \delta_{km}$ for $t \to -\infty$, we conclude from (4.2)

$$a_n(t) = \delta_{mn} + \sum_{k \neq n} \int_{-\infty}^{t} \omega_{nk}^{-1} a_k(t') (\partial H/\partial t')_{nk} \times \exp\left\{i \int^{t'} \omega_{nk}(t'')\, dt''\right\} dt'. \tag{4.3}$$

We apply the iteration method to equation (4.3), taking $\omega_{mn}^{-1}\partial H/\partial t$ as a small quantity. Assuming that $\omega_{nk} \neq 0$ on the real axis, we can close the contour of integration either in the upper or in the lower half plane. Therefore only the poles of the expression under the integral (4.3) will play a role in the iteration series. It is natural to assume that the poles of the expression under the integral (4.3) will coincide with the zeroes and poles of the function $\lambda(t)$.

Let us consider the behavior of the integrand near a zero of the function $\lambda(t)$. (The analytic continuation of the solutions of the stationary equation (4.1) into the complex plane will be taken along the line $\operatorname{Im} \lambda = 0$.) Let us assume that the asymptotes of $V(x)$ follow a power law, which for simplicity we take to be the same in both cases:

$$V(x) \approx A|x|^{2l} \qquad (l > 0) \text{ for } x \to \pm\infty. \tag{4.4}$$

We write $V(x)$ in the form

$$V(x) = A|x|^{2l} + U(x). \tag{4.5}$$

Let us introduce the new variable

$$\xi = \lambda^{1/2(l+1)} x.$$

In this case equation (4.1) takes the form

$$d^2\psi_n/d\xi^2 + [E_n \lambda^{1/(l+1)} + A|\xi|^{2l} + \lambda^{l/(l+1)} U(\xi \lambda^{-1/2(l+1)})]\,\psi_n = 0. \tag{4.6}$$

It is seen from (4.4) that the inequality

$$A|\xi|^{2l} \gg \lambda^{l/(l+1)} U(\xi \lambda^{-1/2(l+1)}) \tag{4.7}$$

is valid everywhere except in a small region of order $\lambda^{1/2(l+1)}$ near $\xi = 0$. For the solution of equation (4.1) near a zero of $\lambda(t)$ we can therefore replace the potential in (4.1) by its asymptotic value. It is then readily verified that (4.3) can be rewritten in the form

$$a_n(t) = \delta_{mn} + \sum_{k \neq n} \int_{-\infty}^{t} c_{nk}\, a_k \lambda' \lambda^{-1} \exp\left\{i \int^{t'} \omega_{nk}\, dt''\right\} dt', \tag{4.8}$$

where c_{nk} is a matrix which depends only on the asymptotic form of $V(x)$ and not on the form of the function $\lambda(t)$.

From (4.8) we obtain for the transition amplitude in first approximation

$$a_{nm} = B'_{nm} \exp\left\{i \int^{t_0} \omega_{mn}\, dt\right\}. \quad (4.9)$$

Here B'_{nm} is a matrix which is completely determined by the first term in the asymptotic expansion of the potential. Since the same zero or pole which determines the first term in the iteration series used for the calculation of the integrals will play an analogous role in all succeeding terms, it is clear that all terms of this series will be proportional to the same exponential $\exp\{i\int^{t_0} \omega_{mn}\, dt\}$ and therefore have the same order of smallness. It is easily shown that the convergence of this series is guaranteed by the fast decrease of the factors multiplying the exponentials. By summing up the whole series we obtain the expression

$$a_{nm} = B_{mn} \exp\left\{i \int^{t_0} \omega_{mn}\, dt\right\}. \quad (4.10)$$

Since the matrix B_{nm} is a universal quantity, it can be obtained from the solution of the Schrödinger equation with an arbitrary potential possessing the given asymptotic values. For example, if the potential has the asymptotic behavior Ax^2, we find for the transition amplitude, using the results of Sec. 3,

$$a_{nm} = \begin{cases} \left(\frac{m!}{n!}\right) 2^{(n-m)/2} \left[\left(\frac{m-n}{2}\right)!\right]^{-1} \exp\left\{i \int^{t_0} \omega_{mn}\, dt\right\} & (m > n) \\ \left(\frac{n!}{m!}\right)^{1/2} 2^{(m-n)/2} \left[\left(\frac{n-m}{2}\right)!\right]^{-1} \exp\left\{i \int^{t_0} \omega_{nm}\, dt\right\} & (m < n). \end{cases} \quad (4.11)$$

I take this opportunity to express my sincere gratitude to Yu. B. Rumer and V. L. Pokrovskiĭ for suggesting this problem and for many valuable comments concerning this work.

APPENDIX

We present here the approximate evaluation of the integral (3.17). We expand the function under the integral into a series in powers of R and Re R. The general term of this series is evidently equal to

$$\frac{R^p(-\operatorname{Re} R)^q}{p!\ q!} \int_{-\infty}^{\infty} \exp(-\xi^2)\, \xi^{2p+q} H_n^{(q)}(\xi) H_k(\xi)\, d\xi. \quad (A.1)$$

This matrix element is different from zero only if

$$2p + q \geqslant |n - k - q|. \quad (A.2)$$

It is seen from (A.1) that for given n and k the term with the lowest value of p+q has the largest value. We must therefore look for the minimum of the expression p+q under the subsidiary condition (A.2).

We discuss the cases $n < k$ and $n > k$ separately. In the first case formula (A.2) becomes $2p \geq k - n$. The minimum of p+q occurs at $q = 0$, $p = (k-n)/2$. We therefore have

$$I_{nk} = \frac{R^p}{p!} (\xi^{k-n})_{nk} = R^{(k-n)/2} \left[\left(\frac{k-n}{2}\right)!\right]^{-1} \left(\frac{k!}{n!}\right)^{1/2} \times 2^{(n-k)/2} + O\left(R^{(k-n)/2+1}\right). \quad (A.3)$$

If $n > k$, (A.2) gives

$$p + q \geqslant (n-k)/2. \quad (A.4)$$

In this case we must sum over all terms of the series which satisfy the condition $p+q = (n-k)/2$. As can be readily seen, this sum is equal to

$$\sum_{p,\,q} \frac{R^p(-\operatorname{Re} R)^q 2^q}{p!\ q!} (\xi^{n-k})_{nk} = \left(-R^*\right)^{(n-k)/2} \times \left[\left(\frac{n-k}{2}\right)!\right]^{-1} \left(\frac{n!}{k!}\right)^{1/2} 2^{(k-n)/2} + O\left(R^{(n-k)/2+1}\right). \quad (A.5)$$

Formulas (A.3) and (A.5) lead to (3.18).

[1] P. Langevin and L. de Broglie, La Theorie du Rayonnement et les Quanta (Report at the Solvay Conference, Brussels, 1911).

[2] H. Alfvén, Cosmical Electrodynamics, Clarendon Press, Oxford (1950).

[3] G. Helwig, Z. Naturforsch. **10a**, 508 (1955).

[4] R. M. Kulsrud, Phys. Rev. **106**, 205 (1957).

[5] A. Lenard, Ann. of Physics **6**, 276 (1959).

[6] Pokrovskiĭ, Savvinykh, and Ulinich, JETP **34**, 1272 and 1629 (1958), Soviet Phys. JETP **7**, 879 and 1119 (1958).

[7] M. Born and V. Fock, Z. Physik **51**, 165 (1928).

[8] V. I. Kogan and V. M. Galitskiĭ, Сб. задач по квантовой механике (Collection of Problems in Quantum Mechanics), Moscow, GITTL (1956).

Translated by R. Lipperheide
111

ANALYSIS BASED ON DISPERSION RELATIONS OF DATA ON PION PHOTOPRODUCTION NEAR THRESHOLD

A. M. BALDIN

P. N. Lebedev Physics Institute, Academy of Sciences, U.S.S.R.

Submitted to JETP editor August 26, 1959

J. Exptl. Theoret. Phys. (U.S.S.R.) **38**, 579-587 (February, 1960)

It is found that in the region near the threshold it is possible to make a direct comparison of data on the photoproduction of π mesons with the dispersion relations. This new method of analysis is applied to the available experimental data on the photoproduction of π^0, π^+, and π^- mesons. An investigation is made of the reasons for the significant discrepancy found earlier[4] between conclusions based on the dispersion relations and experimental data. Experiments are suggested which should ascertain whether this discrepancy is due to a large contribution to the dispersion integrals from the domain of very high energies. The solution of this problem may greatly affect the efforts to construct a theory of pion photoproduction on the basis of dispersion relations.

1. INTRODUCTION

UNTIL very recently the analysis of the photoproduction of π mesons founded on dispersion relations was based on the well known paper by Chew et al.,[1] in which an attempt was made to obtain the amplitudes for the photoproduction of π mesons from dispersion relations.

In a number of papers[1,2] it was noted that these amplitudes, generally speaking, agree with experimental data. In a paper by Govorkov and Baldin[4] an analysis of new experimental data[5] was made, and it was shown that the photoproduction amplitudes given in reference 1 contradict these data. In discussing this contradiction one must bear in mind the fact that the amplitudes in reference 1 were obtained on the basis of a number of assumptions of special nature. In this connection, a method of analysis of photoproduction data which would enable us to compare directly the dispersion relations with experiment would be of considerable interest. Until now the dispersion relations have been investigated in this way only for the case of the scattering of π mesons by nucleons. In the case of photoproduction such a comparison, generally speaking, presents great difficulties. The object of the present article is the application of the dispersion relations to the photoproduction of π mesons in the near-threshold region, where, as it turns out, a number of difficulties disappears and the comparison mentioned previously turns out to be possible.

We have made partial use of this method in reference 4. It was shown there that the contradiction between the experimental data and the conclusions reached on the basis of the dispersion relations, persists to a great extent also in the case of this method of analysis. Thus, the contradiction becomes much more acute since the new approach does not depend on the assumptions made by Chew et al.[1]

Earlier[4] we have investigated only the forward part of the photoproduction amplitude. Without any doubt a complete analysis of the available experimental data on the photoproduction of π mesons in the near-threshold region, an analysis of the possible reasons for the observed contradiction, and also a complete exposition of the method mentioned previously and a proposal of further experiments are topics of definite interest.

The present article is devoted to all these problems.

2. THE METHOD OF ANALYSIS

The dispersion relations for the photoproduction of π mesons have been given in references 1 and 3. In the center-of-mass system they have the following structure:

$$\mathrm{Re}F_i(w, \nu_1) = F_i^B + \frac{1}{\pi}\int_{M+1}^{\infty} dw' \,\mathrm{Im}\sum_j F_j(w', \nu_1)\, Q_{ij}(w', w, \nu_1). \quad (1)$$

Here the quantities F_i are proportional to the individual amplitudes which make up the total amplitude for the process

$$F = i(\sigma\varepsilon)F_1 + \frac{(\sigma q)(\sigma[k\varepsilon])}{qk}F_2 + i\frac{(\sigma k)(q\varepsilon)}{qk}F_3 + i\frac{(\sigma q)(q\varepsilon)}{q^2}F_4, \quad (2)$$

σ is the Pauli matrix, ϵ is the photon polarization vector, $\mathbf{q}$ and $\mathbf{k}$ are respectively the meson and the photon momenta.

In this case the cross section has the following form

$$\frac{d\sigma}{d\Omega} = (q/k)\{|F_1|^2 + |F_2|^2 - 2\,\mathrm{Re}\,F_1^* F_2 \cos\theta + \tfrac{1}{2}\sin^2\theta\,[|F_3|^2 + |F_4|^2 + 2\,\mathrm{Re}\,F_2^* F_3 + 2\,\mathrm{Re}\,F_1^* F_4 + 2\,\mathrm{Re}\,F_3^* F_4 \cos\theta]\}, \quad (3)$$

$w = \sqrt{1+q^2} + \sqrt{M^2+q^2}$ is the total energy,* $Q_{ij}(w, w', \nu_1)$ are certain real functions. The explicit expressions for F_i^B and Q_{ij} are given in references 1 and 3.

An attempt to make a direct comparison of relations (1) with experiment encounters great difficulties. These difficulties are first of all associated with the fact that the experimental data on the amplitudes F_i are very meager. Moreover, the integral in (1) contains a non-physical region ($\cos\theta > 1$) which also introduces some indefiniteness into the comparison of (1) with experiment. Further, the range of integration in (1) over w' extends to infinity, and since the experimental data always refer to a limited range of energies, this reduces the value of the conclusions with respect to the verification of the dispersion relations themselves.

Another difficulty in making a comparison of (1) with experiment involves the numerical evaluation of the principal value of the integrals of functions obtained experimentally with very limited accuracy.

The method utilized by us enables us to a large extent to avoid these difficulties.

We undertake the investigation of the near-threshold region, by which we mean the region of energies such that $q < 1$. In this region the problem of comparing (1) with experiment is simplified.

If we expand the amplitude [and correspondingly Eq. (1)] into a power series in q, we shall be dealing with the amplitude and with its derivatives at $q = 0$. In this case the non-physical region reduces to a point. The difficulty associated with the evaluation of the principal value of integrals is also eliminated since at $q = 0$ the poles of the functions Q_{ij} are cancelled by the zeros of the functions F_i.

Moreover, in virtue of the well known connection between scattering and photoproduction and of the fact that the scattering phases vanish as $q \to 0$, we may obtain the left hand side of (1) from the experimental data without making use of polarization experiments. We have already discussed this point in reference 4.

One might think that the principal difficulty associated with estimating the role played by the region of high values of w' will also be considerably reduced in our case since the integrand falls off quite rapidly as w' increases.

We represent the experimental data on the photoproduction of π mesons in the following form:

$$\frac{d\sigma}{d\Omega} = \sum_{mn} b_{mn} q^m (\cos\theta)^n; \quad (4)$$

the parameters b_{mn} may be evaluated from the dispersion relations and compared with the experimental values, as we shall demonstrate later.

We begin with a few general remarks on the coefficients b_{mn}. In the photoproduction of π^0 mesons, the predominant role is played by the $(3/2, 3/2)$ resonance amplitude, for which the coefficients b_{m0} and b_{m2} differ from zero. Moreover, in accordance with the resonance model the amplitude depends on q through the factor

$$\frac{\sin\alpha_{33}}{q^3} \approx \frac{\alpha_{33}}{q^3} = \mathrm{const}\,\frac{q}{\omega\,[1 - \omega/\omega_r]}, \qquad \omega_r \approx 2,$$

from which it follows that in the expansion of this amplitude the terms of the second, third and fourth degree in q are absent.

Thus, one might expect that the experimental data on the photoproduction of π^0 mesons are described by a small number of coefficients b_{mn} over quite a large interval (as was demonstrated in reference 2).

In the case of charged mesons an essential complication arises because of the "retarded term"

$$q^2 \sin^2\theta / 2k^2 [1 - (q/\omega)\cos\theta]^2,$$

which in the region $q \lesssim 1$ considerably exceeds the contribution of the p-waves. Therefore, the lowest terms in the expansion will describe $d\sigma/d\Omega$ over a considerably smaller range of q, than in the case of neutral mesons.*

In such a case it is apparently useful to make an expansion into a series of type (4) not of the differential cross section $d\sigma/d\Omega$, but of the quantity

$$[1 - (q/\omega)\cos\theta]^2\, d\sigma/d\Omega,$$

which, nevertheless, will lead to the necessity of

*We utilize the system of units such that $\hbar = \mu = c = 1$.

*However, it should be noted that in the neighborhood of $\theta = 0$ and $\theta = \pi$ the contribution of this term becomes small, and possibly these ranges of angles (particularly the angles close to π) are the most suitable ones for analysis by our method.

analyzing a considerably greater number of coefficients than in the case of photoproduction of π^0 mesons.

In order to obtain the theoretical values of the different quantities we shall need expansions of the amplitudes* F in powers of q:

$$F_1 \approx f_1^{(0)} + i f_1^{(1)} q + f_1^{(2)} q \cos\theta + f_1^{(3)} q^2 + \ldots;$$
$$F_2 \approx f_2^{(1)} q + \ldots;\ F_3 \approx f_3^{(1)} q + \ldots;\ F_4 = f_4^{(2)} q^2 + \ldots, \quad (5)$$

$f_i^{(k)}$ is expressed in the form of two terms, one of which is the expansion coefficient of the Born part of the amplitude F_i^B in expression (1) evaluated exactly, while the other term is determined by the dispersion integral. In the case of charged mesons, in order to reduce the necessary number of parameters b_{mn}, it is advantageous to retain the "retarded term" without expanding it. This means that the amplitudes F_2 and F_4 will contain the following terms

$$f_3^{(2)} = \frac{ef}{1+\omega/M}\frac{qk}{\omega k - qk\cos\theta}, \quad f_4^{(2)} = \frac{ef}{1+\omega/M}\frac{-q^2}{\omega k - qk\cos\theta}. \quad (6)$$

Here f is the renormalized coupling constant, and e is the charge.

3. NEUTRAL MESONS

The photoproduction of π^0 mesons was partially investigated by the method just outlined in reference 4. It was shown there that if the forward part of the photoproduction amplitude is calculated on the assumption that the principal contribution to the dispersion integrals is made by the $(3/2, 3/2)$ resonance amplitude, then a significant disagreement with experiment exists (approximately three standard deviations). However, this result depends on the uncertainties associated with the calibration of the beam. Moreover, if the errors in the measurement of the renormalized coupling constant and of the total photoproduction cross section for π^0 mesons are taken into account, this may further reduce the disagreement to some extent. In this connection we have carried out a complete analysis of the photoproduction of π^0 mesons (not only for the forward photoproduction amplitude). In the evaluation of errors we have also taken into account some small errors of the type just indicated. It is also necessary to keep in mind that, strictly speaking, the data of reference 5 are insufficient for the determination of the coefficients b_{mn}.

In reference 4, in order to determine the first few coefficients in expansion (4), we have utilized data for $q > 1$, after correcting them for the $(3/2, 3/2)$ resonance. These corrections strongly depend on the value of the "resonance" frequency* ω_r.

In order to be able to draw more definite conclusions with respect to the coefficients b_{mn} we require additional measurements of cross sections in the region $q < 1$. A more rigorous approach to the available experimental data consists of collecting all the available data on the reaction $\gamma + p \to p + \pi^0$, choosing an appropriate ω_r and then extrapolating to $q = 0$. The diagram shows the experimental results of references 2 and 5 on the determination of A and C presented in the form of

$$(A/q\omega)\,[a_{33}q^2/\sin\alpha_{33}]^2$$

and

$$(C/q\omega)\,[a_{33}q^2/\sin\alpha_{33}]^2.$$

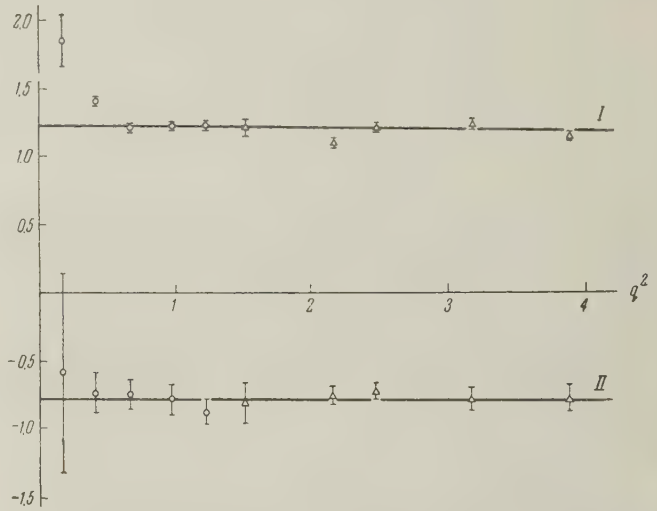

The experimental data of reference 2 (triangles) and of reference 5 (circles) presented in the following form: I – $(A/q\omega)[a_{33}q^2/\sin\alpha_{33}]^2$, II – $(C/q\omega)[a_{33}q^2/\sin\alpha_{33}]^2$.

The resonance frequency satisfying all these data has turned out to be equal to $\omega_r = 1.95$. The values of the coefficients b_{mn} obtained as a result are given in the second line of the table. They differ considerably from those obtained by us earlier[4] with $\omega_r = 2.1$.

b_{12}	b_{21}	b_{30}	b_{10}
−0.78 ±0.10	−0.38 ±0.04	1.23 ±0.03	0.10 ±0.03
+0.32 ±0.03	−0.71 ±0.07	1.04 ±0.1	0.12 ±0.01

In order to determine b_{mn} from the dispersion relations we must obtain $f_k^{(i)}$. A numerical evaluation of the dispersion integrals on the basis of the same assumptions as in reference 4 yields†

*For the sake of simplicity we have omitted everywhere the isotopic indices.

*In reference 4 we assumed $\omega_r = 2.1$.

†Here $f_i^{(k)}$ are amplitudes corresponding to the process $\gamma + p \to p + \pi^0$, and not partial amplitudes referring to a state of definite isotopic spin.

$$f_1^{(0)} = -0.79 + 0.46 = -0.33, \quad f_1^{(2)} = 0.85 + 0.77 = 1.62,$$

$$f_2^{(1)} = 0.0 + 0.61 = 0.61, \quad f_3^{(1)} = -0.98 - 0.77 = -1.75,$$

$$f_4^{(2)} = 0.35 + 0.0 = 0.35. \qquad (7)$$

Here $f_i^{(k)}$ is expressed in units of $10^{-2}\hbar/\mu c = 1.4 \times 10^{-15}$ cm.

The first figures indicate the contribution of the Born part of the amplitude, while the second ones give the contribution of the dispersion integrals.* The statistical error in these quantities amounts to approximately 5%.

These values of the amplitudes correspond to the values of the coefficients b_{mn} shown in the third line of the table. In order to eliminate the uncertainties associated with the calibration of the beam we compare the quantities b_{32}/b_{30} and b_{21}/b_{30}.† Experiment yields for these quantities the following values: -0.63 ± 0.08 and -0.31 ± 0.03 respectively, while from the dispersion relations we obtain: $+0.32 \pm 0.03$ and -0.66 ± 0.07.

Thus, the discrepancy amounts to several standard deviations. The reasons for the discrepancy should be sought only in the evaluation of the dispersion integrals, if we disregard the possible inaccuracies in the extrapolation of the experimental data to $q = 0$. (One should also remember that all our conclusions are based on the data of only a single experiment and require additional experimental confirmation.) We note that the data (7) correspond to approximately equal absolute values and opposite signs of the amplitudes of the magnetic dipole transitions M_{1+} and M_{1-}, while in the integrand we took into account only the imaginary part of the amplitude M_{1+}. We could achieve agreement with experiment at $q = 0$ by assuming that the integral of the imaginary part of M_{1-} is close in magnitude to the integral of the imaginary part of M_{1+} and that these integrals have the same sign. However, this is, in turn, in poor agreement with experimental data on photoproduction and on scattering at energies where the integrands are large, $q \sim 1$.

Indeed, from our analysis[4] it follows that in the region of the threshold energies, M_{1-} is equal to zero within experimental error. At higher energies we may utilize the data of McDonald, Peterson and Corson[2] for the evaluation of the amplitude of M_{1-}.

An estimate of the magnitude of the amplitude of M_{1+} may be obtained from the integrated cross section from which all interference terms drop out. We neglect the squares of the other p-wave amplitudes. Then, on taking into account the relation between scattering and photoproduction, and the fact that the scattering phases α_{11}, α_{31} and α_{13} do not exceed $10 - 15°$, it is not difficult to obtain an estimate for the magnitude of M_{1-} from the general expression for the angular distribution. It turns out to be of the order of magnitude of the experimental error, and certainly less than $0.2\,M_{1+}$. From this we see that the integral of the imaginary part of M_{1-} cannot be close in magnitude to the integral of the imaginary part of M_{1+}. At the present time, because of the inaccuracy of the experimental data, it is difficult to make an estimate of the total value of the discrepancy under discussion taking into account the possible contribution of M_{1-}.

4. CHARGED MESONS

The photoproduction amplitudes for charged mesons differ by the fact that the Born part $f_1^{(0)}$ is much larger than in the case of neutral mesons. This is a reflection of the well known fact that in the near-threshold region the s-wave meson photoproduction plays the dominant role in the case of charged mesons. Moreover, the Born parts of the amplitudes F_2 and F_4, containing the "retarded term," also give a contribution which considerably exceeds the contribution of the dispersion integrals. The value of $f_1^{(0)}$ expressed in terms of our units amounts to 2.56 for the photoproduction of π^+ mesons, the contribution of the "retarded term" in the region $q \sim 1$ in the expressions for F_2 and F_4 amounts to $\sim 0.7\, f_1^{(1)}$, so that it cannot be neglected. The dispersion integrals, obtained under the same assumptions as the dispersion integrals for the photoproduction amplitudes for π^+ mesons, are close to these integrals in magnitude. From this it is clear that only in the region of $q \sim 1$ will the contribution of the dispersion integrals to the cross section be as high as $20 - 25\%$. As q decreases this contribution is reduced significantly and falls outside the limits of the available experimental accuracy. On the basis of this one should expect that the experimental data on the photoproduction of charged mesons in the region of interest to us may be described with a sufficient degree of accuracy by formulas which agree with the first nonvanishing approximation of perturbation theory. The contribution of the dispersion integral to $f_1^{(1)}$ which does not diminish as q decreases requires

*As can be seen from these figures, the overwhelmingly large contribution of the Born part of the amplitude noted in reference 4 is a peculiarity of the forward photoproduction, and not of near-threshold photoproduction in general.

†It is necessary to emphasize that the uncertainty associated with the value of ω_r does not affect these quantities within experimental error, while changes in the values of b_{mn} when ω_r is changed from 2.1 to 1.95 lie far outside the limits of statistical errors.

a separate comment. This contribution, in spite of being small, nevertheless introduces some uncertainty into the determination of the coupling constant from the photoproduction cross section for charged π mesons extrapolated to the threshold.

A comparison of the b_{mn}, obtained by neglecting the contribution of the dispersion integrals, with the experimental data on the photoproduction of π^+ mesons shows good agreement between them. The essential role played by the "retarded term" is demonstrated by the recent results of references 6 and 7 in which an increase in the square of the amplitude in the threshold region was discovered.

Data on the photoproduction of π^- mesons can at present be obtained only by analyzing the data on photoproduction in deuterium. It appears to us that in the near-threshold region this may be done only by analyzing experiments carried out in such a way that all the product particles of the reaction $\gamma + d \to 2p + \pi^-$ are recorded.[8] The squares of the amplitudes of the process $\gamma + n \to p + \pi^-$ were obtained by us[9] on the basis of the experimental data of Adamovich et al.[8]

In the paper by Beneventano et al.[10] it was noted that from these data and from the new data[6] on π^+ the near-threshold ratio $\sigma^-/\sigma^+ \lesssim 1$ is obtained. We do not agree with this statement, since on the basis of the data given in our paper[9] it is quite possible to draw the curve corresponding to $\sigma^-/\sigma^+ \sim 1.35$ where σ^+ is taken from the most recent publications.[6,11] Moreover, the small corrections* introduced recently by Adamovich, Kharlamov, and Larionova[11] show that the curve corresponding to the value of the square of the π^- photoproduction amplitude obtained by neglecting the contribution of the dispersion integrals agrees very well with the improved experimental data. The contribution of the "retarded term" to σ^- lies outside the limits of experimental accuracy.

In connection with the conclusions reached by Beneventano et al.[10] we have analyzed the only doubtful point in our theory of the $\gamma + d \to 2p + \pi^-$ reaction and have obtained a better founded method of dealing with the two-nucleon wave function in the region where the nuclear forces are effective, and we consider it appropriate to describe it here.

It is necessary to emphasize at the outset that the application of this method does not alter our quantitative results, but merely makes them more convincing.

In reference 9, in the evaluation of the cross section for the photoproduction on deuterium, it turned out to be necessary to make estimates of integrals of the form

$$\delta I_s = \int \psi^*_{fs} e^{iqr} \psi_d dr - \int \varphi_{fs} e^{iqr} \varphi_d dr.$$

Here ψ_{fs} and ψ_d are the true wave function for the relative motion of the two nucleons in the final s-state, and the true deuteron wave function. φ_{fs} and φ_d are model wave functions; these functions differ only within the region where the nuclear forces are effective. As was noted in reference 9, δI_s gives a significant correction only in the region of small relative momenta of the nucleons. On integrating over the solid angle and on taking into account the fact that $q \lesssim 1/r_0$, we may easily show that δI_s may be expressed in terms of the integral:

$$\int (u_s u_d - v_s v_d)\, dr. \qquad (8)$$

Here u_s is the true radial wave function, while v_s is the model radial wave function; u_s and v_s coincide outside the range of the forces and are normalized in accordance with the condition $v(0) = 1$. This also applies to u_d and v_d.

We note that the integral (8) coincides with $-\frac{1}{2}\bar{\rho}$, where $\bar{\rho}$ is the "mixed effective radius" defined by Feshbach and Schwinger.[12] On the basis of an investigation of the photomagnetic disintegration of the deuteron, they have obtained

$$\bar{\rho} = (2.18 \pm 0.3) \cdot 10^{-13} \text{ cm}.$$

If we make use of this value for estimating δI_s, then the difference between the value of $A(p, q)$ obtained by the present author[9] and of $A(p, q)$ obtained on the basis of such an estimate lies outside the limits of accuracy of the calculations over the whole range of variation of the arguments p, q.

In summarizing the analysis of data on the photoproduction of charged mesons near the threshold we can say that both σ^- and σ^+ are well described by the Born part of the amplitude alone, if we choose the renormalized coupling constant equal to $f^2 = 0.08$. Within experimental error this value of the coupling constant agrees well with the values estimated on the basis of other effects.

5. DISCUSSION

The method of analyzing experimental data on photoproduction utilized by us has turned out to be quite effective even in the present state of the experimental data. However, if we set as our aim the accumulation of experimental data to which our method is applicable, then as the result of a relatively small effort we can reach quite important conclusions on the properties of the π meson photoproduction amplitude.

*These corrections lie within the 10% accuracy limit previously ensured.

The effective use of the long wavelength approximation in the near-threshold energy region enables us to carry out a generalized phase analysis. Thus, in reference 4 we have obtained the amplitudes for the s-photoproduction in the case of both protons and neutrons, which turned out to be significantly different;* an estimate was given of the value of the amplitude for the magnetic dipole transition M_{1-}. However, the most important results are obtained by applying the dispersion relations in this region. The application of the dispersion relation here turns out to be, on the one hand, particularly simple (a number of difficulties enumerated earlier is avoided), and on the other hand, most productive of results from the point of view of checking the predictions of field theory. The latter is due to the fact that the sharpest predictions of field theory consist of the singularities in the energy and in the angular dependences associated with the existence of a known pole in the nonphysical region. These singularities are expressed by the presence of the Born part in (1). The threshold is that point in the physical region of variation of the variable photoproduction amplitudes, which lies very close to this pole. Therefore the pole exerts a decisive influence on the near-threshold region. Thus, for example, in the case of charged mesons the Born part of the amplitude describes the experimental data satisfactorily, while the contribution of the dispersion integral lies outside the limits of experimental accuracy.

Moreover, it is clear from the foregoing that in the near-threshold region one may measure the "retarded term" sufficiently reliably since its contribution turns out to be considerably greater than the contribution of the dispersion integrals.

The application of the method to the photoproduction of neutral mesons has led to essential difficulties. From the analysis just carried out it is clear that the Born part of the amplitude by no means determines the cross section for the process.

The evaluation of the dispersion integrals on the assumption that the principal contribution to them is made by the $(3/2, 3/2)$ resonance amplitude of the magnetic dipole transition leads to a large discrepancy with the experimental results. The inclusion of the second resonance in the photoproduction changes the situation very little. We do not have much basis for suspecting that the dispersion relations are not valid, since, as we have seen, in the case of charged mesons, for which the contribution of the dispersion integrals is small, good agreement with experiment is obtained even in such details as the "retarded term." From this it is clear that a solution must be sought in a more detailed evaluation of the dispersion integrals. First of all, an analysis should be made as to whether this contradiction might not be an indication of the presence of other partial amplitudes — of the magnetic dipole M_{1-} and the electric quadrupole transitions.

An exact answer to this question could be given by an experiment on the measurement of the polarization of the recoil protons in the reactions $\gamma + p \rightarrow p + \pi^0$ for γ-quanta energies lying in the range 240-270 Mev. Experimental data on the angular distribution enable us to obtain only upper limits on these amplitudes. A preliminary investigation shows that these upper limits give too low values of the amplitudes to eliminate the discrepancy. The discrepancy is considerably reduced if the contribution of the integral of M_{1-} is positive, while the quantity M_{1-} itself is negative in the near-threshold region, while the data of Pontecorvo's group (cf. reference 14) show clearly that the scattering phase α_{11} is positive over a wide range. If we assume that M_{1-} changes sign at an energy in the neighborhood of 200 Mev, then the contribution of the integral, which is already too small, is significantly reduced still further.

In summarizing we can say that the possibility of removing the difficulty should first of all be sought in the evaluation of the dispersion integrals. In our opinion it is of the greatest interest to obtain an answer to the question whether this discrepancy can be removed by considering the contribution to the dispersion integrals made by the small photoproduction amplitudes in the energy range in the neighborhood of the $(3/2, 3/2)$ resonance, or whether in order to remove the discrepancy it is necessary to invoke the contribution of the photoproduction amplitudes in the energy range above 1 Bev.

Additional investigations are required to give an answer to this question. First of all, more accurate measurements than those made in reference 5 are required of the angular distribution for the π^0-meson photoproduction in the near-threshold region. Such measurements would, firstly, give more accurate information on the magnitude of the above discrepancy, and secondly, an estimate could be made of the coefficients b_{mn} in (4) for higher values of m. It may be easily

*We note that this is an interesting example of an exception to the rule[13] on the relationship between the matrix elements of the isotopic scalar and isotopic vector parts of the S-matrix for processes involving photon absorption: $\langle S \rangle \sim (\mu/M)\langle V_3 \rangle$, where μ and M are respectively the meson and nucleon masses.

shown* that the high-energy region has a considerably smaller effect on these coefficients.

In order to determine the magnitude of the small amplitudes it is necessary to obtain more precisely the angular distributions in the $\gamma + p \rightarrow p + \pi^0$ reaction for energies in the 220 — 450 Mev range. Experiments on the measurement of the polarization of the recoil nucleons could yield much information.

In order to evaluate the role played by the dispersion integrals in the amplitudes for charged mesons it is necessary to increase significantly the accuracy of the experimental data in the near-threshold region.

*The coefficients b_{mn} for large values of m are related to the high order derivatives of the amplitude for which the integrands in the dispersion integrals fall off much faster than for the amplitude itself.

[1] Chew, Goldberger, Low, and Nambu, Phys. Rev. **106**, 1345 (1957).

[2] McDonald, Peterson, and Corson, Phys. Rev. **107**, 577 (1957).

[3] Logunov, Tavkhelidze, and Solovyev, Nuclear Phys. **4**, 427 (1957).

[4] A. M. Baldin and B. B. Govorkov, Nuclear Phys. **13**, 193 (1959).

[5] Vasil'kov, Govorkov, and Gol'danskiĭ, Nuclear Phys. **12**, 327 (1959).

[6] Barbaro, Goldwasser, and Carlson-Lee, Bull. Am. Phys. Soc. **4**, 23 (1958).

[7] J. E. Leiss and S. Penner, Bull. Am. Phys. Soc. **4**, 273 (1959).

[8] Adamovich, Kuz'micheva, Larionova, and Kharlamov, JETP **35**, 27 (1958), Soviet Phys. JETP **8**, 21 (1959).

[9] A. M. Baldin, Nuovo cimento **8**, 569 (1958).

[10] Beneventano, Bernardini, Stopini, and Tau, Nuovo cimento **10**, 1109 (1958).

[11] Adamovich, Gorzhevskaya, Larionova, Kharlamov, Popova, and Yagudina, Paper by G. Bernardini at the Kiev 1959 Conference on High Energy Physics.

[12] H. Feshbach and J. Schwinger, Phys. Rev. **84**, 194 (1951).

[13] A. M. Baldin, Nuovo cimento Suppl. **3**, 4 (1956).

[14] S. M. Korenchenko, Author's abstract, Thesis, Joint Institute for Nuclear Research, 1959.

Translated by G. Volkoff
112

SPECTRA OF GAMMA RAYS PRODUCED IN THE CAPTURE OF THERMAL NEUTRONS BY HEAVY NUCLEI. I

L. V. GROSHEV, A. M. DEMIDOV, and V. I. PELEKHOV

Submitted to JETP editor August 28, 1959

J. Exptl. Theoret. Phys. (U.S.S.R.) 38, 588-597 (February, 1960)

The experimental data on the γ spectra from the thermal neutron $(n\gamma)$ reaction are compared with the theoretical spectra calculated for two laws of variation of the level density. The effect of the energy gap in the level spectrum of even-even nuclei on the γ ray spectrum in the 0.8 — 4 Mev region is discussed. The presence of an energy gap leads to a large difference in the spectra of odd-odd and even-even nuclei.

In the last few years we have measured the spectra of gamma rays due to radiation capture of thermal neutrons for a large number of elements. The measurements were conducted with a magnetic Compton spectrometer having a resolution of 2%. The results obtained have been gathered in an atlas published in 1958,[1] and in several subsequent articles.

In the present paper we consider several laws for the gamma spectra of heavy elements (A = 100 — 200), located not too near the magic nuclei. At a resolution of 2%, the principal fraction of the gamma transitions in the spectra of such elements lies in the unresolved part, the form of which is essentially of interest to us. To analyze the general form of the spectrum, measurements with a magnetic Compton spectrometer are quite convenient, since this instrument makes it possible to measure, under identical conditions, almost the entire gamma-ray spectrum from the $(n\gamma)$ reaction, namely in the energy interval from 0.3 to 12 Mev.

The question of the form of the unresolved portion of the gamma spectrum for heavy elements was considered by us earlier in a paper delivered to the Second Geneva Conference on Peaceful Uses of Atomic Energy.[3] In this paper we compared the unresolved portions of the spectrum for heavy nuclei with different parities of the numbers of protons and neutrons and established, in particular, the manifestation of the nucleon pairing effect on the form of the gamma spectrum in its upper portion. The nucleon pairing effect manifests itself in the fact that the upper boundary of the unresolved portion of the spectrum in even-even nuclei lies approximately 1.5 Mev below the binding energy of the neutron in the particular nucleus, whereas in odd-odd nuclei these two quantities practically coincide. This fact illustrates quite clearly the presence of an energy gap near the ground state of even-even nuclei. In this article we consider again the problem of the general form of the spectrum and its dependence on the energy level distribution in heavy nuclei. This is made necessary, on the one hand, by the completion of calculations on the shape of the spectrum, made with the aid of a computer,[4] and on the other hand by the appearance of additional conclusions with respect to the shape of the spectrum of different nuclei at low energies.

To exhibit the singularities of interest to us in the low energy region, it is more convenient to plot the spectrum with the ordinates representing the values of $\nu(E)$ — the number of photons per neutron capture and per unit energy interval in Mev (E — energy of gamma quantum), instead of $\nu(E)H\rho$, as was done in preceding investigations.[3] The absolute values of $\nu(E)$ were usually obtained by normalizing the energy radiated by the nucleus to the neutron binding energy.

Figure 1 shows by way of an example the gamma spectra of the even-even nucleus Gd^{158} and of the odd-odd nucleus Ho^{166}. As can be seen from the diagram, in the case of Gd^{158} separate peaks are separated in the upper and lower regions against the background of the unresolved portion. These peaks correspond to monochromatic lines. An analogous picture is characteristic also of other even-even nuclei. For odd-odd nuclei such peaks are observed only in the upper portion of the spectrum.

In this article we confine ourselves to an examination of gamma spectra only for even-even and odd-odd nuclei with $100 < A < 200$. All the spectra, with the exception of that of gadolinium, are obtained with natural mixtures of isotopes. In the

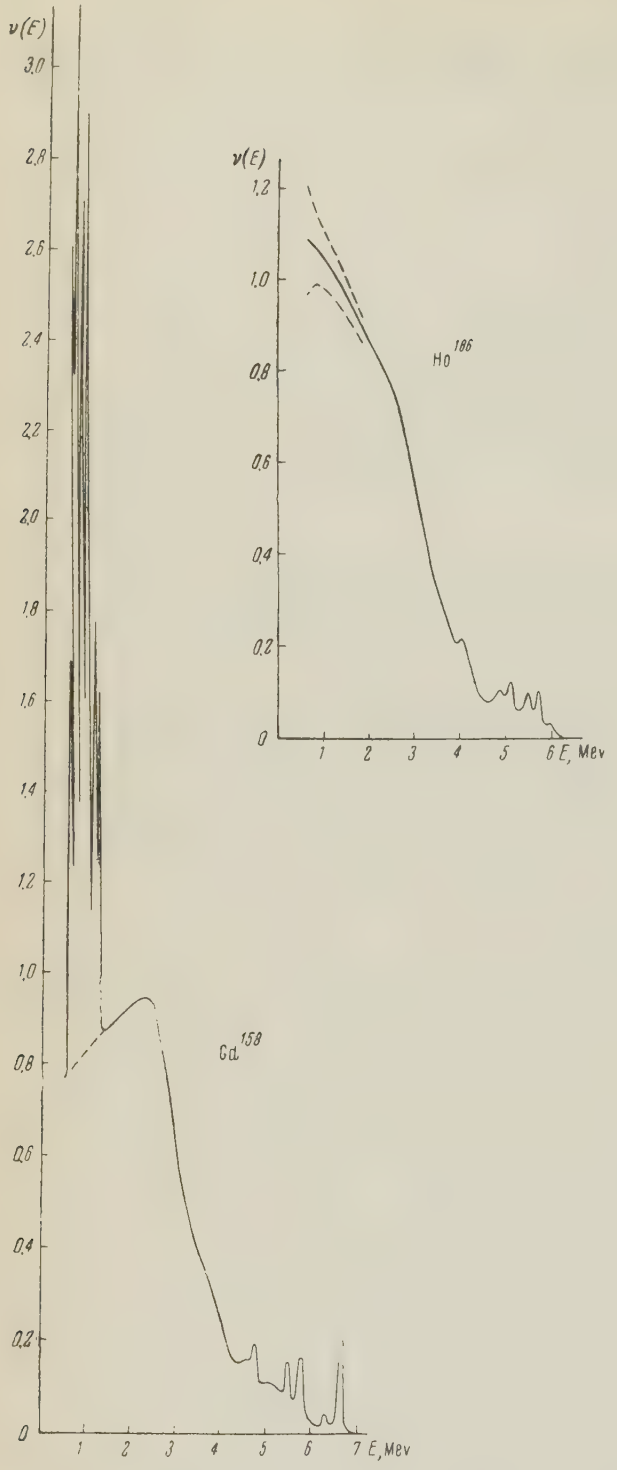

FIG. 1. Gamma ray spectra Gd^{158} and Ho^{166}.

notation given, we shall indicate the isotope (or isotopes) which makes the principal contribution to the investigated spectrum. The atomic weight of the isotope is referred in all cases to the radiating nuclei, produced after neutron capture.

In the case of odd-odd nuclei we have spectra for Rh^{104}, Ag^{108}, Ag^{110}, In^{116}, Sb^{122}, Sb^{124}, La^{140}, Eu^{152}, Ho^{166}, Tm^{170}, Ta^{182}, Re^{186}, Re^{188}, Ir^{192}, Ir^{194}, and Au^{198}. Figure 2a shows spectra for Rh, Ag, In, and Sb, while Fig. 2b shows the spectra for Ho, Tm, Ta, and Ra. The nuclei of the first group have an atomic weight $A \sim 110$ and are spherical. Those of the second group have $A \sim 175$ and are all prolate.

In the case of even-even nuclei we have the spectra of Mo^{96}, Cd^{114}, Sn^{116}, Sn^{118}, Sn^{120}, Nd^{144}, Sm^{150}, Gd^{156}, Gd^{158}, Er^{168}, Hf^{178}, Pt^{196}, and Hg^{200}. Figure 2c shows the spectra for the four prolate nuclei Gd^{156}, Gd^{158}, Er^{168}, and Hf^{178}. These spectra have been obtained from those experimentally measured by cutting off the peaks with energies less than 2 Mev. For Gd^{158} (see Fig. 12) such a cut-off is shown dotted. We discarded the lines in the low-energy regions for convenience in comparison of the spectra of different nuclei.

In the curve for Ho^{166} in Fig. 1, and also later in Figs. 7 and 8b, the dotted lines indicate the experimental errors in the measurement of the spectrum. Since the errors increase with decreasing photon energy, all the experimental spectra were plotted for energies ≥ 0.8 Mev.

It is seen from Fig. 2 that, within the limits of each of three groups, the spectra can be represented by an average curve. The average spectra obtained in this manner are shown separately in Fig. 3. It is seen from this diagram that the spectra for the two groups of odd-odd nuclei (curves I and II) do not differ greatly from each other. One should therefore take an average spectrum for all eight odd-odd isotopes, as we have done in the beginning. However, a more detailed analysis shows the presence of one singularity, which repeats in all spectra with $A \sim 175$, and which is missing in nuclei with $A \sim 110$. We have in mind here the presence of a small convexity in curve II in the energy region 2 — 3 Mev. Such a difference in the spectra appears also in the theoretical calculations (for more details see reference 4).

Another logical reason for breaking up the spectra of the odd-odd nuclei into two groups is that the binding energy of the neutron, B_n, for nuclei with $A \sim 110$, is on the average somewhat higher than that for nuclei with $A \sim 175$, as can be seen from the table.

Nucleus	B_n	Nucleus	B_n
Rh^{104}	6.8	Ho^{166}	6.2
Ag^{108} (30%)	7.27	Tm^{170}	6.6
Ag^{110} (70%)	6.6	Ta^{182}	6.06
In^{116}	6.6	Re^{186} (48%)	6.2
Sb^{122} (66%)	6.8	Re^{188} (52%)	5.94
Sb^{124} (34%)	6.3		
Average	6.7	Average	6.2

The parentheses contain the contribution of the given isotope to the absorption cross section for thermal neutrons.

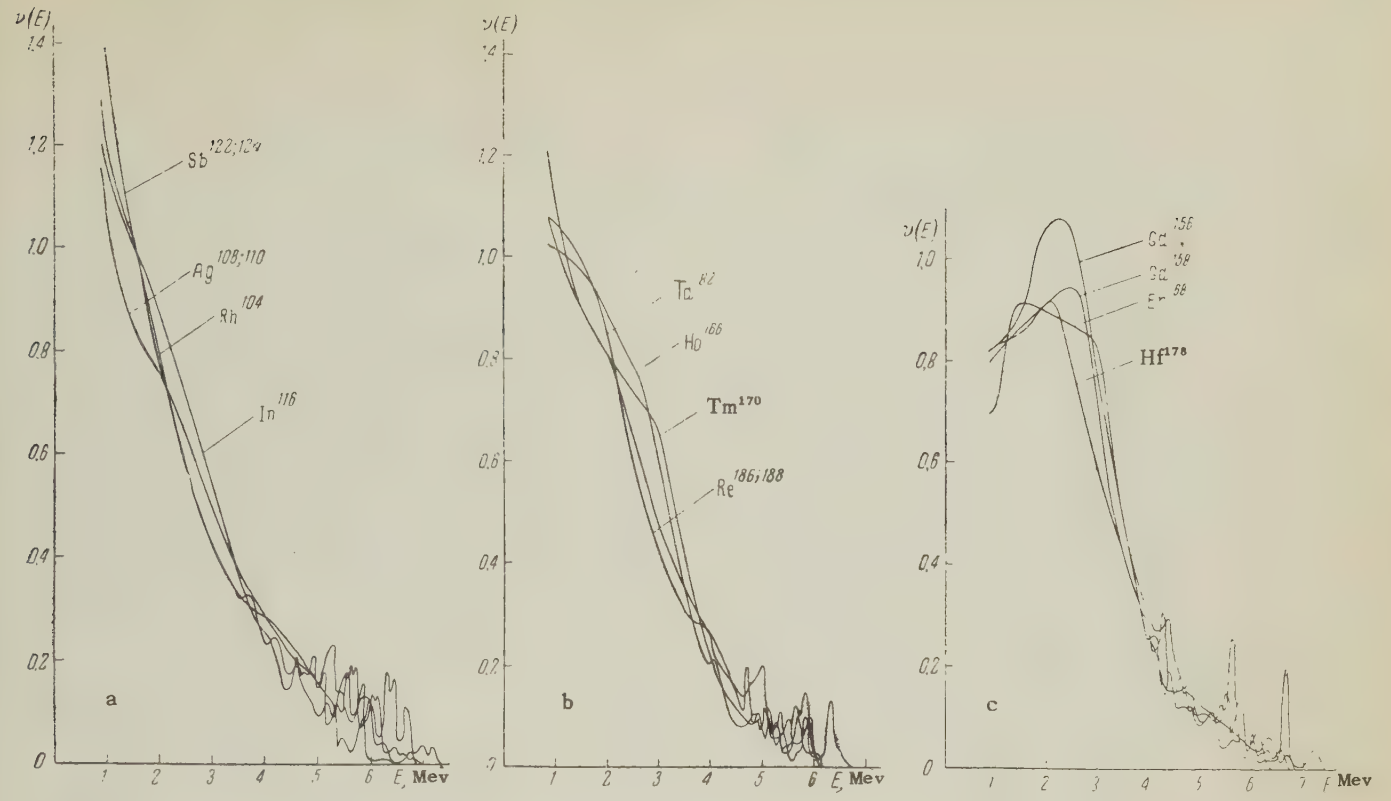

FIG. 2. Experimental gamma-ray spectra: a – odd-odd nuclei with A ~ 110, b – with A ~ 175, c – even-even nonspherical nuclei.

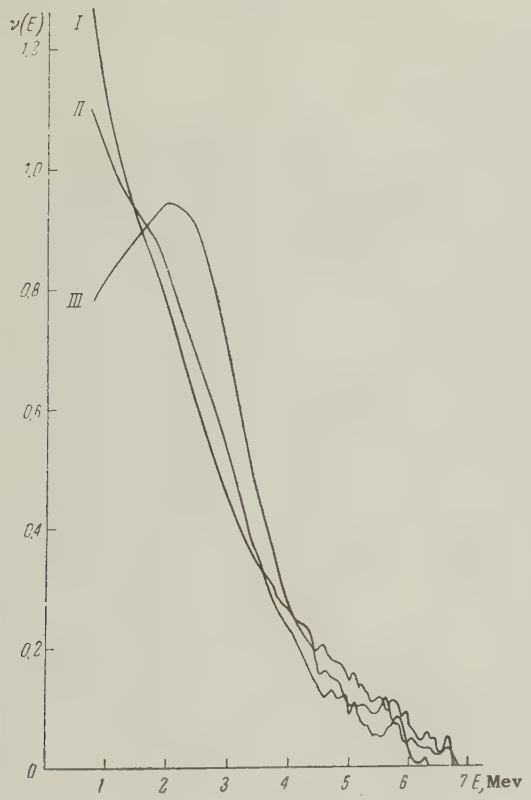

FIG. 3. Average experimental curves: I – for odd-odd nuclei with A ~ 110, II – odd-odd nuclei with A ~ 175, III – even-even non-spherical nuclei.

For the even-even isotopes indicated in Fig. 2c, the binding energy of the neutron is 8.46, 7.87, 7.76, and 7.55 Mev respectively. From the figures given it is seen that as a rule, within the limits of each group of nuclei, the neutron binding energies do not differ greatly. For this reason we have not reduced the spectra to one and the same value of the binding energy.

The average experimental spectra shown in Fig. 3 can be compared with the theoretical calculated spectra (see reference 4). These calculations have been made for a neutron binding energy of 6.4 Mev in odd-odd nuclei and 7.6 Mev in even-even nuclei. The calculations were made for two types of variations of the level density with excitation energy.

$$\rho(u) = \rho_0 \exp \sqrt{au}, \qquad (1)$$

$$\rho(u) = \rho_0 \exp (u/\tau) \qquad (2)$$

At constant a and τ, and in the case of even-even nuclei, it was assumed that these variations hold starting with a certain energy Δ, the width of the energy gap at the ground state.

For even-even nuclei the principal calculations were made for $\Delta = 1.2$ Mev, which is equal to the difference between the neutron binding energy assumed for even-even and odd-odd nuclei. For this reason, the effective excitation energy for even-

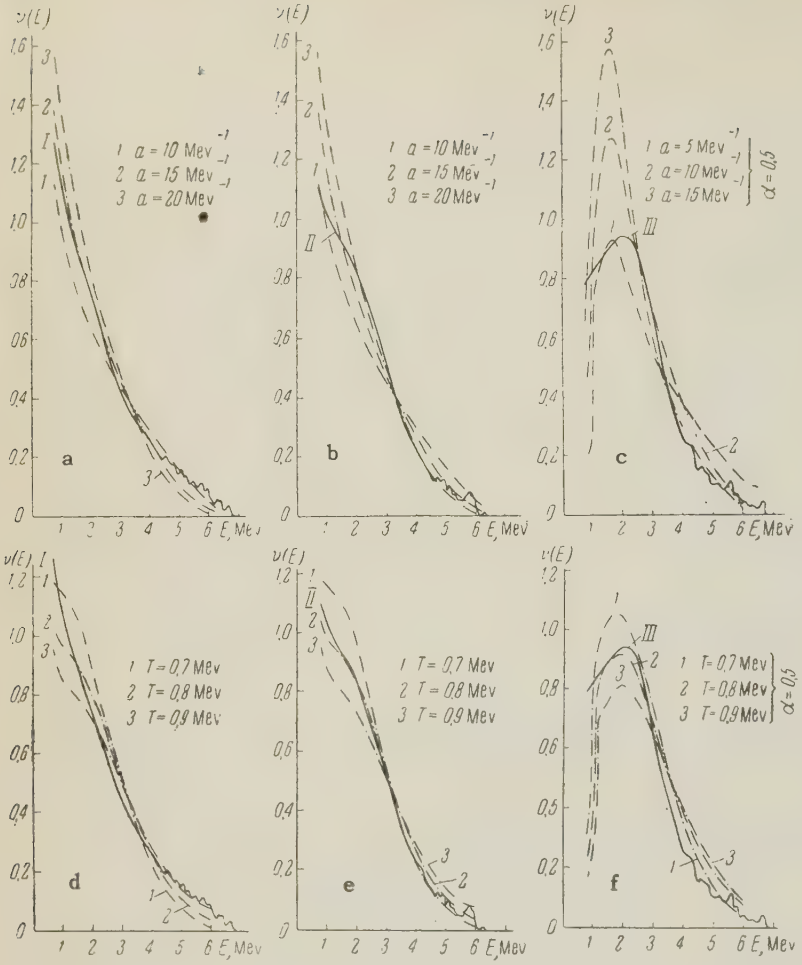

FIG. 4. Comparison of the average experimental spectra for odd-odd nuclei with A ~ 110 (a and d), odd-odd nuclei with A ~ 175 (b and e), and even-even non-spherical nuclei (c and f) with the spectra calculated theoretically for two variations of the level densities: a, b, c – following Eq. (1), and d, e, f – following Eq. (2) (τ has been designated T on the diagram). The theoretical spectra are shown by dash-dot lines.

even nuclei (the energy is measured from the upper ridge of the gap) is 6.4 Mev, and consequently the calculations are carried out in the same energy interval for both categories of nuclei.

For assumed variation (1), the theoretical calculations have been made for values of a in the interval from 5 to 60 Mev^{-1}, and for assumed variation (2) — for values of τ varying in steps of 0.1 Mev from 0.4 to 1 Mev and for $\tau = 1.2$ Mev. In the case of even-even nuclei, the parameter $\alpha = \rho_0^{-1}\overline{M}_B^2/\overline{M}_A^2$ was also varied, where M_B and M_A are the matrix elements of parallel transitions from the given excited state, going respectively through the gap into the ground state or into states located above a gap (for more details see reference 4).

A comparison of the average experimental spectra with the theoretically calculated curves makes it possible to choose the values of the parameter a, if variation (1) is used, or of the parameter τ, if (2) is used. Such a comparison is shown in Fig. 4. It contains, along with the average experimental spectra for nuclei of different categories, three theoretical curves each, calculated for variation (1) (the upper part of Fig. 4) and for variation (2) (lower part of Fig. 4). The theoretical curves have been plotted in all cases for three different values of τ or a, chosen such that at intermediate values of τ and a these curves approach the closest to the experimental spectra (an exception is Fig. 4c).

It is seen from Fig. 4c that in the case of odd-odd nuclei, for either variation of the density, the curves calculated with suitably chosen parameters are sufficiently close to the experimental spectra. However, a more detailed comparison of the curves of Fig. 4 shows (see Figs. 4a and 4d) that in the case of spherical nuclei with A ~ 100, using variation (1) and a = 15 Mev^{-1}, the agreement between the experimental and theoretical spectra is somewhat better than for the other type of variation in ρ. This agreement can be improved even further by changing the value of a somewhat.

The situation is reversed for the prolate nuclei with A ~ 175.

Here the experimental spectrum is in best agreement with the theoretical curve, calculated for variation (2) at $\tau = 0.8$ Mev. The presence of a small difference in the spectra of odd-odd nuclei with A ~ 110 and A ~ 175 may be due (see reference

4) to the difference in the variation of the level densities in spherical and prolate nuclei. It must be recalled again that the difference in the spectra for these two categories of odd-odd nuclei is not particularly essential and appears only in the details of the curves.

In the case of even-even nuclei, the agreement between the experimental and theoretical spectra is not as good (see Figs. 4c and 4f) as for the odd-odd nuclei. However, if (2) is used, the smallest discrepancy between the various curves is obtained for the same value $\tau = 0.8$ Mev, as for the prolate odd-odd nuclei with $A \sim 175$. When using variation (1) and $\alpha = 0.5$, the theoretical curves are in much poorer agreement with the experimental spectra. At a value of $a = 15$ Mev^{-1}, obtained from a comparison of the spectra for odd-odd nuclei, the theoretical curve differs greatly from the experimental spectrum. For smaller values of a, the discrepancy is somewhat reduced, but nevertheless remains considerably greater than in the case of curve 2 of Fig. 4f.

We note still another important fact, that in the foregoing comparison of the experimental and theoretical spectra, we compare not only the overall course of the curves, but also the absolute values of $\nu(E)$.

Let us proceed now to a comparison of the average experimental spectra of odd-odd and even-even nuclei, shown in Fig. 3. It is seen from this figure that there is a substantial difference in the lower portions of these spectra. Due to the fact that in going from odd-odd nuclei to even-even ones, the number of photons of low energy, with $E < 1.5$ Mev, decreases considerably in the unresolved portion of the spectrum, while the number of photons with energies 2 — 4 Mev increases.

This change in the spectrum of the even-even nucleus is readily explained by the presence of an energy gap in the level spectrum of the nucleus, due to evaporation of nucleons. Qualitatively this reduces to the following. When the excited states of an even-even nucleus are de-excited, the presence of the gap results not only in γ transitions, which gradually bring the nucleus to the upper boundary of the gap (type A transitions), but also in parallel transitions (type B), which carry the nucleus through the gap into the ground state or states close to it, corresponding to collective excitations. In the case of an odd-odd nucleus only type A transitions take place. The photons emitted in type B transitions have considerably greater energy than those of type A transitions and result from the exclusion of the latter. Such an outflow of type B photons will play a considerably smaller and smaller role as the nuclear excitation energy increases. On the other hand, as the excitation energy is decreased to 1.5 — 2.0 Mev, although the de-excitation into the ground state is energetically more convenient, such transitions may nevertheless be forbidden. In the case of spherical nuclei, the usual spin forbiddenness will be effective here, and in the case of prolate nuclei K-forbiddenness enters into the picture. These forbiddennesses lead to an increase in the population of levels located in the region ~ 1 Mev, a fact that manifests itself most strongly in non-spherical nuclei. In the spectra of such nuclei, as shown earlier,[5] a group of intense lines of similar energy arises (see, for example, Fig. 1). It follows from the experimental data that the de-excitation of the non-spherical even-even nuclei goes in approximately 50% of the cases through levels which are located directly above the gap and in approximately the same number of cases via type B transitions, which go into the more highly excited levels.

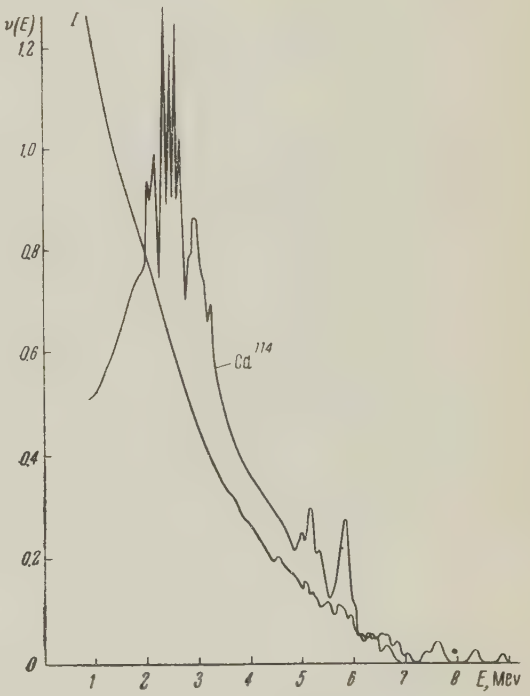

FIG. 5. Comparison of the spectrum of Cd^{114} with the average experimental spectrum for odd-odd nuclei with $A \sim 110$ (curve 1).

Let us consider the γ spectra of other nuclei. Figure 5 shows along with the average spectrum for spherical odd-odd nuclei also the experimental spectrum for Cd^{114} (as in all other even-even nuclei, lines of energy less than 2 Mev have been cut off here). In this case there is approximately the same qualitative difference in the spectra of even-even and odd-odd nuclei, as above. The spectrum of Cd^{114} was not included in the averaging over the

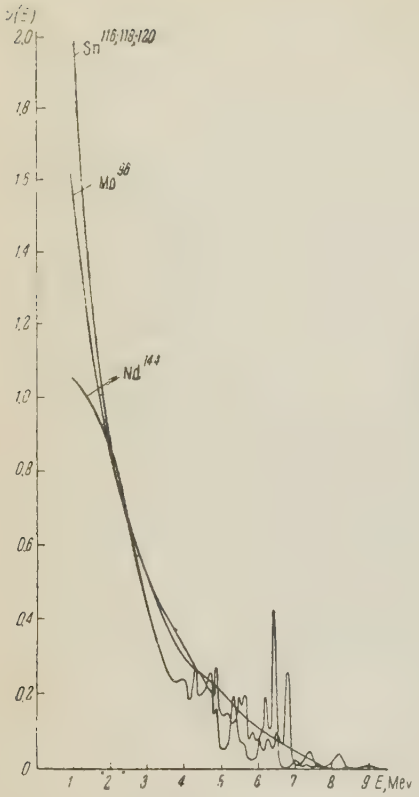

FIG. 6. Gamma-ray spectra of Mo^{96}, Sn^{116}, Sn^{118}, Sn^{120}, and Nd^{144}.

even-even nuclei, since this isotope has a considerably greater neutron binding energy, 9 Mev.

Figure 6 shows the spectra of the following even-even nuclei: Mo^{96}, Sn^{116}, Sn^{118}, Sn^{120}, and Nd^{144}. The unresolved portion of these spectra have a form close enough to that of odd-odd nuclei. This result can be understood by examining in greater detail the type B transitions, i.e., the transitions that cause an outflow into the ground state. The point is that this outflow may go not only to the ground state, but also to the lower excited states. Whereas in the non-spherical even-even nuclei the excited levels, to which the effective outflow is possible, are located at low excitations (100 — 300 kev), in spherical nuclei, particularly in Mo^{96}, Sn^{118}, and Nd^{144}, even the first excited level is located at 0.78, 1.2, and 0.7 Mev respectively. With this, the first level gathers in up to 90% of all the cascades. Inasmuch as the evaporation energy of the nucleons in these nuclei is 1.5 — 2 Mev, a noticeable outflow not into the ground state, but to lower excited levels decreases noticeably the effective width of the energy gap in these nuclei. Thus, in these nuclei the energy of type B transitions differs from that of type A transitions not by 1.5 — 2 Mev, but by a smaller quantity, equal to the effective width of the energy gap, which indeed leads to a considerable smoothing of the difference in the γ spectra of the indicated even-even and odd-odd nuclei.

For the Cd^{114} nucleus we also have a greater population of the first level, which has an energy 0.56 Mev. However, apparently, the effective energy gap in this case is still large, enough to influence substantially the form of the spectrum of Cd^{114}.

Let us dwell now on the two neighboring nuclei, Eu^{152} and Sm^{150}. The spectra of these nuclei differ noticeably from the average spectra given above. For Sm^{150} this difference lies in the greater height of the maximum, and for Eu^{152} by the fact that in the region of lower energies its spectrum lies higher than the spectra of other odd-odd nuclei. It is interesting to note, however, that in comparing the spectra of Sm^{150} and Eu^{152} (see Fig. 7) we observe qualitatively the same picture, which was established above in comparing the spectra of even-even and odd-odd nuclei (see Fig. 3).

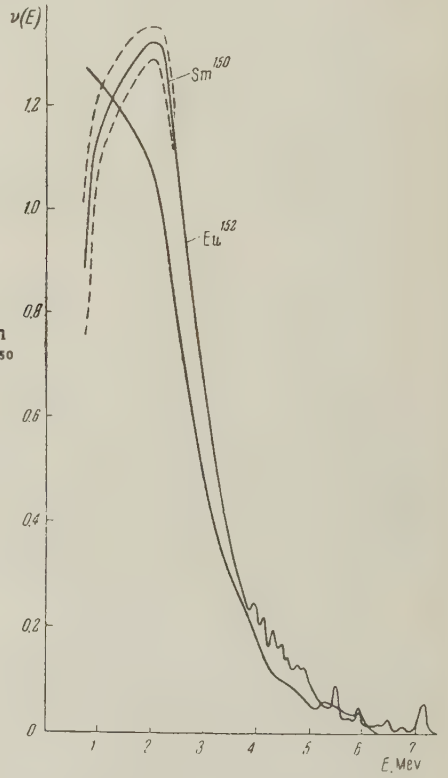

FIG. 7. Comparison of γ-ray spectra of Sm^{150} and Eu^{152}.

As already noted earlier[3,6] for elements located near the twice-magic nucleus Pb^{208}, the γ-ray spectra differ considerably in shape from the foregoing spectra of heavy elements which are far from magic. Figure 8a shows as an example the spectrum of Au^{198}. The same figure shows the theoretical spectrum, calculated under the assumption that the level densities are given by Eq. (1) at $a = 5$ Mev^{-1}. Both curves are quite close to each other. We have already noted, however,[3] that such a great reduction in the value of a for Au^{188} is not verified by other experiments, and another reason was indicated in

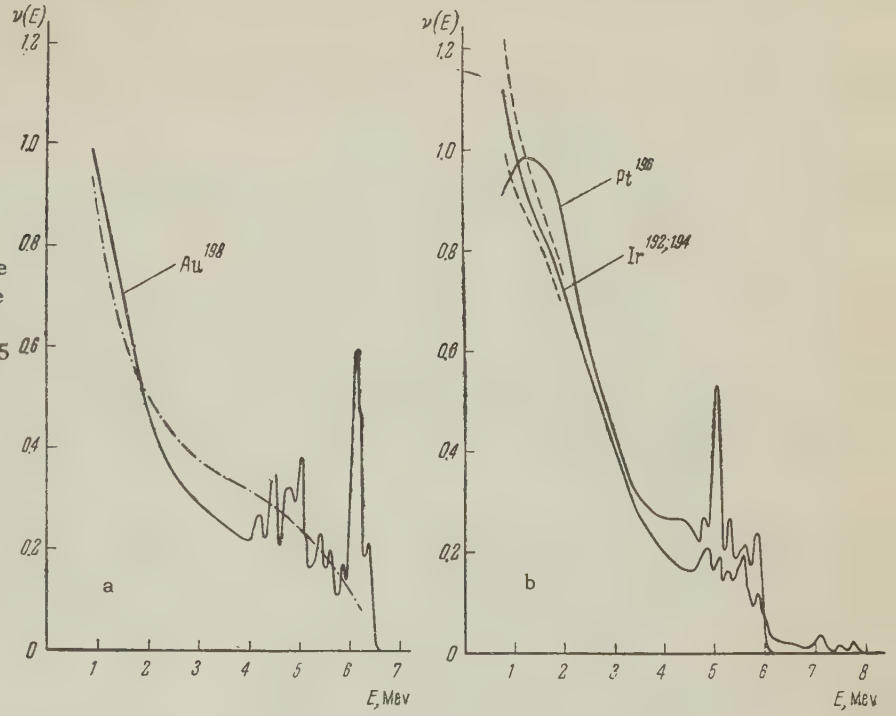

FIG. 8. Gamma-ray spectra of nuclei close to $Z = 82$ and $N = 126$: a – comparison of the experimental spectrum of Au^{188} with the theoretical one, calculated for Eq. (1) and at $a = 5$ Mev^{-1} (dash-dot curve), b – comparison of the spectra of Ir^{192}, Ir^{194}, and Pt^{196}.

that reference for such a substantial change in the form of the Au^{188} spectrum as compared with the spectra of nuclei that are not close to magic.

We note that in this region one sees quite clearly the manifestation of an energy gap in the γ spectra. Figure 8b shows the experimental spectra for the neighboring nuclei, the odd-odd Ir^{192} and Ir^{194} and for the even-even Pt^{196}. It is seen from the figure that if we disregard the change in the form in the upper portion of the spectrum, due to the approach to $Z = 82$ and $N = 126$ (see reference 3), we observe qualitatively the same difference in the spectra of the even-even and odd-odd nuclei, which is illustrated in Fig. 3.

[1] Groshev, Demidov, Lutsenko, and Pelekhov, Атлас спектров γ-лучей радиационного захвата тепловых нейтронов (Atlas of Spectra of Gamma Rays of Radiative Capture of Thermal Neutrons), Atomizdat, 1958.

[2] Groshev, Gavrilov, and Demidov, Атомная энергия (Atomic Energy) **6**, 281 (1959). Groshev, Demidov, and Pelekhov, ibid., in press.

[3] Groshev, Demidov, Lutsenko, and Pelekhov, Доклады советских ученых на Второй международной конференции по мирному использованию атомной энергии, Ядерная физика (Papers of the Soviet Scientists at the Second Geneva Conference, Nuclear Phys.) Vol. 1, Atomizdat, 1958.

[4] Strutinskiĭ, Groshev, and Akimova, JETP **38**, 598 (1960), this issue p. 430.

[5] Groshev, Demidov, Lutsenko, and Pelekhov, Атомная энергия (Atomic Energy) **4**, 5 (1958).

[6] Bartholomew, Campion, Knowles, and Manning, Proc. of the Intern. Conf. on the Neutron Interactions with the Nucleus, N.Y., 1957.

Translated by J. G. Adashko
113

SPECTRA OF GAMMA RAYS PRODUCED IN THE CAPTURE OF THERMAL NEUTRONS BY HEAVY NUCLEI. II

V. M. STRUTINSKIĬ, L. V. GROSHEV, and M. K. AKIMOVA

Submitted to JETP editor August 28, 1959

J. Exptl. Theoret. Phys. (U.S.S.R.) **38**, 598-611 (February, 1960)

The spectra of γ rays accompanying the capture of thermal neutrons are calculated. The calculations are performed for dipole γ radiation and two types of dependence of the nuclear level density on energy. The results for the level density are compared with data derived from other experiments.

THE capture of a thermal neutron by an atomic nucleus leads to the formation of a relatively strongly excited nucleus with excitation energy 6 — 8 Mev. In the case of heavy nuclei with atomic weight A > 100, owing to the great density of the levels, the transition from the excited state that results from the capture of a thermal neutron may proceed via a large number of different paths. Accordingly, the overwhelming portion of the γ transitions in such elements occurs in a portion of the spectrum that is still unresolved by modern measurement procedures. In the case of light nuclei, and in the case of heavy close-to-magic nuclei, the γ-ray spectrum is almost a line spectrum owing to the small level density.[1] In this paper we consider only continuous spectra. Experimental data have shown that the spectra of γ quanta in heavy nuclei change relatively little from nucleus to nucleus. One can therefore assume that the spectrum of the emitted quanta is determined essentially by the general laws of the distribution of the density of the nuclear levels and by the multipolarity of the radiation transition, and depends little on the specific properties of the matrix elements of the transitions.

In accordance with the statistical theory, we assume that the relative probability of emission of a γ quantum with energy E by a nucleus, located in a certain state with energy u, is given by the following formula:[2]

$$w(u, E) = E^{\varkappa}\rho(u - E)/n(u), \tag{1}$$

where $\rho(u - E)$ is the density of the final states of the nucleus. It is assumed that the distribution of the γ quanta is determined only by the energies of the initial and final states of the nucleus. One can see certain justification for this in the fact that the probability $w(u, E)$ has the meaning of a relative transition probability, averaged over a sufficiently large number of initial and final nuclear states. The distribution (1) is normalized to a total decay probability of unity, from which we determine the normalizing factor $n(u)$

$$n(u) = \int_0^u E^{\varkappa}\rho(u - E)\,dE. \tag{2}$$

The average transition matrix element, which we consider to be a constant, is not contained in Eq. (1). The constant κ has a value $2l+1$, where 2^l is the multipolarity of the radiation.

To calculate the total γ-ray spectrum of the nucleus it is necessary to sum the spectra of all the stages of the cascade. This problem is solved most simply when the energy in the emitted quanta can be considered small compared with the excitation energy of the nucleus. The spectrum was calculated in this approximation by Nosov and one of the authors of the present paper (V.S.).[1] This case is characterized by the emission of a large number of quanta during de-excitation of the nucleus. Considering the number of quanta to be a continuous quantity, it is possible to obtain the following expression for the γ-ray spectrum:

$$\nu(E)\,dE = dE\int_E^{u_0} w(u, E)\frac{du}{\bar{E}(u)}, \tag{3}$$

where $\nu(E)\,dE$ is the number of quanta whose energy is in the interval E, E+dE, emitted by the nucleus, u_0 is the initial excitation energy, and $\bar{E}(u)$ is the average energy of the γ quanta of energy u emitted by the nucleus:

$$\bar{E}(u) = \int_0^u Ew(u, E)\,dE. \tag{4}$$

The total number of quanta $\bar{\nu}$ is in this approximation

$$\bar{\nu} \equiv \int_0^{u_0}\nu(E)\,dE = \int_0^{u_0} du/\bar{E}(u). \tag{5}$$

Putting in (1) $\rho = \rho_0 \exp\{S(u)\}$, where $S(u)$ is the entropy of the nucleus, we obtain

$$\bar{E}(u) \approx (\varkappa + 1) T(u), \tag{6}$$

$$\bar{\nu}(u_0) = \int_0^{u_0} \frac{du}{(\varkappa+1) T(u)} = \frac{S(u_0)}{\varkappa+1}. \tag{7}$$

The mean squared fluctuation of the number of quanta is

$$\sqrt{\bar{\nu}^2 - \bar{\nu}^2} = \sqrt{S(u_0)}/(\varkappa+1). \tag{8}$$

In formulas (6) and (7), $T(u)$ is the nuclear temperature, $T(u) = du/dS$.

A comparison has been made previously[1] of the experimental data on the spectra of the γ rays that accompany the capture of thermal neutrons; the calculations there were based on formulas (3) — (7). These formulas yield a fairly good qualitative approximation, but their accuracy when applied to capture of thermal neutrons is insufficient, owing to the small number of emitted quanta ($\sim 3-4$ quanta per capture). The average quantum energy is $\sim 1.5-2$ Mev, i.e., it is far from small compared with the nuclear excitation energy.

A more accurate calculation of the γ-ray spectrum can be made by foregoing one of the premises that underly the derivation of Eqs. (3) — (7), namely that the change in nuclear energy upon emission of the γ quanta is small, and the resultant replacement of the summation of individual decay chains by integration over stages, each of which is characterized by a certain average nuclear excitation energy. Such a calculation can be made on the basis of the kinetic equation that describes a multistage process of γ emission from the nucleus.[3] In our case, when the emission of quanta is the only process, this equation has the following form

$$\partial y_k(u, t)/\partial t = \int_u^{u_0} y_{k-1}(u', t)\,\Gamma(u')\,w(u', u'-u)\,du' - \Gamma(u)\,y_k(u, t), \tag{9}$$

where $y_k(u, t)$ is the probability of finding k quanta and the nucleus in the state with energy u at the instant t in the nucleus-plus-photons system. In Eq. (9) $\Gamma(u)$ is the decay probability per unit time of a nucleus with energy u, multiplied by $\hbar$.

During the initial instant of time, $t = 0$, we have

$$y_k(u_0, 0) = \delta_{k0}\delta(u - u_0) \tag{10}$$

(δ_{ab} is the Kronecker symbol and δ stands for the δ function), since at $t = 0$ there were no quanta in the system, and the nucleus was in the initial state.

One can obtain, on the basis of (9), a simple equation for a certain quantity directly related with the γ-spectrum of interest to us. To derive this equation we introduce the function $N(u, t)$, the probability of having at the instant t a nucleus with energy u with any number of quanta:

$$N(u, t) = \sum_{k=0}^{\infty} y_k(u, t). \tag{11}$$

The function $y_0(u, t)$ satisfies the following differential equation [see (9)]:

$$\partial y_0(u, t)/\partial t = -\Gamma(u)\,y_0(u, t). \tag{12}$$

Taking this into account, we obtain, summing both halves of (9) over k, the following equation for the function $N(u, t)$

$$\partial N(u, t)/\partial t = \int_u^{u_0} \Gamma(u')\,w(u', u'-u)\,N(u', t)\,du' - \Gamma(u)\,N(u, t). \tag{13}$$

Analogously we obtain from (10) the initial condition

$$N(u, 0) = \delta(u - u_0). \tag{14}$$

We now denote by $\nu(E, t)$ the number of quanta with energy E in the system at the instant t. The function $\nu(E, t)$ satisfies the following equation

$$\partial\nu(E, t)/\partial t = \int_E^{u_0} N(u', t)\,\Gamma(u')\,w(u', E)\,du', \tag{15}$$

a solution of which, satisfying boundary condition $\nu(E, 0) = 0$, is the function

$$\nu(E, t) = \int_E^{u_0} w(u', E)\,du' \int_0^t \Gamma(u')\,N(u', t')\,dt'. \tag{16}$$

The function $\nu(E, t)$ at $t = \infty$ yields the number of quanta of energy E, emitted by the nucleus during the decay process:

$$\nu(E) \equiv \nu(E, \infty) = \int_E^{u_0} w(u', E)\,du' \int_0^{\infty} \Gamma(u')\,N(u', t)\,dt. \tag{17}$$

Let us now find the equation satisfied by the function

$$Z(u) = \int_0^{\infty} \Gamma(u)\,N(u, t)\,dt.$$

For this we integrate both parts of (13) with respect to time:

$$N(u, \infty) - N(u, 0) = \int_u^{u_0} Z(u')\,w(u', u'-u)\,du' - Z(u). \tag{18}$$

This is precisely the sought integral equation for the function $Z(u)$. Actually, using the formula (14)

and noting that $N(u, \infty) = 0$ for all $u > 0$, we find

$$Z(u) = \int_u^{u_0} w(u', u' - u) Z(u') du' + \delta(u - u_0). \quad (19)$$

The function $\nu(E)$ can be written

$$\nu(E) = \int_E^{u_0} w(u', E) Z(u') du'. \quad (20)$$

The function $Z(u)$ gives the probability of the nucleus passing through the state with energy u during the process of emission of the γ quanta. Expressions (3) and (20) for the γ spectrum coincide to the same extent that the function $Z(u)$ is equal to $1/\bar{E}(u)$.

It will be more convenient to transform (19) and (20), introducing a new function $\zeta(u) = Z[u - \delta(u) - u_0]$. Then (19) and (20) become

$$\zeta(u) = \int_u^{u_0} w(u', u' - u) \zeta(u') du' + w(u_0, u_0 - u), \quad (21)$$

$$\nu(E) = w(u_0, E) + \int_E^{u_0} w(u', E) \zeta(u') du'. \quad (22)$$

The first term in (22) corresponds to the γ quanta emitted from the initial states of the nuclei, while the second represents the spectrum of the succeeding quanta.

By using the method of successive approximation we obtain from integral equation (21) the well known expression for the γ-ray spectrum

$$\nu(E) = w(u_0, E) + \int_0^{u_0 - E} w(u_0, E') w(u_0 - E', E) dE' + \ldots, \quad (23)$$

where each term of the series represents respectively the probability of emission of a quantum with energy E by the first, second, etc term in the chain. The effective number of terms in this series depends on E. When $E \gtrsim 1 - 2$ Mev it is found to be too large and expression (23) cannot be used in practice to calculate the spectrum, owing to the need for evaluating integrals of high multiplicity.

In that important case, when the function $w(u, E)$ is given by expression (1), the integral equation (21) can be transformed into a differential one. For this purpose, after first inserting into (21) the expression (1), for the function $w(u, E)$, we divide both halves of the equation by $\rho(u)$ and differentiate $\kappa + 1$ times with respect to u. As a result we obtain a differential equation of order $\kappa + 1$ for the function $\zeta(u)$:

$$d^{\varkappa+1} f(u) / du^{\varkappa+1} = (-1)^{\varkappa+1} \varkappa! f(u) \rho(u) / n(u), \quad (24)$$

where $f(u) = \zeta(u)/\rho(u)$ and the boundary condition at the point $u = u_0$ is:

$$(d^\lambda f(u) / du^\lambda)_{u=u_0} = \begin{cases} 0 & \text{for } \lambda = 0, \ldots, \varkappa - 1, \\ (-1)^\varkappa \varkappa! / n(u_0) & \text{for } \lambda = \varkappa. \end{cases} \quad (25)$$

In certain simple cases (24) makes a direct determination of $\zeta(u)$ possible. For a qualitative determination of the properties of the function ζ we note that the function $n(u)$ has a value $\kappa! T^{\kappa+1} \rho(u)$ for large values of u, when $u \gg \kappa T$, and has a value $u^{\kappa+1}/(\kappa+1)$ as $u \to 0$ (we assume here that the level density is a continuous function, starting with $u = 0$). Taking this into account, we can find with the aid of (24) that $\zeta(u)$ behaves like

$$w(u_0, u_0 - u) \approx (u_0 - u)^\varkappa \rho(u) / \varkappa! T(u_0)$$

at values of u close to u_0, which satisfy the inequality

$$u_0 - \bar{E}(u_0) \approx u_0 - (\varkappa + 1) T(u_0) \leqslant u \leqslant u_0,$$

like c/u (where c is a constant) as $u \to 0$, and like $1/\bar{E} \approx 1/\{(\kappa+1) T(u)\}$ in the intermediate region, where $u \gg T(u)$. These properties of $\zeta(u)$ are obvious from the point of view of the aforementioned physical meaning of the function $Z(u)$ [see Eqs. (3) and (6)]. In practice the region of energies in which $\zeta(u)$ can be represented as $[(\kappa+1) T(u)]^{-1}$ is small, and this causes (3) to be inaccurate. A plot of the function $\zeta(u)$ is shown in Fig. 6 (curve 1; the variables u and v are identical for curve 1).

The divergence of the function $\zeta(u)$ as $u \to 0$ signifies that nuclei with small excitation energies accumulate during the process of emission of quanta. As a consequence, the spectrum of the γ quanta emitted by a nucleus will also diverge as $1/E$ as $E \to 0$. This circumstance is common to all cases in which the energy density can be considered continuous, starting with small values of the energy. One can expect such a situation to correspond most closely to the case of odd-odd heavy nuclei, where the presence of two odd unpaired particles causes the level density to increase more or less uniformly, starting directly with the ground state of the nucleus. In even-even nuclei the pairing of the particles leads to the occurrence of a gap between the ground and the first excited state. For nuclei of medium atomic weights this quantity (Δ) is equal to 1.0 or 1.2 Mev. For simplicity we shall assume that in an even-even nucleus (ρ_e) there are no levels at all below an energy Δ, and that above this energy the level density is determined by the same law as in the case of odd-odd nuclei (ρ_o), i.e., we take ρ_e in the form

$$\rho_e(u) = \begin{cases} 0 & \text{for } u = \Delta, \\ \rho_0(u-\Delta) = \rho_0\rho(v) & \text{for } u \geqslant \Delta, \end{cases} \quad (26)$$

where v is the excitation energy of the even nucleus, measured from the gap: $v = u - \Delta$. The function $\rho(v)$ is normalized such that $\rho(0) = 1$.

In the presence of a gap in the spectrum of the nuclear levels, radiative transitions in even nuclei can be divided into two groups, since a high-energy transition into the ground state ($E = u$) is also possible from each excited state of the even-even nucleus, along with transitions to excited states with energies $u > \Delta$ ($E < u - \Delta$). Transitions of the former type will be called type A transitions, while those of the latter type will be called type B (see Fig. 1).

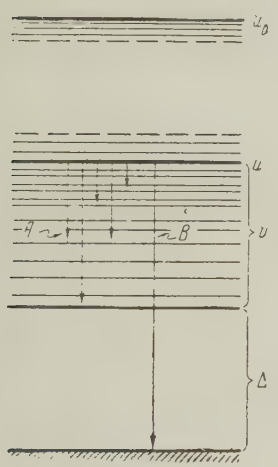

FIG. 1. Qualitative transition scheme in an even-even nucleus.

The function w(u, E) in the case of an even-even nucleus can be written in the following form

$$w_e(u, E) = w_A + w_B, \quad (27)$$

$$w_A = E^3\rho(u - E - \Delta)/n^*(u), \quad (28)$$

$$w_B = \alpha E^3\delta(u - E)/n^*(u). \quad (29)$$

The normalizing factor

$$n^*(u) = \int_0^u \{E^3\rho(u - E - \Delta) + \alpha\delta(u - E)\}\, dE$$
$$= \alpha(\Delta + v)^3 + \int_0^v E^3\rho(v - E)\, dE. \quad (30)$$

The constant $\alpha = (\overline{M_B^2}/\overline{M_A^2})\rho_0^{-1}$, where M_B and M_A are the matrix elements for type B and type A transitions. We assume here that both type A and type B transitions are dipole transitions. In addition, it is assumed, as above, that the mean square of the matrix element for type A transitions is independent of the energy.

If we now introduce instead of the function $\zeta(u)$ the function

$$\zeta(v) = (\zeta(u))_{u=\Delta+v}, \quad (31)$$

it is easy to show that both Eq. (21) and Eqs. (24) — (25) remain valid for the function $\zeta(v)$, provided the function w(u, E) is replaced by $w_A(u, E)$, and we put in the latter $u = \Delta + v$, while the function n(u) is replaced by a function n*(v), of the form

$$n^*(v) = \alpha(\Delta + v)^3 + n(v), \quad (32)$$

where n(v) is given by Eq. (2). We obtain

$$\zeta(v) = \int_0^{v_0} w_A(v', v' - v)\,\zeta(v')\, dv' + w_A(v_0, v_0 - v),$$
$$w_A(v, E) = (w_A(u, E))_{u=\Delta+v}. \quad (33)$$

The γ-quantum spectrum of an even-even nucleus is written in the form

$$\nu_e(E) = w_A(u_0, E) + \nu_A(E) + \nu_B(E), \quad (34)$$

where $w_A(u_0, E)$ is the spectrum of γ quanta emitted by a nucleus in the initial state (in this term we can neglect direct transitions from the initial state of the nucleus to the ground state);

$$\nu_B(E) = \alpha E^3[\zeta(v)/n^*(v)]_{v=E-\Delta} \quad (35)$$

is the γ spectrum of type B transitions, and

$$\nu_A(E) = \int_E^{v_0} (E^3\rho(v - E)/n^*(v))\,\zeta(v)\, dv \qquad (v_0 = u_0 - \Delta) \quad (36)$$

is the γ spectrum for type A transitions. The term $\nu_B(E)$ in (34) is taken into account when $E \geq \Delta$. Inasmuch as it is assumed that in an even-even nucleus at energy $u > \Delta$ the energy-level density coincides, accurate to a non-essential constant factor, with the level density in the odd nucleus, and the initial energy is greater than that of an odd-odd nucleus by exactly the amount Δ, then* the solution of the Eq. (21), the function $\zeta(u)$, and the photon spectrum (22) is obtained for the odd-odd nucleus as a particular case of Eqs. (34) and (36) with $\alpha = 0$. Here the variable v should be considered only as the excitation energy of the odd-odd nucleus, measured from the ground state $\Delta = 0$.

The presence of type B transitions in a nucleus with a gap can be readily analyzed qualitatively. Actually, the presence of type B transitions leads first to a weakening of the accumulation of nuclei with energy close to Δ: the function $\zeta(v)$ re-

*Actually the difference in the neutron binding energies in even-even and odd-odd nuclei somewhat exceeds Δ, which is defined as the size of the energy gap in the level spectrum of the even-even nucleus. This is not significant, since the γ-ray spectrum depends relatively little on the initial excitation energy.

mains finite at $\alpha \neq 0$ as $v \to 0$. Accordingly, the function $\nu_A(E)$ vanishes as $E \to 0$. This reduction in the number of low-energy photons is compensated by a corresponding increase in the number of transitions with energy $E > \Delta$ (see below, Fig. 6).

The parameter α can be roughly estimated by specifying the width of the energy interval δ, $0 < v < \delta$, in which type B transitions are most probable. This obviously occurs when the first term in the expression for $n^*(v)$ [formula (32)] exceeds the second. By equating the two terms, we obtain a relation between the parameters δ and α, from which we find

$$\alpha = n(\delta)/(\Delta + \delta)^3. \quad (37)$$

To obtain tentative values of the parameters we indicate, that, according to Eq. (37), the value $\delta \sim 1$ Mev corresponds to $\alpha \sim 1$ Mev, while $\delta \sim 0.2$ Mev corresponds to $\alpha \sim 0.001$ Mev.

The function $n(v)$ is a rapidly increasing function of v. Therefore when $v \gtrsim \delta$ the first term in (32) is negligibly small compared with the second. As a consequence, the spectrum of an even-even nucleus will differ substantially from that of an odd-odd nucleus only in the interval $0 < E < \delta$, where the spectrum of the even-even nucleus is characterized by a smaller number of quanta, as well as in the interval $\Delta < E \lesssim \Delta + \delta$, where the spectrum of the even-even nucleus will contain an additional contribution due to type B transitions.

Let us proceed now to a report of the results of the calculations and compare them with the experimental data. To calculate the γ-ray spectra we integrated Eqs. (24) and (33) numerically, using the Moscow State University "Strela" electronic computer. Two expressions were used for the level densities of the nucleus [the function $\rho(v)$]

$$\rho(v) = \exp(v/\tau), \quad \tau = \text{const}, \quad (38)$$

$$\rho(v) = \exp\sqrt{av}, \quad a = \text{const}. \quad (39)$$

In the first calculations we used (24) and (25) to find the function $\zeta(v)$. This differential equation was solved with automatic interval selection, insuring accuracy not less than 0.1%, using a standard program based on the Runge-Kutta method. After compiling a program for solving integral equation (33) by the Euler broken-line method, all the calculations were performed with the integral equation. An interval 0.2 Mev was chosen, since a comparison of the solutions of the integral equation with the previously obtained solutions of the differential equation had shown that such an interval insures the stipulated accuracy of 0.1%. Simultaneously with solving an integral equation, we evaluated the integral (36), and the functions $w(v_0, E)$ and $\nu_B(E)$. These functions, together with the function $\zeta(v)$ and $n^*(v)$, were obtained from the computer for points from 0.2 to 6.4 Mev every 0.2 Mev. The parameter v_0 was taken in all cases the same, 6.4 Mev, corresponding approximately to the average neutron binding energy in odd-odd nuclei. In most calculations a value of 1.2 Mev was used for Δ, corresponding approximately to the position of the peak in the experimental spectra of even-even nuclei (see below). Values in the interval from 0.4 to 2.5 Mev were taken for τ in (38), and values in the interval from 2 to 30 Mev^{-1} were used for the parameter a [Eq. (39)]. The constant α was taken to be 0, 1/1000, 1/400, 1/32, and 1/2 Mev.

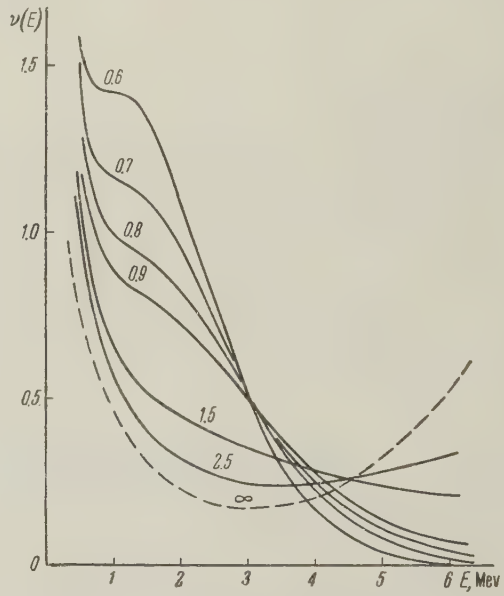

FIG. 2. Spectra of γ quanta, calculated for a level density as given by (38). The values of the parameter τ (in Mev) are indicated in the diagram ($\alpha = 0$).

Figure 2 shows several spectra of odd nuclei ($\alpha = 0$), calculated by means of (38) for level densities at certain values of the parameter τ. Figure 3 also shows several theoretical spectra of odd nuclei, calculated for a level density as given by Eq. (39).

The dotted curve of Fig. 2 shows the photon spectrum for $\tau = \infty$ (or $a = 0$). This spectrum was obtained from an analytic solution of the differential equation (24) and from an evaluation of the integral $\nu_A(E)$, [Eq. (36)], which are possible when $\rho = \text{const}$. As shown in the paper by Groshev et al.,[4] the best agreement with experiment is obtained at $\tau = 0.8$ Mev in the case of (38) or $a = 15$ Mev^{-1} for the case of (39) [corresponding

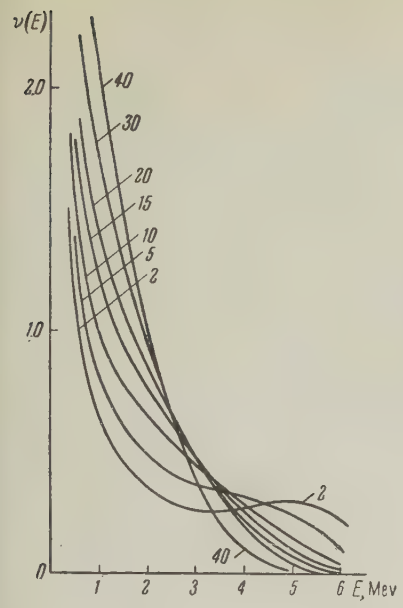

FIG. 3. Gamma spectra calculated for a level density as given by Eq. (39). The curves are labeled with values of the parameter a (in Mev^{-1}) ($\alpha = 0$).

to this value of a is an initial nuclear temperature $T_0 = (4u_0/a)^{1/2} \approx 1.3$ Mev]. Such a ratio between the "equivalent" values of the parameters τ and a is quite natural, if one considers that the average nuclear temperatures should be close.

In exactly the same manner it is possible, for other values of τ, to make the curves $\nu(E)$ obtained in the cases (38) and (39) close to each other by suitable choice of the parameter a. There is, however, a slight qualitative difference between the spectra shown in Figs. 2 and 3. The spectra calculated for an exponential density have a characteristic inflection in the region of $E \sim 1$ Mev. There is no such inflection in curves shown in Fig. 3 [where the density is taken from (39)]. The inflection is due to the fact that the first term in (34) is a bell-shaped curve (see Fig. 4), and the second term $\nu_A(E)$ is a monotonically decreasing function. In the case of version (39), owing to the greater dependence of the level density on the energy at $u \lesssim 1$ Mev, the spectrum $\nu_A(E)$ is greatly enriched by soft quanta, and the presence of the maximum in the function $w(u_0, E)$ does not appear explicitly in the form of the summary spectrum.

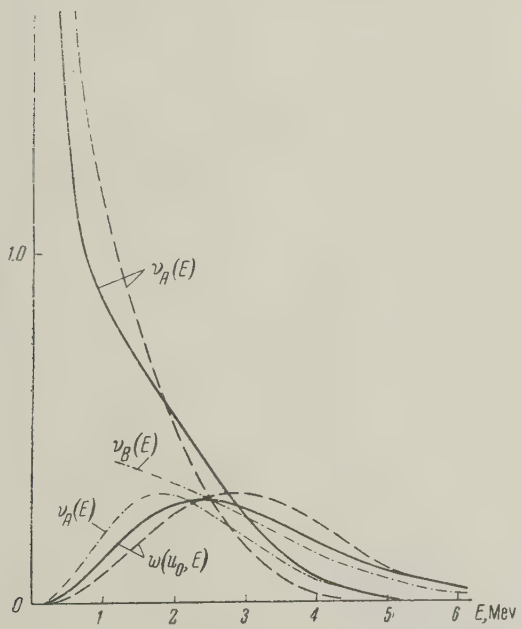

FIG. 4. Component parts of the complete γ spectrum [see (35)]. The solid curves correspond to $\alpha = 0$ for the level density given by (38) ($\tau = 0.8$ Mev); the dotted lines are the same for the case of (39) ($a = 15$ Mev^{-1}), while the dash-dot curve corresponds to $\alpha = 0.5$ Mev and $\tau = 0.8$ Mev.

The presence of an inflection at $E \sim 1$ Mev in the spectra of all the investigated deformed odd-odd nuclei[4] is an indication that in these nuclei the level density increases at low energy ($\lesssim 1$ Mev) more smoothly than $\exp\sqrt{au}$. It is interesting to note that no such inflection is observed in the spectra of spherical nuclei.

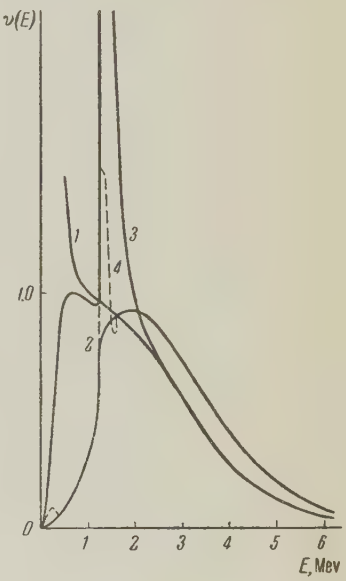

FIG. 5. Spectra of even-even nuclei, calculated for level densities of (38) ($\tau = 0.8$ Mev): curve 1 – at $\alpha = 0$, 2 – $\alpha = 0.5$ Mev, 3 – $\alpha = 1/400$ Mev, 4 – α taken in the form of a step (curve 1 of Fig. 7), $\alpha_1 = 1/400$ Mev, $\alpha_2 = 0.5$ Mev, $v^* = 0.4$ Mev.

We see by comparing the curves shown in Fig. 5 that in the quantum energy region $E \gtrsim 5$ Mev the contribution of the function $\nu_A(E)$ to the total spectrum is quite small (< 10%). Radiative transitions from such an energy are almost exclusively transitions from the initial state. Their average intensity is approximately

$$w(u_0, u_0) \approx u_0^3 \rho(0) / n(u_0) \approx u_0^3 / 6\tau^4 \rho(u_0) \approx 0.5\%, \quad (40)$$

and differs little from the experimental value ($\sim 0.5 - 3\%$).

Figure 5 shows the γ spectra calculated with the aid of (32) – (36) for $\alpha \neq 0$ (even-even nuclei) and $\tau = 0.8$ Mev (exponential energy dependence of the level density). Curves of ζ functions for these values of the parameters are given in Fig. 6.

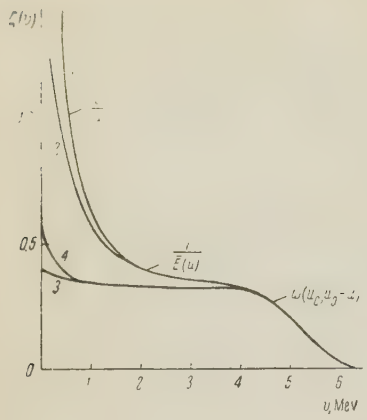

FIG. 6. Plot of the function $\zeta(v)$, calculated for a level density as given by (38) for the following values of the parameters: $1-\alpha = 0$ [odd-odd nucleus, $v = u$, cf. (31)]; $2-\alpha = 1/400$ Mev, $3-\alpha = 0.5$ Mev; $4-\alpha$ as a function of the energy (curve 1 of Fig. 7), $\alpha_1 = 1/400$ Mev; $\alpha_2 = 0.5$ Mev, $v^* = 0.4$ Mev, $\tau = 0.8$ Mev.

When compared with the odd-odd nuclei, the experimental spectra of deformed even-even nuclei are characterized by a large number of quanta of relatively large energies ($\sim 2-4$ Mev), while the spectra contained relatively fewer soft quanta ($E \lesssim 1.5$ Mev) and, in addition, a sharp peak exists with a width $\lesssim 0.5$ Mev at $E \sim 1$ Mev.[4] These first two distinctions suggest the choice of a relatively large value of α. For an exponential density [Eq. (38)] the best agreement from experiment was obtained at $\alpha = 0.5$ Mev and $\tau = 0.8$ Mev,[4] i.e., for the same value of τ as for the odd nuclei located in the same region. The aforementioned similarity in the density as given by (39) leads in the case of even-even nuclei to a considerable difference in the spectra calculated by means of (38) and (39). In the case of (39) the γ spectrum is characterized by much greater values of $\nu(E)$ in the region $E \lesssim 1$ Mev, and diminishes more rapidly with increasing E than the spectrum calculated for an exponential level density. Therefore, in order to make the theoretical spectrum calculated for the density given in (39) closer to the experimental spectrum of the even-even deformed nucleus, it becomes necessary to take $a = 5$ Mev^{-1}. So small a value of this parameter ($T_0 \approx 2.3$ Mev) is very unlikely, particularly if it is considered that the value obtained for a of odd nuclei is 15 Mev^{-1}. It is therefore necessary to conclude that the form of the spectrum of the even-even nuclei is evidence of a weak dependence of the level density of deformed even-even nuclei on the energy above the gap, at least compared with (39).

Let us return now to an examination of the third singularity of the spectra of the even-even deformed nuclei, namely the presence of a sharp peak at E $\sim$ 1 Mev. In principle, such a peak is present at a small value of α, on the order of $1/400 - 1/1000$ (see Fig. 5); however, at such a value of α the theoretical spectrum does not differ in practice from the spectrum for $\alpha = 0$ (i.e., the spectrum of the odd-odd nucleus) and all the remaining region, with the exception of the region of the peak and, accordingly, in the region $E \gtrsim 0.5$ Mev (see curves 1 and 3 in Fig. 5). On the other hand, at α on the order of unity, at which the general form of the theoretical spectrum is in good agreement with the experimental spectrum of deformed even-even nuclei, there is no sharp maximum at all at $E \sim \Delta$; the population of the levels of the nucleus with energy $u \gtrsim \Delta$ is found to be small, owing to the competition of type B transitions, which in this case is substantial even for large nuclear excitation energy.

It is natural to attempt to resolve this contradiction by considering the dependence of α on the excitation energy of the nucleus. In fact, all three singularities of the spectrum of deformed even-even nuclei can be explained qualitatively by assuming that the parameter depends on the energy as shown in Fig. 7 (curve 1), taking $v^* \approx 0.4$ Mev.

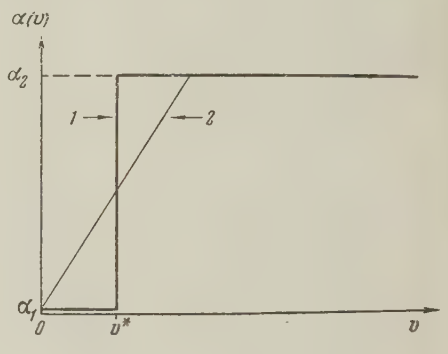

FIG. 7. Two versions of the function $\alpha(v)$ for which the spectra were calculated.

At such a value of α the γ spectrum will coincide with the spectrum calculated for $\alpha = 0.5$ in the quantum energy region $v^* \lesssim E < \Delta$ and $E > \Delta + v^*$, while in the region $\Delta < E \lesssim \Delta + v^*$ the spectrum will have a sharp maximum, as in the case of small α. This can be readily established by considering the dependence of $\nu_B(E)$ on α [$\nu_B(\Delta) = \{\zeta(v)\}_{v=0}$ is independent of α]. The γ spectrum was calculated also for variable α, in the form of a step (curve 1 of Fig. 7), and a ramp function (Fig. 2) for the following values of the parameters: $\alpha_2 = \alpha_1 + 0.5$ Mev, $\alpha_1 = 1/400$ Mev, $v^* = 0.4$ and 0.8, and $\tau = 0.7$, 0.8, and 0.9 Mev. The parameter Δ was taken to be 0.8 and 1.2 Mev. The density of the levels is specified in the form (38).

For illustration, Fig. 5 shows also one of the spectra calculated for the function $\alpha(v)$, taken in the form of a step. The discontinuities there are connected with the presence of a sharp jump in α and, naturally, will be smooth if the region of the sharp variation $\alpha(v)$ is somewhat smeared out. The spectra calculated for the ramp curve 2

of Fig. 7 do not differ in practice from the spectra at constant $\alpha = \alpha_1$. The spectrum shown in Fig. 5 for variable α has all the features of the experimental spectra of even-even nuclei, on the basis of which one can conclude that in the region ~ 0.5 Mev above the gap, the value of the parameter α is very small compared with the entire remaining energy region. The specific value of the parameter α near the gap (α_1) is not important here for the essential singularities of the form of the spectrum.

At the present time the structure of the levels of deformed even-even nuclei in the energy region above the gap has not yet been sufficiently investigated, and one can only guess at the reasons for the forbiddenness of the transitions through the gap for not too high a nuclear excitation. Such a forbiddenness could occur were the emission of the γ quanta to result in production of nuclei with large spins. This, however, can hardly be the cause of the forbiddenness, since near the ground state of even-even deformed nuclei there are always closely-located rotational levels, with sufficiently large spins, to which a radiative transition would be possible. A selection of transitions based on parity can also not lead to a sharp change in α, for the selection of transitions to the ground state by parity takes place also for transitions from strongly excited states.

A possible explanation of an energy dependence of α similar to that shown in Fig. 7 may be the presence of an additional forbiddenness based on the projection of the momentum on the nuclear axis in deformed nuclei (the quantum number K). The ground state is characterized by $K = 0$. A selection rule based on K, $\Delta K = 0$, and 1, would pick out in the case of dipole transitions only those excited states for which $K = 0$ or 1. If it is assumed that states with such K are missing in the vicinity of the gap, with the exception possibly of the lowest state, the dipole transitions would be impossible, and the radiative transitions through the gap would be less probable. Such a picture is confirmed by the well-studied decay schemes of W^{182} (reference 6) and many other deformed even-even nuclei.[7] On the other hand, the quantum number K is only an approximate adiabatic integral of the motion, and one might think that the forbiddenness connected with K does not play a substantial role, if one speaks of a transition into the ground state from strongly excited states of the nucleus: the wave function of such states is apparently a superposition of states with different values of K, including also such for which the transition to $K = 0$ is allowed.

This allows us to assume that the ratio of the matrix elements $\overline{M_A^2}/\overline{M_B^2}$ is close to unity. The factor ρ_0 in front of the exponent in formula (38) then coincides with α^{-1}, whence, using the values of the parameters α and τ, determined from γ spectra of even nuclei, we can estimate the average distance between the nuclear levels at the binding energy. This value should coincide in order of magnitude with the average distance between the neutron resonances (change in the nuclear spin upon emission of quanta is small and can be neglected). One can verify that this actually takes place. Reversing this argument, we could conclude, on the basis of the resultant value of α (~ 0.5 Mev), that the matrix elements are approximately equal. We emphasize, however, that we can speak only of a rough estimate.

For certain values of the parameters we also calculated the spectrum, for constant α, under the assumption that the radiative transitions through the gap (type B) are quadrupole transitions. In all cases the form of the computed spectrum differs greatly from the experimental one.

It is of interest to compare the data on the density distribution of the nuclear levels with results of other methods of determining this quantity. The most direct method is a direct calculation of the number of levels below a given energy. This method was recently used by Erikson[8] to determine the energy dependence of the level density below the neutron binding energy for certain nuclei with $A < 60$. The level distribution agrees with (38), and the parameter τ is found to be $1.0 - 1.2$ Mev. This result agrees with the determination of the level density from the spectrum of secondary particles in the (α, α') reaction in the same region of nuclei.[9] For the (p, p') reaction, a somewhat better agreement with formula (39) is indicated.[10] All these results pertain, unfortunately, to light nuclei, which perhaps explains the discrepancy between the value of the parameter τ, determined from the γ spectra (0.8 Mev), and that determined directly from the level density ($1.0 - 1.2$ Mev). We note incidentally that the results of the analysis of the γ spectra indicate the absence of a strong variation on the parameters that characterize the energy dependence of the level density as A varies from 100 to 200.[4] The absence of a noticeable dependence of the temperature on the atomic weight has been also noted in reference 10. On the other hand, the spectra of nuclei close to magic are characterized by relatively large values of τ (or, respectively, by small values of a). Thus, for gold the best agreement with the experimental

spectrum is obtained when $a = 3 - 5$ Mev^{-1}. We note also that the average distribution of the intensity in the spectra of light odd-odd nuclei[5] is in qualitative agreement with the theoretical values, calculated under the assumption $\rho = \text{const}$ (Fig. 3), which does not contradict other data on the level densities of these nuclei.

The temperature of the nucleus at an energy equal to the binding energy of a neutron can be determined also from the density of the neutron resonances. The value of the initial temperature of nuclei in the rare-earth region is found to be $0.6 - 0.7$ Mev, corresponding to a value of the parameter $a = 40 - 60$ Mev^{-1}. This value differs substantially from the value indicated above, $a = 15$ Mev^{-1}, obtained from the γ spectra. The discrepancy is considerably reduced it it is taken into account that the expression for the density of levels in the given momentum for a Fermi gas contains a factor in front of the exponent, which diminishes as u^{-2} with energy. If we attempt, however, to approximate the function $u^{-2}\exp\sqrt{au}$ by expressions of the form $\exp[(a^*u)^{1/2} + c]$, choosing the constants a^* and c in such a way as to make these expressions coincide at the points, say, $u = 2$ and 6.5 Mev, we obtain for the constant a^* a somewhat smaller value. Thus, at $a = 30$ or 60 Mev^{-1} the constant a^* becomes respectively 20 and 35 Mev^{-1}. It is precisely these values of the "effective" constant a^* that should be compared with the value obtained from the γ spectra or in other similar cases, if the level density is given by an expression of form (39).

If analogously we approximate the function $u^{-2}\exp\sqrt{au}$ by the function $\exp(u/\tau + c)$, we obtain for the constant τ a value ~ 0.7 Mev at $T_0 = 0.65$ Mev, determined from the neutron resonances, i.e., a value which does not greatly differ from the 0.8 Mev obtained from the γ spectra.*

As regards the choice between the distributions (38) and (39), as already noted, both laws lead to quite similar results. The singularities in the form of spectra of odd-odd deformed nuclei, and a comparison of the theoretical spectra with those of even-even deformed nuclei, nevertheless make it preferable to use for these nuclei the exponential law (38), or at least to conclude that the level density depends less on energy near the gap than called for by Eqs. (26) and (39).

This result is in agreement with what is obtained when nucleon pairing is considered. For deformed nuclei the presence of pairing between particles leads to a difference in the law of dispersion of the elementary excitations from the dispersion of free particles. The excitation energy is given by the following expression[11]

$$E_\nu \approx \sqrt{\varepsilon_\nu^2 + (\Delta/2)^2}, \qquad (41)$$

where ϵ_ν is the Fermi energy of the free particle, measured from the boundary. The level density of the elementary excitation $d\nu/dE_\nu$ diminishes with energy. If we speak of an odd-odd nucleus or an even-even nucleus with one broken pair, i.e., at $\Delta < u \lesssim 2\Delta$, where there are two free quasiparticles, the level density remains almost constant. As the excitation energy is increased, the number of broken pairs of particles increases and the level density begins to increase rapidly, and on the average this increase is closer to exponential.[12] In other words, in the presence of the finite energy to be spent on "liberating" the particle, the temperature of the system depends less on the energy than for free particles. Finally, at a certain sufficiently large energy the effect of pairing vanishes, and the level density is given by an expression of the type (39).

The results of the analysis of γ spectra of deformed nuclei are in full agreement with the picture drawn. Unfortunately, in spherical nuclei the grouping of levels in shells and subshells makes it very difficult to describe even qualitatively the dependence of the level density on the energy. The fact that the level density of odd-odd spherical nuclei in the energy region $\lesssim 1$ Mev increases more rapidly than $\exp(u/\tau)$ can be attributed either to the smallness of the pairing energy, or in general to a particle-dispersion law differing from (41). For two free odd particles the level density increases as u^2.

The authors express their gratitude to Professor A. N. Tikhonov and A. V. Luk'yanov for participating in the calculations on the Moscow State University electronic computer.

*These results were obtained jointly with Yu. V. Adamchuk.

[1] Groshev, Demidov, Lutsenko, and Pelekhov, Доклады советской делегации на Второй международной конференции по мирному использованию атомной энергии, Ядерная физика, (Papers of the Soviet Delegation at the Second Geneva Conference, Nuclear Physics) Vol. 1, Atomizdat, 1958, p. 281.

[2] J. Blatt and V. Weisskopf, Theoretical Nuclear Physics, Wiley, N.Y., 1952, Chap. 12.

[3] E. Segre, ed. Nuclear Physics, Vol. 2, (Russ. Transl.) IIL, 1955, Chap. 1.

[4] Groshev, Demidov, and Pelekhov, JETP **38**, 588 (1960), this issue, p. 423.

[5] Groshev, Ad'yasevich, and Demidov, Доклады советской делегации на Первой международной конференции по мирному использованию атомной энергии. Физические исследования, (Papers of the Soviet Delegation at the First Geneva Conference, Physics Research), Acad. Sci. Press, 1955, p .252.

[6] Murray, Boehm, Marmier, and Du Mond, Phys. Rev. **97**, 1007 (1955); Alaga, Alder, Bohr, and Mottelson, Kgl. Danske Videnskab. Selskab **29**, No. 9 (1955).

[7] B. F. Dzhelepov and L. K. Pekar, Схемы распада радиоактивных изотопов (Decay Schemes of Radioactive Isotopes), Acad. Sci. Press, 1958.

[8] T. Erikson, Nucl. Phys. **11**, 481 (1959).

[9] Fullbright, Lassen, and Roy Poulsen, Kgl. Danske Videnskab. Selskab, Mat.-fys. Medd. **31**, No. 10 (1959).

[10] B. L. Cohen and A. G. Rubin, Phys. Rev. **111**, 1658 (1959).

[11] S. T. Belyaev, Kgl. Danske Videnskab. Selskab, Mat.-fys. Medd. **31**, No. 11 (1959).

[12] V. Strutinski, Congr. Int. Phys. Nucl., Paris, 1958.

Translated by J. G. Adashko
114

STABILITY OF EQUILIBRIUM OF A CONDUCTING LIQUID HEATED FROM BELOW IN A MAGNETIC FIELD

V. S. SOROKIN and I. V. SUSHKIN

Ivanovo State Pedagogical Institute

Submitted to JETP editor September 12, 1959

J. Exptl. Theoret. Phys. (U.S.S.R.) **38**, 612-620 (February, 1960)

The general effect of a uniform magnetic field on the stability of the equilibrium of a conducting liquid which is heated from below in a cavity of arbitrary shape is investigated. The time variation of the perturbations which arise in the liquid is always monotonic. The critical value of the Rayleigh number C_0^2, above which the equilibrium is unstable, increases monotonically with the Hartmann number M, so that the inequality in Eq. (4.16) is satisfied. At small values of M the critical value of the Rayleigh number is proportional to M^2 and the coefficient of proportionality can be computed. The asymptotic nature of the function $C_0(M)$ as $M \to \infty$ depends on the shape of the cavity and the direction of the field.

THE most interesting phenomena in magnetohydrodynamics occur when energy dissipation is not important. These effects have been investigated widely in recent years. Cases of motion in small volumes, in which case viscosity is important, are generally considered less interesting. Under these conditions, the magnetic field induces a current in the liquid and this current tends to retard the motion; in principle, no other additional effects arise. Cases of this kind have been considered by Hartmann[1] (plane Poiseuille flow), Chandrasekhar[2] (convection in a plane horizontal layer), Smirnov[3] (convection in a vertical tube heated from below), Velikhov[4] (Poiseuille flow and flow between rotating cylinders) and Regirer[5] (convection in a plane vertical slit).

Of the problems which have been considered, the convection problems are of special interest because of their connection with the theory of hydrodynamic stability. The initial state is an equilibrium state and the analysis of its stability is much simpler than the problem of flow stability. At the same time the presence of the magnetic field means that the equations of motion are not self-adjoint and hence more closely related to typical equations in the theory of hydrodynamic stability. If there is no magnetic field the problem is extremely simple.[6] Hence a general investigation of the effect of the magnetic field on the stability of equilibrium of a conducting liquid heated from below in an external uniform magnetic field is of interest.

1. EQUATIONS OF MOTION

We consider "slow" motion in a conducting liquid which is originally in equilibrium in a gravitational field

$$\mathbf{g} = -g\gamma, \quad \gamma^2 = 1 \tag{1.1}$$

and which is heated from below so that there is a constant vertical temperature gradient (as long as equilibrium prevails)

$$\nabla T_0 = -A\gamma. \tag{1.2}$$

The liquid fills a cavity of arbitrary shape which is cut into an infinite external solid medium. The external magnetic field

$$\mathbf{H}_0 = H_0\beta, \qquad \beta^2 = 1 \tag{1.3}$$

produces a current density $\mathbf{j}$ and an additional magnetic field $\mathbf{h}$ in the liquid.

To the usual convection equations[7] it is now necessary to add the Lorentz force; since the motion is slow we retain only the linear perturbation terms. Then the equations of motion and the heat conduction equation are

$$\dot{\mathbf{v}} = -\rho^{-1}\nabla p - \nu \operatorname{curl}\operatorname{curl}\mathbf{v} + \alpha g\gamma T + (H_0/c\rho)[\mathbf{j}\times\beta],$$
$$\dot{T} = A\gamma v + \chi\nabla^2 T, \qquad \operatorname{div}\mathbf{v} = 0. \tag{1.4}$$

In addition we have Maxwell's equations (in which the displacement current is neglected) and Ohm's law:

$$\operatorname{curl}\mathbf{h} = (4\pi\sigma/c)\{\mathbf{E} + c^{-1}H_0[\mathbf{v}\times\beta]\} = 4\pi\mathbf{j}/c,$$
$$\mathbf{h} = -c\operatorname{curl}\mathbf{E}, \quad \operatorname{div}\mathbf{h} = 0 \tag{1.5}$$

(σ is the electrical conductivity, $\mu = 1$, and $\mathbf{E}$ is the electric field).

We can eliminate $\mathbf{j}$ and $\mathbf{E}$ from these equations, expressing these quantities in terms of $\mathbf{h}$. Then the equations which describe the problem become

$$\dot{\mathbf{v}} = -\rho^{-1}\nabla p - \nu\,\mathrm{curl}\,\mathrm{curl}\,\mathbf{v} + \alpha g\gamma T + (H_0/4\pi\sigma)[\mathrm{curl}\,\mathbf{h}\times\beta],$$
$$\dot{T} = \gamma A\mathbf{v} + \chi\nabla^2 T,$$
$$\dot{\mathbf{h}} = -(c^2/4\pi\sigma)\,\mathrm{curl}\,\mathrm{curl}\,\mathbf{h} + H_0[\mathbf{v}\times\beta],$$
$$\mathrm{div}\,\mathbf{v} = \mathrm{div}\,\mathbf{h} = 0. \qquad (1.6)$$

For the external medium, in these equations we set the velocity equal to zero and replace the coefficients χ and σ by the corresponding coefficients in the medium, $\tilde{\chi}$ and $\tilde{\sigma}$:

$$\dot{T} = \tilde{\chi}\nabla^2 T, \qquad \dot{\mathbf{h}} = -(c^2/4\pi\tilde{\sigma})\,\mathrm{curl}\,\mathrm{curl}\,\mathbf{h}, \quad \mathrm{div}\,\mathbf{h} = 0. \qquad (1.6')$$

At the boundaries of the cavity the velocity, magnetic field, temperature, and normal components of the current and heat flow must be continuous:

$$\mathbf{v}|_s = 0, \qquad \mathbf{h}|_s = \tilde{\mathbf{h}}|_s, \qquad T|_s = \tilde{T}|_s,$$
$$\mathbf{n}\,\mathrm{curl}\,\mathbf{h}|_s = \mathbf{n}\,\mathrm{curl}\,\tilde{\mathbf{h}}|_s, \qquad \mathbf{n}\nabla T|_s = \eta_1\mathbf{n}\nabla\tilde{T}|_s \qquad (1.7)$$

(η is the ratio of the heat conductivities of the medium and the liquid). Both T and $\mathbf{h}$ vanish at infinity.

We now introduce characteristic units: the characteristic dimension of the cavity l, H_0, and the characteristic velocity and temperature, defined by

$$v_1^2 = \left(\frac{H_0 c}{4\pi}\right)^2 \frac{1}{\rho\nu\sigma}, \qquad T_1^2 = \left(\frac{H_0 c}{4\pi}\right)^2 \frac{A}{\alpha\chi\rho\sigma g}. \qquad (1.8)$$

Then Eq. (1.6) assumes the following form:

$$\mathbf{v} = -\nabla p - \mathrm{curl}\,\mathrm{curl}\,\mathbf{v} + C\gamma T + M[\mathrm{curl}\,\mathbf{h}\times\beta],$$
$$P\dot{T} = C\gamma\mathbf{v} + \nabla^2 T, \qquad (1.9)$$
$$N\dot{\mathbf{h}} = -\mathrm{curl}\,\mathrm{curl}\,\mathbf{h} + M\,\mathrm{curl}\,[\mathbf{v}\times\beta],$$
$$\mathrm{div}\,\mathbf{v} = \mathrm{div}\,\mathbf{h} = 0;$$
$$\tilde{P}\dot{\tilde{T}} = \nabla^2\tilde{T}, \quad \tilde{N}\dot{\tilde{\mathbf{h}}} = -\mathrm{curl}\,\mathrm{curl}\,\mathbf{h}, \quad \mathrm{div}\,\mathbf{h} = 0. \qquad (1.9')$$

The boundary conditions (1.7) and the conditions at infinity remain the same as before.

We use the following dimensionless quantities in these equations:

$P = \nu/\chi = \tilde{\chi}\tilde{P}/\chi$ (Prandtl number)
$N = 4\pi\nu\sigma/c^2 = \sigma\tilde{N}/\tilde{\sigma}, \quad \eta_1 = \tilde{\varkappa}/\varkappa,$
$C^2 = \alpha g A l^4/\nu\chi$ (Rayleigh number)
$M^2 = H_0^2\sigma l^2/\rho\nu c^2$ (Hartmann number squared)

(The so-called Lundquist number, which determines the nature of typical processes in magnetohydrodynamics, is $M\sqrt{N}$. This quantity does not contain the viscosity.)

The linear equations (1.9) do not contain the time explicitly so that all quantities may be assumed to be multiplied by a function of the form $e^{-\lambda t}$; we are then concerned with the boundary value problem:

$$\lambda\mathbf{v} = \nabla p + \mathrm{curl}\,\mathrm{curl}\,\mathbf{v} - C\gamma T - M[\mathrm{curl}\,\mathbf{h}\times\beta],$$
$$\lambda PT = -C\gamma\mathbf{v} - \nabla^2 T, \qquad (1.10)$$
$$\lambda N\mathbf{h} = \mathrm{curl}\,\mathrm{curl}\,\mathbf{h} - M\,\mathrm{curl}\,[\mathbf{v}\ \beta],$$
$$\mathrm{div}\,\mathbf{v} = \mathrm{div}\,\mathbf{h} = 0;$$
$$\lambda\tilde{P}\tilde{T} = -\nabla^2 T, \qquad \lambda\tilde{N}\tilde{\mathbf{h}} = \mathrm{curl}\,\mathrm{curl}\,\mathbf{h}, \qquad (1.10')$$

with the boundary conditions (1.7) and the condition $\mathbf{T} = \mathbf{h} = 0$ at infinity. The sign of the real part of λ (the eigenvalue of the boundary-value problem) determines the stability: stability obtains when $\mathrm{Re}\,\lambda > 0$.

In what follows we will be concerned with integrals which are taken over all space. These are written in the form of sums of integrals over the volume of the liquid and the external volume whose integrands differ from each other by the obvious substitution of P by $\tilde{\mathrm{P}}$ and so on. The boundary conditions allow us to use Gauss' theorem over all space since the integrals over the surface of the interface always cancel.

2. STABILITY IN THE ABSENCE OF A MAGNETIC FIELD

This problem has been investigated by one of us.[6] In the absence of a field $\mathbf{M} = 0$ and Eq. (1.10) can be simplified:

$$\lambda\mathbf{v} = \nabla p + \mathrm{curl}\,\mathrm{curl}\,\mathbf{v} - C\gamma T,$$
$$P\lambda T = -C\gamma\mathbf{v} - \nabla^2 T, \quad \mathrm{div}\,\mathbf{v} = 0; \qquad (2.1)$$
$$\tilde{P}\lambda\tilde{T} = -\nabla^2\tilde{T}. \qquad (2.1')$$

The system of equations in (2.1) and (2.1′) is self-adjoint and the eigenvalues λ and eigenfunctions $\mathbf{v}$ and T are real. The equations in (2.1) are the Euler equations for the variational problem

$$J[\mathbf{v}, T] = \frac{1}{2}\int\{(\mathrm{curl}\,\mathbf{v})^2 + (\nabla T)^2 - 2C\gamma\mathbf{v}T\}\,dV + \frac{1}{2}\eta_1\int(\nabla\tilde{T})^2\,d\tilde{V} = \mathrm{extr},$$
$$K[\mathbf{v}, T] = \frac{1}{2}\int\{\mathbf{v}^2 + PT^2\}\,dV + \frac{1}{2}\eta_1\int\tilde{P}\tilde{T}^2 d\tilde{V} = 1,$$
$$\mathrm{div}\,\mathbf{v} = 0 \qquad (2.2)$$

with the earlier conditions (1.7), while the λ's are stationary values of the quotient:

$$\lambda = \mathrm{extr}\,(J/K). \qquad (2.3)$$

The last situation, which does not appear in problems of hydrodynamic stability, makes the analysis much easier. For a given C there exists an infinite set of solutions

$$\lambda_n;\ \{\mathbf{v}_n, T_n, p_n\},\ n = 0, 1, 2, \ldots, \qquad (2.4)$$

which can be designated in order of increasing λ.

These solutions are orthogonal to each other in the following sense:

$$\tfrac{1}{2}\int\{\mathbf{v}_m\mathbf{v}_n + PT_mT_n\}\,dV + \tfrac{1}{2}\eta\int\widetilde{P}\,\widetilde{T}_m\widetilde{T}_n d\widetilde{V} = \delta_{mn},$$

$$\tfrac{1}{2}\int\{\mathrm{curl}\,\mathbf{v}_m\,\mathrm{curl}\,\mathbf{v} + \nabla T_m\cdot\nabla T_n - C\gamma\mathbf{v}_m T - C\gamma\mathbf{v}_n T_m\}\,dV$$
$$+\tfrac{1}{2}\eta\int\nabla\widetilde{T}\cdot\nabla\widetilde{T}_n\,d\widetilde{V} = \lambda_n\delta_{mn}. \qquad (2.5)$$

It is apparent that $J > 0$ when $C = 0$, that is to say, all the $\lambda_n > 0$, and the liquid is stable. By means of a variational technique (2.3) it is shown in reference 6 that when C is increased all the λ_n are diminished, i.e., the damping of the perturbations becomes weaker and for some value $C = C_0$ the eigenvalue λ_0 vanishes. When $C > C_0$, the zeroth motion increases in time and the liquid becomes unstable. With a further increase in C we obtain successive negative values λ_1, λ_2, etc.

In order to find the critical number C_α we solve Eq. (2.1), setting $\lambda = 0$:

$$C\gamma T = \nabla p + \mathrm{curl}\,\mathrm{curl}\,\mathbf{v},\quad C\gamma\mathbf{v} = -\nabla^2 T,\quad \mathrm{div}\,\mathbf{v} = 0; \qquad (2.6)$$

$$\nabla^2\widetilde{T} = 0 \qquad (2.6')$$

with the earlier boundary conditions. Equations (2.6) and (2.6′) are also self-adjoint and are equivalent to the variational problem:

$$I[\mathbf{v}, T] = \tfrac{1}{2}\int\{(\mathrm{curl}\,\mathbf{v})^2 + (\nabla T)^2\}\,dV$$
$$+\tfrac{1}{2}\eta\int(\nabla\widetilde{T})^2\,d\widetilde{V} = \mathrm{extr},$$

$$Q[\mathbf{v}, T] = \int\gamma\mathbf{v}T\,dV = 1,\quad \mathrm{div}\,\mathbf{v} = 0. \qquad (2.7)$$

The eigenvalues for this problem are given by

$$C = \mathrm{extr}\,(I/Q). \qquad (2.8)$$

We shall call the solutions of this problem the critical motions, enumerating them by Greek subscripts in order of increasing C:

$$C_\alpha;\ \{\mathbf{v}_\alpha, T_\alpha, p_\alpha\}, \qquad (2.9)$$

so that C_α^2 is the value of the Rayleigh number at which perturbations characterized by $n < \alpha$ increase, the perturbation characterized by $n = \alpha$ is neutral, and perturbations characterized by $n > \alpha$ are damped. The critical motions satisfy the following orthogonality conditions:

$$\int\gamma\mathbf{v}_\alpha T_\beta dV = \delta_{\alpha\beta},$$

$$\int\mathrm{curl}\,\mathbf{v}_\alpha\,\mathrm{curl}\,\mathbf{v}_\beta dV = C_\alpha\delta_{\alpha\beta},$$

$$\int\nabla T_\alpha\cdot\nabla T_\beta dV + \eta\int\nabla\widetilde{T}_\alpha\cdot\nabla\widetilde{T}_\beta\,d\widetilde{V} = C_\alpha\delta_{\alpha\beta}. \qquad (2.10)$$

It is assumed that Eq. (2.9) defines a complete set and that this set can be used for expansion of any $\mathbf{v}$, T, and p.

3. PERTURBATIONS IN A MAGNETIC FIELD

The system of equations in (1.10) for perturbations in a magnetic field is not self-adjoint and it is not immediately apparent whether or not the eigenvalues are real. From Eq. (1.10) it is easy to derive the integral relation

$$(\lambda - \lambda^*)\left\{\int[\mathbf{v}^*\mathbf{v} + PT^*T - N\mathbf{h}^*\mathbf{h}]\,dV\right.$$
$$\left.+\int[\eta\widetilde{P}\,T^*T - \hat{N}\,\widetilde{\mathbf{h}}^*\widetilde{\mathbf{h}}]\,d\widetilde{V}\right\} = 0, \qquad (3.1)$$

which, strictly speaking, does not prove that the λ are real, although it does suggest that such is the case. It is possible, however, to expand the eigenvalues and eigenfunctions in powers of M^2 and these expansions are real.

These expansions are obtained as follows. When $M = 0$ Eq. (10) has a set of solutions given by (2.4). Physically it is clear that this set must be complete in the sense that any pair of functions $\{\mathbf{v}, T\}$ can be expanded in functions of the set:

$$\{\mathbf{v}, T\} = \sum_n a_n\{\mathbf{v}_n, T_n\} \qquad (3.2)$$

with the same coefficients a_n in both expansions.

We may note that a set of several $\mathbf{v}_n$ (or T_n) is overcomplete for any $\mathbf{v}$; hence any $\mathbf{v}$ can be expanded in different ways in the $\mathbf{v}_n$, depending on the T to which this $\mathbf{v}$ is related. The reason such expansions are real is clear from the fact that any initial $(\mathbf{v}, T)$ vary in accordance with Eq. (1.9); i.e., the expansions must consist of terms which vary exponentially in time.

In Eq. (1.10) we now write

$$\lambda = \lambda_n + M^2\lambda^{(1)} + \ldots + M^{2k}\lambda^{(k)} + \ldots, \qquad (3.3)$$

$$\{\mathbf{v}, T, p\} = \{\mathbf{v}_n, T_n, p_n\}$$
$$+\sum_{m\neq n}[M^2 a_m^{(1)} + \ldots + M^{2k}a_m^{(k)} + \ldots]\{\mathbf{v}_m, T_m, p_m\}, \qquad (3.4)$$

$$\mathbf{h} = M\mathbf{h}^{(1)} + \ldots + M^{2k-1}\mathbf{h}^{(k)} + \ldots\ . \qquad (3.5)$$

Assuming that all terms of these expansions are determined to order $(k-1)$, we now show that it is possible to determine terms of order k. If we substitute the expansions (3.3) and (3.4) in the third equation of (1.10) and consider M^{2k-1} terms we have

$$N\lambda_n\mathbf{h}^{(1)} - \mathrm{curl}\,\mathrm{curl}\,\mathbf{h}^{(1)} = -\mathrm{curl}\,[\mathbf{v}_n\times\beta]\quad (k=1);$$

$$N\lambda_n\mathbf{h}^{(k)} - \mathrm{curl}\,\mathrm{curl}\,\mathbf{h}^{(k)} = -\mathrm{curl}\sum_{m\neq n}a_m^{(k-1)}[\mathbf{v}_m\times\beta]$$
$$-[\lambda^{(1)}\mathbf{h}^{(k-1)} + \ldots + \lambda^{(k-1)}\mathbf{h}^{(1)}] \qquad (k>1). \qquad (3.6)$$

The right sides of these equations are assumed to be known and, solving Eq. (3.6) with the imposed boundary conditions, we obtain the $\mathbf{h}^{(k)}$. We then substitute the expansions in (3.3) and (3.4) and the

$\mathbf{h}^{(k)}$, which are now known, in the remaining equations of (1.10) and consider M^{2k} terms. In this way we obtain

$$\lambda^k \mathbf{v}_n + \sum_{m \neq n} [\lambda^{(k-1)} a_m^{(1)} + \ldots + \lambda_n a_m^{(k)}] \mathbf{v}_m$$
$$= \sum_{m \neq n} a_m^{(k)} [\nabla p_m + \operatorname{curl}\operatorname{curl} \mathbf{v}_m - C\gamma T_m]$$
$$- [\operatorname{curl} \mathbf{h}^{(k)} \times \beta],$$
$$P\left\{ \lambda^{(k)} T_n + \sum_{m \neq n} [\lambda^{(k-1)} a_m^{(\ )} + \ldots + \lambda_n a_m^{(k)}]\, T_m \right\}$$
$$= - \sum_{m \neq n} a_m^{(k)} [C\gamma \mathbf{v}_m + \nabla^2 T_m] \qquad (3.7)$$

and similar equations in the external medium.

Multiplying Eq. (3.7) by

$$\{\mathbf{v}_n, T_n\}$$

and integrating, by virtue of the orthogonality condition (2.5) we obtain

$$\lambda^{(k)} = \int \operatorname{curl} \mathbf{h}^{(k)} [\mathbf{v}_n \times \beta]\, dV, \qquad (3.8)$$

then, multiplying by

$$\{\mathbf{v}_m, T_m\} \quad (m \neq n)$$

and integrating we obtain

$$[\lambda^{(k-1)} a_m^{(1)} + \ldots + \lambda_n a_m^{(k)}] = \lambda_m a_m^{(k)} + \int \operatorname{curl} \mathbf{h}^{(k)} [\mathbf{v}_m \times \beta]\, dV,$$

whence

$$a_m^{(k)} = \frac{1}{\lambda_m - \lambda_n} \left\{ \lambda^{(k-1)} a_m^{(1)} + \ldots + \lambda^{(1)} a_m^{(k-1)} \right.$$
$$\left. - \int \operatorname{curl} \mathbf{h}^{(k)} [\mathbf{v}_m \times \beta]\, dV \right\}. \qquad (3.9)$$

By this method it is then possible to compute successively all terms of the expansions in Eqs. (3.3) to (3.7); it is obvious that when $M \neq 0$ the solutions are real. We may note that the following relation follows from Eqs. (3.3) and (3.8):

$$\lambda = \lambda_n + M \int \operatorname{curl} \mathbf{h}\, [\mathbf{v}_n \times \beta]\, dV, \qquad (3.10)$$

which can also be derived directly from Eq. (1.10).

Taking account of the fact that $\{\lambda, \mathbf{v}, T\}$ are real, from Eq. (1.10) we find that

$$\lambda = \left\{ \int \left[(\operatorname{curl} \mathbf{v})^2 + (\nabla T)^2 - (\operatorname{curl} \mathbf{h})^2 \right.\right.$$
$$\left. - 2C\gamma \mathbf{v} T - 2M \operatorname{curl} \mathbf{h}\, [\beta \times \mathbf{v}] \right] dV$$
$$+ \int [\eta\, (\nabla \tilde{T})^2 - (\operatorname{curl} \mathbf{h})^2]\, dV \Big\} \Big\{ \int [\mathbf{v}^2 + PT^2 - N\mathbf{h}^2]\, dV$$
$$\left. + \int [\eta \tilde{P}\, \tilde{T}^2 - \tilde{N}^2 \mathbf{h}^2]\, dV \right\}^{-1}, \qquad (3.11)$$

and Eq. (1.10) is obtained by the variation of the numerator of this expression with the denominator held constant.

We cannot show starting directly from Eq. (3.11) that in a magnetic field there will be a critical Rayleigh number C_0^2 at which the motion becomes unstable, although this result is almost obvious physically. But if stability is lost at the critical value C_0, the smallest λ is zero. Hence it is possible to investigate Eq. (1.10) directly with $\lambda = 0$, assuming that M is given. Thus we can obtain the spectrum of critical $C_\alpha(M)$.

4. STABILITY IN A MAGNETIC FIELD

Writing $\lambda = 0$ in Eq. (1.10) we obtain the equations for the critical motions. In these equations it is convenient to introduce the current

$$\mathbf{j} = \operatorname{curl} \mathbf{h}, \qquad (4.1)$$

so that the equations assume the form

$$C\gamma T = \nabla p + \operatorname{curl}\operatorname{curl} \mathbf{v} - M [\mathbf{j} \times \beta], \quad C\gamma \mathbf{v} = -\nabla^2 T,$$
$$\operatorname{curl} \{\mathbf{j} - M [\mathbf{v} \times \beta]\} = 0, \quad \operatorname{div} \mathbf{v} = \operatorname{div} \mathbf{j} = 0. \qquad (4.2)$$

In the external medium

$$\nabla^2 \tilde{T} = 0, \quad \operatorname{curl} \mathbf{j} = 0, \quad \operatorname{div} \mathbf{j} = 0. \qquad (4.2')$$

The boundary conditions remain the same as before except that we must take account of the fact that the normal component of the current is continuous.

It is easy to show that Eq. (4.2) is obtained by solution of the following variational problem:

$$I[\mathbf{v}, T, \mathbf{j}] = \frac{1}{2} \int \{(\operatorname{curl} \mathbf{v})^2 + (\nabla T)^2 - \mathbf{j}^2 - 2M\mathbf{j} [\beta \times \mathbf{v}]\}\, dV$$
$$+ \frac{1}{2} \int \{\eta\, (\nabla \tilde{T})^2 - \tilde{\mathbf{j}}^2\}\, d\tilde{V} = \text{extr};$$
$$Q[\mathbf{v}, T] = \int \gamma \mathbf{v} T dV = 1, \qquad \operatorname{div} \mathbf{v} = \operatorname{div} \mathbf{j} = 0 \qquad (4.3)$$

with the same boundary conditions as before. The quantity $C(M)$ can itself be expressed in terms of the extreme of the function $\mathbf{v}$, T, $\mathbf{j}$ by use of any of the following formulas:

$$C(M) = I[\mathbf{v}, T, \mathbf{j}] / Q[\mathbf{v}, T]$$
$$= \left\{ \int (\nabla T)^2 dV + \eta \int (\nabla \tilde{T})^2 d\tilde{V} \right\} \Big/ \int \gamma \mathbf{v} T\, dV$$
$$= \int [(\operatorname{curl} \mathbf{v})^2 + \mathbf{j}^2]\, dV \Big/ \int \gamma \mathbf{v} T dV, \qquad (4.4)$$

where the following relations obtain for the critical values of $\mathbf{v}$, T and $\mathbf{j}$

$$\int \mathbf{j}^2 dV = M \int \mathbf{j}\, [\mathbf{v} \times \beta]\, dV,$$
$$\int [(\operatorname{curl} \mathbf{v})^2 + \mathbf{j}^2]\, dV = \int (\nabla T)^2 dV + \eta \int (\nabla \tilde{T})^2 d\tilde{V}. \qquad (4.5)$$

We now compute the derivative of $C(M)$ with respect to M from the first relation in Eq. (4.4). It is apparent that it is necessary to differentiate only with respect to M, which appears explicitly in the integral I, since the result of differentiation of the functions $\mathbf{v}$, T and $\mathbf{j}$ gives zero by virtue

of Eq. (4.2). Consequently

$$dC(M)/dM = \int \mathbf{j}[\mathbf{v}\times\beta]\,dV \Big/ \int \gamma \mathbf{v} T dV \qquad (4.6)$$

or, from Eqs. (4.5) and (4.6),

$$\frac{M}{C}\frac{dC}{dM} = \int j^2 dV \Big/ \left\{ \int (\nabla T)^2 dV + \eta \int (\nabla \tilde{T})^2 d\tilde{V} \right\}. \qquad (4.7)$$

It follows from Eq. (4.5) that

$$0 \leqslant \int j^2 dV \Big/ \left\{ \int (\nabla T)^2 dV + \eta \int (\nabla \tilde{T})^2 d\tilde{V} \right\}$$
$$= 1 - \int (\mathrm{curl}\,\mathbf{v})^2 dV \Big/ \left\{ \int (\nabla T)^2 dV + \eta \int (\nabla \tilde{T})^2 d\tilde{V} \right\} < 1, \qquad (4.8)$$

whence

$$0 \leqslant d\ln C / d\ln M < 1. \qquad (4.9)$$

At small values of M the dependence of C(M) on M can be determined easily by a perturbation method.* We consider the change, under the effect of a weak magnetic field, in the critical motion ($\mathbf{v}_0$, T_0, p_0, $h_0 = 0$) which corresponds to the smallest critical Rayleigh number $C_0^2(0)$. We expand all quantities in terms of the critical motion (without the magnetic field) (2.9):

$$\mathbf{v} = \mathbf{v}_0 + M^2 \sum_{\alpha\neq 0} \beta_\alpha \mathbf{v}_\alpha \ldots,$$

$$T = T_0 + M^2 \sum_{\alpha} \theta_\alpha T_\alpha + \ldots,$$

$$p = p_0 + M^2 \sum_{\alpha} \pi_\alpha p_\alpha + \ldots,$$

$$C_0(M) = C_0(0) + \Delta C. \qquad (4.10)$$

(In the summation for $\mathbf{v}$ we neglect the term with $\alpha = 0$, which is equivalent to a change of normalization.) Substituting in Eq. (4.2) and keeping only the lowest power of M we have

$$M^2\Big[-\sum_{\alpha}\nabla\pi_\alpha p_\alpha - \sum_{\alpha\neq 0}\beta_\alpha\,\mathrm{curl}\,\mathrm{curl}\,\mathbf{v}_\alpha + C_0(0)\sum_{\alpha}\theta_\alpha\gamma T_\alpha\Big]$$
$$+ \Delta C\gamma T_0 + M[\mathbf{j}\times\beta] = 0,$$

$$M^2 C_0(0)\gamma\sum_{\alpha\neq 0}\beta_\alpha\mathbf{v}_\alpha + \Delta C\gamma\mathbf{v}_0 + M^2\sum_{\alpha}\theta_\alpha\nabla^2 T_\alpha = 0,$$

$$\mathbf{j} = M[\mathbf{v}_0\times\beta] - \nabla\varphi. \qquad (4.11)$$

The current may be assumed known since in determining the potential φ from div $\mathbf{j} = 0$, we get

$$\nabla^2\varphi = M\,\mathrm{div}[\mathbf{v}_0\times\beta]. \qquad (4.12)$$

It is apparent that the current is proportional to M.

In order to compute ΔC we multiply Eq. (4.11) by $\mathbf{v}_0$ and T_0 respectively, integrate over all space, and add. By virtue of the orthogonality condition (2.10) we have

$$\Delta C + M^2 C_0(0)\theta_0 + M\int[\mathbf{j}\times\beta]\,\mathbf{v}_0 dV = 0,$$
$$\Delta C - M^2 C_0(0)\theta_0 = 0,$$

whence

$$\Delta C = \tfrac{1}{2} M \int \mathbf{j}[\mathbf{v}_0\times\beta]\,dV. \qquad (4.13)$$

It follows from the last equation of (4.11) that

$$\tfrac{1}{2}\int \mathbf{j}[\mathbf{j}+\nabla\varphi]\,dV = \tfrac{1}{2}\int j^2 dV - \tfrac{1}{2}\int\varphi\,\mathrm{div}\,\mathbf{j}\,dV,$$

i.e.,

$$\Delta C = \tfrac{1}{2}\int j^2 dV. \qquad (4.14)$$

The current in this expression is computed from the velocity $\mathbf{v}_0$, normalized in accordance with Eq. (2.10). Thus, $\Delta C \sim M^2$.

If we return to the conventional units, in accordance with Eqs. (1.8) and (2.10)

$$\Delta C/C_0(0) = \tfrac{1}{2}\int (j^2/\sigma)\,dV \Big/ \int \nu\rho\,(\mathrm{curl}\,\mathbf{v})^2 dV, \qquad (4.15)$$

so that the change in the critical Rayleigh number in the magnetic field is determined by the ratio of the Joule heat to the viscous dissipation.

The function $C_0(M)$, which is positive for M = 0, first increases as M^2 and then continues to increase monotonically, so that

$$dC_0(M)/dM < C_0(M)/M. \qquad (4.16)$$

The inequality given here cannot become an equality as this would mean that the curl of the velocity vanishes everywhere, (zero velocity everywhere), which cannot be the case. Consequently, the curve $C_0(M)$ at each point intersects a line drawn to this point from the origin of coordinates and cannot touch this line at any other point. When $M \to \infty$ the quantity C_0 cannot increase faster than M but may also approach a constant. This follows from the simple example of convection between two parallel vertical planes.[5] When the external magnetic field is vertical it has no effect on the zeroth critical perturbation, for which the velocity is also vertical, and the critical value C_0 is independent of M. In the case of a horizontal field, however,

$$C_0(M) = \pi^2[1 + M^2/\pi^2]^{1/2},$$
$$C_0(M) \sim \pi M \text{ for } M \to \infty.$$

*This calculation has been carried out by S. V. Ust'-Kachkintseva at the Perm University.

[1] L. Hartmann, Kg. Danske Videnskab. Selskab, Mat.-fys. Medd. **15**, No. 6 (1937).

[2] S. Chandrasekhar, Phil. Mag. **43**, 501 (1952).

[3] A. G. Smirnov, Dokl. Akad. Nauk SSSR **115**, 2, 284 (1957).

[4] E. P. Velikhov, JETP **36**, 1192, 1398 (1959), Soviet Phys. JETP **9**, 848, 995 (1959).

[5] S. A. Regirer, JETP **37**, 212 (1959), Soviet Phys. JETP **10**, 149 (1960).

[6] V. S. Sorokin, Прикладная математика и механика (Applied Math. and Mechanics) **17**, 39 (1953).

[7] L. D. Landau and E. M. Lifshitz, Механика сплошных сред (Mechanics of Continuous Media) Gostekhizdat, M. 1953.

Translated by H. Lashinsky
115

CIRCULAR POLARIZATION OF GAMMA QUANTA ACCOMPANYING NUCLEAR CAPTURE OF SLOW NEUTRONS

D. P. GRECHUKHIN

Moscow State Pedagogical Institute

Submitted to JETP editor February 16, 1959; resubmitted October 8, 1959

J. Exptl. Theoret. Phys. (U.S.S.R.) **38**, 621-630 (February, 1960)

An estimate is made of the order of magnitude of the circular polarization and the anisotropy of the angular distribution of the cascade quanta emitted by a previously polarized compound nucleus. From a determination of the sign of the mean circular polarization for the cascade it is possible to establish the spin of the original state of the compound nucleus, and a study of the spectral distribution of the polarization and the anisotropy of the angular distribution of the quanta can provide information about the way in which the level density of the compound nucleus depends on the spin.

INTRODUCTION

UPON capturing a neutron, the nucleus emits a number of quanta in the process of transition to the ground state. Spectra of the capture γ quanta have recently been studied intensively by Groshev's group[1] and the following relationships have been established: (1) In the region of atomic number $A < 100$, and in the neighborhood of the magic-number nuclei, the capture γ spectra possess a line structure, each isotope having individual peculiarities in the distribution of the lines over the energy interval; (2) In the region $100 < A < 200$, i.e., sufficiently far away from the magic numbers, the spectrum of the n-capture quanta appears to be continuous (or unresolved) with superimposed individual intense lines whose contribution, however, is small compared with that of the continuum.

In the case of the discrete spectra, the problem of studying the nuclear level structure reduces to an investigation of the characteristic lines of the spectrum of each isotope.

Experience has shown that the continuous spectrum of a heavy nucleus, $100 < A < 200$, has a number of properties that are typical of the entire interval of A:

1. The distribution of quanta, $\hbar\omega\nu(\hbar\omega)$, where $\nu(\hbar\omega)$ is the number of quanta with energy $\hbar\omega$, is bell-shaped with parameters varying little from one isotope to its neighbor. The maximum of the distribution occurs in the interval $\hbar\omega \simeq 1.5$ to 2.5 Mev.[1]

2. On the average, $\overline{N} \approx 4 \pm 1$ quanta with energies $\hbar\omega \geq 0.3$ Mev and approximately one quantum with an energy $\hbar\omega < 0.3$ are emitted in a cascade.[1]

3. The mean radiation width for n capture in this region of A varies little over the entire interval from A = 100 to 200.[2]

From the general properties of the n-capture process enumerated above, it can be assumed that within the given range of A the spectra of n-capture quanta can be described by the simple statistical model used in a number of papers[2-4] to calculate the mean radiation widths of neutron resonances. In this model the spectrum $\nu(\hbar\omega)$ is determined by the density of nuclear levels $\rho(\epsilon)$ and on the dependence $W_L(\hbar\omega)$ of the emission probability for a quantum of multipolarity L upon the energy of the quantum. It is usually assumed that all the quanta have the same multipolarity.

The shape of the spectrum $\nu(\hbar\omega)$ of the n-capture quanta for the statistical model was first studied by Nosov and Strutinskiĭ, and the results of their calculations are recorded in a review paper by Groshev.[1] In that paper the form

$$W_L(\hbar\omega) = \text{const} \cdot (\hbar\omega)^{2L+1}$$

is used for the emission probability of a quantum with momentum L and energy $\hbar\omega$, and the nuclear level density $\rho(\epsilon)$ is found in the usual way from the entropy S and the temperature T corresponding to the given excitation energy ϵ of the nucleus:

$$\rho(\varepsilon) = e^{S(T)}/\Delta\varepsilon; \quad T = d\varepsilon/dS,$$

while for the nuclear specific heat $C(T) = d\epsilon/dT$ a power-law dependence $C(T) = aT^{\lambda}$ is assumed.

It has been shown that the observed shape of the spectrum $\nu(\hbar\omega)$ can be explained within the framework of the statistical theory of cascades,

and according to Groshev[1] the best agreement with experiment is attained when $L = 1$ and $\lambda = 1$. In particular, for the probability of emission of N quanta in cascade[1] we have

$$W(N) = \sqrt{(L+1)/2\pi\bar{N}}\exp[-(L+1)(N-\bar{N})^2/2\bar{N}].$$

Comparison of the calculated spectrum with the experimentally observed spectrum $\nu(\hbar\omega)$ permits the parameters a and λ of the nuclear level density $\rho(\epsilon)$ to be determined. However, $\nu(\hbar\omega)$ contains no information on the density $\rho_I(\epsilon)$ of nuclear levels with a particular spin I. Information about $\rho_I(\epsilon)$ can be obtained from data on the angular characteristics of the cascade quanta emitted from a previously polarized compound nucleus, such as: (1) the circular polarization $e(\hbar\omega, \theta)$ of the cascade γ quanta; (2) the angular distribution $F(\hbar\omega, \theta)$ of the cascade γ quanta with respect to the spin orientation direction of the compound nucleus in its initial state, I_0; (3) the residual spin polarization of the compound nucleus in one of the final states taken up by the nucleus after the emission of a cascade of γ quanta; (4) the angular correlation $W_{12}(\theta_{12})$ of any pair of quanta emitted successively in a cascade sequence.

It should be mentioned here that a beam of polarized neutrons and an unpolarized target are sufficient for a study of the circular polarization $e_{I_0}(\hbar\omega, \theta)$ of cascade quanta and the residual spin polarization of the compound nucleus, whereas the investigation of the angular distribution $F_{I_0}(\hbar\omega, \theta)$ of the quanta requires a polarized target.

For the study of the angular correlation between cascade quanta, neither a polarized beam nor a polarized target are required. However, as a result of the averaging of the anisotropy over all the cascade quanta, the angular correlation turns out to be beyond the limits of experiment. To illustrate the relationships of the quantities $e_{I_0}(\theta)$, $F_{I_0}(\theta)$, and $W_{12}(\theta_{12})$, let us consider the simple case of a four-quantum cascade $I_0 \to I_1 \to I_2 \to I_3 \to I_4$ with the fixed values $I_0 = 4$ and $I_4 = 1$. The spins I_1, I_2, and I_3 take on all possible values with equal probability. We shall assume that all the quanta of the cascade are dipole quanta ($L = 1$). In this case there are four distinct cascade chains, 16 quanta are emitted, and a correlation is possible between 24 pairs of quanta. A simple calculation leads to the following values for the quantities $e_{I_0}(\theta)$, $F_{I_0}(\theta)$, and $W_{12}(\theta_{12})$:

$$e_{I_0}(\theta) = 1.34\,\zeta_1(I_0)\cos\theta/(1 + 0.27\zeta_2(I_0)P_2(\cos\theta)),$$
$$F_{I_0}(\theta) = 1 + 0.27\,\zeta_2(I_0)P_2(\cos\theta),$$
$$W_{12}(\theta_{12}) = 1 - 0.025\,P_2(\cos\theta_{12}).$$

Here $\zeta_\kappa(I_0) = \sum_{\mu_0} f_{\mu_0} C^{I_0\mu_0}_{I_0\mu_0\kappa_0}$, where f_{μ_0} is the distribution of the compound nucleus in its initial state according to magnetic quantum number ($\sum_{\mu_0} f_{\mu_0} = 1$), and $C^{a\alpha}_{b\beta c\gamma}$ is a Clebsch-Gordan series coefficient.

If the polarization I_0 of the nuclear spin is accomplished by the capture of a polarized neutron by an unpolarized target nucleus with a spin of $J = 7/2$, then $\zeta_2(I_0) = 0$, and $\zeta_1(I_0) = 3\sqrt{5}\,\eta_n/32$ (η_n being the degree of polarization of the neutron). In this case $e(\theta) = 0.45\,\eta_n \cos\theta$. Thus in this example $e_{I_0}(\theta)$ is approximately twenty times larger than the anisotropy $W_{12}(\theta_{12})$; when the average is taken over a large number of different chains, the ratio will increase even more.

The quantities $e_{I_0}(\hbar\omega, \theta)$ and $F_{I_0}(\hbar\omega, \theta)$ will henceforth be considered only for odd target nuclei, so that the compound nucleus will be even-even. The results of the calculation given below depend in a fundamental way on the cascade scheme which is assumed, and numerical values for $e_{I_0}(\theta)$ and $F_{I_0}(\theta)$ can be obtained only for specific models of the distribution $\rho_I(\epsilon)$. Consequently the calculation is of the nature of a guess at the scale of the quantities e_{I_0} and F_{I_0} from a model.

In what follows we shall make use of the following γ-cascade scheme for an even-even compound nucleus (Fig. 1). Upon resonance capture of a neutron by the target nucleus, the compound nucleus (by the emission of N quanta) drops into one of the levels in an interval of width Δ lying just above the energy gap of the nuclear spectrum (the gap width being 2Δ).

The subsequent transition from this interval to one of the states close to the ground state occurs by the emission of a characteristic quantum which appears as an individual intense line in the spectrum $\nu(\hbar\omega)$.

In the interval Δ above the gap of 2Δ, the density of nuclear levels is relatively low, and the γ transitions between levels in this interval depend on the structural peculiarities of the given nucleus. In this case there may be a violation of the basic assumption of a statistical model for the cascade, which has been assumed to be valid for all the γ transitions, in the neighborhood of the spectral region indicated above. In order to exclude these transitions, it is necessary to limit the continuous spectrum to the portion $\hbar\omega > \Delta$ and to ignore the characteristic lines of the spectrum.

For the cascade scheme chosen above, the final state of the nucleus after the emission of N quanta is not the ground state, but one of the states in the

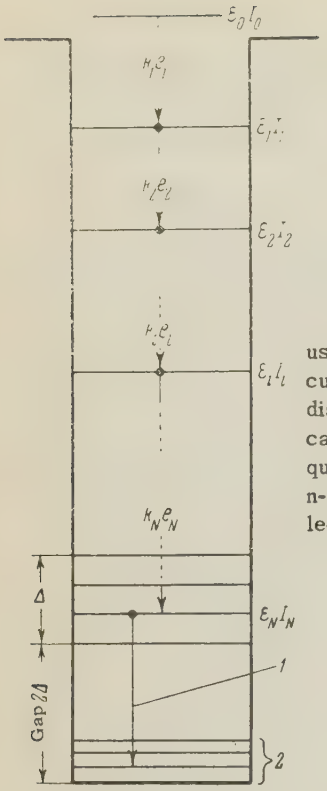

FIG. 1. The cascade scheme used in the estimation of the circular polarization and angular distribution of quanta from (nγ) capture. 1 is the characteristic quantum in the γ spectrum of the n-capture; 2 represents the collective excitation of the nucleus.

interval Δ above the gap. Similarly, the nuclear spin I_N after the cascade emission may take on any value which is permitted in that interval.

At the present time there is no evidence available about the energy dependence $\rho_I(\epsilon)$, either for the interval Δ above the gap or for the remaining portion of the nuclear spectrum. Therefore a calculation of the magnitudes of $e_{I_0}(\hbar\omega, \theta)$ and $F_{I_0}(\hbar\omega, \theta)$ can be made only for specific models of the distribution $\rho_I(\epsilon)$. We shall assume hereafter that the level density for a nucleus with a given spin I can be approximated in the factorable form $\rho_I(\epsilon) \approx \rho(I, \alpha)\rho(\epsilon)$, where $\rho(I, \alpha)$ does not depend on the nuclear excitation energy.

Numerical estimates have been made for two model distributions:

a) In the free nucleon Fermi-gas model, according to Bethe[5] we have for $\rho_I(\epsilon)$

$$\rho_I(\varepsilon) = \text{const} \cdot \rho(\varepsilon)(2I+1)\exp[-I(I+1)/\alpha^2].$$

Here $\alpha^2 = 2J_0\tau/\hbar^2$; $J_0 = \frac{2}{5}MAR_0^2$ is the moment of inertia of the nucleus considered as a solid body; and τ is the nuclear temperature in Mev corresponding to the nuclear excitation energy ϵ. In this model our assumption leads to a value of α^2 which depends weakly on ϵ, instead of being a constant. If the temperature of the initial nuclear state is $\tau = 0.5$ and $A = 150$, we obtain the value $\alpha = 10$, and so the numerical calculation below has been made for the interval $\alpha = 4$ to 10.

b) As a second example, consider $\rho_I(\epsilon)$ in the form

$$\rho_I(\varepsilon) = \text{const} \cdot \rho(\varepsilon)(2I+1)\exp\{-I(I+1)/\alpha^2\},$$

in the interval $\epsilon > 3\Delta$;

$$\rho_I(\varepsilon) = \begin{cases} \text{const} & \text{for } I_N \leqslant I_{N\,max} \\ 0 & \text{for } I_N > I_{N\,max} \end{cases}$$

in the interval $3\Delta > \epsilon > 2\Delta$. Let us assume in addition that the probability of a radiative transition between two levels $I_i \to I_{i+1}$, averaged over the group of nuclear levels with moments I_i and I_{i+1}, may be expressed in the form

$$W_{LI_iI_{i+1}}(\hbar\omega) = W_L(\varepsilon_i, \varepsilon_{i+1}, \hbar\omega)\,\mathfrak{M}_L(I_i\ I_{i+1}),$$

where the factor $\mathfrak{M}_L(I_iI_{i+1})$ does not depend on the excitation energy of the nucleus. In calculations of the radiation widths of neutron resonances (references 2 – 4 and 1) it is assumed that $\mathfrak{M}_L = 1$ and $W_L = \text{const} \cdot (\hbar\omega)^{2L+1}$. As in reference 1, we consider a pure L-cascade, and numerical estimates of $e_{I_0}(\theta)$ and $F_{I_0}(\theta)$ have been made below only for $L = 1$ (M1 and E1 cascades) with spectra $\rho_I(\epsilon)$ of types a and b.

1. RELATIVE PROBABILITY OF AN N-QUANTUM CHAIN

Suppose that, as a result of neutron capture by a target nucleus with spin J, a compound nucleus has been formed in a state with momentum I_0 and energy ϵ_0. The spin I_0 is so oriented in space that the probability of its projection μ_0 on some direction singled out by the experimental conditions is equal to f_{μ_0}; $\sum_{\mu_0} f_{\mu_0} = 1$.

During the emission of N quanta the nucleus passes successively through N – 1 intermediate states with energies ϵ_i and spins I_i and μ_i (i = 1, . . . , N – 1), and appears in one of the states ϵ_N, I_N, μ_N in the interval Δ of the nuclear spectrum above the gap. Let us find the relative probability of emission of a chain of N quanta, in which the nucleus passes through a definite sequence of states $I_0 \to I_1 \to \ldots I_i \to \ldots I_N$. Let us also fix the wave vector k_i and polarization e_i of each quantum. For brevity we shall denote the chain of nuclear states by $I_0 \to c \to I_N$.

For the probability of the nuclear transition

$$\varepsilon_{i-1},\ I_{i-1},\ \mu_{i-1} \xrightarrow{L,\ k_i,\ e_i} \varepsilon_i,\ I_i,\ \mu_i$$

with the emission of a quantum $\hbar\omega_i$ in the direction $n_i = k_i/k_i$ we have:

$$W^{I_{i-1}I_iL}_{\mu_{i-1}\mu_i}(\hbar\omega_i \mathbf{n}_i e_i) = W_{LI_{i-1}I_i}(\hbar\omega_i)\, S_{\mu_{i-1}\mu_i}(\mathbf{n}_i e_i),$$

$$S_{\mu_{i-1}}(\mathbf{n}_i e_i) = 0.5 \left| C^{L+\Lambda_i 0}_{1-1L1} \right|^{-2} \left| \sum_{M_i} C^{I_{i-1}\mu_{i-1}}_{I_i \mu_i LM_i} (\mathbf{e}_i Y^{\Lambda_i}_{LM_i}(\mathbf{n}_i)) \right|^2,$$

$$\sum_{\mu_i e_i} \int d\Omega_i S_{\mu_{i-1}\mu_i}(\mathbf{n}_i e_i) = 1.$$

Let us now proceed to the relative probability of the γ transition

$$\gamma_{I_{i-1}I_i;\,\mu_{i-1}\mu_i}(\hbar\omega_i, \mathbf{n}_i, e_i) = \gamma_{I_{i-1}I_iL}(\hbar\omega_i)\, S_{\mu_{i-1}\mu_i}(\mathbf{n}_i, e_i),$$

where

$$\gamma_{I_{i-1}I_iL}(\hbar\omega_i) = \frac{W_{LI_{i-1}I_i}(\hbar\omega_i)}{\sum_{I_i} \int_0^{\varepsilon_{i-1}} W_{LI_{i-1}I_i}(\hbar\omega_i)\, \rho_{I_i}(\varepsilon_i)\, d\hbar\omega_i};$$

and for the relative probability of the emission of N quanta we find, in the cascade $(I_0, \mu_0, k_1, e_1) \rightarrow \ldots (I_i, \mu_i, k_i, e_i) \ldots \rightarrow (I_N, \mu_N, k_N, e_N)$:

$$P_N = \Big(\prod_{i=1}^{N} \gamma_{I_{i-1}I_iL}(\hbar\omega_i)\Big)\Big(\prod_{i=1}^{N} S_{\mu_{i-1}\mu_i}(\mathbf{n}_i, e_i)\Big).$$

Experimentally, the detector determines the quantum energy $\hbar\omega$, the direction of travel of the quantum $\mathbf{n}$ with respect to the direction of the nuclear spin polarization $\mathbf{I}_0$, and the circular polarization e of the quantum, but not the position of the quantum emission in the sequence, or the form of the cascade chain.

We shall therefore find the relative probability of emission of a quantum with energy $\hbar\omega$ and $\mathbf{n}$ and e at any position in the cascade chain $I_0 - c - I_N$

$$P_{I_0cI_N}(\hbar\omega; \mathbf{n}, e) = \sum_{i=1}^{N} \Big\{ \int\cdots\int_N \delta(\hbar\omega - \hbar\omega_j) \times \prod_{i=1}^{N} d(\hbar\omega_i)\, \gamma_{I_{i-1}I_iL}(\hbar\omega_i)\, \rho_{Ii}(\varepsilon_i)\, \delta\Big(E_{0N} - \sum_{i=1}^{N} \hbar\omega_i\Big)\Big\} \times \Big\{ \sum_{\mu_0} f_{\mu_0} \sum_{e_i \mu_i} \delta_{ee_j} \int\cdots\int_N \delta(\mathbf{n} - \mathbf{n}_j) \prod_{i=1}^{N} d\Omega_i\, S_{\mu_{i-1}\mu_i}(\mathbf{n}_i, e_i)\Big\},$$

where $E_{0N} = \epsilon_0 - \epsilon_N$ is the energy of the nuclear transition. Taking $\rho_{iI}(\epsilon_i) = \rho(I_i, \alpha)\rho(\epsilon_i)$ and $W_{LI_{i-1}I_i} = W_L \mathfrak{M}_L(I_{i-1}, I_i)$, we obtain for

$P_{I_0cI_N}(\hbar\omega; \mathbf{n}, e)$

$$P_{I_0cI_N}(\hbar\omega; \mathbf{n}, e) = \sum_{j=1}^{N} W_{jN}(\hbar\omega)\, G_{jI_0cI_N}(\mathbf{ne}) R_{I_0cI_N};$$

$$W_{jN}(\hbar\omega) = \int\cdots\int_N \delta(\hbar\omega - \hbar\omega_j)\, \delta\Big(E_{0N} - \sum_{i=1}^{N} \hbar\omega_i\Big) \times \prod_{i=1}^{N} d(\hbar\omega_i) \rho(\varepsilon_i)\, \gamma_L(\hbar\omega_i, \varepsilon_{i-1}, \varepsilon_i),$$

$$\gamma_L(\hbar\omega_i, \varepsilon_{i-1}, \varepsilon_i) = W_L(\hbar\omega_i, \varepsilon_{i-1}, \varepsilon_i) \Big/ \int_0^{\varepsilon_{i-1}} W_L(\hbar\omega_i, \varepsilon_{i-1}, \varepsilon_i) \rho(\varepsilon_i) d(\hbar\omega_i);$$

$$R_{I_0cI_N} = \prod_{i=1}^{N} \Big(\mathfrak{M}_L(I_{i-1}, I_i)\rho(I_i, \alpha) \Big/ \sum_{I_i} \mathfrak{M}_L(I_{i-1}, I_i)\rho(I_i, \alpha)\Big);$$

$$G_{jI_0cI_N}(\mathbf{ne}) = \sum_{\mu_0} f_{\mu_0} \sum_{\mu_i e_i} \delta_{ee_j} \int\cdots\int_N \delta(\mathbf{n} - \mathbf{n}_j) \prod_{i=1}^{N} d\Omega_i S_{\mu_{i-1}\mu_i}(\mathbf{n}_i e_i).$$

Here $W_{jN}(\hbar\omega)$ is the probability of emission of quanta with energies $\hbar\omega$ in the j-th position of an N-quantum chain, and $G_{jI_0cI_N}(\mathbf{ne})$ is proportional to the emission probability of quanta in the direction $\mathbf{n}$ with polarization e after $j-1$ quanta have already been emitted. These quantities have been considered in other specific applications by Dolginov.[6]

Considering the relationship

$$\left| C^{I_{j-1}\mu_{j-1}}_{I_j \mu_j LM_j} \right|^2 = \sum_{\varkappa} \frac{2\varkappa + 1}{2L + 1} U(\varkappa L I_{j-1} I_j;\, L I_{j-1})\, C^{I_{j-1}\mu_{j-1}}_{I_{j-1}\mu_{j-1}\varkappa 0} C^{LM_j}_{LM_j \varkappa 0},$$

we find for $G_{jI_0cI_N}(\mathbf{ne})$

$$G_{jI_0cI_N} = (8\pi)^{-1} \sum_{\varkappa} P_\varkappa(\theta)\,[2\varkappa + 1]\, C^{Le}_{Le\varkappa 0} \zeta_\varkappa(I_0) \Big(\prod_{i=1}^{j-1} U_i(\varkappa)\Big) U_j(\varkappa),$$

where $P_K(\theta)$ is the κ-th Legendre polynomial and θ is the angle between the vector $\mathbf{n}$ and the direction of polarization $\mathbf{I}_0$,

$$U_i(\varkappa) = U(L I_{i-1} I_i \varkappa;\; I_i I_{i-1});\; U_j(\varkappa) = U(\varkappa L I_{j-1} I_j;\; L I_{j-1}),$$
$$U(abcd;\; gf) = \sqrt{(2g+1)(2f+1)}\, W(abcd;\; gf),$$

where W(abcd; gf) is the Racah function (see references 7 and 8).

For $P_{I_0cI_N}(\hbar\omega; \mathbf{n}, e)$, using the expression already obtained for $G_{jI_0cI_N}$, we have

$$P_{I_0cI_N}(\hbar\omega;\; \mathbf{n}, e) = (8\pi)^{-1} \sum_{\varkappa} P_\varkappa(\theta)\,[2\varkappa + 1]\, C^{Le}_{Le\varkappa 0} \zeta_\varkappa(I_0) \times \Big[R_{I_0cI_N} \sum_{j=1}^{N} W_{jN} \Big(\prod_{i=1}^{j-1} U_i(\varkappa)\Big) U_j(\varkappa)\Big].$$

In order to obtain the probability of emission of a quantum $(\hbar\omega; \mathbf{n}, e)$ in a cascade, we sum $P_{I_0cI_N}$ over all the types of chains $I_0 \rightarrow c \rightarrow I_N$ and over all attainable values of I_N:

$$P_{I_0}(\hbar\omega;\; \mathbf{n}, e) = (8\pi)^{-1} \sum_{\varkappa} P_\varkappa(\theta)\,[2\varkappa + 1]\, C^{Le}_{Le\varkappa 0} \zeta_\varkappa(I_0)\,\{\varkappa\},$$

$$\{\varkappa\} = \sum_{N=1}^{\infty} \sum_{I_N} \sum_{j=1}^{N} \sum_{c} W_{jN}(\hbar\omega)\, R_{I_0cI_N} \Big[\Big(\prod_{i=1}^{j-1} u_i(\varkappa)\Big) U_j(\varkappa)\Big]_{cI_N}.$$

Hereafter we shall denote by $\{\kappa\}'$ the value of $\{\kappa\}$ for odd κ, and $\{\kappa\}''$ for even κ; the sum $\sum_K'$ is taken over odd κ and $\sum_K''$ over even κ. By definition, the polarization of a quantum is equal to

$$e_{I_0}(\hbar\omega;\; \theta) = [P_{I_0}(\mathbf{n},\; \hbar\omega,\; e = +1) - P_{I_0}(\mathbf{n},\; \hbar\omega;\; e = -1)] / [P_{I_0}(\mathbf{n}, \hbar\omega;\; e = +1) + P_{I_0}(\mathbf{n},\; \hbar\omega,\; e = -1)],$$

and the unnormalized angular distribution is

$$F_{I_0}(\hbar\omega,\; \theta) \propto \sum_{e=\pm 1} P_{I_0}(\mathbf{n},\; \hbar\omega;\; e).$$

Noting that $U_i(0) = 1$, $U_j(0) = 1$, $\sum_{cI_N} R_{I_0cI_N} = 1$, and $\{0\} = \sum_{N=1}^{\infty} \sum_{j=1}^{N} W_{jN}(\hbar\omega)$, we obtain for $e_{I_0}(\hbar\omega, \theta)$ and $F_{I_0}(\hbar\omega, \theta)$:

$$e_{I_0}(\hbar\omega, \theta) = \frac{\sum_{\varkappa=1}' P_\varkappa(\theta)[2\varkappa+1] C^{L1}_{L1\varkappa 0} \zeta_\varkappa(I_0)\{\varkappa\}'}{\sum_{\varkappa=0}'' P_\varkappa(\theta)[2\varkappa+1] C^{L1}_{L1\varkappa 0} \zeta_\varkappa(I_0)\{\varkappa\}''};$$

$$F_{I_0}(\hbar\omega, \theta) = \frac{1 + \sum_{\varkappa=2}'' P_\varkappa(\theta)[2\varkappa+1] C^{L1}_{L1\varkappa 0} \zeta_\varkappa(I_0)\{\varkappa\}''}{\sum_{N=1}^{\infty} \sum_{j=1}^{N} W_{jN}(\hbar\omega)}.$$

Computations have shown that, as a result of the summation over all the cascade chains with all attainable values of I_i, the values of $\{\kappa\}$ are found to become smaller as the value of κ grows larger. In particular, if $\{0\} = 1$, then $\{1\} \approx 0.1$, and $\{2\} \approx 0.01$. Therefore in the sums $e_{I_0}(\hbar\omega, \theta)$ and $F_{I_0}(\hbar\omega, \theta)$ it is sufficient to limit oneself to the first values, $\kappa = 0$, 1, and 2:

$$e_{I_0}(\hbar\omega, \theta) \approx P_1(\theta)\, 3C^{L1}_{L110}\, \zeta_1(I_0)\{1\} \Big/ \sum_{N=1}^{\infty} \sum_{j=1}^{N} W_{jN}(\hbar\omega);$$

$$F_{I_0}(\hbar\omega, \theta) = 1 + P_2(\theta)\, 5C^{L1}_{L120}\, \zeta_2(I_0)\{2\} \Big/ \sum_{N=1}^{\infty} \sum_{j=1}^{N} W_{jN}(\hbar\omega).$$

For the case of a dipole cascade $L = 1$ (an E1 or M1 cascade) this formula is exact.

2. THE AVERAGES $\bar{e}_{I_0}(\theta)$ AND $\bar{F}_{I_0}(\theta)$ TAKEN OVER THE CASCADE

The spectral distributions $e_{I_0}(\hbar\omega, \theta)$ and $F_{I_0}(\hbar\omega, \theta)$ depend on the value of $W_{jN}(\hbar\omega)$. This quantity depends on $\rho(\epsilon)$, and even for a relatively simple form of $\rho(\epsilon)$ the calculation of W_{jN} and $\sum_{j=1}^{N} W_{jN}$ entails great difficulties. We shall therefore consider the averages $\bar{e}_{I_0}(\theta)$ and $\bar{F}_{I_0}(\theta)$, taken over the spectrum, which are simpler for purposes of numerical estimation. Integrating $P_{I_0cI_N}(\hbar\omega, ne)$ with respect to the quantum energy $\hbar\omega$ between the limits $\hbar\omega_{min} = \Delta$ and $\hbar\omega_{max} = \epsilon_0 - 2\Delta$, we obtain

$$\bar{P}_{I_0cI_N}(ne) \approx (8\pi)^{-1} \sum_{\varkappa} P_\varkappa(\theta)[2\varkappa + 1] C^{Le}_{Le\varkappa 0} \zeta_\varkappa(I_0) \times \sum_{N=1}^{\infty} W_N \sum_{cI_N} R_{I_0cI_N} \Big[\sum_{j=1}^{N} \Big(\prod_{i=1}^{j-1} U_i(\varkappa)\Big) U_j(\varkappa)\Big]_{cI_N}.$$

Here we have taken

$$\int_{\Delta}^{\epsilon_0 - 2\Delta} W_{jN}(\hbar\omega)\, d(\hbar\omega) \approx W_N,$$

since for chains with $N \le 5$ the probability of emitting a single soft quantum is relatively small, and the contribution of chains with $N > 5$ is negligible.[1]

Taking into account the fact that, for $\kappa = 0$,

$$\sum_{j=1}^{N} \Big(\prod_{i=1}^{j-1} U_i(\varkappa)\Big) U_j(\varkappa) = N$$

and introducing

$$Q_N(\varkappa) = \sum_{I_N} \sum_{c} \mathfrak{N}_{NI_0cI_N} R_{I_0cI_N},$$

$$\mathfrak{N}_{NI_0cI_N} = N^{-1} \sum_{j=1}^{N} \Big(\prod_{i=1}^{j-1} U_i(\varkappa)\Big) U_j(\varkappa),$$

we find for the polarization and angular distribution

$$\bar{e}_{I_0}(\theta) \approx 3P_1(\theta) C^{L1}_{L110} \zeta_1(I_0) \sum_{N=1}^{\infty} N W_N Q_N(1) \Big/ \sum_{N=1}^{\infty} N W_N,$$

$$\bar{F}_{I_0}(\theta) \approx 1 + 5P_2(\theta) C^{L1}_{L120} \zeta_2(I_0) \sum_{N=1}^{\infty} N W_N Q_N(2) \Big/ \sum_{N=1}^{\infty} N W_N$$

or

$$\bar{e}_{I_0}(\theta) \approx \cos\theta\, A\zeta_1(I_0), \quad \bar{F}_{I_0}(\theta) \approx 1 + P_2(\theta) B\zeta_2(I_0).$$

The value of W_N has been estimated in a study by Nosov and Strutinskiĭ. In particular, for $L = 1$, according to Groshev et al.[1], $W_N = \text{const} \times \exp\{-2(N - \bar{N})^2/\bar{N}\}$. If we make use of the experimental value $\bar{N} \approx 3.5$, we obtain the following values for W_N:

$N =$	1	2	3	4	5	6
$W_N/\text{const} =$	0.05	0.28	0.87	0.87	0.28	0.027

Although Strutinskiĭ and Nosov obtained W_N with a particular model for the level density $\rho(\epsilon)$, it is evident that the distribution of W_N cannot be seriously altered by the use of other models for $\rho(\epsilon)$ which approximate the observed spectrum of nuclear levels. From the values of W_N given above, it can be seen that essentially it is only necessary to take into account chains having $N = 2$, 3, 4, and 5 quanta.

In order to get some idea of the order of magnitude of $e_{I_0}(\theta)$ and $F_{I_0}(\theta)$, and of the sensitivity of $e_{I_0}(\theta)$ and $F_{I_0}(\theta)$ to changes in the parameter α in the spectrum $\rho(I, \alpha)$, a calculation was made of the mean values $\bar{e}_{I_0}$ and $\bar{F}_{I_0}$ for a dipolar cascade of quanta ejected from a nucleus with initial spin $I_0 = 4$ and $I_0 = 3$. The calculations were made for the two models of the distribution $\rho(I, \alpha)$ discussed above — the spectra of types a and b. The results are shown in Tables I and II, where the values of the coefficients A and B for the quantum polarization and the angular distribution are given. Of particular interest is the estimate of the mean polarization of the

TABLE I. The coefficients A and B for $I_0 = 4$, for spectra of types a and b

α	4	6	8	10	∞	ρ_I = const*
A_a	0.49	0.23	0.13	0.09	0	0.215
A_b	0.38	0.23	0.15	0.12	0.05	0.215
B_a	0.046	—	0.014	—	0	0.033

*In this column, for comparison, are given the values of the A and B coefficients for the case where the nuclear level spectrum does not depend on I: $\rho_I(\varepsilon) = \rho(\varepsilon)$.

quanta in a cascade following the capture of a polarized neutron by an unpolarized target nucleus with spin J (we denote the degree of polarization

TABLE II. The A coefficients for $I_0 = 3$, for spectra of types a and b

α	4	6	8	10	∞
A_a	0.40	0.17	0.115	0.075	0
A_b	0.37	0.195	0.15	0.12	0.07

of the neutron by η_n). In this case $\zeta_0(I_0) \equiv 1$; $\zeta_2(I_0) \equiv 0$, and for $\zeta_1(I_0)$ we have

$$\zeta_1(I_0) = \eta_n \frac{(2I_0+1)}{6(2J+1)} \sqrt{(2J+3)/(2J+1)} \text{ for } I_0 = J + 1/2;$$

$$\zeta_1(I_0) = -\eta_n \frac{(2I_0+1)}{6(2J+1)} \sqrt{(2J-1)/(2J+1)} \text{ for } I_0 = J - 1/2.$$

For the limiting quantum polarization with the given values of the parameter α we find ($\theta = 0°$)

$$\xi_{I_0}(\alpha) \equiv \bar{e}_{I_0}(\theta = 0^0)/\eta_N = 3C^{11}_{1110}(\zeta_1(I_0)/\eta_n) \sum_{N=1}^{\infty} NW_N Q_N(1) / \sum_{N=1}^{\infty} NW_N.$$

The results of the calculations for $\xi_{I_0}(\alpha)$ are shown in Fig. 2 for $J = 7/2$.

The estimates which have been made of angular distribution and circular polarization show that these values lie within experimentally attainable limits. An investigation of $e_{I_0}(\theta, \hbar\omega)$ and $F_{I_0}(\theta, \hbar\omega)$ could give information about the relationship $\rho_I(\epsilon)$. It is important to note that the sign of the mean polarization $\bar{e}_{I_0}$ makes it possible to establish the spin of the initial state of the compound nucleus I_0.

In conclusion, I offer my sincerest thanks to L. V. Groshev, V. V. Sklyarevskiĭ, B. A. Obinyakov, and B. T. Geĭlikman for their interest in the work, and to V. G. Nosov and V. M. Strutinskiĭ for the opportunity to become acquainted with the results of their preliminary calculations.

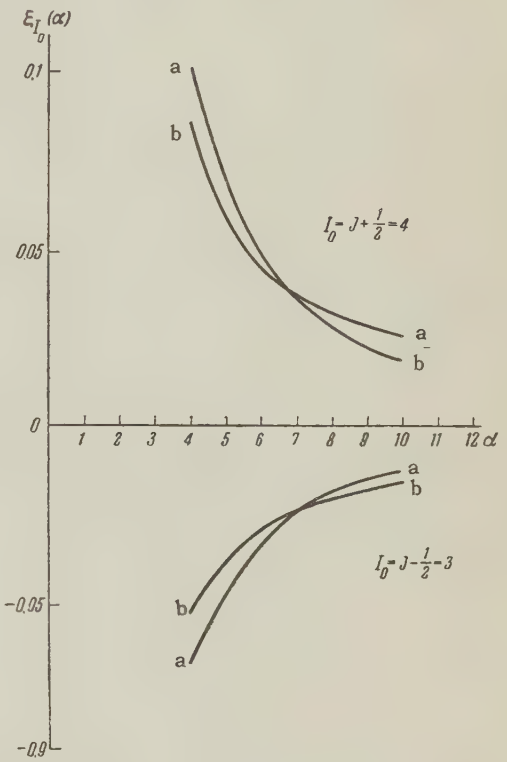

FIG. 2. Dependence of the limiting spectral-mean polarization of the cascade quanta on the parameter α, for nuclear spectra $\rho(I, \alpha)$ of the types a and b, for the case of capture of polarized neutrons by an unpolarized nucleus with spin J = 7/2. The upper curves correspond to an initial spin of $I_0 = J + 1/2 = 4$ for the compound nucleus; the lower curves to $I_0 = J - 1/2 = 3$.

[1] Groshev, Demidov, Lutsenko, and Pelekhov, Report on the Second International U. N. Conference on the Uses of Atomic Energy for Peaceful Purposes, Geneva, (1958). Groshev, Demidov, Lutsenko, and Pelekhov, Атлас спектров γ-лучей радиационного захвата тепловых нейтронов (Atlas of Gamma-Ray Spectra from the Radiative Capture of Thermal Neutrons) Moscow, 1958.

[2] A. Stolovy and I. A. Harvey, Phys. Rev. **108**, 353 (1957).

[3] A. G. W. Cameron, Can. J. Phys. **35**, 666 (1957).

[4] D. F. Newton, Can. J. Phys. **34**, 804 (1956).

[5] H. A. Bethe, Nuclear Physics, vol. II (Russ. Transl.), IIL, (1948).

[6] A. Z. Dolginov, JETP **34**, 931 (1958), Soviet Phys. JETP **7**, 644 (1958); Nucl. Phys. **5**, 512 (1958).

[7] M. E. Rose, Multipole Fields, Wiley, N. Y. 1955.

[8] H. A. Jahn, Proc. Roy. Soc. **A205**, 192 (1951).

Translated by D. C. West
116

Letters to the Editor

ANGULAR DISTRIBUTION OF NEUTRONS IN THE REACTION $C^{13}(d, n)N^{14}$

T. L. ABELISHVILI, T. G. GACHECHILADZE and O. M. MDIVANI

Tbilisi State University; Institute of Electronics, Automation, and Telemechanics, Academy of Sciences, Georgian S.S.R.

Submitted to JETP editor May 23, 1959

J. Exptl. Theoret. Phys. (U.S.S.R.) 38, 631-633 (February, 1960)

In the present note we give the results of a calculation of the angular distribution of neutrons in the reaction $C^{13}(d, n)N^{14}$, studied experimentally by Green, Scanlon, and Willmott[1] for an incident deuteron energy of 0.86 Mev. They managed to obtain four groups of neutrons with respect to energy (g_0, g_1, g_2, and g_3). The first group corresponds to the final N^{14} nucleus in its ground state, and the remainder to transitions to the first three excited states of the final nucleus.

As is well known, the differential cross section for the reaction, taking exchange effects into account, takes the form:[2]

$$\frac{d\sigma}{d\Omega} = c(E)\,|\,i^{l_1} G_D(K_1)\, j_{l_1}(k_1 R_1) - \frac{\Lambda_2}{\Lambda_1}(-1)^l i^{l_2} G_H(K_2)\, j_{l_2}(k_2 R_2)|^2.$$

Here l_1 and l_2 are the angular momenta of the absorbed particles corresponding to normal and "heavy particle" stripping; l describes the relative orbital angular momentum of the odd neutron in the target nucleus; R_1 and R_2 are characteristic interaction radii; Λ_2/Λ_1 is the ratio of the reduced widths; j_l are the spherical Bessel functions of order l;

$$G_i \approx 2\sqrt{2\pi\alpha_i}/(\alpha_i^2 + K_i^2) \quad (i = D, H),$$

$$K_1^2 = k_n^2 + \tfrac{1}{4}k_d^2 - k_n k_d \cos\vartheta,$$

$$k_1^2 = k_d^2 + (M_{12}/M_{14})^2 k_n^2 - 2(M_{12}/M_{14}) k_n k_d \cos\vartheta,$$

$$K_2^2 = k_n^2 + (M_n/M_{13})^2 k_d^2 + 2(M_n/M_{13}) k_n k_d \cos\vartheta,$$

$$k_2^2 = k_d^2 + (M_d/M_{14})^2 k_n^2 + 2(M_d/M_{14}) k_n k_d \cos\vartheta.$$

In these formulas k is the wave number, M the mass, and ϑ the scattering angle in the center-of-mass system.

Besides exchange effects, a significant part is played by the process of spin flip of the liberated nucleon.[3] Taking this effect into account both for normal and "heavy particle" stripping leads in our case to the formula

$$\frac{d\sigma_{D,H}}{d\Omega} = \frac{1}{4\pi^2\hbar^4}\frac{k_n}{k_d}\frac{M_n M_{14}}{M_n + M_{14}}\frac{M_d M_{13}}{M_d + M_{13}} \times \sum_{l,m}\left(\sum_{J,j}(2J+1)\left|\int \Psi^{M*}_{Jj_f^{1/2}} f_{D,H}(\sigma_n, \xi)\Psi^M_{Jjl}\, d\tau\right|^2\right) \times \frac{|\alpha_{D,H}(l,m)|^2}{2l+1},$$

where

$$\alpha_D(l,m) = \int \exp(-i\mathbf{k}_n\mathbf{r}_n)\,\delta(r_n - R_1) \times \exp\left\{\frac{i}{2}\mathbf{k}_d\left[\mathbf{r}_n + \mathbf{R}_1\frac{M_{13}+2M_n}{M_{13}+M_n}\right]\right\} \times \Phi_d\left(\left|\mathbf{R}_1\frac{M_{13}}{M_{13}+M_n} - \mathbf{r}_n\right|\right) Y_l^{m*}(\Omega_p)\, d\Omega_p d\mathbf{r}_n,$$

$$\alpha_H(l,m) = \int \exp(-i\mathbf{k}_n\mathbf{r}_n)\,\delta(r_n - R_2)\exp\left\{-\frac{i\mathbf{k}_d}{M_{13}}\left[M_n\mathbf{r}_n + M_{12}\left(1 + \frac{M_n}{M_d+M_{13}}\right)\mathbf{R}_2\right]\right\}\Phi_{C^{13}}\left(\left|\mathbf{R}_2\frac{M_d}{M_d+M_{12}} - \mathbf{r}_n\right|\right) \times Y_l^{m*}(\Omega)\, d\Omega d\mathbf{r}_n,$$

Φ_d and $\Phi_{C^{13}}$ are the internal functions of the deuteron and the odd neutron in C^{13}. For normal stripping $\mathbf{J} = \mathbf{j}_f + \vec{\tfrac{1}{2}}$, $\mathbf{j} = \mathbf{j}_i + \vec{1}$, and for "heavy particle" stripping $\mathbf{J} = \mathbf{j}_f + \vec{\tfrac{1}{2}}$, $\mathbf{j} = 1 + \vec{\tfrac{1}{2}}$. The subscripts D and H correspond to normal and "heavy particle" stripping.

The calculations show that: (1) the data corresponding to the transition to the ground state can be explained by assuming that the reaction is described by the theory of Butler with exchange effects taken into account (see Fig. 1); (2) that the

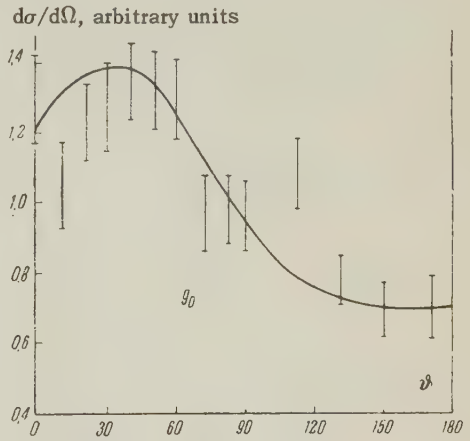

FIG. 1

data corresponding to the transition to the first two excited states is understood if we take the spin-flip process into account for both kinds of stripping without taking account of their interference, since the amplitudes for the two processes are in fact not separated (see Figs. 2 and 3); (3) in the case of a transition to the third excited state, the spin-flip process occurs only for the "heavy particle" stripping, with interference not taken into account (see Fig. 4).

Neutron group	Excitation energy, Mev	Spin of N^{14}	l_1	l_2	10^{13} R_1, cm	10^{13} R_2, cm	A_2/A_1
g_0	0.00	1^+	1	0	4.5	4.5	0.47
g_1	2.31	0^+	0	0	6.0	6.0	—
g_2	3.90	1^+	0	0	5.0	5.0	—
g_3	4.80	0^-,1^-	0	0	6.5	7.5	—

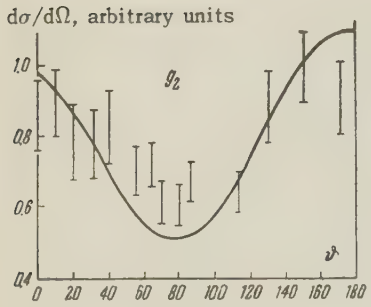

FIG. 2

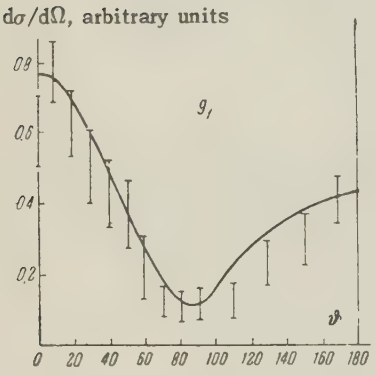

FIG. 3

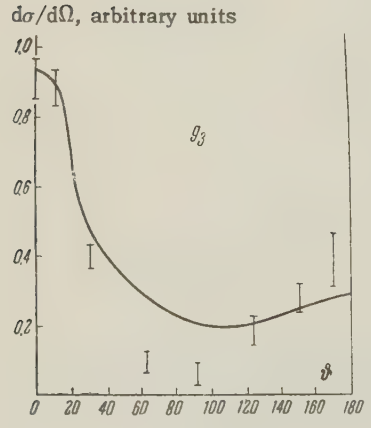

FIG. 4

The values of the parameters used for the calculation are given in the table; $\alpha_D = 0.23 \times 10^{13}$ cm^{-1}, $\alpha_H = 0.47 \times 10^{13}$ cm^{-1}.

[1] Green, Scanlon, and Willmott, Proc. Phys. Soc. A68, 386 (1955).

[2] G. Owen and L. Madansky, Phys. Rev. **105**, 1766 (1957).

[3] J. E. Bowcock, Phys. Rev. **112**, 923 (1958).

Translated by R. F. Peierls
117

POSSIBLE INFLUENCE OF NUCLEON STRUCTURE IN HIGH ENERGY INTERACTIONS

Zh. S. TAKIBAEV

Institute for Nuclear Physics, Academy of Sciences, Kazakh S.S.R.

Submitted to JETP editor July 7, 1959

J. Exptl. Theoret. Phys. (U.S.S.R.) **38**, 633-634 (February, 1960)

CLARIFICATION of the relation between the angular distribution of shower particles and their energy spectrum could provide a means to study the inner structure of the nucleon. In several instances it is more convenient to consider the distribution in the Lorentz-invariant transverse momenta instead of the energy spectrum.

In the majority of showers[1] the average value of the transverse component of the momentum amounts to $\sim (1-1.5)\, m_\pi c$, where m_π stands for the mass of the pion. In his papers[2] devoted to the problem of multiple production of mesons, Heisenberg observed that the average value of the transverse momentum of particles produced in the high energy region should be of just that order of magnitude.

If the primary particle is sufficiently energetic to penetrate inside the nucleon, then depending on the initial conditions of the interaction (i.e., depending on the values of the impact parameter), the production of heavier mesons, e.g., K mesons, is possible and this process probably occurs in a volume characterized by the dimension $\sim \hbar/m_K c$. Such a phenomenological treatment (a different approach is given by Jastrov[3]) is discussed in great detail from various points of view in a series of papers by Blokhintsev et al.[4]

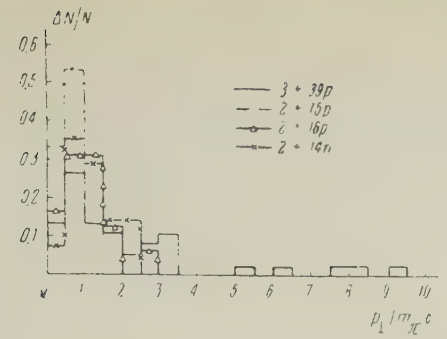

FIG. 1

It seems to us that a discussion of the interesting relation between the degree of anisotropy of shower particles and the character of the distribution of their transverse momenta is not without value. In Fig. 1 is shown the distribution in transverse momenta of particles produced in four showers: the showers 2+16p and 2+14n described by Edwards et al.,[1] the shower 2+15p described by Shein et al.,[5] and the shower 3+39p described by Debenedetti et al.[6] It is reasonably clear from this figure that the distribution of $p_\perp$ in the showers 2+16p, 2+14n and 3+39p corresponds to a significant number of particles with transverse momenta in excess of $m_\pi c$, whereas in the shower 2+15p the values of transverse momenta of the particles do not exceed $1.5\, m_\pi c$. When this fact is related to the character of the angular distributions of the indicated showers, them it becomes possible to reach an interesting conclusion. In Fig. 2 are shown integral angular distributions of

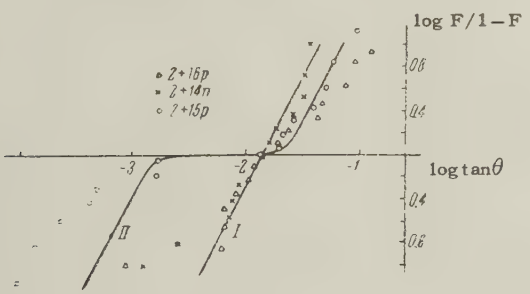

FIG. 2

the particles in the showers 2+16p, 2+14n, and 2+15p. The angular distribution of the particles in the shower 3+39p is nearly identical to that of the showers 2+16p and 2+14n. The straight line I corresponds to a particle distribution in the center of mass system that is isotropic in angle and monoenergetic, curve II corresponds to one anisotropic in angle (of the type $\cos^{2n}\theta^*$) and monoenergetic. We see upon comparison of the data shown in Figs. 1 and 2 that when the angular distribution is anisotropic the values of transverse momenta are essentially of order $m_\pi c$, whereas for a smaller degree of anisotropy (showers 2+16p, 2+14n, and 3+39p) values of transverse momenta in excess of $m_\pi c$ occur frequently. (Let us note that in the case of collisions between a nucleon and a complex nucleus large values of $p_\perp$ may appear as a consequence of scattering.) We propose that in the case of smaller anisotropy (which corresponds approximately to small values of the impact parameter) the production of heavier mesons is more probable, whereas in the case of a strongly anisotropic distribution (which corresponds to larger values of the impact parameter) essentially only π mesons are produced. From this point of view the relation between the degree of angular anisotropy and the character of distribution in transverse momenta of particles produced in the high energy region becomes comprehensible. At the present time we are engaged in an attempt to establish this relation between the degree of angular anisotropy and the distribution in transverse momenta for particles in showers produced by 10-Bev protons from the proton synchrotron of the Joint Institute for Nuclear Research.

[1] Edwards, Losty, Perkins, Pinkau, and Reynolds, Phil. Mag. **3**, 237 (1958). Zh. S. Takibaev, Тр. Института ядерной физики АН КазССР (Trans. Inst. Nuc. Phys. Acad. Sci. Kaz. S.S.R.) **1**, 1958.

[2] H. W. Heisenberg, Kosmische Strahlung, Springer, Berlin-Gottingen-Heidelberg, 1953.

[3] R. Jastrow, Phys. Rev. **81**, 165 (1951).

[4] Blokhintsev, Barashenkov, and Barbashov, Preprint, Joint Inst. Nuc. Res. P-317 (1959).

[5] Shein, Haskin, and Glasser, Nuovo cimento **12**, Suppl. No. 2, 355 (1954).

[6] Debenedetti, Garelli, Tallone, and Vigone, Nuovo cimento **4**, 1142 (1956).

Translated by A. M. Bincer
118

POLARIZATION OF HYDROGEN NUCLEI IN A FREE RADICAL

G. S. LOMKATSI

Submitted to JETP editor July 25, 1959

J. Exptl. Theoret. Phys. (U.S.S.R.) **38**, 635-636 (February, 1960)

BELJERS et al.[1] have shown that Overhauser's[2] method can be used to polarize hydrogen nuclei in the free radical of diphenyl picryl hydrazyl (DPPH).

When the $\Delta M = \pm 1$ and $\Delta m = 0$ transitions (where M and m are the projections of the electron and nuclear spins respectively in the direction

of the magnetic field) are saturated, on account of the electron-nucleus interaction, an increase occurs in the difference in population of the nuclear levels of hydrogen. When the quantity $2(\mu_n + s|\mu_e|)H/kT$ is small, it is easy to show that this difference increases by a factor of $(\mu_n+\mu_e)/\mu_n$ [μ_n and μ_e are the magnetic moments of the proton and electron respectively, and s is the coefficient of saturation of paramagnetic resonance (p.r.)].

We investigated the possibility of polarizing hydrogen nuclei in DPPH at liquid-helium temperatures. We cooled a sample of DPPH down to 4° K and then applied three mutually perpendicular magnetic fields to it: a constant field with $H \approx 3300$ oe, an ultrahigh-frequency (UHF) field of frequency $\nu_e = 9419$ Mcs for the purpose of saturating the p.r., and a high-frequency field with $\nu_n = 14$ Mcs for the purpose of observing the nuclear resonance (n.r.) of the protons.

The frequency and power of the UHF field remained constant in the course of the experiment. We plotted the dependence of the amplitude of the n.r. signal on the constant field. Theory leads one to expect that the n.r. signal will increase by a factor of $(\mu_n+s|\mu_e|)/\mu_n$ at a value of the field $H_0 = h\nu_e/2.003\mu_e$. However, the effect was not observed at the H_0 point. An increase of the n.r. signal was observed for the two values of the field, $H_0 \pm \Delta H$. We gave an incorrect interpretation of this phenomenon earlier.[3]

At the $H_0 + \Delta H$ point the polarity of the n.r. signal indicates that $n_+ > n_-$, while in the case of $H_0 - \Delta H$ we get $n_- > n_+$ (n_- and n_+ are the number of hydrogen nuclei with spins against and along the field respectively). The accompanying figure shows the dependence of the amplitude of the n.r. signal on the constant field.

Uebersfeld et al.[4] observed a similar effect in the case of protons in benzene absorbed by carbon. Abragam et al.[5] have explained this phenomenon.

The UHF field causes $\Delta M = \Delta m = \pm 1$ and $\Delta M = -\Delta M = \pm 1$ transitions. If the probabilities of such transitions are much greater than those of nuclear transitions due to other processes, we obtain in equilibrium

$$n_+/n_- = \exp\{\mp 2|\mu_e|H/kT\},$$

the plus sign in the exponent is taken in the first case. Correspondingly, the magnetic field will be $H = H_0(1 \pm \mu_n/\mu_e)$, which in our case will yield $H = (3360 \pm 5)$ oe. On this basis, when the frequency and power of the UHF field remain constant, one would expect the field dependence of the amplitude of the n.r. signal to have the shape of two Gaussian distributions with maxima of $\pm|\mu_e|/\mu_n$ situated at $H = (H_0 \pm 5)$ oe respectively and half-widths equal to the sum of the half-widths of the p.r. and n.r. lines. If the distributions are so wide that they overlap, these lines of opposite sign will interfere with each other.

We observed a strong temperature dependence of the p.r. line width. At 4° K the half-width of the p.r. line is ~ 40 oe, while that of the n.r. line is ~ 15 oe. We therefore observed the total picture.

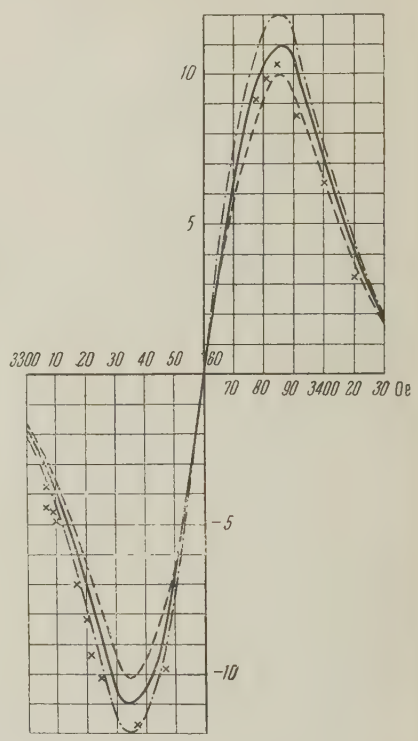

Dependence of the magnitude of the n.r. signal on the field at constant frequency and constant UHF power (the n.r. signal in the absence of the UHF field is taken as the unit of signal magnitude). The crosses designate the experimental points. The lines were obtained by a summation of Gaussian distributions with maxima taken to equal 42 units (solid line), 38 units (broken line), and 46 units (dot-dash line).

For the purpose of comparison with experiment, the figure shows the curves resulting from the summation of two Gaussian distributions of opposite sign with centers at $(H_0 \pm 5)$ oe and half-widths equal to 55 oe. The maximum was selected to obtain the best agreement with the experiment. As can be seen from the figure, it is possible to state, with an accuracy within 10%, that the n.r. signal should have increased by a factor of 42 instead of 660.

At fixed values of ν_e and H the amplitude of the n.r. signal versus the power of the UHF field is given by the following values:

UHF power, mw	0.26	0.85	1.6	18
amplitude of n.r. signal	7.3	10.7	11.1	13.7

From this it can be seen that we were close to saturation.

It is interesting to note that the unpaired electron of the DPPH molecule can cause the polarization of not only the protons of its own molecule but also those of distant molecules.

Before the experiment the sample was subjected to vacuum melting (1 to 0.1 mm Hg) and kept in

that condition for several hours. This led to a decrease in the number of unpaired electrons and a consequent increase in the number of protons per unpaired electron. The accompanying data correspond to a sample in which the number of protons per unpaired electron is of the order of 10^3. As the experiment shows, we had too weak a concentration of unpaired electrons.

Borghini and Abragam[6] have carried out similar experiments.

I wish to express my deep gratitude to S. Ya. Nikitin, G. R. Khutsishvili, V. T. Smolyankin, A. V. Lebedev, and V. Z. Kolganov for their valuable advice and unfailing interest in my work, to V. N. Latyaeva for preparing the DPPH, and to V. S. Zhurkov and M. A. Veselov for assistance with the experiments.

[1] Beljers, van der Kint, and van Weringen, Phys. Rev. **95**, 1683 (1954).

[2] A. W. Overhauser, Phys. Rev. **92**, 411 (1953).

[3] G. S. Lomkatsi, V Всесоюзное совещание по физике низких температур (Fifth All-Union Conference on Low Temperature Physics), Tbilisi, 1958

[4] Uebersfeld, Motchane, and Erb, J. phys. radium **19**, 848 (1958).

[5] A. Abragam and W. G. Proctor, Compt. rend. **246**, 2253 (1958).

[6] M. Borghini and A. Abragam, Compt. rend. **248**, 1803 (1959).

Translated by E. S. Gordon
119

MEASUREMENT OF THE LOGARITHMIC DAMPING DECREMENT OF A HOLLOW CYLINDER IN ROTATING HELIUM II

D. S. TSAKADZE and I. M. CHKHEIDZE

Tbilisi State University

Submitted to JETP editor September 25, 1959

J. Exptl. Theoret. Phys. (U.S.S.R.) **38**, 637-638 (February, 1960)

As is well known, the fundamentals of the theory of the rotation of a superfluid liquid have been set forth in the publications of Feynman, based on Onsager's concept of the existence in rotating helium II of vortex lines. According to these papers, the number of vortex lines grows as the rotational velocity increases, while each such line has a definite energy per unit length. Investigation of the properties of vortex lines in rotating helium II has been carried out both by the stack-of-disks method,[1-3] and by the method of a single disk oscillating about its axis, with the latter parallel to the vortex lines (references 4 and 5, as well as private communication by Hall).

In one of these papers[4] Andronikashvili and Tsakadze have shown that with increasing rotational velocity the logarithmic damping decrement of the disk passes through a maximum, which must be explained (cf. reference 6) by a corresponding change in the elastic-plastic properties of rotating helium II. In accordance with this hypothesis the superfluid component of helium II should, at small velocities of rotation, be regarded as a system of relatively few vortex lines not interacting among themselves, while at large velocities, these lines form a single elastic-plastic tangle. In the two cases, of both low and high velocities, the vortex lines may be considered to be bound at their ends, to a greater or lesser degree, to the surface of the oscillating disk. It was natural to assume that rotating helium II should show different viscous properties in experiments in which the surface of the solid body subjected to retardation moves perpendicular to the direction of the vortex lines and in which it moves parallel to them.

With the object of verifying this hypothesis, the single disk in the previously-described[4,5,7] apparatus was replaced by a hollow cylinder, machined from organic glass and having circular graduations ruled on its cylindrical surface to facilitate its immersion to various depths in the rotating helium II, suspended upside down on an elastic fiber. As in the work with the single disk, the hollow cylinder took part simultaneously in both rotational and oscillatory motion. The cylinder had a diameter of 24.06 mm, a height of 49.80 mm, and a thickness of 0.49 mm. The distance between the rulings was 5.0 mm. The number of rulings was 9. The outer container, which rotated uniformly together with the helium II with which it was filled, had a diameter of 44 mm and a height of 62 mm.

The solution of the hydrodynamic problem of a cylinder immersed in a rotating classical liquid and performing axial-rotational oscillations of small amplitude superimposed upon rotation leads to the formula

$$(\delta_2 - \delta_1)/(l_2 - l_1) = (2\pi^2 r^3/J)\sqrt{2\eta\rho/\Omega}, \quad (1)$$

where $\delta_1(\delta_2)$ is the logarithmic damping decrement for the oscillations of the cylinder when it is immersed in the liquid to a depth $l_1(l_2)$, r is the radius of the cylinder, η and ρ are the viscosity

and density of the liquid, J is the moment of inertia of the suspended system and Ω is the frequency of oscillations.

The experiments which we carried out with stationary helium II showed that the viscosity of helium II as determined with the aid of the hollow cylinder agrees with the viscosity measured formerly by É. L. Andronikashvili using the single-disk method.[8]

Experiments performed in water rotating uniformly within the limits $0 < \omega_0 < 100 \times 10^{-3}$ sec^{-1} led to values for the viscosity agreeing with tabulated data. These circumstances permitted us to apply the "inverted beaker" method to the measurement of the damping in rotating helium II when the surface subjected to drag is parallel to the vortex lines.

The hydrodynamic problem of the damping of the motion of a cylindrical surface placed within rotating helium II and performing uniform-rotational motion, on one hand, and harmonic axial-rotational oscillations, on the other, has been investigated by Mamaladze and Matinyan,[9] who obtained the equation

$$\frac{\delta_2 - \delta_1}{l_2 - l_1} = \frac{2\pi^2 r^3 \sqrt{2\eta\rho}}{J\sqrt{\Omega}} \left[1 + \frac{\rho_s B\omega_0}{2\rho\Omega}\right], \qquad (2)$$

where ρ_S is the density of the superfluid component, ω_0 is the rotational frequency and B is the mutual friction coefficient of Hall and Vinen.[10]

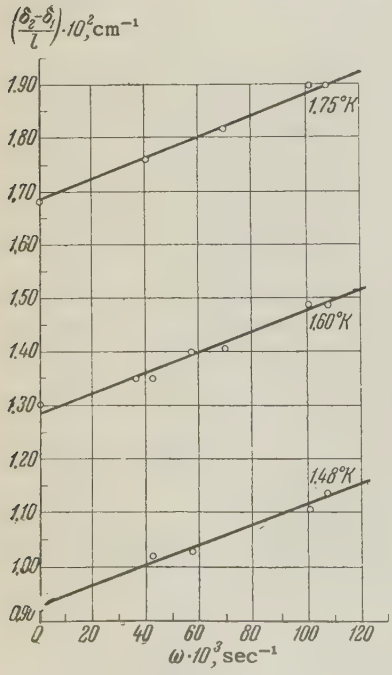

Dependence of the logarithmic damping decrement for a hollow cylinder immersed in helium II upon the rotational frequency. Curves taken for the case $l = l_2 - l_1 = 1$ cm.

The results of experiments carried out by us at three different temperatures agreed within the limits of experimental error with equation (2) over the whole range of velocities investigated. It is evident from the figure that the dependence found experimentally has a linear form, and that the characteristic maximum of the curve $\delta(\omega)$ found previously[5] in the case of the oscillating disk is absent.

We have thus shown that the viscous properties of rotating helium II do in fact depend upon the direction along which the damping is measured, not only in magnitude, but in their very character.

The authors take this opportunity to express their deep gratitude to É. L. Andronikashvili for his valued advice and constant interest in this work. The authors thank Yu. G. Mamaladze and S. G. Matinyan for their discussion of these results.

[1] D. S. Tsakadze, É. L. Andronikashvili, Сообщения АН Груз.ССР (Commun. Acad. Sci., Georgian S.S.R.) **20**, 677 (1958).

[2] H. E. Hall, Proc. V Internat. Conf. on Low Temperature Physics and Chemistry, 1958; p. 66.

[3] H. E. Hall, Proc. Roy. Soc. **A245**, 546 (1958).

[4] É. L. Andronikashvili and D. S. Tsakadze, JETP **37**, 322 (1959), Soviet Phys. JETP **10**, 227 (1960).

[5] É. L. Andronikashvili and D. S. Tsakadze, JETP **37**, 562 (1959), Soviet Phys. JETP **10**, 397 (1960).

[6] Andronikashvili, Tsakadze, Mamaladze, and Matinyan, Paper presented to the Fifth All-Union Conference on Low Temperature Physics, Tbilisi, 1958.

[7] Andronikashvili, Mamaladze, Tsakadze, Тр. Ин-та физики АН Груз.ССР (Trans. Inst. Phys. Acad. Sci. Georgian SSR) **7**, 1 (1959).

[8] É. L. Andronikashvili, JETP **18**, 429 (1948).

[9] Yu. G. Mamaladze and S. G. Matinyan, JETP, this issue, p. 656, Soviet Phys. JETP, this issue, p. 471.

[10] H. E. Hall and W. F. Vinen, Proc. Roy. Soc. **A238**, 215 (1956).

Translated by S. D. Elliott
120

THE SCHWINGER EFFECT WITH ACCOUNT OF THE SCREENING OF THE NUCLEUS BY THE ATOMIC ELECTRONS

V. M. KOPROV

Submitted to JETP editor September 27, 1959

J. Exptl. Theoret. Phys. (U.S.S.R.) 38, 639-641 (February, 1960)

AN important effect in the scattering of neutrons by heavy nuclei at small angles ($\theta \lesssim 10°$) is the interaction of the magnetic moment of the neutron with the electric field of the nucleus. This effect was first considered by Schwinger,[1] who found that the additional cross section for an unpolarized current, $\Delta\sigma(\theta)$, has, in first order perturbation theory, the form

$$\Delta\sigma(\theta) = \frac{\varepsilon^2}{16}\cot^2\frac{\theta}{2}, \quad \varepsilon = 2|\mu_n| Z \frac{e^2}{\hbar c}\frac{\hbar}{mc}, \tag{1}$$

where the zero order functions are taken to be those corresponding to the absence of the scattering center (first Born approximation). We note that this cross section is infinite at the origin. Later Sample[2] calculated $\Delta\sigma(\theta)$ using in zeroth approximation functions corresponding to the scattering from a hard sphere. Sample's cross section is also infinite at the origin and differs very little from that obtained by Schwinger. Both Schwinger and Sample used for the perturbing potential

$$V_1 = \varepsilon \mathbf{LS}/r^3. \tag{2}$$

Experimentally this effect was observed by Voss and Wilson[3] for U (energy ~ 100 Mev) and Aleksandrov and Bondarenko[4] for Pb (energy ~ 3 — 4 Mev). Later Aleksandrov[5] also measured this effect for Cu, Sn, Pb, Bi, U, and Pu at the energy ~ 2 Mev. According to references 4 and 5 the cross section increases as the angle becomes smaller in the region of small θ; this dependence is well described by formula (1) in the cases of Cu, Sn, Pb, and Bi. There is some disagreement for U and Pu, but even in these cases formula (1) does reproduce the general behavior of the cross section.

Owing to the screening of the nucleus by the atomic electrons the electric field of the atom is different from the Coulomb field. Let $\Phi(r)$ describe the screening of the potential U, i.e., $U(r) = (Ze/r)\Phi(r)$. Then $\mathbf{E}(r) = -(Ze/r^3) \times \alpha(r)\mathbf{r}$, where $\alpha(r) = \Phi(r) - r\Phi'(r)$, and

$$V_1 = \varepsilon\alpha(r)\mathbf{LS}/r^3. \tag{3}$$

For $\Phi(r) = 1$ formula (3) coincides with (2). If $\psi_l(r)$ are the zero order functions, i.e., solutions of the radial equation for the scattering from the unperturbed potential and δ_l the corresponding phases, the following formulas hold for the additional cross section in the first order of perturbation theory:

$$\Delta\sigma(\theta) = |a_1(\theta) + a_2(\theta)|^2,$$

$$a_1(\theta) = -\frac{\varepsilon}{4}\cot\frac{\theta}{2}\cdot K\int_0^\infty \Phi(r)\sin Kr\,dr,$$

$$a_2(\theta) = \frac{\varepsilon}{2}\sum_{l=1}^{\infty}(2l+1)\left[\int_0^\infty \frac{j_\nu^2(kr)}{r}\alpha(r)\,dr - e^{i2\delta_l}\right.$$
$$\left.\times\int_0^\infty \frac{[\psi_l(r)]^2}{r}\alpha(r)\,dr\right] P_l^{(1)}(\cos\theta), \tag{4}$$

where $K = 2k\sin(\theta/2)$, k is the wave number, and the $j_\nu = j_{l+1/2}$ are spherical Bessel functions. The ψ_l are normalized by the condition $\psi_l(r) \to \sin(kr - l\pi/2 + \delta_l)/kr$ for $r \to \infty$. It follows from these formulas that

$$\Delta\sigma(0) = 0. \tag{5}$$

The screening factor $\Phi(r)$ can be obtained from the statistical Thomas-Fermi model of the atom:

$$\Phi(r) = \varphi(x), \qquad x = r/\mu,$$
$$\mu = {}^1/_4\,(9\pi^2/2Z)^{1/3}\,(\hbar^2/4\pi^2 m_e e^2), \tag{6}$$

where φ is the solution of the Thomas-Fermi equation.[6]

For the calculation of $\Delta\sigma(\theta)$ according to formulas (4) and (6) with $Z = 92$ we used as the unperturbed potential

$$V_0(r) = -V_0(1 + i\zeta)/\{1 + \exp[(r - R)/a]\}$$

with $V_0 = 44$ Mev, $R = 7.72 \times 10^{-13}$ cm, $a = 0.5 \times 10^{-13}$ cm, $\zeta = 0.075$; the energy is 2.5 Mev. The contribution from the term $a_2(\theta)$ which is determined by the functions and phases of the zeroth approximation appeared to be negligible for $\theta \lesssim 10°$: $|a_2(\theta)| \ll |a_1(\theta)|$ for $\theta \lesssim 10°$. The screening changes the angular distribution considerably at very small angles. The behavior of the cross section for $\theta < 16'$ is shown in the figure. The relative magnitude of the correction to the screening,

$$\left[\Delta\sigma(\theta) - (\varepsilon^2/16)\cot^2\frac{\theta}{2}\right]/(\varepsilon^2/16)\cot^2\frac{\theta}{2}$$

is 2.6% for $\theta = 20'$. For larger angles it decreases as $\sin^{-3/2}(\theta/2)$. In the region of angles in which the measurements[4,5] were carried out the correction to the screening is somewhat smaller than the experimental error.

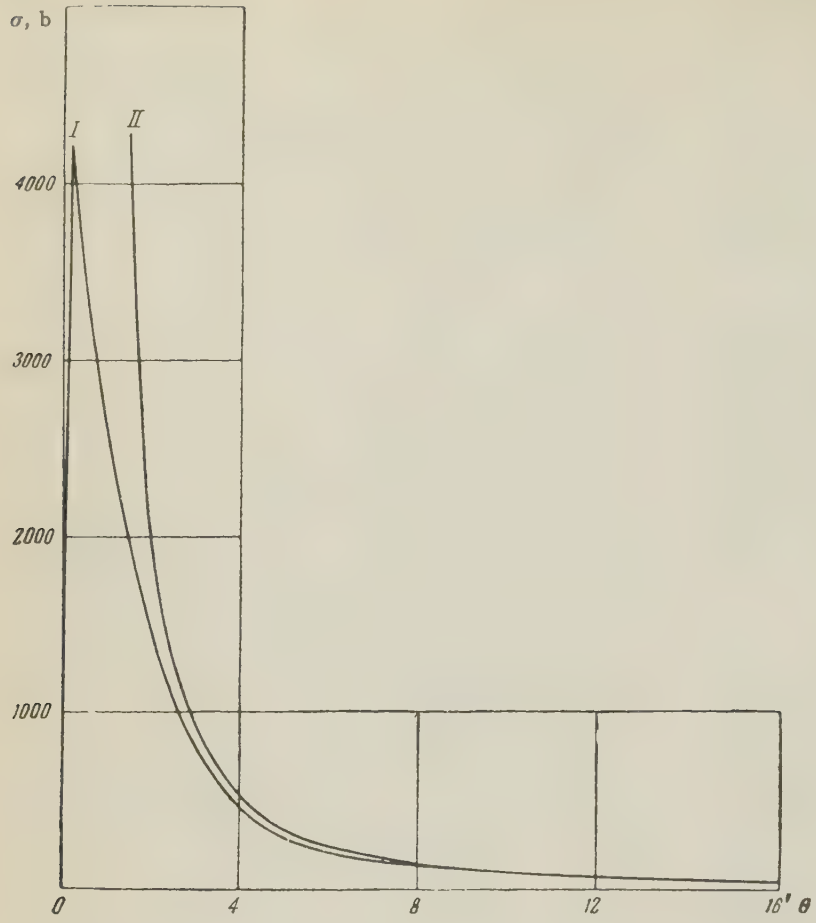

Curve I: cross section of Schwinger scattering with screening; curve II: the same cross section without screening.

[1] J. Schwinger, Phys. Rev. **73**, 407 (1948).
[2] J. T. Sample, Canad. J. Phys. **34**, 36 (1956).
[3] R. G. P. Voss and R. Wilson, Phil. Mag. **1**, 175 (1956).
[4] Yu. A. Aleksandrov and I. I. Bondarenko, JETP **31**, 726 (1956), Soviet Phys. JETP **4**, 612 (1957).
[5] Yu. A. Aleksandrov, JETP **33**, 294 (1957), Soviet Phys. JETP **6**, 228 (1958).
[6] P. Gombas, Die statistische Theorie des Atoms und ihre Anwendungen, Springer, Wien, 1949.

Translated by R. Lipperheide
121

INVESTIGATION OF BETA RADIATION OF Nb^{95} *AND* Ce^{144} *BY THE METHOD OF ABSORPTION IN AIR*

N. E. TSVETAEVA and L. A. ROZENFEL'D

Submitted to JETP editor September 29, 1959

J. Exptl. Theoret. Phys. (U.S.S.R.) **38**, 641-642 (February, 1960)

1. Beta radiation of Nb^{95}. A spectroscopic investigation of this radiation has been the subject of many papers. The values of the β radiation energy of Nb^{95}, obtained by different authors, range over sufficiently wide limits, 0.140 — 0.171 Mev, i.e., the outermost values differ by 20%.[1-4] These investigations were performed with spectrometers of different constructions.

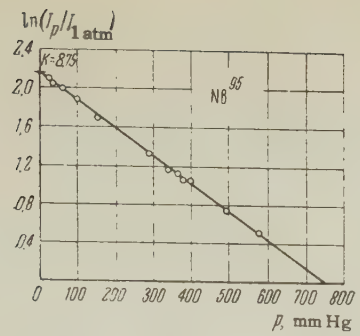

FIG. 1

We have investigated the β radiation of Nb^{95} by the previously described method of absorption in air.[5] The absorption curve of β radiation from Nb^{95} in air (Fig. 1) was obtained by varying the air pressure p between the BFL T-25 counter and a compound located 8 cm from the counter window. Using the empirical relation for $K(E_0)$, where $K = I(p = 0)/I(p = 1 \text{ atmos})$ (Fig. 2), we have determined from the value of $K_{Nb^{95}} = 8.75$ (Fig. 1) the energy of β radiation from Nb^{95}, found to be $E_0 = (0.166 \pm 0.004)$ Mev. The error $\Delta E_0 = 0.004$ Mev was determined from the statistical measurement error, $\delta = 2\%$.

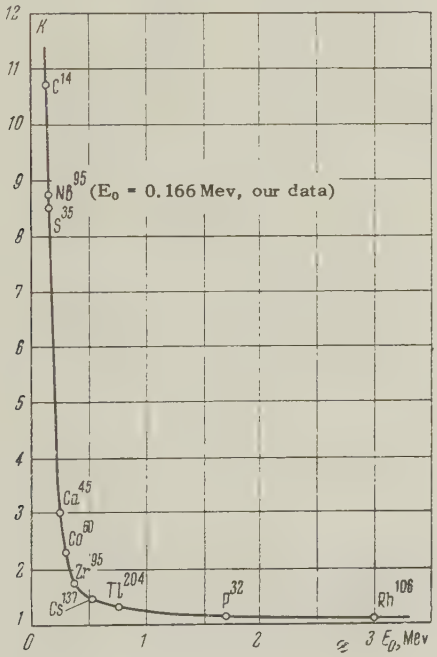

FIG. 2

In determining the empirical relation for $K(E_0)$ at small energies, we used isotopes with simple β spectra, such as C^{14} ($E_0 = 0.155$ Mev) and S^{35} ($E_0 = 0.167$ Mev). The results of the measurements of these β emitters, obtained by different authors, agree well with each other.[6]

2. Beta radiation from Ce^{144}. One of the most interesting objects for spectroscopic investigation is Ce^{144}. For a long time this substance was associated with a β radiation of energy on the order of 0.3 Mev.[7] An investigation in regions of small energies with the aid of the Fermi-Curie graph is difficult in this case, owing to the presence of a large number of conversion electron peaks in the soft part of the spectrum. Porter and Cook[8] were first to propose the existence of a softer component in Ce^{144}, with an energy $E_0 = 0.170$ Mev, at a content of approximately 30%. This assumption was based on the investigation of conversion lines of γ rays from Pr^{144}. These data were later confirmed by other authors.[9,10]

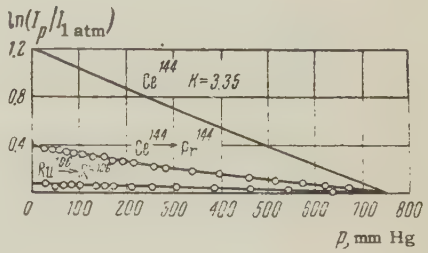

FIG. 3

We have investigated the β radiation of Ce^{144} by the method of absorption in air. Figure 3 shows an absorption curve in air of the summary β radiation of Ce^{144} and Pr^{144}. By means of absorption in an aluminum foil we have eliminated from the total curve the β radiation of Pr^{144} ($E_0 = 3$ Mev). With this, we extrapolated the curve of absorption in aluminum for Pr^{144} to zero thickness of absorber in accordance with the variation of the absorption curve* for $Ru^{106} - Rh^{106}$.

The elimination of Pr^{144} from the total curve of absorption in air at less than atmospheric pressure was also carried out in accordance with the course of the absorption curve in air for $Ru^{106} - Rh^{106}$. As a result we obtain for Ce^{144} the absorption curve in air shown in Fig. 3.

As can be seen from Fig. 2, the value of the air coefficient of Ce^{144}, equal to 3.35, differs greatly from the assumption that only a single β-radiation component with energy ~ 0.3 Mev exists in Ce^{144}, as stated by several authors.[7] The 0.3-Mev β radiation corresponds to a considerably lower value of air coefficient, namely 2.30. Therefore, in addition to the 0.3-Mev component, one must assume that Ce^{144} has at least one other softer component. Investigating the graph of the variation of $K(E_0)$, and also the formulas derived earlier,[5] we obtained a β-radiation component with energy $E_0 = (0.168^{+0.032}_{-0.020})$ Mev, with a content

of (40 ± 12)%. These data agree with the results obtained by Porter and Cook, and also by other authors.[8-10]

*The β radiation of Ru^{106} is completely absorbed by the counter window and by the air, and the character of the absorption of β radiation from Pr^{144} and Rh^{106} in aluminum is approximately the same.

[1] Mandeville, Scherb, and Keighton, Phys. Rev. **74**, 888 (1948).
[2] E. F. Sturcken and A. H. Weber, Phys. Rev. **91**, 484 (1953).
[3] P. S. Mittelman, Phys. Rev. **94**, 99 (1954).
[4] V. S. Shpinel', Doctoral Thesis, Moscow State University, 1957.
[5] N. E. Tsvetaeva and L. A. Rozenfel'd, Атомная энергия (Atomic Energy) **7**, 482 (1959).
[6] Seaborg, Perlman, and Hollender, Revs. Modern Phys. **25**, 469 (1953).
[7] H. B. Keller and J. M. Cork, Phys. Rev. **84**, 1079 (1951).
[8] F. T. Porter and C. S. Cook, Phys. Rev. **87**, 464 (1952).
[9] I. Pullman and P. Axel, Phys. Rev. **102**, 1366 (1956).
[10] Parfenova, Farafontov, and Shpinel', Izv. Akad. Nauk SSSR, Ser. Fiz. **21**, 1601 (1957), Columbia Tech. Transl. p. 1590.

Translated by J. G. Adashko
122

THE REACTION p + d → t + π^+ AT PROTON ENERGY 670 Mev

Yu. K. AKIMOV, O. V. SAVCHENKO, and L. M. SOROKO

Joint Institute for Nuclear Research

Submitted to JETP editor October 15, 1959

J. Exptl. Theoret. Phys. (U.S.S.R.) **38**, 643-644 (February, 1960)

A comparison of the cross sections for the reactions

$$p + d \to t + \pi^+, \quad (1)$$

$$p + d \to He^3 + \pi^0 \quad (2)$$

allows us to test the principle of the charge independence of nuclear forces, since, for isotopic spin conservation, the angular distributions for the two processes should be the same, and the ratio of their total or differential cross sections in the center-of-mass system should be 2:1.[1,2] A study of these two processes is interesting in itself, since they are connected with analogous processes of meson production in the reactions

$$p + p \to d + \pi^+, \quad (3)$$

$$p + n \to d + \pi^0 \quad (4)$$

and they admit of a simple theoretical interpretation.[1,3]

A measurement of the cross sections for reactions (1) and (2) was carried out earlier at energies of 340 Mev,[4] 450 Mev,[5] and 600 Mev.[6] In the present work, measurements were carried out to clarify the conditions for comparing processes (1) and (2) for the incident proton energy E_p = 670 Mev.

The examination of the reaction p + d → t + π^+ was carried out on a proton beam with an intensity 10^{11} protons/sec. The secondary charged particles formed in the heavy polyethylene or carbon target were identified by momentum, specific ionization, and range. The selection by specific ionization was made simultaneously by five scintillation counters in a telescope,[7] so that rare emissions of particles with high ionization could be detected against a background of irrelevant particles with smaller ionization. The emission of low-energy tritium nuclei in reaction (1) was measured for angles 5.4° and 11° in the laboratory system. The calibration of absolute cross sections was carried out with the aid of a measurement of the path of the deuterons in reaction (3), since the angular distribution there was well known for an energy of 660 Mev.[8] The differential cross sections for reaction (1), calculated in the center-of-mass system and relative to the pion emission angle, are equal to

$$d\sigma(12^\circ)/d\Omega = (9.3 \pm 1.5) \cdot 10^{-30}, \text{ cm}^2/\text{sr},$$

$$d\sigma(25^\circ)/d\Omega = (3.1 \pm 0.5) \cdot 10^{-30} \text{ cm}^2/\text{sr}.$$

These results are shown in the figure, together with the data obtained at different proton energies. As the energy of the incident protons is increased, a change is observed in the differential cross section of reaction (1), which tends to peak more in the forward, meson-emission direction. This kind of change in the differential cross section can be got qualitatively from the relation between the π^+ formation processes in reaction (1) and in reaction (3). This relation was obtained by interpreting process (1) on the basis of a hard-core nucleon model and by application of the impulse approximation.[3]

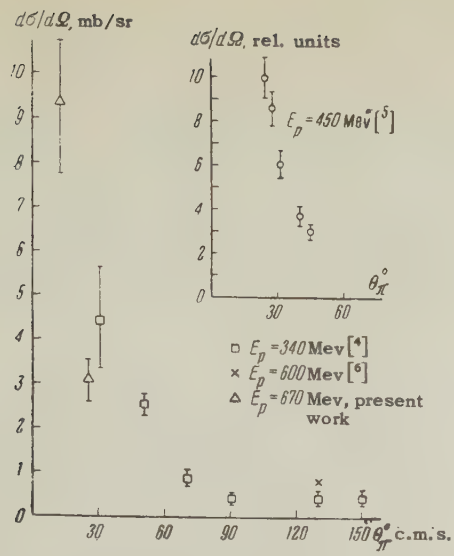

Since, for example, if the ratio of the pion formation cross sections in reaction (1) for incident proton energy 340 Mev for 0° and 180°, calculated on the basis of this theory with a core radius $0.5\hbar/m_\pi c$ is equal to ~ 10, then this ratio for 670-Mev protons increases to ~ 120 if the same wave function parameters are used and if the dependence of the angular distribution of reaction (3), which is indispensable for the calculation, is obtained by extrapolating the data for the inverse reaction for the meson energy region 174 to 370 Mev.[9] The differential cross sections calculated by this model for the incident proton energy 670 Mev, is

$$d\sigma(12^\circ)/d\Omega = 3.1\cdot 10^{-30}, \quad d\sigma(25^\circ)/d\Omega = 2.4\cdot 10^{-30}\ \text{cm}^2/\text{sr}$$

The quantitative disagreement between the calculated values and the experimental data is evidently due to the fact that in all these calculations one looks at the formation of positive pions from the collision of the incident proton with the proton of the deuteron only as reaction (3), and one does not take into account the contribution from pion formation in the reaction $p + p \rightarrow n + p + \pi^+$, whose total cross section exceeds by a factor of a few tens the total cross section for (3) in the incident proton energy region near 900 Mev, that used in the impulse approximation theory calculations.

[1] M. Ruderman, Phys. Rev. **87**, 383 (1952).

[2] L. I. Lapidus, JETP **31**, 865 (1956), Soviet Phys. JETP **4**, 740 (1957).

[3] S. Bludman, Phys. Rev. **94**, 1722 (1954).

[4] Frank, Bandtel, Medey, and Moyer, Phys. Rev. **94**, 1716 (1954).

[5] Crewe, Garwin, Ledey, Lillethun, March, and Marcowitz, Phys. Rev. Letters **2**, 269 (1959).

[6] Harting, Kluyver, Kusumegi, Rigopoulos, Sacks, Tibell, Vanderhaeghe, and Weber, Phys. Rev. Letters **3**, 52 (1959).

[7] Akimov, Komarov, Savchenko, and Soroko, Приборы и техника эксперимента (Instrum. and Meas. Engg.), in press.

[8] M. G. Meshcheryakov and B. S. Neganov, Dokl. Akad. Nauk SSSR **100**, 677 (1955).

[9] B. S. Neganov and L. B. Parfenov, JETP **34**, 767 (1958), Soviet Phys. JETP **7**, 528 (1958).

Translated by W. Ramsay
123

ON THE MAGNETIC SUSCEPTIBILITY OF A RELATIVISTIC ELECTRON GAS

A. A. RUKHADZE and V. P. SILIN

P. N. Lebedev Physics Institute, Academy of Sciences, U.S.S.R.

Submitted to JETP editor October 24, 1959

J. Exptl. Theoret. Phys. (U.S.S.R.) **38**, 645-646 (February, 1960)

LANDAU[1] was the first to show that a gas consisting of free electrons is diamagnetic, if one neglects the electron spins, and that its diamagnetism is equal to one third of the spin paramagnetism. Landau evaluated the magnetic susceptibility of an electron gas, starting from the expression of the energy spectrum of a non-relativistic electron in a magnetic field.

To evaluate the magnetic susceptibility of a relativistic electron gas one could use the solution of the Dirac equation for an electron in a magnetic field.[2] It is, however, simpler to use the method of the quantum transport equation with a self-consistent interaction.[3] Starting from the Dirac equations for an electron in an external transverse electromagnetic field, we obtain the following transport equation with a self-consistent interaction for the quantum distribution function which depends on the momentum $\mathbf{p}$, the coordinate $\mathbf{r}$ and the spin indices α, β, γ

$$\frac{\partial}{\partial t} f_{\alpha\beta}(\mathbf{p},\mathbf{r}) = \frac{1}{(2\pi)^6}\frac{i}{\hbar}\int d\tau\, d\eta_1\, d\mathbf{k}\, d\mathbf{r}_1 e^{i\tau(\eta-\mathbf{p})+i\mathbf{k}(\mathbf{r}_1-\mathbf{r})}$$
$$\times\left\{\left[\left(\boldsymbol{\alpha}, c\left(\boldsymbol{\eta}_1+\frac{\hbar\mathbf{k}}{2}\right)-e\mathbf{A}\left(\mathbf{r}_1-\frac{\hbar\tau}{2}\right)\right)+\beta\mu\right]_{\beta\gamma} f_{\alpha\gamma}(\boldsymbol{\eta}_1,\mathbf{r}_1)\right.$$
$$\left.-\left[\left(\boldsymbol{\alpha}, -c\left(\boldsymbol{\eta}_1-\frac{\hbar\mathbf{k}}{2}\right)+e\mathbf{A}\left(\mathbf{r}_1+\frac{\hbar\tau}{2}\right)\right)-\beta\mu\right]_{\gamma\alpha} f_{\gamma\beta}(\boldsymbol{\eta}_1,\mathbf{r}_1)\right\}, \quad (1)$$

where $\boldsymbol{\alpha}$ and β are the Dirac matrices, $\mu = mc^2$, A is the vector potential of the transverse electro-

magnetic field. To determine the magnetic susceptibility it is necessary to evaluate the current density which in the case of the relativistic electron gas is of the form

$$j = ec \int dp\ (\alpha_{\alpha\beta} f_{\alpha\beta}). \qquad (2)$$

The magnetic susceptibility of the gas χ^* is determined using a solution of the stationary linearized equation (1) as follows: $j_k = ck^2 \chi A_k$, where j_k and A_k are the Fourier components of the current and the vector potential. After simple calculations we find the magnetic susceptibility of a relativistic electron gas

$$\chi = \pi e^2 \hbar^2 \left\{1 - \frac{1}{3}\right\} \int_0^\infty \frac{f_0(p)}{E_p}\, dp, \qquad E_p = \sqrt{c^2 p^2 + \mu^2}, \quad (3)$$

where $f_0(p)$ is the equilibrium momentum distribution function of the electrons normalized to the total number of electrons per unit volume. The one in the curly brackets in (3) is caused by the electron spins and corresponds to the spin paramagnetism of the electron gas, while the second term $\frac{1}{3}$ corresponds to the diamagnetism of the free electrons. The diamagnetism of a relativistic, as of a non-relativistic, electron gas is thus equal to one third of its spin paramagnetism. In the non-relativistic limit $E_p = \mu = mc^2$ and Eq. (3) goes over into Landau's well-known expression.

For a relativistic degenerate electron gas a simple evaluation of the integral in (3) gives

$$\chi_\Phi = \left(\frac{e\hbar}{2mc}\right)^2 \frac{m^2 c}{\pi^2 \hbar^3} \left\{1 - \frac{1}{3}\right\} \ln \frac{p_0 + \sqrt{p_0^2 + m^2 c^2}}{mc}, \qquad (4)$$

where $p_0 = \hbar (3\pi^2 N)^{1/3}$. In the ultrarelativistic limit, $p_0 \gg mc$, we get from Eq. (4)

$$\chi_\Phi = \left(\frac{e\hbar}{2mc}\right)^2 \frac{m^2 c}{\pi^2 \hbar^3} \left\{1 - \frac{1}{3}\right\} \left[\ln \frac{2\hbar (3\pi^2 N)^{1/3}}{mc} + \frac{m^2 c^2}{4\hbar^2 (3\pi^2 N)^{2/3}}\right]. \qquad (5)$$

It follows from Eq. (5) that the magnetic susceptibility of an ultrarelativistic degenerate electron gas increases logarithmically with increasing density

$$\chi_\Phi \approx 0.5 \cdot 10^{-3} \ln (2\hbar (3\pi^2 N)^{1/3} / mc).$$

In real cases $\chi_\Phi \ll 1$.

For an ultrarelativistic Boltzmann electron gas ($\kappa T \gg mc^2$) Eq. (3) goes over into the following expression for the magnetic susceptibility

$$\chi_B = \left(\frac{e\hbar}{2mc}\right)^2 \frac{N}{2\kappa T} \left(\frac{mc^2}{\kappa T}\right)^2 \left\{1 - \frac{1}{3}\right\} \left[\ln \frac{\kappa T}{mc^2} + 0.116\right]. \qquad (6)$$

In the equilibrium state of the system the number of electron-positron pairs formed through collisions is for $\kappa T \gg mc^2$ equal to[4] $N^+ = N^- = 0.183\ (\kappa T/\hbar c)^3$. Taking this into account in Eq. (6) we conclude that the magnetic susceptibility of the system increases logarithmically with increasing temperature, $\chi_B \approx 10^{-4} \ln (\kappa T/mc^2)$. In real systems $\chi_B \ll 1$.

We express our gratitude to V. L. Ginzburg for his interest and for discussions of this paper.

*We emphasize that we are dealing with the susceptibility of an electron gas in a thermodynamic equilibrium state. The magnetic moment of the system may in a non-equilibrium state be appreciably higher.

[1] L. Landau, Z. Phys. **64**, 629 (1930).

[2] V. A. Fock, Начала квантовой механики (Principles of Quantum Mechanics) Leningrad, 1932.

[3] V. P. Silin, Proc. Inst. Phys. Acad. Sci., U.S.S.R. **6**, 201 (1955).

[4] L. D. Landau and E. M. Lifshitz, Статистическая физика (Statistical Physics) Gostekhizdat, 1951, Statistical Physics, Pergamon Press, London, 1958.

Translated by D. ter Haar
124

ELECTRICAL RESISTANCE MAXIMUM FOR FERROMAGNETS AT THEIR CURIE POINTS AT LOW TEMPERATURES

E. I. KONDORSKIĬ, O. S. GALKINA, and L. A. CHERNIKOVA

Moscow State University

Submitted to JETP editor October 27, 1959

J. Exptl. Theoret. Phys. (U.S.S.R.) **38**, 646-648 (February, 1960)

We showed earlier[1] that for nickel the ratio $\Delta\rho/\Delta I$ (where $\Delta\rho$ is the change of electrical resistivity for a change in magnetization of ΔI produced by a magnetic field, in the region of magnetic saturation) is approximately equal to the ratio $(\rho_T - \rho_0)/(I_0 - I_T)$, where ρ_T and I_T are the specific resistivity and saturation magnetization at temperatures $T < 20°K$, ρ_0 is the residual resistivity and I_0 is the saturation magnetization derived by extrapolation to absolute zero. It was also established that at hydrogen temperatures and below, the law $\rho_T - \rho_0 = aT^{3/2}$ holds for iron and nickel, where a is the constant of proportionality, and that above hydrogen temperatures the difference $\rho_T - \rho_0 - aT^{3/2}$ is roughly proportional to T^5. From this it was deduced that at hydrogen and he-

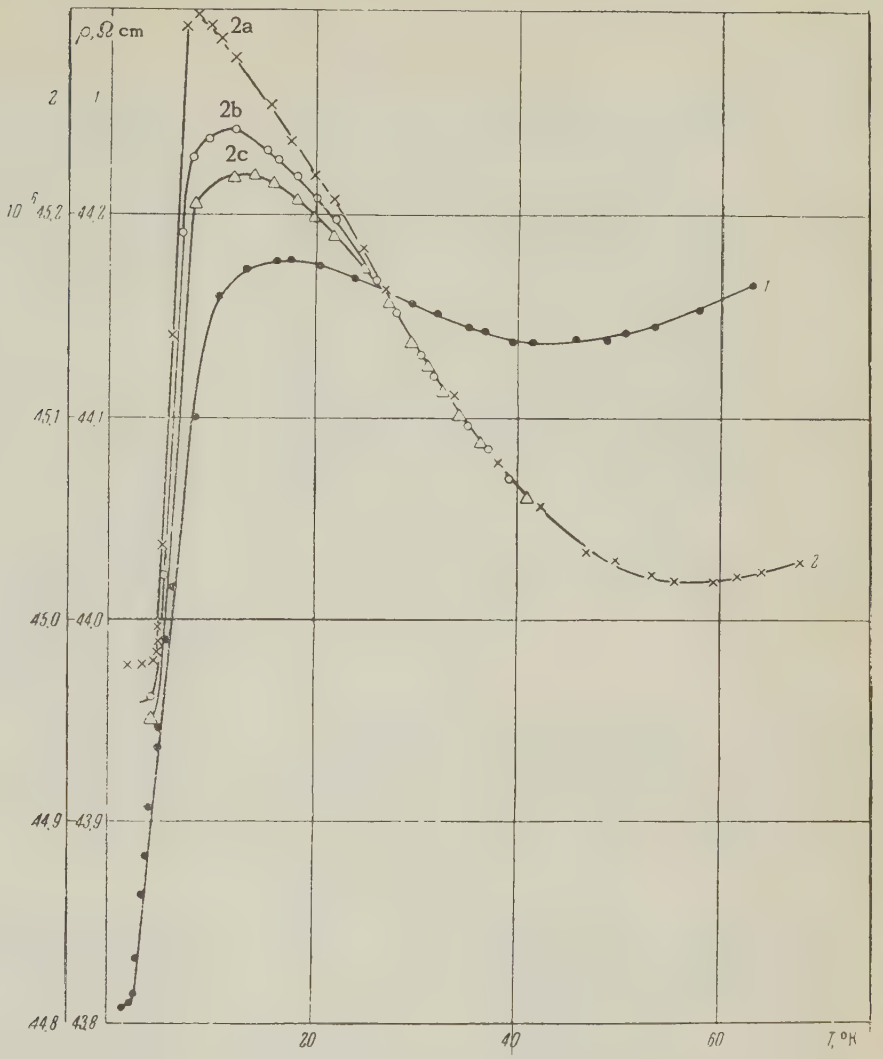

Dependence of electrical resistivity of copper-nickel alloys on temperature. Curve 1 – alloy with 58% copper; H = 0; 2a – 59.25% Cu, H = 0; 2b – 59.25% Cu, H = 1540 oe; 2c – 59.25% Cu, H = 2310 oe.

lium temperatures, the main cause of the increase in resistivity with temperature for ferromagnetic metals is the increase in disorder of the magnetic moment of the lattice (the increase in the number of ferromagnons, which scatter conduction electrons), and above hydrogen temperatures it is due to the greater intensity of lattice vibrations (the increase in the number of phonons).

In the region of the Curie point, where fluctuations in the magnetic ordering occur, a maximum in the resistivity could be expected. This maximum should be most marked when the Curie point lies at hydrogen or helium temperatures, where the phonon part of the resistivity is small.

The first indication of the existence of such a maximum occurred in the work of Krivoglaz and Rybak,[2] where the effect of various kinds of static disorder of the lattice was examined, and a theoretical study made of the influence of fluctuations in the magnetic moment on the conductivity of ferromagnetic semiconductors. It follows from equations (43), (44), and (54) of that paper that the mean free path and mobility of the electrons due to scattering by the fluctuations of magnetic moment increases on application of a magnetic field which reduces these fluctuations.

The purpose of the present work was an experimental verification of the existence of the resistivity maximum in the region of magnetic saturation for ferromagnets with low transition temperatures. The specimens used were copper-nickel alloys with 58 and 59.25% copper, for which the Curie points lie below 20°K. The resistivity was determined by the method described previously.[1]

The figure shows the dependence of resistivity on temperature. There are maxima in the region of the magnetic transition, and that for the 59.25% Cu specimen with a Curie point near to helium temperatures is especially marked. These maxima are smoothed out when a magnetic field is applied. At the maximum of the 59.25% Cu specimen the value of $\rho - \rho_0$ is 0.7% of the residual resistivity and agrees with the calculation given by Krivoglaz and Rybak.[2] We should point out that this cal-

culation was made for semiconductors, whereas our result is for a metal, so that a quantitative comparison is hardly possible. Nevertheless the existence of a resistivity maximum in the region of the magnetic transition of metals confirms the theory and the deductions made from our previous work about the effect of disorder of the magnetic moment on the electrical resistivity of ferromagnets at low temperatures.

[1] E. I. Kondorskiĭ, O. S. Galkina, and L. A. Chernikova, JETP **34**, 1070 (1958), Soviet Phys. JETP **7**, 741 (1958).

[2] M. A. Krivoglaz and S. A. Rybak, J. Tech. Phys. (U.S.S.R.) **28**, 940 (1958), Soviet Phys.-Tech. Phys. **3**, 876 (1958).

Translated by R. Berman
125

POSSIBILITY OF AN EXPERIMENTAL TEST FOR FORM FACTORS IN THE THEORY OF THE UNIVERSAL FERMI INTERACTION

HE TSO-HSIU

Joint Institute for Nuclear Research

Submitted to JETP editor October 28, 1959

J. Exptl. Theoret. Phys. (U.S.S.R.) **38**, 648-650 (February, 1960)

THERE is great interest at present in a test of the form factors in the theory of the weak interaction. These form factors are commonly expressed by "weak magnetism" terms and by pseudoscalar interaction terms.[1] Unfortunately, however, this effect is small in beta decay, is difficult to examine, and up to now has not been observed.[2] In the present note we calculate the process of μ capture by spin-$\frac{1}{2}$ nuclei without emission of neutrons and protons, supposing that after the capture the nucleus makes a transition from the spin-$\frac{1}{2}$ state to the spin-$\frac{3}{2}$ state. The density matrix of the initial state has the form[3]

$$\tfrac{1}{4}(1+\sigma_p\xi_p+\sigma_\mu\xi_\mu+\varepsilon\sigma_p\sigma_\mu), \qquad (1)$$

ξ_ρ and ξ_μ are the polarizations of the nucleus and the muon; they are equal to each other for the triplet state and equal to zero for the singlet state; $\epsilon = \frac{1}{3}$ for the triplet state and $\epsilon = -1$ for the singlet state. The density matrix can also be written in an analytic form for a mixed state. Here ϵ takes on values between -1 and $\frac{1}{3}$ and characterizes the distribution of muons between the singlet and triplet states. We will take as the nuclear matrix element that of Chou Kuang-Chao and Maevskiĭ.[4] We neglect the momenta of the proton and muon in the initial state. After calculation we get the probability for the transition of the nucleus from spin-$\frac{1}{2}$ to spin-$\frac{3}{2}$ in the form

$$W = (G^2Z^3/2\pi^2a_\mu^3)\,N_0\,|M_{G.T.}|^2q^2(1-q/Am_p),$$

$$N_0 = (1+\varepsilon)\left[\lambda^2+\frac{\lambda\beta}{3}(2\mu+2-f+\lambda)-\frac{\beta^2}{12}(\mu+1)(2f-2\lambda-\mu+1)\right]+\frac{\beta^2}{12}(\mu+f+1-\lambda)^2. \qquad (2)$$

Here G is the Fermi constant; a_μ is the muon Bohr-orbit radius; q is the neutrino energy, λ is the ratio of the Gamow-Teller and Fermi constants, equal to 1.25 for beta decay; μ is the anomalous gyromagnetic ratio which characterizes "weak magnetism" and is equal to 3.7; f is the pseudoscalar coupling constant, equal to about 8λ for muon capture by protons; $\beta = q/m_p$; A is the atomic number; $|M_{GT}|^2$ is the square of the matrix element for Gamow-Teller transitions, which, as Ioffe showed,[5] is equal to

$$|M_{GT}|^2 = |M^\beta_{GT}|^2(1-\tfrac{1}{3}q^2\langle r^2\rangle_A), \qquad (3)$$

where M^β_{GT} is the matrix element for the corresponding beta decay, $\langle r^2\rangle_A$ is the mean square charge radius, corresponding to the axial vector transition and equal to the square of the radius obtained from the transition of nuclei related to a single isotopic multiplet.

We see from (2) that if the muon is captured by a nucleus in the singlet state, that is, $\epsilon = -1$, and if the process is considered without form factors, then $\mu = f = 0$ and $\lambda = 1$, and this process is completely forbidden in our approximation. But if a form factor exists, then this transition is possible and its probability is on the order of $\frac{1}{8}$ of the ordinary transition. In such a way, an experiment on capture in the singlet state can serve as a criterion for the presence of form factors.

The result obtained is connected with the fact that in the transition considered the neutrino is always in the $J = \frac{1}{2}$ state if the muon and nucleus are in the singlet state, and conservation of angular momentum completely forbids this process, except when the neutrino carries away orbital momentum. As is well known, a form factor is always tied up with $l = 0$. Therefore, if the number of neutrinos with $J = \frac{1}{2}$ is small, the contribution from the form factors is comparable to that from other terms which we neglect. An analogous situation exists in nuclei with spin greater than $\frac{1}{2}$.

It is well known that for μ capture from a singlet state in a metal, a muon which is in a higher state in the hyperfine structure has a large probability of making a transition into a lower state and giving its energy to a conduction electron.[6] For example, the probability of such a transition in Al is $\sim 10^6$ sec^{-1}. Thus for light nuclei we can test for the presence of a form factor by comparing the transition probabilities in metals and nonmetals. The muons in nonmetals are distributed statistically among the hyperfine state levels (if there is not some other kind of transition mechanism). In addition, a muon in a higher hyperfine state can also make a magnetic dipole transition to a lower state. It is known[7] that the probability of this transition varies as Z^{*q}, where Z^* is the effective charge. Thus for nuclei heavy enough to have an effective charge greater than 35, almost all the muons at a high hyperfine level make the transition to a lower state. Of course, a strong magnetic field would effect the magnetic dipole transition, and we could change the distribution of muons among the states of the hyperfine distribution.

The authors express their gratitude to Ya. A. Smorodinskiĭ for his interest in the work and his examination of the results, and also to Chou Huang-Yuan, Chou Kuang-Chao, A. E. Ignatenko, and I. S. Shapiro for useful comments and advice.

[1] Ya. A. Smorodinskiĭ, Usp. Fiz. Nauk **48**, 653 (1959).

[2] A. I. Alikhanov, Report at the Kiev Conference on High Energy Physics, 1959 (preprint).

[3] I. M. Shmushkevitch, Nuclear Phys. **11**, 419 (1959).

[4] Chou Kuang-Chao and V. Maevskiĭ, Acta Physica Sinica **15**, 377 (1959).

[5] B. L. Ioffe, JETP **37**, 159 (1959), Soviet Phys. JETP **10**, 113 (1960).

[6] V. L. Telegi, Phys. Rev. Letters **3**, 59 (1959).

[7] H. Primakoff, Revs. Modern Phys. **31**, 803 (1959).

Translated by W. Ramsay
126

MOMENTUM DISTRIBUTION OF PARTICLES PRODUCED IN INELASTIC N-N COLLISIONS AT E = 9 Bev

V. S. BARASHENKOV, WANG PEI, and V. M. MAL' TSEV

Joint Institute for Nuclear Research

Submitted to JETP editor November 13, 1959

J. Exptl. Theoret. Phys. (U.S.S.R.) **38**, 650-652 (February, 1960)

FIGURES 1 and 2 show theoretical and experimental momentum spectra of particles of different kinds, produced in inelastic collisions between nucleons (in the center-of-mass system of the colliding nucleons). The theoretical spectra are calculated with the statistical theory,[1] while the experimental results are taken from reference 2. Statistical measurement errors are indicated.

The table lists the values of the average momenta of the nucleons and pions, $\bar{p}$, calculated from the data of Figs. 1 and 2. The experimental values of $\bar{p}$ for the laboratory system of coordinates were obtained by the Lorentz transformation from the mass system under the assumption that in the p-p collisions the angular distributions of

	Pions		Protons	
	Experiment	Theory	Experiment	Theory
$\bar{p}_{l.s.}$, Bev/c	1.0±0.2	1.46	3.6±0.5	2.9
$\bar{p}_{c.m.s.}$, Bev/c	0.40±0.1	0.57	1.24±0.25	0.79

the pions and nucleons in the center-of-mass system are symmetrical with respect to the angle $\theta = \pi/2$. (This assumption agrees with the theoretical and experimental results obtained in references 3 and 4.) The values obtained are close to the values of $\bar{p}$ obtained in reference 5 from an analysis of the interaction between protons and photoemulsion nuclei, $\bar{p} \approx p_{sp} = (3.0 \pm 0.5)$ Bev/c for protons and $p \approx p_{s\pi} = (1.0 \pm 0.2)$ Bev/c for pions (p_{sp} is the momentum of fast protons, $p_{s\pi}$ is the momentum of fast pions).

It is seen from the table and from the diagrams that the experimental momentum spectra of the nucleons are harder and the spectra of the pions are softer than those calculated theoretically. Accordingly, the theoretical energy losses to the production of new particles in one act of inelastic p-p interaction, ΔE, is equal to $\sim 58\%$ of the primary-nucleon energy (of which approximately 50% is consumed for the production of pions and approxi-

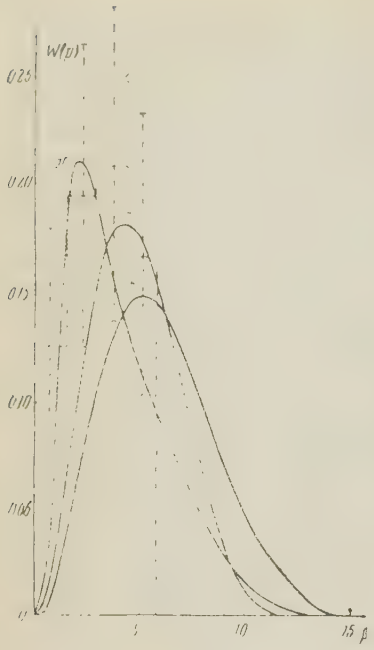

FIG. 1. Momentum spectra of π, K, and $\bar{K}$, mesons. Dotted curve – experimental histogram for pions. The momenta p are given in $m_\pi c$ units, W(p) – probability of momentum p normalized to unity.

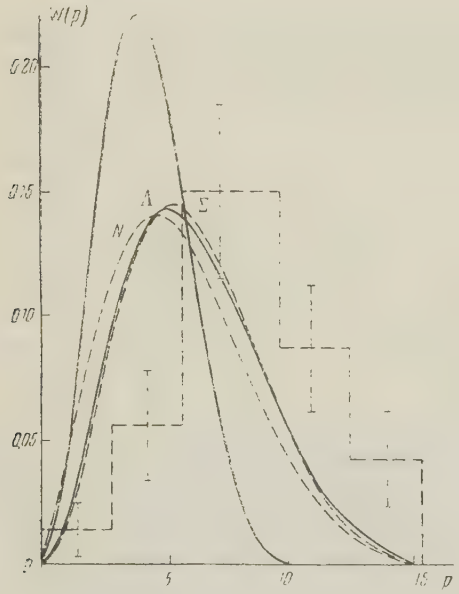

FIG. 2. Momentum spectra of nucleons, antinucleons, Λ hyperons, and Σ hyperons. The dotted curves show the theoretical and experimental spectra of the nucleons, and also the spectrum of Σ hyperons. The momenta p are given in units of $m_\pi c$; W(p) – probability of momentum p normalized to unity.

mately 8% for the production of strange particles,)* are found to be considerably higher than the average experimental values, namely ΔE = (30 to 40)%,[3] (40 ± 10)%,[5] and (35 ± 2)% (private communication from Bunyatov).

The difference between the theoretical and experimental values of the spectra and energy losses can be understood qualitatively, if it is considered that in the experimental investigations[2,3,5] the central N-N collisions were not separated in the measurements from the peripheral ones. On the other hand, the nucleon spectrum after a peripheral collision is on the average harder than the spectrum of nucleons produced in a central collision. To the contrary, the pions produced in a peripheral collision are on the average softer than the pions due to central collisions.

It was shown in reference 4 that an allowance for the peripheral collisions is also essential to explain the angular distributions of the particles produced in N-N collisions.

*Theoretical values of the energy losses are calculated on the basis of the momentum distributions, given in Figs. 1 and 2. This is followed by a changeover to the laboratory system under the assumption that the angular distributions of the particles, produced in p-p collisions, are symmetrical in the center-of-mass system about the angle $\theta = \pi/2$.

[1] Barashenkov, Barbashev, and Bubelev, Nuovo cimento **7**, Suppl. 1, 117 (1958).

[2] Bogachev, Bunyatov, Merekov, Sidorov, and Yarba, Материалы ежегодной конференции по физике высоких энергий (Materials of the Annual Conference on High-Energy Physics, Kiev, 1959).

[3] Bogachev, Bunyatov, Gramenitskiĭ, Lyubimov, Merekov, Podgoretskiĭ, Sidorov, and Tuvdendorzh, JETP **37**, 1225 (1959), Soviet Phys. JETP **10**, 872 (1960).

[4] Barashenkov, Mal'tsev, and Mikhul, JETP **37**, 1484 (1959), Soviet Phys. JETP **10**, 1052 (1960); Nucl. Phys. **13**, 583 (1959).

[5] Barashenkov, Belyakov, Wang Shu-Fen, Glagolev, Dolkhazhav, Kirillova, Lebedev, Mal'tsev, Markov, Tolstov, Tsyganov, Shafranova, and Yao Ch'ing-Ze, Атомная энергия (Atomic Energy), **7**, 376 (1959).

Translated by J. G. Adashko
127

ON THE QUESTION OF A RESONANT $\pi\pi$ INTERACTION

V. M. MAKSIMENKO

P. N. Lebedev Physics Institute, Academy of Sciences, U.S.S.R.

Submitted to JETP editor November 16, 1959

J. Exptl. Theoret. Phys. (U.S.S.R.) 38, 652-654 (February, 1960)

THE question of a resonant $\pi\pi$ interaction has been the subject of much discussion[1-9] in the recent past. So far, however, there is no convincing experimental proof that such an interaction exists. It is therefore of value to discuss experiments in which this interaction may manifest itself. In the present note the angular correlation of π mesons is analyzed for the case of stopped antinucleons annihilating according to the scheme

$$\bar{p} + p \text{ (or } \bar{n} + n) \to \pi^+ + \pi^- + \pi^0. \quad (1)$$

Let us make the assumption which was made by other authors[5-9] and which is in agreement with Belenkiĭ's[10] ideas regarding the inclusion of a resonant interaction between particles, that the reaction (1) may proceed through two channels:

$$N + N \to 3\pi, \quad (2)$$

$$N + N \to \sigma + \pi \to 3\pi. \quad (3)$$

where the symbol σ denotes a π-mesic "isobar" — a "particle" of mass $m_\sigma = (3-4)\mu$ (where μ is the mass of the pion), spin J and isospin I, which decays into two pions with a lifetime of the order of, or somewhat larger than, nuclear times. By making use of isotopic invariance we obtain the probabilities for the final states in reaction (3) for various possible values of I (see table; the decay products of the isobar are put in parentheses).

Final state	$I=0$	$I=1$	$I=2$
$(\pi^+\pi^-)\,\pi^0$	$5/6$	$1/6$	$2/15$
$(\pi^-\pi^0)\,\pi^+$	—	$5/12$	$3/10$
$(\pi^+\pi^0)\,\pi^-$	—	$5/12$	$3/10$
$(\pi^0\pi^0)\,\pi^0$	$1/6$	—	$4/15$

Assuming that the σ decays isotropically in its proper coordinate system, we find the distribution of the number N of pairs of pions as a function of the angle ψ between them in the laboratory system. It turns out that the pions from the decay of the σ form narrow pairs whereas the pion produced directly together with one of the "decay" pions form a wide pair.

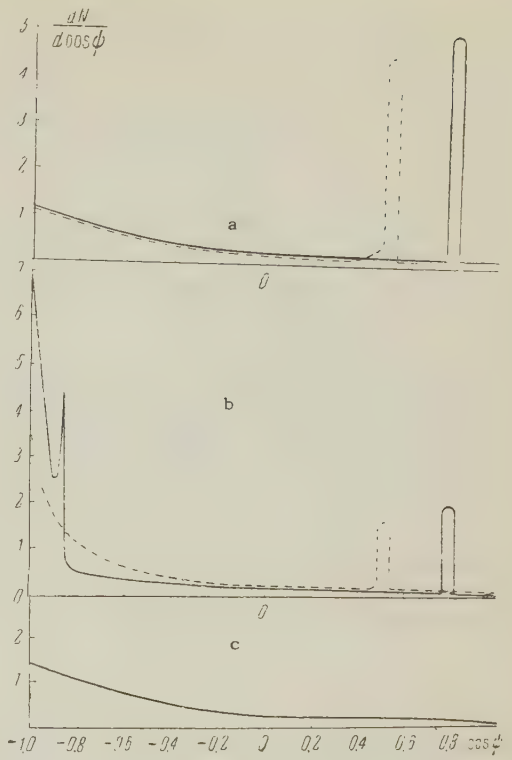

As can be seen from the table, the relative fraction of pairs of the first and second type in the case of charged pions in reaction (1) will be significantly different depending on the value of I. The figure shows the dependence of $dN/d\cos\psi$ on $\cos\psi$ for $I = 0$, $J = 0$ (a) and $I = 1$, $J = 1$ (b) for two values of m_σ: $m_\sigma = 3\mu$ (solid curve) and $m_\sigma = 4\mu$ (dotted curve). In constructing these curves statistical theory* was used to determine the relation between processes (2) and (3). The curves for $I = 2$ are not shown since in this case the situation qualitatively differs little from the case $I = 1$ as can be seen from the table. The analogous graph for the process (2) alone (absence of a resonant interaction) is shown in Fig. (c). The curves differ significantly from each other and therefore a comparison with appropriate experimental data may yield some information on the resonant $\pi\pi$ interaction. The curves in the Figs. (a) and (b) are calculated for the minimum possible values of J; for larger values of J the relative contribution of process (3) will increase and the difference between the curves will be even more pronounced.

In conclusion I express my gratitude to I. L. Rozental' and M. I. Podgoretskiĭ for a discussion of these problems, and also to Z. S. Maksimova for numerical calculations.

*The peaks for small angles have almost a "δ-function" character and are therefore shown in a somewhat distorted form in order to make it easier to see the relation between the areas under various portions of the curves.

[1] F. J. Dyson, Phys. Rev. **99**, 1037 (1955).
[2] G. Takeda, Phys. Rev. **100**, 440 (1955).
[3] H. Miyazawa, Phys. Rev. **97**, 1399 (1955).
[4] W. Frazer and J. Fulco, Phys. Rev. Lett. **2**, 365 (1959).
[5] E. Eberle, Nuovo cimento **8**, 610 (1958).
[6] T. Gotô, Nuovo cimento **8**, 625 (1958).
[7] V. I. Rus'kin, JETP **36**, 164 (1959), Soviet Phys. JETP **9**, 113 (1959); JETP **37**, 105 (1959), Soviet Phys. JETP **10**, 74 (1960)
[8] F. Cerulus, Preprint (1959).
[9] V. S. Barashenkov and V. M. Mal'tsev, JETP **37**, 884 (1959), Soviet Phys. JETP **10**, 630 (1960).
[10] S. Z. Belen'kiĭ, JETP **32**, 1171 (1957), Soviet Phys. JETP **5**, 952 (1957).

Translated by A. M. Bincer
128

DESTRUCTION OF SUPERCONDUCTIVITY BY A CURRENT

E. TROĬNAR

Moscow State University

Submitted to JETP editor November 17, 1959

J. Exptl. Theoret. Phys. (U.S.S.R.) **38**, 654-655 (February, 1960)

IT was shown by Shubnikov and Alekseevskiĭ[1] as early as 1936 that when the superconductivity of a cylindrical specimen is destroyed by a current, there is a sharp jump in resistance to a value which is less than that in the normal state, and then the resistivity gradually returns to its normal value. This phenomenon was examined theoretically by London[2] and by Landau.[3] It was shown that the resistance jump must be $0.5\,R_n$ (R_n being the resistance in the normal state).

In the first experiments[1,4] the jump was greater than the theoretical value and reached $0.7-0.8\,R_n$, and Scott[5] suggested a dependence of R_c/R_n (R_c is the resistance of the specimen for the critical current) on the specimen diameter, due to the surface energy. It therefore seemed interesting to carry out measurements on specimens of different diameters. In addition, by using specimens of different purity, it would be possible to test Kuper's[6] view on the connection between the magnitude of the resistance jump and the ratio of specimen diameter to the mean free path.

Specimen No.	Diameter, cm	Length, cm	$10^3\rho_n$, Ω·cm at 3.8° K	$\frac{10^4 R_{3.8°}}{R_{300°}}$
1	0.050	6.3	1.37	0.80
2	0.032	3.7	1.70	0.96
3	0.0181	0.81	1.97	1.28
4	0.0083	0.50	2.30	1.51
5	0.0041	0.90	2.65	2.0
6	0.034	1.65	18	15
7	0.0181	0.82	20	17
8	0.0083	0.43	20	17
9	0.0041	0.78	20	17

We made two series of specimens from two tin samples of different purity. The specimens were prepared from wires obtained by extruding the metal through fine holes. The specimen characteristics are shown in the table. They were mounted on a frame and placed horizontally in a Dewar vessel to avoid a temperature gradient along the specimen. The earth's magnetic field was compensated to an accuracy of 3%. From the measurements, curves were obtained of the dependence of R_c/R_n on the temperature of the helium bath for various specimens (Fig. 1). In the value of R_n

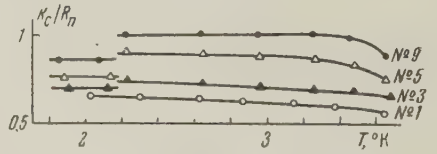

FIG. 1

account was taken of the effect of the magnetic field of the current. When the values of R_c/R_n at temperatures above and below the λ-point are compared, it can be seen that the heating of the specimen above the temperature of the helium bath has a considerable effect. The dependence of R_c/R_n on the heat flow from the specimen per unit area, q, is shown in Fig. 2. (The points on the curves for each temperature correspond to the specimens 1, 2, 3, 4, 5, 6, 7, 8 and 9 of the table.) The shapes of the curves suggest that R_c/R_n depends primarily on q. It is probable that the dependence, found by Scott, on the diameter of the specimen is mainly determined by the dependence of q on d, since $q \sim H_c^2\rho_n/d$ (ρ_n is the specific resistivity of the specimen).

If the variation of R_c/R_n with q is extrapolated to $q = 0$, the limiting value depends on temperature (increasing with falling temperature) and is about 0.5 only near T_c. It is not impossible that the reason for this is the surface forces between the superconducting and normal phases, which increase with decreasing temperature.

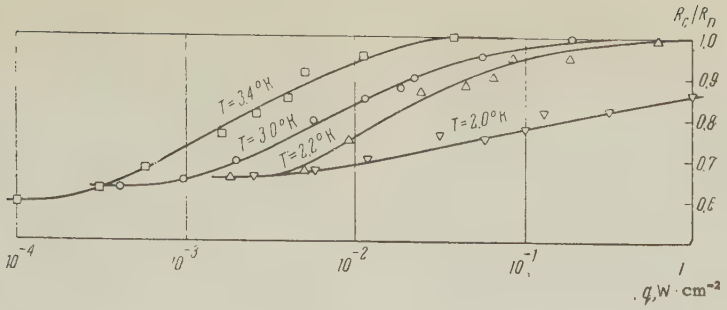

FIG. 2

The data presented thus indicates that it is only possible to elucidate the influence of surface forces (Scott) and mean free path (Kuper) if overheating of the specimen is avoided.

[1] L. W. Shubnikov and N. E. Alexejevski, Nature **138**, 804 (1936).

[2] F. London, Superfluids, Wiley, New York 1950, Vol. 1, p. 120.

[3] D. Shoenberg, Superconductivity, (Russ. Transl.) IIL, 1955, p. 128, [Cambridge, 1952].

[4] N. E. Alekseevskiĭ, JETP **8**, 342 (1938).

[5] R. B. Scott, J. Res. Nat. Bur. Stand. **41**, 581 (1948).

[6] C. G. Kuper, Phil. Mag. **43**, 1264 (1952).

Translated by R. Berman
129

DAMPING OF THE OSCILLATIONS OF A CYLINDER IN ROTATING HELIUM II

Yu. G. MAMALADZE and S. G. MATINYAN

Institute of Physics, Academy of Sciences, Georgian S.S.R.

Submitted to JETP editor November 20, 1959

J. Exptl. Theoret. Phys. (U.S.S.R.) **38**, 656-657 (February, 1960)

WE have previously shown[1] that the interaction of a disk oscillating in rotating helium II with the Onsager-Feynman vortex lines leads to a specific dependence of the damping upon the rotational velocity, with a characteristic maximum[2,3] which is not to be explained by consideration of the influence on the disk of the normal component of the helium II alone (even when the mutual friction between the normal and superfluid liquids is taken into account). A decisive role in the explanation of the formulas derived in reference 1 is played by the circumstance that the vortex lines, being perpendicular to the plane surface of the disk, lie with one end upon this surface. Distorted by the perpendicular displacement of the surface, they act upon it with a force which depends upon their tension. The relation between the tension of a vortex line and its circulation, moreover, determines the effective viscosity of the superfluid component (the quantity η_s in reference 1).

From what has been said, it is clear that if the disk be replaced by a cylinder whose surface is parallel to the axes of the vortex lines, then the possibility of direct interaction of the oscillating body with the vortices which form when a superfluid liquid is rotated is completely excluded. The presence of the vortices manifests itself solely in mutual friction effects.

Solving the system of hydrodynamic equations for rotating helium II,[4,1] for boundary conditions corresponding to small oscillations of an infinite cylinder rotating together with an unbounded liquid about their common axis,* one can readily verify that the force acting upon the surface of the cylinder is wholly determined by the momentum flow of the normal component.

The sum of the moments of the forces acting upon unit length of the outer and inner surfaces of a thin-walled cylinder of radius R turns out to be

$$M = -2\pi i R^3 \eta_n \Omega \varphi_0 k \left[H_2^{(1)}(kR)/H_1^{(1)}(kR) - J_2(kR)/J_1(kR)\right] e^{i\Omega t}. \quad (1)$$

Here, η_n is the viscosity of the normal component, Ω and φ_0 are the frequency and amplitude of the oscillations of the cylinder, J_p is a Bessel function, $H_p^{(1)}$ is a Hankel function, and k is the complex wave number, determined by the equation

$$k^2 = -\frac{i\Omega}{\nu_n}\left[1 + i\frac{2\omega_0}{\Omega}\beta_s\left(1 - i\frac{2\omega_0}{\Omega}\frac{\beta_n}{1 + 2i\omega_0\beta_n/\Omega}\right)\right], \quad (2)$$

with $\mathrm{Im}\, k > 0$. Here ν_n is the kinematic viscosity of the normal component, ω_0 is the angular velocity of rotation, and β_n and β_s are the coefficients for the mutual friction between the superfluid and normal components (cf. reference 1).

As was to be expected, Eqs. (1) and (2) show that the dependence of M upon the rotational velocity vanishes for $\beta_n = \beta_s = 0$. Consequently, the influence of rotation upon the damping of the oscillations of a cylinder is characteristic only of helium II. Measurements[5,6] have confirmed the absence of such an effect in a classical fluid.

Using Eq. (2) it is not difficult to show that over a broad range of frequencies ω_0 and Ω and for $R \approx 1$ cm the penetration depth of the cylindrical waves excited by the oscillations of a cylinder in rotating helium II is appreciably less than the radius of the cylinder. This makes it possible to use an asymptotic expansion of the cylindrical functions for large values of the argument.

As a result, the damping γ' at the surface of a unit length of the cylinder is

$$\gamma' = \frac{\pi R^3 \sqrt{2\eta_n \rho_n \Omega}}{I_1}\left(1 - \frac{\omega_0}{\Omega}\beta_s\right)\left(1 - \frac{3\delta_0}{R}\right), \qquad (3)$$

Where I_1 is the moment of inertia of the cylinder (per unit length), $\delta_0 = \sqrt{2\nu_n/\Omega}$ is the penetration depth in the absence of rotation, and ρ_n is the normal component density. Equation (3) is written in the linear approximation to the product of $2\omega_0/\Omega$ and the mutual friction coefficients.

To eliminate boundary effects it is convenient to measure the quantity $(\gamma_2 - \gamma_1)/(l_2 - l_1)$, which is equivalent to γ'; here γ_2 and γ_1 are the values of the damping for immersion of the cylinder to depths l_2 and l_1, respectively. (In addition, I_1 should be replaced in Eq. (3) by the moment of inertia of the suspended system I, which is presumed to be sufficiently great that the period of the oscillations is the same in both stationary and rotating helium, and for various depths of immersion.)

It can readily be seen that the ratio of the quantities $\gamma_2 - \gamma_1$ as measured in rotating and in stationary helium II is

$$(\gamma_2 - \gamma_1)/(\gamma_2 - \gamma_1)_{\omega_0 = 0} = 1 + \omega_0 \rho_s B/2\Omega\rho, \qquad (4)$$

where ρ_s/ρ is the relative density of the superfluid component, and B is the coefficient of Hall and Vinen[7,8] ($\beta_s = -\rho_s B/2\rho$). Equations (3) and (4) are also confirmed by experiment.[6]

The authors regard it their pleasant duty to thank É. L. Andronikashvili and his colleagues in the cryogenic laboratory of the Tbilisi State University for their constant interest in this work.

*In solving this problem the necessity of using additional boundary conditions for the velocity of the superfluid liquid does not arise (cf. references 1 and 4), since its components turn out to be proportional to the corresponding components of the normal fluid velocity.

[1] Yu. G. Mamaladze, S. G. Matinyan, JETP **38**, 184 (1960), Soviet Phys. JETP **11**, 134 (1960).

[2] Andronikashvili, Tsakadze, Mamaladze, and Matinyan, Fifth All-Union Conference on Low Temperature Physics, Tbilisi, 1958.

[3] É. L. Andronikashvili and D. S. Tsakadze, JETP **37**, 562 (1959), Soviet Phys. JETP **10**, 397 (1960).

[4] H. E. Hall, Proc. Roy. Soc. **A245**, 546 (1958).

[5] Andronikashvili, Tsadkadze, Chkheidze, Тр. Института физики АН ГрузССР (Trans. Inst. Phys. Acad. Sci. Georgian SSR), in press.

[6] D. S. Tsakadze and I. M. Chkheidze, JETP, this issue, p. 637, Soviet Phys. JETP this issue, p. 457.

[7] H. E. Hall and W. F. Vinen, Proc. Roy. Soc. **A238**, 204, 215 (1956).

[8] E. M. Lifshitz and L. P. Pitaevskiĭ, JETP **33**, 535 (1957), Soviet Phys. JETP **2**, 418 (1958).

Translated by S. D. Elliott
130

ON THE POSSIBILITY OF MEASURING A GRAVITATIONAL FREQUENCY SHIFT IN THE SUN'S FIELD

B. D. OSIPOV

P. N. Lebedev Physics Institute, Academy of Sciences, U.S.S.R.

Submitted to JETP editor November 20, 1959

J. Exptl. Theoret. Phys. (U.S.S.R.) **38**, 657-658 (February, 1960)

SEVERAL authors[1,2] have discussed the possibility of using artificial earth satellites to measure the gravitational frequency shift. However, they have considered only the shift due to the earth's field. We wish to present a calculation which shows that the frequency shift due to the sun's field can also be measured with earth satellites.

The frequency shift due to the sun is

$$\Delta\nu/\nu = -kM_\odot/c^2 r, \qquad (1)$$

where k is the gravitational constant, $M_\odot = 2.0 \times 10^{33}$ g is the mass of the sun and r is the dis-

tance from the satellite to the sun. If the satellite travels on a circular orbit lying in the plane of the earth's orbit, then the distance r can be written in the form $r = r_0 + \Delta r \cos \Omega t$, where Δr is the radius of the satellite's orbit, Ω is its frequency and r_0 is the distance between the earth and sun. The time-dependent part of (1) is then

$$\Delta\nu/\nu = (kM_\odot/c^2 r_0^2)\,\Delta r \cdot \cos \Omega t. \qquad (2)$$

This experiment could be done by putting a stable oscillator on either an artificial satellite or on the moon.

For a generator on the moon ($\Delta r = 3.8 \times 10^{10}$ cm) the fractional frequency change amounts to 5×10^{-11} (which can be compared with a maximum change of 7×10^{-10} in the earth's field). Although the effect due to the sun is smaller than that due to the earth, the experiment using the sun's field has the advantages that the frequency of the oscillator need not be unaffected by the rocket flight to put the satellite in orbit, and the effect is periodic with the period of the satellite.

[1] V. L. Ginzburg, JETP **30**, 213 (1956), Soviet Phys. JETP **3**, 136 (1956).

[2] S. F. Singer, Phys. Rev. **104**, 11 (1956).

Translated by R. Krotkov
131

ON THE APPLICABILITY OF THE FERMI-TELLER "Z-LAW" TO A PHOTOEMULSION CONTAINING URANIUM

G. E. BELOVITSKIĬ

P. N. Lebedev Physics Institute, Academy of Sciences, U.S.S.R.

Submitted to JETP editor July 30, 1959

J. Exptl. Theoret. Phys. (U.S.S.R.) **38**, 658-660 (February, 1960)

IT has been shown recently[1,2] that the relative probability of capture of slow μ^- mesons by various atoms in chemical compounds, (such as Al_2O_3, AgCl, UF_4, etc) does not follow the expected law (proportionality to Z) obtained by Fermi and Teller,[3] but is proportional to the number of atoms of the given element in the molecule.

This unexpected result dictates a cautious approach to the conclusions previously drawn in many investigations, particularly those devoted to the investigation of fission of uranium by slow π^- mesons. In these works it has been assumed in the calculation of the fission probability P_f that the probability of capture of a π^- meson by various atoms contained in the photoemulsion gelatine obeys the Fermi-Teller "Z-law." In this connection it becomes advisable to clarify the applicability of the Fermi-Teller "Z-law" to an emulsion to which some other substance (uranium) has been added.

To make the experimental data more precise (the previously obtained values of P_f range from 0.18 to 0.5), the experiments on the fission of uranium by slow π^- mesons were repeated in this investigation. The value of P_f was calculated under several assumptions, and it has been demonstrated by comparison with electronically-performed experiments that the capture of π^- mesons by various atoms in a medium comprising gelatine + uranium obeys the Fermi-Teller Law.

NIKFI-R emulsions 200 μ thick and impregnated with uranyl acetate were used in the experiments. The number of uranium nuclei introduced into the emulsions was determined by counting the alpha particles from the natural radioactivity of the uranium. The plates were irradiated in the slow π^--meson beam of the synchrocyclotron of the Joint Institute for Nuclear Research. The μ^--meson admixture was found to be 20%. Since P_f of uranium is very low for μ^- mesons (0.07),[4] the fissions due to the μ^- mesons did not exceed 3% of the total and were taken into account in the final result. The experimental data are listed in the table.

Number of experiments		1	2
Number of fissions		20	61
Number of stopped π- mesons		1445	5560
Number of uranium nuclei per cm³ of emulsion		$1.8 \cdot 10^{20}$	$1.5 \cdot 10^{20}$
Probability of capture of π- mesons in uranium	"Z-law"	$7.3 \cdot 10^{-2}$	$6.3 \cdot 10^{-2}$
	number of atoms	$5.9 \cdot 10^{-3}$	$5.0 \cdot 10^{-3}$
Fission probability	"Z-law"	0.45 ± 0.11	0.42 ± 0.07
	number of atoms	~6	~6

The probability of uranium fission by π^- mesons was calculated on the following assumptions: 1) the uranium is completely adsorbed in the gelatine, as established experimentally by Lozhkin and Shamov;[5] 2) the probability of capture of the π^- meson by the various elements in the gelatine (with the exception of hydrogen) was calculated under two assumptions: a) the capture of π^- mesons is proportional to Z, and b) the capture of the π^- meson is proportional to the number of atoms of the

given element in the gelatine.[1,2] As can be seen from the table, in the former case $P_f \approx 4$ and in the latter case $P_f \approx 6$, which is impossible. This excludes the applicability of item b) to the gelatine + uranium medium.

To the contrary, the applicability of the Fermi-Teller "Z-law" to the gelatine + uranium medium can be corroborated by comparing P_f for the fission of uranium by π^- mesons and the fission of Th^{232} by protons[6] (experiments with thorium were performed electronically). In either case, isotopes of the same substance are first produced (Pa^{238} and Pa^{233}). In the fission of Th^{232} by protons of energies from 10 to 340 Mev, P_f increases rapidly with energy and reaches a constant value, 0.45 ± 0.07, at approximately 50 Mev. At equal excitation energies (noticeably higher than the fission-threshold energies), P_f is smaller for the isotopes with the larger mass number. Therefore P_f (Pa^{238}) cannot be greater than 0.45.

Nor can P_f (Pa^{238}) be noticeably less than this quantity, as will now be shown. The mean excitation energy of uranium upon capture of slow π^- mesons is 60 to 80 Mev. At such excitation energies, fission of the nucleus is preceded by emission of several neutrons. Upon emission of five neutrons, the nuclear excitation energy diminishes by the amount of the binding energy (~ 25 Mev) and the kinetic energy carried away by these neutrons (~ 10 Mev).[7] The result is the nucleus Pa^{233} (the same isotope as in the fission of thorium by protons) with excitation energy 25 — 45 Mev. It follows from the experiments on the fission of Th^{232} by protons that at such excitation energies $0.35 < P_f \leq 0.45$. If $P_f \approx 0.35$, then by putting the probability of π^--meson capture by the various nuclei to be proportional to Z^n, a value close to unity is obtained for n ($n = 1.25$).

Thus, the probability of π^--meson capture in a gelatine + uranium medium (which is not a homogenous chemical compound) obeys more readily the "Z-law" than the proportionality to the number of atoms. This conclusion holds also for other types of mesons, since the capture of mesons on the atomic shells does not depend on the nuclear properties of the mesons.

These results, in conjunction with earlier experiments,[1,2] indicate that the probability of meson capture by various atoms in inhomogeneous media depends apparently on the structure of the medium.

[1] Sens, Swanson, Telegdi, and Iovanovitch, Nuovo cimento 7, 536 (1958).

[2] Backenstoss, Bloch, Chidley, Reiter, Romanowski, Siegel, and Sutton, Bull. Amer. Phys. Soc. 4, 273 (1959).

[3] E. Fermi and E. Teller, Phys. Rev. 72, 399 (1947).

[4] Belovitskiĭ, Kochukeev, Mikhul, Petrashku, Romanova, and Tikhomirov, JETP 38, 404 (1960), this issue p. 296.

[5] O. V. Lozhkin and V. P. Shamov, JETP 28, 739 (1955), Soviet Phys. JETP 1, 587 (1955).

[6] H. M. Steiner and I. A. Junderman, Phys. Rev. 101, 807 (1956).

[7] G. H. Harding and D. M. Skyrme, Nuovo cimento 9, 1083 (1958).

Translated by J. G. Adashko
132

DETERMINATION OF THE COUPLING CONSTANT FOR THE PION-NUCLEON INTERACTION FROM CROSS SECTIONS FOR THE ELASTIC SCATTERING OF 630-Mev NEUTRONS BY PROTONS

N. S. AMAGLOBELI, B. M. GOLOVIN, Yu. M. KAZARINOV, S. V. MEDVED', and N. M. POLEV

Joint Institute for Nuclear Research; Physics Institute, Academy of Sciences, Georgian S.S.R.

Submitted to JETP editor November 17, 1959

J. Exptl. Theoret. Phys. (U.S.S.R.) 38, 660-661 (February, 1960)

IN reference 1, the differential cross sections for elastic n-p collisions, $\sigma_{np}(\theta)$, for $E_n = 630$ Mev and for the center-of-mass angular interval $160° \leq \theta \leq 180°$ were used to determine the pion-nucleon coupling constant f^2 by the Chew method.[2] For this the measured cross sections $\sigma_{np}(\theta)$ were multiplied by the quantity

$$x^2 = (1 + \mu^2/2k^2 + \cos\theta)^2$$

(μ is the pion mass, $\mathbf{k}$ is the nucleon c.m.s. momentum) and the values obtained $x^2\sigma_{np}(\theta)$ by the method of least squares were approximated by a power series of the form

$$x^2 \sigma_{np}(\theta) = A + Bx + Cx^2 + \ldots + dx^m. \qquad (1)$$

According to present meson theory, the coefficient A of this series can be directly expressed

by the constant f^2. In order to approximate the experimental values $x^2\sigma_{np}(\theta)$ a series of trial functions was used, beginning from a linear dependence up to and including a fourth-power parabola. Using polynomials of higher order ($m > 4$) was not reasonable, since the number of points $x^2\sigma_{np}(\theta)$ was relatively small. The results of the calculations showed that the best values of f^2 were 0.04 and 0.085. However, the relatively low statistical accuracy and the small number of points on the curve $\sigma_{np}(\theta)$ in the angular interval mentioned above prevented choosing one of these two values of the constant. Here it also appeared that in all the remaining cases (excluding the linear dependence $A+Bx$) $0.04 \leq f^2 \leq 0.085$. Averaging all the values of f^2 found gave $f^2 = 0.06 \pm 0.02$.

The necessity of getting supplementary information to more accurately determine the constant f^2 led us to continue the measurements and to markedly increase the number of points on the curve $\sigma_{np}(\theta)$ in the angular interval $160° \leq \theta \leq 180°$ ($0° \leq \varphi \leq 9°$, φ is the recoil angle in the laboratory system). The measurements of the differential cross sections for n-p collisions at 630 Mev were carried out by two methods: by the method of a ring scatterer[3] and by an ordinary detector which records the recoil proton.

The ring scatterer method, as is well known, has the advantage that for small angular resolutions a detector encompasses a relatively large solid angle. By this method, however, it is possible to investigate only a limited angular region ($2.5° \leq \varphi \leq 8°$). An ordinary detector of proton recoil can function in the whole angular interval under investigation, but since in our case a small angular resolution (0.5°) and a high-energy threshold were required, after a short time it was impossible to carry through the experiment for the available intensity of the neutron beam. In this way, these two methods supplemented one another. The differential cross sections were measured in relative units. Their absolute values were found from the known differential cross section for elastic n-p scattering at $\varphi = 8°$, measured previously in reference 1.

As a result of the measurements the number of points on the curve $\sigma_{np}(\theta)$ in the angular interval $160° \leq \theta \leq 180°$ which were suitable for determining the pion-nucleon coupling constant was increased to twice that of the preceding work (ten points were established).

The approximation to the experimentally obtained dependence of $x^2\sigma_{np}(\theta)$ by a power series of the form (1) was carried out by the computing department of the Joint Institute for Nuclear Research. In this, by the method of least squares, curves for trial functions were fitted to the experimental points, the functions beginning with a linear dependence and ending with a fifth-order polynomial.

As has been explained, a further increase in the number of terms of the series was not sensible, since the calculations showed that the coefficients for powers of x higher than the fifth had values small compared with the error, which exceeded 100%. A series of the form $A + Bx^2$, according to the criteria of reliability, seemed the best of the calculated trial series. The coefficient A gives there the value $f^2 = 0.04 \pm 0.005$ for the pion-nucleon coupling constant.

Not long ago we received a letter from Moravcsik, Cziffra, and Larsen at Berkeley, in which they kindly report that, using the data from elastic n-p scattering for $E_n = 630$ Mev[1] which was communicated earlier at the International Conference on High-Energy Physics (Kiev, 1959), they got a most probable value of $f^2 = 0.04 \pm 0.015$. Here, however, at variance with reference 1, they used the whole investigated region of scattering angles $11° \leq \theta \leq 180°$, just as they had for energies $E_n = 90$ and 400 Mev.[4]

The result of the present work and, equally, the values of f^2 calculated by Cziffra and Moravcsik[4] for values of $\sigma_{np}(\theta)$ at energies $E_n = 90$ and 400 Mev show that, in determining f^2 from the scattering of neutrons from protons by the method suggested by Chew, the constant f^2 takes on an evidently smaller value than the 0.08 obtained from experiments on pion-proton scattering.

The authors take pleasure in expressing their gratitude to Yu. N. Simonov for his help in the work, to S. N. Sokolov and T. P. Kochkina for carrying out necessary calculations and for examining the results of the work.

[1] N. S. Amaglobeli and Yu. M. Kazarinov, JETP **37**, 1587 (1959), Soviet Phys. JETP **10**, 1125 (1960).

[2] G. F. Chew, Phys. Rev. **112**, 1380 (1958).

[3] Golovin, Dzhelepov, Katyshev, Konin, and Medved', Приборы и техника эксперимента (Instruments and Meas. Engg.), in press.

[4] P. Cziffra and M. J. Moravcsik, Preprint.

Translated by W. Ramsay
133

DEPENDENCE OF THREE-DIMENSIONAL DEVELOPMENT OF A CASCADE SHOWER ON THE ENERGY OF THE PRIMARY PARTICLE

V. V. GUZHAVIN and I. P. IVANENKO

Institute of Nuclear Physics, Moscow State University

Submitted to JETP editor October 8, 1959

J. Exptl. Theoret. Phys. (U.S.S.R.) **38**, 662-664 (February, 1960)

IN three-dimensional cascade theory, the functions of angular and spatial distribution of particles are usually calculated under the assumption that the energy of the primary particle is infinitely large. However, the energy of the electrons and photons near the axis of the shower is comparable with the energy E_0 of the primary particle, and therefore E_0 cannot be assumed infinite. We give here a convenient approximate method of calculating these functions, which yields a sufficiently accurate account of the influence of the finite E_0 on the form of the distribution function. Let, for example, $N_p(E_0, E, r, t)\,dr$ be the number of electrons with energy greater than E at a depth t and a distance r, r+dr from the shower axis, due to a primary particle with energy E_0. If we introduce $x = Er/E_s$, where $E_s = 21$ Mev, then when $E_0 = \infty$ the function $N_p^{\infty}(E_0, E, r, t)$ can be represented in the form*[1]

$$N_p^{\infty}(E_0, E, r, t) = f_p^{\infty}(x, s)\, N_p(E_0, E, t)\, E^2 E_s^2, \qquad (1)$$

where $N_p(E_0, E, t)$ is a function that describes the one-dimensional development of the shower. The function of lateral distribution $f_p^{\infty}(x, s)$ is normalized as follows:

$$\int_0^{\infty} f_p^{\infty}(x, s)\, x\,dx = 1.$$

In one-dimensional cascade theory, the quantities E_0, E, and t are related as follows

$$-\lambda_1'(\bar{s})\, t = y, \qquad (2)$$

where $\bar{s}$ is the cascade parameter, $y = \ln(E_0/E)$, and $\lambda_1'(s)$ is a tabulated function. In three-dimensional theory for a finite value of E_0, the quantities E_0, E, x and t are related by

$$-\lambda_1(s)\, t = y + \ln x, \qquad (3)$$

which holds when $1 > x > E/E_0$. It is seen from (3) that at a finite value of E_0 and a fixed depth t, the quantity x is a function of s, and as r decreases s increases, reaching a limiting value $s = \infty$ when $x_{min} = E/E_0$. If we let E_0 approach infinity in (3), then the dependence $x = x(s)$ becomes weaker and weaker, and in the limit $E_0 = \infty$ it disappears entirely. In this case the parameter s is constant for $0 < x < \infty$ and coincides with the parameter $\bar{s}$ of the one-dimensional theory. Taking this into account, the function of lateral distribution of particles at a depth t in a shower, induced by a primary particle of energy E_0, can be represented in the form

$$N_p(E_0, E, x(s), t(\bar{s})) = f_p^{E_0}(x, s)\, N_p(E_0, E, s, t(\bar{s}))\, E^2/E_s^2, \qquad (4)$$

where the dependence $x(s)$ at constant E_0, E, and t is determined from (3), while $t(\bar{s})$ is determined from (2). To calculate $N_p[E_0, E, x(s), t(\bar{s})]$, we can use the functions $f_p^{\infty}(x, s)$ which were previously calculated[2] by the method of moments. Actually, the moments $\overline{\theta^n}(E_0, E, s)$ and $\overline{r^n}(E_0, E, s)$ of the functions of angular and spatial distribution depend little on E_0 if s is constant and $E_0/E > 10$, (reference 3). Consequently, one can assume approximately that at constant s the functions $f_p^{E_0}(x, s)$ depend little on $E_0/E > 10$, i.e., $f_p^{E_0}(x, s) \approx f_p^{\infty}(x, s)$. Therefore, if we determine the variation of $x(s)$ from (3) at constant E_0, E, and t, we get

$$N_p(E_0, E, x(s), t(\bar{s})) \approx f_p^{\infty}(x, s)\, N_p(E_0, E, s, t(\bar{s}))\, E^2/E_s^2. \qquad (5)$$

We introduce the function of spatial distribution of electrons for a finite value of E_0, normalized to one particle:

$$f_p(E_0, E, x(s), t) = N_p(E_0, E, x(s), t(\bar{s}))\, E_s^2/N_p(E_0, E, \bar{s}, t(\bar{s}))\, E^2. \qquad (6)$$

We then obtain finally

$$f_p(E_0, E, x, t) = f_p^{\infty}(x, s)\, N_p(E_0, E, s, t)/N_p(E_0, E, \bar{s}, t). \qquad (7)$$

It is easy to calculate analogously the functions of spatial distribution of photons with energy greater than E, and also the corresponding distribution functions of particles with energies $E > 0$, with allowance for ionization losses. The method used for the calculation can be applied to the calculation of angular-distribution functions.

Let us obtain the lateral distribution function of electrons with energy greater than E for the case of equilibrium. In reference 4 it was shown that if the electrons and photons of energy E_0 are generated over the entire thickness of the substance in

accordance with the law $e^{-\mu t}\delta(E_0 - E)$, then $\bar{s}$, t and y are related by

$$-\lambda_1'(\bar{s})[t - 1/(\lambda_1(\bar{s}) + \mu)] = y, \tag{8}$$

where μ is the coefficient of absorption of the component that generates the primary electrons or photons. The integral energy spectrum of the electrons has the form

$$N_p(E_0, E, t) = \frac{H_1(\bar{s})}{\bar{s}} \exp\left\{y\bar{s} + \lambda_1(\bar{s})\, t - \ln[\lambda_1(\bar{s}) + \mu]\right\} \times \left[2\pi\left\{\lambda_1''(\bar{s})\, t - \frac{\lambda_1''(\bar{s})[\lambda_1(\bar{s}) + \mu] - \lambda_1'^2(\bar{s})}{[\lambda_1(\bar{s}) + \mu]^2}\right\}\right]^{-1/2}. \tag{9}$$

It can be shown that in the case of continuous generation in depth, the quantities s, t, y, and x in three-dimensional theory are related by

$$-\lambda_1'(s)[t - 1/(\lambda_1(s) + \mu)] = y + \ln x. \tag{10}$$

We used the foregoing method to calculate the following functions: the laterial distribution function of electrons and photons with energy greater than E (approximation A) at $\bar{s} = 0.4$, 0.6, 0.8, 1.0, 1.2, 1.4, and 1.6 for various values of the ratio $E_0/E = 10^6$, 10^4, 10^3, 10^2 and 10; the functions of lateral distribution of electrons with energy $E > 0$ (approximation B) for $\bar{s} = 0.6$, 0.8, 1.0, 1.2, 1.4, 1.6 and for values of the ratio $E_0/\beta = 10^6$, 10^4, 10^3, 10^2 and 10. We also calculated the equilibrium functions of angular and lateral distributions of electrons for several values of the parameters.

*The condition $E_0 = \infty$ is used here only for calculating the function $f_p^{\infty}(x, s)$.

[1] S. Z. Belen'kiĭ, Лавинные процессы в космических лучах (Cascade Processes in Cosmic Rays), Gostekhizdat, 1948.

[2] V. V. Guzhavin and I. P. Ivanenko, Dokl. Akad. Nauk SSSR **115**, 1089 (1957), Soviet Phys.-Doklady **2**, 407 (1958).

[3] L. Eyges, Phys. Rev. **74**, 1801 (1948).

[4] S. Z. Belen'kiĭ and I. P. Ivanenko, Usp. Fiz. Nauk **69**, 591 (1959), Soviet Phys.-Uspekhi **2**, 912 (1960).

Translated by J. G. Adashko
134

ON THE PRODUCTION OF AN ELECTRON-POSITRON PAIR BY A NEUTRINO IN THE FIELD OF A NUCLEUS

A. M. BADALYAN and CHOU KUANG-CHAO

Submitted to JETP editor November 26, 1959

J. Exptl. Theoret. Phys. (U.S.S.R.) **38**, 664-665 (February, 1960)

PRESENT experimental possibilities have allowed a rather close approach to a measurement of the cross section for scattering of a neutrino by an electron.[1] This process is a very important one for testing the theory of the universal weak interaction.

In the laboratory system, in which the electron is at rest, and for incident neutrino energy $\omega_1 \gg m$, the cross section for scattering of a neutrino by an electron is

$$\sigma_1 = (g^2/3\pi)\, m\omega_1, \tag{1}$$

i.e., a linear function of ω_1.

There is another process, $\nu + Z \to \nu + Z + e^+ + e^-$, for which the laboratory system coincides with the center-of-mass system. On one hand, it could be expected that the cross section for this process would be smaller than that for scattering, since it contains the factor $(Ze^2)^2$, and the phase volume gives an additional numerical factor $(2\pi)^{-2}$. On the other hand, the phase volume is proportional to ω_1^8, since there are three particles in the final state.

This process is described by two second-order diagrams. The calculation of the contributions of the two diagrams to the cross section leads to extremely cumbersome formulas. We shall, however, get the right order of magnitude for the total cross section if we confine ourselves to the contribution of one diagram. The differential cross section for the process then has the form

$$d\sigma_2 = \frac{16g^2(Ze^2)^2}{\omega_1\omega_2\varepsilon_-\varepsilon_-} \frac{dp_- dp_+ dk_2}{q^4(2\pi)^5} \frac{(k_1k_2)}{m^2 - f^2} \times \left[2\varepsilon_+\varepsilon_- - (p_+p_-) + 2fp_+ \frac{2\varepsilon_-^2 + m^2 - (fp_-)}{m^2 - f^2}\right] \times \delta(\omega_1 - \omega_2 - \varepsilon_+ - \varepsilon_-), \tag{2}$$

where

$$f = k_1 - k_2 - p_-, \qquad q = k_1 - k_2 - p_+ - p_-.$$

Here k_1, k_2, p_+, and p_- are four-vectors that refer respectively to the neutrino in its initial and

final states and to the positron and electron; ω_1, ω_2, ϵ_+, and ϵ_- are the corresponding energies.

For high energies of all the particles involved in the process the differential cross section $d\sigma_2$ has a sharp maximum near the direction of the momentum of the incident neutrino. All of the emerging particles are concentrated in a narrow cone around this direction, with angular aperture $\vartheta \approx m/\omega_1$. This follows from the fact that the denominator of the expression (2) contains the factor

$$[\omega_1\omega_2(1-\cos\vartheta_{12}) + \omega_1\varepsilon_+(1-v_+\cos\vartheta_{1+}) - \omega_2\varepsilon_+(1-v_+\cos\vartheta_{2+})]$$

(ϑ_{ik} is the angle between the momenta of the i-th and k-th particles, and v_+ is the velocity of the positron), together with the fact that the effective recoil momentum of the nucleus is $q \sim m$.

The reduction of the "effective" solid angle sharply lowers the degree of the energy dependence of the total cross section. Apart from terms of second order in m/ω_1 the total cross section is

$$\sigma_2 = \frac{8g^2(Ze^2)^2\omega_1^2}{3(2\pi)^3}\alpha\left(\ln\frac{\omega_1}{m}-\beta\right), \qquad \omega_1 \gg m, \qquad (3)$$

where α, $\beta \sim 1$; $1 < \beta < 2$. Comparison of Eqs. (1) and (3) shows that for $Z/137 \approx 1/2$ the cross section σ_2 becomes comparable with σ_1 only for incident neutrino energy $\omega_1 \approx 10$ Mev. It is only at energies higher than this that the process of production of an electron-positron pair may become observable.

The writers express their gratitude to Ya. A. Smorodinskiĭ for his interest in this work and for a discussion of the results.

[1] C. L. Cowan, Jr. and F. Reines, Phys. Rev. **107**, 528 (1957).

Translated by W. H. Furry
135

INSTABILITY IN A SEMICONDUCTOR AMPLIFIER WITH NEGATIVE EFFECTIVE CARRIER MASS

A. L. ZAKHAROV

Submitted to JETP editor December 8, 1959

J. Exptl. Theoret. Phys. (U.S.S.R.) **38**, 665-667 (February, 1960)

KRÖMER has shown[1] that a crystal of germanium or silicon, of the p type, in which there exists a strong field in the [100] direction ("longitudinal" direction), will have in any direction perpendicular to the [100] ("transverse directions") a negative conductivity. The use of this negative conductivity for amplification and generation is precisely the idea of the new semiconductor instrument proposed by Krömer, the NEMAG (negative effective mass amplifier and generator).

This device differs from diodes with negative conductivity (for example, tunnel or parametric) in that its negative conductivity is specific. This circumstance leads to an unstable operating state of the device, as can be seen from the following consideration. Assume that in a certain microvolume, the thermal fluctuations of the hole concentrations result in an accumulation of a small positive charge. Then the field produced by this charge causes in the surrounding medium a current flowing not from the charge (as in the case of positive specific conductivity) but to the charge (more accurately, to the [100] line, passing through the charge). The charge will start increasing exponentially with a time constant called the time of dielectric relaxation ($\tau = |\epsilon\rho|$ where ϵ is the dielectric constant and ρ the negative specific resistivity of the semiconductor) and this process will slow down and cease only when a transverse field E_t is produced strong enough to make the conductivity in it positive (a negative conductivity is observed only at sufficiently small transverse fields).

An analogous process leads to the formation of a negative charge (region where the concentration of the holes is less than the concentration of the charged impurity centers — acceptors), if the initial fluctuation reduces the concentration of the holes compared with the equilibrium value.

In the stationary state the charge is arranged around the [100] axis with a density that decreases with the distance from this axis. The state with negative conductivity (weak transverse field) is retained only in a thin cylinder about this axis, and the finite thickness of the cylinder is determined only by the diffusion loss of holes, and amounts to a fraction of a micron (of the order or less than kT/eE_t). Such cylinders are attracted to each other when their charges are of the same polarity, and are repelled when they are different, and consequently, as can be shown, the distances between the cylinders in the state of stable equilibrium are of the same order as or greater than the thickness of the crystal in the transverse direction. But this thickness is always much greater than the thickness of the cylinder and furthermore the lineary density of the charge in the cylinder is negligible (on the order of $kT/2$); therefore the contribution of the cylinders to the total con-

ductivity of the crystal is negligibly small. This conductivity will be determined essentially by the conductivity of the regions with strong transverse field (the region of the crystal outside the cylinders), i.e., it will be positive.

It may turn out that the qualitative considerations given by us clearly refute the idea of using the negative effective mass for amplification and generation. This is not so, however. Let us consider the NEMAG to be a carrier-poor layer, produced in a reverse-biased junction,* in which we introduce holes one by one at time intervals greater than the travel time of the holes. Clearly in such an instrument there will be no transverse field produced and its action will obey in its entirety the Krömer theory. Naturally, in order for the device to have resistance, the hole need not be alone; one merely needs a sufficiently small number of holes. In terms of the phenomenological theory, this condition will be formulated as follows: the negative specific conductivity should be so small, and the length of the device in the longitudinal direction should be so short, that the time of the dielectric relaxation be greater than, or at least of the same order as the travel time of the carrier through the entire device. The point is that since the positive electrode producing the longitudinal field is an equipotential surface (the field is perpendicular to the surface), it causes the material to have a negative conductivity. The process of charge formation and the formation of the transverse field requires a finite time, equal to several times the dielectric relaxation time. But simultaneously with accumulation of charge, the charges are carried away by drift motion towards the negative electrode and leave the device. The meaning of the requirement formulated above is that the device can have a negative conductivity only when the process of formation of the transverse field has not yet a chance to be completed and the charges formed have already drifted out from the instrument. It is possible to obtain negative conductivity without limitations on the lengths of the structure by operating in the pulsed mode.

Thus, although the possibility of using the negative effective mass is not completely eliminated by the appearance of instability, it is considerably restricted, and the idea of the device loses a considerable portion of its attractiveness. Probably the NEMAG as an amplifier will be a highly noisy device (in contrast to what Krömer predicts), since the initial stage of the process of charge formation should be subject to very strong fluctuations. On the other hand, small negative conductivities and short structures, which are required for continuous operation, necessitate a large value of RC (on the order of the time of flight) and a small thickness of the device. One should indicate that the device could be used as a noise generator.

Although all the foregoing is in the nature of rough qualitative ideas, they indicate undoubtedly that the distribution of the charges and fields in this device, and also its properties, will be much more complicated than proposed by Krömer's theory.

*I.e., in the double charge layer of the donor and acceptor impurities, which are formed around the junction (separation boundary) between the regions of the semiconductor with n and p conductivities, when a reverse voltage is applied to the semi-conductor: plus to the electron region and minus to the hole region.

[1] H. Krömer, Proc. IRE 47, 231 (1959).

Translated by J. G. Adashko
136

SOVIET PHYSICS JOURNALS

Published in English by the American Institute of Physics

Soviet Physics—JETP

A translation, beginning with 1955 issues of "Zhurnal Eksperimental'noi i Teoreticheskoi Fiziki" of the USSR Academy of Sciences. Leading physics journal of Soviet Union. Similar to "The Physical Review" in quality and range of topics. Outstanding new work is most likely to appear in this journal.

Twelve issues, approximately 4000 pages. $75 domestic, $79 foreign. Libraries $35 domestic, $39 foreign. Single copies, $8.*

Soviet Physics—SOLID STATE

A translation, beginning with 1959 issues of "Fizika Tverdogo Tela" of the USSR Academy of Sciences. Offering results of theoretical and experimental investigations in the physics of semiconductors, dielectrics, and on applied physics associated with these problems. Also publishes papers on electronic processes taking place in the interior and on the surface of solids.

Twelve issues, approximately 2000 pages. $55 domestic, $59 foreign. Libraries $25 domestic, $29 foreign. Single copies, $8.*

Soviet Physics—TECHNICAL PHYSICS

A translation, beginning with 1956 issues of "Zhurnal Tekhnicheskoi Fiziki" of the USSR Academy of Sciences. Contains work on plasma physics and magnetohydrodynamics, aerodynamics, ion and electron optics, and radio physics. Also publishes articles in mathematical physics, the physics of accelerators, and molecular physics.

Twelve issues, approximately 2000 pages, $55 domestic, $59 foreign. Libraries $25 domestic, $29 foreign. Single copies, $8.*

Soviet Physics—ACOUSTICS

A translation, beginning with 1955 issues of "Akusticheskii Zhurnal" of the USSR Academy of Sciences. Devoted principally to physical acoustics but includes electro-, bio-, and psychoacoustics. Mathematical and experimental work with emphasis on pure research.

Four issues, approximately 500 pages. $12 domestic, $14 foreign. (No library discounts.) Single copies, $4.

Soviet Physics—DOKLADY

A translation, beginning with 1956 issues of the physics sections of "Doklady Akademii Nauk SSSR," the proceedings of the USSR Academy of Sciences. All-science journal offering four-page reports of recent research in physics and borderline subjects.

Six issues, approximately 1500 pages. $35 domestic, $38 foreign. Libraries $15 domestic, $18 foreign. Single copies Vols. 1 and 2, $5; Vol. 3 and later issues, $7.*

Soviet Physics—CRYSTALLOGRAPHY

A translation, beginning with 1957 issues of the journal "Kristallografiya" of the USSR Academy of Sciences Experimental and theoretical papers on crystal structure, lattice theory, diffraction studies, and other topics of interest to crystallographers, mineralogists, and metallurgists.

Six issues, approximately 1000 pages. $25 domestic, $27 foreign. Libraries $10 domestic, $12 foreign. Single copies, $5.*

SOVIET ASTRONOMY—AJ

A translation, beginning with 1957 issues of "Astronomicheskii Zhurnal" of the USSR Academy of Sciences. Covers various problems of interest to astronomers and astrophysicists including solar activity, stellar studies, spectroscopic investigations of radio astronomy.

Six issues, approximately 1100 pages. $25 domestic, $27 foreign. Libraries $10 domestic, $12 foreign. Single copies, $5.*

Soviet Physics—USPEKHI

A translation, beginning with September, 1958, issue of "Uspekhi Fizicheskikh Nauk" of the USSR Academy of Sciences. Offers reviews of recent developments comparable in scope and treatment to those carried in "Reviews of Modern Physics." Also contains reports on scientific meetings within the Soviet Union, book reviews, and personalia.

Six issues, approximately 1700 pages. (Contents limited to material from Soviet sources.) $45 domestic, $48 foreign. Libraries $20 domestic, $23 foreign. Single copies $9.*

*For libraries of nonprofit academic institutions.
Subscription prices subject to annual variation, depending on size of Russian originals.

Please send orders and inquiries to

American Institute of Physics

335 East 45 Street, New York 17, N.Y.